

# The Muon Magnetic Moment and Physics Beyond the Standard Model

Peter Athron<sup>a,b</sup>, Kilian Möhling<sup>c</sup>, Dominik Stöckinger<sup>c,\*</sup>, Hyejung Stöckinger-Kim<sup>c</sup>

<sup>a</sup>*Institute of Theoretical Physics and Institute of Physics Frontiers and Interdisciplinary Sciences, Nanjing Normal University, Wenyuan Road, Nanjing, Jiangsu, 210023, China*

<sup>b</sup>*Nanjing Key Laboratory of Particle Physics and Astrophysics, Nanjing, 210023, China*

<sup>c</sup>*Institut für Kern- und Teilchenphysik, TU Dresden, Zellescher Weg 19, 01069 Dresden, Germany*

---

## Abstract

We review the role of the anomalous magnetic moment of the muon  $a_\mu$  as a powerful probe of physics beyond the Standard Model (BSM), taking advantage of the final result of the Fermilab  $g - 2$  experiment and the recently updated Standard Model value. This review provides both a comprehensive summary of the current status, as well as an accessible entry point for phenomenologists with interests in dark matter, Higgs and electroweak or neutrino and flavour physics in the context of a wide range of BSM scenarios. It begins with a qualitative overview of the field and a collection of key properties and typical results. It then focuses on model-independent, generic formulas and classifies types of BSM scenarios with or without chiral enhancements. A strong emphasis of the review are the connections to a large number of other observables — ranging from the muon mass and the muon–Higgs coupling and related dipole observables to dark matter, neutrino masses and high-energy collider observables. Finally, we survey a number of well-motivated BSM scenarios such as dark photons, axion-like particles, the two-Higgs doublet model, supersymmetric models and models with leptoquarks, vector-like leptons or neutrino mass models. We discuss the impact of the updated Standard Model value for  $a_\mu$  and of complementary constraints, exploring the phenomenology and identifying excluded and viable parameter regions.

---

---

\*Corresponding author

*Email addresses:* [peter.athron@coepp.org.au](mailto:peter.athron@coepp.org.au) (Peter Athron), [kilian.moehling@tu-dresden.de](mailto:kilian.moehling@tu-dresden.de) (Kilian Möhling), [dominik.stoeckinger@tu-dresden.de](mailto:dominik.stoeckinger@tu-dresden.de) (Dominik Stöckinger), [hyejung.stoeckinger-kim@tu-dresden.de](mailto:hyejung.stoeckinger-kim@tu-dresden.de) (Hyejung Stöckinger-Kim)

# Contents

<b>1</b>	<b>Introduction</b>	<b>5</b>
1.1	Motivation and overview . . . . .	6
1.1.1	Status of $a_\mu$ and current values . . . . .	8
1.1.2	Sensitivity to fundamental interactions and generic BSM contributions . . . . .	9
1.1.3	Key properties of $a_\mu$ and complementarities to other observables . . . . .	11
1.1.4	Structure of BSM contributions and the role of chirality flips and electroweak gauge invariance . . . . .	12
1.1.5	Overview of BSM scenarios . . . . .	16
1.2	Definition of $a_\mu$ . . . . .	17
1.3	Status of the $a_\mu$ Measurement . . . . .	23
1.4	Status of $a_\mu$ in the Standard Model . . . . .	27
<b>2</b>	<b>Generic BSM scenarios</b>	<b>33</b>
2.1	General one-loop formulas for $\Delta a_\mu$ . . . . .	33
2.2	Contributions from minimal extensions of the Standard Model . . . . .	38
2.3	Three-field extensions with chiral enhancements and mass-insertion approximations . . . . .	43
2.4	Effective field theory description . . . . .	48
<b>3</b>	<b>Relationships to other observables</b>	<b>53</b>
3.1	Muon mass and generic estimates of possible $a_\mu$ contributions . . . . .	53
3.2	Other leptonic dipole observables and charged lepton flavour violation . . . . .	57
3.3	Muon–Higgs coupling . . . . .	62
3.4	Electroweak precision observables . . . . .	66
3.5	Neutrino masses . . . . .	69
3.5.1	Overview of neutrino mass terms . . . . .	70
3.5.2	Seesaw mechanism and radiative mass generation . . . . .	71
3.5.3	Example contributions of neutrino mass generation mechanisms to $a_\mu$ . . . . .	75
3.6	Dark Matter . . . . .	77
3.6.1	The relic density of dark matter, WIMPs and the detection of dark matter . . . . .	78
3.6.2	Single-field extensions of the SM . . . . .	81
3.6.3	Two-field extensions . . . . .	82
3.6.4	Three-field extensions . . . . .	86
3.7	Collider observables . . . . .	90
3.7.1	Mass limits from Colliders and $\Delta a_\mu$ . . . . .	91
3.7.2	Two-field models and compressed spectra . . . . .	94
<b>4</b>	<b>Higher-order contributions to <math>a_\mu</math></b>	<b>97</b>
4.1	Form factor trace projectors . . . . .	97
4.2	Two-loop Barr-Zee diagrams . . . . .	98
4.3	Leading logarithms and EFT resummation . . . . .	100

4.3.1	The EFT renormalisation group equation . . . . .	101
4.3.2	Photonic logarithms for purely heavy BSM scenarios . . . . .	103
4.3.3	More general logarithms . . . . .	104
<b>5</b>	<b>Specific BSM scenarios</b> . . . . .	<b>106</b>
5.1	Light Dark Sectors . . . . .	106
5.1.1	Analytical results for light-particle contributions . . . . .	107
5.1.2	Dark Photons . . . . .	109
5.1.3	$Z'$ and $U(1)_{L_\mu-L_\tau}$ . . . . .	111
5.1.4	Axion-like particles and other light scalar particles . . . . .	115
5.1.5	Models modifying $\sigma(e^+e^- \rightarrow \text{had})$ . . . . .	120
5.2	Supersymmetry . . . . .	123
5.2.1	Brief account of the MSSM . . . . .	124
5.2.2	MSSM contributions to $a_\mu$ . . . . .	127
5.2.3	Complementary constraints on MSSM parameters . . . . .	131
5.2.4	Baseline SUSY scenarios . . . . .	136
5.2.5	Phenomenological results for heavy sparticles in the MSSM . . . . .	139
5.2.6	Phenomenological results with light Bino-like LSP in the MSSM . . . . .	142
5.2.7	Phenomenological results with light Higgsino- or Wino-like LSP in the MSSM . . . . .	144
5.2.8	SUSY beyond the R-parity conserving MSSM . . . . .	146
5.2.9	Summary . . . . .	148
5.3	Two-Higgs-doublet models . . . . .	149
5.3.1	Type I, II, X, Y and Flavour-aligned 2HDM . . . . .	151
5.3.2	2HDM contributions to $a_\mu$ . . . . .	152
5.3.3	Constraints from $a_\mu$ and other observables on the Type I, II, X, Y and Flavour-aligned 2HDM . . . . .	154
5.3.4	General 2HDM and summary . . . . .	157
5.4	Leptoquark models . . . . .	158
5.4.1	Leptoquark types with and without chiral enhancements . . . . .	159
5.4.2	Leptoquark contributions to $a_\mu$ . . . . .	160
5.4.3	Constraints on leptoquarks from $a_\mu$ and related observables . . . . .	162
5.4.4	Brief survey of leptoquark scenarios with specific flavour structures . . . . .	165
5.5	Vector-like fermion models . . . . .	167
5.5.1	Vector-like lepton models and chiral enhancement . . . . .	168
5.5.2	Vector-like lepton contributions to $a_\mu$ . . . . .	171
5.5.3	Collider searches and precision constraints . . . . .	174
5.5.4	Vector-like fermions with extended scalar sectors . . . . .	177
5.6	Muon $g - 2$ and neutrino mass . . . . .	179
5.6.1	Extensions of the scotogenic model . . . . .	180
5.6.2	Neutrino mass models based on other mechanisms . . . . .	185



# 1. Introduction

Magnetic dipole moments are among the most precisely known observables in physics, with a long and rich history. They represent simple and yet characteristic particle properties reflecting details of the fundamental interactions. The anomalous magnetic moments of leptons  $a_\ell = (g-2)_\ell/2$  are also among the most precisely computed quantities in physics. Their values originate exclusively from loop diagrams in renormalisable quantum field theories and are thus sensitive to quantum fluctuations of all particles that can interact with leptons. For elementary particle physics, the anomalous magnetic moment of the muon  $a_\mu = (g-2)_\mu/2$  is of particular interest. Compared to the electron, the muon is much heavier and enables higher-energetic quantum fluctuations, and although the muon lifetime is finite, it is long enough to allow measurements almost as precise as for the electron, which is not the case for the even heavier  $\tau$ -lepton. Thus in combination  $a_\mu$  is the most sensitive to heavy elementary particles and constitutes an excellent probe of the fundamental laws of physics.

Recently, two landmark results were obtained for the experimental and theoretical determination of  $a_\mu$ . The Fermilab muon  $g-2$  experiment has obtained its final result, decreasing the uncertainty of the world average to 125 ppb [1]. Meanwhile, the SM theory prediction has been scrutinised, and the immense effort of the community has led to two White Papers [2, 3] detailing the involved calculations. These two White Papers differ in their evaluation of the non-perturbative leading-order hadronic vacuum polarisation (HVP) contributions. The most recent prediction is based on lattice gauge theory computations, which have become very precise and consistent and are now cross-checked by several groups in multiple ways. The previous prediction was instead based on data-driven evaluations of the HVP contribution using experimental data for  $e^+e^- \rightarrow$  hadrons together with dispersion relations. However, at the time of Ref. [2] some tensions between these data sets were already present and have subsequently become more severe with the appearance of additional measurements. These tensions are under intense scrutiny and further improvements on the SM prediction can be expected in the forthcoming years.

The earlier SM prediction based on Ref. [2] is lower than the experimental value, favouring a sizeable and positive contribution to  $a_\mu$  from physics beyond the SM (BSM). In contrast, the current SM prediction of Ref. [3] is in full agreement with the experimental result for  $a_\mu$ . The newly obtained agreement may mark the emergence of  $a_\mu$  as an important constraint on many BSM scenarios, allowing only (positive or negative) contributions to  $a_\mu$  of sufficiently small magnitude.

In this review we show the power and significance of  $a_\mu$  as a precision test for BSM physics, provide detailed insights into calculations, describe correlations with other observables and discuss the phenomenological behaviour for many models. The first sections of the review focus on generic statements and relationships that can be described in a model-independent way or with the help of simplified examples. The last section focuses on a broad range of motivated BSM scenarios and presents up-to-date constraints from  $a_\mu$  and complementary observables. We mostly use  $a_\mu$  as a constraint on new physics rather than as a signal, using the new White Paper result and uncertainty. However the current SM prediction is a snapshot of the present situation and progress on the SM prediction might lead to a resolution of the tensions between lattice and data-driven results and could end up pointing at a new deviation from the experimental value. In this case, all the calculations and correlations we discuss would still apply, and the phenomenological plots would still display the preferred parameter regions. In either case, the present review thus aims to provide a timely overview of the impact of  $a_\mu$  as a precision test for new physics at the beginning of this new era for muon  $g-2$ .

In the following Section 1.1 we provide a brief overview of the field and motivate  $a_\mu$  as a probe of fundamental physics with unique properties. In addition, we also summarise the content of the review in more detail and preview selected results in a qualitative manner. The remainder of this Introduction then contains details on the quantum field theoretical definition of  $a_\mu$  in Sec. 1.2, and the status of the experiment and SM theory are reviewed in Secs. 1.3, 1.4. After this extended Introduction the review is structured into three essentially model-independent, generic sections and one section with detailed model-specific results.

In the model-independent, generic part of the review we describe in detail the general properties of the observable  $a_\mu$  from the perspective of BSM physics and correlations and complementarities to other observables ranging from low-energy dipole moments and the Higgs–muon interaction to neutrino masses and dark matter. We further analyse generically which classes of BSM scenarios can lead to large or small contributions to  $a_\mu$  and link characteristic properties to fundamental motivations such as dark matter or the origin of mass or flavour. Specifically, generic formulas for  $a_\mu$  together with their interpretation and applications to simple and generic models are explained in Sec. 2. Section 3 describes the relationships of  $a_\mu$  with the muon mass, with other dipole observables, the muon–Higgs interaction, electroweak precision observables and other collider observables as well as with neutrino masses and dark matter. Section 4 provides additional technical details on model contributions including higher orders both in Feynman diagrammatic and in effective field theory approaches.

The model-specific part of the review is Sec. 5, where we present an extensive survey of up-to-date results on a large set of motivated BSM scenarios. They cover models with light or heavy new particles, with or without dark matter, and with a wide range of relevant complementary observables. For each model the theory and phenomenology, and particularly the interplay of  $a_\mu$  and complementary constraints is explained. Viable model parameter regions are characterised, and it is shown which scenarios could lead to sizeable contributions to  $a_\mu$  and which scenarios are preferred by the new measurement and SM prediction.

There exist already several reviews and surveys with full or partial focus on  $a_\mu$  and BSM, such as Refs. [4–9] and [10–13]. Although there is some unavoidable overlap, the present review aims to be complementary in several respects. In the past years, a combination of general, model-independent analyses and explicit investigations in specific models have led to a detailed understanding of how  $a_\mu$  is related to a number of other observables, and how properties of BSM scenarios are relevant for such relationships. Here we provide a coherent and self-contained discussion of these insights with the goal of serving as a reference and summary but also as a possible entry point into the field.

In addition, the review appears after the final result of the Fermilab muon  $g - 2$  experiment and after significant progress on the SM theory prediction, although further SM theory progress is expected. It takes advantage of the current status and provides a detailed account of how the recent developments affect the constraints on BSM models. In our selection of models we are broad but focus particularly on a wide range of models which are intrinsically motivated independently of  $a_\mu$  and explain how they are constrained by the combination of  $a_\mu$  and other appropriate observables.

## 1.1. Motivation and overview

The use of  $a_\mu$  as a precision test of the SM and probe of new physics follows many decades of investigations into magnetic moments that have continuously helped shape our understanding of fundamental laws of nature. The discovery that the Dirac equation predicts the gyromagnetic ratio  $g = 2$  for the electron [14], in agreement with experiments at the time, was the first example of the fruitful interplay between theory and experiment.

Key progress was made by Schwinger, who realised that quantum effects, i.e. loop Feynman diagrams in QED lead to a deviation from  $g = 2$ , the anomalous magnetic moment  $a = (g - 2)/2$  [15, 16]. The agreement between the one-loop result  $a_e = \alpha/2\pi$  for the electron and experiments at the time confirmed relativistic quantum field theory (QFT) as the correct framework for fundamental interactions. The essential QFT property entering here is the possibility for quantum fluctuations of particle number, in modern language equivalent to the contributions of loop diagrams with the exchange of virtual particles.

Subsequently over the decades  $a_e$  and  $a_\mu$  were measured and computed at increasingly high levels of precision, finally arriving at the latest Fermilab measurement and SM theory prediction mentioned above. With this precision, the comparison between experiment and theory for  $a_\mu$  is sensitive to all known particles and interactions of the SM — even the heaviest particles such as  $W^-$ ,  $Z^-$  and Higgs boson and the top quark enter the theory prediction in a relevant way.

The SM is a mathematically rigorous, consistent, renormalisable QFT, and it is in excellent agreement with a multitude of experimental tests. Nevertheless it leaves open important questions and hence cannot be the ultimate description of nature. It cannot describe observational facts such as the evidence for dark matter in the universe and the existence of neutrino oscillations and neutrino masses. It also cannot explain the baryon-antibaryon asymmetry of the universe unless one assumes ad hoc asymmetric initial conditions. Beyond these observations, the structure of the SM with the gauge group  $SU(3)_c \times SU(2)_L \times U(1)_Y$ , three generations of quark and lepton doublets and singlets, and one scalar Higgs doublet, suggests that a deeper understanding of the origin of this structure might be possible: What is the origin of this particular gauge group or the number of three generations? What is the origin of the Higgs field, the Higgs potential and of electroweak symmetry breaking, and what sets the interactions of quarks and leptons with the Higgs field and ultimately the fermion masses?

Achieving progress on such questions requires the investigation of physics beyond the SM in an interplay of theory and experiment. Here the muon anomalous magnetic moment  $a_\mu$  plays a special role. Via quantum fluctuations,  $a_\mu$  could be influenced by any currently unknown BSM particles as long as these have direct or indirect interactions with muons.  $a_\mu$  is thus sensitive to a large set of hypothetical BSM scenarios, e.g. scenarios with extended scalar, fermion or gauge boson sectors which may be motivated by the open questions listed above. The new states may be light or heavy, strongly or weakly interacting, they may be similar to the known SM leptons, quarks or Higgs, or may have very different properties such as leptoquarks or dark matter particles.  $a_\mu$  can also test elaborate constructions such as supersymmetric models or extended non-abelian gauge groups. Importantly,  $a_\mu$  is complementary to high-energy experiments at colliders such as the LHC, where detector acceptances and SM backgrounds are relevant, and to many lower-energy observables which correspond to symmetry violations such as charge-parity (CP) violating or flavour-violating observables.

In this Section 1.1 we give an extended motivation and an overview of the field. We briefly describe the current status and provide the experimental and SM numbers. We highlight the distinctive properties of  $a_\mu$  as a probe of fundamental interactions and constraint on new physics and describe the important role of chirality flips. A table at the end of Sec. 1.1 also collects useful generic formulas and illustrative model-specific results for BSM contributions to  $a_\mu$ . This section also describes the content of the review in more detail, including forward references to later sections.

### 1.1.1. Status of $a_\mu$ and current values

The anomalous magnetic moment of the muon  $a_\mu$  can be measured via the spin precession of the muon in a homogeneous, weak magnetic field, and computed in quantum field theory in terms of the one-particle irreducible muon–photon 3-point function. This definition is reviewed in Sec. 1.2, including a discussion of suppressed effects, e.g. from non-linearities or inhomogeneities in the  $B$ -field or radiation effects, which are neglected in the quantum field theoretical derivation.

Measurements of  $a_\mu$  have been carried out by experiments at CERN [17, 18], Brookhaven [19–22] and Fermilab [1, 23–25] using the same experimental principle. All results are in full agreement, and the final uncertainties are statistics dominated, leading to a very satisfactory experimental status. The recent final result of the Fermilab experiment, and the resulting world average experimental value are

$$a_\mu^{\text{FNAL,Run-1-6}} = 11\,659\,207.05(1.48) \times 10^{-10}, \quad (1.1)$$

$$a_\mu^{\text{Exp}} = 11\,659\,207.15(1.45) \times 10^{-10}. \quad (1.2)$$

In Sec. 1.3 we provide further details on the experimental method and the results of the individual measurements.

In parallel to the experimental progress, the SM theory prediction has continuously been scrutinised. It can essentially be divided into four contributions, from QED alone, from the hadronic vacuum polarisation (HVP), from hadronic light-by-light scattering (HLbL), and from the weak interactions and all remaining SM particles. The individual definitions and values are given in Sec. 1.4. Already the precision of the Brookhaven measurement required the evaluation of all these SM contributions, and in preparation of the Fermilab experiment, a worldwide theory initiative was formed to obtain the best possible SM evaluation based on a coordinated, conservative and inclusive community effort. The theory initiative has published two extensive White Papers [2, 3], with the results

$$a_\mu^{\text{SM,WP2020}} = 11\,659\,181.0(4.3) \times 10^{-10}, \quad (1.3)$$

$$a_\mu^{\text{SM,WP2025}} = 11\,659\,203.3(6.2) \times 10^{-10}. \quad (1.4)$$

The result from the year 2020 is based on original references on QED [26, 27], electroweak [28, 29], HVP [30–36] and HLbL contributions [11, 37–50]. The 2020 SM prediction deviates substantially from the experimental result. At the time of the Fermilab Run-1 publication [23] the significance was  $4.2\sigma$ , leading to great enthusiasm in the community and many attempts to explain the deviation in terms of BSM physics.

The SM prediction from 2025 is based on the following original references for QED [26, 51–56], electroweak [28, 29, 57, 58], HVP [35, 36, 59–76], and HLbL contributions [38–40, 42, 49, 50, 57, 77–99]. Its value is now very close to the experimental result and in full agreement within uncertainties.

Sec. 1.4 will explain this change in more detail; in brief, crucial new results have appeared for the HVP contributions. The HVP contributions are non-perturbative, and two possible evaluation strategies are based on dispersion relations, the optical theorem and experimental low-energy hadronic data on the one hand, and on lattice gauge theory on the other hand. In recent years there was tremendous progress on lattice calculations. A first milestone was the result of the BMW collaboration [61], which was then confirmed by a number of further lattice results using a multitude of different approaches. In contrast, the dispersive analysis relies on measurements of  $e^+e^- \rightarrow$  hadrons at low energies. Different available data sets used to be in sufficient, though not perfect agreement. Now the recent CMD3 measurement of  $e^+e^- \rightarrow$  hadrons [100, 101] is in stronger tension with previous  $e^+e^-$  data. At present no concrete reason has been identified to dismiss any of the  $e^+e^-$  data sets [3] and the origin of the disagreements is unknown. The current tensions therefore do

not allow a meaningful dispersive evaluation of the HVP contributions. Hence, Ref. [3] evaluates the LO HVP correction based on lattice calculations only, which are, however, internally very consistent.

After these recent developments, the deviation between the experimental world average and the SM prediction is [3] (all numbers are rounded appropriately to the level of  $10^{-11}$ )

$$\Delta a_\mu^{\text{Exp-WP2025}} = 3.8(6.3) \times 10^{-10}, \quad (1.5)$$

where the uncertainties are summed in quadrature. This corresponds to full agreement and shows no sign for physics beyond the SM. Nevertheless, it corresponds to an important constraint on BSM scenarios. The current result in Eq. (1.5) will be the basis of the phenomenological discussions in the present review. In order to understand the development of the field over the past years it is useful to also record the discrepancy between the experimental result (1.2) and the SM prediction based on the first White Paper Eq. (1.3),

$$\Delta a_\mu^{\text{Exp-WP2020}} = 26.2(4.5) \times 10^{-10}, \quad (1.6)$$

which would correspond to a  $> 5\sigma$  deviation.

Given the rapid progress and intense effort of the community, further progress on the HVP contributions can be expected [3, 102, 103]. The result of such progress is unknown at present, but we can highlight the following logical possibilities from the point of view of BSM interpretations:

- The agreement (1.5) is consolidated and sharpened with smaller uncertainty. In this case, BSM contributions will be allowed to be zero, positive, or negative, but their magnitude must be sufficiently small.
- The central value of  $\Delta a_\mu$  remains compatible with the  $1\sigma$  band of Eq. (1.5) and thus much smaller than the previous deviation  $\Delta a_\mu^{\text{Exp-WP2020}}$ , but the uncertainty goes down such that an indication for non-zero BSM contributions re-emerges. In this case, BSM contributions will be constrained to be non-zero and positive, but of a smaller magnitude  $\lesssim 10 \times 10^{-10}$ .
- The central value of  $\Delta a_\mu$  increases towards a value similar to the value after the 2020 White Paper, as Eq. (1.6). In this case, there will be a strong indication for BSM contributions to  $a_\mu$ , which will be constrained to be positive and approximately of the order  $20 \times 10^{-10}$ .

In the present review we will also comment on the impact of such possible future developments. Mostly, however, we will explain the impact of the dramatically shifted result (1.5) on BSM physics. As a first result, we record here the  $2\sigma$  interval around the new result,

$$\Delta a_\mu(2\sigma) = [-8.8 \dots 16.5] \times 10^{-10}. \quad (1.7)$$

The interval (1.7) is now the allowed region for BSM contributions to  $a_\mu$ .

### 1.1.2. Sensitivity to fundamental interactions and generic BSM contributions

Magnetic dipole moments are some of the most precisely measured observables in physics and play a very important role in understanding elementary particles and how they interact. Their sensitivity to details of fundamental interactions becomes immediately apparent by comparing the gyromagnetic ratios  $g$  for the electron [104], the muon (Eq. (1.2)) and

the proton [104],

$$g_e^{\text{exp}} = 2.002\,319\,304\,361\,24\,(24), \quad (1.8a)$$

$$g_\mu^{\text{exp}} = 2.002\,331\,841\,43\,(29), \quad (1.8b)$$

$$g_p^{\text{exp}} = 5.585\,694\,689\,26\,(164). \quad (1.8c)$$

The electron  $g$ -factor is most precisely known. Its value is very close to 2, the value predicted by the Dirac equation, and the per-mille level deviation from the Dirac value is consistent with Schwinger’s calculation  $a_e = \alpha/2\pi$ . Section 3.2 will provide details on the relationships between the dipole moments of the muon and the electron, and further important leptonic dipole observables. As described there, the full value of  $g_e^{\text{exp}}$  is in good agreement with theory, confirming the electron as a fundamental elementary spin 1/2 particle of the SM.

From a low-energy and long-distance perspective, the proton seems no less elementary than the electron. Its  $g$ -factor, however, dramatically differs from the electron and from the Dirac values, establishing that the proton behaves fundamentally differently than the electron. In this way the  $g$ -factor, which corresponds to a long-distance/low-energy observable, directly reflects the fact that the proton actually is not elementary but a strongly interacting bound state.

For the muon, comparing the three  $g$ -factors immediately shows that the muon behaves fundamentally similarly to the electron, in line with the SM where the muon is the 2nd-generation sibling of the electron, with identical interactions except for the Yukawa interaction to the Higgs field and the resulting heavier muon mass. Eq. (1.8b) highlights several digits in boldface. At the 5th decimal place the muon and electron  $g$ -factors start to differ due to the higher muon mass providing higher energy for quantum fluctuations. The major difference results from two-loop diagrams with electron loops contributing to the muon versus muon loops contributing to the electron. At the 7th decimal place the muon  $g$ -factor is influenced by hadronic effects, i.e. by strongly interacting particles. At the 9th decimal place the muon  $g$ -factor is influenced by the weak interactions and the heaviest SM particles.

This discussion shows that the muon magnetic moment  $a_\mu$  at the current level of precision is sensitive to all elementary particles and interactions we know. The digits of the single number reflect our combined understanding of fundamental physics. Clearly, in the same way  $a_\mu$  can also be sensitive to possible BSM particles depending on their mass and their interactions.

In the present review, Sec. 2 describes the most important general ways how BSM particles can impact  $a_\mu$ . Starting from generic expressions for one-loop Feynman diagrams of renormalisable QFTs, it becomes apparent that different types of BSM scenarios can lead to very different contributions. If only two gauge multiplets enter the loop, the contributions have a very simple structure and are typically small and automatically in agreement with the new result in Eq. (1.5), though there are exceptions if BSM masses are very small. Often the sign of such contributions is fixed by the quantum numbers of the relevant gauge multiplets, and several tables in Sec. 2.2 list large classes of models of this kind, and their contributions to  $a_\mu$ .

If three or more gauge multiplets enter the loop, so-called chiral enhancements are possible. Corresponding BSM scenarios are often stringently constrained by Eq. (1.5). The characteristic model properties leading to chiral enhancements are discussed with the help of explicit simplified examples and the mass-insertion approximation in Sec. 2.3. An instructive qualitative account of the interplay between chirality, chirality flips, the Higgs mechanism and  $a_\mu$  will be given further below in Sec. 1.1.4.

A very useful approach both for qualitative discussions and for precision calculations is the one of effective field theories. These can provide systematic low-energy approximations for more fundamental theories involving heavy degrees

of freedom. Two particularly important effective field theories for  $a_\mu$  are LEFT and SMEFT, which extend QED/QCD or the full Standard Model by higher-dimensional operators, respectively. These theories, and the description of  $a_\mu$  within them, are explained in Sec. 2.4.

A later section 4 complements the one-loop discussions by describing typical and important higher-order contributions, both using Feynman diagrams and effective field theory arguments.

### 1.1.3. Key properties of $a_\mu$ and complementarities to other observables

Via quantum effects and loops,  $a_\mu$  is an inclusive probe of many candidate BSM scenarios. Unravelling the existence and the properties of potential new physics requires complementary experimental information from high-energy colliders such as LHC, from astrophysics and low-background measurements related e.g. to dark matter or neutrinos, and from low-energy observables such as flavour-violating rare decays and dipole moments.

The muon magnetic moment has a special role because it is sensitive to a large class of models and it combines several properties in a unique way:  $a_\mu$  is

- *flavour conserving,*
- *CP conserving,*
- *loop induced,*
- *chirality flipping.*

In contrast, many other low-energy precision observables are CP or flavour violating, and many high-energy collider observables at the LHC are not loop induced or not chirality flipping. The four properties are thus the reason why  $a_\mu$  is complementary to many other important observables and why  $a_\mu$  can help to disentangle the nature of BSM physics. Sec. 3 explores and discusses such complementarities in detail, but still in a model-independent way.

The last item in particular means that the QFT operator for  $a_\mu$  connects left-handed and right-handed muon fields, similar to the muon mass operator. Sec. 1.1.4 below will explain how this feature helps to obtain a qualitative and quantitative understanding of possible BSM contributions to  $a_\mu$ , and how investigating  $a_\mu$  may shed light on the origin of the muon mass. The relationship between  $a_\mu$  and the muon mass is then further explored in Sec. 3.1, where it becomes clear that BSM scenarios that change the way the muon receives its mass can be particularly strongly constrained by  $a_\mu$ . Also special cases are considered such as models with radiative muon mass generation and models with the maximum possible contributions to  $a_\mu$  compatible with perturbative unitarity.

$a_\mu$  has especially close relationships to other dipole observables, which share the chirality-flipping nature. Among these, the electron magnetic moment  $a_e$  is however less sensitive to heavy BSM contributions, the electric dipole moments  $d_\mu$  and  $d_e$  are CP-violating observables and hence only sensitive to BSM effects which violate CP, and the decay  $\mu \rightarrow e\gamma$  is only sensitive to BSM effects which violate lepton flavour. These relations are quantified in Sec. 3.2. Via chirality flips  $a_\mu$  is also related to the muon–Higgs interaction which itself is strongly related to the muon mass and which can be directly constrained at the LHC. The nature of this relation and the resulting constraints on models are discussed in Sec. 3.3. A difference is that  $a_\mu$  is loop-induced while the muon–Higgs coupling arises at tree level. This has specific implications for the strength of the correlation and the class of models with particularly large effects.

Clearly,  $a_\mu$  has only weak or no correlations with many important high-energy collider observables. This makes constraints on BSM from  $a_\mu$  complementary to the ones from direct BSM particle searches at LHC or high-precision measurements of electroweak interactions. It is instructive to discuss this complementarity in a model-independent way.

This is done in Secs. 3.4, 3.7 on a qualitative level and with the help of simplified models. In case of electroweak precision observables discussed in Sec. 3.4 there exists one interesting connection to  $a_\mu$  via the quantity  $\Delta\alpha$  and the hadronic vacuum polarisation, which enters both kinds of observables in an important way. Sec. 3.7 on the other hand focuses on the reach of direct collider searches for new particles and describes how this reach compares to constraints from  $a_\mu$  for different classes of models.

Some of the most pressing open questions of particle physics are related to the nature of neutrino masses and the nature of dark matter. Perhaps surprisingly,  $a_\mu$  has a stronger impact on many candidate explanations of dark matter often more straightforwardly than on many neutrino mass generation models. There are, however, specific classes of neutrino mass models which potentially lead to significant contributions to  $a_\mu$  and which therefore are constrained by  $a_\mu$ . These connections are explained in Secs. 3.6 and 3.5.

#### 1.1.4. Structure of BSM contributions and the role of chirality flips and electroweak gauge invariance

Here we begin discussing quantitatively how BSM physics can contribute to  $a_\mu$ . As a preview, the very simplest type of one-loop BSM contributions take the generic form

$$\Delta a_\mu \sim \frac{|c|^2}{16\pi^2} \frac{m_\mu^2}{M^2}. \quad (1.9)$$

The first factor involves a generic BSM coupling  $c$  and a one-loop suppression. The second factor provides a squared mass suppression by the ratio of the muon and the heavier BSM masses  $m_\mu, M$ . The symbol  $\sim$  denotes equality up to order-one factors. The sign can be positive or negative but is often fixed for a given model with this type of contributions.

It turns out that the need for chirality flips mentioned above in subsection 1.1.3 is of pivotal importance for the BSM phenomenology of  $a_\mu$  [4, 7, 105]. Accordingly, in some BSM scenarios there can be so-called *chiral enhancements*, leading to modified formulas such as

$$\Delta a_\mu \sim R_\chi \times \frac{c_L c_R}{16\pi^2} \frac{m_\mu^2}{M^2}, \quad (1.10)$$

where  $R_\chi$  represents a dimensionless chiral enhancement factor, and the formula also highlights that two different kinds of coupling constants  $c_{L,R}$  are in general required to invoke chiral enhancements. Phenomenologically, in such scenarios the contributions to  $a_\mu$  can often be large and involve intricate parameter dependencies, leading to non-trivial constraints. In such contributions, often the sign of the product  $c_L c_R$ , and sometimes also of the factor  $R_\chi$ , can be positive or negative.

Here we explain how the basic structure of these or other model-specific formulas emerges and discuss the role of chirality flips. The discussion will make explicit a fundamental connection to the muon mass and later allow us to elucidate how different fundamental BSM mechanisms can contribute to  $a_\mu$ . It will also help us classify BSM scenarios and understand parameter dependences, as well as correlations to other observables.

First we note that massless fermions cannot have a non-vanishing anomalous magnetic dipole moment, i.e.  $a_\mu = 0$ , if  $m_\mu = 0$ . The reason is that the spin of massless particles reduces to helicity and cannot undergo the continuous spin precession as is needed and measured for an anomalous magnetic dipole moment. Hence, non-vanishing  $a_\mu$  requires non-vanishing  $m_\mu$ , establishing a deep link.

Next, on a more technical level, the operators describing the mass and the anomalous magnetic dipole moment of the

muon can be written as

$$\mathcal{L}_m = -m_\mu (\overline{\mu}_L \mu_R + \overline{\mu}_R \mu_L), \quad (1.11a)$$

$$\mathcal{L}_{a_\mu} = -a_\mu \frac{Qe}{4m_\mu} (\overline{\mu}_L \sigma^{\mu\nu} \mu_R + \overline{\mu}_R \sigma^{\mu\nu} \mu_L) F_{\mu\nu}. \quad (1.11b)$$

Here the spin-1/2 muon with charge  $Q$  is described by a Dirac spinor  $\mu = \mu_L + \mu_R$ , with chirality eigenstates  $\gamma_5 \mu_{L,R} = \mp \mu_{L,R}$  and  $F_{\mu\nu}$  denotes the photon field strength tensor. More details on the definition of  $a_\mu$  and such Lagrangians will be provided in Secs. 1.2 and 2.4.

These Lagrangians allow us to introduce the notions of *chirality flips*, *chiral transformations* and *chiral symmetry*. Interpreted as a Feynman rule, both the mass term and the  $a_\mu$ -term correspond to an incoming right-handed and outgoing left-handed muon  $\mu_R \rightarrow \mu_L$  or vice versa. This is called a chirality flip.

In general, a chiral transformation is a transformation where the left- and right-handed fields transform with opposite phases. Specifically for the muon, a chiral transformation reads

$$\mu_R \rightarrow e^{i\alpha} \mu_R \quad \mu_L \rightarrow e^{-i\alpha} \mu_L. \quad (1.12)$$

A theory is chirally symmetric if this transformation is a symmetry (possibly by assigning suitable transformation laws for other fields). Importantly, the mass term and the  $a_\mu$ -term in Eqs. (1.11a) and (1.11b) are never chirally symmetric.

The need for chirality flips and breaking of the chiral symmetry Eq. (1.12) has very important consequences especially in the SM and BSM scenarios defined at the weak scale or above. These theories must include electroweak interactions and respect the associated  $SU(2)_L \times U(1)_Y$  gauge invariance. In contrast to QED or QCD, in such theories no gauge invariant Dirac mass terms for leptons or quarks are possible. Specifically the left-handed muon  $\mu_L$  is part of an  $SU(2)_L$  doublet with hypercharge  $-1/2$  while the right-handed muon  $\mu_R$  is an  $SU(2)_L$  singlet with hypercharge  $-1$ . The only way to generate a muon mass in a theory with electroweak gauge invariance (SM or beyond) is to have *spontaneous electroweak symmetry breaking* (EWSB) and to couple the muon in a gauge invariant way to the corresponding vacuum expectation value ( $vev$ ). In the SM, the muon mass generated at tree-level can be written as

$$m_\mu^{\text{SM, tree}} = \frac{y_\mu v}{\sqrt{2}}. \quad (1.13)$$

Here  $y_\mu$  is the strength of the muon–Higgs Yukawa coupling, which acts as the breaking parameter of the muon-specific chiral symmetry, and  $v$  is the EWSB Higgs  $vev$ .

Analogously, any extension of the SM which has electroweak gauge invariance must have one or several vacuum expectation values responsible for EWSB. These may be expectation values of fundamental or of composite fields. The physical muon mass  $m_\mu$  will always be generated from (tree-level and/or loop-induced) couplings to these  $vevs$ . And any such theory must contain one or several parameters which break the relevant chiral symmetry Eq. (1.12).

As a result, any contribution to the physical muon mass in any such theory will involve the factors

$$\Delta m_\mu \sim \left[ \left( \text{chirality-flipping parameter(s)} \right) \times \left( \text{EWSB } vev \right) \right] \times (\text{other factors}). \quad (1.14)$$

This expresses that any contribution to  $m_\mu$  must be proportional to the combination of parameters responsible for chiral symmetry breaking and to the vacuum expectation values responsible for EWSB; Fig. 1.1 shows illustrative Feynman diagrams with different insertions of  $vevs$ . The “other factors” can involve any couplings of the theory in question which appear in appropriate Feynman diagrams and do not have to be related to EWSB or chiral symmetry breaking. They can also include numerical prefactors or dimensionless loop functions.

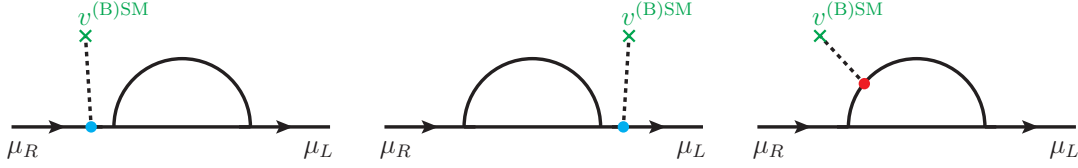


**Figure 1.1:** One-loop Feynman diagrams illustrating Eqs. (1.14,1.15) and the possibility of chiral enhancements. Each contribution to the muon mass and to  $a_\mu$  must involve one factor of some SM or BSM  $vev$   $v^{(B)SM}$  breaking electroweak symmetry, as well as a chirality flip between  $\mu_L$  and  $\mu_R$ . In order to obtain a contribution to  $a_\mu$ , a photon (not shown in the diagrams) needs to couple to any of the charged internal lines. In the first two diagrams, the chirality is flipped at the external line, producing an explicit factor  $m_\mu$  in the computation of the diagrams. In these two diagrams, the loop only couples to  $\mu_L$  or  $\mu_R$ , respectively. In the third diagram, the chirality is flipped via the loop, possibly via virtual BSM particles.

Exactly the same kind of discussion applies to  $a_\mu$  in view of the analogous structure of Eqs. (1.11a) and (1.11b). We can therefore write the generic relationship

$$\Delta a_\mu \sim m_\mu \times \left[ (\text{chirality-flipping parameter(s)}) \times (\text{EWSB } vev) \right] \times \frac{(\text{other factors})}{M^2} \quad (1.15)$$

for any contribution to  $a_\mu$  in any model with electroweak gauge invariance. The factors in the square bracket reflect the need for chirality flips and EWSB. Since the coefficient in the Lagrangian Eq. (1.11b) actually corresponds to  $a_\mu/m_\mu$ , solving for  $a_\mu$  produces the explicit factor  $m_\mu$  on the r.h.s. of Eq. (1.15). The denominator  $M^2$  represents a typical mass scale of the theory and must appear for dimensional reasons. The “other factors” have the same properties as the ones in Eq. (1.14). We note that the separation into these factors is not necessarily unique but always possible, as will also be apparent from results in concrete models discussed later.

The formulas in Eqs. (1.14) and (1.15) demonstrate the deep relationship between the muon mass and  $a_\mu$  and lead to the notion of models with or without chiral enhancements as indicated at the beginning of this subsection in Eqs. (1.9) and (1.10). In the SM, the factors in the square brackets of these formulas simply amount to the product of the SM Yukawa coupling and Higgs  $vev$ , i.e. to the muon mass,  $[\dots] \rightarrow m_\mu$ . There is a class of BSM scenarios where the same is true, e.g. the ones illustrated by the first two Feynman diagrams in Fig. 1.1 where the chirality is flipped at the external muon line, necessarily producing the factor  $m_\mu$ . Such contributions have the straightforward behaviour of Eq. (1.9).

In another class of BSM scenarios, however, the factors in the square brackets can be very different and potentially larger. This is illustrated by the third diagram in Fig. 1.1 where the  $vev$  is inserted at an internal line possibly corresponding to a BSM particle. The new couplings relevant for chirality flips might be generalised Yukawa couplings to  $vevs$  from extended Higgs sectors; they can also correspond to a suitable product of couplings which break chiral symmetry in combination. With such new sources of symmetry breakings, it can happen that some terms in the square brackets in Eqs. (1.14) and (1.15) are enhanced,  $[\dots] \gg m_\mu$ . This is the case for the chiral enhancement exemplified in Eq. (1.10). In this case it is always possible to define a characteristic quantity  $R_\chi \gg 1$  which is given by enhancement factors appearing in  $[\dots]$  divided by the muon mass. For example the  $vev$  insertion in the third diagram in Fig. 1.1 could come from the Yukawa coupling to a heavier fermion in the loop with mass  $m_F$ , in which case one can get an enhancement factor  $R_\chi = \frac{m_F}{m_\mu} = \frac{y_F}{y_\mu}$ . The enhanced diagram in Fig. 1.1 also illustrates that two different couplings  $c_{L,R}$  to left- and right-handed muon are typically required, such that the generic formula (1.10) becomes valid.

<b>Generic one-loop results</b>	
(a) <i>without</i> chiral enhancement, discussed in Secs. 2.1 and 2.2	$\Delta a_\mu \sim \pm \frac{ c ^2}{64\pi^2} \frac{m_\mu^2}{M^2} \qquad \approx \pm 1.8 \times 10^{-9}  c ^2 \left( \frac{100 \text{ GeV}}{M} \right)^2$
(b) <i>with</i> chiral enhancement, discussed in Secs. 2.3 and 3.7	$\Delta a_\mu \sim \pm R_\chi \times \frac{c_L c_R}{16\pi^2} \frac{m_\mu^2}{M^2} \qquad \approx \pm 6.7 \times 10^{-8} c_L c_R \frac{R_\chi}{100} \left( \frac{1 \text{ TeV}}{M} \right)^2$
(c) radiative muon mass generation ( $m_\mu = \Delta m_\mu$ ). See Eq. (3.4) in Sec. 3.1	$\Delta a_\mu \sim \pm \frac{16\pi^2 \Delta m_\mu}{\lambda_L \lambda_R m_\mu} \times \frac{\lambda_L \lambda_R}{16\pi^2} \frac{m_\mu^2}{M^2} = \pm \frac{m_\mu^2}{M^2} \qquad \approx \pm 2 \times 10^{-9} \left( \frac{2.4 \text{ TeV}}{M} \right)^2$
(d) maximal contribution compatible with perturbativity: $R_\chi, c_i \sim \sqrt{8\pi}$ . See Eq. (3.15)	$\Delta a_\mu \sim \pm \frac{\sqrt{8\pi} v}{m_\mu} \times \frac{1}{2\pi} \frac{m_\mu^2}{M^2} \qquad \approx \pm 2 \times 10^{-9} \left( \frac{100 \text{ TeV}}{M} \right)^2$
<b>Model-specific results</b>	
(e) <u>Supersymmetry</u> : WHL one-loop contribution. See Eq. (5.44a) in Sec. 5.2.2	$\Delta a_\mu \approx \tan \beta \times \frac{5g_2^2}{192\pi^2} \frac{m_t^2}{M^2} \qquad \approx +2.1 \times 10^{-9} \frac{\tan \beta}{40} \left( \frac{500 \text{ GeV}}{M} \right)^2$
(f) <u>2HDM</u> : two-loop Barr-Zee contribution. See Eqs. (5.89) and (5.90) in Sec. 5.3	$\Delta a_\mu \approx -\zeta_t \zeta_u \frac{m_t^2}{v^2} \times \frac{N_c Q_t^2 \alpha}{8\pi^3} \frac{m_\mu^2}{M^2} (\mathcal{F}_1 - \mathcal{F}_2) \qquad \approx -7 \times 10^{-10} \frac{\zeta_t \zeta_u}{100} \left( \frac{1 \text{ TeV}}{M} \right)^2$
(g) <u>Leptoquarks</u> : $S_1$ + top one-loop contribution. See Eqs. (5.98) and (5.101) in Sec. 5.4	$\Delta a_\mu \approx \frac{m_t}{m_\mu} \times \frac{N_c \lambda_L^{32} \lambda_R^{32}}{16\pi^2} \frac{m_\mu^2}{M^2} \mathcal{F}^{\text{FS}} \qquad \approx +3.3 \times 10^{-9} \frac{\lambda_L^{32} \lambda_R^{32}}{0.01} \left( \frac{2 \text{ TeV}}{M} \right)^2$
(h) <u>Vector-like leptons</u> : $L \oplus E$ one-loop contribution. See Eq. (5.126) in Sec. 5.5	$\Delta a_\mu \approx -\frac{\bar{\lambda}_\Phi v}{m_\mu} \times \frac{\lambda_L \lambda_R}{16\pi^2} \frac{m_\mu^2}{M^2} \qquad \approx -4 \times 10^{-10} \frac{\lambda_L \lambda_R \bar{\lambda}_\Phi}{0.01} \left( \frac{2 \text{ TeV}}{M} \right)^2$

**Table 1.1:** A collection of BSM contributions to  $\Delta a_\mu$  in different scenarios. The first column shows approximate analytical formulas and the second the corresponding seminumerical approximation. As indicated by the  $\sim$  symbol, the generic results are given up to  $\mathcal{O}(1)$  factors depending e.g. on the  $SU(2)_L$  representations and electric charges, while the model-specific formulas are approximations to the full results explained in the indicated sections. The first factors on the left of the  $\times$  symbols correspond to the chiral enhancement factors in the form of Eq. (1.10) and discussed in Sec. 1.1.4, see also Sec. 3.7. In case of the leptoquark and 2HDM we have suppressed the arguments of the loop-functions and neglected the resulting  $\ln(M)$  dependence in the seminumerical results. In case of the radiative muon mass model, the chiral enhancement corresponds to an inverse one-loop expression.

### 1.1.5. Overview of BSM scenarios

As explained above, the chirality-flipping interactions have a key influence on the behaviour of BSM contributions to  $a_\mu$ . The instructive relations Eqs. (1.14) and (1.15) for  $m_\mu$  and  $a_\mu$  highlight the relevance of factors related to EWSB and to chirality flips. This insight allows for a straightforward understanding of how different models can contribute to  $a_\mu$ , including a distinction between models with or without chiral enhancements.

In the following we give a brief overview of important types of contributions and important models. Table 1.1 summarises corresponding analytical and numerical results for contributions to  $a_\mu$  in a selection of relevant models and generic model classes. First, there are many models without chiral enhancement, where EW and chiral symmetry are broken by the SM Higgs  $vev$  and the SM Yukawa coupling. Examples include the SM itself, as well as many BSM scenarios such as dark photon, dark  $Z$ , more general *dark matter* (DM) and dark sector models, and also several leptoquark models. Generally, models where the new states can couple either only to the left-handed muon or only to the right-handed muon cannot lead to chiral enhancement. The contributions of such models to  $a_\mu$  have a simple structure and depend on the involved couplings and masses. As shown in the table, they can only lead to significant contributions to  $a_\mu$  if the masses are smaller than around 100 GeV and/or couplings are very large. This is essentially only viable if the models have very weak or no interactions at colliders, i.e. with electrons, photons, or quarks. Hence models with DM candidates or a larger dark sector with light particles can often lead to potentially visible effects in  $a_\mu$ ; conversely such models can be strongly constrained by  $a_\mu$ . This will be explored in Sec. 5.1.

There are also many well-motivated models with chiral enhancement. The reason is that fundamental questions related to the Higgs sector and electroweak symmetry breaking or to the origin of flavour and the three generations motivate the study of modified Higgs sectors and extended fermion or Yukawa sectors — these often contain new sources of breaking of the chiral symmetry in Eq. (1.12). Such models can lead to modifications of the factors in square brackets in Eq. (1.15), i.e. potentially to chiral enhancements. Similarly, models with the goal to explain the origin of neutrino masses often include new fields which as a by-product also contribute to the muon mass and thereby also to  $a_\mu$ . Many such models can potentially lead to large contributions to  $a_\mu$ , and their parameter space can be significantly constrained by  $a_\mu$ .

Table 1.1 shows several well-known examples. *Supersymmetry* (SUSY) is one of the best motivated and most studied ideas for BSM physics, and it has been known for a long time that the parameter  $\tan\beta$ , the ratio of two Higgs vacuum expectation values, can lead to a chiral enhancement which brings SUSY contributions into a very interesting ballpark for SUSY mass ranges which are motivated for other reasons. SUSY also provides very promising potential explanations of dark matter. The current LHC and dark matter limits together with  $a_\mu$  constrain the SUSY parameter space in a complementary way. This will be discussed in detail in Sec. 5.2, focusing both on constrained scenarios motivated by GUT- or Planck-scale assumptions and on phenomenological SUSY with different ways to accommodate dark matter.

The *Two-Higgs doublet model* (2HDM) is one of the simplest extensions of the Higgs sector, but its leading contributions to  $a_\mu$  arise in a rather complicated way on the two-loop level from so-called Barr-Zee diagrams where a second Higgs state connects the muon to a loop of e.g. the top quark. Such contributions are chirally enhanced if the additional Higgs field has enhanced Yukawa couplings to the muon. However, there is a multitude of constraints from collider, leptonic and quark flavour observables on the new Yukawa couplings and Higgs masses. Depending on the type and flavour structure of the 2HDM, these constraints complement constraints from  $a_\mu$  in different ways. This interplay and resulting viable 2HDM scenarios are discussed in Sec. 5.3.

The existence of *leptoquarks* (LQ), i.e. spin-0 or spin-1 particles which directly connect leptons and quarks, can be

motivated e.g. by attempts to unify quarks and leptons. Specific versions of leptoquarks allow gauge invariant couplings both to the left- and the right-handed muon and the left- and right-handed top quark. Such models lead to a strong chiral enhancement where e.g. the top- or charm-quark mass governs the chirality flip instead of the muon mass. Even though there are strong lower mass limits on leptoquarks from the LHC, such leptoquarks can very significantly contribute to  $a_\mu$  as well as to many quark flavour and lepton flavour observables. This is discussed in Sec. 5.4.

The SM contains three generations of chiral quarks and leptons, and it is known that no fourth chiral generation can exist. However, additional vector-like leptons or quarks with TeV-scale masses are possible. Specifically *vector-like leptons* (VLL) can contribute to the muon mass not only via loop corrections but also through mixing already at tree level in a way similar to the seesaw mechanism for neutrino masses. Because of this difference in loop order, the relationships between  $a_\mu$ , the muon mass, and in particular also the muon–Higgs coupling are of special interest in this class of models. In addition collider and electroweak observables also yield important complementary constraints. In Sec. 5.5 we discuss how the combination of these observables can significantly constrain such VLL models and we also characterise the remaining viable regions in parameter space.

Another open question, not addressed by the SM, is the origin of the *neutrino masses*. These tiny but non-zero masses were thoroughly established with the discovery of neutrino oscillation, but so far none of the proposed explanations could be confirmed experimentally. The close connection between neutrinos and charged leptons via the electroweak symmetry might suggest that the answer could also have a profound impact on the charged lepton sector. The simplest possible solutions discussed in Sec. 3.5 typically require extremely heavy new particles or very weak coupling, such that  $a_\mu$  remains mostly unaffected. However, there are nonetheless many models that simultaneously explain the tiny neutrino masses while also resulting in a significant contribution on  $a_\mu$ . A wide range of such models will be discussed in detail in Sec. 5.6

Table 1.1 also includes several special model-independent cases of chirally enhanced contributions. First it is possible that the tree-level muon mass vanishes and the muon mass is instead radiatively generated by BSM loop effects. In terms of Eqs. (1.14) and (1.15) this means that the chiral enhancement must be large enough to compensate all loop suppression factors such that  $\Delta m_\mu = m_\mu$  and  $\Delta a_\mu \sim m_\mu^2/M^2$ . This is possible in a variety of SUSY and non-SUSY scenarios. Models with radiative muon mass generation lead to  $\Delta a_\mu \sim 10^{-9}$  for a relevant mass scale of around 3 TeV.

Finally, the maximum possible chiral enhancement from one-loop diagrams where all appearing couplings are as large as allowed by perturbative unitarity and the relevant *vev* is the full SM *vev*. In such a case  $\Delta a_\mu \sim 10^{-9}$  can be obtained even for a mass scale of order 100 TeV. Conversely speaking, the scale of 100 TeV is the heaviest mass scale that can be constrained by  $a_\mu$  in perturbative models.

## 1.2. Definition of $a_\mu$

Like mass and charge, the magnetic dipole moment is an intrinsic property of the muon that influences its motion in the presence of an external classical electromagnetic field  $A_\mu^{\text{ext}}(x)$ . Writing the magnitude of the magnetic moment  $\boldsymbol{\mu}$  in terms of the spin  $\boldsymbol{s}$  and the total charge  $q$  as

$$|\boldsymbol{\mu}| = g_\mu \frac{q}{2m_\mu} |\boldsymbol{s}|, \quad (1.16)$$

the gyromagnetic ratio  $g_\mu$  and the anomalous magnetic moment  $a_\mu = (g_\mu - 2)/2$  is defined. Interestingly, the value of  $a_\mu$  always vanishes at tree level and is a prediction arising from quantum effects in any renormalisable quantum field theory. The derivation of  $a_\mu$  from first principles within QFT has been pioneered by Schwinger [16] and can be found in many

textbooks and reviews. We reproduce it here, particularly highlighting and quantifying several of the approximations that are made in the process. For an alternative definition in the context of axiomatic QFT, see Ref. [106].

The physical situation relevant for the definition and measurement of  $a_\mu$  is in essence nonrelativistic. In its rest frame the muon only interacts with the external quasiclassical electromagnetic field, which is assumed to be weak compared to the intrinsic energy scale set by the muon rest mass. The available energy is not sufficient to create new particles. Here, photon radiation emitted off the accelerated charge is neglected, and the muon decay is neglected as well.

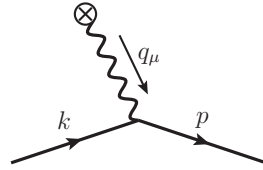
In QFT, this single-particle system in the presence of an external field can be described as follows. The muon is described by a 4-component Dirac spinor field  $\mu(x)$  and its interaction with the photon field is given by the renormalisable Lagrangian term

$$\mathcal{L} \supset -Qe\bar{\mu}A\mu, \quad (1.17)$$

which follows from gauge invariance. The quasiclassical external field  $A_\mu^{\text{ext}}$  can be introduced via a coherent quantum state under which the quantum field operator  $A_\mu$  develops the expectation value  $\langle A^\mu \rangle = A_\mu^{\text{ext}}$ . Then, computations in the presence of the coherent state are simply equal to computations after the variable shift  $A_\mu \rightarrow A_\mu + A_\mu^{\text{ext}}$  in the action [107, 108], see also Refs. [109, 110] for further progress. The variable shift effectively leads to an additional term in the interaction Lagrangian,

$$\mathcal{L} \supset -Qe\bar{\mu}A^{\text{ext}}\mu. \quad (1.18)$$

We assume the field is weak and can be treated perturbatively. Then the interaction with the external field is described by an additional Feynman given by



$$= -iQe\gamma^\mu \tilde{A}_\mu^{\text{ext}}(q) \quad (1.19)$$

where  $\tilde{A}_\mu^{\text{ext}}$  denotes the Fourier transform. For a discussion of the Furry picture, where the external field is resummed and incorporated in the unperturbed propagator, we refer to the recent Refs. [110, 111].

In this setup, the 2-point Green function  $G(x, y) = \langle T\mu(x)\bar{\mu}(y) \rangle^{(A_\mu^{\text{ext}})}$  computed in the presence of the additional Feynman rule of Eq. (1.19) thus describes the time-dependent motion of a fermion subject to the external field. In a perturbative treatment of the external field it is useful to also define  $G^{\text{amp}}$  as the amputated Green function obtained by dropping the trivial tree-level contribution and removing the external unperturbed propagators. Assuming time-independence of the external field and thus energy conservation, the Green function only depends on the 7 arguments  $\mathbf{x}$ ,  $\mathbf{y}$  and  $y^0 - x^0$ . It is useful to define its momentum-space version  $\tilde{G}^{\text{amp}}(\mathbf{p}, \mathbf{k}, k^0)$  as the 7-fold Fourier transformation where  $\mathbf{k}$  and  $\mathbf{p}$  are incoming and outgoing 3-momenta and  $k^0 = p^0$  is enforced by energy conservation.

To later match the QFT description to a single-particle quantum theory it is useful to also consider scattering of the muon off the external field. This is described by the amplitude of an in-state with definite 4-momentum  $k_\mu$  and polarisation  $s_\mu$  scattering into an out-state with four momentum  $p_\mu$  and polarisation  $s'_\mu$ , where  $(k, s) \neq (p, s')$ ,

$$\langle p, s' | k, s \rangle_{\text{in}} = -2\pi i \delta(k_0 - p_0) T_{ps'; ks}. \quad (1.20)$$

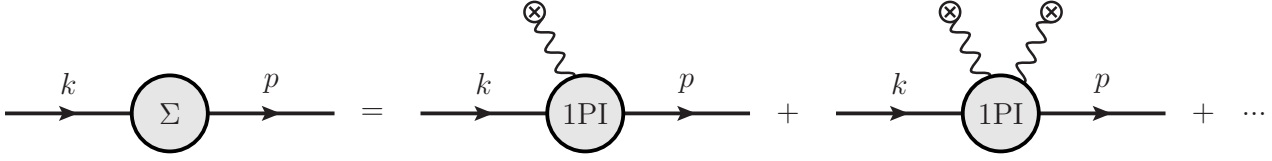


**Figure 1.2:** 1PI on-shell self-energy of the muon. The crosses correspond to insertions of the interaction vertex with the external field  $A_\mu^{\text{ext}}$ . Note that for off-shell momenta the r.h.s. would contain an additional 1PI term without insertions of the external field.

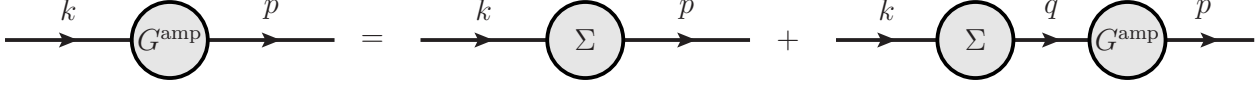


**Figure 1.3:** Dyson-Schwinger equation for the two-point Green function, corresponding to Eq. (1.26).

The T-matrix element  $T_{ps';ks}$  is also defined assuming energy conservation and is given by the LSZ formula<sup>1</sup> in terms of the amputated two-point function introduced before,

$$-iT_{ps';ks} = \bar{u}(p, s') G^{\text{amp}}(\mathbf{p}, \mathbf{k}, k^0) u(k, s). \quad (1.21)$$

As mentioned above, if the external field is strong, the Furry picture provides a more appropriate starting point. In that context, the recent Refs. [110–112] have also considered the situation where infrared real radiation is relevant.

Generally, we use Dirac spinors  $u(k, s)$  describing a free muon with on-shell momentum  $k$  and polarisation  $s$  satisfying the conditions

$$(\not{k} - m)u(k, s) = 0, \quad \text{and} \quad \gamma^5 \not{s} u(k, s) = u(k, s) \quad (1.22)$$

where the 4-vectors fulfil  $k^2 = m_\mu^2$ ,  $s^2 = -1$  and  $k \cdot s = 0$ . Similarly, the negative frequency solution  $v(k, s)$  obeying  $(\not{k} + m)v(k, s) = 0$  is also an eigenspinor of the helicity operator fulfilling  $\gamma^5 \not{s} v(k, s) = -v(k, s)$ . Explicitly, the Dirac spinors are given by [113–116]

$$u(k, s) = \frac{\not{k} + m}{\sqrt{2(k_0 + m)}} \begin{pmatrix} \xi(s) \\ \xi(s) \end{pmatrix}, \quad v(k, s) = \frac{\not{k} - m}{\sqrt{2(k_0 + m)}} \begin{pmatrix} -\xi(-s) \\ \xi(-s) \end{pmatrix}, \quad (1.23)$$

in terms of 2-spinors  $\xi$ , which allows to derive the following projection operators

$$u(k, s)\bar{u}(k, s) = \frac{1}{2}(\not{k} + m)(\mathbb{1} + \gamma^5 \not{s}) \quad (1.24)$$

$$v(k, s)\bar{v}(k, s) = \frac{1}{2}(\not{k} - m)(\mathbb{1} + \gamma^5 \not{s}). \quad (1.25)$$

From now on we assume a fixed polarisation axis, such that there are only two discrete possible values  $\pm s$  for the polarisation vector; a corresponding completeness relation is  $\sum_s u(k, s)\bar{u}(k, s) = \not{k} + m$ .

<sup>1</sup>For simplicity, here we assume on-shell renormalisation such that the LSZ factor  $\mathcal{Z} = 1$ .

As pioneered by Schwinger, the Green function  $G^{\text{amp}}(\mathbf{p}, \mathbf{k}, k_0)$  and the T-matrix element  $T_{ps';ks}$  allow to read off the value of the gyromagnetic ratio  $g_\mu$  [16]. In order to proceed it is useful to derive a Dyson-Schwinger like equation adapted to the non-relativistic situation. Introducing the self-energy  $\Sigma(\mathbf{p}, \mathbf{k}; k_0)$  as the sum of the one-particle irreducible (1PI) diagrams in the presence of the external field (see Fig. 1.2) allows us to write down the Dyson-Schwinger equation for  $G^{\text{amp}}$  described e.g. in the review Ref. [117] and illustrated in Fig. 1.3,

$$G^{\text{amp}}(\mathbf{p}, \mathbf{k}; k_0) = i\Sigma(\mathbf{p}, \mathbf{k}; k_0) + \int \frac{d^4q}{(2\pi)^4} (2\pi)\delta(k_0 - q_0) i\Sigma(\mathbf{p}, \mathbf{q}; q_0) \frac{i}{\not{q} - m_\mu + i\epsilon} G^{\text{amp}}(\mathbf{q}, \mathbf{k}; k_0). \quad (1.26)$$

After rewriting the tree-level fermion propagator in terms of positive-time and negative-time contributions we arrive at

$$G^{\text{amp}}(\mathbf{p}, \mathbf{k}; p_0) = i\Sigma(\mathbf{p}, \mathbf{k}; p_0) - \sum_r \int \frac{d^3q}{(2\pi)^3 2\omega_q} \left\{ \Sigma(\mathbf{p}, \mathbf{q}; p_0) \frac{u(q, r)\bar{u}(q, r)}{p_0 - \omega_q + i\epsilon} G^{\text{amp}}(\mathbf{q}, \mathbf{k}; p_0) + \Sigma(\mathbf{p}, -\mathbf{q}; p_0) \frac{v(q, r)\bar{v}(q, r)}{p_0 + \omega_q - i\epsilon} G^{\text{amp}}(-\mathbf{q}, \mathbf{k}; p_0) \right\}, \quad (1.27)$$

where  $\omega_q = \sqrt{\mathbf{q}^2 + m_\mu^2}$  corresponds to the relativistic energy-momentum relation. The first term in the brackets corresponds to the exchange of a forward propagating muon and the second to a backward propagating anti-muon.

At this point the non-relativistic limit can be used. In this limit, the energies  $p_0 = k_0$  and  $\omega_q$  are approximately equal to the rest mass  $m_\mu$ . Hence the forward propagator is unsuppressed while the denominator of the backward propagator leads to a relative  $1/m_\mu$  suppression. Up to  $1/m_\mu$  corrections, this backward propagator term can be neglected.

The Dyson-Schwinger equation for the Green function implies a similar equation for the T-matrix element. Defining  $T_{ps';ks}^{\text{1PI}} \equiv -\bar{u}(p, s')\Sigma(\mathbf{p}, \mathbf{k}; p_0)u(k, s)$  for the 1PI part we can write the following iterative integral equation,

$$T_{ps';ks} = T_{ps';ks}^{\text{1PI}} + \sum_r \int \frac{d^3q}{(2\pi)^3 2\omega_q} \frac{T_{ps';qr}^{\text{1PI}} T_{qr;ks}}{k_0 - \omega_q + i\epsilon}. \quad (1.28)$$

This represents an approximate equation that includes the interaction with the external fields to all orders, but where  $1/m_\mu$ -suppressed terms were neglected.<sup>2</sup>

This integral equation provides a starting point to match the full QFT description to the one of non-relativistic single-particle quantum mechanics, which then allows to extract the effective value of the magnetic moment. There, the muon is described by a 2-spinor wave function  $\psi(t, \mathbf{x}; \mathbf{s}) = \langle t, \mathbf{x}; \mathbf{s} | \psi \rangle$  whose time-dependence is governed by the Schrödinger equation

$$i \frac{\partial}{\partial t} \psi(t, \mathbf{x}; \mathbf{s}) = H(\mathbf{x}) \psi(t, \mathbf{x}; \mathbf{s}). \quad (1.29)$$

Here  $\mathbf{s}$  denotes the polarisation 3-vector and the Hamiltonian  $H$  is constrained by gauge invariance and takes the general form

$$H = \frac{1}{2m_\mu} [\hat{\mathbf{p}} - q\mathbf{A}^{\text{ext}}]^2 + q\phi^{\text{ext}} - \boldsymbol{\mu} \cdot \mathbf{B} - \mathbf{d} \cdot \mathbf{E} + H_{\text{eff}}. \quad (1.30)$$

Here  $\phi^{\text{ext}}$  and  $\mathbf{A}^{\text{ext}}$  are the same external fields as in the QFT description, and  $\mathbf{B}$ ,  $\mathbf{E}$  are the corresponding physical magnetic and electric fields. The first term of the Hamiltonian gives the Pauli kinetic term and the coefficients  $\boldsymbol{\mu}$  and  $\mathbf{d}$  of the second and third term by definition correspond to the magnetic and electric dipole moments, respectively. These dipole coefficients  $\boldsymbol{\mu}$  and  $\mathbf{d}$  are of the order  $1/m_\mu$ . The last term  $H_{\text{eff}}$  represents an infinite tower of additional effective

<sup>2</sup>The equation would become exact if the 1PI self energy were replaced by a redefined self energy that is 1-particle irreducible only with respect to the forward propagator  $\sim \frac{1}{p_0 - \omega_q + i\epsilon}$ .

	S.I.	natural units	Ratios	numerical value
$m_\mu$	0.113 u	0.105 GeV	$\gamma\tau_\mu\omega_c$	2700
$\Gamma_\mu$	$4.55 \times 10^5$ Hz	$3 \times 10^{-19}$ GeV	$v \approx R_0\omega_c$	0.9994
$B_0$	1.45 T	$2.68 \times 10^{-15}$ GeV <sup>2</sup>	$\frac{B_0}{m_\mu^2}$	$2.54 \times 10^{-14}$
$R_0$	7.112 m	$3.6 \times 10^{16}$ GeV <sup>-1</sup>	$\frac{\Gamma_\mu}{m_\mu}$	$2.84 \times 10^{-18}$
$\frac{1}{R_0} \partial_\phi B_0 _{\max}$	$100 \frac{\text{ppm}}{\text{deg}} \times \frac{B_0}{R_0}$	$4 \times 10^{-34}$ GeV <sup>3</sup>	$\frac{\partial_\phi B_0}{R_0 m_\mu^3}$	$4 \times 10^{-31}$
$\omega_c = \frac{eB_0}{\gamma m_\mu}$	$4.21 \times 10^7$ Hz	$2.77 \times 10^{-17}$ GeV	$\Delta_{\text{synch}} = \frac{4\pi\alpha\gamma^4}{3R_0 m_\mu \gamma}$	$2 \times 10^{-13}$
$\omega_a = a_\mu \frac{eB_0}{m_\mu}$	$1.44 \times 10^6$ Hz	$9.47 \times 10^{-19}$ GeV		

**Table 1.2:** Magnitude of quantities relevant to  $a_\mu$  and neglected contributions in the derivation. The left table contains dimensionful quantities in S.I. and natural units, the right table contains dimensionless combinations. Here  $\Gamma_\mu$  is the muon width,  $B_0$  and  $R_0$  are the magnetic field and the radius of the ring used in the Fermilab experiment,  $\omega_{c,a}$  are the frequencies for the circular motion and the spin precession relative to the motion. The “magic”  $\gamma$  used for the muons is  $\gamma = 29.3$ .  $\Delta_{\text{synch}}$  is the relative energy loss per turn caused by synchrotron radiation, and  $\frac{1}{R_0} \partial_\phi B_0|_{\max}$  corresponds to the maximum field inhomogeneity in azimuthal direction. See Refs. [118–120].

contributions suppressed by higher powers of  $1/m_\mu$ . These include e.g. higher-order derivatives and non-linear terms in the external fields.<sup>3</sup>

The single-particle quantum theory allows to describe the same scattering of the non-relativistic particle off the external field. In this approach, the full Hamiltonian Eq. (1.30) is split into  $H = H_0 + V$  with the free part  $H_0 = \frac{\hat{\mathbf{p}}^2}{2m_\mu}$  and the interaction potential  $V$ ; the scattering T-matrix element corresponding to Eq. (1.20) can be written as [126]

$$T_{ps';ks}^{\text{QM}} = {}^{\text{QM}}_0 \langle \mathbf{p}; \mathbf{s}' | V | \mathbf{k}; \mathbf{s} \rangle_{\text{in}}^{\text{QM}}, \quad (1.31)$$

which corresponds to a matrix element of  $V$  between an asymptotically free in-state and a free momentum eigenstate satisfying  $H_0 | \mathbf{p}; \mathbf{s} \rangle_0^{\text{QM}} = p_0 | \mathbf{p}; \mathbf{s} \rangle_0^{\text{QM}}$  (with the non-relativistic dispersion relation  $p_0 = \frac{\mathbf{p}^2}{2m_\mu}$ ), and the normalisation  $\langle t, \mathbf{x}; \mathbf{s}' | \mathbf{p}; \mathbf{s} \rangle_0^{\text{QM}} = e^{-i(p_0 t - \mathbf{p}\mathbf{x})} \delta_{ss'} \xi(\mathbf{s})$ , where the 2-spinors  $\xi(\mathbf{s})$  are the same as those in Eq. (1.23) in the rest frame.

This T-matrix element fulfils the Lippmann-Schwinger equation

$$T_{ps';ks}^{\text{QM}} = V_{ps';ks} + \sum_r \int \frac{d^3 q}{(2\pi)^3} \frac{V_{ps';qr} T_{qr;ks}^{\text{QM}}}{k_0 - q_0 + i\epsilon}, \quad (1.32)$$

where  $V_{ps';ks} = {}^{\text{QM}}_0 \langle \mathbf{p}; \mathbf{s}' | V | \mathbf{k}; \mathbf{s} \rangle_0^{\text{QM}}$ . Obviously this Lippmann-Schwinger equation is an iterative integral equation of the same form as Eq. (1.28) which followed from the Dyson-Schwinger equation of the QFT Green function. Matching the QM and the QFT T-matrix elements thus yields the equation<sup>4</sup>

$$T_{ps';ks}^{\text{1PI}} = 2p_0 V_{ps';ks}. \quad (1.33)$$

To complete the matching, we are left with computing  $T_{ps';ks}^{\text{1PI}}$  and interpreting its result in terms of contributions to

<sup>3</sup>Sample terms in  $H_{\text{eff}}$  can be  $\frac{e}{m_f^2} (\partial \cdot \mathbf{E})$ ,  $\frac{e}{m_f^2} (\mathbf{p} - Qe\mathbf{A}^{\text{ext}}) \cdot (\mathbf{E} \times \boldsymbol{\sigma})$ , or  $\frac{e^2}{m_f^3} \mathbf{E}^2$  which are analogous to terms appearing in effective field theories such as NRQED or the leptonic equivalent of HQET [121–125], although these field theories are still different from the single-particle quantum theory described here.

<sup>4</sup>the factor of  $2p_0$  accounts for the relativistic normalisation of the QFT states

$V_{ps';ks}$ , which can be rewritten as  $\xi(\mathbf{s}')^\dagger \tilde{V}(\mathbf{p}, \mathbf{k}) \xi(\mathbf{s})$ , where the Fourier transform of the interaction potential is given by

$$\tilde{V}(\mathbf{p}, \mathbf{k}) = -\frac{q}{2m_\mu} \tilde{\mathbf{A}}(\mathbf{q}) \cdot \mathbf{P} + q\tilde{\phi}(\mathbf{q}) + i\boldsymbol{\mu} \cdot (\mathbf{q} \times \tilde{\mathbf{A}}(\mathbf{q})) - i\mathbf{d} \cdot \mathbf{q}\tilde{\phi}(\mathbf{q}) + \dots \quad (1.34)$$

Here  $\mathbf{q} = \mathbf{k} - \mathbf{p}$  and  $\mathbf{P} = \mathbf{k} + \mathbf{p}$ , and the dots denote terms of higher order in  $1/m_\mu$  that we neglect in the following.

As discussed above, the field relevant for the  $a_\mu$  experiments is weak. Hence only terms of first order in  $A_\mu^{\text{ext}}$  have to be taken into account in the computation of the self energy  $\Sigma$  and to  $T_{ps';ks}^{\text{1PI}}$ ; higher powers of the field would contribute to terms in  $H_{\text{eff}}$  suppressed by additional factors  $eA_\mu^{\text{ext}}/m_\mu$ .<sup>5</sup> Accordingly, in Fig. 1.2 only the first term on the r.h.s. is required. In this approximation the 1PI T-matrix element can be written as

$$\text{Diagram} \equiv -iQe\bar{u}(p, s')\Gamma^\mu(p, k)u(k, s) \times \tilde{A}_\mu^{\text{ext}}(q). \quad (1.35)$$

Equivalently, in this approximation we have the relationship  $\Sigma(\mathbf{p}, \mathbf{k}; p_0) = -Qe\Gamma^\mu(p, k)\tilde{A}_\mu^{\text{ext}}(q)$ . The computation of the vertex function  $\Gamma^\mu$  is now independent of the external field and can be done utilising ordinary Feynman rules in vacuum.

In general,  $\Gamma^\mu$  can be written in terms of the covariant decomposition

$$\Gamma^\mu(p, k) = \gamma^\mu \left[ A_1(q^2) + A_2(q^2)\gamma^5 \right] + \frac{P^\mu}{2m_\mu} \left[ A_3(q^2) + iA_4(q^2)\gamma^5 \right] + \frac{q^\mu}{2m_\mu} \left[ A_5(q^2) + A_6(q^2)\gamma^5 \right], \quad (1.36)$$

where  $q = p - k$  and  $P = p + k$  is defined also for the 4-momenta. Because the muon momenta are on-shell the prefactors  $A_i$  are Lorentz invariant and depend only on  $q^2$ . Furthermore, gauge invariance for the external field implies the Ward identity

$$q_\mu \cdot \bar{u}(p, s')\Gamma^\mu(p, k)u(k, s) = 0 \quad (1.37)$$

and requires  $A_5(q^2) = 0$  as well as  $q^2 A_6(q^2) = -(2m_\mu)^2 A_2(q^2)$ . The vertex function can therefore be written in terms of only four form factors

$$\Gamma^\mu(p, k) = \gamma^\mu A_1(q^2) + \left[ \gamma^\mu - \frac{2m_\mu}{q^2} q^\mu \right] \gamma^5 A_2(q^2) + \frac{P^\mu}{2m_\mu} \left[ A_3(q^2) + iA_4(q^2)\gamma^5 \right] \quad (1.38)$$

or, using the Gordon identities to rewrite the spinor products, equivalently as

$$\Gamma^\mu(p, k) = \gamma^\mu F_E(q^2) + \frac{i\sigma^{\mu\nu} q_\nu}{2m_\mu} \left[ F_M(q^2) - iF_D(q^2)\gamma^5 \right] + \left[ \gamma^\mu - \frac{2m_\mu}{q^2} q^\mu \right] \gamma^5 A_2(q^2), \quad (1.39)$$

where  $F_E = A_1 + A_3$ ,  $F_M = -A_3$  and  $F_D = A_4$ . Using the explicit results for the Dirac spinors Eq. (1.23) we can expand the vertex function in the non-relativistic limit. To first order in  $\mathbf{q}$  and  $\mathbf{P}$  this gives

$$\bar{u}(p, s')\Gamma^0(p, k)u(k, s) \approx \xi^\dagger(\mathbf{s}') \left\{ 2mF_E(0) + F_D(0)i\mathbf{q}\boldsymbol{\sigma} \right\} \xi(\mathbf{s}) \quad (1.40a)$$

$$\bar{u}(p, s')\Gamma^k(p, k)u(k, s) \approx \xi^\dagger(\mathbf{s}') \left\{ F_E(0) \left( \mathbf{P}^k - i\epsilon^{kij} \mathbf{q}_i \sigma_j \right) - F_M(0)i\epsilon^{kij} \mathbf{q}_i \sigma_j \right\} \xi(\mathbf{s}). \quad (1.40b)$$

<sup>5</sup>Note that the same would not be true for reducible diagrams, where higher powers of the external field can appear with the weaker suppression  $A_\mu^{\text{ext}}/(\not{q} - m_\mu)$ .

We may then insert this expansion together with  $\tilde{A}_\mu^{\text{ext}}(\mathbf{q}) = (2\pi)\delta(q_0)(\tilde{\phi}(\mathbf{q}), -\tilde{\mathbf{A}}(\mathbf{q}))$  into Eq. (1.35) after which Eq. (1.33) reduces to

$$\tilde{V}(\mathbf{p}, \mathbf{k}) \approx QeF_E(0)\left(\tilde{\phi}(\mathbf{q}) - \frac{1}{2m_\mu}\tilde{\mathbf{A}}(\mathbf{q}) \cdot \mathbf{P}\right) + i\frac{Qe}{2m_\mu}\left(F_E(0) + F_M(0)\right)\boldsymbol{\sigma} \cdot (\mathbf{q} \times \tilde{\mathbf{A}}(\mathbf{q})) + i\frac{Qe}{2m_\mu}F_D(0)\boldsymbol{\sigma} \cdot \mathbf{q}\tilde{\phi}(\mathbf{q}) \quad (1.41)$$

After comparing the coefficients with Eq. (1.34) we arrive at

$$q = F_E(0)Qe \quad (1.42a)$$

$$\boldsymbol{\mu} = 2\left(F_E(0) + F_M(0)\right)\frac{Qe}{2m_\mu}\frac{\boldsymbol{\sigma}}{2} \equiv g_\mu\frac{Qe}{2m_\mu}\frac{\boldsymbol{\sigma}}{2} \quad (1.42b)$$

$$\mathbf{d} = -2F_D(0)\frac{Qe}{2m_\mu}\frac{\boldsymbol{\sigma}}{2} \quad (1.42c)$$

If the electric charge is on-shell renormalised,  $F_E(0) = 1$ , and we obtain the usual simple expression for the anomalous magnetic moment as

$$a_\mu = \frac{g_\mu - 2}{2} = F_M(0). \quad (1.43)$$

This result provides the starting point for quantum field theoretical computations of  $a_\mu$ . We note that it also corresponds to the effective Lagrangian already announced in Eq. (1.11b) which was used to explain the importance of chirality flips in Sec. 1.1.4.

The derived effective single-particle Pauli quantum theory is appropriate to describe the setup of  $g - 2$  measurements both for the electron and the muon. In the latter case, the muon and its spin behave quasiclassically, and the time-dependence of the spin expectation value is described by the classical Bargmann-Michel-Telegdi equation [127]

$$\frac{d\mathbf{s}}{dt} = -\frac{Qe}{m_\mu}\left[\left(\frac{g_\mu}{2} + \frac{1 - \gamma}{\gamma}\right)\mathbf{B} - \frac{a_\mu\gamma}{1 + \gamma}(\mathbf{v} \cdot \mathbf{B})\mathbf{v} - \left(\frac{g_\mu}{2} - \frac{\gamma}{1 + \gamma}\right)\mathbf{v} \times \mathbf{E}\right] \times \mathbf{s} \quad (1.44)$$

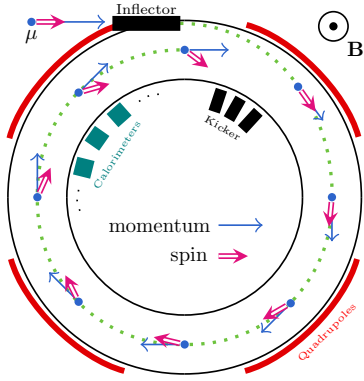
which can be derived starting from the quantum theory neglecting the  $1/m_\mu^2$ -suppressed terms as described in Ref. [128], §41.

As indicated at the beginning, the derivation has involved several approximations. Synchrotron radiation emitted by the accelerated muon and the muon decay were ignored in setting up a single-particle description, and terms with relative  $1/m_\mu$  suppression were neglected. As the derivation showed, the  $1/m_\mu$ -suppressed terms can correspond to inhomogeneities in the field  $\sim \boldsymbol{\partial} \cdot \mathbf{B}$ , higher orders in the field, or relativistic corrections to the energy-momentum relation. In Tab. 1.2 we collect a number of experimental quantities, converted into natural units and combined to dimensionless suppression factors. While a more complete evaluation of impact of the neglected contributions on the definition of  $a_\mu$  in Eq. (1.43) is beyond the scope of this review, the small values of these factors confirm that the experimental measurements of  $a_\mu$  are quite immune to such corrections.

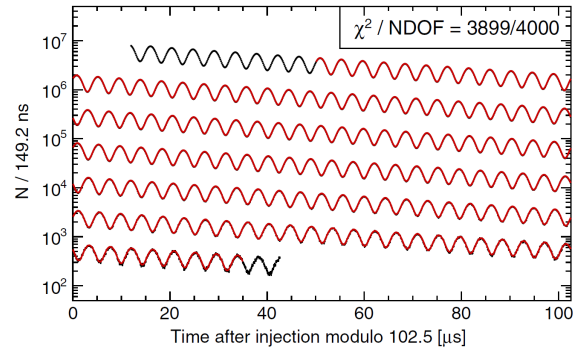
### 1.3. Status of the $a_\mu$ Measurement

In this section we summarise the history of the  $g - 2$  experiments and discuss the current status after the latest results of the final run of the Fermilab experiment [1]. For a more complete historic overview and experimental details we refer to the reviews in Refs. [13, 129, 130] and to the original literature.

The first experimental measurements of  $a_\mu$  were performed as early as 1957 at Nevis [131, 132] in an effort to test the prediction of parity violation in the weak interaction by Lee and Yang a year earlier [133]. In their seminal paper Lee and Yang proposed several processes in which parity violation could be tested. In particular, they noted that parity



(a) Illustration of the spin precession in storage ring



(b) Fit of the positron count in FNAL run-1d [118]

**Figure 1.4:** (a) Schematic of the storage ring and illustration of the muon spin precession in the constant magnetic field. In total, 24 calorimeters distributed evenly around the ring measure the positrons emitted by the decaying muon beam. (b) Fit of the positron count overlaid on top of the measured data in the FNAL run-1d [118].

violation and conservation of angular momentum in the pion decay  $\pi \rightarrow \mu + \nu$  as well as the subsequent decay of the muon  $\mu \rightarrow e + \nu_\mu \bar{\nu}_e$  leads to a strong correlation between the momentum and polarisation of the muon (and electron). After the experimental confirmation [131, 134] this fact became crucial to control the initial polarisation and observe the final spin of the muons in the measurements of  $a_\mu$ .

Initially, several experiments determined  $g_\mu$  through the spin precession of a muon at rest in an external magnetic field  $\mathbf{B}$ . Here the spin precession is described by [135]

$$\frac{d\mathbf{s}}{dt} = \boldsymbol{\omega}_s \times \mathbf{s}, \quad (1.45)$$

and the precession rate (Larmor frequency) is given by  $\boldsymbol{\omega}_s = -g_\mu(Qe/2m_\mu)\mathbf{B}$  and can thus be adjusted by varying the value of the external field. The experiments were set up to first produce polarised muons ( $\mu^+$ ) from an incoming beam of pions ( $\pi^+$ ) which were stopped in a target inside of a static magnetic field. A scintillator then counted the emitted positrons over a fixed interval, and the precession frequency  $\boldsymbol{\omega}_s$  could be measured for several values of  $|\mathbf{B}|$ , to extract the magnetic moment. By 1960 the results were precise enough to confirm Schwingers one-loop correction term  $\alpha/2\pi$  [136]

$$a_\mu^{1960} = 0.00122(8), \quad (1.46)$$

and by 1965 the first CERN experiment (CERN I) reached the precision of the QED two-loop contribution [137–139],

$$a_\mu^{\text{CERN I}} = 0.001162(5). \quad (1.47)$$

However, while very successful early on this approach was ultimately limited. For one, performing the experiment with negatively charged muons ( $\mu^-$ ) was not possible as these would be captured by the target after stopping. In addition, the lifetime of the muon at rest  $\tau_\mu \approx 2.2 \mu\text{s}$  only allowed for a short measurement period and consequently limited statistics.

These issues prompted the development of a new method using relativistic muons resulting in longer lifetimes and thereby significantly extending the measurement period. This technique was pioneered by the second CERN experiment (CERN II) where, for the first time, a storage ring was used to contain the muon ( $\mu^+$  or  $\mu^-$ ) beam [17, 140]. Because of the (relativistic) velocities of the muon, its spin precession frequency is modified by the Bargmann-Michel-Telegdi-equation

[127], see Eq. (1.44),

$$\boldsymbol{\omega}_s = -\frac{Qe}{m_\mu} \left[ \left( \frac{g_\mu}{2} + \frac{1-\gamma}{\gamma} \right) \mathbf{B} - \frac{a_\mu \gamma}{1+\gamma} (\mathbf{v} \cdot \mathbf{B}) \mathbf{v} - \left( \frac{g_\mu}{2} - \frac{\gamma}{1+\gamma} \right) \mathbf{v} \times \mathbf{E} \right]. \quad (1.48)$$

At the same time, the muon velocity also rotates

$$\frac{d\mathbf{v}}{dt} = \boldsymbol{\omega}_c \times \mathbf{v} + \frac{Qe}{\gamma m_\mu} \frac{1}{\gamma^2 - 1} (\mathbf{v} \cdot \mathbf{E}) \mathbf{v}, \quad (1.49)$$

with the cyclotron frequency

$$\boldsymbol{\omega}_c = -\frac{Qe}{m_\mu} \left[ \frac{1}{\gamma} \mathbf{B} - \frac{\gamma}{\gamma^2 - 1} \mathbf{v} \times \mathbf{E} \right]. \quad (1.50)$$

Because of the difference between Eq. (1.48) and Eq. (1.50) over time the polarisation of the muon beam deviates from the direction of the velocity as sketched in Fig. 1.4a. This difference can be tracked through the positrons (or electrons) emitted from the muon beam and measured by detectors arranged around the inside of the ring. Up to experimental corrections, the number of positrons varies with time as

$$N(t) = N_0 e^{-t/\gamma\tau_\mu} \left[ 1 + \mathcal{A} \cos(|\boldsymbol{\omega}_a|t + \phi_0) \right], \quad (1.51)$$

where  $N_0$  and  $\phi_0$  denote the initial beam density and average initial polarisation angle,  $\mathcal{A}$  stems from the weak decay asymmetry and dictates the amplitude of the oscillation around the average exponential decay with the anomalous precession frequency

$$\boldsymbol{\omega}_a = \boldsymbol{\omega}_s - \boldsymbol{\omega}_c = -\frac{Qe}{m_\mu} \left[ a_\mu \mathbf{B} - \frac{a_\mu \gamma}{1+\gamma} (\mathbf{v} \cdot \mathbf{B}) \mathbf{v} - \left( a_\mu - \frac{1}{\gamma^2 - 1} \right) \mathbf{v} \times \mathbf{E} \right]. \quad (1.52)$$

The magnetic field is typically measured using nuclear magnetic resonance (NMR) probes that yield  $|\mathbf{B}| = \omega_p/2\mu_p$  in terms of the proton Larmor frequency and magnetic moment  $\omega_p$  and  $\mu_p$ . After extracting  $|\boldsymbol{\omega}_a|$  from fitting the positron count, subtracting experimental corrections and writing  $e = 4m_e\mu_e/g_e$  in terms of the electron mass  $m_e$  and magnetic moment  $\mu_e$ ,  $a_\mu$  is given by

$$a_\mu = \frac{\omega_a \mu_p m_\mu g_e}{\omega_p \mu_e m_e 2}. \quad (1.53)$$

Here the ratios  $\mu_p/\mu_e$  and  $m_\mu/m_e$  as well as  $g_e$  are taken from independent experiments and are sufficiently well known.

CERN II relied solely on weak magnetic focusing, such that no external electric field was present ( $\mathbf{E} = 0$ ) and the Lorentz factor  $\gamma \approx 12$  was set by the ring geometry ( $r = 2.5$  m) and the external magnetic field  $|\mathbf{B}| \approx 1.71$  T. This first measurement using a relativistic muon beam [140] already improved the precision by a factor of 16 compared to CERN I

$$a_\mu^{\text{CERN II}} = 0.00116610(31). \quad (1.54)$$

However, there were a number of drawbacks with the first design, the most severe stemming from the inclusion of the pion production target as a muon kicker inside of the storage ring. While this avoided the technical challenge of producing and injecting the polarised muon beam into the storage ring, it also resulted in a large hadronic background and decreased statistics due to the small number of muons kicked into the correct orbit. To improve on this result a cleaner muon beam with longer lifetime was required.

This was achieved at the CERN III experiment, where the  $g - 2$  experiment in its modern form was implemented for the first time [18]. Instead of the weak magnetic focusing, electric quadrupoles were used to provide vertical stability.

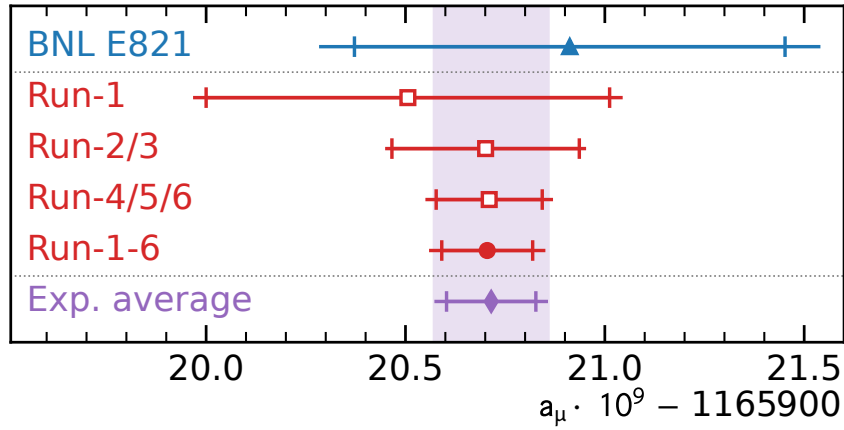


**Figure 1.5:** Reprinted from Ref. [1]. Summary plot of the experimental values of  $a_\mu$  obtained from the FNAL run-1, run-2/3 and run-4/5/6 measurements (red squares) as well as the final BNL E821 result (blue triangle). The FNAL final value Eq. (1.1) is indicated by the red circle and the current world average Eq. (1.2) by the purple diamond. The additional results can be found in Eqs. (1.56) and (1.57). The vertical bars indicate the statistical uncertainties, the horizontal lines the total uncertainties.

According to Eq. (1.52), this additional electric field would enter the frequency  $\omega_a$ , potentially leading to uncertainties. However, it was noted that this effect could be suppressed by choosing the magic  $\gamma = \sqrt{1 + 1/a_\mu} \approx 29.3$ . To achieve this with a comparable magnetic field  $|\mathbf{B}| \approx 1.45$  T, a new ring with radius  $r = 7.112$  m needed to be constructed. Further upgrades were the injection of a pion instead of proton beam, the development of an inflector magnet and the uniform magnetic field allowing for a simpler averaging over the muon distribution. In combination, CERN III yielded another factor of 36 improvement over the previous results [18],

$$a_\mu^{\text{CERN III}} = 11\,659\,240(85) \times 10^{-10}. \quad (1.55)$$

Famously, this measurement was precise enough to verify the relevance of the hadronic vacuum polarisation contributions in the SM theory prediction, which contribute at the level of  $7 \times 10^{-7}$ .

A decade after CERN III the next  $g-2$  experiment E821 [19] at Brookhaven National Laboratory (BNL) was approved. The basic measurement principle from the CERN collaboration was kept, however with a number of further upgrades, most notably a new superconducting storage ring magnet (that would also be reused at Fermilab) and the injection of a much more intense beam. The magnetic field was closely monitored by a number of NMR probes installed around the ring as well as an NMR trolley that could map the magnetic field in the ring when the muon beam was inactive. A new muon kicker allowed for the injection of a much cleaner muon beam, which significantly decreased the number of remaining pions compared to CERN. Altogether these upgrades yielded another factor of 15 improvement in  $a_\mu$  [20–22] (the number was updated in Ref. [118] to reflect changes of CODATA values for external inputs)

$$a_\mu^{\text{BNL}} = 11\,659\,209.1(6.3) \times 10^{-10}. \quad (1.56)$$

This was precise enough to come within reach of the electroweak SM contribution, which contributes at the  $10^{-9}$  level; in addition, this result differed by around  $3\sigma$  from the SM prediction at the time, motivating considering BSM contributions to  $a_\mu$  as well as further experimental scrutiny.

In order to scrutinise this result, the follow-up experiment E989 at the Fermilab National Accelerator Laboratory (FNAL) was commissioned with the goal to improve the overall uncertainty by another factor of 4 [141]. The central part, the 14 m ring magnet, was moved from Brookhaven to the Fermilab campus, but (apart from the inflector) essentially

all of the electronics were replaced. The new calorimeters provided a much higher spatial and timing resolution, and an additional monitoring system was used to stabilise the energy measurement. An in-vacuum tracking system was developed in order to measure the beam profile. Another major improvement was the much longer muon delivery path from the production target to the injector, that allowed for most of the excess pions to decay before arriving at the storage ring. In addition a delivery ring was constructed that helped separating remaining protons from the muon bunches. With these upgrades, already the results from Run-1 published in 2021 [23, 118–120] reached the precision of the BNL experiment, and together with the Run-2 and 3 results published in 2023 [24, 25] further improved on this result by more than a factor of 2.

The final analysis of Run-4 to 6 was presented earlier this year [1]. Within uncertainties, it is in full agreement with all previous measurements at Fermilab and Brookhaven. The total Run-1–6 result has surpassed its design goal and reduced the statistical and systematic uncertainties to  $(1.14)^{\text{stat}}(0.91)^{\text{syst}} \times 10^{-10}$ , in total to better than 4 times the precision of the Brookhaven measurement.<sup>6</sup> In total, the results of the Fermilab muon  $g - 2$  experiment, and the resulting current world average are (taking into account updates reflecting experimental corrections that were applied after the original publications)

$$a_{\mu}^{\text{FNAL,Run-1}} = 11\,659\,205.1 (5.4) \times 10^{-10}, \quad (1.57\text{a})$$

$$a_{\mu}^{\text{FNAL,Run-2,3}} = 11\,659\,207.0 (2.5) \times 10^{-10}, \quad (1.57\text{b})$$

$$a_{\mu}^{\text{FNAL,Run-4,5,6}} = 11\,659\,207.10(1.62) \times 10^{-10}, \quad (1.57\text{c})$$

$$a_{\mu}^{\text{FNAL,Run-1-6}} = 11\,659\,207.05(1.48) \times 10^{-10}, \quad (1.57\text{d})$$

$$a_{\mu}^{\text{Exp}} = 11\,659\,207.15(1.45) \times 10^{-10}. \quad (1.57\text{e})$$

These numbers are also illustrated in Fig. 1.5.

Finally, let us give a brief outlook for the planned  $a_{\mu}$  experiment at J-PARC [142–146]. This experiment aims to be complementary in that it minimises the electric-field term in Eq. (1.52) not by choosing a magic  $\gamma$  but instead by vanishing electric field. A key requirement for this is a lower emittance of the muon beam compared to the Fermilab and Brookhaven experiments. To achieve this, the polarised muon beam produced by the pion decay is cooled and then re-accelerated before injection into storage ring. Such cooling will eliminate the need for additional electric focusing, and thereby the constraint to the magic  $\gamma$ , and generally significantly reduce the systematics associated with the muon beam. The novel technology required for the cooling was recently demonstrated for the first time [147].

#### 1.4. Status of $a_{\mu}$ in the Standard Model

Here we describe the SM theory prediction and explain the origin of the results obtained in the Theory Initiative White Papers [2, 3] and given in Eqs. (1.3,1.4). Generally, the theory prediction is given in terms 1PI Feynman diagrams with external on-shell muons and an external photon, see Eq. (1.43). As mentioned before, for the SM prediction all SM particles and interactions matter in a relevant way. The hadronic contributions are responsible for the largest part of the theory uncertainty; for this review it is also of interest to highlight certain aspects of the QED and electroweak contributions which are similar to many potential BSM contributions.

---

<sup>6</sup>Experimental numbers which cannot be found in the references cited in the main text are from the internal Muon  $g - 2$  collaboration document #GM2-doc-32016-v10, revised 11th June 2025, by A. Lusiani.

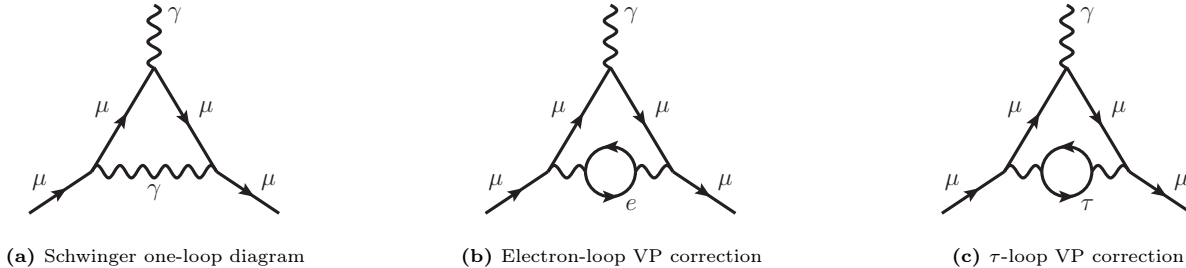


**Figure 1.6:** One- and two-loop QED contributions to  $a_\mu$  in the Standard Model. Diagram (a) corresponds to the well-known Schwinger correction, while diagrams (b) and (c) show two-loop leptonic vacuum-polarisation (VP) corrections from an electron and  $\tau$  loop inserted into the photon propagator.

Traditionally, the full SM theory prediction for  $a_\mu$  is split into

$$a_\mu^{\text{SM}} = a_\mu^{\text{QED}} + a_\mu^{\text{EW}} + a_\mu^{\text{HVP}} + a_\mu^{\text{HLbL}}, \quad (1.58)$$

where the abbreviations denote QED, electroweak, hadronic vacuum polarisation and hadronic light-by-light contributions, respectively.

The QED and electroweak (EW) contributions are very accurately known. Their uncertainties were already negligible in Ref. [2], and their values have changed only by tiny amounts in Ref. [3]. The QED contributions are given by Feynman diagrams involving only photons and muons or other leptons. They have been evaluated including the 5-loop level to [3, 26, 27, 51–56]

$$a_\mu^{\text{QED}} = 11\,658\,471.88(2) \times 10^{-10}. \quad (1.59)$$

Three QED diagrams of particular interest are shown in Fig. 1.6. The diagram in Fig. 1.6a is the well-known QED one-loop diagram leading to Schwinger’s result  $a_\mu^{\text{QED},1\text{L}} = \alpha/2\pi$  [16]. The diagrams in Fig. 1.6b and 1.6c illustrate important features of mass-dependent contributions. They are two-loop corrections where either an electron loop or a  $\tau$ -lepton loop is inserted into the photon propagator. The electron mass  $m_e$  is lighter than the muon mass, leading to a logarithmic enhancement

$$a_\mu^{\text{QED, Fig. 1.6b(b)}} = \left(\frac{\alpha}{\pi}\right)^2 \left[ -\frac{25}{36} + \frac{1}{3} \ln\left(\frac{m_\mu}{m_e}\right) \right] \sim 6 \times 10^{-6}. \quad (1.60)$$

This logarithmic enhancement is the main reason why the muon magnetic moment  $a_\mu$  is larger than the electron magnetic moment  $a_e$ , see also the comparison in Eqs. (1.8a,1.8b). The  $\tau$ -lepton mass in contrast is larger than the muon mass, leading to a quadratic mass suppression

$$a_\mu^{\text{QED, Fig. 1.6c(c)}} = \left(\frac{\alpha}{\pi}\right)^2 \left[ \frac{1}{45} \frac{m_\mu^2}{m_\tau^2} + \mathcal{O}\left(\frac{m_\mu^4}{m_\tau^4}\right) \right] \sim 4 \times 10^{-10}. \quad (1.61)$$

Such a quadratic mass suppression is typical of the contributions of heavy particles also in the context of BSM physics.

The EW contributions are given by all Feynman diagrams which contain any of the non-QED/QCD particles, i.e. the heavy  $W$ ,  $Z$  or Higgs boson or neutrinos. The one-loop EW diagrams are shown in Fig. 1.7. For example, the  $W$ -boson contribution is essentially determined by

$$a_\mu^{\text{W}} \propto \frac{g_2^2}{16\pi^2} \frac{m_\mu^2}{M_W^2} \sim 10^{-9}, \quad (1.62)$$

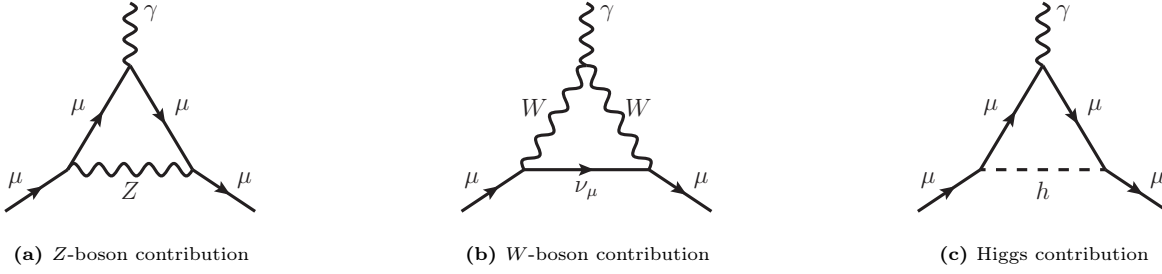


**Figure 1.7:** Complete electroweak one-loop contribution to  $a_\mu$  in unitary gauge. Diagrams (a) and (b) correspond to the leading  $Z$ - and  $W$ -boson correction, while diagram (c) gives the suppressed Higgs correction. In other gauges (like  $R_\xi$ ) additional contributions from the appropriate Goldstone bosons need to be included.

where  $g_2^2/16\pi^2$  corresponds to a loop factor involving the weak  $SU(2)_L$  gauge coupling, and  $m_\mu^2/M_W^2 \sim 10^{-6}$  is again a mass suppression factor arising from the heavy  $W$ -boson. This shows that the EW contributions are six orders of magnitude smaller than the QED contributions and affect the total  $g$ -factor of the muon at the 9th decimal place, as announced in Eq. (1.8b) in Sec. 1.1.2. Nevertheless, the EW contributions are relevant at the current level of precision. In detail, the EW contributions can be split into

$$a_\mu^{\text{EW}} = a_\mu^{\text{EW}(1)} + a_{\mu;\text{bos}}^{\text{EW}(2)} + a_{\mu;\text{ferm}}^{\text{EW}(2)} + a_\mu^{\text{EW}(\geq 3)}, \quad (1.63)$$

corresponding to one-loop diagrams, two-loop diagrams without/with fermion loop, and  $\geq 3$ -loop diagrams. The analytic evaluation of the diagrams in Fig. 1.7 (together with the corresponding Goldstone boson contributions) gives

$$a_\mu^{\text{EW}(1)} = \frac{G_F}{\sqrt{2}} \frac{m_\mu^2}{24\pi^2} \left\{ \underbrace{\left(1 - 4s_W^2\right)}_Z - 5 + 10 \underbrace{- \frac{m_\mu^2}{M_W^2} \left[7 + 6 \ln\left(\frac{m_\mu^2}{M_W^2}\right)\right]}_W + \underbrace{\mathcal{O}\left(\frac{m_\mu^2}{M_Z^2} \ln\left(\frac{m_\mu^2}{M_Z^2}\right)\right)}_h \right\} \quad (1.64)$$

The one-loop and bosonic two-loop contributions [29, 148–151] essentially depend on the heavy  $W$ ,  $Z$ , and Higgs boson masses and amount to  $a_\mu^{\text{EW}(1)} = 19.479(1)$  and  $a_{\mu;\text{bos}}^{\text{EW}(2)} = -1.9962(3)$  in units of  $10^{-10}$ , respectively. The large, negative two-loop correction is mainly due to large QED-like logarithms and appears also in the context of BSM contributions [28, 152], see also Sec. 4.3. The fermionic two-loop contributions [28, 29, 57, 58, 153] together with the  $\geq 3$ -loop contributions amount to  $-2.04(4) \times 10^{-10}$ , where about half of this value originates from loops of the 3rd-generation fermions  $\tau$ -lepton, top- and bottom-quarks and the uncertainty is mainly caused by 2nd-generation hadronic contributions [58] and by unknown  $\geq 3$ -loop contributions [28]. In total, therefore,

$$a_\mu^{\text{EW}} = 15.44(4) \times 10^{-10}. \quad (1.65)$$

The hadronic vacuum polarisation (HVP) contributions correspond to diagrams such as Fig. 1.8 and appropriate higher-order corrections, where a hadronic vacuum polarisation is inserted into a QED one-loop diagram. They are almost two orders of magnitude larger than the EW contributions and enter the muon  $g$ -factor at the 7th digit in Eq. (1.8b). This can be understood by noting the diagrammatic similarity to the electron-loop and  $\tau$ -loop diagrams of Fig. 1.6b and 1.6c together with the value of the lightest hadron masses.

These HVP contributions are the cause of the largest SM theory uncertainty and are subject to intense current scrutiny. They require non-perturbative techniques, and two approaches are established. The more traditional approach is based on the optical theorem and dispersion relations and relates  $a_\mu^{\text{HVP}}$  to cross sections for  $e^+e^- \rightarrow \gamma^* \rightarrow \text{hadrons}$  processes, which are experimentally measurable. The result used in the first White Paper [2] is based on this approach. Ref. [2]

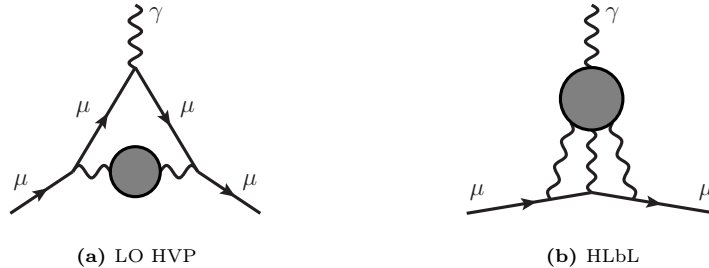


**Figure 1.8:** Non-perturbative hadronic contributions to  $a_\mu$  in the SM. Diagram (a) shows the leading-order hadronic vacuum polarisation (HVP) correction and diagram (b) the hadronic light-by-light (HLbL) scattering correction.

obtained

$$a_\mu^{\text{HVP,LO,[2]}} = 693.1(4.0) \times 10^{-10} \quad (1.66)$$

for the most important leading-order HVP contributions. This result is based on original references [30–34], and it needs to be combined with known next- and next-to-next-to-leading order corrections [35, 36]. In evaluating Eq. (1.66), the most critical hadronic channel is  $e^+e^- \rightarrow \pi^+\pi^-$  at energies between 0.6...0.9 GeV. This had been measured most precisely by KLOE [154], Babar [155], CMD-2 [156, 157], SND [158, 159] and BESIII [160]. However, there were significant tensions between these data sets. For instance, evaluating  $a_\mu$  by using just one of the two individually most precise data sets KLOE and Babar in this energy region leads to results that differ by  $10 \times 10^{-10}$ . The tensions were taken into account by locally and globally rescaling uncertainties to obtain the result (1.66) and its uncertainty. For detailed discussions we refer to Refs. [30–34], Refs. [2, 3] and references therein.

The second approach to evaluate the HVP contributions is based on lattice gauge theory, which allows a direct non-perturbative computation without relying on experimental data. When Ref. [2] appeared, the lattice results were not yet sufficiently consolidated to be used. However, around the same time the Budapest-Marseille-Wuppertal (BMW) lattice collaboration [61] published the first lattice determination of the HVP contribution with an uncertainty estimate that is small enough to be competitive with the data-driven estimates. This BMW prediction is not in agreement with the data-driven results used in Ref. [2] but is significantly larger. The disagreement is strengthened with the recent update [69] which obtains

$$a_\mu^{\text{HVP,LO,[69]}} = 714.1(3.3) \times 10^{-10}. \quad (1.67)$$

Recent further lattice groups have found agreement with the BMW calculation, and full HVP,LO results were obtained by the BMW [61, 69], Mainz/CLS [65, 68, 72] and RBC/UKQCD collaborations [59, 67, 71]. Further important results, partially for intermediate/long- or short-distance Euclidean time windows where specific optimisations are possible, are given in Refs. [60, 62–64, 66, 70, 73–75]. All these lattice results are consistent with each other and uniformly show a tension between lattice and the data-driven results used in Ref. [2].

The situation is further complicated by experimental data from the recent CMD-3 experiment [100] which gives systematically larger cross-sections for  $e^+e^- \rightarrow \pi^+\pi^-$  than the previous CMD-2, SND, Babar, KLOE and BESIII measurements. The reasons for the disagreement between the HVP contributions based on earlier  $e^+e^- \rightarrow \pi\pi$  data, based on CMD-3 data, or based on lattice gauge theory are under intense scrutiny [3, 161–165]. Currently, the reasons are unknown, and as discussed in detail in the second White Paper [3], there are no scientific grounds on which any of the  $e^+e^-$  data sets could be disregarded. However, the increased tensions between the different data sets make it currently impossible to obtain a reliable update of the HVP result using the dispersive and data-based approach.

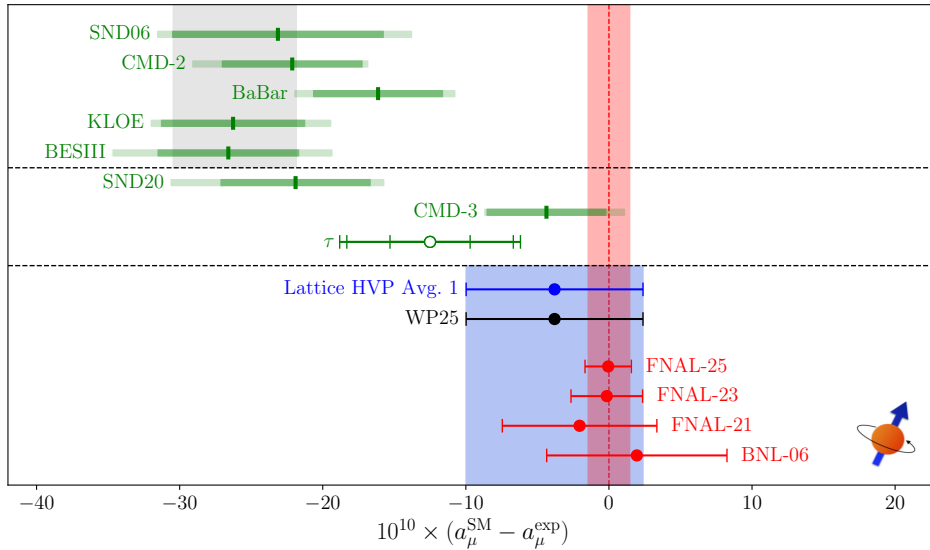


**Figure 1.9:** Reprinted from Ref. [3]. Summary plot of the SM predictions for  $a_\mu$ , based on different evaluations of the LO HVP. The black point and blue band correspond to the new WP2025 value Eq. (1.4) obtained from the lattice-QCD results, while the grey band shows the old WP2020 value Eq. (1.3), derived from the  $e^+e^-$  data sets collected above the upper dashed line. The values between the dashed lines were obtained from the SND20 and CMD-3 data sets that appeared after the WP2020 [2] as well as a reevaluation of the LO HVP based on  $\tau$ -decay data and are not included in either WP value for  $a_\mu$ . The red points and band correspond to the experimental values already shown in Fig. 1.5.

Notwithstanding these complications, the lattice gauge theory results on their own are now sufficiently precise, obtained by several independent groups, fully consistent and cross-checked in multiple ways. Hence the second Theory Initiative White Paper Ref. [3] evaluates the HVP,LO contributions based on the lattice results from Refs. [59–75] and obtains

$$a_\mu^{\text{HVP,LO,[3]}} = 713.2(6.1) \times 10^{-10}. \quad (1.68)$$

Here, the value (1.67) has not been used since it employs a combination of lattice (95%) and  $e^+e^-$  data (5%), but both values agree very well. Including higher orders, the full HVP result reads [3]

$$a_\mu^{\text{HVP,[3]}} = 704.5(6.1) \times 10^{-10}. \quad (1.69)$$

Figure 1.9 from Ref. [3] summarises the different evaluations of the HVP contributions and compares the full SM prediction to the experimental value (1.2).

Finally we briefly comment on the hadronic light-by-light contributions. They are given by diagrams of the form given in Fig. 1.8b where a non-perturbative hadronic light-by-light scattering subdiagram is attached to the muon line. They are the smallest of the four classes of SM contributions in Eq. (1.58) but still highly relevant. Significant progress has been achieved in their evaluation in the past decades. After earlier computations via hadronic models summarised in Refs. [12, 166], more recent phenomenological approaches based on dispersion relations have been developed in Refs. [11, 37–48, 50] and [86, 89, 92, 94, 167, 168], and also lattice gauge theory computations have become feasible [49, 96, 98, 99]. All approaches lead to compatible results, and the White Paper Ref. [3] obtains the value

$$a_\mu^{\text{HLbL}} = 115.5(9.9) \times 10^{-11}. \quad (1.70)$$

In total, adding up the values given in Eqs. (1.59,1.65,1.69,1.70) yields the full SM theory prediction for  $a_\mu$  given

already in Eq. (1.4). The difference between the values obtained in the two White Papers Refs. [2, 3] and shown in Eqs. (1.3,1.4) and Fig. 1.9 is mainly caused by the new result for the HVP contributions as discussed above.

While the current SM prediction agrees very well with the experimental determination of  $a_\mu$ , significant progress and updates can be expected. Specifically the leading-order HVP prediction is under intense scrutiny [3, 161–165]. The understanding of  $e^+e^-$  data can improve via new measurements, new analyses also including rigorous validation of theory ingredients such as higher-order calculations and Monte Carlo tools [169]. Ideally, the current tensions among the  $e^+e^-$  data can be resolved. In addition, the inclusion of  $\tau$ -decay data [3, 162, 170] and the MUonE experiment [171–176] measuring the vacuum polarisation in the space-like instead of the time-like region can provide further cross-checks and independent input.<sup>7</sup>

Forthcoming lattice computations by many groups will employ a wide range of methods. This progress promises even more precise and consolidated results for the full SM prediction of  $a_\mu$ , further sharpening its role as a test of all aspects of the SM and a unique constraint on BSM physics.

---

<sup>7</sup>The MUonE experiment can also be used to study physics beyond the SM, as discussed in Refs. [177–182].

## 2. Generic BSM scenarios

Physics beyond the SM can contribute to  $a_\mu$  via loop Feynman diagrams. The contributions have an anatomy governed by the need for chirality flips and electroweak symmetry breaking, and there are classes of models with or without chiral enhancements. In this section we provide technical details and connect them to such qualitative discussions. Sec. 2.1 provides generic one-loop results which are applicable to all renormalisable quantum field theories. The form of one-loop Feynman diagrams that can contribute to  $a_\mu$  is restricted by the requirement that there must be couplings to a photon and two muons, in addition to the usual restrictions from gauge and Lorentz invariance and renormalisability. As a result the possible one-loop contributions to muon  $g-2$  are well known and depend only on the couplings, masses and topology of the diagrams. The formulas of Sec. 2.1 allow mass eigenstates with arbitrary couplings to left-handed and right-handed muons.

If the particles in the loop are assumed to coincide with gauge eigenstates or with mixtures of only two gauge eigenstates, the possible gauge quantum numbers are quite restricted. Such specific BSM extensions are discussed in Secs. 2.2 and 2.3, where only one, two, or three new BSM fields with specific gauge quantum numbers and with gauge-invariant interactions are added to the SM. The set of such extensions is quite limited and the possible models can be systematically categorised, and immediate consequences can be drawn regarding the possible signs and magnitudes of the BSM contributions to  $a_\mu$ . The comparisons of the generic mass eigenstate formulas with the behaviour of two-field and three-field models also sheds additional light on the role of chirality flips and illustrates the usefulness of mass-insertion approximations. Finally, Sec. 2.4 introduces the description of dipole moments in important effective field theories. These frameworks are useful to study general properties of  $a_\mu$  and correlations to other observables in model-independent ways, although renormalisability is given up. The LEFT framework can be used for observables below the electroweak scale, and the SMEFT framework is appropriate for observables above the electroweak scale as long as no BSM particles exist at the considered mass scale. The effective theory description will also be used later to obtain higher-order corrections that are applicable to wide classes of models.

### 2.1. General one-loop formulas for $\Delta a_\mu$

In this section we collect the general formulas for  $\Delta a_\mu$  at one-loop order in generic renormalisable relativistic quantum field theories. Such theories may contain scalar fields, spin 1/2 fermion fields and vector fields which interact via operators of dimension 4 or less. The generically possible one-loop Feynman diagrams that contribute to  $a_\mu$  can be classified into FS-type contributions shown in Fig. 2.1a, FV-type contributions shown in Fig. 2.1b and FSV-type contributions shown in Fig. 2.1c. All diagrams can be computed in a model-independent way based on a generic Lagrangian.

Details and discussions of the calculation have been presented in the literature many times in the past. Specifically, results for unitary gauge can be found in Refs. [8, 12, 183–185] and for t’Hooft Feynman gauge in Refs. [9, 186, 187].

To list the results, we start from the generic interaction Lagrangian in the mass basis after EWSB. The relevant terms for the interaction between the muon and the additional fields read

$$\mathcal{L}_\mu^{\text{SFV}} = \bar{F}(c_L P_L + c_R P_R)\mu S^\dagger + \bar{F}\gamma^\nu(g_L P_L + g_R P_R)\mu V_\nu^\dagger + h.c., \quad (2.1)$$

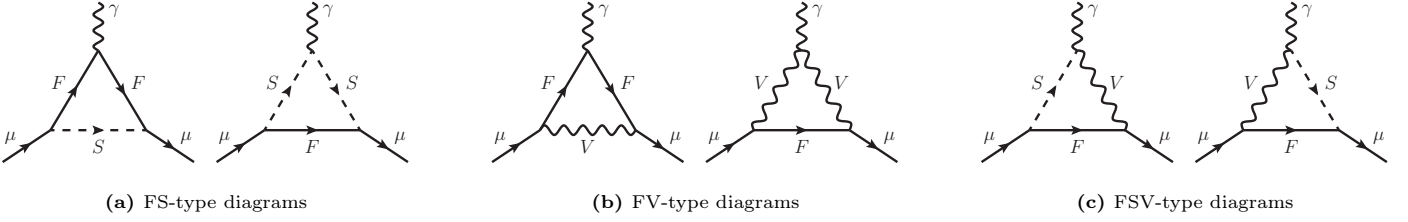


**Figure 2.1:** All possible one-loop diagrams contributing to  $a_\mu$  in generic renormalisable QFTs, with internal scalars (S), spin 1/2 fermions (F) or vector-bosons (V).

while the interaction terms involving the photon are given by

$$\begin{aligned} \mathcal{L}_\gamma^{\text{SFV}} = & e\bar{\mu}A\mu - Q_F e\bar{F}AF - iQ_S e(S^\dagger\partial_\mu S - S\partial_\mu S^\dagger)A_\mu \\ & - iQ_V e(F^{\mu\nu}V_\mu V_\nu^\dagger - V^{\mu\nu}A_\mu V_\nu^\dagger + V_{\mu\nu}^\dagger A^\mu V^\nu) - \mu_0 e A^\mu (V_\mu^\dagger S + V_\mu S^\dagger). \end{aligned} \quad (2.2)$$

Here  $F = F_L + F_R$  is a new fermion field,  $S$  and  $V_\nu$  are new scalar and vector fields, and  $\mu = \mu_L + \mu_R$  is the muon field. The muon electric charge is set to  $Q = -1$ , and for non-vanishing contributions to  $a_\mu$ , charge conservation implies  $Q_S = Q_V = -1 - Q_F$ . In Fig. 2.1 the charges always flow from left to right. Further,  $V_{\mu\nu} = \partial_\mu V_\nu - \partial_\nu V_\mu$  and  $\mu_0$  denotes a model-dependent mass parameter, e.g. for Goldstone bosons  $\mu_0 = Q_V m_V$ . The appearing fields are assumed to be mass eigenstates with masses  $m_{F,S,V}$ , but are not required to be gauge eigenstates with well-defined gauge quantum numbers. The Lagrangian of any concrete model can be mapped to these Lagrangians, leading to specific values of the coupling prefactors. In general, the full contribution to  $a_\mu$  must be gauge independent. However, propagator and vertex Feynman rules and individual Feynman diagrams can depend on the choice of gauge. Here we present the results in unitary gauge, where the vector boson propagators take a specific form and Goldstone-boson contributions vanish. We note that, while absent in the SM, physical FSV-type contributions can exist in extensions to the SM (e.g. in the type-II see-saw mechanism).

After the charge  $Q_F$  is eliminated, the physical results corresponding to the generic diagrams Fig. 2.1a, 2.1b and 2.1c can be written compactly as

$$\Delta a_\mu^{\text{FS}} = \frac{1}{16\pi^2} \frac{m_\mu^2}{m_S^2} \left( \text{Re}\{c_L^* c_R\} \frac{m_F}{m_\mu} \mathcal{F}^{\text{FS}}(x_\mu, x_F; Q_S) + \{|c_L|^2 + |c_R|^2\} \mathcal{G}^{\text{FS}}(x_\mu, x_F; Q_S) \right), \quad (2.3a)$$

$$\Delta a_\mu^{\text{FV}} = \frac{1}{16\pi^2} \frac{m_\mu^2}{m_V^2} \left( \text{Re}\{g_L^* g_R\} \frac{m_F}{m_\mu} \mathcal{F}^{\text{FV}}(z_\mu, z_F; Q_V) + \{|g_L|^2 + |g_R|^2\} \mathcal{G}^{\text{FV}}(z_\mu, z_F; Q_V) \right), \quad (2.3b)$$

$$\Delta a_\mu^{\text{FSV}} = \frac{\mu_0}{16\pi^2} \frac{m_\mu}{m_V^2} \left( \text{Re}\{g_R^* c_L + g_L^* c_R\} \mathcal{F}^{\text{FSV}}(z_\mu, z_F, z_S) + \text{Re}\{g_R^* c_R + g_L^* c_L\} \frac{m_F m_\mu}{m_V^2} \mathcal{G}^{\text{FSV}}(z_\mu, z_F, z_S) \right), \quad (2.3c)$$

where  $x_i \equiv m_i^2/m_S^2$  and  $z_i \equiv m_i^2/m_V^2$ . The fully general expressions for the loop functions are listed at the end of this subsection.<sup>8</sup>

All of the formulas contain two different kinds of terms, corresponding to different chirality combinations and involving different fermion mass combinations. As explained in Sec. 1.1.4, any contribution to  $a_\mu$  requires a  $L \leftrightarrow R$  flip of the muon chirality. This flip can happen at the external muon line or via the internal loop. In the FS- and FV-type diagrams the terms involving  $|c_{L,R}|^2$  or  $|g_{L,R}|^2$  are exemplified by the diagram in Fig. 2.2 (left), where only the right-handed (or similarly only the left-handed) muon couples to the loop and the chirality is flipped at an external muon line. In the

<sup>8</sup>We mention that one-loop contributions from non-renormalisable models with spin-3/2 particles have been considered in Ref. [188] and from spin-2 Kaluza-Klein excitations of gravitons in Ref. [189].

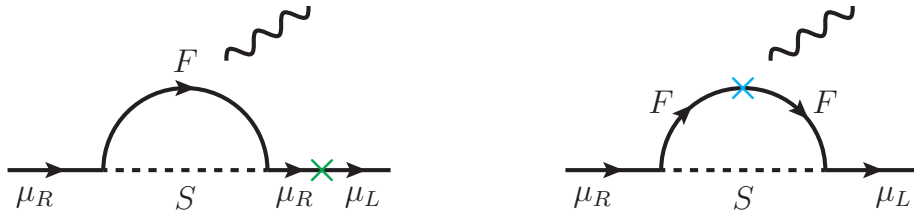


**Figure 2.2:** Illustration of the chirality flips in the FS-type one-loop contribution Eq. (2.3a) to  $\Delta a_\mu$ . The photon can couple to any charged internal line. The left diagram corresponds to a chirality flip on the external line, producing the  $|c_{L,R}|^2 m_\mu$  term, while the right diagram corresponds to an internal chirality flip resulting in the  $c_L^* c_R m_F$  term. There exist similar diagrams with the roles of  $\mu_{L,R}$  exchanged, and the FV- and FSV-type contributions can be understood analogously.

diagrammatic computation this corresponds to an application of the Dirac equation  $\not{p}u(p) = m_\mu u(p)$  on the external muon spinor, and the resulting contributions to  $a_\mu$  are suppressed by  $m_\mu^2/M^2$ , where  $M$  is the potentially heavy internal scale. In terms of the discussion of Sec. 1.1.4 and Eqs. (1.14) and (1.15), the factors in square brackets simply amount to  $[\dots] \rightarrow m_\mu$ , corresponding to no chiral enhancement.

The other kind of terms of the FS- and FV-type results are illustrated by the Feynman diagram of Fig. 2.2 (right), where one of the vertices connects to a right-handed muon, the other vertex to a left-handed muon, and where the chirality is flipped via the loop. In the computation of the diagram, the fermion mass  $m_F$  arises via the propagator of the fermion  $F$  in the loop, leading to the relative, potential enhancement factor  $m_F/m_\mu$ . In terms of Eqs. (1.14) and (1.15), the factors in the square brackets  $[\dots]$  correspond to the combinations  $c_L^* c_R m_F$  and  $g_L^* g_R m_F$ . In order to enable these potentially chirality-flip enhanced contributions, there must be mixing, i.e. the particles in the loop must be linear combinations of states with different gauge quantum numbers. This mixing affects the potential enhancement since it requires the explicit or implicit appearance of a factor of an EWSB  $vev$  as illustrated by the  $vev$  insertion in Fig. 1.1 (right). For example the fermion mass  $m_F$  may arise from an EWSB  $vev$ , or the vertex factors  $c_{L,R}$ ,  $g_{L,R}$  might involve mixing matrix elements which effectively again depend on some EWSB  $vev$ . The role of the two kinds of terms in the FSV-type diagrams is analogous but reversed compared to the cases of the FS- and FV-type diagrams.

The numerical behaviour of all these terms and their appearance in concrete models will be discussed at length in subsequent sections. As a first illustration, already the EWSM one-loop diagrams shown in Fig. 1.7 are of all the above types. The  $W$ -boson diagram only involves left-handed muon couplings, whereas the  $Z$ - and Higgs-boson diagrams lead to terms of both chirality combinations. However, in these diagrams the internal fermion is a muon, hence the factor  $m_F/m_\mu = 1$  is no enhancement. In contrast, in many BSM scenarios, the terms with a chirality flip on the internal line are potentially enhanced, see also Tab. 1.1.

The generic formulas in Eq. (2.3) depend on loop functions of the appearing masses. We first provide these loop functions in approximations for important limits. Very often, BSM particles are heavy and the muon mass can be neglected. In the corresponding limits  $x_\mu, z_\mu \rightarrow 0$ , the loop functions for FS-type diagrams depend only on the single

ratio  $y \equiv m_F^2/m_S^2$  and are given by <sup>9</sup>

$$\mathcal{F}^{\text{FS}}(0, y; Q_S) = -\frac{3 - 4y + y^2 + 2 \ln(y)}{(1-y)^3} - \frac{2Q_S(1-y + \ln(y))}{(1-y)^2}, \quad (2.7a)$$

$$\mathcal{G}^{\text{FS}}(0, y; Q_S) = \frac{2 + 3y - 6y^2 + y^3 + 6y \ln(y)}{6(1-y)^4} + \frac{Q_S(1-y^2 + 2y \ln(y))}{2(1-y)^3}, \quad (2.7b)$$

for the FV-type diagrams 2.1b the loop functions depend on  $y \equiv m_F^2/m_V^2$  and are given by<sup>10</sup>

$$\mathcal{F}^{\text{FV}}(0, y; Q_V) = \frac{4 - 3y - y^3 + 6y \ln(y)}{(1-y)^3} + \frac{2Q_V(4 - 5y + y^2 + 3y \ln(y))}{(1-y)^2}, \quad (2.8a)$$

$$\mathcal{G}^{\text{FV}}(0, y; Q_V) = -\frac{8 - 38y + 39y^2 - 14y^3 + 5y^4 - 18y^2 \ln(y)}{6(1-y)^4} - \frac{3Q_V(2 - 7y + 6y^2 - y^3 - 2y^2 \ln(y))}{2(1-y)^3}, \quad (2.8b)$$

and for the FSV-type diagrams 2.1c the loop functions become

$$\mathcal{F}^{\text{FSV}}(0, y, z) = \frac{y^2(1-z) - 2(y-z)}{2(1-y)(1-z)(y-z)} - \frac{(1-z)y^3 \ln(y)}{2(1-y)^2(y-z)^2} + \frac{[2(y-z) + y(1-z)]z^2 \ln(z)}{2(1-z)^2(y-z)^2}, \quad (2.9a)$$

$$\mathcal{G}^{\text{FSV}}(0, y, z) = \frac{2yz(1-y) - y(3+y)(y-z)}{6(1-y)^2(y-z)^2} + \frac{[y(1+z)(3z-y) - z^2(3+y^2)]y \ln(y)}{3(1-y)^3(y-z)^3} + \frac{z^3 \ln(z)}{3(1-z)(y-z)^3}. \quad (2.9b)$$

Generally, the loop functions take values of the order one, and it is of interest to collect further limiting cases. Equally heavy internal masses correspond to  $y = 1$ , very heavy boson mass  $m_{S,V} \gg m_F \gg m_\mu$  corresponds to  $y \rightarrow 0$  and very heavy fermion mass corresponds to  $y \rightarrow \infty$ . In case of FSV, equal boson masses  $m_S = m_V$  corresponds to  $z = 1$ . In these limits, the loop functions become

$$\mathcal{F}^{\text{FS}}(0, y; Q_S) \stackrel{y \rightarrow 1}{=} \frac{2}{3} + Q_S \quad \mathcal{G}^{\text{FS}}(0, y; Q_S) \stackrel{y \rightarrow 1}{=} \frac{1 + 2Q_S}{12} \quad (2.10a)$$

$$\mathcal{F}^{\text{FS}}(0, y; Q_S) \stackrel{y \rightarrow 0}{\simeq} -2(1 + Q_S) \ln(y) - 3 - 2Q_S \quad \mathcal{G}^{\text{FS}}(0, y; Q_S) \stackrel{y \rightarrow 0}{=} \frac{2 + 3Q_S}{6} \quad (2.10b)$$

$$\mathcal{F}^{\text{FS}}(0, y; Q_S) \stackrel{y \rightarrow \infty}{=} \frac{1 + 2Q_S}{y} \quad \mathcal{G}^{\text{FS}}(0, y; Q_S) \stackrel{y \rightarrow \infty}{=} \frac{1 + 3Q_S}{6y}, \quad (2.10c)$$

and

$$\mathcal{F}^{\text{FV}}(0, y; Q_V) \stackrel{y \rightarrow 1}{=} 2 + 5Q_V \quad \mathcal{G}^{\text{FV}}(0, y; Q_V) \stackrel{y \rightarrow 1}{=} -\frac{13}{12} - \frac{5Q_V}{2} \quad (2.10d)$$

$$\mathcal{F}^{\text{FV}}(0, y; Q_V) \stackrel{y \rightarrow 0}{=} 4 + 8Q_V \quad \mathcal{G}^{\text{FV}}(0, y; Q_V) \stackrel{y \rightarrow 0}{=} -\frac{4 + 9Q_V}{3} \quad (2.10e)$$

$$\mathcal{F}^{\text{FV}}(0, y; Q_V) \stackrel{y \rightarrow \infty}{=} 1 + 2Q_V, \quad \mathcal{G}^{\text{FV}}(0, y; Q_V) \stackrel{y \rightarrow \infty}{=} -\frac{5 + 9Q_V}{6}, \quad (2.10f)$$

<sup>9</sup> In the literature the loop functions are often given for the individual diagrams of Fig. 2.1 instead of the combined contributions in Eq. (2.3). It is straightforward to translate between these results. For example the FFS, FSS, FFV and FVV functions defined in Ref. [9, 12, 190] correspond to setting either  $Q_S = 0$ ,  $Q_F = 0$ , or  $Q_V = 0$  and can be recovered as

$$F_2^C(y) = F(y) = \frac{3}{2} \mathcal{F}^{\text{FS}}(0, y, 0), \quad F_2^N(y) = C(y) = -3 \mathcal{F}^{\text{FS}}(0, y, -1), \quad (2.4)$$

$$F_4^C(y) = \frac{2}{3} C(y) + \frac{y}{3} F(y) = \frac{1}{2} \mathcal{F}^{\text{FV}}(0, y, 0), \quad F_4^N(y) = 2K(y) + \frac{y}{6} C(y) = -\frac{1}{2} \mathcal{F}^{\text{FV}}(0, y, -1). \quad (2.5)$$

Further useful loop functions are obtained by taking differences,

$$F_a(x, y) = -\frac{F_2^C(x) - F_2^C(y)}{3(x-y)}, \quad F_b(x, y) = -\frac{F_2^N(x) - F_2^N(y)}{6(x-y)}. \quad (2.6)$$

<sup>10</sup>In t'Hooft Feynman gauge ( $\xi = 1$ ), the loop functions obtained from Fig. 2.1b are instead given in terms of the definitions in Ref. [9] by  $\mathcal{F}_{\xi=1}^{\text{FV}}(0, y; Q_V) = \frac{4}{3}(1 + Q_V)C(y) + 3Q_V K(y)$  and  $\mathcal{G}_{\xi=1}^{\text{FV}}(0, y; Q_V) = -\frac{(1+Q_V)}{3}M(y) - \frac{Q_V}{6}J(y)$ . The physical result Eq. (2.8) is recovered once the Goldstone boson contributions are added.

and

$$\mathcal{F}^{\text{FSV}}(0, y, 1) \stackrel{y \rightarrow 1}{=} -\frac{1}{2} \qquad \mathcal{G}^{\text{FSV}}(0, y, 1) \stackrel{y \rightarrow 1}{=} \frac{1}{12} \qquad (2.10g)$$

$$\mathcal{F}^{\text{FSV}}(0, y, 1) \stackrel{y \rightarrow 0}{=} -\frac{1}{2} \qquad \mathcal{G}^{\text{FSV}}(0, y, 1) \stackrel{y \rightarrow 0}{=} \frac{1}{3} \qquad (2.10h)$$

$$\mathcal{F}^{\text{FSV}}(0, y, 1) \stackrel{y \rightarrow \infty}{=} -\frac{1}{2}, \qquad \mathcal{G}^{\text{FSV}}(0, y, 1) \stackrel{y \rightarrow \infty}{=} \frac{1}{6y}. \qquad (2.10i)$$

It is worth noting that none of the above functions are singular in the limits  $y, z \rightarrow 1, \infty$  (or  $z \rightarrow y$ ), and only  $\mathcal{F}^{\text{FS}}$  develops a logarithmic enhancement for  $y \rightarrow 0$  in the term proportional to the fermion charge  $Q_F = -1 - Q_S$ . This enhancement is present e.g. in the EWSM Higgs-boson one-loop contribution shown in Fig. 1.7, where the internal muon is much lighter than the internal Higgs boson, however due to the small Yukawa couplings that diagram is nevertheless negligible.

**General expressions of the loop functions** Finally, we list the general results for the loop functions in Eq. (2.3) valid for arbitrary masses of the muon and internal particles. We make use of the following abbreviation

$$\tilde{\Lambda}(x, y, z) \equiv \frac{\sqrt{\lambda(x, y, z)}}{x} \ln \left( \frac{\sqrt{\lambda(x, y, z)} - x + y + z}{2\sqrt{yz}} \right) \qquad (2.11)$$

where  $\lambda(x, y, z) = (x - y - z)^2 - 4yz$  denotes the the Källén function. For the FS-diagrams Fig. 2.1a the loop functions are given by

$$\mathcal{F}^{\text{FS}}(x, y; Q) = \frac{2}{x} + \frac{\ln(y)}{x^2} \left[ 1 + x - y + Qx \right] + \frac{2\tilde{\Lambda}(x, y, 1)}{x\lambda(x, y, 1)} \left[ 1 - 2y + (x - y)^2 + Qx(1 + x - y) \right] \qquad (2.12a)$$

$$\begin{aligned} \mathcal{G}^{\text{FS}}(x, y; Q) = & -\frac{1 + 2Q}{2x} - \frac{1 - y}{x^2} - \frac{\ln(y)}{2x^3} \left[ (1 - y)^2 - yx + Qx(1 - y) \right] \\ & - \frac{\tilde{\Lambda}(x, y, 1)}{x^2\lambda(x, y, 1)} \left[ (1 - y)^3 - x(1 - y)(1 + 2y) - yx^2 + Qx \{ (1 - y)^2 - x(1 + y) \} \right], \end{aligned} \qquad (2.12b)$$

for the FV Fig. 2.1b diagrams by

$$\begin{aligned} \mathcal{F}^{\text{FV}}(x, y; Q) = & 4(1 + Q) - \frac{2(2 + y)}{x} - \frac{\ln(y)}{x^2} \left[ 2 - (x + y) - (x - y)^2 + Qx(2 - x + y) \right] \\ & - \frac{2\tilde{\Lambda}(x, y, 1)}{x\lambda(x, y, 1)} \left[ 2 - 3(x + y) - (x - y)^3 + Qx \{ 2(1 - x) - (x + y) - (x - y)^2 \} \right] \end{aligned} \qquad (2.13a)$$

$$\begin{aligned} \mathcal{G}^{\text{FV}}(x, y; Q) = & -\frac{Q(2 + x + y)}{x} + \frac{y(2 - 3x + 2y) - (2 - x)^2}{2x^2} - \frac{\ln(y)}{2x^3} \left[ 2 - 3(x + y) + y(2x + (x - y)^2) \right] \\ & + Qx \left\{ 2 - 3x - y(1 - x + y) \right\} - \frac{\tilde{\Lambda}(x, y, 1)}{x^2\lambda(x, y, 1)} \left[ 2 - 5x(1 - x) - 5y(1 - y) \right. \\ & \left. - (x - y)^2(2 - y(1 + x - y)) + Qx \left\{ 2(1 - x) - 3(x + y) + 3x^2 + y(x + (x - y)^2) \right\} \right], \end{aligned} \qquad (2.13b)$$

and for the FSV diagrams Fig. 2.1c by

$$\begin{aligned}
\mathcal{F}^{\text{FSV}}(x, y, z) = & \frac{x - y + z^2}{3x(z - 1)} - \frac{2 + 2x + y}{6x} - \frac{(1 - z)\ln(y)}{12x^2} \left[ 2 - 3(x + y) + 2z \right] + \frac{\ln(z)}{12x^2(1 - z)^2} \left[ (x - y)^3(1 + z) \right. \\
& - 3z(x + y)(2x - 2y + 3z - z^2) + 2z^3(2 - z) \left. \right] + \frac{\tilde{\Lambda}(1, \frac{1}{x}, \frac{y}{x})}{6x(1 - z)^2} \left[ (x - y)^2(1 + z) + (x + y)(1 - 5z) + 2(2z - 1) \right] \\
& - \frac{\tilde{\Lambda}(1, \frac{z}{x}, \frac{y}{x})}{6x(1 - z)^2} \left[ (x - y)^2(1 + z) + z(x + y)(z - 5) + 2z^2(2 - z) \right]
\end{aligned} \tag{2.14a}$$

$$\begin{aligned}
\mathcal{G}^{\text{FSV}}(x, y, z) = & -\frac{2 + x - 4y + 2z}{6x^2} - \frac{\ln(y)}{6x^3} \left[ 1 - 3y(1 + x - y + z) + z(1 + z) \right] - \frac{\ln(z)}{6x^3(1 - z)} \left[ (x - y)^3 \right. \\
& \left. - 3yz(x - y + z) + z^3 \right] - \frac{\tilde{\Lambda}(1, \frac{1}{x}, \frac{y}{x})}{3x^2(1 - z)} \left[ (x - y)^2 + 1 + x - 2y \right] + \frac{\tilde{\Lambda}(1, \frac{z}{x}, \frac{y}{x})}{3x^2(1 - z)} \left[ (x - y)^2 + z(x - 2y + z) \right].
\end{aligned} \tag{2.14b}$$

## 2.2. Contributions from minimal extensions of the Standard Model

The one-loop diagrams discussed in the previous section can provide new contributions to  $a_\mu$  from physics beyond the standard model when BSM particles enter these loops. There are many possibilities and some popular BSM theories have many particles that can contribute. Here however we want to consider minimal contributions from a limited number of new fields. The key difference to the generic diagrams considered above is that here each new field is required to have specific quantum numbers under the SM gauge group and gauge invariant interactions. In contrast, the generic Lagrangian in Eq. (2.1) was not required to be gauge invariant by itself and the appearing mass-eigenstate fields could be mixtures of fields with different gauge quantum numbers.

The scenarios considered here represent minimal BSM extensions that give non-trivial effects to  $a_\mu$ , which can be relevant on their own or which can be part of larger theories when only a few particles are light and constitute building blocks for contributions from theories with many new particles. Their understanding provides a useful basis for the general discussion of BSM contributions to  $a_\mu$ .

We therefore systematically categorise the simplest extensions of the standard model that give new physics contributions to the anomalous magnetic moment of the muon. Drawing on similar systematic investigations in the literature [9, 191–196] we focus here on one-field and two-field extensions, defined as BSM scenarios where the SM is extended by exactly one or two new fields that have renormalisable and gauge invariant interactions involving the muon.

In both the one-field and two-field cases only specific gauge quantum numbers of such fields allow couplings to the muon and thus one-loop contributions to  $a_\mu$ . For example, if a single scalar field  $\phi$  is added to the SM, it must be paired with an internal SM fermion to get a contribution via one of the diagrams in Fig. 2.1. Hence at least one of the field combinations  $\phi \mu_L f$  and  $\phi \mu_R f$  must allow a gauge invariant operator, where  $f$  can be any of the SM fermion multiplets  $f \in \{l_{Li}, e_{Ri}, q_{Li}, u_{Ri}, d_{Ri}\}$ , possibly involving hermitian conjugation. Using such arguments leads to Tab. 2.1. This table contains all possibilities for one-field extensions with possible one-loop contributions to  $a_\mu$ . Similar considerations gives Tab. 2.2 containing two-field extensions where two new BSM states of different spins enter the one-loop contributions to muon  $g - 2$ .

To be specific on the considered class of models, we use the following requirements: The added fermions are 4-component Dirac spinors, matching conventions in Ref. [191]. For the one-field models, each proposed new field must have renormalisable and gauge invariant couplings to the muon, together with some other SM field. This excludes models such as a scalar singlet from the table, where the singlet could contribute to  $a_\mu$  via mixing with the SM Higgs doublet.

For the two-field models, we require that both new fields together have direct couplings to the muon and can form a loop without any further SM fields. This excludes models with two different vector-like leptons or so-called bridge models [197] with one vector-like lepton and a scalar singlet. Many models that go beyond the tables will be discussed in later sections.

We first focus on the models with the table entry “Chiral enhancement=No” in Tabs. 2.1 and 2.2. This set includes most one-field models and all two-field models with two fields of different spin. A prominent feature of most of these models is that the sign of the contributions to  $a_\mu$  is fixed to be positive or negative definite, as given in the table in column 4 of Tab. 2.1 and column 3 of Tab. 2.2. In terms of the formulas of the previous subsection 2.1, the reason is that these models allow either only left-handed or only right-handed couplings to the muon, as indicated in column 5 of Tab. 2.1 and column 4 of Tab. 2.2. In such cases with only single chiralities, only the  $|c_{L,R}|^2$ -type terms of Eqs. (2.3) play a role. These terms have essentially a fixed sign which depends on the loop functions and the particle charges as can be seen e.g. in the limits in Eqs. (2.10). Exceptions can arise in models with larger gauge multiplets where several Feynman diagrams with loop functions with different signs and different mass-dependencies can contribute.

For example, the one-field model with a single scalar triplet  $\phi_T$  in line 4 of Tab. 2.1 with quantum numbers  $(1, 3, -1)$  allows only the gauge invariant term  $\phi_T^\dagger l_L l_L$ ; hence it only interacts with left-handed muons. The charges of the appearing physical scalars are  $Q_S = 0, -1, -2$ , and the overall sign of the contribution to  $a_\mu$  is always negative. Similarly, the one-field model 20 is a spin-1 leptoquark which couples to the right-handed muon and to right-handed up-type quarks. The relevant vector boson charge is  $Q_V = -5/3$ , and in line with Eq. (2.10) the contribution to  $a_\mu$  is positive. For all two-field models with two fields of different spin, the situation is the same. Whatever the quantum numbers of the new states are, at most either the coupling to the left-handed muon or to the right-handed muon can be gauge invariant, but not both. As a result in most cases the sign of the contribution to  $a_\mu$  is fixed.

Such models where there are only gauge invariant couplings to either left- or right-handed muons cannot have muon  $g - 2$  contributions with a chiral enhancement by a factor  $m_F/m_\mu$ , since the muon chirality must be the same at each vertex. However, assuming flavour conserving couplings, there are also several examples which can couple to both but still do not get the chiral enhancement. For example Model 16 adds a new gauge boson that can have couplings to both left- and right-handed muons (as indicated in the gauge invariant muon interactions column of Table 2.2), but the only possibility for flipping the chirality is through a muon mass insertion which therefore does not lead to a chiral enhancement, even if it is done at an internal line. Another case is given by e.g. model 3 where we have a second scalar doublet that can have Yukawa couplings connecting left- and right-handed muons (written as L-R in the respective column). This Yukawa coupling does flip the chirality, but since Yukawa coupling must appear at both vertices one has an even number of chirality flips. Thus there is no net change in chirality from the one-loop diagram and no chiral enhancement at one-loop order.

Thus for the models with only single muon chiralities as well as the exceptional additional models without chiral enhancement discussed above the magnitude of the muon  $g - 2$  contributions are rather limited. For all models with the table entry “Chiral enhancement=No”, the contributions to  $a_\mu$  are of the order

$$\Delta a_\mu \sim \frac{|c|^2(1 + 2Q_S)}{192\pi^2} \frac{m_\mu^2}{M^2} \sim \frac{|c|^2}{64\pi^2} \frac{m_\mu^2}{M^2} \approx |c|^2 \left( \frac{100 \text{ GeV}}{M} \right)^2 \times 18 \times 10^{-10}, \quad (2.15)$$

where the FS-type result Eq. (2.3a) in the equal-mass limit of Eq. (2.10) has been used as a reference; in the second equation  $Q_S = 1$  has been used as an example to obtain a numerical estimate of the typical magnitude of the contribution. Note that the charges can be negative, where  $Q_F + Q_S = -1$ , so the sign of the contributions depends on the values of

Model	Spin	$SU(3)_c \times SU(2)_L \times U(1)_Y$	$\text{Sign}(\Delta a_\mu^{\text{BSM}})$	Muon interactions	Chiral enhancement?
1	0	$(\mathbf{1}, \mathbf{1}, 1)$	-	L	No
2	0	$(\mathbf{1}, \mathbf{1}, 2)$	-	R	No
3	0	$(\mathbf{1}, \mathbf{2}, -1/2)$	$\pm$	L-R	only with FV
4	0	$(\mathbf{1}, \mathbf{3}, -1)$	-	L	No
5	0	$(\bar{\mathbf{3}}, \mathbf{1}, 1/3)$	$\pm$	L and R	Yes
6	0	$(\bar{\mathbf{3}}, \mathbf{1}, 4/3)$	-	R	No
7	0	$(\bar{\mathbf{3}}, \mathbf{3}, 1/3)$	+	L	No
8	0	$(\mathbf{3}, \mathbf{2}, 7/6)$	$\pm$	L and R	Yes
9	0	$(\mathbf{3}, \mathbf{2}, 1/6)$	-	L	No
10	1/2	$(\mathbf{1}, \mathbf{1}, 0)$	-	L	No
11	1/2	$(\mathbf{1}, \mathbf{1}, -1)$	$\pm$	L	No
12	1/2	$(\mathbf{1}, \mathbf{2}, -1/2)$	+	R	No
13	1/2	$(\mathbf{1}, \mathbf{2}, -3/2)$	-	R	No
14	1/2	$(\mathbf{1}, \mathbf{3}, 0)$	-	L	No
15	1/2	$(\mathbf{1}, \mathbf{3}, -1)$	-	L	No
16	1	$(\mathbf{1}, \mathbf{1}, 0)$	$\pm$	L and R	only with FV
17	1	$(\mathbf{1}, \mathbf{2}, -3/2)$	+	L-R	only with FV
18	1	$(\mathbf{1}, \mathbf{3}, 0)$	+	L	No
19	1	$(\bar{\mathbf{3}}, \mathbf{1}, -2/3)$	$\pm$	L and R	Yes
20	1	$(\bar{\mathbf{3}}, \mathbf{1}, -5/3)$	+	R	No
21	1	$(\bar{\mathbf{3}}, \mathbf{2}, 5/6)$	$\pm$	L and R	Yes
22	1	$(\bar{\mathbf{3}}, \mathbf{2}, -1/6)$	-	L	No
23	1	$(\bar{\mathbf{3}}, \mathbf{3}, -2/3)$	+	L	No

**Table 2.1:** Gauge invariant single field extensions with one-loop contributions to the anomalous magnetic moment of the muon. Column two specifies the spin of the state where we consider spin 0, 1/2 and 1. Column three specifies the representations under SM gauge groups  $SU(3)_c$  and  $SU(2)_L$  and the hypercharge. The fourth column shows the sign of the one-loop contribution to  $a_\mu$ , while the fifth column shows which kind of gauge invariant and renormalisable couplings to the muon are possible: “L”, “R” denote couplings to the left-handed or right-handed muon (and some other unspecified SM field), respectively, and “L-R” denotes a Lagrangian term involving a product of left- and right-handed muon. The sixth column states whether there is a chirality flipping enhancement in the one-loop diagrams allowing large new physics contributions to  $a_\mu$ . Special cases where a chirality enhancement at one-loop is only possible by introducing lepton flavour violating couplings are marked as “only with FV”. Note these models were originally grouped together in [9] which itself drew upon previous systematic investigations and classifications in Ref. [191–194].

Model	$(SU(3)_c \times SU(2)_L \times U(1)_Y)_{\text{spin}}$	$\text{sign}(\Delta a_\mu^{\text{BSM}})$	Muon interactions	Chiral enhancement?
24	$(\mathbf{1}, \mathbf{1}, 0)_0 - (\mathbf{1}, \mathbf{1}, -1)_{1/2}$	+	R	No
25	$(\mathbf{1}, \mathbf{1}, -1)_0 - (\mathbf{1}, \mathbf{1}, 0)_{1/2}$	-	R	No
26	$(\mathbf{1}, \mathbf{2}, -1/2)_0 - (\mathbf{1}, \mathbf{1}, 0)_{1/2}$	-	L	No
27	$(\mathbf{1}, \mathbf{1}, 0)_0 - (\mathbf{1}, \mathbf{2}, -1/2)_{1/2}$	+	L	No
28	$(\mathbf{1}, \mathbf{2}, -1/2)_0 - (\mathbf{1}, \mathbf{1}, -1)_{1/2}$	+	L	No
29	$(\mathbf{1}, \mathbf{1}, -1)_0 - (\mathbf{1}, \mathbf{2}, 1/2)_{1/2}$	-	L	No
30	$(\mathbf{1}, \mathbf{2}, -1/2)_0 - (\mathbf{1}, \mathbf{2}, -1/2)_{1/2}$	$\text{sign}(M_S - M_F)$	R	No
31	$(\mathbf{1}, \mathbf{2}, 1/2)_0 - (\mathbf{1}, \mathbf{3}, 0)_{1/2}$	+	L	No
32	$(\mathbf{1}, \mathbf{2}, 1/2)_0 - (\mathbf{1}, \mathbf{3}, -1)_{1/2}$	+	L	No
33	$(\mathbf{1}, \mathbf{3}, 0)_0 - (\mathbf{1}, \mathbf{2}, -1/2)_{1/2}$	-	L	No
34	$(\mathbf{1}, \mathbf{3}, 0)_0 - (\mathbf{1}, \mathbf{3}, -1)_{1/2}$	+	R	No
35	$(\mathbf{1}, \mathbf{3}, 1)_0 - (\mathbf{1}, \mathbf{2}, -1/2)_{1/2}$	-	L	No
36	$(\mathbf{1}, \mathbf{3}, -1)_0 - (\mathbf{1}, \mathbf{3}, 0)_{1/2}$	-	R	No
37	$(\mathbf{1}, \mathbf{3}, -1)_0 - (\mathbf{1}, \mathbf{2}, -3/2)_{1/2}$	+	L	No
38	$(\mathbf{1}, \mathbf{2}, -3/2)_0 - (\mathbf{1}, \mathbf{3}, 1)_{1/2}$	-	L	No
39	$(\mathbf{1}, \mathbf{2}, -3/2)_0 - (\mathbf{1}, \mathbf{2}, 1/2)_{1/2}$	-	R	No
40	$(\mathbf{1}, \mathbf{2}, 1/2)_0 - (\mathbf{1}, \mathbf{2}, -3/2)_{1/2}$	+	R	No
41	$(\mathbf{1}, \mathbf{3}, -2)_0 - (\mathbf{1}, \mathbf{3}, 1)_{1/2}$	-	R	No
42	$(\mathbf{1}, \mathbf{3}, 1)_0 - (\mathbf{1}, \mathbf{3}, -2)_{1/2}$	+	R	No
43	$(\mathbf{1}, \mathbf{1}, -1)_{1/2} - (\mathbf{1}, \mathbf{1}, 0)_1$	-	R	No
44	$(\mathbf{1}, \mathbf{2}, -1/2)_{1/2} - (\mathbf{1}, \mathbf{1}, 0)_1$	-	L	No
45	$(\mathbf{1}, \mathbf{2}, -1/2)_{1/2} - (\mathbf{1}, \mathbf{3}, 0)_1$	+	L	No
46	$(\mathbf{1}, \mathbf{1}, 0)_{1/2} - (\mathbf{1}, \mathbf{1}, 1)_1$	+	R	No
47	$(\mathbf{1}, \mathbf{2}, -1/2)_{1/2} - (\mathbf{1}, \mathbf{1}, -1)_1$	+	L	No
48	$(\mathbf{1}, \mathbf{3}, -1)_{1/2} - (\mathbf{1}, \mathbf{3}, 0)_1$	-	R	No

**Table 2.2:** Gauge invariant two-field extensions with one-loop contributions to the anomalous magnetic moment of the muon where both new fields enter the loop diagrams. Column two shows the representations under SM gauge groups  $SU(3)_c$  and  $SU(2)_L$  and the hypercharge of each state inside brackets and the spin of the states is shown as the subscript. Column three shows the sign of the one-loop contribution to  $a_\mu$ , while the fourth column shows which kind of gauge invariant couplings to the muon are possible: “L”, “R” denote couplings to the left-handed or right-handed muon, respectively. The fifth and final column states whether there is a chirality flipping enhancement in the one-loop diagrams allowing large new physics contributions to  $a_\mu$ . Note most of these models were originally grouped together in [9] which itself drew upon previous systematic investigations and classifications in Ref. [191, 195, 196].

the particle charges appearing in the loop. This illustrates how the different sign predictions visible in the tables emerge.

This result allows a general understanding of the  $a_\mu$  phenomenology which applies to many of the one- and two-field models. If the BSM masses are sufficiently heavy,  $M \gtrsim 200$  GeV, and couplings at most  $\mathcal{O}(1)$ , the contributions to  $a_\mu$  are typically smaller than  $\sim 5 \times 10^{-10}$  and hence in agreement with the new result  $\Delta a_\mu^{\text{Exp-WP2025}}$ . Previously, such scenarios could not explain the large deviation  $\Delta a_\mu^{\text{Exp-WP2020}}$ . Now, because of the automatic agreement such scenarios are not nontrivially constrained by  $a_\mu$ .

For smaller masses, the models can potentially contribute sizeably to  $a_\mu$  but are also constrained by complementary limits e.g. from collider searches. Such complementary limits are very model dependent. For example, leptoquarks as light as  $100 \dots 200$  GeV are strongly excluded, while a light neutral boson can be viable. If complementary constraints allow light masses, the models can be constrained by  $a_\mu$ .

Here the new result changes the conclusions significantly. Previously,  $\Delta a_\mu^{\text{Exp-WP2020}}$  preferred a non-zero positive result, which excludes many models and forces models with positive contributions into parameter regions with small masses and rather large couplings. Now,  $\Delta a_\mu^{\text{Exp-WP2025}}$  is compatible with positive or negative  $\Delta a_\mu$  contributions. However the contributions must be sufficiently small, resulting in upper limits on couplings in such models.

These remarks will be refined for specific models in later sections. Here we highlight two special classes of models. First, there is a class of models with only electrically and colour neutral BSM particles. Within the minimal models considered here, these are in particular the one-field models with gauge quantum number  $(\mathbf{1}, \mathbf{1}, 0)$  such as a  $Z'$ , dark photon or neutral scalar. Such new particles easily evade collider limits and hence can be rather light. They could be part of a dark sector and related to dark matter. Due to their lightness,  $a_\mu$  can place significant constraints on their parameter space. Such light dark sector particles are the subject of Sec. 5.1. Similarly, there are certain two-field models where compressed spectra provide more challenging scenarios for the LHC, allowing gaps in the exclusion at lower masses. Thus special scenarios may be found where larger  $\Delta a_\mu$  contributions generated by light masses are not ruled out. Again, such models are also interesting in view of dark matter, and a more detailed discussion will be given in Sec. 3.6.

Second, the one-field model 3 corresponds to the two-Higgs doublet model, where very important two-loop Barr-Zee diagrams can dominate the  $\Delta a_\mu$  contributions and strongly alter the one-loop discussion here. Such two-loop diagrams will be discussed in Sec. 4.2, and the resulting phenomenology of the two-Higgs doublet model will be discussed in Sec. 5.3.

Finally we discuss the models with chiral enhancement, i.e. models where the  $m_F/m_\mu$ -terms in Eq. (2.3) can contribute. As is clear from the previous discussion and visible in the tables, a necessary condition for such an enhancement is the existence of gauge invariant couplings both to left-handed muons and to right-handed muons. The crucial common feature of all these chirally enhanced contributions is that not two, but three different gauge multiplets appear inside the loop contributing to  $a_\mu$ .

Since the mechanism of chiral enhancements and the models with chiral enhancements are of particular importance, the following subsection 2.3 is devoted to an analysis of generic 3-field models representing minimal models with chiral enhancements, and Sec. 5 contains detailed discussions of concrete important models. Here we briefly explain how one- and two-field models can combine with SM fields to get three gauge multiplets in the loop.

Indeed, in the one-field case most models with chiral enhancement are leptoquark models where the leptoquark couples left-handed muons to quarks of one chirality and right-handed muons to quarks of the opposite chirality. Then, in the  $a_\mu$  Feynman diagrams of Fig. 2.1 the internal fermion is a quark and the chirality can be flipped from a left-handed to a right-handed quark. The three relevant fields are therefore the single BSM leptoquark and two SM multiplets, a

quark singlet and a quark doublet. In addition to the leptoquark examples there are also special cases where the factor  $m_F/m_\mu$  is only large when the new BSM state has lepton flavour-violating couplings, allowing the internal lepton to be the  $\tau$ -lepton. These exceptions are model 3 which can be interpreted as the two-Higgs doublet model, model 16 which can be interpreted as a  $Z'$  model, and model 17 which could be embedded in a 331 model [198].

Though excluded from our Table 2.2, there are classes of two-field models which allow chiral enhancements. Examples are models with two different new vector-like fermions which can combine e.g. with the SM Higgs field in a one-loop diagram. Such models will be discussed later in Sec. 5.5 and Eq. (5.111) provides a complete list. Another type of examples are bridge models [197] where one vector-like lepton and a scalar can combine e.g. with a SM lepton to give a one-loop contribution to  $a_\mu$ .

In general we see that extending the SM by only one or two fields typically leads to small contributions to muon  $g-2$ , though we have highlighted special cases where they can be larger and are thus constrained by  $\Delta a_\mu^{\text{Exp-WP2025}}$ . In the next sections we will show that when we consider extensions with three BSM fields, many more models with an internal chirality flip are possible allowing a much wider variation in the size of the contributions.

### 2.3. Three-field extensions with chiral enhancements and mass-insertion approximations

We now focus in detail on a set of simple and generic models which lead to chirally enhanced contributions to  $a_\mu$ . The key point is that the potential chiral enhancement via the  $m_F$ -terms in the generic formulas (2.3) requires a chirality flip on one of the internal lines in the one-loop diagrams. It must correspond to an additional source of chiral symmetry breaking besides  $m_\mu$  as discussed in Sec. 1.1.4 and illustrated in Eqs. (1.10) and (1.15). To achieve this within a minimal setup, three distinct gauge-eigenstate fields are needed that allow for additional gauge invariant couplings to the left- and right-handed muons as well as to the SM Higgs.

The models with chiral enhancements discussed in Sec. 2.2 combine one BSM field with two SM fields, and later in Sec. 5.5 we will discuss models where one SM field and two BSM fields are combined to give chiral enhancements. The generic models discussed here illustrate such cases, but they also cover the case of three BSM fields. This last case of 3-field models represents a wide class of very important BSM scenarios in a simplified and generic way. Here we specifically focus on models with either two new fermions and one additional scalar or one new fermion and two additional scalars, which have often been used to illustrate the generic behaviour in scenarios with chiral enhancement [195, 196, 199–202].

We essentially follow the conventions of Refs. [199, 200] and introduce three classes of 3-field models. Class I and II contain two new Dirac fermions  $\psi$  and  $\chi$  and one scalar field  $\phi$ , while Class III instead contains a single new Dirac fermion  $\psi$  and two scalar fields  $\phi$  and  $\eta$ <sup>11</sup>. Both Dirac fermions are formed from left-handed and right-handed fields of equal gauge quantum numbers, such that explicit Dirac masses, denoted by  $m_\psi$  and  $m_\chi$ , are allowed by gauge invariance. Similarly, the scalar masses are written as  $m_\phi$  and  $m_\eta$ . The interaction Lagrangians connecting the new fields to the SM

---

<sup>11</sup>In the literature, Class I and III correspond to FLR and SLR of Ref. [196], Class II and III were considered in Refs. [199, 200], the other references cited above consider very similar models corresponding to combinations of the classes, and Ref. [195] also considers additional simple models. Similar models are also studied in Ref. [203], and several of the references also study dark matter in the context of these models. We note that the same kind of three-field models can also be used as a starting point to discuss the constraints of asymptotic safety on values of couplings and the magnitude of contributions to  $a_\mu$ , and corresponding results are obtained in Refs. [204–206]

are defined as<sup>12</sup>

$$\text{Class I: } \quad \mathcal{L} \supset -\lambda_L \bar{l}_L \psi_R \phi^\dagger - \lambda_R \bar{\chi}_L \mu_R \phi - \lambda_\Phi \bar{\psi}_R \chi_L \Phi + h.c., \quad (2.16a)$$

$$\text{Class II: } \quad \mathcal{L} \supset -\lambda_L \bar{l}_L \psi_R \phi^\dagger - \lambda_R \bar{\chi}_L \mu_R \phi - \bar{\lambda}_\Phi \bar{\psi}_L \chi_R \Phi + h.c., \quad (2.16b)$$

$$\text{Class III: } \quad \mathcal{L} \supset -\lambda_L \bar{l}_L \psi_R \phi^\dagger - \lambda_R \bar{\psi}_L \mu_R \eta - a_\Phi \eta^\dagger \Phi \phi + h.c., \quad (2.16c)$$

where  $l_L, \mu_R$  and  $\Phi$  denote the left-/right-handed muon and Higgs fields respectively (cf. [Appendix A](#)) and we have used 4-spinor notation for the fermion fields. In order to ensure  $U(1)_Y$  invariance the hypercharges of the Class I/II fields  $(\phi^\dagger, \psi, \chi)$  and Class III fields  $(\psi, \phi^\dagger, \eta^\dagger)$  need to be of the form  $Y = (X, -\frac{1}{2} - X, -1 - X)$ , where  $X$  can be an arbitrary constant. Possible  $SU(2)_L$  quantum number assignments of  $(\psi, \phi^\dagger, \eta^\dagger)$  and  $(\phi^\dagger, \psi, \chi)$  include the combinations  $(\mathbf{1}, \mathbf{2}, \mathbf{1})$ ,  $(\mathbf{2}, \mathbf{1}, \mathbf{2})$ ,  $(\mathbf{2}, \mathbf{3}, \mathbf{2})$ ,  $(\mathbf{3}, \mathbf{2}, \mathbf{3})$ , (where  $\mathbf{1}, \mathbf{2}, \mathbf{3}$  denote singlets, doublets and triplets). Note that the  $SU(2)_L$  contractions in Eq. (2.16) have been suppressed but are, in general, non-trivial in order to ensure gauge invariance. For further details and more explicit Lagrangians see e.g. Refs. [195, 196, 202]. To be definite, we focus on the  $(\mathbf{1}, \mathbf{2}, \mathbf{1})$  case for the explicit calculations and refer to the literature for further results. The  $SU(3)_c$  representations are left implicit, i.e. the new fields may also carry appropriate colour charges.

In each model class,  $\lambda_{L,R}$  are Yukawa couplings of the the new fields to the left-/right-handed muons, and the coupling of the new fields to the SM Higgs is denoted either by  $\lambda_\Phi$  and  $\bar{\lambda}_\Phi$  in case of two fermions or by the dimensionful coupling  $a_\Phi$  in case of two new scalars. The difference between Class I and II is the chirality of the fermions interacting with the Higgs field. In Class I, only  $\psi_R$  and  $\chi_L$  interact with the muon and the Higgs, whereas  $\psi_L$  and  $\chi_R$  only have gauge interactions that play no role for the current discussion. In Class II the muon interactions are unchanged, but the opposite chiralities of the new fields  $\psi_L$  and  $\chi_R$  interact with the Higgs. Although the chirality is different, in both Class I and II the third term implies a mass mixing between  $\psi$  and  $\chi$  after EWSB. Similarly in Class III a mass mixing between the scalars is induced by their coupling to the Higgs boson.

As mentioned in the beginning, the chirally enhanced models in Tab. 2.1 are connected to the classes introduced above by identifying two of the fields  $\psi, \chi, \phi$  and  $\eta$  with SM fields. For example, the 1-field leptoquark models 5 and 8 discussed in Sec. 5.4 correspond to Class I where the fermions  $\psi_R$  and  $\chi_L$  are identified with the SM quark singlets and doublets while  $\phi$  constitutes the leptoquark. Similarly, the two-Higgs doublet model (model 3 in Tab. 2.1) is recovered from Class I identifying  $\psi_R$  and  $\chi_L$  with the lepton singlets and doublets (and dropping the Dirac masses) and  $\phi$  with the second Higgs doublet. In this case the parameter  $\lambda_\Phi$  corresponds to a lepton Yukawa coupling and is thus  $\propto m_l$ , such that chiral enhancement is present if the fermions are identified with the  $\tau$  and the Yukawa couplings to  $\phi$  are lepton-flavour violating. For a detailed discussion of the 2HDM see Sec. 5.3. The 1-field models with a BSM spin-1 particle and chiral enhancements appearing in Tab. 2.1 have no correspondence to the 3-field models considered here, but their behaviour is similar and has been discussed in the literature (see in particular Ref. [194]). Furthermore, many 2-field models with chiral enhancement, like the vector-like leptons discussed in Sec. 5.5, also correspond to special cases of the Class I, II or III models.

We will now analyse the models and exhibit their essential new features related to  $a_\mu$ , chirality flips and the impact of mixing in several complementary ways. We will begin with the mass-insertion approximation method and connect it to the discussion of chirality flips of Sec. 1.1.4, then we describe the explicit calculation of  $a_\mu$  via results of Sec. 2.1.

The mass-insertion approximation method (M.I.A.) is a generally useful tool to obtain insight into the behaviour

---

<sup>12</sup>For simplicity we assume all couplings to be real.

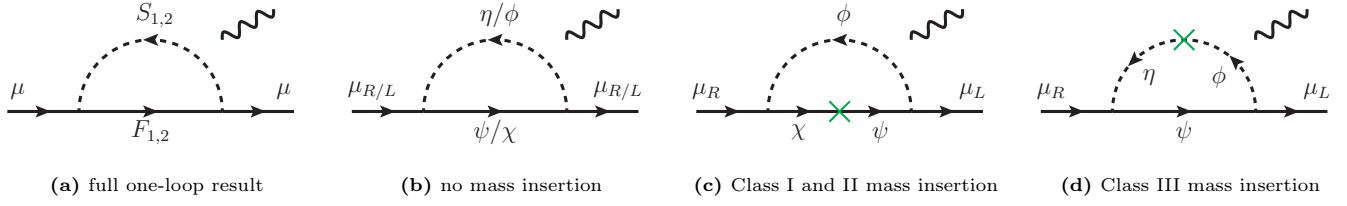


**Figure 2.3:** Diagrams generating  $\Delta a_\mu$  at one-loop in Class I, II and III. Diagram (a) corresponds to the full calculation in the mass-basis, (b) to the zero-order mass-insertion and diagrams (c) and (d) to the single mass-insertion in Class I/II and III, respectively.

of Feynman diagrams in case of mixing. It allows to qualitatively understand the dominant parameter dependences, and can also be used for quantitatively accurate computations, see e.g. Refs. [5, 207–209]. Its main idea is to treat bilinear Lagrangian terms which mix different fields and are  $\propto v$  as small interaction terms giving bilinear vertices in Feynman diagrams. In the models considered here, the  $\lambda_\Phi v$ -,  $\bar{\lambda}_\Phi v$ - and the  $a_\Phi v$ -terms arising after inserting the Higgs  $vev$   $\langle \Phi \rangle = (0, v/\sqrt{2})^T$  into the Lagrangian, are of this kind.

In general, these bilinear terms from couplings to the Higgs  $vev$  give rise to mass mixing between the fields. For example, in the  $(\mathbf{1}, \mathbf{2}, \mathbf{1})$  representation the mass matrices for the gauge-eigenstate fields are given by

$$\text{Class I: } \begin{array}{c} \psi_{2R} \quad \chi_R \\ \overline{\psi_{2L}} \begin{pmatrix} m_\psi & 0 \\ \lambda_\Phi \frac{v}{\sqrt{2}} & m_\chi \end{pmatrix} \\ \overline{\chi_L} \end{array} \quad \text{Class II: } \begin{array}{c} \psi_{2R} \quad \chi_R \\ \overline{\psi_{2L}} \begin{pmatrix} m_\psi & \bar{\lambda}_\Phi \frac{v}{\sqrt{2}} \\ 0 & m_\chi \end{pmatrix} \\ \overline{\chi_L} \end{array} \quad \text{Class III: } \begin{array}{c} \phi_2 \quad \eta \\ \phi_2^\dagger \begin{pmatrix} m_\phi^2 & a_\Phi \frac{v}{\sqrt{2}} \\ a_\Phi \frac{v}{\sqrt{2}} & m_\chi \end{pmatrix} \\ \eta^\dagger \end{array}, \quad (2.17)$$

where  $\psi_2$  and  $\phi_2$  denote the lower-components of the respective doublets.

Fig. 2.3 compares the full diagram with several mass-insertion diagrams where either zero or one of the off-diagonal entries are inserted as a bilinear vertex. The mass-insertion diagrams thus correspond to a Taylor expansion in  $v$ ; the exact result would be obtained by resumming diagrams with any number of insertions, however often the leading contributions are sufficient. In this way one can avoid explicitly diagonalising the mass matrices and obtain a useful analytic approximation of the main behaviour.

The zeroth-order M.I.A. diagram Fig. 2.3b is present in all three classes. It can only contain two out of the three fields of each class and thus behaves like the one- or two-field models without chiral enhancement discussed in the previous subsection. These diagrams contribute to  $a_\mu$  only via the non-enhanced  $|c_{L,R}|^2$ -terms in Eq. (2.3a), and the magnitude of this contribution can hence be estimated as (cf. Eq. (2.15))

$$|\Delta a_\mu^{\text{no insertion}}| \sim \frac{|\lambda_{L,R}|^2 m_\mu^2}{64\pi^2 M^2}, \quad (2.18)$$

where  $M$  is the typical mass scale of the particles in the loop.

The diagrams 2.3c and 2.3d with single mass insertions are the crucial new contribution present in the three-field models. They involve all three of the new couplings, resulting in a chirality flip inside of the loop. A straightforward estimate based on the structure of the diagrams gives

$$|\Delta a_\mu^{\text{one insertion}}| \sim \frac{\lambda_L \lambda_R}{16\pi^2} \frac{m_\mu v}{\sqrt{2} M^2} \left\{ \lambda_\Phi, \bar{\lambda}_\Phi \frac{m_\psi m_\chi}{M^2}, \frac{m_\psi a_\Phi}{M^2} \right\}. \quad (2.19)$$

for Class I, II and III respectively. Here the coupling factors in the numerator correspond to the three vertices of the diagrams. The different powers of the internal fermion masses arise because the numerator of each fermion propagator (each of the form  $(\not{k} + m)$ ) is sandwiched between specific combinations of the projectors  $P_{L/R}$ , the factor  $v/\sqrt{2}$  comes

from the mass insertions and the muon mass  $m_\mu$  stems from the definition of  $a_\mu$ . The mass in the denominator is then fixed by the dimensionality and again corresponds to the typical mass scale of the loop.

It is instructive to relate these explicit results to the generic discussion of chirality flips and gauge invariance in Sec. 1.1.4. First, the single mass insertions in Fig. 2.3 correspond to the coupling to the EWSB  $vev$  in Fig. 1.1 (right) and to the “(EWSB  $vev$ )” factor in Eq. (1.15). Since we assume the additional scalars to not develop vacuum expectation values, the only relevant  $vev$  is the one of the SM Higgs. Diagrams with several mass insertions would correspond to terms of higher power in the mixing and to higher-order corrections to formulas such as Eq. (1.15).

As a second connection, the different combinations of couplings appearing in Eq. (2.19) can be understood in terms of new sources of (muon) chiral symmetry breaking present in these models. The chiral transformation of Eq. (1.12) may be extended to the new fields as

$$\psi_{L/R} \rightarrow e^{-i\mathcal{C}_{L/R}^\psi \alpha} \psi_{L/R}, \quad \chi_{L/R} \rightarrow e^{-i\mathcal{C}_{L/R}^\chi \alpha} \chi_{L/R}, \quad \phi \rightarrow e^{-i\mathcal{C}_\phi \alpha} \phi, \quad \text{and} \quad \eta \rightarrow e^{-i\mathcal{C}_\eta \alpha} \eta \quad (2.20)$$

with initially unspecified chiral charges  $\mathcal{C}_i$  for the new fields. These transformations would leave the Lagrangians in Eq. (2.16) invariant if the following equations

$$\text{Class I/II: } 0 = \begin{cases} 1 + \mathcal{C}_\phi - \mathcal{C}_R^\psi \\ 1 + \mathcal{C}_L^\chi - \mathcal{C}_\phi \\ \mathcal{C}_{R/L}^\psi - \mathcal{C}_{L/R}^\chi \end{cases}, \quad \text{Class III: } 0 = \begin{cases} 1 + \mathcal{C}_\phi - \mathcal{C}_R^\psi \\ 1 + \mathcal{C}_L^\psi - \mathcal{C}_\eta \\ \mathcal{C}_\eta - \mathcal{C}_\phi \end{cases} \quad (2.21)$$

could hold. However, in Class I there is no simultaneous solution, and in Class II and III the only possible solutions require  $\mathcal{C}_L^{\psi,\chi} \neq \mathcal{C}_R^{\psi,\chi}$ . The latter inequality is then inconsistent with the invariance of the Dirac mass terms in the respective models. Note however that dropping any one of the equations does yield consistent solutions in all three classes. Consequently, this implies that the order parameters of chiral symmetry breaking in Class I, II and III respectively are the following specific combinations,

$$\lambda_L \lambda_\Phi \lambda_R, \quad \lambda_L \bar{\lambda}_\Phi \lambda_R m_\psi m_\chi, \quad \text{and} \quad \lambda_L \lambda_R a_\Phi m_\psi. \quad (2.22)$$

It is precisely those combinations that appear in Eq. (2.19) and lead to the chiral enhancement.<sup>13</sup> In this way they represent an explicit realisation of the “(chirality flipping parameters)” in Eqs. (1.14) and (1.15), while the “(other factors)” here correspond to the  $1/16\pi^2$  loop suppression as well as group factors depending on the specific representations. The essential relative chiral enhancement between Eq. (2.18) and the single-insertion diagrams is (assuming  $\lambda_L \sim \lambda_R$  and  $m_\psi, m_\chi \sim M$ )

$$\frac{|\Delta a_\mu^{\text{one insertion}}|}{|\Delta a_\mu^{\text{no insertion}}|} \sim \frac{v}{m_\mu} \left\{ \lambda_\Phi, \bar{\lambda}_\Phi, \frac{a_\Phi}{m_\psi} \right\}. \quad (2.23)$$

As mentioned in Sec. 2.1, the true chiral enhancement is therefore not just the factor  $m_F/m_\mu$  as might have been guessed from the formulas in Eq. (2.3), but the behaviour is more complicated due to the presence of mixing.

<sup>13</sup> Some of the additional models of Ref. [195] provide an interesting negative illustration of chiral symmetry breaking as a prerequisite for large chiral enhancements. While e.g. their Models 3 or 9 are similar to our Classes I, II and lead to chiral enhancements, their Model 6 does not. Model 6 corresponds to combination of Class I and Class II but with a crucial modification where the replacement  $\lambda_L \bar{l}_L \phi^\dagger \psi_R \rightarrow \lambda_L \bar{l}_L \phi \psi_R$  is applied to the Lagrangian. After this difference, the Lagrangian always is chirally symmetric under  $\mu_R \rightarrow e^{i\alpha} \mu_R$ ,  $l_L \rightarrow e^{-i\alpha} l_L$ , and  $\phi \rightarrow e^{-i\alpha} \phi$ . Hence, the product of the couplings  $\lambda_L \lambda_R \lambda_\Phi$  in this case would not break chiral symmetry and could not contribute to  $a_\mu$ , as also pointed out in Ref. [195].

With this qualitative understanding we now proceed with the exact computation of the one-loop contributions to  $a_\mu$  in the model and elucidate how it reproduces the above estimates. Although the calculations proceed similarly for all representations, we again take  $(\mathbf{1}, \mathbf{2}, \mathbf{1})$  as the explicit example. To calculate the full diagram in Fig. 2.3 and employ the generic one-loop formulas (2.3), we first introduce the mass-basis fields  $F_i$  and  $S_i$  in the different classes as

$$\text{Class I/II: } \begin{pmatrix} F_1 \\ F_2 \end{pmatrix}_{L/R} = \begin{pmatrix} \cos \theta_{L/R} & -\sin \theta_{L/R} \\ \sin \theta_{L/R} & \cos \theta_{L/R} \end{pmatrix} \begin{pmatrix} \psi_2 \\ \chi \end{pmatrix}_{L/R}, \quad S = \phi, \quad (2.24a)$$

$$\text{Class III: } \begin{pmatrix} S_1 \\ S_2 \end{pmatrix} = \begin{pmatrix} \cos \theta & -\sin \theta \\ \sin \theta & \cos \theta \end{pmatrix} \begin{pmatrix} \phi_2 \\ \eta \end{pmatrix}, \quad F = \psi, \quad (2.24b)$$

where the rotation matrices are chosen to diagonalise the mass matrices (2.17), such that the corresponding terms in the Lagrangians become

$$\text{Class I/II: } \mathcal{L} \supset -m_1 \bar{F}_1 F_1 - m_2 \bar{F}_2 F_2 - m_\phi^2 |S|^2, \quad (2.25)$$

$$\text{Class III: } \mathcal{L} \supset -m_1^2 |S_1|^2 - m_2^2 |S_2|^2 - m_\psi \bar{F} F. \quad (2.26)$$

In Class I and II two independent transformations of the left- and right-handed fields with mixing angle  $\theta_{L,R}$  are required and fulfil the following useful relation [200]

$$\sin \theta_L \cos \theta_R = \cos \theta_L \sin \theta_R \left\{ \frac{m_1}{m_2}, \frac{m_2}{m_1} \right\} = \frac{1}{m_2^2 - m_1^2} \frac{v}{\sqrt{2}} \left\{ m_1 \lambda_\Phi, m_2 \bar{\lambda}_\Phi \right\}. \quad (2.27)$$

In Class III only a single mixing angle is required which also fulfils a similar relation

$$\sin \theta \cos \theta = \frac{a_\Phi v}{\sqrt{2}(m_2^2 - m_1^2)}. \quad (2.28)$$

The scalar mass-eigenstate(s) coupling to the muon in Class I and II (Class III) have the electric charge  $Q_S = X$  ( $Q_S = -1 - X$ ), and the relevant products of mass-basis Yukawa couplings appearing in Eq. (2.3a) are given by

$$\text{Class I/II: } \begin{cases} F_1 : & c_L^* c_R = -\lambda_L \lambda_R \sin \theta_L \cos \theta_R \\ F_2 : & c_L^* c_R = +\lambda_L \lambda_R \sin \theta_R \cos \theta_L \end{cases} \quad \text{Class III: } \begin{cases} S_1 : & c_L^* c_R = -\lambda_L \lambda_R \sin \theta \cos \theta \\ S_2 : & c_L^* c_R = +\lambda_L \lambda_L \sin \theta \cos \theta. \end{cases} \quad (2.29)$$

Similar expressions hold for the non-enhanced  $|c_{L/R}|^2$  terms which we neglect for the discussion here. With this, the enhanced contributions to  $\Delta a_\mu$  read

$$\text{Class I: } \Delta a_\mu^{\text{enhanced}} = \frac{\lambda_L \lambda_R}{16\pi^2} \frac{\lambda_\Phi v m_\mu}{\sqrt{2} m_\phi^2} \times \frac{1}{x_2 - x_1} \left[ x_2 \mathcal{F}^{\text{FS}}(0, x_2; Q_S) - x_1 \mathcal{F}^{\text{FS}}(0, x_1; Q_S) \right], \quad (2.30a)$$

$$\text{Class II: } \Delta a_\mu^{\text{enhanced}} = \frac{\lambda_L \lambda_R}{16\pi^2} \frac{\bar{\lambda}_\Phi v m_\mu}{\sqrt{2} m_\phi^2} \times \frac{\sqrt{x_1 x_2}}{x_2 - x_1} \left[ \mathcal{F}^{\text{FS}}(0, x_2; Q_S) - \mathcal{F}^{\text{FS}}(0, x_1; Q_S) \right], \quad (2.30b)$$

$$\text{Class III: } \Delta a_\mu^{\text{enhanced}} = \frac{\lambda_L \lambda_R}{16\pi^2} \frac{a_\Phi v m_\mu}{\sqrt{2} m_\psi^3} \times \frac{z_1 z_2}{z_1 - z_2} \left[ z_2 \mathcal{F}^{\text{FS}}(0, z_2; Q_S) - z_1 \mathcal{F}^{\text{FS}}(0, z_1; Q_S) \right], \quad (2.30c)$$

where  $x_i = m_i^2/m_\phi^2$  and  $z_i = m_i^2/m_\psi^2$ . For small mixing the mass eigenvalues  $m_{1,2}$  appearing in these exact results correspond to  $m_{\psi,\chi}$  in Class I/II and  $m_{\phi,\eta}$  in Class III. Since the loop-functions are of order one this result is in full agreement with the naive estimate Eq. (2.19). This is further illustrated by the following simple limits. Taking  $x_i = z_i \equiv m_F^2/m_S^2 \equiv x$ , the limits  $m_F \ll m_S$ ,  $m_F = m_S$  and  $m_F \gg m_S$  are of the form

$$\Delta a_\mu^{\text{enhanced}} = \frac{\lambda_L \lambda_R}{16\pi^2} \frac{m_\mu v}{\sqrt{2} m_S^2} \left\{ \lambda_\Phi, \bar{\lambda}_\Phi, \frac{a_\Phi}{m_F} \right\} \begin{cases} \{1, 1, x\} [a_1 + b_1 \ln(x)] & m_F \ll m_S \\ \frac{1}{6} a_2 & m_F = m_S \\ \left\{ \frac{1}{x^2}, \frac{1}{x}, \frac{1}{x} \right\} [a_3 + b_3 \ln(x)] & m_F \gg m_S \end{cases} \quad (2.31a)$$

Rep.	Class	$a_1$	$b_1$	$a_2$	$a_3$	$b_3$
(1, 2, 1)	I	$-5 - 4X$	$-2 - 2X$	$1 + 2X$	$1 - 4X$	$2X$
	II	$-2 - 2X$	0	$-3 - 4X$	$-1 - 2X$	0
	III	$1 - 4X$	$-2X$	$1 + 2X$	$-5 - 4X$	$2 + 2X$
(2, 1, 2)	I	$3 + 4X$	$1 + 2X$	$-2X$	$-3 + 4X$	$1 - 2X$
	II	$1 + 2X$	0	$1 + 4X$	$2X$	0
	III	$-3 + 4X$	$-1 + 2X$	$-2X$	$3 + 4X$	$-1 - 2X$
(2, 3, 2)	I	$-17 - 12X$	$-7 - 6X$	$4 + 6X$	$1 - 12X$	$1 + 6X$
	II	$-7 - 6X$	0	$-11 + 12X$	$-4 - 6X$	0
	III	$1 - 12X$	$-1 - 6X$	$4 + 6X$	$-17 - 12X$	$7 + 6X$
(3, 2, 3)	I	$-7 - 12X$	$-2 - 6X$	$-1 + 6X$	$11 - 12X$	$-4 + 6X$
	II	$-2 - 6X$	0	$-1 - 12X$	$1 - 6X$	0
	III	$11 - 12X$	$4 - 6X$	$-1 + 6X$	$-7 - 12X$	$2 + 6X$

**Table 2.3:** Coefficients of the limits in Eq. (2.31) for different  $SU(2)_L$  representations of the Class I/II fields ( $\phi^\dagger, \psi, \chi$ ) and Class III fields ( $\psi, \phi^\dagger, \eta^\dagger$ ). As described in the text, their respective hypercharges are given in terms of the arbitrary constant  $X$  as  $(X, -\frac{1}{2} - X, -1 - X)$ .

where the entries in the brackets correspond to Class I, II and III respectively. The coefficients  $a_i$  and  $b_i$  depend on the representation of the field multiplets as well as the hypercharge  $X$  and are listed in Tab. 2.3. There are interesting relations between the Class I and III coefficients, namely  $a_{1,2,3}^I = a_{3,2,1}^{III}$  and  $b_{1,3}^I = -b_{3,1}^{III}$ . Furthermore, for Class II,  $b_i = 0$  for all listed representations, i.e. in this case none of the limits results in logarithmic enhancement. On the other hand, both Class I and III develop logarithmic enhancements not only in the limit  $x \rightarrow 0$  as expected from Eq. (2.10), but also for  $x \rightarrow \infty$ . This is another consequence of the mixing between the gauge-eigenstates and once again confirms that this mixing is crucial to understand the chirally enhanced contribution.

As mentioned, the behaviour found in these simple 3-field models is characteristic for a large number of BSM scenarios which involve new couplings to both left-handed and right-handed muons. Examples are supersymmetric models, vector-like leptons, certain leptoquarks and the flavour-violating 2HDM and more general models. We will also use the 3-field models later to illustrate connections to other observables such as the muon mass and the muon-Higgs coupling.

## 2.4. Effective field theory description

To conclude the section on generic BSM scenarios we discuss  $\Delta a_\mu$  in the context of effective field theories (EFT). Over the past decades, EFT has become one of the most important tools for studying new physics at or above the electroweak scale, particularly as it allows for model independent analyses of BSM effects on a wide range of observables. EFT is especially potent for low-energy observables, like  $\Delta a_\mu$ , where the expansion in  $E/M_{\text{BSM}}$  converges rapidly. For recent reviews we refer to Refs. [210–212].

The first appropriate effective theory of this kind is known as low-energy EFT (LEFT) [213] or weak effective theory

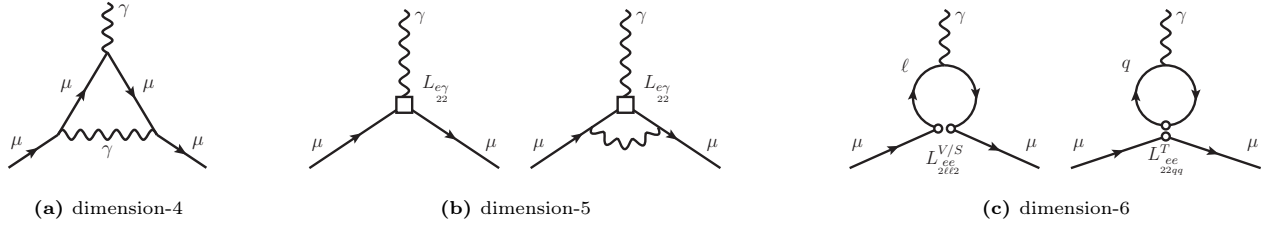


**Figure 2.4:** Sample diagrams of contributions to  $a_\mu$  in the LEFT. The dimension-4 contribution is just the usual QED Schwinger diagram already shown in Fig. 1.6a, the dimension-5 contribution stems solely from the muon dipole operator in Eq. (2.32), and the dimension-6 four-fermion contributions come from scalar or vector operators defined in Eq. (2.37) involving the leptons and tensor operators involving the heavy quarks.

(WET) [214]. Here heavy states like the  $W^-$ ,  $Z^-$  or Higgs boson and potential heavy BSM fields are integrated out and the resulting EFT is an  $SU(3)_c \times U(1)_{em}$  gauge theory which contains QED and QCD, the light SM fields and non-renormalizable terms suppressed by inverse powers of the electroweak scale in the Lagrangian. It is a valid description of phenomena below the electroweak scale as long as there is no light BSM physics.

The Lagrangian of this low-energy EFT contains the dipole operator (we follow the conventions of Ref. [213])

$$\mathcal{L}_{\text{LEFT}} \supset L_{e\gamma} \left( \overline{\mu}_L \sigma^{\alpha\beta} \mu_R \right) F_{\alpha\beta} + h.c. \quad (2.32)$$

where  $L_{e\gamma}$  is a Wilson coefficient assumed to scale as  $\propto M^{-1}$ , where  $M$  is the relevant heavy scale. The Wilson coefficient is defined in the  $\overline{\text{MS}}$  scheme,  $\mu_{L,R}$  are the left- and right-handed muon fields and  $F_{\mu\nu}$  denotes the photon field-strength tensor defined in Eq. (A.14). Like the mass and Yukawa terms, this dimension-5 term connects the left- and right-handed muons resulting in an additional breaking of the muon chiral symmetry (cf. Sec. 1.1.4). The dipole operator yields a contribution to  $a_\mu$  already at tree-level,

$$a_\mu^{\text{LEFT,tree}} = \frac{4m_\mu}{e} \text{Re} L_{e\gamma}. \quad (2.33)$$

Further contributions, shown in Fig. 2.4, arise at the one-loop level e.g. from four-fermion operators, but also the usual QED corrections. The total  $a_\mu$  at one-loop order in the  $\overline{\text{MS}}$  renormalised LEFT is given by [212]

$$a_\mu^{\text{LEFT}} = \frac{\alpha}{2\pi} + \frac{4m_\mu}{e} \text{Re} L_{e\gamma}(\mu) \left\{ 1 - \frac{\alpha}{4\pi} \left[ 2 + 5 \ln \left( \frac{\mu^2}{m_\mu^2} \right) \right] \right\} + \Delta a_\mu^{4l} + \Delta a_\mu^{2l2q} + \mathcal{O}(L_{e\gamma}^2). \quad (2.34)$$

Here,  $e \equiv e(\mu)$  and  $L_{e\gamma}$  denote the QED gauge-coupling and the Wilson coefficient in the  $\overline{\text{MS}}$  scheme, and  $m_\mu$  is the physical muon pole mass.<sup>14</sup> The first term corresponds to Fig. 2.4a and to Schwinger's one-loop QED result, which is part of the LEFT prediction for  $a_\mu$ . The second term corresponds to the tree-level and one-loop corrections of Fig. 2.4b involving the dimension-5 dipole operator. Specifically the logarithmic term is a higher-order correction to Eq. (2.33).<sup>15</sup>

The one-loop corrections  $\Delta a_\mu^{4l}$  and  $\Delta a_\mu^{2l2q}$  illustrated in Fig. 2.4c arise from the following dimension-6 four-fermion operators involving two muons and either two leptons or two quarks,

$$\begin{aligned} \mathcal{L}_{\text{LEFT}} \supset & L_{2ij}^{V,LR} (\overline{\mu}_L \gamma^\mu e_{Li}) (\overline{e}_{Rj} \gamma_\mu \mu_R) + L_{2ij}^{S,RR} (\overline{\mu}_L e_{Ri}) (\overline{e}_{Lj} \mu_R) \\ & + L_{2ij}^{T,RR} (\overline{\mu}_L \sigma^{\mu\nu} \mu_R) (\overline{u}_{Lj} \sigma_{\mu\nu} u_{Rj}) + L_{2ij}^{T,RR} (\overline{\mu}_L \sigma^{\mu\nu} \mu_R) (\overline{d}_{Lj} \sigma_{\mu\nu} d_{Rj}), \end{aligned} \quad (2.35)$$

<sup>14</sup>For more details on the scheme definition of the running quantities we refer to the original literature, and to Ref. [215] for an overview of variants of dimensional regularisation.

<sup>15</sup>If  $m_\mu$  is also taken in the  $\overline{\text{MS}}$  scheme at the scale  $\mu$ , the coefficient of the leading one-loop logarithm in Eq. (2.34) is modified. For a detailed discussion of the logarithmic terms see Sec. 4.3.

and result in the contributions

$$\Delta a_\mu^{4l} = \frac{m_\mu}{4\pi^2} \sum_i m_{e_i} \left\{ \ln \left( \frac{\mu^2}{m_{e_i}^2} \right) \operatorname{Re} L_{\frac{ee}{2i2}}^{S,RR}(\mu) - \operatorname{Re} L_{\frac{ee}{2i2}}^{V,LR}(\mu) \right\} \quad (2.36a)$$

$$\Delta a_\mu^{2l2q} = \frac{m_\mu}{\pi^2} \sum_{q_j, i} N_c Q_{q_j} m_{q_j} \ln \left( \frac{\mu^2}{m_{q_j}^2} \right) \operatorname{Re} L_{\frac{eq}{22ii}}^{T,RR}(\mu), \quad (2.36b)$$

where the sum runs over the heavy quarks  $q_j$  active the scale  $\mu$  (i.e. usually  $c$  and  $b$ ). The light quark contributions, not included here, have to be computed non-perturbatively and are discussed in Refs. [212, 216].

In the LEFT result Eq. (2.34), the dipole operator contributes at tree-level while the four-fermion operators contribute first at one-loop order. When applying this result to concrete renormalizable theories it is important to keep in mind that this loop counting might not reflect the loop counting of the underlying theories. For example, in many UV completions  $L_{ee}$  and  $L_{eq}$  arise at tree-level while  $L_{e\gamma}$  is generated radiatively, such that their overall contributions will be of similar size.

It is instructive to illustrate the application of LEFT to the EWSM contributions where the above comment is relevant. For example, integrating out the  $Z$  and  $W$ -boson from the SM yields (in the  $\overline{\text{MS}}$  scheme with naive dimensional regularisation)

$$L_{\frac{ee}{2222}}^{V,LR}(M_Z) = \frac{4G_F}{\sqrt{2}} (1 - 2s_W^2) s_W^2, \quad \text{and} \quad L_{22}^{e\gamma}(M_Z) = \frac{em_\mu}{48\pi^2} \frac{G_F}{\sqrt{2}} (3 + 8s_W^2 - 16s_W^4) \quad (2.37)$$

and the SM one-loop contribution Eq. (1.64) discussed in Sec. 1.4 is recovered once both Wilson coefficients are inserted into Eq. (2.34). This agreement includes the absence of a large logarithm of the form  $\log(M_Z/m_\mu)$  in the  $Z$ -boson contribution. Applying the same procedure to the SM Higgs one-loop contribution yields a non-vanishing tree-level result for  $L_{ee}^{S,RR}$ , and inspecting Eqs. (2.34) and (2.36a) shows that this Higgs contribution contains a large logarithm, in line with the limit of the relevant loop function in Eq. (2.10).

Similarly, certain BSM scenarios such as many one-field models of Tab. 2.1 can yield non-vanishing Wilson coefficients of all these types. There are, however, also many BSM scenarios such as the models with two fields of different spin in Tab. 2.2 which contribute to  $a_\mu$  only via the dipole operator. For all such models there can be no large logarithm at the one-loop level, but the logarithm present explicitly in Eq. (2.34) constitutes an important two-loop correction. This universal logarithmically enhanced QED correction will be discussed in more detail in Sec. 4.3.

The LEFT description is valid up to the scale  $\mu_{\max} \sim \min(v, M_{\text{BSM}})$ . If the new physics is significantly heavier than  $v$ , it may be appropriate to first integrate out the BSM modes before going to the LEFT. Generically, this yields a non-renormalizable  $\text{SU}(3)_c \times \text{SU}(2)_L \times \text{U}(1)_Y$  gauge theory referred to as Standard Model EFT (SMEFT), whose operators and Lagrangian have been systematically analysed in Refs. [217, 218]. Similar to Eqs. (2.32) and (2.33) the SMEFT contains dipole operators that contribute to  $a_\mu$  at tree-level. In the conventions of Ref. [218] the relevant part of the Lagrangian reads

$$\mathcal{L}_{\text{SMEFT}} \supset C_{eB} (\overline{l_{L2}} \sigma^{\mu\nu} e_{R2}) \Phi B_{\mu\nu} + C_{eW} (\overline{l_{L2}} \sigma^{\mu\nu} e_{R2}) \sigma^a \Phi W_{\mu\nu}^a, \quad (2.38)$$

where the  $C_i$  are SMEFT Wilson coefficients with the assumed scaling  $\propto M_{\text{BSM}}^{-2}$ . Here we slightly differ from the conventions of Ref. [218] and absorb the BSM scale in the dimensionful Wilson coefficients  $C_i$ . As an alternative parametrisation of SMEFT Wilson coefficients we will use

$$C_i \equiv \frac{c_i}{M_{\text{BSM}}^2} \quad (2.39)$$

with dimensionless coefficients  $c_i$ . Like the dimension-4 Yukawa interaction, these dipole operators connect the left-handed lepton doublet with the right-handed singlet. Thus, similar to LEFT, the corresponding Wilson coefficients both individually break the muon chiral symmetry.

Note that in this case gauge invariance results in the appearance of the Higgs fields and the electroweak field strength tensors defined in Eq. (A.5), rather than  $F_{\mu\nu}$  directly. The lowest-order contribution to  $a_\mu$  from the SMEFT dipole operators is then

$$\Delta a_\mu^{\text{SMEFT,tree}} = \frac{4m_\mu v}{e\sqrt{2}} \text{Re} C_{e\gamma}^{22}, \quad (2.40)$$

where  $C_{e\gamma} \equiv c_W C_{eB} - s_W C_{eW}$ . The result can be compared to its LEFT counterpart and related to the need for chirality flips. In contrast to Eq. (2.32), the SMEFT dipole operators are of dimension 6 and consequently their contribution to  $a_\mu$  is suppressed by a factor of  $1/M_{\text{BSM}}^2$ . Because of the appearance of the Higgs field  $\Phi$ , this contribution scales like  $\Delta a_\mu \propto m_\mu v/M_{\text{BSM}}^2$ . This SMEFT behaviour corresponds to the discussion of chirality flips and electroweak symmetry breaking leading to the structure (1.15) for contributions to  $a_\mu$ . In contrast, LEFT ignores electroweak gauge invariance and hence leads to a simpler scaling of  $\Delta a_\mu \propto m_\mu/M_{\text{BSM}}$ . However, the two behaviours coincide when  $M_{\text{BSM}} \sim v$ , which is the heaviest possible scale in LEFT.

More generally, the LEFT dipole operator emerges from Eq. (2.38) after EWSB as can be seen after decomposing the SMEFT operators in terms of the gauge-boson mass eigenstates

$$(\bar{l}_{L2} \sigma^{\mu\nu} e_{R2}) \left[ C_{eB}^{22} B_{\mu\nu} + C_{eW}^{22} \sigma^a W_{\mu\nu}^a \right] \Phi \xrightarrow{\text{EWSB}} \frac{v}{\sqrt{2}} C_{e\gamma}^{22} (\bar{\mu}_L \sigma^{\mu\nu} \mu_R) F_{\mu\nu} + \dots \quad (2.41)$$

where  $C_{e\gamma}$  has been defined above and the dots denote additional terms involving the  $W$ ,  $Z$  and Higgs bosons. Results for the complete matching of SMEFT to LEFT at tree-level and one-loop order have been presented in Refs. [213, 219]. Similar to above, a BSM UV theory will typically give rise to correlations between the SMEFT Wilson coefficients and the related observables, several examples of which will be discussed in Sec. 3.

If we ignore such correlations and assume coefficients of equal size, the largest SMEFT contribution to  $\Delta a_\mu$  stems from the two dipole operators in Eq. (2.38) as well as the following four-fermion operator

$$\mathcal{L}_{\text{SMEFT}} \supset C_{lequ}^{(3)}{}_{2233} (\bar{l}_{L2}^a \sigma^{\mu\nu} e_{R2}) \epsilon_{ab} (\bar{q}_{L3}^b \sigma_{\mu\nu} u_{R3}) \quad (2.42)$$

involving the left- and right-handed muon and top-quark multiplets. Together their leading contributions are given by [211, 220]

$$\Delta a_\mu^{\text{SMEFT}} = \frac{4m_\mu v}{e\sqrt{2}} \text{Re} \left[ c_W C_{eB}^{22}(\mu) - s_W C_{eW}^{22}(\mu) \right] - \frac{2m_\mu m_t}{\pi^2} \ln \left( \frac{\mu^2}{m_t^2} \right) \text{Re} C_{lequ}^{(3)}{}_{2233}(\mu). \quad (2.43)$$

For a more elaborate seminumerical version of this equation that takes into account higher-order corrections from RGE running we refer to Ref. [212]. Similarly, Ref. [221] has obtained the analogous result in an extended EFT,  $\nu\text{SMEFT}$ , where neutrino masses are taken into account and where additional operators can contribute.

In Fig. 2.5 the contributions to  $a_\mu$  from the individual SMEFT Wilson coefficient are plotted, illustrating how a non-zero deviation like  $\Delta a_\mu^{\text{Exp-WP2020}}$  restricts the possible BSM mass scale from above, while the current result  $\Delta a_\mu^{\text{Exp-WP2025}}$  restricts the possible mass scale from below. We show the two cases where either  $C_i = 1/M_{\text{BSM}}^2$ , corresponding to strongly interacting new physics (dashed), or  $C_i = 1/(16\pi^2 M_{\text{BSM}}^2)$ , corresponding to weakly interacting new physics with large chiral enhancement (solid).

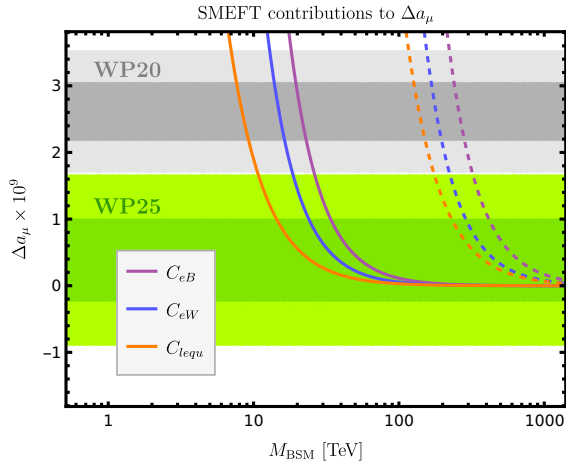


**Figure 2.5:** Contribution of the SMEFT Wilson coefficients  $C_{eB}$ ,  $C_{eW}$  and  $C_{lequ}$  to  $\Delta a_\mu$  as a function of the BSM scale  $M_{\text{BSM}}$ . The continuous (dashed) lines correspond to coefficients generated by weakly (strongly) coupled new physics as described in the text. The green bands indicate the new result  $\Delta a_\mu^{\text{Exp-WP2025}}$  and the grey bands the previous  $\Delta a_\mu^{\text{Exp-WP2020}}$  (at the  $1\sigma$  and  $2\sigma$  levels).

The plot shows the general behaviour in the simplest cases. Clearly, the quantitative mass dependence in actual models depends also on other model parameters and can differ from the ones shown in the plot. It is instructive to connect the SMEFT framework to the results of explicit models. The simple 1-field and 2-field models without chiral enhancement lead to

$$C_{22}^{e\gamma} \sim \frac{y_\mu |c|^2}{16\pi^2} \frac{e}{M_{\text{BSM}}^2} \quad (2.44)$$

in line with the behaviour of  $\Delta a_\mu$  in Eq. (2.15). As an example of a model with chiral enhancement, the Class I model with a common mass scale  $m_F, m_S \sim M_{\text{BSM}}$  leads to (cf. Eq. (2.19))

$$C_{22}^{e\gamma} \sim \frac{\lambda_L \lambda_R \lambda_\Phi}{16\pi^2} \frac{e}{M_{\text{BSM}}^2}. \quad (2.45)$$

Refs. [211, 220] have used the SMEFT framework to classify plausible values of  $\Delta a_\mu$  from very heavy new physics in general: For strongly interacting new physics with large chiral enhancement, the relevant couplings can be assumed to compensate the  $1/16\pi^2$  suppression,<sup>16</sup> such that

$$C_{22}^{e\gamma} \sim \frac{e}{M^2} \quad \Delta a_\mu \sim \frac{m_\mu v}{M^2} \sim \left( \frac{100 \text{ TeV}}{M} \right)^2 \times 20 \times 10^{-10}. \quad (2.46)$$

This is arguably the largest plausible magnitude of  $\Delta a_\mu$  for any given mass scale  $M$ , and it shows that measurable contributions to  $a_\mu$  can be generated even by new physics as heavy as 100 TeV, without violating constraints from unitarity [211]. Similarly, for weakly coupled new physics with large chiral enhancement, a suitable estimate is

$$C_{22}^{e\gamma} \sim \frac{1}{16\pi^2} \frac{e}{M^2} \quad \Delta a_\mu \sim \frac{m_\mu v}{16\pi^2 M^2} \sim \left( \frac{10 \text{ TeV}}{M} \right)^2 \times 15 \times 10^{-10}. \quad (2.47)$$

For each of these cases the SMEFT framework then allows to evaluate the implication of a sizeable  $\Delta a_\mu$  on other observables. It turns out that the same new physics producing a deviation around  $3 \times 10^{-9}$ , i.e. as large as the previous deviation (1.6), would inevitably lead to observable effects at a future muon collider [220, 222], see also Ref. [223] for an analogous study in a related EFT HEFT.

<sup>16</sup>The additional factor  $e$  in this and the following formula compared to the generic formulas used for all Wilson coefficients in Fig. 2.5 is natural for couplings to the photon but inconsequential for the following arguments.

### 3. Relationships to other observables

The observable  $a_\mu$  is flavour and CP conserving, loop induced and chirality flipping. This set of properties implies similarities, differences and complementarities to many other observables. Such relationships are explored and described in this section. We work on generic, model-independent levels and use qualitative arguments, and we also use simple models for quantitative details and technical explanations. Sec. 3.1 continues the discussion of Sec. 1.1.4 and focuses on the connection to the muon mass implied by the common need for chirality flips and electroweak symmetry breaking. It also explains special cases such as models with radiative muon mass generation. Sec. 3.2 discusses differences and relations with other dipole observables such as  $a_e$ , electric dipole moments and flavour-violating decays. The muon–Higgs coupling also shares many properties with  $a_\mu$ , though it appears at tree-level and is measured at the LHC. Its connection with  $a_\mu$  is explored in Sec. 3.3. Electroweak precision observables such as  $M_W$  or  $\sin^2\theta_W$  depend on quite different properties such as custodial symmetry, but they share the importance of the hadronic vacuum polarisation with  $a_\mu$ . The consequences are described in Sec. 3.4. Sections 3.5 and 3.6 focus neutrino masses and dark matter — two phenomena which both require BSM physics. These sections describe how models explaining neutrino masses or dark matter can contribute to  $a_\mu$  and can be constrained by it. Finally, Sec. 3.7 focuses on the general complementarity of  $a_\mu$  with collider constraints, particularly from the LHC.

#### 3.1. Muon mass and generic estimates of possible $a_\mu$ contributions

The analysis of chirality flips, electroweak gauge invariance and muon-chiral symmetry has revealed a deep connection between the muon mass and the muon magnetic moment. Here we provide further details and phenomenological conclusions for generic classes of BSM scenarios, as already illustrated in Tab. 1.1. The relationship between the two observables is expressed by the patterns Eqs. (1.14) and (1.15) for any contribution to  $m_\mu$  and  $a_\mu$  in the SM or any BSM extension. These patterns can also be summarised by the following expressions for contributions to  $a_\mu$  and  $m_\mu$  in any given BSM scenario as (see also Refs. [4, 7, 105]),

$$\Delta a_\mu^{\text{BSM}} = C_{\text{BSM}} \frac{m_\mu^2}{M_{\text{BSM}}^2}, \quad \frac{\Delta m_\mu^{\text{BSM}}}{m_\mu} = \mathcal{O}(C_{\text{BSM}}), \quad (3.1)$$

where  $M_{\text{BSM}}$  is the relevant mass scale. This equation highlights that a BSM scenario contributing to  $a_\mu$  generically also contributes to  $m_\mu$  and the contributions are related. The complicated origin of the muon mass, the necessity for EWSB and chiral symmetry breaking are all encapsulated in the dimensionless coefficient  $C_{\text{BSM}}$ . This coefficient summarises the interesting chirality-flipping and EWSB factors in the square brackets in Eqs. (1.14) and (1.15) together with the “other factors”, and is normalised to the full muon mass  $m_\mu$ . This factor reflects interesting dynamical details of the model in question and is thus very model-dependent. In exceptional cases it can happen that the contributions to either  $m_\mu$  or  $a_\mu$  in a model vanish or dominant terms arise at different loop orders. In such cases the  $\mathcal{O}(1)$  factors between the two formulas in Eq. (3.1) correspond to zero or infinity, and in such BSM scenarios, Eq. (3.1) does not capture the dominant behaviour.

A qualitative conclusion of the relationship is that  $a_\mu$  can provide a window to the muon mass generation mechanism: According to the SM the muon mass is generated by EWSB generating a Higgs  $vev$  and the Yukawa interaction which couples the muon to the Higgs  $vev$ . But many open questions remain. Hence many BSM scenarios modify the Higgs sector and/or the Yukawa sector. Technically, the muon mass generation mechanism is reflected by the factors in square brackets in Eqs. (1.14) and (1.15), hence many BSM scenarios substantially modify these factors. The three-field models

discussed in Sec. 2.3 provide simple examples of such modifications, and many models discussed in Sec. 5 provide further examples.

For this reason, the  $a_\mu$  phenomenology of such BSM scenarios with modified Higgs/Yukawa sectors is particularly rich. They can lead to strong chiral enhancements and thereby provide potentially large and highly model-dependent contributions to  $a_\mu$ . Such models were often considered promising explanations of a deviation as large as  $\Delta a_\mu^{\text{Exp-WP2020}}$ . In general, the parameter spaces of such models are severely constrained by  $a_\mu$ , and the new result  $\Delta a_\mu^{\text{Exp-WP2025}}$  sets an upper limit on chirally enhanced contributions which in individual models translates into limits on the modified Higgs, Yukawa and related sectors.

On a technical level, the validity of Eq. (3.1) in a wide range of scenarios can be illustrated by juxtaposing generic one-loop formulas for  $\Delta a_\mu$  and for the muon mass correction  $\Delta m_\mu$ . Using the same conditions and notations as in Sec. 2.1, and specialising for concreteness to the case of the FS type contributions, we have

$$\Delta m_\mu = \frac{1}{16\pi^2} m_\mu \left( \{|c_L|^2 + |c_R|^2\} \frac{1}{2} B_1 - \frac{m_F}{m_\mu} \text{Re}\{c_L^* c_R\} B_0 \right), \quad (3.2a)$$

$$\Delta a_\mu = \frac{1}{16\pi^2} \frac{m_\mu^2}{m_S^2} \left( \{|c_L|^2 + |c_R|^2\} \mathcal{G}^{\text{FS}} + \frac{m_F}{m_\mu} \text{Re}\{c_L^* c_R\} \mathcal{F}^{\text{FS}} \right). \quad (3.2b)$$

Here the loop functions  $B_{0,1} \equiv B_{0,1}(m_\mu^2, m_F, m_S)$  are standard Passarino-Veltman functions, and the  $\Delta a_\mu$  result corresponds to Eq. (2.3a) with suppressed arguments. As an illustration, in the limit  $m_S = m_F \gg m_\mu$  the loop functions reduce to  $B_0 = -2B_1 = 1/\bar{\epsilon} + \ln(\mu^2/m_S^2)$  and  $\mathcal{G}^{\text{FS}} = (1 + 2Q_S)/12$ ,  $\mathcal{F}^{\text{FS}} = (2 + 3Q_S)/3$ , where  $\mu$  is the renormalisation scale and where  $1/\bar{\epsilon}$  is the dimensional regularisation parameter which is set to zero in the  $\overline{\text{MS}}$ -renormalisation scheme. Hence in general all appearing loop functions have values of  $\mathcal{O}(1)$ . The analogous structure of  $\Delta m_\mu$  and  $\Delta a_\mu$  is apparent. In both cases there are terms without chiral enhancement governed by  $|c_{L,R}|^2$  and a term with potential chiral enhancement governed by  $c_L^* c_R$ . For each term, the contributions to  $a_\mu$  and  $m_\mu$  differ in the relative factor  $m_\mu/m_S^2$  and in the  $\mathcal{O}(1)$  coefficients and loop functions. Hence each term reflects the general relationship stipulated by Eqs. (1.14) and (1.15).

Relations such as Eq. (3.1) and the discussion of chiral enhancements allow to obtain a qualitative understanding of the behaviour of  $a_\mu$  in many BSM scenarios, and Tab. 1.1 already presented a collection of estimates. Here we specifically provide details on three classes of BSM scenarios with particularly large contributions to  $\Delta m_\mu$  and  $\Delta a_\mu$ . All of these can be exemplified by the three-field models of Sec. 2.3 but are also relevant beyond this simple setup. The classes are

- models with radiative muon mass generation,
- models with “finetuning in the muon mass”,
- models saturating perturbative unitarity for chiral enhancements.

Models with radiative muon mass generation realise the idea that the tree-level muon mass vanishes and instead the entire muon mass arises via BSM loop effects, such that

$$\Delta m_\mu^{\text{BSM}} = m_\mu. \quad (3.3)$$

The idea is appealing since it offers a chance to explain the smallness of the muon mass; it might be accompanied by radiative generation of the electron mass or other fermion masses [4, 199]. As emphasised in Ref. [4] (and highlighted in Tab. 1.1 (c)), combining Eq. (3.3) with Eq. (3.1) shows that models with radiative muon mass lead to a specific, large value of  $\Delta a_\mu$ ,

$$\Delta a_\mu = \mathcal{O}(1) \frac{m_\mu^2}{M_{\text{BSM}}^2}. \quad (3.4)$$

In Refs. [4, 200, 224] the impact of radiative muon mass generation on  $a_\mu$  has been investigated using several simple examples, in Refs. [225–227] the idea is expanded to more elaborate models which explain the lepton masses radiatively and study connections to neutrino and dark matter physics. In the context of supersymmetry, the tree-level muon mass can be set to zero either by setting one of two Higgs *vevs* to zero, or by setting the muon Yukawa coupling to zero, and the corresponding impact on  $a_\mu$  has been investigated in Refs. [228] and [229–231], respectively. Here we follow Ref. [200] and illustrate radiative muon mass generation using the three-field models of Class II, III in Sec. 2.3 in the special case where the muon Yukawa coupling is set to zero; later in Sec. 5.2.5 we discuss it in the context of supersymmetry. In the two three-field models, setting  $y_\mu = 0$  restores muon-specific chiral symmetry on the dimension-4 level, while the BSM parameters made explicit in Eq. (2.22) break chiral symmetry only softly on the dimension-3 level. Hence in these cases, the loop contribution  $\Delta m_\mu$  is guaranteed to be finite and unaffected by renormalisation. In contrast, setting  $y_\mu = 0$  in the three-field Class I model does not restore chiral symmetry on the dimension-4 level.

For example, in the Class II model, the chirally enhanced muon mass correction and  $\Delta a_\mu$  can be written as

$$\frac{\Delta m_\mu^{\text{Class II}}}{m_\mu} = C^{\text{II}} \times \left[ B_0(0, m_1, m_\phi) - B_0(0, m_2, m_\phi) \right], \quad (3.5a)$$

$$\Delta a_\mu^{\text{Class II}} = C^{\text{II}} \frac{m_\mu^2}{m_\phi^2} \left[ \mathcal{F}^{\text{FS}}(0, x_2; Q_S) - \mathcal{F}^{\text{FS}}(0, x_1; Q_S) \right], \quad (3.5b)$$

using the common prefactor

$$C^{\text{II}} = \frac{\lambda_L \lambda_R}{16\pi^2} \frac{\bar{\lambda}_\Phi v}{\sqrt{2} m_\mu} \times \frac{m_1 m_2}{m_2^2 - m_1^2}. \quad (3.6)$$

Here the generic result Eq. (3.2) has been specialised to the Feynman rules given around Eq. (2.27) and where  $x_i = m_i^2/m_\phi^2$  as in Eq. (2.30). By requiring radiative muon mass generation,  $m_\mu = \Delta m_\mu^{\text{Class II}}$ , the prefactor can be eliminated, and the resulting  $\Delta a_\mu$  can be expressed via a ratio of loop functions,

$$\Delta a_\mu^{\text{Class II, rad } m_\mu} = \frac{m_\mu^2}{m_\phi^2} \left[ \frac{\mathcal{F}^{\text{FS}}(0, x_2; Q_S) - \mathcal{F}^{\text{FS}}(0, x_1; Q_S)}{B_0(0, m_1, m_\phi) - B_0(0, m_2, m_\phi)} \right]. \quad (3.7)$$

It is further illuminating to record the result for the simple case where all masses are similar,  $m_1 \approx m_2 \approx m_\phi$ . In this case, the muon mass and  $\Delta a_\mu$  can be written as

$$m_\mu^{\text{Class II, rad } m_\mu} \approx \frac{\lambda_L \lambda_R}{32\pi^2} \frac{\bar{\lambda}_\Phi v}{\sqrt{2}}, \quad \Delta a_\mu^{\text{Class II, rad } m_\mu} \approx \frac{m_\mu^2}{m_\phi^2} \left[ \frac{1}{3} + \frac{4Q_F}{3} \right]. \quad (3.8)$$

These equations are all in line with the discussion above. The contributions to the muon mass and to  $a_\mu$  are related in the expected way, the model-dependent prefactors are the same, and the final  $\Delta a_\mu$  behaves as expected in Eq. (3.4). The  $\mathcal{O}(1)$  prefactor of that equation corresponds to the ratio of dimensionless loop functions in the square brackets in Eqs. (3.7) or (3.8). Interestingly, this prefactor can be positive or negative, and in exceptional cases it can also vanish. For the important cases where the charges of the BSM fermion is either  $Q_F = -1$  or  $Q_F = 0$ , the prefactor becomes  $-1$  or  $+1/3$ , respectively.

Similarly, for the Class III model, the results are

$$\frac{\Delta m_\mu^{\text{Class III}}}{m_\mu} = C^{\text{III}} \times \left[ B_0(0, m_1, m_\psi) - B_0(0, m_2, m_\psi) \right], \quad (3.9a)$$

$$\Delta a_\mu^{\text{Class III}} = C^{\text{III}} \frac{m_\mu^2}{m_\psi^2} \left[ z_2 \mathcal{F}^{\text{FS}}(0, z_2; Q_S) - z_1 \mathcal{F}^{\text{FS}}(0, z_1; Q_S) \right], \quad (3.9b)$$

using the common prefactor

$$C^{\text{III}} = \frac{\lambda_L \lambda_R}{16\pi^2} \frac{a_\Phi v}{\sqrt{2}m_\mu} \times \frac{m_\psi}{m_2^2 - m_1^2}, \quad (3.10)$$

the result for the case of radiative muon mass generation is

$$\Delta a_\mu^{\text{Class III}} = \frac{m_\mu^2}{m_\psi^2} \left[ \frac{z_2 \mathcal{F}^{\text{FS}}(0, z_2; Q_S) - z_1 \mathcal{F}^{\text{FS}}(0, z_1; Q_S)}{B_0(0, m_1, m_\psi) - B_0(0, m_2, m_\psi)} \right], \quad (3.11)$$

and the approximate results in the equal-mass limit are

$$m_\mu^{\text{Class III}} \approx \frac{\lambda_L \lambda_R}{32\pi^2} \frac{a_\Phi v}{\sqrt{2}m_\psi}, \quad \Delta a_\mu^{\text{Class III}} \approx \frac{m_\mu^2}{m_\psi^2} \left[ \frac{1}{3} + \frac{2Q_F}{3} \right]. \quad (3.12)$$

The results for these two explicit models are representative for the general class of radiative muon mass generation models. In all cases, there is a strong chiral enhancement that at first depends on the chirality-flipping model parameters. These model parameters can be eliminated, leaving a prediction for  $\Delta a_\mu$  that involves the typical factor  $m_\mu^2/M_{\text{BSM}}^2$  and where the complicated model parameter dependence has cancelled. Most prominently, the overall sign of  $\Delta a_\mu$  is essentially fixed and does not depend on the sign of the model parameters. Numerically, the contributions can be large even for BSM masses in the multi-TeV region. Conversely,  $a_\mu$  constitutes a strong constraint on radiative muon mass models.

In the general case with non-zero tree-level muon mass it is possible to consider the situation

$$|\Delta m_\mu^{\text{BSM}}| > m_\mu. \quad (3.13)$$

Here the radiative corrections are larger than required by radiative muon mass generation, and the total muon mass arises from a cancellation between tree-level and higher-order effects. Accordingly, the contributions to  $a_\mu$  can be larger than in Eq. (3.4), i.e.

$$|\Delta a_\mu| \gtrsim \frac{m_\mu^2}{M_{\text{BSM}}^2}. \quad (3.14)$$

It is clear from the above that already the simple three-field models considered above allow this to happen if the model couplings are larger than what is required by Eqs. (3.8) and (3.12). Nevertheless, the possible values can be limited from above by two relevant considerations.

First, a cancellation between contributions to the muon mass might be considered as undesirable finetuning. If no cancellation at all is allowed, Eq. (3.4) constitutes an upper limit on  $\Delta a_\mu$ ; conversely, a value of  $\Delta a_\mu \sim 10^{-9}$  can only be reached for  $M_{\text{BSM}} \lesssim 3 \text{ TeV}$ . If a finetuning to a degree of e.g. 10% [232] or 1% [201] is allowed, the maximum value of  $\Delta a_\mu$  increases accordingly.

A second consideration is perturbative unitarity. While finetuning constraints can be considered optionally, unitarity constraints are quantum field theoretically stricter. Such unitarity constraints can be derived within explicit models such as the three-field models defined in Sec. 2.3 [201, 233]. In this context, the unitarity constraints are equivalent to the absence of non-perturbative new physics at the energy scale of consideration, and e.g. for the three-field models of Classes I, II, Refs. [201, 233] obtain the unitarity limits  $|\lambda_{L,R}| < \sqrt{8\pi}$  and  $|\lambda_\Phi, \bar{\lambda}_\Phi| < \sqrt{4\pi}$ ; the limits for the Class III model are similar. Thus perturbative unitarity implies an upper limit on  $\Delta a_\mu$  for any given mass scale. However this upper limit is huge; for example even in models where  $M_{\text{BSM}} \lesssim 100 \text{ TeV}$ ,  $\Delta a_\mu \sim 20 \times 10^{-10}$  is possible [201, 233], confirming EFT results described in Sec. 2.4. In general, the results obtained in these references can be summarised

$$\Delta a_\mu^{\text{max,perturbative unitarity}} \sim \frac{1}{16\pi^2} \frac{m_\mu [(8\pi)^{3/2} v]}{M^2} \approx \left( \frac{100 \text{ TeV}}{M} \right)^2 \times 20 \times 10^{-10}. \quad (3.15)$$

Hence even such heavy BSM scenarios can be constrained by  $\Delta a_\mu^{\text{Exp-WP2025}}$ . At the same time, the results of these references and the related Refs. [220, 234] imply that muon colliders have a strong sensitivity to essentially all high-scale models which involve sizeable corrections to  $a_\mu$ .

### 3.2. Other leptonic dipole observables and charged lepton flavour violation

Next to  $a_\mu$ , there is a number of further related dipole observables in the lepton sector. This includes the anomalous magnetic moment of the electron  $a_e$ , the electric dipole moments (EDM) of the electron and muon  $d_{e,\mu}$  as well as several charged lepton flavour violating (CLFV) processes such as  $\mu \rightarrow e\gamma$ . The magnetic dipole moments  $a_e$  and  $a_\mu$  are CP- and flavour-conserving observables, but correspond to different generations, and comparing them as in Eq. (1.8) provides a high precision test of the universality of the lepton interactions. The other dipole observables violate CP and flavour conservation and hence test different aspects of fundamental interactions. At the same time, all mentioned observables arise via very similar operators and are all sensitive to chirality flips in the sense discussed in Sec. 1.1.4. For this reason, BSM contributions to all dipole observables could be related. Here we explore relationships between these and further related CLFV observables in a generic, model-independent way.

We begin with a collection of the SM predictions and experimental results. For the electron  $a_e$ , the current experimental measurement reads [56, 104]

$$a_e^{\text{Exp}} = 1\,159\,652\,180.62(12) \times 10^{-12} \quad [104], \quad (3.16)$$

and the SM prediction is given by

$$a_e^{\text{SM}} = \begin{cases} 1\,159\,652\,181.61(23) \times 10^{-12} & \text{for } \alpha_{\text{Cs}}, [54] \\ 1\,159\,652\,180.252(95) \times 10^{-12} & \text{for } \alpha_{\text{Rb}}, [55] \end{cases} \quad (3.17a)$$

$$(3.17b)$$

The two SM values were compiled in Ref. [13] and are based on a long series of high-precision theory calculations reviewed in Ref. [27] and two different measurements of the fine-structure constant  $\alpha$  using atomic interferometry via either caesium or rubidium [54, 55]. These  $\alpha$  measurements differ by more than 5 standard deviations; hence at present there is no clear evidence for BSM physics in  $a_e$ .<sup>17</sup> Clearly, though, the magnitude of BSM contributions to  $a_e$  is bounded to be below  $|\Delta a_e^{\text{BSM}}| \lesssim 10^{-12}$ .

The EDMs  $d_\ell$  are CP-violating observables. So far, the only known source of CP violation (CPV) stems from the CKM matrix in the quark sector of the SM. The lepton EDMs resulting from this CPV are first generated at the 4-loop level yielding [236–239]

$$d_{e,\mu,\tau}^{\text{SM}} \sim 10^{-40} \dots 10^{-38} \text{ e} \cdot \text{cm}. \quad (3.18)$$

Similarly, LFV has so far only been established firmly in the neutral sector through the discovery of neutrino oscillation. The required (tiny) neutrino masses induce CLFV through radiative corrections, however, this is again very strongly suppressed [240–242]

$$\text{BR}(\mu \rightarrow e\gamma)_{\text{SM}} \sim 10^{-50}. \quad (3.19)$$

---

<sup>17</sup> At the time the result (3.17a) was published, the difference between experiment and the SM prediction of  $\Delta a_e$  was negative, and a variety of studies analysed to what extent this deviation could be explained by BSM physics, in particular in conjunction with the positive  $\Delta a_\mu$  at the time. For an overview we refer to Ref. [235], further studies will be mentioned in Sec. 5.

Consequently, a measurement of non-vanishing electric dipole moments (within the projected future sensitivities) or observation of CLFV processes would pose an unambiguous signal for physics beyond the Standard Model.

For the CP-violating EDMs  $d_e$  and  $d_\mu$ , so far no nonzero signals have been found. The most sensitive searches for the electron and muon EDM have been obtained using electrons confined in  $\text{HfH}^+$  ions and thus subjected to huge intramolecular fields and in the Brookhaven Muon g-2 experiment, respectively,

$$|d_e| < 4.1 \times 10^{-30} e \cdot \text{cm} \quad [243], \quad (3.20a)$$

$$|d_\mu| < 1.9 \times 10^{-19} e \cdot \text{cm} \quad [244]. \quad (3.20b)$$

Similarly, the CLFV decays  $\ell_i \rightarrow \ell_j \gamma$  have not yet been observed. The best available limits have been obtained by the MEG experiment at PSI and the BaBar and Belle collaborations

$$\text{BR}(\mu \rightarrow e \gamma) < 3.1 \times 10^{-13} \quad [245], \quad (3.21a)$$

$$\text{BR}(\tau \rightarrow e \gamma) < 3.3 \times 10^{-8} \quad [246], \quad (3.21b)$$

$$\text{BR}(\tau \rightarrow \mu \gamma) < 4.2 \times 10^{-8} \quad [247]. \quad (3.21c)$$

The absence of signals in these experiments puts strong constraints on the possible CP and flavour textures of potential BSM scenarios. Still, there is good potential that such signals could be seen in future experiments. On the one hand, it has been known for a long time that the CPV of the SM is insufficient to address the baryon-antibaryon asymmetry in the early universe. Many models introduced to resolve this issue also induce lepton EDMs significantly above the SM value. On the other hand, lepton flavour is an accidental symmetry of the SM that is generically broken by higher-dimensional terms like the four-fermion and, in particular, dipole operators. Thus new physics scenarios above the electroweak scale often induce new sources of CPV and/or CLFV, leading to enhanced rates potentially observable in the future, for reviews see e.g. [8, 237, 248, 249].

Since all observables considered here are defined at low energies, it is appropriate to describe them using an effective Lagrangian. The appropriate framework is the one of LEFT, discussed in Sec. 2.4. In particular, the dipole operator introduced in Eq. (2.32) can be generalised to

$$\mathcal{L} \supset L_{e\gamma} \bar{e}_{Li} \sigma^{\mu\nu} e_{Rj} F_{\mu\nu} + h.c. \quad (3.22)$$

The diagonal Wilson coefficients induce the dipole moments

$$\Delta a_i = \frac{4m_i}{e} \text{Re} L_{e\gamma} \quad (3.23)$$

$$d_i = 2 \text{Im} L_{e\gamma} \quad (3.24)$$

while the off-diagonal Wilson coefficients contribute to the CLFV processes, most notably [8, 250, 251]

$$\text{BR}(\ell_i \rightarrow \ell_j \gamma) = \frac{m_i^3}{4\pi\Gamma_i} \left( |L_{e\gamma}{}_{ij}|^2 + |L_{e\gamma}{}_{ji}|^2 \right). \quad (3.25)$$

These equations make the connections between the dipole observables manifest. Although the different coefficients  $L_{e\gamma}{}_{ij}$  are in general independent, in many concrete BSM scenarios they arise simultaneously from common origins and, as a consequence, are correlated [8, 235, 249, 252]. The nature of these relationships is of course model-dependent and can manifest in different ways. For a general, qualitative discussion we follow Refs. [235, 252]. As e.g. in Ref. [252] we first

introduce generic CPV phases  $\phi_i$  and effective flavour mixing angles  $\theta_{ij}$  (for  $i \neq j$ ) as

$$\tan \phi_i \equiv \frac{\text{Im } L_{e\gamma}^{ii}}{\text{Re } L_{e\gamma}^{22}}, \quad \text{and} \quad \theta_{ij} \equiv \frac{L_{e\gamma}^{ij}}{L_{e\gamma}^{22}}, \quad (3.26)$$

where we will assume  $\theta_{ij}$  to be real for simplicity. It is instructive to use these generic parameters to express several potential BSM properties as

$$\text{no CPV : } |\tan \phi_i| = 0 \quad \text{no LFV : } |\theta_{ij}| = 0, \quad (3.27a)$$

$$\text{weak CPV : } |\tan \phi_i| \ll 1 \quad \text{weak LFV : } |\theta_{ij}| \ll 1, \quad (3.27b)$$

$$\text{generic CPV : } |\tan \phi_i| \sim 1 \quad \text{generic LFV : } |\theta_{ij}| \sim 1. \quad (3.27c)$$

In the absence of any fundamental mechanism, one may expect that BSM contributions generically violate both CP and lepton flavour; however, certain fundamental BSM properties might guarantee that these symmetries are only weakly or not at all violated.

Using the parametrisation (3.26) we can express generic and qualitative relationships between the observables in semi-numerical form. For the EDMs we can write

$$d_e \approx \left( \frac{\Delta a_e}{10^{-12}} \right) \left( \frac{\tan \phi_e}{2 \times 10^{-7}} \right) 4.1 \times 10^{-30} e \cdot \text{cm}, \quad (3.28a)$$

$$d_\mu \approx \left( \frac{\Delta a_\mu}{10^{-9}} \right) \left( \frac{\tan \phi_\mu}{2000} \right) 1.9 \times 10^{-19} e \cdot \text{cm}. \quad (3.28b)$$

A similar expression for  $\mu \rightarrow e\gamma$  reads

$$\text{BR}(\mu \rightarrow e\gamma) \approx \left( \frac{\Delta a_\mu}{10^{-9}} \right)^2 \left( \frac{\theta_{12}^2 + \theta_{21}^2}{(4.3 \times 10^{-5})^2} \right) (1 + \tan^2 \phi_\mu)^2 3.1 \times 10^{-13}. \quad (3.29)$$

These three equations illuminate the relationships between the dipole observables in various ways. First, comparing to the experimental bounds in Eqs. (3.20) and (3.21) the product of the brackets on the r.h.s. must be smaller than 1. In addition, the  $\Delta a_i$  are normalised to their current experimental sensitivities, such that these terms must also be  $\lesssim 1$ . In the electron sector, Eq. (3.28a) for the EDM  $d_e$  therefore implies that BSM contributions to  $a_e$  are either far below the current experimental sensitivity, or that they must be essentially CP conserving with  $\tan \phi_e \lesssim 10^{-7}$ . In contrast, Eq. (3.28b) for the muon EDM  $d_\mu$  still allows for a sizeable  $\Delta a_\mu$  even in the presence of large CPV  $\tan \phi_\mu \gg 1$ .

Similarly, Eq. (3.29) shows that sizeable contributions to the muon magnetic moment  $\Delta a_\mu$  at the level of the current sensitivity are only possible in models with  $\theta_{12,21} \lesssim 10^{-5}$ , i.e. which are essentially flavour conserving. Such a suppression typically requires some additional symmetries or underlying mechanisms that impose specific flavour structures. This is illustrated e.g. in Ref. [8] where a number of simplified models have been explored in the context of CLFV and  $a_\mu$ . In addition, Refs. [253, 254] consider the connection between  $a_\mu$  and CLFV in models with discrete flavour symmetries, and Ref. [255] considers the generic situation also including renormalisation-group running, which further strengthens the conclusion that sizeable BSM contributions to  $a_\mu$  are only viable in the presence of non-trivial flavour symmetry properties of the underlying BSM mechanisms.

Here we will consider two particular general patterns of BSM contributions that appear in a variety of scenarios. First, if the SM Yukawa couplings are the only source of chiral symmetry breaking, the discussion of Sec. 1.1.4 shows that the contributions are typically related by

$$\frac{L_{11}^{e\gamma}}{L_{22}^{e\gamma}} \sim \frac{m_e}{m_\mu}. \quad (3.30)$$

This behaviour is often called *naive scaling* (n.s.) [252]. It also arises in BSM scenarios when additional chirality breaking BSM parameters are present but are forced to be proportional to the SM Yukawa couplings by an underlying mechanism. If naive scaling holds, the coefficient  $C_{\text{BSM}}$  introduced in Eq. (3.1) is generation-independent. A discussion on the related minimal flavour violation in the lepton sector can be found in Ref. [256].

In case of naive scaling, additional and tighter relationships between the electron and muon dipole moments emerge,

$$\Delta a_e^{(\text{n.s.})} \sim \frac{m_e^2}{m_\mu^2} \Delta a_\mu \approx 2.3 \times 10^{-5} \Delta a_\mu, \quad (3.31a)$$

$$d_e^{(\text{n.s.})} \sim \frac{m_e}{m_\mu} d_\mu \approx 4.8 \times 10^{-3} d_\mu. \quad (3.31b)$$

As a consequence, the currently strongest experimental bounds on  $\Delta a_\mu$  and  $d_e$  imply mutually stronger constraints of the orders

$$|\Delta a_e^{(\text{n.s.})}| \lesssim 10^{-13}, \quad \text{and} \quad |d_\mu^{(\text{n.s.})}| \lesssim 10^{-27} e \cdot \text{cm} \quad (3.32)$$

on the dipole moments of the opposite generations. In particular, combined with Eq. (3.28) we arrive at a relation between  $d_e$  and  $\Delta a_\mu$ ,

$$d_e^{(\text{n.s.})} \approx \left( \frac{\Delta a_\mu}{10^{-9}} \right) \left( \frac{\tan \phi_\mu}{10^{-5}} \right) 4.1 \times 10^{-30} e \cdot \text{cm}. \quad (3.33)$$

Together with Eq. (3.28a), this requires either  $\Delta a_\mu$  to be well below current experimental sensitivities, or CP conservation to an excellent degree in both the muon and the electron sector,  $\tan \phi_{\mu,e} < 10^{-5}$ .

As a second special pattern of BSM contributions we consider the relations implied by a *single particle contribution* (s.p.c.) [235]. This corresponds to the special case of a single BSM particle which couples to leptons with generation-dependent couplings  $c_i$  and produces a contribution to the dipole operators. In this case, the Wilson coefficients scale as  $L_{ij}^{e\gamma} \propto c_i c_j$  and are thus related as

$$L_{ij}^{e\gamma} \sim L_{ji}^{e\gamma} \sim \sqrt{L_{ii}^{e\gamma} L_{jj}^{e\gamma}}. \quad (3.34)$$

Under this assumption,  $\text{BR}(\mu \rightarrow e\gamma)$  can be written as

$$\text{BR}(\mu \rightarrow e\gamma)^{(\text{s.p.c.})} \approx \left( \frac{\Delta a_e}{10^{-12}} \right) \left( \frac{\Delta a_\mu}{10^{-9}} \right) \left( 2.2 \times 10^8 \right) \left( 1 + \tan^2 \phi_\mu \right)^2 3.1 \times 10^{-13}. \quad (3.35)$$

In the case of such simple scenarios the existing  $\mu \rightarrow e\gamma$  bounds thus exclude simultaneously sizeable contributions to  $\Delta a_e$  and  $\Delta a_\mu$  at the level of the current sensitivities [235]. This observation was of interest particularly before the result (3.17b) became available. As mentioned in footnote 17, the slight discrepancy between Eqs. (3.16) and (3.17a) sparked numerous attempts to explain the negative  $\Delta a_e$  simultaneously with positive  $\Delta a_\mu$ , which are constrained by Eq. (3.35).

In the following we focus more broadly on CLFV observables. Table 3.1 collects a selection of promising observables and the sensitivities of planned experiments. In the  $\mu$ - $e$  sector, there are two particularly important CLFV processes complementary to  $\mu \rightarrow e\gamma$ . These are the decay  $\mu^+ \rightarrow e^+ e^- e^+$  ( $\mu \rightarrow 3e$  for short) and  $\mu \rightarrow e$  conversion  $\mu\text{N} \rightarrow e\text{N}$ , where a muon bound in the field of a nucleus N converts into an electron, where the nucleus absorbs the recoil. These processes receive contributions not only from the dipole terms in Eq. (3.22) but also from chirality-preserving four-fermion operators. Such observables are therefore particularly relevant in scenarios without chiral enhancements, where the bounds from  $\mu \rightarrow e\gamma$  and the dipole moments are much less stringent, and Refs. [262, 263] provide an overview of the interplay between various CLFV observables.

Observable	Future sensitivity	Experiment
$\text{BR}(\mu \rightarrow e\gamma)$	$6 \times 10^{-14}$	MEG II [257]
$\text{BR}(\mu \rightarrow 3e)$	$2 \times 10^{-15}$	Mu3e (phase 1) [258]
$\text{BR}(\mu \rightarrow 3e)$	$10^{-16}$	Mu3e (phase 2) [258]
$\text{BR}(\mu\text{Al} \rightarrow e\text{Al})$	$7 \times 10^{-15}$	COMET (phase 1) [259]
$\text{BR}(\mu\text{Al} \rightarrow e\text{Al})$	$3 \times 10^{-17}$	COMET (phase 2) [259], Mu2e [260]
$\text{BR}(\tau \rightarrow \mu\gamma)$	$10^{-9}$	Belle II [261] (Figure 189)
$\text{BR}(\tau \rightarrow e\gamma)$	$3 \times 10^{-9}$	
$\text{BR}(\tau \rightarrow 3\mu)$	$3.5 \times 10^{-10}$	
$\text{BR}(\tau \rightarrow \mu\pi)$	$4.5 \times 10^{-10}$	
$\text{BR}(\tau \rightarrow \mu ee)$	$3 \times 10^{-10}$	

**Table 3.1:** Future experimental sensitivities to a selection of CLFV observables. The first set involves  $\mu \rightarrow e$  transitions, the second set involves  $\tau$ -lepton decays into final states involving muons and/or electrons. The decays of the type  $\ell_i \rightarrow \ell_j \gamma$  are generated by dipole operators, the other decays can be generated also by other operators.

For our purposes in connection with  $a_\mu$  it is interesting to estimate the impact of the additional muon decay observables in the case of *dipole dominance* (d.d.), i.e. in the case where the non-enhanced BSM contributions are absent or can be neglected. In this case the expressions for the branching ratios reduce to [8, 250, 264–266]

$$\text{BR}(\mu \rightarrow 3e)^{\text{(d.d.)}} \simeq \frac{\alpha m_\mu^3}{48\pi^2 \Gamma_\mu} \left[ 8 \ln\left(\frac{m_\mu}{m_e}\right) - 11 \right] \times \left( |L_{12}^{e\gamma}|^2 + |L_{21}^{e\gamma}|^2 \right) \approx \text{BR}(\mu \rightarrow e\gamma) 6 \times 10^{-3} \quad (3.36)$$

and

$$\text{BR}(\mu N \rightarrow eN)^{\text{(d.d.)}} \simeq \frac{m_\mu^3 D_N^2}{4\Gamma_{\text{capt}}^N} \left( |L_{12}^{e\gamma}|^2 + |L_{21}^{e\gamma}|^2 \right) \approx \text{BR}(\mu \rightarrow e\gamma) \begin{cases} 2.7 \times 10^{-3} & (\text{Al}), \\ 3.9 \times 10^{-3} & (\text{Au}), \end{cases} \quad (3.37)$$

where the result in the second case depends on the nucleus  $N$ . Thus in case of dipole dominance all these processes are strictly correlated by fixed, known factors; the additional suppression factors appearing here arise from an additional phase space factor and from nuclear overlap integrals, respectively. The branching ratios dictated by dipole dominance are therefore roughly a factor of 1000 smaller than for  $\mu \rightarrow e\gamma$ . Comparing to the bounds set by SINDRUM and SINDRUM II,

$$\text{BR}(\mu \rightarrow 3e) < 10^{-12} \quad [267], \quad (3.38a)$$

$$\text{BR}(\mu\text{Au} \rightarrow e\text{Au}) < 7 \times 10^{-13} \quad [268], \quad (3.38b)$$

and to Eq. (3.21a), shows that currently these processes do not constitute additional constraints beyond  $\mu \rightarrow e\gamma$  on BSM scenarios with dipole dominance. However, as Tab. 3.1 shows, the sensitivities in the measurements are expected to improve by a factor of more than  $10^4$  in the upcoming Mu3e experiment at PSI for  $\mu \rightarrow 3e$  as well as the COMET and Mu2e experiments at J-PARC and Fermilab for  $\mu \rightarrow e$  conversion in the presence of an Al-nucleus. These future

experiments will have a sensitivity to CLFV that can surpass the one of  $\mu \rightarrow e\gamma$  even in case of dipole dominance, and they additionally have a unique sensitivity to non-dipole operators.

Finally we also provide qualitative comments on CLFV observables involving  $\tau$  decays. Table 3.1 lists a small selection of  $\tau$ -decay modes that can be investigated at the Belle II experiment. Specifically the so-called “golden modes” [261]  $\tau \rightarrow \mu\gamma$  and  $\tau \rightarrow 3\mu$  behave analogously to  $\mu \rightarrow e\gamma$  and  $\mu \rightarrow 3e$ . Similarly to the discussion above in the  $\mu$ - $e$  sector, the correlation of  $\tau \rightarrow \mu\gamma$  to  $a_\mu$  and the correlation between  $\tau \rightarrow \mu\gamma$  and  $\tau \rightarrow 3\mu$  in case of dipole dominance can be analysed in analogous ways. The  $\tau$ -lepton sector offers a wide range of additional observables. There are observables with  $\tau$ - $e$  transitions or even observables that involve all three lepton flavours (such as  $\tau \rightarrow \mu ee$  in the table), and observables with leptons and hadrons in the final state (illustrated by  $\tau \rightarrow \mu\pi$  in the table). The latter may be sensitive to special classes of BSM physics, e.g. to leptoquarks. For a brief account of how the  $\tau$ -decay observables provide complementary constraints on BSM physics and on EFT operators we refer to section 15.2.1 of Ref [261].

To summarise, the three observables with  $\mu \rightarrow e$  transitions provide the highest-sensitivity probes of CLFV, and their interplay can specifically test the hypothesis of dipole dominance, which in turn relates to the discussion of  $a_\mu$ . In general, the constraints from all CLFV observables including muons or  $\tau$ -leptons are sensitive to different properties of BSM physics and are therefore complementary. Positive or negative signals combined with limits from magnetic and electric dipole moments provide key information on the chiral and flavour structure of BSM physics.

### 3.3. Muon–Higgs coupling

In the previous sections 3.1 and 3.2 we have considered several cases where large BSM effects in  $\Delta a_\mu$  also leave an imprint in other low-energy chirality-flipping observables. Here we extend this discussion into the high-energy regime by exploring the connection between  $\Delta a_\mu$  and the muon–Higgs coupling  $\lambda_{\mu\mu}$  probed at the LHC. Like the magnetic moment and the muon mass, the Higgs coupling  $\lambda_{\mu\mu}$  is flavour conserving and chirality flipping. Much of the discussion of chirality flips in Sec. 1.1.4 can also be applied to this quantity, suggesting that large chiral enhancements present in  $\Delta a_\mu$  generically translate into similar enhancements in  $\lambda_{\mu\mu}$ . This has been observed and evaluated in the context of concrete models such as vector-like lepton models [269, 270], leptoquark models [271–273], the two-Higgs doublet model [273] and generalised within EFT frameworks [202, 273–275].

Over the past decade many of the Higgs decay channels have been measured with impressive accuracy. In particular, the current world average for the di-muon signal strength is given by [104, 276, 277]

$$\mu(H \rightarrow \mu\mu) = \frac{\sigma \cdot \text{BR}(H \rightarrow \mu\mu)}{[\sigma \cdot \text{BR}(H \rightarrow \mu\mu)]_{\text{SM}}} = 1.21 \pm 0.35. \quad (3.39)$$

In many BSM scenarios the modifications to both the production cross section  $\sigma$  and the total decay width of the Higgs are negligible, such that this measurement provides a direct constraint on the effective interaction strength between muon and the Higgs, the muon–Higgs coupling  $\lambda_{\mu\mu}$ ,

$$\mu(H \rightarrow \mu\mu) \simeq \frac{\Gamma(H \rightarrow \mu\mu)}{\Gamma(H \rightarrow \mu\mu)_{\text{SM}}} = \left| \frac{\lambda_{\mu\mu}}{\lambda_{\mu\mu}^{\text{SM}}} \right|^2. \quad (3.40)$$

The LHC result Eq. (3.39) is consistent with the SM prediction but also allows BSM contributions of more than 20% to  $\lambda_{\mu\mu}$ .

The relationship between the muon–Higgs coupling and  $a_\mu$  is illustrated by the generic diagrams in Fig. 3.1 (left) where the same chiral structure generates both a correction to the muon Yukawa coupling and thus the muon mass

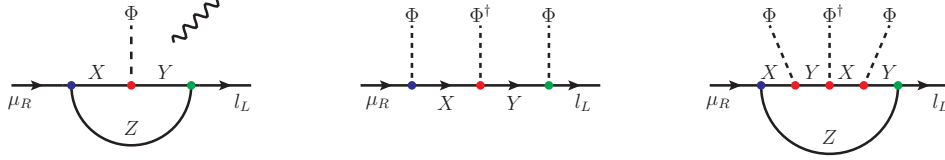


**Figure 3.1:** Generic diagrams from Ref. [274] contributing to the muon–Higgs vertex or SMEFT dipole operator (*left*) as well as to  $C_{e\Phi}$  at tree-level (*middle*) and one-loop (*right*). Rather than the genuine 1PI one-loop topologies displayed here in some models there are instead only one-*light*-particle-irreducible contributions, like e.g. obtained by connecting two of the Higgs lines in the middle diagram.

(without external photon) and also to the magnetic moment  $\Delta a_\mu$  (with external photon). This diagram is similar to the ones illustrating the relationship between  $a_\mu$  and the muon mass in Fig. 1.1 and to the mass-insertion diagrams for three-field models in Fig. 2.3, but it highlights the possible appearance of a physical Higgs boson, not only of the Higgs  $vev$ . As Fig. 3.1 shows, the couplings responsible for the left diagram can also generate effective interactions between the muon and three Higgs fields, either at tree level (middle) or at one-loop order (right). We note that the left and middle diagrams involve the same power of couplings, however of different couplings. Hence depending on the model, the tree-level diagram might vanish or might be of the same order as the diagram on the left. In contrast, the left and right diagrams involve the same type of couplings, however in different powers.

The relationships between contributions of these kinds to  $a_\mu$ ,  $m_\mu$  and  $\lambda_{\mu\mu}$  can be understood well by using the framework of SMEFT introduced in Sec. 2.4. Here we follow particularly Refs. [274, 275], which considered all types of contributions in Fig. 3.1. In this context, the left diagram in Fig. 3.1 gives rise to a matching correction to the fundamental muon Yukawa coupling  $y_\mu$ , which then differs from its SM value, and to the dipole operator, and the other two diagrams induce the dimension-6 mass operator  $\bar{l}_L \mu_R \Phi |\Phi|^2$ . The relevant resulting effective Lagrangian is

$$\mathcal{L} \supset -y_\mu (\bar{l}_L \mu_R \Phi) + C_{e\Phi} (\bar{l}_L \mu_R \Phi) |\Phi|^2 + C_{e\gamma} (\bar{l}_L \sigma^{\mu\nu} \mu_R) \Phi F_{\mu\nu} + h.c., \quad (3.41)$$

where the first term is the usual dimension-4 muon–Higgs Yukawa coupling, the second term is a dimension-6 muon–Higgs coupling with three powers of the Higgs doublet, the third term is the muon dipole operator. The first two terms contribute to the muon mass and the physical muon–Higgs coupling  $\lambda_{\mu\mu}$ , the third term to  $a_\mu$  and  $d_\mu$ . The Lagrangian can be easily augmented by few four-fermion operators to form a closed system under renormalisation-group equations [273]; here it has been simplified and written in terms of the photon dipole by using Eq. (2.38), which is sufficient for the following discussion.

The diagrammatic relationship in Fig. 3.1 translates into a correlation between the two dimension-6 Wilson coefficients that can be parametrised in terms of a model-dependent factor  $\kappa$  [274, 275],

$$C_{e\Phi} = \frac{\kappa}{e} C_{e\gamma}. \quad (3.42)$$

In general, the factor  $\kappa = |\kappa| e^{i\phi_\kappa}$  is complex and depends on the BSM masses and couplings. It plays a similar role as the model-dependent  $\mathcal{O}(1)$  factor between  $a_\mu$  and  $\Delta m_\mu/m_\mu$  implicit in Eq. (3.1). In contrast, however,  $\kappa$  does not have to be  $\mathcal{O}(1)$ . Instead its order of magnitude is determined by the relative loop suppression between the contributions to the dipole and dimension-6 mass operator. Typically the dipole operator is induced at one-loop, while  $\mathcal{O}_{e\Phi}$  can be induced at tree-level (by diagrams as in Fig. 3.1 (middle) if they exist) or at one-loop level (by diagrams as in Fig. 3.1 (right)).

Hence, typical values can be

$$|\kappa| \sim \begin{cases} 16\pi^2 & \text{if tree-level diagrams for } C_{e22}^\Phi \text{ exist,} \\ |\lambda_{XY}|^2 & \text{if one-loop is leading order,} \end{cases} \quad (3.43)$$

where  $\lambda_{XY}$  are the additional coupling factors present in Fig. 3.1 (right). To see how Eq. (3.42) translates into a correlation between the Higgs decay and  $\Delta a_\mu$  we consider the muon mass and effective Higgs coupling generated in the SMEFT (at dimension 6) after EWSB. At leading order, these are given by

$$m_\mu = \frac{1}{\sqrt{2}}(y_\mu v - \frac{1}{2}C_{e22}^\Phi v^3), \quad (3.44a)$$

$$\lambda_{\mu\mu} = \frac{1}{\sqrt{2}}(y_\mu - \frac{3}{2}C_{e22}^\Phi v^2). \quad (3.44b)$$

The important factor 3 arises from the expansion  $(v+h)^3 = v^3 + 3v^2h + \dots$  and results in a modification of the correlation between the muon mass and the muon–Higgs coupling. While the SM correlation is simply  $\lambda_{\mu\mu}^{\text{SM}} = m_\mu/v$ , the above equations can be combined by eliminating the SMEFT Yukawa coupling  $y_\mu$ , yielding the correlation

$$\lambda_{\mu\mu} = \frac{m_\mu}{v} - C_{e22}^\Phi \frac{v^2}{\sqrt{2}}. \quad (3.45)$$

In this approximation the modification is thus caused solely by the dimension-6 mass operator involving three Higgs fields; further, subleading effects are discussed in Ref. [275].

Using Eq. (3.42), the SMEFT expressions for the muon dipole moments discussed in sec. 2.4 and sec. 3.2 give

$$\text{Re} \{ e^{-i\phi_\kappa} C_{e22}^\Phi \} = \frac{|\kappa| \Delta a_\mu}{2\sqrt{2}v m_\mu} \quad (3.46a)$$

$$\text{Im} \{ e^{-i\phi_\kappa} C_{e22}^\Phi \} = -\frac{|\kappa| d_\mu}{\sqrt{2}ve}. \quad (3.46b)$$

After eliminating EFT Yukawa coupling  $y_\mu$  in favour of  $m_\mu$  and expressing  $C_{e\Phi}$  in terms of the above equations, we arrive at the following correlation between the muon–Higgs coupling and dipole moments

$$\left| \frac{\lambda_{\mu\mu}}{\lambda_{\mu\mu}^{\text{SM}}} \right|^2 = \left( \cos(\phi_\kappa) - \frac{|\kappa|}{728} \left( \frac{\Delta a_\mu}{10^{-9}} \right) \right)^2 + \left( \sin(\phi_\kappa) - \frac{|\kappa|}{684} \left( \frac{d_\mu}{10^{-22} e \cdot \text{cm}} \right) \right)^2, \quad (3.47)$$

where the numerical prefactors correspond to the factors  $\frac{v^2}{4m_\mu^2}$  and  $\frac{v^2}{2m_\mu}$ , respectively.

A shift of the muon–Higgs coupling of a relevant magnitude can therefore be expected if e.g. the dipole moments are significant,  $\Delta a_\mu \sim 10^{-9}$  or  $d_\mu \sim 10^{-22} e \cdot \text{cm}$ , and if  $|\kappa| \sim \mathcal{O}(100)$ . Here the value  $d_\mu = 10^{-22} e \cdot \text{cm}$  is of interest since it is in reach of the future PSI experiment described in Ref. [278], and a value of  $|\kappa| \sim \mathcal{O}(100)$  is particularly possible in models where the tree-level diagram Fig. 3.1 (middle) is generated.

In Refs. [274, 275] it was stressed that for any given model with fixed  $\kappa$ , the correlation in Eq. (3.47) defines an ellipse in the  $\Delta a_\mu$ – $d_\mu$  plane. Here we use the correlation to study allowed values for the model factor  $\kappa$  for different values of  $\Delta a_\mu$  and  $d_\mu$ . Specifically, Fig. 3.2 shows the  $\kappa$ – $\Delta a_\mu$  regions allowed by Eq. (3.39) and Eq. (3.47) for four example scenarios with either  $d_\mu = 0$  or  $d_\mu = 10^{-22} e \cdot \text{cm}$  and with real or imaginary  $\kappa$ . The first case with  $d_\mu = 0$  and  $\phi_\kappa = 0$  is particularly simple but interesting in its own right. Here in the correlation formula the second bracket on the r.h.s. vanishes, and the relation can be simplified to

$$\left| \frac{\lambda_{\mu\mu}}{\lambda_{\mu\mu}^{\text{SM}}} \right| = \left| 1 - \frac{|\kappa|}{728} \left( \frac{\Delta a_\mu}{10^{-9}} \right) \right|. \quad (3.48)$$

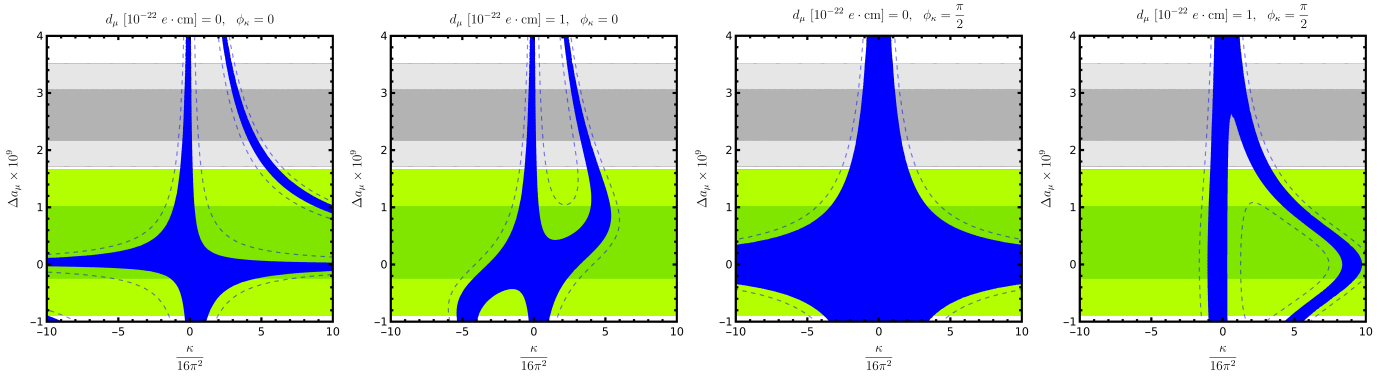


**Figure 3.2:** Contour plots for the correlation between  $\Delta a_\mu$  and the muon–Higgs coupling, in the  $\kappa - \Delta a_\mu$  plane, assuming the tree-level correlation Eq. (3.47). The current experimental bounds Eq. (3.39) on the muon–Higgs coupling at  $1\sigma$  ( $2\sigma$ ) are shown in blue (dashed blue). The green bands indicate the new result  $\Delta a_\mu^{\text{Exp-WP2025}}$  and the grey bands the previous  $\Delta a_\mu^{\text{Exp-WP2020}}$  (at the  $1\sigma$  and  $2\sigma$  levels), and negative  $\kappa$  correspond to the case  $\phi_\kappa \rightarrow \phi_\kappa + \pi$ .

The LHC constraints on the muon–Higgs coupling act only on absolute values and require the left-hand side of this equation to be close to one. Hence there are two distinct ways to fulfil these LHC constraints: Either  $\lambda_{\mu\mu} \approx +\lambda_{\mu\mu}^{\text{SM}}$ , which implies small  $\kappa$  and/or small  $\Delta a_\mu$ . Or  $\lambda_{\mu\mu} \approx -\lambda_{\mu\mu}^{\text{SM}}$ , which requires a very specific value of the product  $\kappa\Delta a_\mu$  where both factors are rather large. Both cases are visible in the first plot of Fig. 3.2. The large cross-like regions centred around the origin corresponds to  $\lambda_{\mu\mu} \approx +\lambda_{\mu\mu}^{\text{SM}}$ . It contains the two limits where  $\Delta a_\mu = 0$  (and  $\kappa$  is unconstrained) and where  $\kappa = 0$  (and  $\Delta a_\mu$  is unconstrained). The allowed region towards larger  $\kappa$  corresponds to  $\lambda_{\mu\mu} \approx -\lambda_{\mu\mu}^{\text{SM}}$ .

The second plot of the same figure shows the case with non-zero  $d_\mu$ , where the general correlation Eq. (3.47) applies. Here the two allowed regions merge at small  $\Delta a_\mu$ , and there is an upper limit on  $|\kappa|$  even at small  $\Delta a_\mu$ . The third and fourth plots of Fig. 3.2 show the case of imaginary  $\kappa = i|\kappa|$ . Here, Eq. (3.47) is purely quadratic in  $\Delta a_\mu$  and its effect therefore suppressed. Consequently, in the case of  $d_\mu = 0$  the allowed ranges of  $|\kappa|$  are larger and the flipped-sign region is absent. For non-zero  $d_\mu$  the scenario is essentially opposite to the one with real  $\kappa$ ; now  $\sin(\phi_\kappa) = 1$  and for small  $\Delta a_\mu$  there are two distinct regions where the second bracket in Eq. (3.47) is close to either  $+1$  or  $-1$ ; these two regions merge as  $\Delta a_\mu$  becomes large where the  $|\kappa|^2$  term in Eq. (3.47) starts to dominate.

As expected, in all scenarios the constraints are relevant for large  $|\kappa| \sim \mathcal{O}(16\pi^2)$ , which are expected only in models where the tree-level diagram Fig. 3.1 (middle) exists. In this case the allowed quantum numbers of the new fermions are strongly constrained and  $\kappa$  can be written as

$$\kappa = \frac{64\pi^2}{\mathcal{Q}} \quad (3.49)$$

where the  $\mathcal{O}(1)$  values of  $\mathcal{Q}$  are listed in Tab. 5.5. These scenarios will be discussed in more detail later in Sec. 5.5.

In contrast, in a much wider class of models,  $C_{e\Phi}$  is generated at one-loop order. Suitable examples are again the generic three-field extensions with chiral enhancements discussed in Sec. 2.3, and a corresponding detailed analysis has been carried out in Refs. [202, 275]. These references have computed the relevant and the relevant matching conditions for the Wilson coefficients. The corresponding values of  $\kappa$  are necessarily real, and translated to our conventions for the Class I, II, III models they can be written as (for simplicity we set  $m_{\phi,\eta} = m_{\psi,\chi} \equiv M$ )

$$\kappa^I = \frac{|\lambda_H|^2}{\mathcal{Q}}, \quad \kappa^{II} = \frac{|\bar{\lambda}_H|^2}{\mathcal{Q}}, \quad \kappa^{III} = \frac{|a|^2}{\mathcal{Q}M^2}. \quad (3.50)$$

The coefficients  $\mathcal{Q}$  depend on the gauge quantum numbers of the BSM fields, and their values for the different classes and representations are listed in Tab. 3.2. In these models,  $\kappa$  is thus typically small, and in this case the muon–Higgs

$SU(2)_L$ rep.	(1, 2, 1)	(2, 1, 2)	(3, 2, 3)	(2, 3, 2)
Class I	$-\frac{1}{6}(1 + 2X)$	$-\frac{1}{3}X$	$\frac{1}{30}(1 - 6X)$	$-\frac{1}{15}(2 + 3X)$
Class II	$-\frac{1}{2}(3 + 4X)$	$-\frac{1}{2}(1 + 4X)$	$-\frac{1}{10}(1 + 12X)$	$-\frac{1}{10}(11 + 12X)$
Class III	$-\frac{1}{2}(1 + 2X)$	$-X$	$\frac{1}{10}(1 - 6X)$	$-\frac{1}{5}(2 + 3X)$

**Table 3.2:** Values of  $\mathcal{Q}$  in Eq. (3.50) for the class I, II and III models and different possible representations of  $(\phi^\dagger, \psi, \chi)$  and  $(\psi, \phi^\dagger, \eta^\dagger)$ . Here,  $X$  denotes the hyper-charge of  $\phi^\dagger$  (class I or II) or  $\psi$  (class III).

coupling currently provides no relevant constraint on  $\Delta a_\mu$  via the correlation in Eq. (3.47), though this could change with increased precision that can be reached at the future FCC-hh [279].

In exceptional cases, however, the hypercharges  $X$  are such that  $\mathcal{Q}$  vanishes. This corresponds to scenarios with a cancellation of the chirally enhanced contributions to  $\Delta a_\mu$ . For values of  $X$  close to this point,  $\kappa$  is strongly enhanced and the constraints from the muon–Higgs coupling become more relevant [202].

### 3.4. Electroweak precision observables

Electroweak precision observables (EWPO) provide stringent tests of the electroweak sector of the SM at the quantum level as well as strong bounds on new physics scenarios. Key electroweak observables are the electroweak boson masses  $M_{W,Z,h}$ , the muon life time and the related Fermi constant  $G_F$ , and effective weak mixing angles  $\sin^2 \theta_{\text{eff}}^f$  for the interaction of a fermion  $f$  with the  $Z$  boson at the  $Z$ -pole. Like  $a_\mu$ , the EWPOs are strongly sensitive to loop effects. But while  $a_\mu$  is related to chirality flips and can be chirally enhanced, EWPOs instead are sensitive to so-called custodial symmetry, an approximate  $SU(2)_{L+R}$  symmetry of the electroweak vacuum [280].<sup>18</sup> In short, the phenomenology of EWPOs is quite independent and complementary to the one of  $a_\mu$ , but there is one important common ingredient, which we will discuss in the following.

The EW sector of the SM at tree level is parametrised by the  $SU(2)_L \times U(1)_Y$  gauge couplings  $g_2$  and  $g_1$  as well as the quartic Higgs coupling  $\lambda$  and the mass parameter  $\mu^2$  that characterise the Higgs potential and govern the EWSB scale. In precision calculations, these four parameters are typically traded for the finestructure constant  $\alpha$ ,  $G_F$ ,  $M_Z$  and  $M_h$  which is the minimal set of experimental input parameters with the smallest relative uncertainty. To illustrate the behaviour of higher orders and compare with  $a_\mu$ , we list the leading shifts to two important EWPOs, the  $W$ -boson mass and the effective weak mixing angle (for a review we refer to Ref. [281]),

$$\frac{\Delta M_W^2}{M_W^2} = \frac{s_W^2}{s_W^2 - c_W^2} \Delta\alpha(M_Z^2) + \frac{c_W^2}{c_W^2 - s_W^2} \Delta\rho + \dots, \quad (3.51)$$

$$\frac{\Delta \sin^2 \theta_{\text{eff}}^f}{\sin^2 \theta_{\text{eff}}^f} = \frac{c_W^2}{c_W^2 - s_W^2} \Delta\alpha(M_Z^2) + \frac{c_W^2}{s_W^2 - c_W^2} \Delta\rho + \dots \quad (3.52)$$

Here  $\Delta\rho$  is the universal correction to the  $\rho$  parameter defined via the neutral- to charged-current ratio at low energies. It is also related to the ratio  $\frac{M_W^2}{c_W^2 M_Z^2}$ , which is equal to  $\rho^{\text{tree}} = 1$  in the SM at tree level because of custodial symmetry, but  $\Delta\rho$  arises from breakings of this symmetry such as the large top-bottom mass splitting and similar properties of BSM extensions [280, 282, 283]. The behaviour of  $\Delta\rho$  depends on very different physical mechanisms and is therefore typically

<sup>18</sup>In the SM this symmetry becomes exact in the limit  $g_1 \rightarrow 0$  and  $y_u = y_d$ .

quite unrelated to the behaviour of  $a_\mu$ .

The intriguing connection to  $a_\mu$  arises via the quantity  $\Delta\alpha(q^2)$  appearing in the above corrections to the EWPOs. This quantity corresponds to the relative shift of the finestructure constant between its value in the Thomson limit in the on-shell scheme,  $\alpha$ , and the effective  $\alpha(q^2)$  at higher energies. This shift arises from the photon vacuum polarisation, which also plays an important role in the evaluation of  $a_\mu$ .

While the leptonic contributions to  $\Delta\alpha$  are uncontroversial and precisely known, the hadronic corrections are of particular interest here. The hadronic vacuum polarisation (HVP) can be defined as

$$\text{had} \equiv -i\Pi_{\text{had}}(q^2) \left( q^2 g^{\mu\nu} - q^\mu q^\nu \right). \quad (3.53)$$

In case of  $a_\mu$  the leading HVP contribution (cf. Sec. 1.4) generated by Fig. 1.8a can be expressed in terms of the following dispersion integral [2, 284, 285]

$$a_\mu^{\text{HVP, LO}} = \frac{\alpha}{\pi^2} \int_{s_{th}}^{\infty} \frac{ds}{s} K(s) \text{Im}\{\Pi_{\text{had}}(s)\}, \quad (3.54)$$

where the integration starts at the  $\pi^0\gamma$  production threshold  $s_{th} = m_{\pi^0}^2$  and the kernel function is given by

$$K(s) = \int_0^1 dz \frac{(1-z)z^2}{z^2 + (1-z)\frac{s}{m_\mu^2}}. \quad (3.55)$$

This is the basic origin of  $a_\mu^{\text{HVP, LO}}$ . As discussed in Sec. 1.4, non-perturbative techniques are required to obtain accurate values for  $\Pi_{\text{had}}(s)$ , though currently there are unresolved tensions between different data-driven evaluations based on experimental  $e^+e^- \rightarrow \gamma^* \rightarrow \text{hadrons}$  measurements, and between data-driven evaluations and lattice simulations.

This hadronic vacuum polarisation also enters the EWPO through the hadronic correction  $\Delta\alpha_{\text{had}}^{(5)}(q^2)$  to the effective fine structure constant, given by

$$\Delta\alpha_{\text{had}}^{(5)}(q^2) = -\text{Re} \left( \Pi_{\text{had}}(q^2) - \Pi_{\text{had}}(0) \right). \quad (3.56)$$

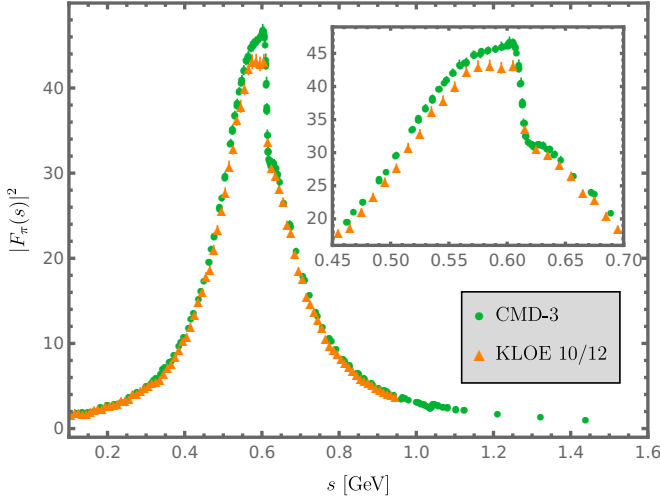
This hadronic correction can be expressed in terms of a dispersion integral similar to Eq. (3.54),

$$\Delta\alpha_{\text{had}}^{(5)}(M_Z^2) = \frac{M_Z^2}{\pi} \text{p.v.} \int_{s_{th}}^{\infty} ds \frac{\text{Im}\{\Pi_{\text{had}}(s)\}}{s(M_Z^2 - s)}. \quad (3.57)$$

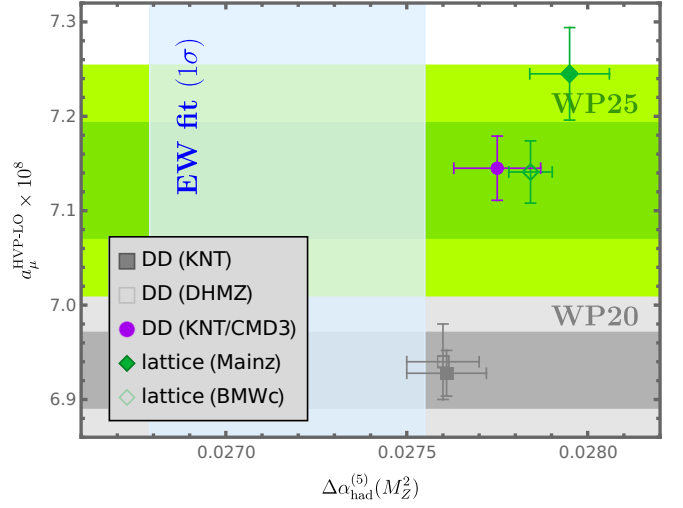
however with a qualitatively different kernel function. While  $K(s)$  decreases monotonically as  $1/s$  and thus gives the greatest weight to the low-energy region around  $s \gtrsim s_{th}$ , the kernel for  $\Delta\alpha_{\text{had}}^{(5)}(M_Z^2)$  remains nearly constant for  $s \ll M_Z^2$  resulting in an increased sensitivity to the contributions also from  $s \gg s_{th}$ .

Notably the HVP contributions to  $a_\mu^{\text{HVP, LO}}$  and  $\Delta\alpha_{\text{had}}^{(5)}(M_Z^2)$  are positively correlated, that is, an increase of  $\text{Im}\Pi_{\text{had}}$  (e.g. due to a larger measured  $e^+e^-$  cross section in case of the data-driven extraction) leads to an increase in both of these quantities, and a resulting decrease of the prediction for  $M_W$ , see Eq. (3.51) [286]. After the Brookhaven measurement, the SM prediction for  $a_\mu$  was about  $3\sigma$  lower than the experimental value, and the SM prediction for  $M_W$  was slightly lower than the measurement at the time. The above correlation means that assuming an increased HVP to reduce the discrepancy for  $a_\mu$  inevitably worsens the discrepancy for  $M_W$  and thus generally worsens the fit of EWPOs to experiment [286].

However, because of the significantly different energy dependence of the two kernel functions the impact on the EW fit depends on the energy scale at which  $\text{Im}\Pi_{\text{had}}$  is modified. After Ref. [286] appeared, several major developments



(a) Comparison between  $|F_\pi(s)|^2$  determined by KLOE and CMD-3



(b) Compilation of  $\Delta\alpha_{\text{had}}^{(5)}(M_Z^2)$  and  $a_\mu^{\text{HVP,LO}}$  from different references

**Figure 3.3:** (a) Comparison between the pion form factor  $F_\pi(s)$  obtained from the KLOE 10/12 [299, 300] and CMD-3 [100, 101] measurements of  $\sigma(e^+e^- \rightarrow \pi^+\pi^-(\gamma))$  for c.o.m. energies around the  $\rho$ -peak. (b) Compilation of values for  $\Delta\alpha_{\text{had}}^{(5)}(M_Z^2)$  and  $a_\mu^{\text{HVP,LO}}$  obtained from the data driven KNT [35, 288] (grey square), DHMZ [34] (empty grey square) and the KNT analysis with CMD-3 data substituted in the available energy range [76] (purple circle) as well as the lattice results from the Mainz [72] (green diamond) and BMW [69] (empty green diamond) collaborations where the corresponding  $\Delta\alpha_{\text{had}}^{(5)}(M_Z^2)$  was taken from Ref. [301]. The blue band shows the  $1\sigma$  region for  $\Delta\alpha_{\text{had}}^{(5)}(M_Z^2)$  determined from the EW fit [302] and the grey and green bands correspond to  $a_\mu^{\text{HVP,LO}}$  obtained in the WP20 [2] and WP25 [3], respectively.

took place. First, the discovery of the Higgs boson and measurement of  $M_h$  removed an important source of uncertainty. Secondly, subsequent updates of the analysis [287–290], particularly in light of the first lattice QCD results [61] for  $a_\mu^{\text{HVP,LO}}$ , as well as further theoretical considerations [291, 292] and more detailed comparisons between data driven and lattice evaluations [161, 163] confirmed that a modification of  $\text{Im}\Pi_{\text{had}}$  at very low energies (e.g. around the  $\rho$  peak at  $s \sim 0.6 \text{ GeV}^2$ ) are actually consistent with EWPO within uncertainties. And finally, as described in Sec. 1.4 there is now strong evidence from many lattice results that  $\text{Im}\Pi_{\text{had}}$  actually is indeed larger than previous  $e^+e^-$ -data based determinations at the time of Refs. [286] or [2] suggested. This is also supported by the more recent CMD-3 measurement of the pion form factor [100, 101] (see Fig. 3.3a), although despite extensive efforts [162, 169, 293, 294] so far no causes of the discrepancies to earlier  $e^+e^-$ -data based results have been identified.<sup>19</sup> Finally, the fit of the EWPO to data has also itself further improved e.g. through the known Higgs boson mass and recent LHC measurements of the  $W$ -boson mass,

$$M_W^{\text{ATLAS}} = 80.3665(159) \text{ GeV} [295], \quad (3.58a)$$

$$M_W^{\text{CMS}} = 80.3602(99) \text{ GeV} [296]. \quad (3.58b)$$

These recent measurements are the two of the most precise  $M_W$  measurements and are both in full agreement with the SM prediction.<sup>20</sup>

In Fig. 3.3b we show a comparison between results for  $\Delta\alpha_{\text{had}}^{(5)}(M_Z^2)$  and  $a_\mu^{\text{HVP,LO}}$  obtained by different groups as well

<sup>19</sup>The persisting discrepancies between  $e^+e^-$ -data based and lattice-based results have led to speculations whether BSM effects could be the cause. We will discuss such ideas in Sec. 5.1.5.

<sup>20</sup>This is in contrast to the CDF result 80.4335(94) GeV [297], which is in significant tension with the SM and with other measurements, leading to a poor fit if combined with the other measurements [298], and is therefore excluded from the global average, as discussed in Ref. [104].

as (for reference) the value preferred by (extracted indirectly from) the EW fit of Ref. [302]<sup>21</sup>

$$\Delta\alpha_{\text{had}}^{(5)}(M_Z^2)[\text{EW fit}] = 0.02716(39). \quad (3.59)$$

The data points are from  $e^+e^-$ -data driven evaluations of  $\text{Im}\Pi_{\text{had}}$  without [34, 35, 288] and with the recent CMD-3 data [76] as well as the lattice results from the Mainz [72] and BMW [69] collaborations. For details see the figure caption. The plot illustrates how the increased low-energy contributions found by CMD-3 and the lattice evaluations resolve the  $a_\mu$  discrepancy without significantly affecting the EW fit. It is worth pointing out that the uncertainty of Eq. (3.59) is driven mainly by the uncertainties of the experimental input and thus further experimental improvements could eventually establish strong tensions within the EW fit. Furthermore, additional observables like  $a_e$  and the muonium hyper-fine splitting also appear promising for future tests of the hadronic contributions [76].

### 3.5. Neutrino masses

One of the important breakthroughs of the past decades in particle physics is the observation of neutrino oscillations [303, 304], which has confirmed the existence of nonvanishing neutrino masses. A number of measurements have resulted in precise determinations of the mass-squared differences  $\Delta m_{ij}^2 \equiv m_i^2 - m_j^2$  between mass eigenvalues as well as the entries of the Pontecorvo-Maki-Nakagawa-Sakata (PMNS) matrix, relating the mass-eigenstates to the flavour eigenstates  $\nu_{e,\mu,\tau}$ . This PMNS matrix can be expressed in terms of three mixing angles  $\theta_{ij}$  for  $i, j = 1, 2, 3$  and one CP violating phase,  $\delta_{CP}$ . In total, the current combined experimental constraints for the case of normal ordering (inverted ordering) are [305]<sup>22</sup>

$$\Delta m_{21}^2 = 7.49_{-0.19}^{+0.19} \quad (7.49_{-0.19}^{+0.19}) \quad \times 10^{-5} \text{eV}^2, \quad (3.60)$$

$$\Delta m_{3l}^2 = 2.513_{-0.019}^{+0.021} \quad (-2.484_{-0.020}^{+0.020}) \quad \times 10^{-3} \text{eV}^2, \quad (3.61)$$

$$\sin^2 \theta_{12} = 0.308_{-0.011}^{+0.012} \quad (0.308_{-0.011}^{+0.012}), \quad (3.62)$$

$$\sin^2 \theta_{23} = 0.470_{-0.013}^{+0.017} \quad (0.550_{-0.015}^{+0.012}), \quad (3.63)$$

$$\sin^2 \theta_{13} = 0.02215_{-0.00058}^{+0.00056} \quad (0.02231_{-0.00056}^{+0.00056}), \quad (3.64)$$

$$\delta_{CP}/^\circ = 212_{-41}^{+26} \quad (274)_{-25}^{+22}. \quad (3.65)$$

For normal ordering (NO) the mass hierarchy and the largest mass splitting are  $m_1 < m_2 < m_3$  and  $\Delta m_{3l}^2 = \Delta m_{31}^2$ , and for inverted ordering (IO) they are  $m_3 < m_1 < m_2$  and  $\Delta m_{3l}^2 = \Delta m_{32}^2$ . This observation implies at least two massive neutrinos and three different mass eigenvalues.

In addition there are absolute upper limits on the maximum neutrino mass from cosmology (see Ref. [305] and references therein, and see Ref. [306] for further discussions of BOSS, eBOSS and Planck CMB data),

<sup>21</sup>We use Ref. [302] since it provides  $\Delta\alpha_{\text{had}}^{(5)}(M_Z^2)$ , however it appeared before the recent measurements of  $M_W$  [295, 296], both of which would improve the agreement or the EW fit with data. As an example, the fit result of Ref. [302] for  $M_W$  without using the experimental  $M_W$  input is 80.354(7) GeV, in excellent agreement with Eqs. (3.58).

<sup>22</sup>see NuFIT, [www.nu-fit.org](http://www.nu-fit.org).

$$m_{\text{tot}} = \sum m_\nu < 3 \times 10^{-10} \text{ GeV}, \quad (3.66)$$

and on the effective electron (anti-)neutrino mass from the KATRIN experiment [305, 307],

$$m_{\nu_e}^{(\text{eff})} < 4 \times 10^{-10} \text{ GeV}. \quad (3.67)$$

One important fact is that all experiments so far observed only interactions of left-handed neutrinos (or right-handed antineutrinos), corresponding to maximal parity violation. Accordingly the Standard Model (SM) contains only left-handed neutrino fields as part of the left-handed lepton doublets. Therefore, Yukawa interaction terms of neutrinos to the Higgs field, which would generate Dirac neutrino masses similarly to the masses of all other charged SM fermions, are not allowed. Hence neutrinos remain massless in the Standard Model and BSM physics is needed to generate and explain neutrino masses. It is natural to ask whether neutrino masses can be linked to charged lepton observables such as  $a_\mu$ . Here we will briefly review ideas to explain the origin of neutrino masses and give generic arguments on how the mechanism to generate neutrino masses could contribute to  $a_\mu$ .

### 3.5.1. Overview of neutrino mass terms

Since neutrinos are electromagnetically neutral they can be either Dirac or Majorana fermions, i.e. fermions which are equal to their antiparticles. Dirac masses are compatible with lepton number conservation and lead to the existence of a neutrino magnetic dipole moment [308]. Majorana masses imply lepton number violation by  $|\Delta L| = 2$ , and consequently processes such as neutrinoless double  $\beta$ -decay ( $0\nu 2\beta$ ) are possible — these are intensely searched for in various experiments [309, 310]. There are many attractive ways to generate Majorana neutrino masses, such as the seesaw mechanism [311–314] discussed below. Currently it is unknown how neutrino masses arise and whether neutrinos are of Majorana or Dirac type.

For a brief overview of neutrino mass terms we allow both Dirac and Majorana masses, and we assume the existence of  $m + n$  neutrino gauge eigenstate fields, combined into  $\omega_R \equiv (\nu_{L1}^C, \dots, \nu_{Lm}^C, N_{R1}, \dots, N_{Rn})^T$ , where the  $\nu_{Li}$  contain the  $m = 3$  generations of SM neutrino fields and where  $N_{Ri}$  denotes the additional neutral right-handed fermions, which can be called right-handed neutrinos or sterile neutrinos or neutral leptons, depending on the context. We can define a combined Majorana field  $\Omega \equiv \omega_R + \omega_R^C$  and write the general form of the neutrino mass Lagrangian in terms of these neutrino gauge eigenstate fields as

$$\mathcal{L}_{\nu\text{-mass}} = -\frac{1}{2} \bar{\Omega} \mathcal{M}_\nu \Omega, \quad (3.68)$$

where the mass matrix takes a block form

$$\mathcal{M}_\nu = \begin{pmatrix} \delta \mathcal{M}_L & \mathcal{M}_D \\ \mathcal{M}_D^T & \mathcal{M}_R \end{pmatrix}. \quad (3.69)$$

We do not consider CP violation here and keep  $\mathcal{M}_\nu$  real for simplicity. Depending on the model, the number  $n$  of additional neutrino fields might be zero or non-zero, and some of the blocks might be zero or non-zero. Generally,  $\mathcal{M}_D$  denotes Dirac neutrino masses which can be generated from Yukawa-type interactions e.g. if right-handed  $SU(2)_L$  singlet

neutrinos  $N_R$  exist. The block  $\mathcal{M}_R$  denotes the Majorana mass of the additional right-handed neutrinos. Finally,  $\delta\mathcal{M}_L$  is a potential Majorana mass of the SM-like left-handed neutrinos.

We can use this general structure to classify the BSM scenarios which aim to explain the neutrino mass generation. There are four general possibilities:

- (a)  $\mathcal{M}_R = 0$ ,  $\mathcal{M}_D \neq 0$  obtained e.g. from Yukawa interaction terms (e.g. pure Dirac masses),
- (b)  $\mathcal{M}_D = \mathcal{M}_R = 0$  (e.g. seesaw type II, Zee and Babu models),
- (c)  $\mathcal{M}_R \neq 0$ , and  $\mathcal{M}_D \neq 0$  (e.g. seesaw type I, III),
- (d)  $\mathcal{M}_D = 0$ ,  $\mathcal{M}_R \neq 0$ , non-zero  $\delta\mathcal{M}_L \neq 0$  obtained from loop diagrams (e.g. Ma/scotogenic model).

In all cases where  $\delta\mathcal{M}_L$  is not specified, it may be generated either at the tree-level or at the loop level, depending on model details.

Scenario (a) together with  $\delta\mathcal{M}_L = 0$  corresponds to the only scenario with Dirac masses and lepton number conservation. In the simplest case, the neutrino masses can arise in the same way as the mass generation of the up-type quarks of the SM. This requires at least three generations of right-handed singlet neutrinos  $N_{Ri}$ , ( $i = 1, 2, 3, \dots$ ) and the additional Yukawa interaction terms

$$\mathcal{L}_{\nu\text{-Dirac mass}} = -y_\nu^{ij} \bar{l}_{Li} \tilde{\Phi} N_{Rj} + \text{h.c.} \quad (3.70)$$

In this case the neutrinos obtain (matrix-valued) Dirac masses  $m_\nu = y_\nu v / \sqrt{2}$ . The required Yukawa coupling values are however extremely tiny,  $|y_\nu| \lesssim \mathcal{O}(10^{-12})$ .

Before exemplifying the other scenarios (b,c,d) we mention that neutrino masses can also be described using the approach of low-energy effective theories. Especially if SMEFT is the correct EFT, see Sec. 2.4, then neutrino masses can arise via the following dimension-5 operator [218, 315]<sup>23</sup>

$$\begin{aligned} Q_{\nu\nu}^{ab} &= \epsilon_{jk} \epsilon_{mn} \Phi^j \Phi^m (l_{La}^k)^T C l_{Lb}^n \\ &= \epsilon_{jk} \epsilon_{mn} \Phi^j \Phi^m \overline{(l_{La}^k)^C} l_{Lb}^n, \end{aligned} \quad (3.71)$$

where  $a$  and  $b$  denote the flavour (generation) indices. This operator violates lepton number by  $|\Delta L| = 2$  [218, 315], and upon inserting the Higgs  $vev$  it generates Majorana masses for neutrinos

$$(M_\nu)_{ab} = c_{\nu\nu}^{ab} \frac{v^2}{2M_\Lambda}, \quad (3.72)$$

where the suppression scale  $M_\Lambda$  has been pulled out of the Wilson coefficient  $C_{\nu\nu}^{ab} = c_{\nu\nu}^{ab} / M_\Lambda$ .

This neutrino mass term has the structure and effect of the block matrix  $\delta\mathcal{M}_L$  in Eq. (3.69), so one may also say that this block matrix often arises in a low-energy EFT upon integrating out heavy fields in the fundamental theory.

### 3.5.2. Seesaw mechanism and radiative mass generation

Here we briefly survey six different ways to generate neutrino masses, exemplifying cases (b,c,d) above. All these models lead to Majorana neutrino masses described at low energies by the formula (3.72). In this way the small neutrino masses

<sup>23</sup>We use the convention of Ref. [218]. The general expression of the dimension-5 operator for more than one Higgs doublet is  $Q_{\nu\nu}^{ab} = f_{abrp} \overline{l_{jaL}^C} l_{kbL} \phi_r^m \phi_p^n \epsilon_{jm} \epsilon_{kn} + f'_{abrp} \overline{l_{jaL}^C} l_{kbL} \phi_r^m \phi_p^n \epsilon_{jk} \epsilon_{mn}$  [315].

Model	Field	$(\mathcal{G}_{EW})_{\text{spin}}$	Parameters
Seesaw Type I	$N_{Ri}$	$(\mathbf{1}, 0)_{\frac{1}{2}}$	$(\mathbf{y}_\nu)_{ij}, M_{Ri}$
Seesaw Type II	$\Delta$	$(\mathbf{3}, 1)_0$	$(\mathbf{y}_\nu)_{ij}, M_\Delta, \boldsymbol{\mu}$
Seesaw Type III	$\Sigma_{Ri}$	$(\mathbf{3}, 0)_{\frac{1}{2}}$	$(\mathbf{y}_\nu)_{ij}, M_{Ri}$

**Table 3.3:** Field content of three tree-level seesaw models. The respective spins and representations with respect to  $\mathcal{G}_{EW} = \text{SU}(2)_L \times \text{U}(1)_Y$  are given in the brackets. The indices  $i, j$  are generation indices, while  $\text{SU}(2)_L$  indices are suppressed. In Type-I and III the number of fields corresponds to the number of neutrino masses generated at tree-level. All fields are singlets under  $\text{SU}(3)_c$ .

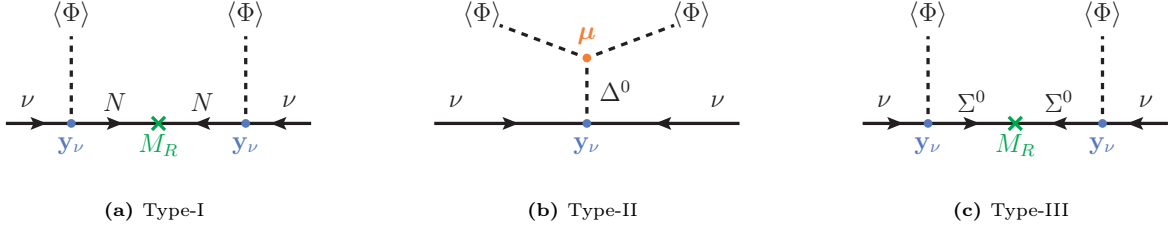


**Figure 3.4:** Diagrams generating neutrino masses and the effective operator Eq. (3.71) at tree-level in the type I, II and III seesaw mechanism.

are explained either by very heavy fundamental masses  $M_\Lambda \approx 10^{15}$  GeV with  $c_{\nu\nu} \approx \mathcal{O}(1)$ , or by tiny lepton-number violating couplings leading to a very small coefficient  $c_{\nu\nu}$ .

The seesaw mechanism is a particularly attractive and simple way to generate neutrino masses. Here, new fields are added to the SM such that a mass matrix of the form (3.69) arises and effectively neutrino masses of the form (3.72) are generated at tree-level. The three types that allow this are illustrated in Fig. 3.4. The additional fields for each seesaw types are displayed in Table 3.3. Type I [311–314] involves right-handed neutrino singlets  $N_R$  with heavy Majorana mass term and gauge invariant Yukawa interaction with the SM lepton doublets and Higgs field. Type III [316] is similar to type I but adds right-handed fermion triplets  $\Sigma_{Ri}$  to the SM. Type II [317] instead adds a triplet scalar field  $\Delta$  with gauge invariant interactions of the form  $ll\Delta$  and  $\Phi\Phi\Delta^\dagger$ . The essential Lagrangian terms can be written as

$$\text{type I: } \mathcal{L} \supset - \left[ (\mathbf{y}_\nu)_{ij} \bar{l}_{Li} \tilde{\Phi} N_{Rj} + \text{h.c.} \right] - \frac{1}{2} M_{Ri} \overline{N_{Ri}^C} N_{Ri}, \quad (3.73a)$$

$$\text{type III: } \mathcal{L} \supset - \left[ (\mathbf{y}_\nu)_{ij} \bar{l}_{Li} \Sigma_{Rj}^a \sigma^a \tilde{\Phi} + \text{h.c.} \right] - \frac{1}{2} M_{Ri} \overline{\Sigma_{Ri}^C} \Sigma_{Ri}, \quad (3.73b)$$

$$\text{type II: } \mathcal{L} \supset - \left[ (\mathbf{y}_\nu)_{ij} \bar{l}_{Li}^C \Delta^a \sigma^a l_{Lj} + \text{h.c.} \right] - M_\Delta^2 |\Delta|^2 - \boldsymbol{\mu} \Phi^\dagger (\Delta^a \sigma^a) \tilde{\Phi}, \quad (3.73c)$$

The tree-level mass matrices  $\mathcal{M}$  arising from replacing the Higgs  $vev$  into the Lagrangians have the structures

$$\text{type I, III: } \delta\mathcal{M}_L = 0 \quad \mathcal{M}_D \sim \mathbf{y}_\nu v \quad \mathcal{M}_R \sim M_R \quad (3.74a)$$

$$\text{type II: } \delta\mathcal{M}_L = \frac{v^2 \boldsymbol{\mu} \mathbf{y}_\nu}{2M_\Delta^2} \quad \mathcal{M}_D = 0 \quad \mathcal{M}_R = 0. \quad (3.74b)$$

They correspond to the above scenarios (c) and (b), respectively. After integrating out all heavy BSM fields, the resulting

values of the dimensionful coefficients of the dimension-5 operator have the form<sup>24</sup>

$$C_{\nu\nu} \sim \frac{\mathbf{y}_\nu^2}{M_R^2} \text{ (type I, III)} \qquad C_{\nu\nu} \sim \frac{\boldsymbol{\mu}\mathbf{y}_\nu}{M_\Delta^2} \text{ (type II)}, \quad (3.75)$$

suppressing flavour indices.

In type II, the mass matrix arises from a triplet  $vev$   $v_\Delta$  which arises automatically as  $v_\Delta \sim \mu v^2/M_\Delta^2$  because the potential receives a linear term  $\sim \mu v^2 \Delta$  after EWSB. The light eigenvalues of the mass matrices in Eq. (3.74) agree with the neutrino masses obtained via  $v^2 C_{\nu\nu}$  from Eq. (3.75).

In all cases the neutrino masses follow the general pattern in Eq. (3.72), but the detailed parameter dependences differ between the types. Of course, the total particle spectrum and wider phenomenology of the three types are very different. We note in passing that the general idea of generating small neutrino masses at tree-level via the exchange of BSM states can be extended in many ways. Two illuminating examples are the inverse seesaw and the linear seesaw mechanisms, proposed in Refs. [320, 321] and Refs. [322, 323], respectively. Both cases may be regarded as extensions of the Type I seesaw mechanism and likewise correspond to our above scenario (c). Compared to Type I seesaw, the number of BSM neutrinos is doubled, and our matrices  $\mathcal{M}_R$  and  $\mathcal{M}_D$  become  $2 \times 2$  and  $1 \times 2$  block matrices. These block matrices and the resulting active neutrino masses have the structure

$$\text{inverse seesaw:} \quad \mathcal{M}_R \sim \begin{pmatrix} 0 & M \\ M^T & \mu \end{pmatrix} \quad \mathcal{M}_D \sim \begin{pmatrix} \mathbf{y}_\nu v & 0 \end{pmatrix} \quad M_\nu \sim \mu(\mathbf{y}_\nu v)^2/M^2, \quad (3.76)$$

$$\text{linear seesaw:} \quad \mathcal{M}_R \sim \begin{pmatrix} 0 & M \\ M^T & 0 \end{pmatrix} \quad \mathcal{M}_D \sim \begin{pmatrix} \mathbf{y}_\nu v & M_L \end{pmatrix} \quad M_\nu \sim M_L \mathbf{y}_\nu v/M. \quad (3.77)$$

In the inverse seesaw case,  $M$  is a Dirac mass in the BSM neutrino sector and  $\mu$  is a lepton-number violating parameter. The smallness of the active neutrino masses is then explained by small  $\mu$  without the need for very large  $M$ . In the linear seesaw case,  $M_L$  acts as a lepton-number violating mass parameter, and the active neutrino masses turn out to depend only linearly on the Yukawa couplings.

A very attractive alternative to the three seesaw types mentioned above or their tree-level extensions is the idea of radiative neutrino mass generation, where  $\delta\mathcal{M}$  is effectively obtained from loop diagrams, providing additional suppression. We illustrate the idea again by briefly reviewing three well-known models by Zee [324], Babu [325], and by Ma [326], respectively. In the Zee and Babu models only the scalar sector is enlarged whereas in the scotogenic model (or Ma model) the fermion and scalar sectors are enlarged with Majorana fermions and an inert Higgs doublet. The field contents in each model are listed in Table 3.4. The Zee model can be understood as an extended two Higgs doublet model (2HDM), of which the scalar sector is enlarged by one more charged scalar singlet  $h^+$ . The Babu model is built on the SM by adding two charged scalar singlets: one singly charged scalar  $h^+$  and one doubly charged scalar  $k^{++}$ . The scotogenic model can be considered an extended inert two Higgs doublet model where three right-handed neutrinos  $N_{R1,2,3}$  are included

---

<sup>24</sup>We note that in these seesaw models, it is possible that some neutrinos remain massless at tree level. In such a case, loop corrections can still generate viable, non-vanishing neutrino masses. For instance in the seesaw type I case, Ref. [318] shows that specific textures of the mass matrices  $\mathcal{M}_R$  and  $\mathcal{M}_D$  lead to vanishing tree-level neutrino masses. Non-vanishing masses and effective contributions to  $\delta\mathcal{M}_L$  then arise from loop diagrams with  $Z$ - or Higgs-boson exchange. In the seesaw type III case, it is also possible to generate three massive active neutrinos with just a single  $\Sigma_R$  field. Here, there can be only a single massive light neutrino at tree level, but the other light neutrino masses can be generated by two-loop diagrams involving two  $W$ -bosons [319].

Model	Symmetry	Fields	Rep.	Parameters
Zee Model	$\mathcal{G}_{EW}$	$h^+$ $\Phi_2$	$(\mathbf{1}, 1)_0$ $(\mathbf{2}, \frac{1}{2})_0$	$\mathbf{f}_{ij}, \mathbf{y}_{ij}^\alpha, \mathbf{M}_{\alpha\beta}$
Babu Model	$\mathcal{G}_{EW}$	$h^+$ $k^{++}$	$(\mathbf{1}, 1)_0$ $(\mathbf{2}, 2)_0$	$\mathbf{f}_{ij}, \mathbf{h}_{ij}, \mu$
Ma Model (scotogenic)	$\mathcal{G}_{EW}; \mathbb{Z}_2$	$N_{Ri}$ $\eta$	$(\mathbf{1}, 0; -)_{\frac{1}{2}}$ $(\mathbf{2}, \frac{1}{2}; -)_0$	$M_{Ri}, \mathbf{h}_{ij}, \lambda_5$

**Table 3.4:** One-loop neutrino mass models. The respective spins and representations with respect to  $\mathcal{G}_{EW} = \text{SU}(2)_L \times \text{U}(1)_Y$  (or  $\mathbb{Z}_2$ ) are given in the brackets. All fields are singlets under  $\text{SU}(3)_c$ .

in addition to the inert Higgs doublet  $\eta$ . All three models are based on the SM gauge invariance, but in the scotogenic model also a discrete  $\mathbb{Z}_2$  invariance is imposed. The additional fields are odd under  $\mathbb{Z}_2$  and the SM fields even. As no additional Majorana fermions are added,  $\mathcal{M}_R$  and  $\mathcal{M}_D$  vanish in the Zee and Babu models, corresponding to scenario (b) above, while the scotogenic model represents scenario (d).

The additional Lagrangians of the three models can be written as

$$\text{Zee-model: } \mathcal{L} \supset \mathbf{f}_{ij} \overline{l_{Li}^C} l_{Lj} h^+ - \mathbf{y}_{ij}^\alpha \overline{l_{Li}} \Phi_\alpha e_{Rj} + \mathbf{M}_{\alpha\beta} \tilde{\Phi}_\alpha^\dagger \Phi_\beta h^+ + \text{h.c.}, \quad (3.78a)$$

$$\text{Babu-model: } \mathcal{L} \supset \mathbf{f}_{ij} \overline{l_{Li}^C} l_{Lj} h^+ + \mathbf{h}_{ij} \overline{e_{Ri}^C} e_{Rj} k^{++} + \mu (h^+ h^+ k^{--}) + \text{h.c.}, \quad (3.78b)$$

$$\text{Ma-model: } \mathcal{L} \supset \frac{1}{2} M_{Ri} \overline{N_{Ri}^C} N_{Ri} - \mathbf{h}_{ij}^\dagger \overline{l_{Li}} N_{Rj} \tilde{\eta} - \frac{1}{2} \lambda_5 (\eta^\dagger \Phi) (\eta^\dagger \Phi) + \text{h.c.} \quad (3.78c)$$

In the Zee and Babu models the scalar singlet  $h^+$  has charge  $Q = +1$  and Lepton number  $L = 2$ ; the Higgs doublet(s) in the Zee model are called  $\Phi_a$ ,  $a \geq 2$  (the SM Higgs doublet is denoted as  $\Phi \equiv \Phi_1$  in this context). As the  $vev$  of  $h^+$  vanishes it does not contribute the gauge boson masses.

In the Zee model the cubic interaction term  $\sim M_{ab}$  is responsible for the one-loop Majorana mass generation for the neutrinos. Similarly, in the Babu model, the triple scalar coupling term  $\sim \mu$  is responsible for the two-loop generation of Majorana neutrino masses.

In the Ma/scotogenic model the parameter  $\lambda_5$  is lepton-number violating and responsible for the loop generation of Majorana neutrino masses. Note that the parameter  $\mathbf{h}$  in the scotogenic model has a different meaning than the parameter  $\mathbf{h}$  in the Zee and Babu models.

The lowest-order contributions to the dimension-5 operator is then given by the one- and two-loop diagrams in Fig. 3.5. Like in the seesaw case, the neutrino masses are then generated via the effective dimension-5 operator with the schematic form

$$\text{Zee-model: } C_{\nu\nu} \sim \frac{1}{16\pi^2} \frac{\mathbf{f} y v m_\ell}{M_h^2} \mathbf{M} \ln(M_h^2/M_\Phi^2), \quad (3.79a)$$

$$\text{Babu-model: } C_{\nu\nu} \sim \frac{1}{16\pi^2} \frac{\mathbf{f} m_\ell \mathbf{h} m_\ell \mathbf{f}^\dagger}{2\pi^2 M_{k^{++}}^2} \mu \ln^2 \left( \frac{M_{h^+}^2 + M_{k^{++}}^2}{M_{h^+}^2} \right), \quad (3.79b)$$

$$\text{Ma-model: } C_{\nu\nu} \sim \frac{1}{16\pi^2} 2\lambda_5 \frac{\mathbf{h} \mathbf{h} M_R}{m_0^2 - M_R^2} \left( 1 - \frac{M_R^2}{m_0^2 - M_R^2} \ln \frac{m_0^2}{M_R^2} \right), \quad (3.79c)$$

where all indices corresponding to flavour or the number of the Higgs doublet have been suppressed and where  $m_\ell$  denotes

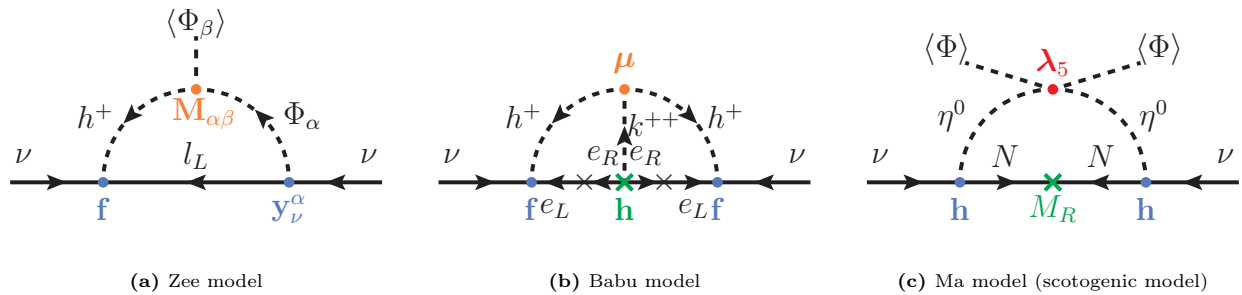


**Figure 3.5:** Lowest-order one-loop or two-loop diagrams contributing to the dimension-5 operator Eq. (3.71) in three well-known radiative neutrino mass scenarios, the Zee-, Babu- and Ma/scotogenic models. See Eqs. (3.79). The lepton-number violating vertices are highlighted in orange.

a lepton mass of any generation. In the scotogenic model,  $m_0$  denotes the new scalar mass scale. The loop-generated masses are suppressed by the loop factor  $\frac{1}{16\pi^2}$  which allows lower BSM masses for small neutrino masses.

The six sketched models represent basic ways how neutrino masses can be generated. They can of course be extended and generalised. For example, tree-level and loop generation can be combined as mentioned in footnote 24 or as in Ref. [327], where additional scalar doublets and right-handed singlet neutrinos are added; mass generation may arise only at higher loop orders, or models may use an extended gauge group. Finally it is possible that the dimension-5 operator in Eq. (3.71) does not provide an appropriate description because higher-dimension operators or a different EFT should be used. We will discuss a variety of modified models in Sec. 5.6, together with their impact on  $a_\mu$ .

### 3.5.3. Example contributions of neutrino mass generation mechanisms to $a_\mu$

We can now return to the question how neutrino masses can be related to  $a_\mu$ . In essence, not the light neutrinos themselves, but the BSM particles which are responsible to generate the neutrino masses can often cause potentially significant contributions to  $a_\mu$ .<sup>25</sup>

Two simple considerations illustrate this point. First, nonvanishing neutrino masses directly modify the value of the EWSM diagram with W- $\nu$ -loop in Fig. 1.7, see also Eq. (1.64). Technically, the second argument of the appearing  $\mathcal{F}^{\text{FV}}, \mathcal{G}^{\text{FV}}$  loop function is then  $z_\nu = m_\nu^2/M_W^2$  instead of zero. Given the absolute neutrino mass bound, the variable  $z_\nu \lesssim 10^{-24}$  and the absolute impact of neutrino masses on this diagram is

$$\Delta a_\mu^W(\nu\text{-mass}) \lesssim 10^{-33} \quad (3.80)$$

and thus totally negligible.<sup>26</sup> Second we can consider the EFT point of view and compare the dimension-5 term Eq. (3.71) for neutrino masses with the dimension-6 dipole operator term Eq. (2.41). The neutrino masses and  $a_\mu$  contributions are then parametrised as

$$m_\nu \sim c_{\nu\nu} \times \frac{v^2}{M_\Lambda} \quad \Delta a_\mu \sim c_{e\gamma} \times \frac{vm_\mu}{M_\Lambda^2}, \quad (3.81)$$

again pulling out appropriate powers of  $M_\Lambda$  to obtain dimensionless Wilson coefficients. Here the neutrino masses have only a single  $M_\Lambda$  suppression, while  $\Delta a_\mu$  has a suppression  $vm_\mu/M_\Lambda^2$ . In addition, both contributions involve Wilson coefficients  $c_{\nu\nu}, c_{e\gamma}$  which can in principle be independent.

<sup>25</sup>For similar connections between  $a_\mu$  and neutrino transition moments see Ref. [328].

<sup>26</sup>Here we do not yet consider the effects of any mixing or contributions from new states that may accompany neutrino masses.

In the simplest case where  $c_{\nu\nu}^{ab} \sim 1$  and the small neutrino masses require  $M_\Lambda \sim 10^{15}$  GeV, we again obtain entirely negligible values of  $\Delta a_\mu$ . However, it is possible that the BSM scale  $M_\Lambda$  is significantly smaller and the smallness of neutrino masses is instead explained by a strongly suppressed  $L$ -violating parameter  $c_{\nu\nu} \ll c_{e\gamma}$ . In this case, the above relation implies the numerical relationship

$$\Delta a_\mu \sim 10^{-9} \left( \frac{1 \text{ TeV}}{M_\Lambda} \right) \left( \frac{c_{e\gamma}}{c_{\nu\nu}} \times 10^{-8} \right). \quad (3.82)$$

Here a neutrino mass of the order 0.05 eV, slightly below the current upper limit, has been assumed. The formula shows that in scenarios where the neutrino masses arise from underlying BSM physics not far above the TeV scale, and where the  $\Delta L = 2$  operators receive an additional suppression, significant  $\Delta a_\mu$  can arise from the same underlying physics. Such neutrino mass models are constrained by  $\Delta a_\mu$ .

The possible connections between  $a_\mu$  and neutrino masses thus depend strongly on details of the underlying mechanisms. Here we illustrate the possible relationships with the help of few simple and well-motivated models as a background for further discussions in later sections. We begin with two examples pointed out in Ref. [329], which first asked the question whether neutrinos and contributions to  $a_\mu$  could be related. The first example is the seesaw type II model (3.73c) with scalar triplet  $\Delta$  and two mass parameters  $\mu$ ,  $M_\Delta$  and the neutrino mass scale given via Eq. (3.75) as  $\mu y_\nu v^2 / M_\Delta^2$ . The small neutrino masses can be well explained by a low seesaw scale  $M_\Delta \sim 1$  TeV, if the lepton-number violating parameter  $\mu$  is tiny. A one-loop diagram for  $a_\mu$  is obtained via two muon–triplet–anti-lepton vertices governed by the Yukawa coupling  $y_\nu$ , as shown in Fig. 3.6a. The contributions correspond to the one-field model 4 in Tab. 2.1 discussed in Sec. 2.2. They cannot contain a chiral enhancement, and the sign is fixed to be negative. Hence,  $\Delta a_\mu$  in the seesaw type II model is of the order

$$\Delta a_\mu \sim - \frac{|\mathbf{y}_\nu|^2}{64\pi^2} \frac{m_\mu^2}{M_\Delta^2}. \quad (3.83)$$

The statement on the negative sign of  $\Delta a_\mu$  has been generalised to all seesaw type I and III models in Ref. [330].

Another example is the scotogenic model (3.78c) with loop-generated neutrino masses via loops of  $\mathbb{Z}_2$ -odd right-handed neutrinos and Higgs doublet  $\eta$ . Again, the formula for the resulting neutrino masses allows a low seesaw scale  $M_R$  if the lepton-number violating coupling  $\lambda_5$  is tiny. Contributions to  $a_\mu$  correspond to model 26 in Tab. 2.2; they are given by a diagram of the same kind as in the seesaw type II case, see Fig. 3.6b. The result is thus of the same form, with the appropriate coupling of the lepton to the right-handed neutrino and the new Higgs doublet  $\eta$ ,

$$\Delta a_\mu \sim - \frac{|\mathbf{h}|^2}{64\pi^2} \frac{m_\mu^2}{M_\Delta^2}. \quad (3.84)$$

Both of these examples, together with the neutrino masses in Eqs. (3.75) and (3.79c), are concrete illustrations of the relationship given in Eq. (3.82). The role of the BSM scale  $M_\Lambda$  is taken by the triplet or right-handed neutrino masses, and the role of  $c_{\nu\nu}^{ab}/c_{e\gamma}$  is taken by either the small ratio  $\mu/M_\Delta$  or by the small parameter  $\lambda_5$ , respectively. Note that  $\mu$  and  $\lambda_5$  are both lepton-number violating and can therefore be assumed to be small in a technically natural way. Due to the negative signs, none of the tree-level models are candidates to explain large positive deviations like  $\Delta a_\mu^{\text{Exp-WP2020}}$ . Beyond that, Ref. [329] showed that the correlations to lepton flavour violation of the kind discussed in Sec. 3.2 are strong and essentially exclude sizeable magnitudes of contributions to  $a_\mu$  in both models. Hence the new result  $\Delta a_\mu^{\text{Exp-WP2025}}$  does not exclude additional parameter regions.

Though  $\Delta a_\mu$  in these two examples turns out to be ultimately small, the examples illustrate how sizeable  $\Delta a_\mu$  may arise in neutrino mass models and how such models may be constrained by  $a_\mu$  results. In Sec. 5.6 we will discuss further



**Figure 3.6:** One-loop contributions to  $a_\mu$  in two neutrino mass models. See Eqs. (3.83,3.84). The chirality flip is shown explicitly on the external line; similar diagrams with the chirality flip on the other line exist as well.

concrete neutrino mass models. The models show a great diversity of ideas how to explain neutrino masses and their smallness, and some are motivated also by other phenomenological goals. Many of them are elaborate constructions extending the scotogenic/Ma model, see Tab. 5.6, but several others are distinct, see Tab. 5.7. Sec. 5.6 will also discuss the contributions to  $a_\mu$  in these models. In many of them, chirally enhanced contributions to  $a_\mu$  arise of the kind present in the three-field models of Classes I/II/III in Sec. 2.3. For this reason, these models are non-trivially constrained by  $a_\mu$ .

### 3.6. Dark Matter

Dark Matter (DM) is one of the primary motivations for physics beyond the standard model, and is evidenced by galaxy rotation curves (see e.g. [331, 332]), gravitational lensing (e.g. [333, 334]) and the cosmic microwave background [335]. Furthermore cold dark matter is one of the postulates of the standard model of cosmology and is required to reproduce the structure formations of galaxies. See Refs. [336–338] for detailed, pedagogical reviews of the evidence and further references to the original work.

To contribute to the dark matter inferred from astrophysics observations a particle dark matter candidate should be electromagnetically neutral<sup>27</sup> and non-baryonic and is thus expected to interact with the SM at most through weak or gravitational interactions or some new interaction between the SM and the dark sector. DM can influence the anomalous magnetic moment of the muon ( $a_\mu$ ) when the stable dark matter particle enters the loops, and/or from loops involving other new states that are introduced to make a consistent gauge invariant theory explaining dark matter. This can lead to a positive or negative shift away from SM prediction of  $a_\mu$  and means that a measurement of  $a_\mu$  with a large deviation from the SM prediction could be experimental evidence of particle dark matter, while measurements consistent with the standard model prediction serve as an important constraint on theories that explain dark matter.

The possible topologies for one-loop diagrams that can influence  $a_\mu$  are shown in Fig. 2.1 in Sec. 2.1 where they are discussed in detail and the form of the corrections they imply may be found. Since it should be electromagnetically neutral the dark matter particle cannot couple to the photon, and since it should also be stable it must not have kinematically allowed channels through which it decays. Thus in one-loop corrections to  $a_\mu$ , the dark matter candidate may then only play the role of the particle connecting the muons in the loop and must therefore have couplings between the DM candidate, the muon and the charged particle in the loop. These properties significantly constrain the possible quantum numbers, and can also constrain the mass of the DM candidate, since decays through this coupling must be kinematically forbidden.

<sup>27</sup>The possibility of milli-charged dark matter has also been considered in the literature, see e.g. [339–341], and remains possible as long as the charges are small enough [342], but we will not discuss it further here.

In the following we discuss the possible impact of the new  $a_\mu$  result on models for dark matter. We begin with general discussions of dark matter properties and possible contributions of dark matter candidates to  $a_\mu$ , then we systematically discuss dark matter models with one, two, or three new fields.

### 3.6.1. The relic density of dark matter, WIMPs and the detection of dark matter

Any particle with the properties described above is a dark matter candidate and *may* contribute to the observed dark matter. However, this is not sufficient to explain dark matter observations, one also needs to check that the correct abundance of dark matter can be generated in order to agree with these observations. More precisely the relic density of dark matter should be in agreement with the value measured by the Planck collaboration [335],

$$\Omega_{\text{DM}}h^2 = 0.120 \pm 0.001. \quad (3.85)$$

Here,

$$\Omega_{\text{DM}} = \frac{\rho_{\text{DM}}}{\rho_c} = \frac{n_{\chi,0}m_\chi}{\rho_c} \quad (3.86)$$

is the DM density normalised to the critical value for the total energy density for a flat Universe  $\rho_c := 3H_0^2/(8\pi G)$  where  $G$  is Newton's Gravitational constant and  $H_0$  is the present day value of the Hubble parameter. In Eq. (3.85) the measured value is presented by convention with the square of the dimensionless Hubble rate  $h = H_0/(100 \text{ km s}^{-1}\text{Mpc}^{-1}) = 0.6736 \pm 0.0054$  [335]. On the right-hand side of Eq. (3.86) we have written the density of dark matter in terms of the present day number density of the dark matter  $n_{\chi,0}$  and the mass of the dark matter candidate  $m_\chi$ , as is appropriate for particle dark matter, and in the case where the dark matter is composed of multiple components with different masses this should be interpreted as a sum over the components  $\chi$ .

Satisfying the relic density provides an important test for standard model extensions that provide dark matter candidates and typically places strong restrictions on the parameter space or even excludes scenarios entirely. Even if one does not require an explanation of all the dark matter within the model, justifying this by assuming some or most of the dark matter is made of other essentially orthogonal new physics<sup>28</sup>, this still provides an important test or constraint on new physics. This is because it should still be checked that the model does not predict an over abundance of dark matter, i.e. the above Planck measurement should still be used to give an upper bound on  $\Omega h^2$ .

The most commonly considered mechanism for generating the DM is the freeze-out mechanism [343, 344] where the DM is thermally produced. When there are very high temperatures in the early universe the particle DM candidates and SM particles are in thermal equilibrium, such that the production and annihilation rates of the DM candidates are equal. When the temperature drops below the mass of the dark matter, production is suppressed and the dark matter is no longer in thermal equilibrium with the SM states and annihilation of the dark matter then drives a rapid decrease in their number densities. As the Universe then cools down and expands, reducing the number densities, we reach a point where the DM can no longer annihilate. The relic abundance of the dark matter freezes out at this time/temperature and subsequently DM number densities evolve according to only the expansion of space, leading to a prediction for the relic density for the dark matter today.

---

<sup>28</sup>For example when considering a model with a WIMP candidate one could allow for the possibility that there is also an axion dark matter candidate that can contribute.

The number density of the dark matter evolves during this process according to the Boltzmann equation,

$$\frac{dn_\chi}{dt} = -3Hn_\chi - \langle\sigma_{\text{eff}}v\rangle(n_\chi^2 - n_{\chi\text{eq}}^2) \quad (3.87)$$

where  $\langle\sigma_{\text{eff}}v\rangle$  is the thermal average of the effective annihilation cross-section which is computed for the specific particle physics model and  $n_{\chi\text{eq}}$  is the number density at equilibrium. The first term in Eq. (3.87) is present because the number density is affected by the expansion of space as well as by the annihilations. When freeze out occurs  $n_\chi/a^3$  becomes constant, where  $a$  is the scale factor for the expansion of space.

The Boltzmann equations should be solved numerically, as is done in public software packages, e.g. MicrOMEGAs and DarkSUSY [345–347]. However rough approximations can also be used to give crude estimates of the relic density [344],

$$\Omega_{\text{DM}} \approx \frac{x_f T_0^3}{\rho_c M_{\text{Pl}} \langle\sigma_{\text{eff}}v\rangle} \approx \frac{x_f T_0^3}{\rho_c M_{\text{Pl}}} \frac{16\pi^2 m_\chi^2}{g^4}, \quad (3.88)$$

where  $x_f = \frac{m_\chi}{T_f}$  is the ratio of dark matter mass to the freeze-out temperature  $T_f$ ,  $T_0$  is the present day temperature of the Universe and  $M_{\text{Pl}}$  is the Planck mass. In the last step we have used a simple ansatz for the thermally averaged annihilation cross-section based on the dimensionality and assuming weak interactions, with  $m_\chi$  being the only mass scale involved. Eq. (3.88) shows that higher annihilation cross sections lead to later freeze-out and hence reduced relic density. The resulting sensitivity to the mass  $m_\chi$  and coupling  $g$  via the ratio  $m_\chi^2/g^4$  illustrates that the freeze-out mechanism can easily produce too much or too little dark matter, depending on the parameter choices. In fact since collider experiments are typically placing lower limits on masses and/or upper limits on interactions, avoiding overabundance can be the biggest challenge with the freeze-out mechanism and is also the constraint which is hardest to argue away, as discussed above.

In Eq. (3.88) we have used  $g$  to denote the coupling to indicate the connection to the weak gauge coupling. While there can be other possibilities where the dark matter (or more generally dark sector) interacts with the standard model via new couplings, if we assume it is the weak gauge coupling then it implies the full relic density is explained when  $m_\chi \sim 100 \text{ GeV} - 1 \text{ TeV}$ , which is known as the WIMP miracle. The apparent miracle here is it just so happens that a weak gauge coupling and weak scale mass give the annihilation cross-section needed to predict the observed relic density of dark matter. This led to the common Weakly Interacting Massive Particle (WIMP) paradigm, with WIMPs being the most popular dark matter candidate. Now, the term WIMP is generally used for a dark matter candidate that is a thermal relic, generating the relic abundance via the freeze-out mechanism, with a mass around the weak scale. For example singlet Higgs portal dark matter couples to the standard model through quartic interactions with the Higgs, e.g.  $\lambda|H|^2SS$  where  $S$  is the dark matter candidate. Although the mass and coupling  $\lambda$  are typically close to those of the Weak scale and Weak force, the DM candidate is a singlet under the SM gauge group and does not interact via the Weak force. Nonetheless for such candidates the freeze-out mechanism generates the relic density and they are typically referred to as WIMPs.

However in recent years the WIMP paradigm has come under increased pressure from non-observation in both direct and indirect detection experiments as well as LHC searches, leading to a reduction in the favouritism towards WIMPs [348]. While LHC searches (see Sec. 3.7) focus on the production of the DM from SM particles, direct detection experiments instead try to detect the recoil of the nucleus in ordinary matter from the scattering of incident dark matter particles with the nucleons. The first direct detection limits on DM appeared in 1987 [349], and since then many experiments have successively increased sensitivity over the years, producing strong constraints in the plane of the mass of the DM candidate and (spin-independent and spin-dependent) WIMP-nucleon cross section. Fig. 3.7 shows a compilation of

experimental results including the most recent results of the LZ experiment [350], which provide the strongest direct detection constraints on WIMPs [350]. To obtain these limits the flux of the DM particles passing through the earth has to be estimated. In dark matter direct detection experiments this estimate is typically based on the Standard Halo Model, see Ref. [351] for recommended values (used by LZ) and the references that these value are based upon. To apply these limits to a new physics model the WIMP-nucleon cross-section for the new physics model must be computed. This cross-section depends on what interactions the DM candidate has with the SM and as a result so does the impact of direct detection. DM interacting via the weak force may interact with the nucleons via tree level  $Z$  boson exchange or, if the DM candidate is a gauge multiplet with a heavier charged state, through inelastic upscattering to the charged state mediated by the  $W$  boson. The Higgs boson may also act as a mediator if the DM couples with the Higgs. Alternatively the mediator may be a BSM state and/or the DM may only couple to nucleons at the loop level.

Indirect detection experiments instead look for excesses in cosmic rays made up of known particles (charged particles, photons, neutrinos) which could result from dark matter annihilation in regions where the dark matter density is large enough, or dark matter decay products if unstable states are present<sup>29</sup>[352, 353]. In the former case, if the annihilation cross-section determines the abundance via the freeze-out mechanism, observation of the annihilation products would probe the mechanism for generating the observed relic abundance. In contrast to the well-controlled low background direct detection experiments, indirect detection has significant uncertainties due to the astrophysical backgrounds and the distribution of the dark matter in the galaxy. Furthermore, unknown or poorly modelled astrophysical sources can make assessing signals and limits challenging. Nonetheless indirect detection experiments using gamma-ray telescopes (e.g. Fermi-LAT [354], MAGIC [355], VERITAS [356]), neutrino detectors (e.g. IceCube [357], ANTARES [358]) and cosmic rays (e.g. AMS-02 [359], PAMELA [360]), looking for signals from sources such as dwarf spheroidal galaxies and the galactic centre can be an important source of potential signals and constraints on new physics [361].

Here we note that the above discussion of WIMPs is rather crude, and in specific models the actual results for cross-sections and dark matter annihilation can be quite different. These differences can matter especially for the correlation with  $a_\mu$  or other particle physics observables. For example, mechanisms to boost the dark matter annihilation cross-section have been explored in various WIMP scenarios where experimental constraints otherwise push the mass limits beyond those where the relic density can be naturally explained. Secondly, it is easy to vary the coupling and mass simultaneously in Eq. (3.88) such that the cross-section does not change. Thirdly, besides DM production via freeze-out other possibilities, like the freeze-in mechanism [368], can be considered. Finally it is worth noting that the relic density can also be affected by non-standard cosmologies (see e.g. [347]) and explanations through exotic macroscopic objects like primordial black holes remain possible [369, 370]. Such explanations, however, also require the existence of new physics.

Thus there is a vast range of mass scales (ranging from  $10^{-21}$  eV to  $10^{73}$  eV) and many different types of dark matter candidates to consider. However since the dark matter could not enter the diagrams for  $a_\mu$  with strong interactions, dark matter candidates with masses far in excess of the TeV scale can be expected to contribute negligibly. In Sec. 5.1 we will discuss  $a_\mu$  predictions for light dark sectors, while in the remainder of the present section we will briefly discuss the simplest possibilities for fitting both dark matter and  $a_\mu$ , focusing mainly on the standard freeze-out mechanism and WIMPs.

---

<sup>29</sup>This applies if one considers dark matter that is not perfectly stable, but rather decays on time scales longer than the cosmological scales needed to explain the data.

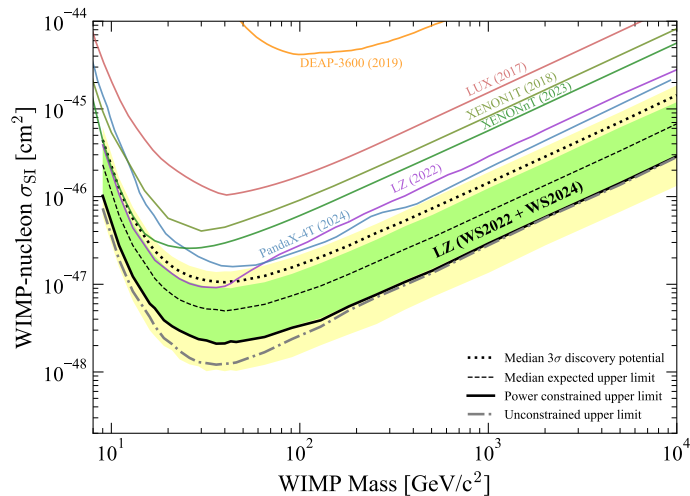


**Figure 3.7:** The latest direct detection limits on WIMP-nucleon cross-section, plotted against the mass of the dark matter candidate, from the LZ collaboration [350] which is shown as the solid black line. Also shown for comparison are  $1\sigma$  limits from their 2022 release [362] and from other collaborations: PandaX-4T [363], LUX [364], XENONnT [365], XENON1T [366] and DEAP-3600 [367], while the green and yellow regions show the range of expected upper limits based that would be seen 68% and 95% of the time respectively assuming background only. This figure is taken from Ref. [350] where more details on the analysis and precise meaning of the limits can be found.

### 3.6.2. Single-field extensions of the SM

As we have discussed in Sec. 2.2, it is possible for an extension of the standard model by a single field to contribute to  $a_\mu$ , with the possibilities listed in Table 2.1. At the same time there are a number of proposed explanations of dark matter that only extend the standard model by a single field, including scalar singlet dark matter [371, 372], inert Higgs doublet dark matter [373] and minimal dark matter [374]. Nonetheless these two sets of models are mostly disjoint since to be a DM candidate the particle should be stable on cosmological time scales, while to enter the one-loop corrections to  $a_\mu$  it must couple to the muon and another SM state, introducing a potential decay channel. Therefore unlike multi-field extensions, typically single field DM models do not contribute to  $a_\mu$  and thus can neither be discovered nor constrained by this observable.

More systematically, requiring colour singlets with an electromagnetically (EM) neutral component cuts the one-field models in Table 2.1 down to: scalar (3, 4), fermion (10, 12, 14, 15), vector (16, 18). Avoiding decays then restricts us to very light DM in all cases. At the same time as argued earlier the freeze-out mechanism implies DM with  $SU(2)_L$  interactions should fit the observed relic density when the mass is  $\mathcal{O}(100 - 1000\text{GeV})$ .<sup>30</sup> This is clearly too large for the erstwhile DM candidate to avoid decaying into muons through the Yukawa coupling that allows the inert Higgs doublet to contribute to  $a_\mu$  at the one-loop level. Furthermore  $SU(2)_L$  doublets and triplets also contain EM charged components and interact via  $Z$ - or  $W$ -exchange. In addition lower bounds on their masses from collider limits, which we will discuss in Sec. 3.7, imply they must be too heavy to avoid decays into SM states.

Thus we are left with singlet fermion and vector states that must be very light.<sup>31</sup> Thanks to the Pauli exclusion principle, the lower bound on the mass of fermion dark matter is  $\mathcal{O}(100\text{eV})$  [375, 376].<sup>32</sup> Furthermore Model 10 can

<sup>30</sup>For example Model 3 is a scalar  $SU(2)_L$  doublet, which could be interpreted as inert Higgs doublet dark matter [373] and it will have the annihilation cross-section needed to deplete the relic density to the observed value (Eq. (3.85)) when its mass is about 600 GeV [373].

<sup>31</sup>There is no scalar singlet in Table 2.1 since it does not have direct couplings to the muon.

<sup>32</sup>This limit could be significantly reduced by introducing very large numbers of different fermion species [377] but this would be very far

be interpreted as a right-handed neutrino or a vector-like lepton (VLL; specifically the VLL model with singlet  $N$  state shown in later Sec. 5.5). For the right handed neutrino, the Yukawa coupling is constrained by the seesaw mechanism and upper limits on neutrino masses, so only negligible contributions arise from providing a mass to the neutrino (see Eq. (3.80) in Sec. 3.5) or from mixing effects. At the same time the VLL can decay virtually through heavier SM states into neutrinos, and in order to suppress these decays sufficiently to allow it to explain DM, the couplings would have to be so small that it also contributes negligibly to muon  $g-2$ .

This leaves only Model 16, a new spin-1 vector boson that is a singlet under the SM gauge group, as a potential single-field dark matter model which can contribute to  $a_\mu$ . One realisation of Model 16 is the dark photon [378–381] (see also Sec. 5.1.2) where the couplings to SM states come only from gauge kinetic mixing. If the dark photon has a mass that is lighter than two times the lightest neutrino mass then it could be an example of very light dark matter. In this case the DM relic is not produced via the freeze-out mechanism as discussed earlier, but non-thermal mechanisms that have been developed for light dark matter including vacuum misalignment [382, 383], quantum fluctuations during inflation [384] or abundance transfer from e.g. axions [385] or the inflation [386] via tachyonic instabilities. See also Ref. [387] for a recent brief review on dark photons. This model may also be extended in various ways, e.g. by including direct mass mixing with the  $Z$  boson, referred to as a dark  $Z$  [388–392]. Direct couplings to the SM are possible through the charge assignments of the new  $U(1)$  gauge group. Importantly, these assignments are restricted by the anomaly cancellation conditions. Without additional matter fields besides the SM leptons and quarks, the only allowed possibilities are  $U(1)_{B-L}$ ,  $U(1)_{L_e-L_\mu}$ ,  $U(1)_{L_e-L_\tau}$  and  $U(1)_{L_\mu-L_\tau}$ . Again, in order for the  $Z'$  to be a stable dark matter candidate it must be light enough so that it cannot decay into the SM particles. The  $U(1)_{L_\mu-L_\tau}$  is special because it avoids couplings to the electron (which are strongly constrained) and, compared to the other possibilities, can give the largest contributions to  $\Delta a_\mu$ . It is worth noting that these models can also be part of a wider dark matter sector where the new gauge boson may not be the stable dark matter but instead acts as a mediator between the visible and dark sectors. Such scenarios and their implications for  $\Delta a_\mu$  are discussed in more detail in Sec. 5.1.

In that section we also discuss another interesting exception to the arguments given above against scalar candidates: the axion or axion-like particles (ALPs) [393]. The axion is a pseudoscalar state introduced to solve the strong CP problem [394–396], and as briefly mentioned earlier it can be a viable dark matter candidate. ALPs are a generalisation of the axion that do not necessarily solve the strong CP problem, but interact with SM states through shift-invariant (but suppressed) effective couplings. As such, they do not really satisfy the selection criteria for our Table 2.1, but can nonetheless have important implications for both DM and  $a_\mu$ .<sup>33</sup> In this case the DM relic abundance can be produced through the vacuum misalignment mechanism [397–399] or from topological defects such as cosmic strings or domain walls, see e.g. Ref. [400] and references therein. The  $a_\mu$  contributions from axions are discussed in detail in Sec. 5.1.4.

### 3.6.3. Two-field extensions

Compared to the one-field extensions, the situation where two new fields enter the loop corrections to  $\Delta a_\mu$  is very different. In particular, there are far more DM models of this nature that may contribute non-negligibly to  $a_\mu$ . In models with two

---

from the single field extensions we consider here.

<sup>33</sup>Similarly one can also add a real scalar singlet that couples via effective couplings or by mixing with the Higgs field. The latter can only affect the one loop result through mixing and the impact should be small, but the former is could be very light dark matter similar to the axion.

new fields of different spin, both neutral and charged states can enter  $\Delta a_\mu$  via the diagrams in Fig. 2.1. The neutral state provides a dark matter candidate as long as it is lighter than the charged state and also does not have further interactions through which it can decay. The latter can be easily realised within a specific model by e.g. imposing a  $\mathbb{Z}_2$  symmetry.

If the two new fields have the same spin then they can only enter the same one-loop diagram via mixing, and there must also be a SM state in the loop that couples to the photon. Therefore the possibilities for dark matter models of this kind with significant contributions to  $\Delta a_\mu$  are restricted in a similar way to the one-field extensions as discussed above. Thus although models like this are of interest because they can get a large chiral enhancement (see e.g. Sec. 5.5.1) they are not particularly interesting for dark matter explanations and we will not discuss them further here.

Therefore we now focus on the case of two fields with different spin. Models of this nature are collected in Table 2.2 in Sec. 2.2 and, as discussed there, these models cannot result in chirally enhanced contributions to  $\Delta a_\mu$ . Instead for all of these models the couplings at the vertices of the one-loop diagram must either be to right handed muons only (written as ‘R’ in Table 2.2) or to left handed muons only (written as ‘L’ in Table 2.2). This means the  $a_\mu$  contributions are roughly given by the simple formula in Eq. (2.15) or Tab. 1.1 (a), and even before looking at the details, we already understand that while we are no longer pushed towards very light dark matter, the contributions to the anomalous magnetic moment from these states are limited. Large contributions beyond the  $2\sigma$  range corresponding to  $\Delta a_\mu^{\text{Exp-WP2025}}$  (see Eq. (1.7)) are only possible for states with  $\mathcal{O}(1)$  couplings with  $\mathcal{O}(100)$  GeV masses or lighter. Nonetheless these models appear to be the simplest class of models that can generically offer a dark matter candidate and provide non-negligible contributions to the anomalous magnetic moment of the muon.

In the following we consider models with a new scalar and a new Dirac fermion, which have been studied in Refs. [9, 195, 196], see also Ref. [401] for an earlier study. Following Ref. [196] we will refer to these as RR or LL models respectively and construct the Dirac fermion to be composed of two Weyl spinors from conjugate representations, i.e. we consider vector-like fermions for which we can write an explicit gauge invariant mass term. The form of a generic Lagrangian, without specifying field representations, can be written in terms of only left-handed Weyl spinors as

$$\mathcal{L}_{\text{LL}} = \left( \lambda_L l_{L2} \psi \phi - M_\psi \psi^c \psi + h.c. \right) - M_\phi^2 |\phi|^2, \quad (3.89)$$

$$\mathcal{L}_{\text{RR}} = \left( \lambda_R \mu_R^\dagger \phi \psi - M_\psi \psi^c \psi + h.c. \right) - M_\phi^2 |\phi|^2, \quad (3.90)$$

where  $l_{L2}$  is the  $\text{SU}(2)_L$  doublet containing left-handed Weyl spinors for the muon and muon-neutrino, while  $\mu_R^\dagger$  is a left-handed Weyl spinor that is the hermitian conjugate of the Weyl spinor for the right-handed muon. For the LL models  $\text{SU}(2)_L$  indices for contractions between  $l_{L2}$  and the new fermion  $\psi$  or new scalar  $\phi$  (depending on the particular representations of the model) are suppressed and similarly for the RR models any  $\text{SU}(2)_L$  indices for contractions between the new scalar and fermion are also suppressed. The possible quantum numbers for one-loop contributions from fermion-scalar loops (i.e. the FS type diagrams in Fig. 2.1) where both the fermion and scalar are BSM states are systematically listed in Table 1 of Ref. [196]. These models are also possible realisations<sup>34</sup> of Models 24 to 42 included in our Table 2.2.

For simplicity, like Refs. [9, 195, 196] we assume muon-philic couplings, which avoids both severe constraints from direct detection of dark matter that would be induced by tree-level couplings to quarks as well as constraints from flavour violating processes. Note however, that the latter in general also play an important role in constraining models that can both explain dark matter and provide large contributions to  $\Delta a_\mu$ . For further details on the LFV constraints see Sec. 3.2 as well as the model-specific discussions in Sec. 5.

<sup>34</sup>Alternatively, for example, Ref. [191] included realisations of Models 24 to 36 without the  $Z_2$  symmetry.

Now that we have specified the models we can go beyond the simple estimate of Eq. (2.15), and in particular obtain expressions showing the dependence on multiplicities from the dimension of the representations. This allows us to further discriminate between the different LL or RR models. For LL models the dimension of the  $SU(2)_L$  representations of the fermion  $N_\psi$  and scalar  $N_\phi$  must be related by  $N_\phi = N_\psi \pm 1$ , while for the RR models  $N_\phi = N_\psi$ . Neglecting mass splittings amongst the components of the  $SU(2)_L$  multiplets, the one-loop  $\Delta a_\mu$  results can be expressed as,

$$\Delta a_\mu^{\text{LL}} = -\frac{|\lambda_L|^2 m_\mu^2}{16\pi^2 M_\phi^2} \frac{2N_\psi(N_\psi \pm 1)}{2N_\psi - (1 \mp 1)} \left[ f_{\text{LL}}^S + \left( Y_S + \frac{1}{6}(\pm N_\psi - 4) \right) (f_{\text{LL}}^S + f_{\text{LL}}^F) \right], \quad (3.91)$$

$$\Delta a_\mu^{\text{RR}} = -\frac{N_\psi |\lambda_R|^2 m_\mu^2}{8\pi^2 M_\phi^2} [f_{\text{LL}}^S + Y_{F_L} (f_{\text{LL}}^S + f_{\text{LL}}^F)], \quad (3.92)$$

where the sum over all  $N_\psi$  multiplet components has been carried out with the hypercharges  $Y_{F_L, S}$  corresponding to the average electric charges of the multiplets; after this summation the result is conveniently expressed in terms of loop functions satisfying  $\mathcal{G}^{\text{FS}}(0, x; Q_S) = 2f_{LL}^F(x) + 2Q_S(f_{LL}^S(x) + f_{LL}^F(x)) = 2Q_S f_{LL}^S(x) + 2(1 + Q_S)f_{LL}^F(x)$  in terms of the loop function defined in Sec. 2.1.<sup>35</sup>

For models that couple only to left-handed muons, or only to right-handed muons, the sign of the new physics contributions is often fixed. More precisely for RR models Ref. [196] show that the sign of  $\Delta a_\mu$  depends on the hypercharge of the new fermion  $Y_F$ , as follows,

$$\text{RR sign rules: } \begin{cases} Y_F \geq -1/3 & \Rightarrow & \text{sign}(\Delta a_\mu) = -1 \\ Y_F \leq -2/3 & \Rightarrow & \text{sign}(\Delta a_\mu) = +1 \\ Y_F = -\frac{1}{2} & \Rightarrow & \text{sign}(\Delta a_\mu) = \text{sign}(M_\phi - M_\psi), \end{cases} \quad (3.93)$$

where  $M_\phi$  is the mass of the scalar and  $M_\psi$  is the mass of the fermion. Note here that  $Y_F$  is the hypercharge of the left-handed Weyl spinor in Eqs. (3.90) and matches the hypercharge assignments given in Ref. [196], which can differ from those given in Table 2.2.

For LL models the rule they found is a little more complicated. The sign of  $a_\mu$  depends on the dimension of the  $SU(2)_L$  representation of the fermion field,  $N_F$ , and the hypercharge of the new scalar,  $Y_S$ . Then for models where the the dimension of the  $SU(2)_L$  representation of the scalar is  $N_S = N_F \pm 1$  the sign of  $\Delta a_\mu$  is determined as follows,

$$\text{LL sign rules: } \begin{cases} Y_S \geq (\mp N_F + 2)/6 & \Rightarrow & \text{sign}(\Delta a_\mu) = -1 \\ Y_S \leq \mp N_F/6 & \Rightarrow & \text{sign}(\Delta a_\mu) = +1 \\ Y_S = (\mp N_f + 1)/6 & \Rightarrow & \text{sign}(\Delta a_\mu) = \text{sign}(M_\phi - M_\psi). \end{cases} \quad (3.94)$$

Note that similar to above, here the  $Y_S$  matches the hypercharge assignments given in Ref. [196], which can differ from those given in Table 2.2 due to differing conventions. Nonetheless these rules are reflected in signs shown in Table 2.2, which we have explicitly checked by translating between conventions.

<sup>35</sup>Generally, the loop-functions used in Ref. [196] are related to the ones of Sec. 2.1 as:

$$\begin{aligned} f_{LL}^F(x) &= +\frac{1}{2}\mathcal{G}^{\text{FS}}(0, x; 0), & f_{LR}^F(x) &= +\frac{1}{2}\mathcal{F}^{\text{FS}}(0, x; 0), \\ f_{LL}^S(x) &= -\frac{1}{2}\mathcal{G}^{\text{FS}}(0, x; -1), & f_{LR}^S(x) &= -\frac{1}{2}\mathcal{F}^{\text{FS}}(0, x; -1). \end{aligned}$$

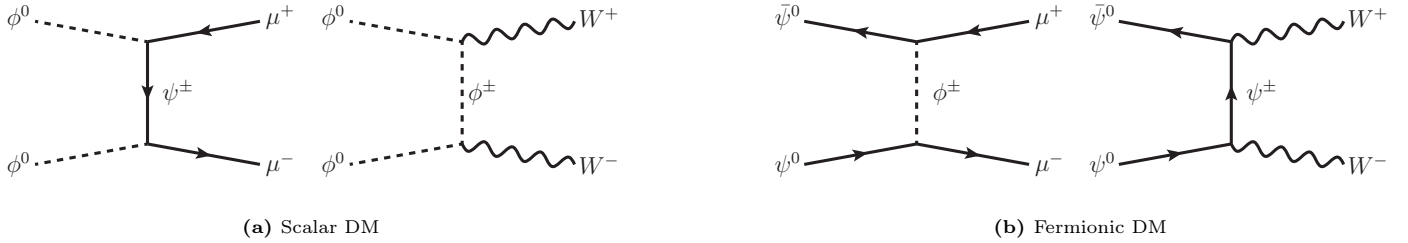


**Figure 3.8:** The dominant annihilation channels for scalar (a) and fermionic (b) dark matter in two-field extensions of the SM discussed in the text.

These RR and LL models may contain fermionic or scalar dark matter with a relic density generated by the freeze-out mechanism discussed earlier. For both fermionic and scalar dark matter, the dark matter predominantly annihilates into muons or  $W^\pm$  gauge bosons before the relic density freezes out, as indicated in Fig. 3.8 where the dominant annihilation diagrams are shown. Note that the annihilation into gauge bosons involves only the states from a single  $SU(2)_L$  multiplet, and depends only on the hypercharge of that multiplet as well as the SM gauge couplings  $g_{1,2}$ . The thermally averaged annihilation cross section for this channel is given by results obtained for minimal dark matter [374],

$$\langle\sigma v\rangle^{\phi\phi\rightarrow WW} \approx \frac{1}{128\pi M_\phi^2 N_\phi} [(N_\phi^4 - 4N_\phi^2 + 3) + 16Y_\phi^2 g_1^2 + 8g_2^2 g_1^2 Y_\phi^2 (N_\phi^2 - 1)], \quad (3.95)$$

$$\langle\sigma v\rangle^{\psi\psi\rightarrow WW} \approx \frac{1}{512\pi M_\psi^2 N_\psi} [(2N_\psi^4 + 17N_\psi^2 - 19) + 4Y_\psi^2 g_1^2 (41 + 8Y_\psi^2) + 16g_2^2 g_1^2 (N_\psi^2 - 1)], \quad (3.96)$$

where we assume here a complex scalar  $\phi$  and a Dirac fermion  $\psi$ , but the result for a real scalar or Majorana fermion is trivially obtained by multiplying with a factor 2. This annihilation channel is active even if the  $a_\mu$  contribution is zero. The annihilation channels into muons, on the other hand, depend on the couplings  $\lambda_L$  or  $\lambda_R$ . Neglecting velocity suppressed terms and assuming real couplings for simplicity, these channels are given by [196],

$$\langle\sigma v\rangle^{\phi\phi\rightarrow\mu^+\mu^-} \approx \frac{\lambda_{L,R}^4}{16\pi} \frac{m_\mu^2}{(M_\psi^2 + M_\phi^2)^2}, \quad (3.97)$$

$$\langle\sigma v\rangle^{\psi\psi\rightarrow\mu^+\mu^-} \approx \frac{\lambda_{L,R}^4}{32\pi} \frac{M_\psi^2}{(M_\phi^2 + M_\psi^2)^2}, \quad (3.98)$$

where we again have given the result for a complex scalar and Dirac fermion. In this case the result for a real scalar is obtained by multiplying with a factor of 4, while for the cross-section for a Majorana fermion additional factor of  $m_\mu^2/M_\psi^2$  must be included<sup>36</sup>. Although not considered in Ref. [196] for scalar dark matter, depending on the quantum numbers of the particular states, couplings from the scalar potential may also play a role. For example the Higgs portal (i.e. mixed quartic) coupling plays an important role in the scalar singlet dark matter, see e.g. Ref. [195].

To maximise the  $\Delta a_\mu$  contribution one can set  $\lambda_{L,R}$  to the perturbative limit and this also means that both channels for DM annihilations will be active. However note that the annihilation cross-section in Eqs. (3.95) and (3.96) increases with the dimension of representation; schematically for  $N = \{N_\psi, N_\phi\}$  and  $M = M_{\psi,\phi}$  if the annihilation into  $W^+W^-$  dominates, the scaling is

$$\langle\sigma v\rangle \sim \frac{N^3}{M^2}. \quad (3.99)$$

<sup>36</sup>If one includes velocity suppressed terms there are additional differences in both cases, as can be seen from the expressions in Ref. [196].

Thus for higher dimensional representations the relic density will be lower for the same masses and couplings,

$$\Omega \sim \frac{M^2}{N^3}. \quad (3.100)$$

To adjust for this the mass can be increased, such that the observed relic density will be explained fully in higher dimensional models at higher masses (assuming fixed  $\lambda_{L,R}$ ), with a scaling

$$M^2(\Omega_{\text{Planck}}) \sim N^3, \quad (3.101)$$

where  $\Omega_{\text{Planck}}$  refers to the measured value given in Eq. (3.85). However increasing the mass will reduce  $\Delta a_\mu$ . Although  $\Delta a_\mu$  also increases with the dimension of the representation, the reduction dominates and we have

$$\Delta a_\mu \sim \frac{N}{M^2} \sim N^{-2}, \quad (3.102)$$

Thus as  $N$  is increased the maximum  $\Delta a_\mu$  that is consistent with the model explaining all the dark matter reduces.

The above argument was originally presented in Ref. [196]. There they were interested in explaining the large anomaly from the BNL measurement and data driven estimates of the SM prediction and therefore they subsequently applied a more careful analysis to derive an upper limit on the relic density that can be obtained when explaining this large deviation within  $2\sigma$ . This ruled out most models of this type from providing dual solutions, i.e. simultaneously explaining dark matter and giving such a large contribution to  $a_\mu$ , with Models 24, 27 and 28 being the only three models that were capable of the dual explanation. These three models have the lowest dimensional representations of  $SU(2)_L$  that could give a positive contribution to  $a_\mu$ .

In the present context based on  $\Delta a_\mu^{\text{Exp-WP2025}}$  in Eq. (1.5) where the SM theory prediction and experimental result are consistent within errors, restricting us to only small deviations, it is these lowest dimensional models where constraints from  $a_\mu$  will be strongest and have the most impact. For higher dimensional representations muon  $g - 2$  predictions are suppressed further, due to the heavier masses needed to fulfil the total measured relic density of dark matter. Thus for higher dimensional representations that explain dark matter, the maximum  $\Delta a_\mu$  contributions they can predict are even smaller than the simple estimate using Eq. (2.15).

In summary, two-field models with a dark matter candidate(s) cannot have a chirality flipping enhancement; hence the contributions to  $a_\mu$  can be sizeable at most in the region of large couplings and small masses. Dark matter constraints however require sufficiently high masses, and large multiplicities further strengthen this requirement. Hence for most of these DM explanations the current  $a_\mu$  bounds do not provide strong complementary parameter constraints. The few cases where small masses and sizeable  $\Delta a_\mu$  are allowed by DM constraints are constrained by collider data. This will be discussed in Sec. 3.7. However before moving onto that section we will first discuss another class of models where explaining dark matter does not place strong restrictions of the size of  $a_\mu$  contributions. In these models, constraints from  $\Delta a_\mu^{\text{Exp-WP2025}}$  or signals from a large deviation like  $\Delta a_\mu^{\text{Exp-WP2020}}$ , may go beyond the reach of the LHC and will be a very important test of models explaining DM.

### 3.6.4. Three-field extensions

Solutions to DM with much larger new physics contributions to  $a_\mu$  are possible when there is both a chiral enhancement and a stable dark matter candidate. The minimum number of new fields where this is possible is three.<sup>37</sup> For models with

---

<sup>37</sup>Interestingly a similar result including also flavour physics was derived in Ref. [402], where the requirements of sizeable  $\Delta a_\mu$  and explanation of dark matter were combined with accommodating  $B$ -physics anomalies present at the time, and at least four BSM fields were found to be

two fermions and one scalar or two scalars and one fermion the relevant Lagrangian interactions allowing the chirality flip are given in Sec. 2.3, Eqs. (2.16a,2.16b,2.16c). As described there, these models introduce two particles of the same spin that can mix, allowing a chirality flip in the internal loop diagram. At the same time they also contain a particle of different spin to enter the loop diagram and as a result the new physics states may have couplings that only involve the muon and another BSM state. Thus there is no longer any requirement that new physics states must decay into SM states and if the lightest of the new states is neutral it can be a dark matter candidate as long as no other couplings through which it decays are present in the model (this could be achieved by imposing a  $\mathbb{Z}_2$  symmetry for example).

Models of this nature have been studied in Refs. [9, 195, 196]. All of these papers (like Sec. 2.3) consider classes of models involving fermions and scalars. The models in Ref. [9, 196] correspond to the three-field models of Class I and Class III given in Sec. 2.3, while Ref. [195] also considers two models that correspond to a combination of Class I and Class II.

Ref. [196] systematically constructed all models of Class I and Class III types in dimensions of the  $SU(2)_L$  representations, up to triplets. We reproduce this classification of the models in Tables 3.5 and 3.6. We again follow Refs. [9, 195, 196] and show the Lagrangian here in terms of left-handed Weyl spinors, and we label the BSM left-handed Weyl spinors  $\psi$  and  $\chi$ .

$$\mathcal{L}_{2F1S} = \left( \lambda_\Phi \Phi \chi \psi + \lambda_L l_{L2} \phi \psi + \lambda_R \chi \mu_R^\dagger \phi^\dagger - M_\psi \psi^c \psi - M_\chi \chi^c \chi + h.c. \right) - M_\phi^2 |\phi|^2, \quad (3.103)$$

$$\mathcal{L}_{2S1F} = \left( a_\Phi \Phi \cdot \phi_a \phi_b + \lambda_L \phi_a l_{L2} \psi + \lambda_R \phi_b \mu \psi^c - M_\psi \psi^c \psi_s + h.c. \right) - M_{\phi_a}^2 |\phi_a|^2 - M_{\phi_b}^2 |\phi_b|^2. \quad (3.104)$$

Note that although Ref. [196] writes the generic Lagrangians in this form, additional couplings allowed by gauge invariance may be included for specific models where they perform detailed numerical investigations.

The dominant channels for dark matter annihilations that deplete the relic density are typically the same as described in the previous Sec. 3.6.3, though the coupling to the Higgs means additional co-annihilation processes are possible and at low masses near resonant annihilation through the Higgs can also be important. The cross-sections for annihilations into  $W$  Bosons are still given by Eqs. (3.95) and (3.96), while the annihilations into muons are significantly modified with a new contribution that requires both  $\lambda_L$  and  $\lambda_R$  to be non zero,

$$\langle \sigma v \rangle^{\phi\phi \rightarrow \mu^+ \mu^-} \approx \frac{1}{16\pi} \left( (\lambda_L^4 + \lambda_R^4) \frac{m_\mu^2}{M_\psi^2} + 4\lambda_L^2 \lambda_R^2 \right) \frac{M_\psi^2}{(M_\psi^2 + M_\phi^2)^2}, \quad (3.105)$$

$$\langle \sigma v \rangle^{\psi\psi \rightarrow \mu^+ \mu^-} \approx \frac{(\lambda_L^2 + \lambda_R^2)^2}{32\pi} \frac{M_\psi^2}{(M_\phi^2 + M_\psi^2)^2}. \quad (3.106)$$

As before, some modifications for the case of a real scalar and for a Majorana fermion are required, with the full expressions given in Ref. [196]. As discussed in Ref. [9] in certain scenarios where this latter channel is dominant, the  $m_\mu/M_F$  suppression of the first term in Eq. (3.105) can lead to the relic density following a similar parabolic curve in the  $\lambda_L$ - $\lambda_R$  plane to contours of fixed  $\Delta a_\mu$ .

With direct couplings to the quarks avoided by the muon-philic choice of couplings, the most important remaining direct detection channels for these models are tree-level  $Z$  exchange, tree-level Higgs exchange induced by the new coupling to the Higgs and loop-level contributions that play an important role in constraining lepto-philic dark matter [403]. The tree-level scattering via  $Z$  exchange applies to models where the dark matter is in a multiplet where the hyper-charge

---

necessary.

Model	$\psi$	$\chi$	$\phi$	DM candidates (DD channel)
FLR1	(1, 1, 0)	(1, 2, -1/2)	(1, 2, 1/2)	$\psi$ (H-ex), $\chi^0$ (H-ex), $\phi^0$ (Z-ex)
FLR2	(1, 1, 1)	(1, 2, -3/2)	(1, 2, -1/2)	– – $\phi^0$ (Z-ex)
FLR3	(1, 2, -1/2)	(1, 1, 0)	(1, 1, 1)	$\psi^0$ (H-ex), $\chi$ (H-ex), –
FLR4	(1, 2, -1/2)	(1, 3, 0)	(1, 3, 1)	$\psi^0$ (H-ex), $\chi^0$ (H-ex), $\phi^0$ (Z-ex)
FLR5	(1, 2, 1/2)	(1, 1, -1)	(1, 1, 0)	$\psi$ (Z-ex), – $\phi$ (H-ex)
FLR6	(1, 2, 1/2)	(1, 3, -1)	(1, 3, 0)	$\psi^0$ (Z-ex), $\chi^0$ (Z-ex), $\phi^0$ (H-ex)
FLR7	(1, 2, 3/2)	(1, 3, -2)	(1, 3, -1)	– – $\phi^0$ (Z-ex)
FLR8	(1, 3, -1)	(1, 2, 1/2)	(1, 2, 3/2)	$\psi^0$ (Z-ex), $\chi^0$ (Z-ex), –
FLR9	(1, 3, 0)	(1, 2, -1/2)	(1, 2, 1/2)	$\psi^0$ (H-ex), $\chi^0$ (H-ex), $\phi^0$ (Z-ex)
FLR10	(1, 3, 1)	(1, 2, -3/2)	(1, 2, -1/2)	$\psi^0$ (Z-ex), – $\phi^0$ (Z-ex)

**Table 3.5:** Models with dark matter candidates that have a chiral enhancement with precisely two new Dirac fermions and one new scalar field. For each field from the Lagrangian (3.103) the representations under  $SU(3)_c \times SU(2)_L \times U(1)_Y$  are shown in columns 2,3 and 4. The last column shows the possible dark matter candidates together with the direct detection channel expected to be most constraining for each of these DM candidates. Here,  $H - ex$  stands for tree-level Higgs exchange and  $Z - ex$  stands for tree-level Z-exchange. If all DM candidates are constrained by tree-level Z-exchange the entry is coloured red reflecting the fact that constraint is strong enough to exclude the model, as discussed in the text. This table is based on similar tables presented in Ref. [196].

Model	$\psi$	$\phi_a$	$\phi_b$	DM candidates (DD channel)
SLR1	(1, 1, 1)	(1, 2, -1/2)	(1, 1, 0)	– $\phi_a^0$ (H-ex), $\phi_b$ (H-ex)
SLR2	(1, 1, 0)	(1, 2, 1/2)	(1, 1, -1)	$\psi$ (Z-ex), $\phi_a^0$ (H-ex), –
SLR3	(1, 2, 1/2)	(1, 1, 0)	(1, 2, -1/2)	$\psi^0$ (Z-ex), $\phi_a$ (H-ex), $\phi_b^0$ (H-ex)
SLR4	(1, 2, 1/2)	(1, 3, 0)	(1, 2, -1/2)	$\psi^0$ (Z-ex), $\phi_a^0$ (H-ex), $\phi_b^0$ (H-ex)
SLR5	(1, 2, 3/2)	(1, 3, -1)	(1, 2, 1/2)	– $\phi_a^0$ (Z-ex), $\phi_b^0$ (Z-ex)
SLR6	(1, 2, -1/2)	(1, 1, 1)	(1, 2, -3/2)	$\psi^0$ (Z-ex), – –
SLR7	(1, 2, -1/2)	(1, 3, 1)	(1, 2, -3/2)	$\psi^0$ (Z-ex), $\phi_a^0$ (Z-ex), –
SLR8	(1, 3, 1)	(1, 2, -1/2)	(1, 3, 0)	$\psi^0$ (Z-ex), $\phi_a^0$ (H-ex), $\phi_b^0$ (H-ex)
SLR9	(1, 3, 0)	(1, 2, 1/2)	(1, 3, -1)	$\psi^0$ (H-ex), $\phi_a^0$ (Z-ex), $\phi_b^0$ (Z-ex)
SLR10	(1, 3, -1)	(1, 2, 3/2)	(1, 3, -2)	$\psi^0$ (Z-ex), – –

**Table 3.6:** Models with dark matter candidates that have a chiral enhancement with precisely one new Dirac fermions and two new scalar fields. For each field from the Lagrangian (3.103) the representations under  $SU(3)_c \times SU(2)_L \times U(1)_Y$  are shown in columns 2,3 and 4. The last column shows the DM candidates and direct detection channel as described in the caption for Table 3.5.

is non-zero ( $Y \neq 0$ ) and if the scattering is elastic this provides very strong exclusions essentially ruling out them out as WIMP dark matter, with cross-sections far above the limits set by direct detection experiments across their full mass range. This limit cannot be avoided by adjusting BSM couplings, since it proceeds through gauge interactions. However if there is a small mixing this suppresses or forbids the elastic scattering and therefore can be evaded, see e.g. [374, 404]. When this is not active, Higgs exchange will typically provide the dominant direct detection limits where the impact depends on the Higgs mixing parameter ( $a_H$  or  $\lambda_H$ ) and the masses, but this can also potentially exclude states up to multi TeV masses. The dominant direct detection channel is indicated in Tables 3.5, 3.6.

If the interactions with the Higgs and either  $\lambda_L$  or  $\lambda_R$  are set to zero we return to the situation discussed in the previous subsection for two-field models.<sup>38</sup> Therefore here we take the natural assumption that all the new couplings are  $\mathcal{O}(0.1-1)$ , implying a large chiral enhancement to  $\Delta a_\mu$  which can generate much larger contributions to the anomalous magnetic moment of the muon. Even with all of these couplings non-zero though, in principle a similar argument to that presented above in Sec. 3.6.3 regarding the dimensionality of these models applies here too. That is, as the dimensionality of the representation increases, the maximum size of the muon  $g-2$  contributions that are consistent with explaining the observed relic density of dark matter decreases. However due to the chirality enhancement this maximum value is much larger for a given representation in this class of models than in the models discussed in Sec. 3.6.3. As a result, as long as one does not consider huge representations, far above the triplet representations categorised here<sup>39</sup>, large  $a_\mu$  corrections well in excess of the  $2\sigma$  bound on  $\Delta a_\mu$  are possible for scenarios that fully explain the observation of DM by fitting the measured relic density.

Dark matter models must also respect complementary constraints e.g. from dark matter direct detection (DMDD) experiments shown in Fig. 3.7. In fact, in such three-field DM scenarios with large chiral enhancements there is a complex interplay between muon  $g-2$ , the relic density and direct detection constraints that must be studied carefully to understand whether or not it is possible to explain dark matter in these models. For example a model with a Lagrangian of the form of Eq. (3.104) is studied in detail in Ref. [9]. There it is shown that parameter regions exist where the DMDD constraints are fulfilled while  $\Delta a_\mu$  is as large as the old deviation  $\Delta a_\mu^{\text{Exp-WP2020}}$ . But there are also parameter regions where  $\Delta a_\mu$  is small while the DMDD constraints are violated. Presently, with the small value  $\Delta a_\mu^{\text{Exp-WP2025}}$  both such parameter regions are excluded, demonstrating the complementarity of  $a_\mu$  and DMDD constraints in probing DM models. The reason for this complementarity is that the two couplings  $\lambda_{L,R}$  and the two masses  $M_{\phi,\psi}$  enter the relic density,  $\Delta a_\mu$  and the DMDD cross section in different ways. Later in Sec. 5.2 we will encounter an analogous situation in the context of supersymmetric models.

Away from these equal mass scenarios other possibilities include scenarios where the relic density and  $\Delta a_\mu$  contours are orthogonal, such that fitting the combination can dramatically shrink the parameter space or where they are roughly parallel contours allowing muon  $g-2$  constraints to exclude fitting the relic abundance entirely in these planes. In general the direct detection limits typically depend on  $a_H$ , a small mass splitting between the two states that are mixed via the

---

<sup>38</sup>Introducing non-zero couplings to the Higgs boson introduces tree-level Higgs exchange as an important channel for direct detection of dark matter via nuclei recoil, as well as allowing the new (co-)annihilation channels mentioned above for the relic density. Thus the effect would be to just further constrain scenarios in comparison to the situation in Sec. 3.6.3, and in parameter regions where the new (co-)annihilation channels are active, further increasing the mass at which the dark matter can be fully explained and thus suppressing  $\Delta a_\mu$  further. If the mixing with the Higgs is zero but both  $\lambda_L$  and  $\lambda_R$  are non-zero then one effectively gets an extra contribution to  $\Delta a_\mu$ , and there is some modification to the DM annihilation cross-sections, but the situation is qualitatively unchanged from that described in Sec. 3.6.3.

<sup>39</sup>Ref. [196] found that large contributions consistent with  $\Delta a_\mu^{\text{Exp-WP2020}}$  were possible for representations smaller than  $\mathcal{O}(20)$ .

Higgs and the general mass scale, whereas constraints from muon  $g-2$  strongly depend also on  $\lambda_L$  and  $\lambda_R$ , and the relic density is typically more sensitive to  $\lambda_L$  and  $\lambda_R$  away from special regions where the co-annihilations between the scalar and fermion are important (i.e. when the fermion and scalar mass are very close) or for very light masses tuned such that resonant annihilation via the Higgs boson is an active channel. As a result it is clear that to truly understand the allowed parameters space, one needs to perform global fits including the relic density, direct detection and muon  $g-2$ .

The situation is similar for other models of this type given in Table 3.6 and for models with a Lagrangian of the form of Eq. (3.103) given in Table 3.5, as has been illustrated by detailed studies of specific cases in Refs. [9, 195, 196]. Thus  $a_\mu$  and direct detection both play important roles in constraining such explanations of dark matter, and may both play a role in further testing or even discovering such scenarios in the future and the inclusion of muon  $g-2$  in global fits of models of these types (or similar) should be mandatory.

### 3.7. Collider observables

Searches for new particles produced in collider experiments provide the most direct probes of new physics and are applicable to a very wide variety of new physics scenarios. This both competes with and complements precision measurements on new physics. In this section we discuss this complementarity and competition between the muon  $g - 2$  measurement and collider searches and discuss the impact collider limits have on possible NP signals in  $\Delta a_\mu$ .

Determining the limits from the Large Hadron Collider (LHC) can be highly model dependent and should be done by identifying possible collider signatures of the specific model, finding the collider searches that can be relevant for this and reinterpreting their results. This is most easily done through publicly available reinterpretation software, e.g. [405–407]. Nonetheless, as a generality, the LHC typically provides much stronger constraints on new physics with strong interactions, since the LHC collides protons and can these particles through strong interactions between the constituent quarks and gluons. Constraints on strongly interacting fundamental new physics tend to reach into the multi-TeV range, with examples being simplified model limits on supersymmetric states like the gluinos and first and second generation squarks reaching up to around 2.4 TeV [408–411] and 1.8 TeV [412, 413] respectively. Similarly for scalar leptoquarks the mass reaches from 2 to 5 TeV are possible depending for some specific states and couplings [414–417]. Note however these limits can be weaker depending on the specific model. For example the limits on stops are weaker than on the light squarks, with current limits reaching around 1.3 TeV at most [418, 419] but also varying significantly depending on the specifics of the simplified model.

In contrast to this, typical limits on weakly interacting states from the LHC do not reach so high and tend to be lower than around 1 TeV.<sup>40</sup> For example the LHC limits on sleptons reach at most 700 GeV [423], while for charginos they can extend at most to around 1.1 TeV [424]. As stated above these limits are very model dependent, for example it has been previously shown that while in certain simplified models of neutralinos and charginos the LHC was placing quite tough limits on these states, when a careful reinterpretation for the MSSM was applied there was no general exclusions in the mass plane of the lightest neutralino and the lightest chargino [425]. When the all relevant degrees of freedom for realistic MSSM scenarios are tested, for every point in this plane there are at least some realistic scenarios with those masses that escape the LHC limits. Since then ATLAS and CMS have produced studies that can close various holes in

---

<sup>40</sup>An important exception to this are  $Z'$  bosons, that tend to have multi-TeV limits [420–422] because through its couplings to quarks it can be produced resonantly and its decay into two leptons is a very clean signal with low backgrounds.

the exclusions, but this result still emphasises how the collider limits depend on models and specific parameter values that influence decay kinematics.

### 3.7.1. Mass limits from Colliders and $\Delta a_\mu$

As indicated in Tables 2.1 and 2.2 (as well as Tables 3.5 and 3.6 in Sec. 3.6), typically states that contribute to muon  $g - 2$  at one-loop have  $SU(2)_L$  and/or electromagnetic interactions, but only a few examples have strong interactions. Thus for the models of interest here we are typically dealing with an LHC reach that does not extend much beyond 1 TeV and can in many cases be much weaker than this depending on model-specific details. However if the model contains charged states then there should at least be very robust limits from LEP of around 100 GeV of the mass of the charged state (e.g. Refs. [426, 427]). Therefore we are typically comparing limits from the precision measurement of  $a_\mu$  to collider limits that vary between  $\mathcal{O}(100\text{--}1000)$  GeV. The limits from muon  $g - 2$  can be broadly understood by looking at the schematic form of the one-loop new physics contributions discussed in Sec. 1.1.4, where it is pointed out that typically the one-loop new physics contributions can be brought into the form

$$\Delta a_\mu = R_\chi \times \frac{c_L c_R}{16\pi^2} \frac{m_\mu^2}{M^2}. \quad (3.107)$$

Here  $R_\chi$  is a chiral enhancement factor,  $c_{L,R}$  are the relevant couplings and  $M$  is the mass scale of the new physics, and there can be additional factors from particle multiplicities and an order one loop-function. Since the production of new particles needs sufficiently large couplings and sufficiently low masses, non-observation of new physics at colliders typically places limits on large couplings and small masses. If the couplings are fixed or one requires that the couplings at least stay perturbative, this generally implies a lower limit on the masses. Using Eq. (3.107) the  $2\sigma$  limits on  $\Delta a_\mu$  from Eq. (1.7) translate into

$$M \gtrsim |R_\chi c_L c_R|^{\frac{1}{2}} \begin{cases} 206 \text{ GeV} & \text{for } \Delta a_\mu > 0 \\ 282 \text{ GeV} & \text{for } \Delta a_\mu < 0 \end{cases}. \quad (3.108)$$

This can be used to illustrate the generic behaviour of mass (and coupling) limits on new physics scenarios that are set from chirally enhanced muon  $g - 2$  contributions in the new physics model. Note that without chiral enhancement ( $R_\chi = 1$ ) and order one couplings  $c_{L,R} \sim \mathcal{O}(1)$  this limit excludes masses below  $\lesssim 200$  GeV, which is already stronger than the generic LEP bound of 100 GeV for heavy charged and neutral particles [426]. On the other hand, this limit lies well below the possible reach of  $\sim \mathcal{O}(1 \text{ TeV})$  for production of weakly interacting states at the LHC. Thus, in such cases a careful (re)interpretation of the LHC data is typically necessary and often leads to competing or stronger exclusion limits.

However, if the NP contributions yield a large chiral enhancement ( $R_\chi \gg 1$ ), the mass exclusion range from  $\Delta a_\mu$  is substantially increased and can easily extend beyond the typical reach of the LHC. This is illustrated in Fig. 3.9 where we plot the mass exclusion contour from Eq. (3.108) (assuming  $\Delta a_\mu > 0$ ) as a function of  $R_\chi$  for fixed  $c_{L,R} \equiv c = 1$  and 0.1. This generic limit is compared to various collider mass bounds on specific new particles, shown as solid or dashed lines with shading indicating the corresponding models. Besides the 100 GeV LEP limit shown in blue, we have included the reach for sleptons  $m_{\tilde{e}} > 700$  GeV and charginos  $m_{\chi^\pm} > 1.1$  TeV in the MSSM (in green), the bounds on VLL singlets  $M_E > 400$  GeV and doublets  $M_L > 1270$  GeV (in orange), the  $S_1$  leptoquark bound  $M_{S_1} > 1400$  GeV for  $\mu t$  final states (in purple) as well as a generic bound applicable to the charged scalar in the 2HDM-X  $M_{H^\pm} > 340$  GeV (in brown).

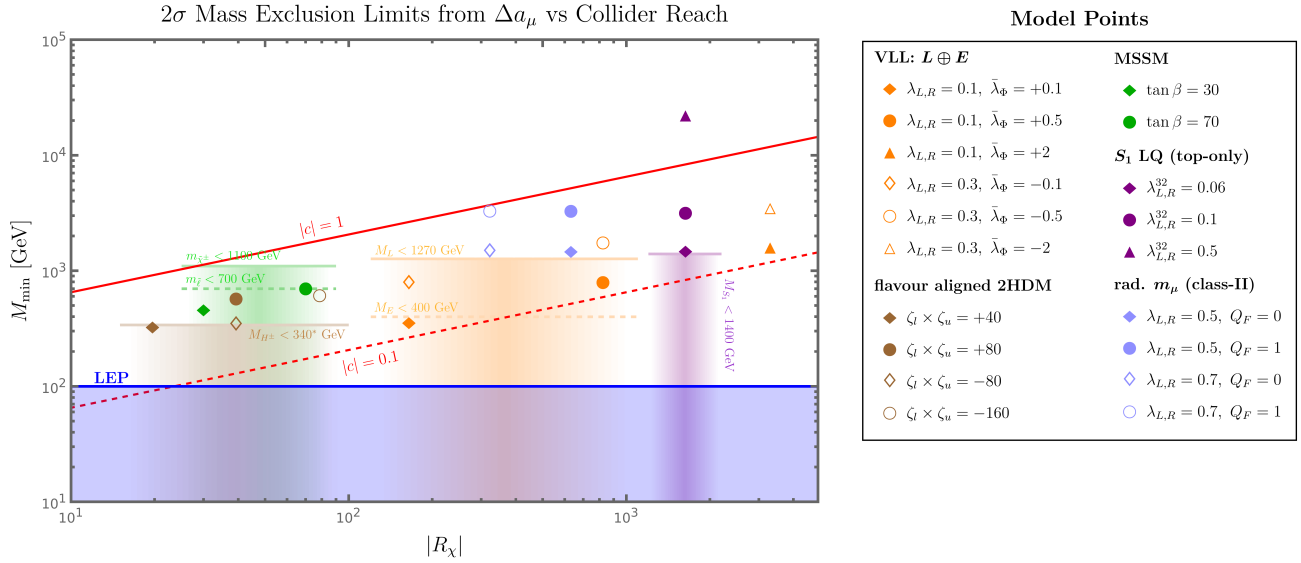


**Figure 3.9:** Comparison of mass limits on new physics coming from the measurement of the anomalous magnetic moment of the muon, and the mass reach and limits of the LHC and LEP. The LEP limit is indicated by the solid blue line and blue shading. The mass reach from the LHC is shown for charginos (solid green) and sleptons (dashed green) from simplified models of supersymmetry, vector-like leptons  $L$  (solid orange) and  $E$  (dashed orange),  $S_1$  scalar leptoquarks coupling to the top and the muon (purple) and finally the flavour aligned 2HDM (brown). The limits on sleptons and charginos should be interpreted as the maximum masses that could be constrained by current LHC data, but are not robust limits that exclude all lighter possibilities. Similarly the relevant VLLs and leptoquarks should be safe when heavier than the LHC reaches indicated, while it may be possible for lighter states to avoid the bound if the branching ratio is suppressed. On the other hand the solid brown line is not a maximum mass reach, but rather a robust limit on the charged Higgs mass in a specific parameter region of the 2HDM discussed in Sec. 5.3.3 and the LHC does also restrict masses heavier than this. These collider constraints can be compared to both the red lines and the points. The solid and dashed red lines show the mass limits from the generic one-loop contributions given in Eq. (3.107) (with couplings  $c := \sqrt{c_L c_R} = 1$  and  $c = 0.1$  respectively), which also appears in Sec. 1.1.4 and Table 1.1. These are just rough generic expectations and the actual limits may deviate substantially from these as demonstrated by diamonds, circles and triangles, where the colour coding indicating the model matches that of the collider limits. The exact choice of couplings are given in the key beside the plot and all  $\Delta a_\mu$  used to obtain these results are computed from the fit formulae in Table 1.1.

As will be discussed in Sec. 5.2, the slepton and chargino bounds do not represent strict exclusion limits, but rather indicate the upper reaches beyond which MSSM scenarios are generally safe from current LHC searches. Nevertheless, significant room for scenarios with masses below these reaches remains viable.

In contrast, the limits on VLL from searches at ATLAS [428–430] and CMS [431–433] are much more robust and essentially completely exclude scenarios with lighter masses. The main reason for the stronger limit in case of the VLL doublet is the larger production cross section resulting from the additional  $SU(2)_L$  interactions. Consequently, limits for similar states like e.g. VLL triplets are expected to be comparable or even stronger. For more details see Sec. 5.5.

Similarly, many searches for scalar leptoquarks with a variety of possible final states have been performed at the LHC in recent years [414–418, 434–446]. The resulting limits typically range between 1 to 2 TeV [414, 415], and even as far 3 to 5 TeV in some specific scenarios [416, 417]. In the context of  $a_\mu$ , the largest chiral enhancement is achieved for LQs coupling to the muon and top-quark (discussed in Sec. 5.4) for which the ATLAS and CMS searches [414, 447] apply, resulting in the comparatively modest bound shown in Fig. 3.9. In fact, this bound may be slightly weakened if additional decay modes are allowed and are dominant. Such scenarios again require a more dedicated recasting of the LHC results.

Finally we note that limits on additional Higgs bosons are very model dependent. Here, the limit  $M_{H^\pm} > 340$  GeV stems from a CMS search for  $\tilde{\tau}_L$  [448], that can be directly reinterpreted as a bound on the type-X 2HDM assuming

$\text{BR}(H^\pm \rightarrow \tau^\pm \nu) \simeq 100\%$ . This limit again differs if additional decay channels are allowed, however, in this case the bounds resulting from a dedicated recasting are typically more stringent. For a detailed discussion on the current constraints on the 2HDM see Sec. 5.3.3.

While we have only shown limits from a few selected searches here, it is worth noting that many LHC analyses often obtain limits in a vast array of models that can be very different from the original interpretation or motivation given for the search. Therefore the limits presented here can also be considered as representative examples of the kind of limits that may be set in other models for which no dedicated LHC searches have been performed. Comparing these to the generic one-loop chirally enhanced contribution shown by the solid and dashed red lines provides a rough indication of how mass limits from the  $a_\mu$  measurement and the direct collider limits compete.

However specific models do not match the generic one-loop result precisely. Often there are further significant factors that can arise from e.g. colour or logarithmic enhancements in the loop functions. Therefore, for a more accurate comparison, in Fig. 3.9 we also show mass limits from  $\Delta a_\mu$  in specific models. We compute these using the expressions for  $R_\chi$  given in Table 1.1, including the full mass-dependent loop functions. These points are shown with the same colour coding as the corresponding collider limits.

For the MSSM we have  $R_\chi = \tan \beta$  and we show examples for  $\tan \beta = 30$  (green diamonds) and  $\tan \beta = 70$  (green circle) where the Wino, Higgsino and left smuon and smuon neutrino are the light states and give the dominant contribution. All these points lie below the chargino collider reach indicated for the MSSM, but nonetheless as discussed above and later in Sec. 5.2, many viable scenarios can be found well below these limits. In these cases the  $a_\mu$  measurement can be stronger than the direct collider limit and plays an important role in exclusions and determining the allowed region. Note that in supersymmetric models the couplings to gauginos are fixed by the gauge couplings, while couplings between muons and Higgsinos are given by Yukawa couplings. As a result of this and the specific loop factors they lie well below the solid red line for the generic one-loop contribution with the couplings set to 1, as could be anticipated by comparing the expression in table 1.1.

Next to the MSSM, we show several points in the flavour aligned 2HDM where the chiral enhancement factor  $R_\chi = -\zeta_l \zeta_u m_t^2 / v^2$  is also typically of  $\mathcal{O}(10)$ . The 2HDM is unique compared to the other examples shown, because here the largest correction to  $\Delta a_\mu$  comes from two-loop Barr-Zee diagrams (see also Sec. 4.2). While this contribution is suppressed by an additional loop factor, this suppression is easily compensated by the logarithmic enhancement in the loop function as well as further combinatoric and colour factors. The brown symbols indicate specific values of  $\zeta_l \zeta_u = 40, 80, -80, -160$ , corresponding to solid diamond, solid circle, empty diamond and empty circle respectively. While the chiral enhancement and the mass limit increases with  $|\zeta_l \zeta_u|$ , the sign is also important as can be seen by comparing the solid circle and empty diamond. The latter effect is entirely due to the different limits on positive and negative  $\Delta a_\mu$  shown in Eq. (3.108). The phenomenology and the impact of the  $a_\mu$  measurement on 2HDM models is discussed in more detail in Sec. 5.3.

For vector-like lepton models which the chiral enhancement is given by  $R_\chi = -\bar{\lambda}_\Phi v / m_\mu$ . Here  $\bar{\lambda}_\Phi$  is a free parameter that can be varied to increase the size of the chirality flip with different choices represented by the orange diamonds, circles and triangles showing how increasing  $|\bar{\lambda}_\Phi|$  increases the chiral enhancement and the mass limit. At the same time the mass limit increases with  $|\lambda_L \lambda_R|^{\frac{1}{2}}$  and again becomes more severe if the sign is chosen so that  $\Delta a_\mu < 0$ , as indicated by comparing the filled and unfilled symbols in orange. These points demonstrate how the mass limit obtained from the  $a_\mu$  measurement can be stronger than collider limits for  $\mathcal{O}(1)$  values of the couplings. Note, however, that in some cases additional constraints apply which are discussed in detail in Sec. 5.5.

In case of the  $S_1$  scalar leptoquarks coupling to the top-quark and muon the resulting chiral enhancement  $R_\chi = m_t/m_\mu \approx 1700$  is fixed, but rather large. Additionally, there is again a colour factor and sizeable loop function, such that the actual limits for these models easily exceed the generic one-loop bounds indicated by the red lines. Since the chiral enhancement is fixed by the measured SM fermion masses, the mass limit only varies with the couplings to left- and right-handed muons. For example, the current collider limit on  $M_{S_1}$  is surpassed for couplings  $\sqrt{\lambda_L^{32}\lambda_R^{32}} > 0.06$ , as indicted by comparing to the purple diamond in Fig. 3.9. The mass limit from the  $a_\mu$  measurement for larger couplings of 0.1 and 0.5 are indicated by the purple circle and triangle respectively, with the latter showing that even masses well above 10 TeV can be excluded by the  $a_\mu$  measurement emphasising the power of this observable.

Finally, we have also shown some points corresponding to the radiative muon mass scenarios listed in Table 1.1 and discussed in more detail in Sec. 3.1. Here the chiral enhancement is given by  $R_\chi \sim 16\pi^2/(\lambda_L\lambda_R)$ , however, since the couplings are always adjusted to produce the correct muon mass, the resulting mass limits are independent of the model parameters and instead depend only on the representation and charges. In turn, the resulting bounds are quite rigid and now typically exclude masses in such scenarios to below the TeV scale.

### 3.7.2. Two-field models and compressed spectra

As we have seen muon  $g - 2$  can be a very powerful observable for constraining models with large chiral enhancements. On the other hand generically for models without any enhancement, direct collider limits on masses are higher than the limit from the  $a_\mu$  measurement. However precision measurements of muon  $g - 2$  still play an important role in the phenomenology of models without an internal chirality flip. As discussed above the collider bounds are very model dependent and can often be evaded. The limits depend significantly on very specific signal regions that can change in realistic and well motivated models where multiple states may be light or due to other factors influencing the kinematics. In these cases rather than competing, collider searches and the precision  $a_\mu$  measurement can provide complementary constraints and cross-checks.

We will illustrate this complementarity in the context of models that extend the SM by two new fields with different spin, which we discussed in Sec. 2.2 and classified in in Table 2.2. As already discussed there these models can only achieve large  $\Delta a_\mu$  contributions, exceeding the  $2\sigma$  bound, for masses that are well within the reach of the LHC searches. These models are particularly interesting as they are the simplest extensions that can both explain dark matter and contribute non-negligibly to  $a_\mu$  and they were also discussed in this context in Sec. 3.6.3. There it was shown that the DM relic density can only be explained for such low masses for the lowest dimensional representations. Nonetheless this does not exclude lower mass scenarios, as it is possible the dark matter candidate provides only a small fraction of the full relic density of dark matter or in fact for the model to have no dark matter candidate at all if one does not assume a  $\mathbb{Z}_2$  symmetry (models like this were considered in Ref. [191]). However both collider constraints and the precision  $a_\mu$  measurement are very relevant for these masses in all cases, i.e. for the models that can explain dark matter, for models that predict an under abundance of DM and for models that have no DM candidate at all.

In particular we will consider two models with a scalar  $\phi$  and Dirac fermion  $\psi$ , one that couples only to left-handed muons, which we will call Model L here, and one that couples to only right-handed muons, which we will call Model R. Model L and Model R have the Lagrangian's given Eq. (3.89) and (3.90), respectively, in Sec. 3.6.3. In both models the scalar and fermion are  $SU(3)_c$  singlets and for the  $SU(2)_L$  representation we choose from the models of this type with the lowest dimensional representations to improve the chances of explaining dark matter. In Model L  $\phi$  is a scalar singlet and

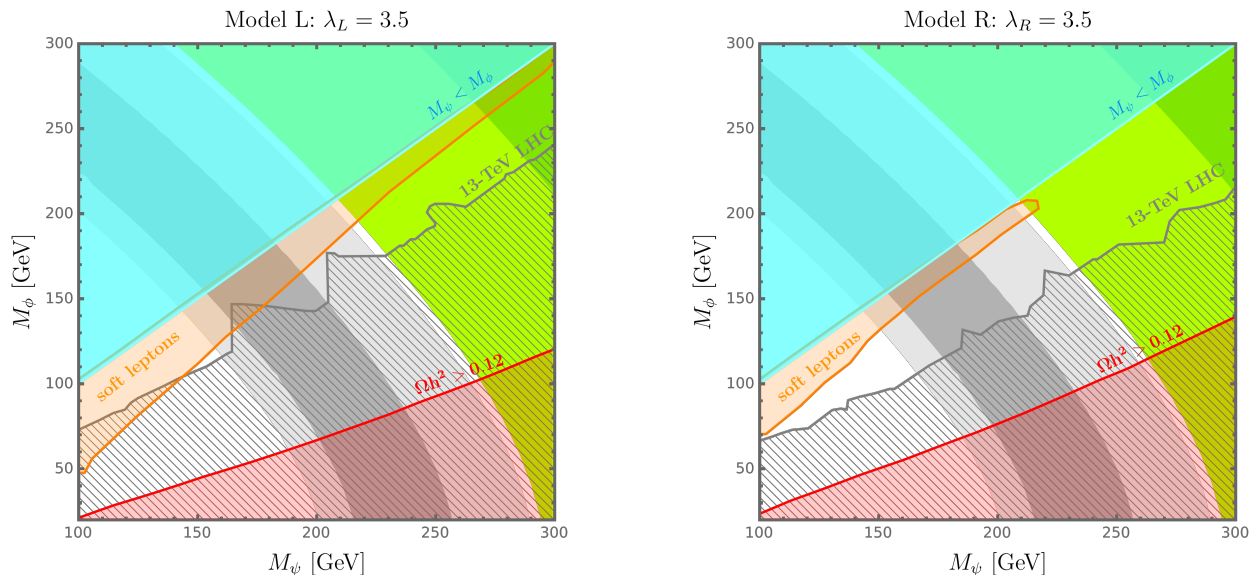


**Figure 3.10:** LHC, dark matter and  $\Delta a_\mu$  exclusion contours in the  $M_\psi - M_\phi$  plane of the Model L (*left*) and R (*right*) discussed in the text. In both cases the scalar  $\phi \sim (\mathbf{1}, 0)$  is a singlet with hyper-charge 0 under  $SU(2)_L \times U(1)_Y$ , while in Model L  $\psi \sim (\mathbf{2}, \frac{1}{2})$  and in Model R  $\psi \sim (\mathbf{1}, -1)$ . The (light) green contour shows the  $1\sigma$  ( $2\sigma$ ) region allowed by  $\Delta a_\mu^{\text{Exp-WP2025}}$ , while the (light) grey contour shows the  $1\sigma$  ( $2\sigma$ ) region allowed by the previous deviation  $\Delta a_\mu^{\text{Exp-WP2020}}$ . Compared to Ref. [9] which took into account higher-order corrections to  $\Delta a_\mu$ , here we have only used the leading one-loop contribution. The resulting difference is, however, negligible for the present discussion. The exclusion limits from 13-TeV LHC (grey hatched region), soft lepton searches (orange shading) and dark matter overabundance  $\Omega h^2 > 0.12$  (red shading) have been directly adapted from Ref. [9]. The region with  $M_\psi < M_\phi$  (cyan contour) is excluded by the fact that the lightest state is electrically charged.

$\psi$  is an  $SU(2)_L$  doublet, while in Model R both the scalar and the fermion are  $SU(2)_L$  singlets, with the scalar having hypercharge zero such that it is a dark matter candidate and the fermion has hypercharge  $-1$  such that it is a charged state that can couple to the photon in the one-loop diagram from  $\Delta a_\mu$ .

Even in these relatively simple models, with only two new physics states, there is a generic challenge in constraining so-called compressed spectra where the mass of the fermion and scalar are close in size. For a sufficiently small mass splitting the kinetic energy of the decay products is too low, resulting in soft leptons or soft jets that can be below the detection threshold. In the past such gaps in the collider exclusion have been interpreted as a possible way that models without a chiral enhancement could explain a large deviation in muon  $g - 2$ , as illustrated in Fig. 3.10 which we reproduce from Ref. [9].

There we see a substantial gap between the exclusion from LHC searches and the  $M_\phi = M_\psi$  line, which borders the cyan region that is excluded because it has a stable charged particle. This is nonetheless further constrained by dedicated searches for compressed spectra [449].<sup>41</sup> Despite these efforts, gaps in the exclusions remain for small enough mass splittings.

By contrast contours of  $\Delta a_\mu$  cross the whole  $M_\phi - M_\psi$  plane with no gaps. This is illustrated by the light and dark, grey and green shaded contours in Fig. 3.10. Here the light (dark) grey contours show the region compatible within  $2\sigma$  ( $1\sigma$ ) with the deviation  $\Delta a_\mu^{\text{Exp-WP2020}}$ . Previously the mass gaps discussed above and plots such as those in Fig. 3.10 were used to provide a way in which these models could explain the then large deviation between experiment and SM

<sup>41</sup>Since Ref. [9] was released there have been further papers tightening constraints on compressed spectra, see e.g. Refs. [450–455]. Nonetheless things do not change qualitatively as there always remains a mass gap in the LHC exclusions.

predictions for  $a_\mu$  and the grey contours show where that was possible. However in the present context where the 2025 White Paper prediction is very close to the measured value, such plots should be reinterpreted. Therefore we have added the light (dark) green contours that show the current  $2\sigma$  ( $1\sigma$ ) limit for these models on top of the results from Ref. [9]. The precision  $a_\mu$  measurement then excludes the entire plane below the light green region, including the previously preferred region in grey.

In this way although the mass reach of the FNAL muon  $g - 2$  experiment does not currently extend to masses large enough to escape the LHC sensitivity, the precision  $a_\mu$  measurement can exclude various gaps in the collider constraints at lower masses where colliders lack sensitivity. Thus muon  $g - 2$  experiments provide a complementary test on light new physics that can close holes in the exclusion limits from colliders. While we have only discussed two particular examples above, this behaviour is typical of the whole class of models extending the SM by a Dirac fermion and a scalar singlet that we have also discussed in previous sections. Furthermore when one considers models with many new states at low energies, as is predicted by some models based on fundamental principles, such as supersymmetry, there are many more ways for holes in the collider limits to be introduced. Therefore the precision measurement of  $a_\mu$  provides a complementary constraint on new physics masses of  $\mathcal{O}(100)$  GeV that is of great importance to particle physics phenomenology.

## 4. Higher-order contributions to $a_\mu$

In this section we discuss several techniques and results for calculations of  $\Delta a_\mu$  in BSM scenarios beyond the one-loop level. We first explain in Sec. 4.1 how the scalar form factors can be obtained from the tensor amplitude using trace projectors. This methods helps to avoid the tedious reductions of the Dirac covariants via Gordon Identities and, in particular for higher order calculation, drastically reduces the computational complexity. Section 4.2 then focuses on the important class of Barr-Zee two-loop diagrams, which are relevant or even dominant in a variety of different models, including e.g. the 2HDM or vector-like fermion extensions. Finally, in Sec. 4.3 we discuss logarithmically enhanced higher-order corrections arising e.g. from QED. There, the origin and structure of such contributions is explained using EFT methods and the impact on various BSM scenarios is sketched.

### 4.1. Form factor trace projectors

On-shell amplitudes like Eq. (1.39) typically consist of a small number of relevant covariants that define the physical form factors. However, especially at higher loop orders, many additional Dirac structures can appear at intermediate steps that require further simplifications in order to bring the result in the desired form. It is therefore often much more efficient to project out the relevant terms already at the amplitude level by using trace projectors. This technique was first developed in 4-dimensions [456–460] and later adapted to dimensional regularisation [10–12, 461], for which we collect the results here. In case of the photon vertex, we denote the projectors as  $\mathcal{P}_i^\mu$  such that the corresponding form factors are given by

$$F_i(q^2) = \text{Tr} \left\{ \mathcal{P}_i^\mu(p, p') \cdot \Gamma_\mu(p, p') \right\}. \quad (4.1)$$

After moving the trace to the integrand level only scalar integrals remain on the right-hand side which directly yield the desired contribution to the respective form factors. The main purpose of the projectors is to enforce the Dirac equation, that is, to remove terms of the form  $\dots(\not{p} - m_\mu)$  and  $(\not{p}' - m_\mu)\dots$  from  $\Gamma^\mu$ . This is achieved by the following ansatz,

$$\mathcal{P}_i^\mu = (\not{p} + m_\mu) \left[ \gamma^\mu \left( C_1 + C_2 \gamma^5 \right) + \frac{P^\mu}{2m_\mu} \left( C_3 + iC_4 \gamma^5 \right) + \frac{q^\mu}{2m_\mu} \left( C_5 + C_6 \gamma^5 \right) \right] (\not{p}' + m_\mu), \quad (4.2)$$

where the momenta are taken on-shell,  $p^2 = p'^2 = m_\mu^2$ . The terms vanishing due to the Dirac equation then drop out automatically. The coefficients  $C_i$  can be determined by inserting this ansatz together with the generic vertex function Eq. (1.39) into Eq. (4.1) and collecting the coefficients in front of the form factors. Solving the resulting system of linear equations assuming  $D = 4 - 2\epsilon$  space-time dimensions yields the coefficients

$$\mathcal{P}_E^\mu : \quad C_1 = \frac{1}{2(D-2)(q^2 - 4m_\mu^2)} \quad C_3 = \frac{2(D-1)m_\mu^2}{(D-2)(q^2 - 4m_\mu^2)^2}, \quad (4.3)$$

$$\mathcal{P}_M^\mu : \quad C_1 = \frac{-2m_\mu^2}{(D-2)q^2(q^2 - 4m_\mu^2)} \quad C_3 = \frac{-2m_\mu^2((D-2)q^2 + 4m_\mu^2)}{(D-2)q^2(q^2 - 4m_\mu^2)^2}, \quad (4.4)$$

$$\mathcal{P}_D^\mu : \quad C_4 = \frac{2m_\mu^2}{q^2(q^2 - 4m_\mu^2)}. \quad (4.5)$$

Note that the projectors for  $F_M(q^2)$  and  $F_D(q^2)$  are both divergent in the limit  $q^2 \rightarrow 0$ . Although this divergence cancels after the evaluation of the loop integrals, it constitutes an inconvenience for the calculation of  $a_\mu$ . For this, it is instead desirable to obtain dedicated projectors that immediately yield the form factors at  $q^2 = 0$ . A simple way to achieve this is by expanding the amplitude in  $q_\mu$  after setting  $p = (P - q)/2$  and  $p' = (P + q)/2$ . Since the dipole covariants are linear in  $q_\nu$  it is sufficient to expand to first order

$$\Gamma^\mu(P, q) \simeq \Gamma^\mu(P, 0) + \left. \frac{\partial}{\partial q_\nu} \Gamma^\mu(P, q) \right|_{q=0} q_\nu \equiv V^\mu + T^{\mu\nu} q_\nu. \quad (4.6)$$

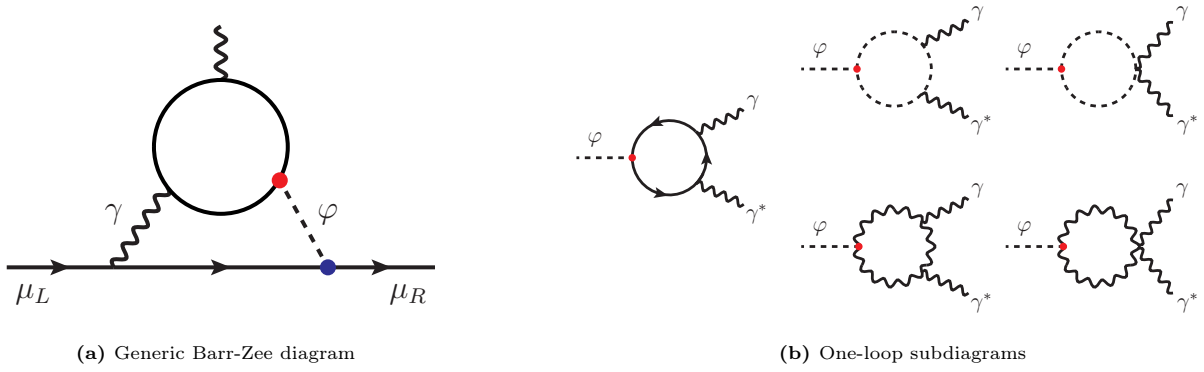


**Figure 4.1:** (a): Generic two loop Barr-Zee diagram with internal photon and real scalar. The blue vertex denotes the small Yukawa coupling of the scalar to the muon while the red vertex denotes the (potentially enhanced) coupling of the scalar to the virtual loop. (b): one-loop contributions of fermions, scalars and gauge bosons to the  $\varphi\gamma\gamma$  subdiagram.

We can then average  $\mathcal{P}_i \cdot \Gamma$  over the spatial directions of  $q_\mu$  which leaves the trace unchanged but allows us to replace [11, 461]

$$\overline{q^\mu}, \overline{q^\mu q^\nu q^\rho} \rightarrow 0 \quad \text{and} \quad \overline{q^\mu q^\nu} \rightarrow \frac{q^2}{D-1} \left( g^{\mu\nu} - \frac{P^\mu P^\nu}{P^2} \right). \quad (4.7)$$

The resulting expressions for the trace projectors are given by

$$F_M(0) = \frac{1}{4(D-1)m_\mu^2} \text{Tr} \left\{ \left[ m_\mu^2 \gamma^\alpha - (D-1)p^\alpha m_\mu - Dp^\alpha \not{p} \right] V_\alpha(p) \right\} + \frac{1}{8(D-2)(D-1)m_\mu} \text{Tr} \left\{ (\not{p} + m_\mu) [\gamma^\alpha, \gamma^\beta] (\not{p} + m_\mu) T_{\alpha\beta}(p) \right\}, \quad (4.8a)$$

$$F_D(0) = \frac{ip^\alpha}{4(D-1)m_\mu^2} \text{Tr} \left\{ (\not{p} + m_\mu) \gamma^\alpha \gamma^5 (\not{p} + m_\mu) T_{\alpha\beta}(p) \right\} - \frac{ip^\alpha}{16m_\mu} \text{Tr} \left\{ \gamma^5 V_\alpha(p) \right\}. \quad (4.8b)$$

Here we have substituted  $P = 2p$  which holds for  $q \rightarrow 0$ . Since both  $V$  and  $T$  depend only on  $p$ , the computation of  $F_M(0)$  and  $F_D(0)$  reduces to an evaluation of on-shell self-energy amplitudes rather than the full three-point function. Furthermore, for  $a_\mu$  only the anti-symmetric part of  $T_{\mu\nu}$  contributes due to the appearance of the commutator.

## 4.2. Two-loop Barr-Zee diagrams

One important class of two-loop diagrams (some of which are shown in Fig. 4.1) with potentially large contributions to  $\Delta a_\mu$  was first identified by Barr and Zee in Ref. [462]. In these diagrams, an inner fermion or boson loop generates an effective  $\gamma\text{-}\gamma\text{-}\varphi$  vertex, which then couples to the muon via a second loop.  $\varphi$  can be the SM Higgs or a new scalar. Barr and Zee initially studied possibility of CP violation mediated by an extended Higgs sector, where  $\varphi$  corresponds to a BSM Higgs. The diagrams can then generate important effects on the EDM of the electron, but the same enhancement mechanism can also lead to a large contribution to  $\Delta a_\mu$ . The main reason for this enhancement is that, compared to a one-loop diagram of the kind in Fig. 2.1a with a virtual  $\varphi$ , one of the scalar vertices is lifted from the muon line into the virtual loop. On the one-hand, this exchanges one of the muon Yukawa couplings  $y_\mu$  for the (potentially) much larger coupling of the scalar  $\varphi$  to the particle running in the inner loop and on the other hand, no further chirality flip on the muon line is necessary, removing a factor of  $m_\mu$ . The compensating mass parameter is given either by the triple boson coupling or, in case of a fermion loop, by an additional required chirality flip on one of the internal heavy fermion lines. In both cases this results in a significant potential enhancement factor, which can often overcome the additional loop suppression.

To specify the diagrams generically, we denote the generic Yukawa and scalar interaction terms in a mass-basis Lagrangian by

$$\mathcal{L}_Y = y_f^\varphi \bar{f} P_R f \varphi + h.c., \quad \mathcal{L}_{\varphi S^2} = -\lambda_{\varphi S^2} \varphi |S|^2, \quad \mathcal{L}_{\varphi V^2} = g_{\varphi V^2} \varphi V_\mu^\dagger V^\mu, \quad (4.9)$$

while the photon interactions are taken from Eq. (2.2). We assume fermion flavour changing couplings to be absent and  $\varphi$  to be a real scalar.

With these couplings, the above discussion can be made concrete. The one-loop diagram with virtual  $\varphi$  and muon has the chirality-flipping and EWSB factors  $[\dots] \rightarrow |y_\mu^\varphi|^2 m_\mu$  in the notation of Eq. (1.15). The two-loop diagram with fermion loop instead involves the factors  $y_\mu^\varphi y_f^\varphi m_f \alpha / 4\pi$ , hence it is relatively enhanced by

$$\left| \frac{\Delta a_\mu^{\text{BZ}}}{\Delta a_\mu^{\text{FS}}} \right| \sim \frac{\alpha}{4\pi} \frac{m_f y_f^\varphi}{m_\mu y_\mu^\varphi}. \quad (4.10)$$

In the typical case where  $m_f \propto y_f^\varphi$ , the two-loop Barr-Zee diagram is bigger than the one-loop FS-type diagram if the mass  $m_f \gtrsim \text{few GeV}$ . The Barr-Zee type diagrams with internal boson loops behave similarly.

Thus, particularly in BSM scenarios with new scalars (such as the 2HDM discussed in Sec. 5.3 or extensions thereof) the Barr-Zee diagrams often provide very substantial or even dominant contributions to  $a_\mu$ .

In the following we collect some of the results previously presented in the literature. We focus particularly on the photonic Barr-Zee diagrams shown in Fig. 4.1. In principle, there are further Barr-Zee type diagrams where the internal photon is exchanged for a massive gauge boson. Although these will have a relative suppression due to the massive propagator, they can still give significant contributions e.g. in case of a charged scalar or as a consequence of other enhancements. For further discussion and details on the calculation for  $\Delta a_\mu$  we refer to Refs. [463, 464] for the fermionic loops and Ref. [465] for more general Barr-Zee diagrams.

The calculation of the diagrams is conveniently split into two steps. First, the sub-loops depicted in Fig. 4.1b are evaluated for off-shell momenta  $p$  and  $k$  of the scalar and one of the photons, while the external photon momentum  $q$  can be treated on-shell. The resulting effective vertex has the following relevant gauge invariant structure

$$i\Gamma^{\mu\nu}(k, q) = i\Gamma(k, q) [g^{\mu\nu} k \cdot q - k^\mu q^\nu] + i\Gamma^5(k, q) \epsilon^{\mu\nu\alpha\beta} k_\alpha q_\beta. \quad (4.11)$$

Note that gauge-variant covariants like  $k^\mu k^\nu$  can also appear during the calculation, but they do not contribute to the final result and can therefore be dropped [466]. After inserting this effective vertex back into the two-loop amplitude, the remaining integral can be evaluated, yielding the contributions to the dipole moments. It is also worth pointing out that the sub-loop is finite and the effective vertex has the structure of a propagator. Therefore also the full amplitude is finite and does not require sub-renormalisation.

With the couplings defined in the Lagrangian (4.9), the results of the diagrams in Fig. 4.1 (neglecting higher orders in  $m_\mu$ ) are given by<sup>42</sup>

$$\Delta a_\mu^{\text{BZ},f} = \frac{\alpha}{8\pi^3} N_c^f Q_f^2 \frac{m_\mu m_f}{m_\varphi^2} \left[ \text{Re} \{y_f^\varphi\} \text{Re} \{y_\mu^\varphi\} \mathcal{F}_1 \left( \frac{m_f^2}{m_\varphi^2} \right) + \text{Im} \{y_f^\varphi\} \text{Im} \{y_\mu^\varphi\} \mathcal{F}_2 \left( \frac{m_f^2}{m_\varphi^2} \right) \right], \quad (4.12)$$

$$\Delta a_\mu^{\text{BZ},S} = \frac{\alpha}{16\pi^3} N_c^S Q_S^2 \frac{m_\mu \lambda_{\varphi S^2}}{m_\varphi^2} \text{Re} \{y_\mu^\varphi\} \mathcal{F}_3 \left( \frac{m_S^2}{m_\varphi^2} \right), \quad (4.13)$$

$$\Delta a_\mu^{\text{BZ},V} = \frac{\alpha}{32\pi^3} Q_V^2 \frac{m_\mu g_{\varphi V^2}}{M_V^2} \text{Re} \{y_\mu^\varphi\} \mathcal{F}_4 \left( \frac{m_V^2}{m_\varphi^2} \right), \quad (4.14)$$

<sup>42</sup>The vector contribution is generalised from the 2HDM diagrams with  $W$ -boson loops computed in Ref. [465] and corresponds to the physical result including appropriate Goldstone boson contributions.

	$x \rightarrow 0$	$x \rightarrow \infty$	$x \rightarrow 1$
$\mathcal{F}_1$	$-\ln(x)^2 - 2\ln(x) - 4 - \frac{\pi^2}{3}$	$-\frac{6\ln(x)+13}{9x}$	-1.66
$\mathcal{F}_2$	$\ln(x)^2 + \frac{\pi^2}{3}$	$\frac{\ln(x)+2}{x}$	2.34
$\mathcal{F}_3$	$-\ln(x) - 2$	$\frac{3\ln(x)+5}{18x}$	0.34
$\mathcal{F}_4$	$-\ln(x) - 2$	$-7\ln(x) - \frac{89}{6}$	-16.76

**Table 4.1:** Asymptotic expressions for the Barr-Zee loop functions.

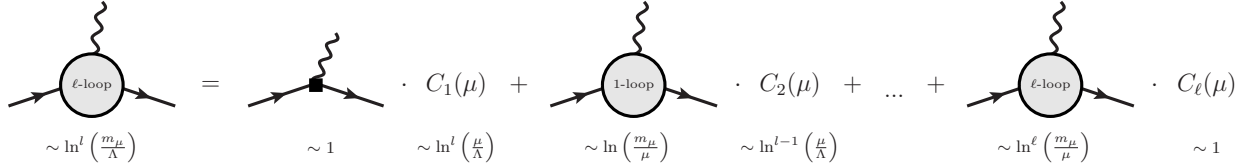


**Figure 4.2:** Illustration of the decomposition of an  $\ell$ -loop contribution to  $\Delta a_\mu$  into EFT (loop) diagrams and Wilson coefficients with the corresponding logarithmic scaling.

where the loop functions are normalised slightly differently compared to Ref. [465] and are given by

$$\mathcal{F}_i(x) = \int_0^1 du \frac{\mathcal{N}_i(u; x)}{x - u(1-u)} \ln\left(\frac{x}{u(1-u)}\right), \quad (4.15)$$

and the numerators for the respective integrals read

$$\mathcal{N}_1(u; x) = 2u(1-u) - 1 \quad (4.16a)$$

$$\mathcal{N}_2(u; x) = 1 \quad (4.16b)$$

$$\mathcal{N}_3(u; x) = u(1-u) \quad (4.16c)$$

$$\mathcal{N}_4(u; x) = u(1-u) - xu[3u(4u-1) + 10]. \quad (4.16d)$$

The loop functions depend on the mass ratios  $x = m_{f,S,V}^2/m_\varphi^2$  between the two involved internal masses. Often the two masses both correspond to heavy states and are of similar order, but sometimes the cases of light  $\varphi$ ,  $x \rightarrow \infty$ , or heavy  $\varphi$ ,  $x \rightarrow 0$ , are of interest. Table 4.1 collects all these limits.

For phenomenological applications not only the magnitude but also the signs of the contributions are of high interest. Taking again the corresponding one-loop diagrams with virtual  $\varphi$  and muon as a reference, its result in the limit of large  $m_\phi$  can be written as (see Sec. 2.1)

$$\Delta a_\mu^{\text{one-loop}} \approx \frac{1}{4\pi^2} \frac{m_\mu^2}{m_\varphi^2} \ln\left(\frac{m_\varphi}{m_\mu}\right) \left[ \text{Re}\{y_\mu^\varphi\}^2 - \text{Im}\{y_\mu^\varphi\}^2 \right] \quad (4.17)$$

in the notation of the Lagrangian (4.9). For a scalar, the couplings are real and the one-loop contribution is positive; for a pseudoscalar the one-loop contribution is negative. In contrast, e.g. the fermionic Barr-Zee diagrams of Eq. (4.12) have exactly the opposite behaviour. This was first observed and used for the 2HDM in Refs. [463, 464, 467, 468].

### 4.3. Leading logarithms and EFT resummation

Another class of important higher-order corrections can arise in BSM scenarios with heavy masses of the order of a scale  $\Lambda \gg m_\mu$ . In such models, large logarithms  $\ln(\Lambda/m_\mu)$  involving the two physical scales can appear, where e.g. for  $\Lambda = 1$

TeV,

$$\ln\left(\frac{\Lambda}{m_\mu}\right) \approx 9.2. \quad (4.18)$$

For example, the electroweak SM contributions involve heavy particles and behave similar to many BSM scenarios. The one-loop  $W$ - and  $Z$ -boson contributions involve no large logarithm, but the one-loop Higgs-boson contribution involves a large logarithm  $\ln(M_h/m_\mu)$ , see Eq. (1.64) in Sec. 1.4. As discussed there, the two-loop electroweak corrections reduce the one-loop result by about 20% and are dominated by large logarithms. These and further logarithms were analysed and computed in Ref. [152], and a prediction valid in many BSM scenarios was derived,

$$\Delta a_\mu^{2\text{L,leading log}} = \Delta a_\mu^{1\text{L}} \left(1 - \frac{4\alpha}{\pi} \ln\left(\frac{\Lambda}{m_\mu}\right)\right), \quad (4.19)$$

i.e. the one-loop contributions are reduced by a large log, and the reduction amounts to about 9% for  $\Lambda \sim 1$  TeV. This holds in scenarios where the one-loop results are governed by purely heavy loops and are proportional to  $m_\mu^2$ , i.e. where the necessary chirality flip (see Sec. 1.1.4) is proportional to the muon Yukawa coupling or some generalisation. The analysis of SM logarithms was refined in Ref [28], the result (4.19) was rederived together with non-logarithmic corrections by Feynman diagrammatic computations in Ref. [469], and more general results were obtained in Ref. [212].

Our aim in this subsection is to show how the techniques of effective field theory (EFT) and renormalisation group equations (RGE) allow to compute such logarithms and discuss the corresponding results. While we focus here on applications to  $\Delta a_\mu$ , we stress that the method is much more general and has been applied e.g. in the context of quark flavour physics [214] and can be applied to a large number of other observables using full one-loop RGEs available for both LEFT [470] and SMEFT [471–473].

### 4.3.1. The EFT renormalisation group equation

In sec. 2.4 we have already discussed how EFT can be applied to analyse BSM contributions to  $a_\mu$  in a model-independent way. A prominent feature of this approach is the separation of the BSM (or electroweak) scale  $\Lambda$  and the muon mass scale  $m_\mu$ . The BSM scale only enters in the Wilson coefficients after matching to the UV theory, while the muon mass (and other light particle masses) appears only in the EFT diagrams. As an important consequence, large *physical* logarithms  $\ln(m_\mu/\Lambda)$  appearing in the full result of the UV theory are split into  $\ln(m_\mu/\mu)$  contributions from EFT (loop) diagrams and  $\ln(\mu/\Lambda)$  contributions from running Wilson coefficients (WCs). In this way, the physical logarithms are connected to the unphysical logarithms  $\ln(\mu)$  of the EFT renormalisation scale  $\mu$ . In particular, as illustrated in Fig. 4.2, the highest powers of  $l$ -loop logarithms  $\ln^l(m_\mu/\Lambda)$  (leading logarithms) are contained entirely in the tree-level Wilson coefficient. This connection can be exploited to obtain the leading (or subleading) higher-order corrections from the RGEs within the EFT which govern the WCs, rather than from explicit multi-loop integrals involving several scales.

As a setup we consider first a generic EFT Lagrangian in terms of the bare composite operators  $\mathcal{O}_i^0$  and corresponding Wilson coefficients  $C_i^0$

$$\mathcal{L} = \sum_i C_i^0 \mathcal{O}_i^0. \quad (4.20)$$

In dimensional regularisation with dimension  $D = 4 - 2\epsilon$  we denote the operator mass dimension by  $[\mathcal{O}_i^0] = n_i - (2 + \varsigma_i)\epsilon$  (with  $n_i = 1, 2, \dots$ ), such that  $[C_i^0] = 4 - n_i + \varsigma_i\epsilon$ . The bare quantities are given in terms of the renormalised ones as

$$C_i^0 = \mu^{\varsigma_i\epsilon} \left( C_i(\mu) + \delta C_i(\mu) \right), \quad \mathcal{O}_i^0 = Z_{\mathcal{O}_i}(\mu) \mathcal{O}_i(\mu), \quad (4.21)$$

where  $Z_{\mathcal{O}_i}$  is the product of composite field wave-function renormalisations and the renormalisation scale  $\mu$  was introduced in such that the renormalised Wilson coefficients are integer dimensional (in the following we suppress the argument). In the  $\overline{\text{MS}}$ -scheme the renormalisation constants can be written as

$$\delta C_i = \sum_{n=1}^{\infty} \frac{\delta C_i^{[n]}}{\epsilon^n}, \quad Z_{\mathcal{O}_i} = 1 + \sum_{n=1}^{\infty} \frac{Z_{\mathcal{O}_i}^{[n]}}{\epsilon^n}. \quad (4.22)$$

The fact that the bare coupling parameters are independent of  $\mu$  and that the  $(\overline{\text{MS}})$  renormalisation constants  $\delta C_i^{[n]}$  depend on  $\mu$  only through the renormalised couplings results in the following RGE

$$\mu \frac{dC_i}{d\mu} = - \left( \delta_{ij} + \frac{\partial \delta C_i}{\partial C_j} \right)^{-1} \varsigma_j \epsilon (C_j + \delta C_j) \stackrel{\epsilon \rightarrow 0}{\equiv} \frac{\partial \delta C_i^{[1]}}{\partial C_j} \varsigma_j C_j - \varsigma_i \delta C_i^{[1]}. \quad (4.23)$$

While this equation is generally valid for all couplings, it can often be significantly simplified for the WCs of the non-renormalisable operators:

- It is often sufficient to consider effects only up to  $1/\Lambda^2$ . In this case only terms linear in the dimension-6 coefficients and (at most) quadratic in the dimension-5 coefficients have to be taken into account.
- In addition, the dimension-5 coefficients are usually generated radiatively, such that two insertions of the dimension-5 operator are loop suppressed by the matching condition. In this case also the  $\sim C^2$  terms can be dropped.

Under these assumptions, the renormalisation constants of the WCs are then given by  $\delta C_i = Z_{ij} C_j$  where the matrix  $Z_{ij}$  depends only on the renormalisable (dimension $\leq 4$ ) couplings (denoted  $\alpha_k$  in the following), and the RGE Eq. (4.23) takes the simple form

$$\mu \frac{dC_i}{d\mu} = (\gamma^T)_{ij} C_j \quad \text{where} \quad \gamma_{ji} = (\varsigma_j - \varsigma_i) Z_{ji}^{[1]} + \frac{\partial Z_{ij}^{[1]}}{\partial \alpha_k} \varsigma_k \alpha_k. \quad (4.24)$$

This simplified RGE can be solved iteratively giving

$$\mathbf{C}(\mu) = \sum_{n=0}^{\infty} \int_{\Lambda}^{\mu} \frac{dt_1}{t_1} \dots \int_{\Lambda}^{t_{n-1}} \frac{dt_n}{t_n} \gamma^T(t_1) \dots \gamma^T(t_n) \mathbf{C}(\Lambda) \equiv \mathcal{T} \left\{ e^{\int_{\Lambda}^{\mu} \frac{dt}{t} \gamma^T(t)} \right\} \mathbf{C}(\Lambda). \quad (4.25)$$

The coefficient matrix  $\gamma$  is therefore also called anomalous dimension matrix (ADM) since the RGE running changes the naive scaling  $C_i \sim \Lambda^{4-n_i}$  to (symbolically)  $C_i \sim \Lambda^{4-n_i-\gamma}$ . The ADM depends on  $\mu$  only through the renormalisable couplings  $\alpha_k(\mu)$ . In principle, the RGEs for these couplings also receive corrections from the higher-dimensional operators, however, under the above assumptions these corrections can be neglected in the RGE of the Wilson coefficients. The running couplings are therefore given by the usual results in QED and QCD (if the EFT is LEFT, see Sec. 2.4) or the SM (for SMEFT). In particular, for the following discussion we will need the one-loop RGEs for LEFT given by

$$\mu \frac{de}{d\mu} = \frac{e^3}{12\pi^2} \left( n_e + \frac{4}{3} n_u + \frac{1}{3} n_d \right) \equiv \frac{\beta_e e^3}{16\pi^2}, \quad (4.26a)$$

$$\mu \frac{dg_s}{d\mu} = \frac{g_s^3}{16\pi^2} \left( \frac{2}{3} (n_u + n_d) - 11 \right) \equiv \frac{\beta_s g_s^3}{16\pi^2}, \quad (4.26b)$$

where  $n_e = n_d = 3$  and  $n_u = 2$  count the number of charged fermions in the LEFT. In addition we also need the running fermion masses and expressions for the wave-function renormalisations

$$\mu \frac{dm_f}{d\mu} = - \frac{3m_f}{8\pi^2} \left( Q_f^2 e^2 + C_F^f g_s^2 \right) = 6m_f Z_f^{[1]}, \quad (4.27)$$

where  $C_F^e = 0$  and  $C_F^{u,d} = \frac{4}{3}$ .

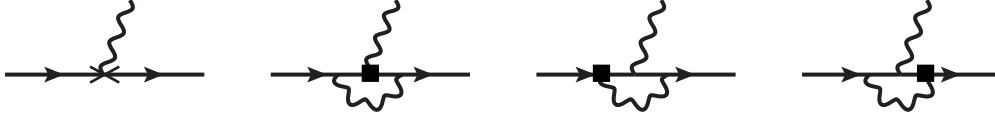


**Figure 4.3:** Diagrams contributing to the  $\mathcal{O}_{e\gamma}$  self-mixing at one-loop order in LEFT.

### 4.3.2. Photonic logarithms for purely heavy BSM scenarios

We first focus on a simple but important case, where new physics contributions to  $a_\mu$  arise from purely heavy one-loop diagrams. This is the case for many 2- and 3-field models as well as e.g. in supersymmetric or leptoquark+top-loop diagrams. Counterexamples are contributions from heavy  $Z'$  or leptoquark+charm-loop diagrams. In this purely heavy case, the dipole operator is the single relevant operator, and only the corresponding diagonal entry of the ADM matters. The corresponding important one-loop diagrams in the EFT are shown in Fig. 4.3 and correspond to the dipole self-mixing via photon loops. In the full BSM theory they correspond to two-loop diagrams with a heavy one-loop  $a_\mu$  subdiagram and an additional photon loop, plus the appropriate renormalisation [469], and the following computation will yield the leading two-loop photonic logarithms.

Including the counterterm diagram, the total amplitude corresponding to Fig. 4.3 gives

$$i\Gamma^\mu = -L_{e\gamma}^{[1]} \left[ Z_{L_{e\gamma}L_{e\gamma}}^{[1]} + Z_{\mathcal{O}_{e\gamma}}^{[1]} - \frac{\alpha}{\pi} \right] \frac{2}{\epsilon} \sigma^{\mu\nu} q_\nu + \text{finite terms.} \quad (4.28)$$

According to Sec. 4.3.1, the operator renormalisation  $Z_{\mathcal{O}_{e\gamma}} = Z_\mu \sqrt{Z_A} = Z_\mu Z_e^{-1}$  is given by

$$Z_{\mathcal{O}_{e\gamma}}^{[1]} = Z_\mu^{[1]} - Z_e^{[1]} = -\frac{\alpha}{8\pi} (2 + \beta_e), \quad (4.29)$$

hence the resulting diagonal renormalisation constant and ADM element of the Wilson coefficient must be (the complete dimension-6 ADM results are listed in Ref. [470])

$$Z_{L_{e\gamma}L_{e\gamma}}^{[1]} = \frac{\alpha}{8\pi} (10 + \beta_e) \quad \implies \quad \gamma_{\mathcal{O}_{e\gamma}\mathcal{O}_{e\gamma}} = \frac{5\alpha}{2\pi} + \frac{\alpha}{4\pi} \beta_e. \quad (4.30)$$

Integrating this equation gives an expression of the running Wilson coefficient  $L_{e\gamma}^{[1]}(Q)$  as a function of the high-scale  $L_{e\gamma}^{[1]}(\Lambda)$  at the leading-logarithmic level. Using  $\Delta a_\mu = 4m_\mu/e(m_\mu)L_{e\gamma}^{[1]}(m_\mu)$ , we obtain the leading-logarithmic result

$$\Delta a_\mu = m_\mu \left[ 4 \frac{L_{e\gamma}^{[1]}(\Lambda)}{e(\Lambda)} \right] \left\{ 1 + \frac{5\alpha}{2\pi} \ln\left(\frac{m_\mu}{\Lambda}\right) + \mathcal{O}(\alpha^2) \right\}, \quad (4.31)$$

where the running of  $e(m_\mu)$  has cancelled the  $\beta_e$  appearing in the running of  $L_{e\gamma}^{[1]}(m_\mu)$ . We note in passing that values of the ADM matrix and Wilson coefficients in general can depend on the regularisation scheme [474] and we refer to the original literature for the scheme specifications and Ref. [215] for a review. Physical results and the dipole coefficient  $L_{e\gamma}^{[1]}(\Lambda)$  in the purely heavy models, however, are scheme independent.

This formula can be applied e.g. to the contributions of a heavy leptoquark+top-loop to  $a_\mu$ , where the one-loop result can be sketched as (see also the discussion in Sec. 1.1.5 and Tab. 1.1)

$$\Delta a_\mu^{\text{LQ,1L}} = c \frac{m_\mu [m_t \lambda_L \lambda_R]}{M^2} \quad (4.32)$$

with a dimensionless constant  $c$  which depends on details such as loop functions and loop factors. Apart from the factor  $m_\mu$  this defines the matching value for the square bracket in Eq. (4.31), such that the leading-logarithmic two-loop correction is

$$\Delta a_\mu^{\text{LQ,1L+2LLL}} = \Delta a_\mu^{\text{LQ,1L}}|_{\overline{\text{MS}}} \left\{ 1 + \frac{5\alpha}{2\pi} \ln\left(\frac{m_\mu}{\Lambda}\right) + \mathcal{O}(\alpha^2) \right\}, \quad (4.33)$$

where the one-loop term, except the factor  $m_\mu$ , needs to be evaluated in the  $\overline{\text{MS}}$ -scheme at the high scale  $\Lambda$ .

A useful, slightly different way to write the same result has been obtained in Ref. [152]. There, the WC is normalised differently by pulling out a factor of the running muon mass, effectively  $C_{H_\mu}(\mu) = -\frac{16\pi^2}{e(\mu)m_\mu(\mu)} \text{Re} L_{22}^{e\gamma}(\mu)$ . The running of this WC differs from Eq. (4.31) by the anomalous dimension of the muon mass, such that

$$\Delta a_\mu = -\frac{m_\mu^2}{4\pi^2} [C_{H_\mu}(\Lambda)] \left\{ 1 + \frac{4\alpha}{\pi} \ln\left(\frac{m_\mu}{\Lambda}\right) + \mathcal{O}(\alpha^2) \right\}. \quad (4.34)$$

This formula is particularly naturally applicable in models, where a factor  $m_\mu^2$  arises in the one-loop computation of  $\Delta a_\mu$ . An example is the MSSM, where the one-loop contributions can be sketched as

$$\Delta a_\mu^{\text{MSSM,1L}} = c \frac{m_\mu^2 \tan \beta}{M^2} \quad (4.35)$$

with a dimensionless constant  $c$  which also depends e.g. on gauge couplings and further model details. Then, the result including leading two-loop logarithms is the one announced in Eq. (4.19), i.e.

$$\Delta a_\mu^{\text{MSSM,1L+2LLL}} = \Delta a_\mu^{\text{MSSM,1L}}|_{\overline{\text{MS}}} \left\{ 1 + \frac{4\alpha}{\pi} \ln\left(\frac{m_\mu}{\Lambda}\right) + \mathcal{O}(\alpha^2) \right\}, \quad (4.36)$$

where now the one-loop contribution, except the factor  $m_\mu^2$ , must be evaluated in the  $\overline{\text{MS}}$ -scheme at the high scale  $\Lambda$ . These leading photonic two-loop logarithms have also been obtained in an explicit diagrammatic two-loop computation in Ref. [469], where also the dependence on the renormalisation scheme was discussed and additional non-logarithmic photonic corrections were obtained.

### 4.3.3. More general logarithms

In the more general case, not only the dipole operator but also further LEFT operators are relevant, corresponding to 4-fermion operators involving leptons and quarks and to 4-lepton operators. The general RGE for  $L_{e\gamma}$  reads

$$\mu \frac{d}{d\mu} L_{22}^{e\gamma} = \frac{\alpha}{4\pi} (10 + \beta_e) L_{22}^{e\gamma} - \frac{eQ_d}{2\pi^2} N_c m_{d_i} L_{22ii}^{T,RR} - \frac{eQ_u}{2\pi^2} N_c m_{u_i} L_{22ii}^{T,RR} - \frac{em_{e_i}}{8\pi^2} L_{2ii2}^{S,RR} + \mathcal{O}(L^2). \quad (4.37)$$

Integrating this equation from the high scale  $\Lambda$  to a scale  $m_\mu$  gives the leading-logarithmic corrections

$$\begin{aligned} L_{22}^{e\gamma}(m_\mu) &\simeq L_{22}^{e\gamma}(\Lambda) \left\{ 1 + \frac{\alpha}{4\pi} (10 + \beta_e) \ln\left(\frac{m_\mu}{\Lambda}\right) + \mathcal{O}(\alpha^2) \right\} \\ &\quad - \frac{e}{8\pi^2} \left\{ 4N_c Q_d m_{d_i} L_{22ii}^{T,RR}(\Lambda) + 4N_c Q_u L_{22ii}^{T,RR}(\Lambda) + m_{e_i} L_{2ii2}^{S,RR}(\Lambda) + \mathcal{O}(\alpha) \right\} \ln\left(\frac{m_\mu}{\Lambda}\right). \end{aligned} \quad (4.38)$$

It is instructive to compare this calculation to the full LEFT one-loop result including non-logarithmic terms from Ref. [212], which was discussed in Sec. 2.4. The logarithmic contributions (up to logarithms between the light scales) from Eq. (2.34) are reproduced here by identifying  $\Lambda = \mu$ . As in the context of Eq. (4.31), the running of  $e$  cancels the appearance of  $\beta_e$  in Eq. (2.34). If desired, Eq. (4.38) can be extended to include higher orders. In this way, Refs. [28, 152] evaluated leading logarithms for the EW SM contributions up to the 3-loop level. Similarly, the formalism explained here can also be used to understand the structure of the logarithms appearing in the two-loop Barr-Zee diagrams of Sec. 4.2,

see Tab. 4.1. If the particles running in the sub-loop are heavy ( $x \rightarrow \infty$ ), the dimension-5  $\phi F_{\mu\nu} F^{\mu\nu}$  operator obtained from integrating out the heavy particles mixes directly into  $\mathcal{O}_{e\gamma}$  at one-loop. Combined with Eq. (4.25) this leads to the two-loop  $\ln^1$  terms. On the other hand if the scalar is heavy ( $x \rightarrow 0$ ), integrating out  $\phi$  leads to a tree-level matching condition for operators like  $\bar{\mu}\mu|S|^2$ ,  $\bar{\mu}\mu\bar{f}f$  and  $\bar{\mu}\mu|V|^2$ . These either mix directly into  $\mathcal{O}_{e\gamma}$  at two-loop leading again to a two-loop  $\ln^1$  term or, only in case of a light fermion loop, first into  $\mathcal{O}_{ee}^T$  which then mixes into the dipole operator leading to a two-loop  $\ln^2$  term.

## 5. Specific BSM scenarios

In this section we focus on a large set of concrete and well-motivated BSM scenarios. For each of them we explain the motivation, the theory and the contributions to  $a_\mu$ , survey the literature and discuss complementary constraints and viable parameter space. We begin with models with light new particles in Sec. 5.1, which can be connected to dark matter and larger dark sectors. The considered models include dark photon,  $Z'$  and ALPs models as well as models trying to explain the existing discrepancies related to the hadronic vacuum polarisation.

Section 5.2 focuses on supersymmetry, both in its minimal form and in alternative realisations that change the phenomenology. Supersymmetric models contain dark matter candidates and lead to chiral enhancements in  $\Delta a_\mu$ , hence there is an important interplay between constraints from  $a_\mu$ , from dark matter, and from the LHC, with significant recent progress.

The two-Higgs doublet model is discussed in Sec. 5.3, allowing the well-known types I II, X, Y but also more general variants. For  $a_\mu$  this model is special since the main contributions arise typically at the two-loop level, and recent LHC and flavour observables significantly narrow down the viable parameter space.

Leptoquark models have been discussed frequently in the context of  $B$ -physics anomalies, but also in the context of  $a_\mu$  because of potentially very large chiral enhancements. In Sec. 5.4 we describe cases with and without chiral enhancement and determine parameter constraints from  $a_\mu$  and flavour physics.

Section 5.5 focuses on models with new fermions. Especially vector-like leptons constitute a special class of models with particularly strong connections between  $a_\mu$  and the muon–Higgs coupling. The constraints from the interplay between these and further collider observables is explained for the complete set of such models and some of their generalisations.

Finally, Sec. 5.6 discusses a wide range of neutrino mass models. The neutrino masses are generated at the tree-level or the loop level, up to three-loop order. These models involve many ideas and elements discussed in other sections such as new gauge groups, new fermions or new scalars; the new particles can be vector-like leptons, leptoquarks, a second Higgs doublet, or dark matter candidates. In many models the contributions to  $a_\mu$  are strongly chirally enhanced, such that  $a_\mu$  places an important complementary parameter constraint on the models.

The phenomenology of  $a_\mu$  has also been studied in additional BSM scenarios. In most cases, the general remarks made in Sec. 2 on models with one, two, or three new fields apply and the relationships to other observables explained in Sec. 3 provide a good understanding of many properties, but a dedicated model-specific discussion is beyond the scope of this review. Examples are heavy new gauge bosons [475–484] including the 331-model [485–495], studies of specific models with heavy dark matter particles beyond the discussions in Secs. 2.2, 3.6 [496–500], models with extra dimensions, technicolour or compositeness [501–521], non-commutative geometry, Lorentz violation and spin-2 particles [522–525]. For detailed discussions we refer to the literature.

### 5.1. Light Dark Sectors

Some of the big open questions in fundamental physics are related to the nature of dark matter and of neutrino masses. Answers could possibly be related to light BSM particles which interact very weakly with ordinary matter. In particular the evidence for dark matter may not only point towards the existence of a single kind of dark matter particle but also indicate a richer dark sector, possibly with a number of different states and non-trivial interactions between them. Such states may contain scalars, fermions and there may be dark gauge sectors with dark vector bosons. The weakness of their interactions with detectors allows their masses to be light, i.e. below the GeV-scale. There is growing interest and activity

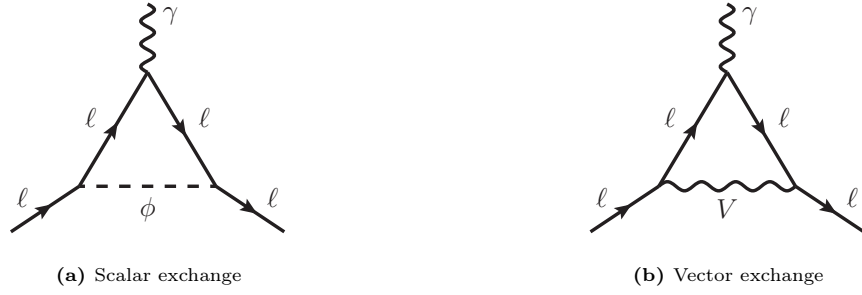


**Figure 5.1:** Light dark sector one-loop contribution to  $a_\ell$  from a neutral scalar  $\phi$  or vector boson  $V$ .

in detailed investigations of such light dark sectors, as reviewed in Refs. [526–531].

In connection with  $a_\mu$  the possible existence of such light dark sectors is of high interest. Even without chirality-flip enhancement, see Sec. 1.1.4, significant BSM contributions are possible provided dark sector particles have some interactions with muons. Particular classes of light dark sectors can therefore be candidates to explain a potential large  $\Delta a_\mu$  effect, and generally  $a_\mu$  provides relevant constraints on such dark sector parameter spaces. Similarly, electric dipole moments provide constraints on dark sectors which violate CP [532].

In general, dark sector states and their interactions are often classified according to so-called “portal interactions” with the SM, which are couplings of dark sector operators to gauge invariant SM operators. In the notation of Sec. 1.2 of Ref. [529],

$$B^{\mu\nu} F'_{\mu\nu} \quad \text{kinetic mixing portal} \quad (5.1)$$

$$(\Phi^\dagger \Phi)(AS + \lambda S^2) \quad \text{Higgs portal} \quad (5.2)$$

$$(\bar{I}\Phi)N \quad \text{neutrino portal} \quad (5.3)$$

$$(\bar{\psi}\gamma^\mu\psi)A'_\mu \quad \text{generic gauge portal} \quad (5.4)$$

$$(\bar{\psi}\gamma^\mu\psi)\partial_\mu a/f_a, (F\tilde{F})a/f_a \quad \text{axion-like portal.} \quad (5.5)$$

Here, the first factors are always gauge invariant SM operators,  $\psi$  is a generic SM fermion and  $F$ ,  $\tilde{F}$  a generic SM field strength/dual field strength tensor. The dark sector fields are an abelian gauge field  $A'_\mu$ , a neutral scalar  $S$ , a neutral fermion  $N$ , an axion-like pseudoscalar  $a$ , and  $A$ ,  $\lambda$ ,  $f_a$  are parameters.

Only specific dark sector particles and interactions can contribute to  $a_\mu$  in one-loop diagrams involving only light fields. New neutral bosons of spin 0 or spin 1 can contribute if they couple to muons, possibly in a lepton flavour-violating way with couplings of the form  $\text{boson}-\mu-e/\mu/\tau$ ; in contrast, new neutral fermions on their own cannot give non-negligible contributions. Here we will focus on several cases of particular interest: the dark photon and kinetic mixing, a light  $U(1)_{L_\mu-L_\tau}$  gauge boson and the gauge portal, and axion-like particles. We will briefly also comment on extensions and generalised scenarios. For general studies of many neutral singlet particles with either spin 0 or spin 1 and the interplay of contributions to  $a_\mu$  with collider constraints and we also refer to Ref. [533], and for the interplay with quark flavour physics to Ref. [534].

### 5.1.1. Analytical results for light-particle contributions

Here we provide basic one-loop formulas for  $a_\mu$  and the dipole moments the other leptons for the case of light neutral bosons. We specifically focus on the two kinds of diagrams in Fig. 5.1, with the exchange of either a neutral vector

boson  $V^\mu$  with vector-like couplings or a neutral real scalar  $\phi$  with scalar and pseudoscalar couplings, with masses  $M_{V,\phi}$  respectively.

We take the Lagrangians for the interactions with a SM lepton  $\ell = e, \mu, \tau$  as

$$\mathcal{L}_{\text{int}}^V = -gV^\mu \bar{\ell} \gamma_\mu \ell, \quad (5.6)$$

$$\mathcal{L}_{\text{int}}^\phi = -\lambda_S^\ell \phi \bar{\ell} \ell - i\lambda_P^\ell \phi \bar{\ell} \gamma_5 \ell. \quad (5.7)$$

The resulting contributions to  $a_\ell$  corresponding to Fig. 5.1 are given by<sup>43</sup>

$$\Delta a_\ell^V = \frac{g^2}{8\pi^2} \int_0^1 dx \frac{2x(1-x)^2}{(1-x)^2 + rx}, \quad (5.8a)$$

$$\Delta a_\ell^\phi = \frac{1}{8\pi^2} \int_0^1 dx \frac{(1-x)^2}{(1-x)^2 + rx} \left[ \lambda_S^{\ell 2} (1+x) - \lambda_P^{\ell 2} (1-x) \right], \quad (5.8b)$$

where  $r = M_{V,\phi}^2/m_\ell^2$  for the vector and scalar case respectively. Note that the vector and the scalar contributions are always positive while the pseudoscalar contributions are always negative. Analytic formulas for more general cases with e.g. lepton-flavour violating couplings, or with couplings of a muon to two different light new particles can be readily obtained from Sec. 2.1, see also Ref. [8], see also Ref. [535] for possible additional correction terms appearing in certain cases.

It is instructive to consider the limiting cases

$$\Delta a_\ell^V = \frac{g^2}{8\pi^2} \begin{cases} 1 & m_\ell \ll M_V \\ \frac{2}{3r} & m_\ell \gg M_V \end{cases} \quad (5.9a)$$

$$\Delta a_\ell^\phi = \frac{1}{16\pi^2} \begin{cases} 3\lambda_S^{\ell 2} - \lambda_P^{\ell 2} & m_\ell \ll M_\phi \\ \frac{\lambda_S^{\ell 2}}{3r} [6 \ln(r) - 7] - \frac{\lambda_P^{\ell 2}}{3r} [6 \ln(r) - 11] & m_\ell \gg M_\phi \end{cases} \quad (5.9b)$$

The limit of heavy  $M_{V,\phi}$  is similar to the limits considered in Sec. 2.1 and can be relevant for light particles with masses around 1 GeV, while the opposite limit is of interest for very light BSM particles. Here the behaviour differs, and the contributions to  $a_\ell$  approach mass-independent constants. The light-vector limit in Eq. (5.9a) corresponds to Schwinger's result  $\alpha/2\pi$ . A noteworthy general property of  $\Delta a_\mu$  in this limit is that naive scaling between the different lepton generations in the sense discussed in Sec. 3.2 is typically violated. Concretely, in the case where the couplings are lepton-generation independent, the ratio of contributions to the electron and muon behave as

$$\frac{\Delta a_\mu}{\Delta a_e} \simeq \begin{cases} 1 & M_{V,\phi} \ll m_e \\ \frac{m_\mu^2}{m_e^2} & M_{V,\phi} \gg m_\mu. \end{cases} \quad (5.10a)$$

$$\quad (5.10b)$$

Here the behaviour corresponds to naive scaling for sufficiently heavy masses; but the ratio becomes 1 for very small masses, and it interpolates between these two limiting values in the mass range between the electron and muon masses.

In general, models with very light particles and generation-independent couplings behaving as Eq. (5.10a) are severely constrained by the electron  $a_e$  value (3.16) and therefore cannot lead to observable contributions to  $a_\mu$  within the current

<sup>43</sup>In terms of the generic loop functions defined in Sec. 2.1 the results can be expressed as

$$\Delta a_\ell^V = \frac{g^2}{16\pi^2} z_\ell \left\{ \mathcal{F}^{\text{FV}}(z_\ell, z_\ell; 0) + 2\mathcal{G}^{\text{FV}}(z_\ell, z_\ell; 0) \right\}$$

$$\Delta a_\ell^\phi = \frac{1}{16\pi^2} x_\ell \left\{ \left[ \lambda_S^{\ell 2} - \lambda_P^{\ell 2} \right] \mathcal{F}^{\text{FS}}(x_\ell, x_\ell; 0) + \left[ \lambda_S^{\ell 2} + \lambda_P^{\ell 2} \right] 2\mathcal{G}^{\text{FS}}(x_\ell, x_\ell; 0) \right\}$$

where  $x_\ell = m_\ell^2/M_\phi^2$  and  $z_\ell = m_\ell^2/M_V^2$ .

sensitivities. In contrast, models with particle masses between  $m_e$  and  $m_\mu$  or slightly larger than  $m_\mu$  can lead to sizeable effects, and their parameter space can be constrained by  $a_\mu$ .

### 5.1.2. Dark Photons

A particularly simple and attractive kind of dark sector particle is the dark photon. This term refers to a BSM vector boson  $A'_\mu$  which in a low-energy EFT only interacts via kinetic mixing [378] with the photon, as

$$\mathcal{L}_{\text{dark photon}} = -\frac{1}{4}F^{\mu\nu}F_{\mu\nu} - \frac{\epsilon}{2}F^{\mu\nu}F'_{\mu\nu} - \frac{1}{4}F'^{\mu\nu}F'_{\mu\nu} - J_{\text{em}}^\mu A_\mu + \frac{M_{A'}^2}{2}A'^\mu A'_\mu. \quad (5.11)$$

Here  $A_\mu$  and  $A'_\mu$  are the ordinary photon and the new vector field, the field strength tensors are defined accordingly, and  $J_{\text{em}}^\mu$  is the electromagnetic current to which the photon couples.  $M_{A'}^2$  is the dark photon mass parameter, which may arise due to some Higgs mechanism associated with the dark gauge group. As mentioned above, the only interaction between the dark sector and the SM happens via the kinetic mixing term, which is a product of two different gauge invariant abelian field strength tensors. Direct couplings of SM quarks and leptons to  $A'_\mu$  are assumed to be absent, i.e. the SM fermions are uncharged under the dark gauge group.

Via the non-unitary transformation  $A_\mu \rightarrow A_\mu + \epsilon A'_\mu$ , the Lagrangian can be transformed to

$$\mathcal{L}_{\text{dark photon}} = -\frac{1}{4}F^{\mu\nu}F_{\mu\nu} - \frac{1+\epsilon^2}{4}F'^{\mu\nu}F'_{\mu\nu} - J_{\text{em}}^\mu (A_\mu + \epsilon A'_\mu) + \frac{M_{A'}^2}{2}A'^\mu A'_\mu. \quad (5.12)$$

Thus we get, up to  $\mathcal{O}(\epsilon^2)$ -terms, canonically normalised kinetic terms and no mixing between  $A_\mu$  and  $A'_\mu$ . After the redefinition, the  $A'_\mu$  corresponds to a physical mass-eigenstate which couples to the electromagnetic current with the suppression factor  $\epsilon$ . I.e. it inherits all couplings of the ordinary photon but multiplied by  $\epsilon$ .

The dark photon especially couples to muon and electron with the equal coupling strength  $\epsilon Qe$ , leading to the behaviour displayed in Eq. (5.10) and the resulting pattern of naive-/non-naive scaling depending on  $M_{A'}$ .

Dark photon contributions to  $g-2$  of the muon and to  $g-2$  of the electron have been first discussed in Ref. [381] and further investigated in Refs. [388–391, 536].

Here we focus on the simplest original dark photon case and discuss its current status. Fig. 5.2 was obtained using public data and code of Ref. [537], and it displays the two-dimensional parameter space  $(\epsilon e, M_{A'})$  of the dark photon and shows a set of constraints. The constraints have been derived from a multitude of experiments as indicated in the plot (for original references we refer to Ref. [537]). We first focus only on  $a_\mu$  and  $a_e$ . The triangular shaded region at the top is excluded by  $g-2$  of the electron  $a_e$ . The shape is due to the simple  $m_e^2/M_{A'}^2$  behaviour of  $\Delta a_e$  in this regime. The contours for  $\Delta a_\mu$  interpolate between the  $m_\mu^2/M_{A'}^2$  behaviour at high masses and approaching a constant at low masses. As a result, and as explained after Eq. (5.10), the bounds on  $a_e$  automatically exclude sizeable contributions  $\Delta a_\mu$  for low masses. For example, in the plot  $\Delta a_\mu > 5 \times 10^{-10}$  is excluded by  $a_e$  for  $M_{A'} \lesssim 10$  MeV. Only higher dark photon masses are of relevance for discussing  $a_\mu$ .

As the plot shows, other constraints now restrict the parameter space more strongly than  $a_e$ . Values of  $\Delta a_\mu$  from dark photons as large as the previous deviation  $\Delta a_\mu^{\text{Exp-WP2020}}$  were ruled already for some time. Nevertheless, a wedge-like region around  $M_{A'} = 10 \dots 100$  MeV and  $\epsilon e = \mathcal{O}(10^{-4})$  is not excluded. This is the region that allows the largest  $\epsilon e/M_{A'}$  ratio and hence the overall largest viable contribution to  $a_\mu$  in the dark photon scenario.

This maximum contribution, obtained from Eq. (5.8a) with  $g = \epsilon e$ , is

$$\Delta a_\mu^{\text{dark photon, max}} \approx 5 \times 10^{-10} \quad \text{for} \quad M_{A'} \approx 20 \text{ MeV} \quad \text{and} \quad \epsilon e \approx 25 \times 10^{-5}. \quad (5.13)$$

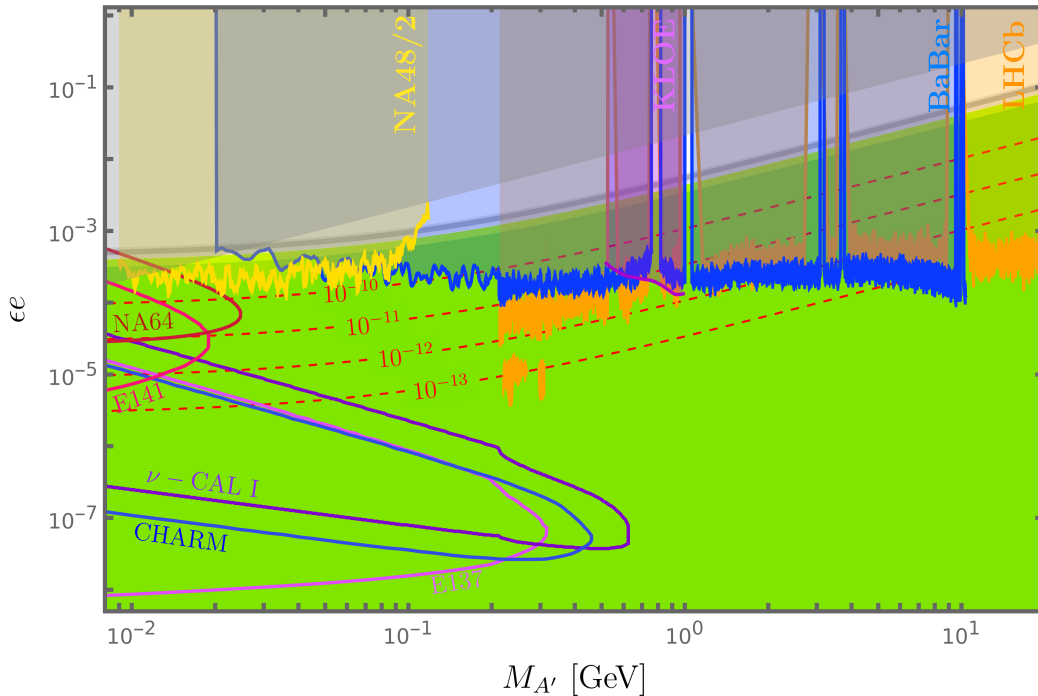


**Figure 5.2:** Constraints on the dark photon parameter space based on the recasting performed in Ref. [537] (Fig. 4) and the accommodating code `DarkCast`. The  $1\sigma$  ( $2\sigma$ ) contour of  $\Delta a_\mu^{\text{Exp-WP2025}}$  is shown in (light) green, while the (light) grey contour shows the  $1\sigma$  ( $2\sigma$ ) range of  $\Delta a_\mu^{\text{Exp-WP2020}}$  for reference.

Especially the NA48/2 and NA64 searches limit this parameter region. Smaller masses are excluded by NA64 [538], which searched for visible  $A' \rightarrow e^+e^-$  decays with a particular  $A'$  lifetime and decay length in beam dump bremsstrahlung events. Larger couplings are excluded by the NA48/2 experiment [539], which searched for the decay chain  $\pi^0 \rightarrow \gamma A'$ ,  $A' \rightarrow e^+e^-$ , assuming that the dark photon decays promptly, i.e. at the production point.

In most of the remaining parameter space the total contribution of the dark photon to  $a_\mu$  is extremely small and thus fully compatible with the current value  $\Delta a_\mu^{\text{Exp-WP2025}}$  in Eq. (1.5). Presently  $\Delta a_\mu$  therefore does not yield a complementary constraint on the dark photon parameter space. Conversely, if a smaller but non-zero deviation within experimental sensitivities should emerge from future progress on the SM prediction,  $\Delta a_\mu$  will provide a strong lower bound on both  $M_{A'}$  and  $\epsilon\epsilon$  and the viable parameter regions will be tiny.

Dark photon contributions to  $a_\mu$  have also been considered in Refs. [388–391, 535, 536, 540–549], partly with the same results, partly in combinations with further BSM states by which bounds can be weakened,  $\Delta a_\mu$  increased, or other observables become relevant.

The straightforward dark photon scenario discussed so far can be changed in several ways. Most importantly, the dark photon is motivated in the context of dark sectors involving also dark matter candidates. In this context it is possible that the dark photon decays mainly invisibly,

$$A' \rightarrow \chi\chi \quad (5.14)$$

into a dark matter particle  $\chi$ . This additional decay channel can significantly weaken the collider bounds shown in Fig. 5.2 [391]. However, in this case other searches become applicable and tend to yield even stronger exclusion limits. Most recently, a dedicated search for invisible  $A'$  decays via missing-energy signatures was performed at the NA64 experiment [550]. In the relevant mass range the constraints on the dark photon coupling are actually stronger than the

ones shown in Fig. 5.2, hence the possible values of  $\Delta a_\mu$  for dark photons with invisible decays are even smaller than Eq. (5.13).

In general, the experimental bounds depend on the details of the dark sector. For example, Refs. [542, 547, 551] found scenarios with extended dark sectors under which the bounds from both visible and invisible decays of the dark photon can be circumvented, and where also neutrino masses can be described. One possibility includes inelastic dark matter, where the dark photon decays dominantly into two different dark-sector particles  $A' \rightarrow \chi_1 \chi_2$  (with very similar masses) the heavier of which subsequently decays to  $\chi_2 \rightarrow \chi_1 e^+ e^-$ . In this case the  $A'$  decay is semivisible and the bounds on the parameter space are weaker. Consequently, larger contributions to  $a_\mu$  are possible and  $\Delta a_\mu^{\text{Exp-WP2025}}$  provides a complementary constraint in such models.

Similarly, in case the dark photon has more general couplings, specifically if there is also a dark fermion  $F$  which allows the vertex  $A'-F-\mu$ , the contribution to  $a_\mu$  from an  $A'-F$  loop could be chirally enhanced by the potentially larger  $F$ -mass [545] as in the three-field models of Sec. 2.3.<sup>44</sup>

Another generalisation of the dark photon scenario is to allow mass mixing via a  $2 \times 2$  mass matrix involving the SM  $Z$  boson and the dark gauge boson, now called dark  $Z$  in this setup. Such a mass mixing can arise e.g. if the SM Higgs carries a dark charge and thus its  $vev$  contributes to the dark  $Z$  mass [388–390, 392]. The main effect is that the dark  $Z$  couples to a linear combination of currents  $\epsilon J_{\text{em}}^\mu + \epsilon_Z J_{\text{NC}}^\mu$ , where  $J_{\text{NC}}^\mu$  is the neutral current which couples to the SM  $Z$  boson. Again, this scenario is viable but does not lead to significant changes in the conclusion for  $a_\mu$  compared to Fig. 5.2.

In light of the new  $\Delta a_\mu^{\text{Exp-WP2025}}$  value, the simplest dark photon model remains an appealing candidate for light new physics with viable parameter space as shown in Fig. 5.2, while  $\Delta a_\mu$  now enters as an important constraint in models with a larger dark sectors where complementary constraints can be weakened.

### 5.1.3. $Z'$ and $U(1)_{L_\mu-L_\tau}$

Now we turn to a wider class of a new neutral spin-1 gauge bosons, generically called  $Z'$ . In distinction from the previous case of the dark photon or dark  $Z$ , we now allow that the SM fermions can be charged under the new gauge group. Hence there can be direct couplings of the  $Z'$  to fermions, i.e. couplings of the form (5.4) corresponding to the generic gauge portal, with prefactors given by the assignments of the new quantum number  $X$ . Kinetic mixing or mass mixing remains allowed and possible but is typically subdominant.

The phenomenology depends on the gauge group and the  $X$  charges. For a large variety of cases, the couplings of electron and muon to  $Z'$  are equal or at least of the same order. A prime example of a gauge group with similar couplings to all SM fermions is  $U(1)_{B-L}$  corresponding to the gauged baryon minus lepton number that often arises in Grand Unified Theories (GUTs). In such models the phenomenology is similar to the one of the dark photon discussed in the previous section. In particular, the correlation between  $a_\mu$  and  $a_e$  combined with the bounds from experiments sensitive to  $Z' \rightarrow e^+ e^-$  leads to similar constraints on the parameter space as Fig. 5.2. Models of this kind have been studied already in Ref. [476]. More recent investigations for  $Z'$  with couplings to quarks and leptons can be found in Refs. [552–556], where different charge assignments were used and different complementary low-energy observables were studied. Similarly, Refs. [557–560] studied  $Z'$  models with couplings to muons and electrons, which can also be interesting

---

<sup>44</sup>Note that the current discussion is at the level of an effective low-energy theory where only QED is relevant; in this case the discussion of chirality flips simplifies compared to the one of Sec. 2.3.

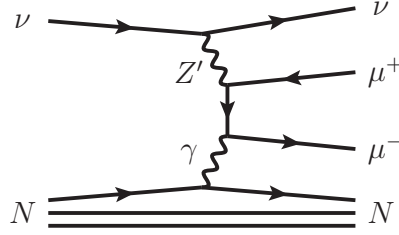


**Figure 5.3:** Tree-level  $Z'$  contribution to the *neutrino trident* production of a  $\mu^+\mu^-$  pair in the scattering of neutrinos on nucleons.

in view of neutrino physics, and Ref. [561] gave a general overview of such models.

The similarity between models with couplings to electrons, muons and quarks of the same order and the dark photon scenario is particularly demonstrated in Ref. [537], where the same experimental constraints are applied to a variety of models including the original dark photon model as well as  $Z'$  models based on various quantum number assignments. Here we focus on  $Z'$  models that differ from such scenarios, i.e. in particular where the couplings to the electron and muon are noticeably different.

In general, the choice of the quantum number  $X$  is constrained by the absence of gauge anomalies. It turns out that this requirement is very restrictive. For instance,  $U(1)_{B-L}$  only becomes anomaly free once three generations of right-handed neutrinos are added to the SM fermion content. Without adding BSM fermions, all viable options for  $U(1)_X$  involve generation-dependent quantum numbers [562]. It has been found that viable options are the quantum numbers

$$X = L_\mu - L_\tau, \quad L_\mu - L_e \quad \text{or} \quad L_e - L_\tau, \quad (5.15)$$

where  $L_i$  corresponds to lepton number of generation  $i$ . Such gauge groups are also of interest in view of flavour model building, and they are of particular interest here, in view of their distinct properties.

Among these,  $L_\mu - L_\tau$  is special since it implies no direct  $Z'$ -coupling to electrons and quarks, such that many of the usual experimental constraints are evaded. Similar models with slightly different gauge groups which nevertheless only allow couplings to muons and  $\tau$ -leptons were studied in Refs. [563, 564]. In the following we therefore focus on the  $U(1)_{L_\mu - L_\tau}$  gauge group and the corresponding  $Z'$  contributions to  $a_\mu$ . These were first pointed out to be potentially significant in Refs. [565–567], where also appropriate parameter constraints and links to neutrino masses were discussed. The relevant Lagrangian is given by

$$\mathcal{L}_{\text{int}, U(1)_{L_\mu - L_\tau}} \supset -g_{Z'} Z'_\mu (\bar{\mu} \gamma^\mu \mu - \bar{\tau} \gamma^\mu \tau + \bar{\nu}_\mu \gamma^\mu \nu_\mu - \bar{\nu}_\tau \gamma^\mu \nu_\tau) + \frac{M_{Z'}^2}{2} Z'^\mu Z'_\mu, \quad (5.16)$$

where the  $Z'$  mass originates as  $M_{Z'} = g_{Z'} v'$  from some unspecified Higgs mechanism which spontaneously breaks  $U(1)_{L_\mu - L_\tau}$ . The contribution to  $a_\mu$  is given by Eq. (5.8a) and simplifies to the following expression for masses  $M_{Z'} \gg m_\mu$ ,

$$\Delta a_\mu^{Z'} = \frac{1}{12\pi^2} \frac{g_{Z'}^2 m_\mu^2}{M_{Z'}^2} = \frac{1}{12\pi^2} \frac{m_\mu^2}{v'^2}, \quad (5.17)$$

where the  $vev$   $v'$  remains as the only relevant model parameter.

Refs. [568, 569] identified the so-called neutrino trident process as a very important constraint on this model. The process is illustrated by the diagram in Fig. 5.3 and corresponds to nucleon–neutrino scattering where the  $Z'$  interaction produces a  $\mu^+\mu^-$  pair. In the large-mass region  $M_{Z'} \gg m_\mu$ , the correction to the trident production cross section results in the simple formula [568]

$$\frac{\sigma(\nu N \rightarrow \nu N + \mu^+ \mu^-)}{\sigma(\nu N \rightarrow \nu N + \mu^+ \mu^-)_{\text{SM}}} \approx \frac{1 + (1 + 4s_W^2 + 2v^2/v'^2)^2}{1 + (1 + 4s_W^2)^2}. \quad (5.18)$$

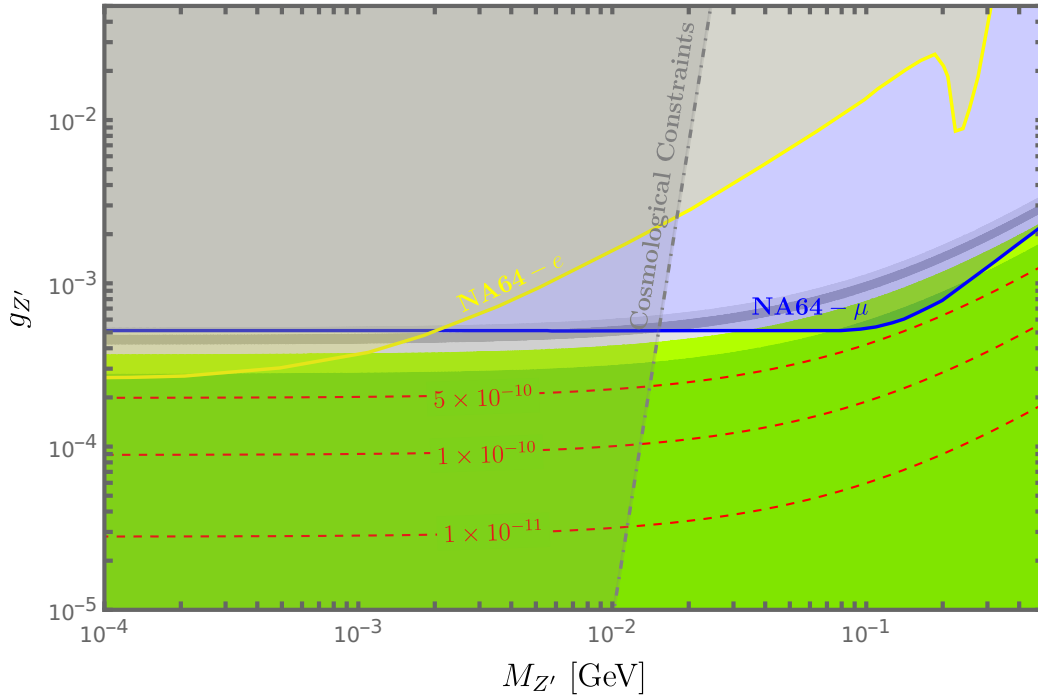


**Figure 5.4:** The  $M_{Z'} - g_{Z'}$  plane of the  $U(1)_{L_\mu - L_\tau}$  model. Regions excluded by NA64-e, NA64- $\mu$  and cosmological bounds are shown in yellow, blue and light grey, respectively. The (light) green area shows the  $1\sigma$  ( $2\sigma$ ) range of  $\Delta a_\mu^{\text{Exp-WP2025}}$ , while the (light) grey band shows the  $1\sigma$  ( $2\sigma$ ) range of the old deviation  $\Delta a_\mu^{\text{Exp-WP2020}}$ .

This process has been measured in several experiments including Charm-II [570], CCFR [571] and NuTeV [572], yielding the combined limit  $\sigma_{\text{Exp}}/\sigma_{\text{SM}} = 0.83 \pm 0.18$  obtained in Ref. [568]. This limit results in a strong lower bound on  $v'$  given by

$$v' \gtrsim 750 \text{ GeV}. \quad (5.19)$$

Even though there has been discussion about the applicability of various neutrino trident experiments [569] it is clear that this bound severely limits the possible  $Z'$  contributions to  $a_\mu$ . If  $M_{Z'} \gg m_\mu$  (such that Eq. (5.19) holds), the contributions are as small as

$$\Delta a_\mu^{Z'} < 1.7 \times 10^{-10} \quad (5.20)$$

However, for smaller  $Z'$  masses the behaviour of the neutrino trident cross section is different (see Ref. [569] for the full calculation), and larger contributions to  $a_\mu$  become possible.

After Refs. [567–569], the region of lower  $M_{Z'}$  has been investigated, a multitude of further constraints on the model have been identified and dedicated experiments have been carried out. An overview is given in Ref. [573].

The resulting parameter space for  $M_{Z'} \lesssim 1 \text{ GeV}$  is shown in Fig. 5.4, together with the strongest current exclusion limits. One important constraint comes from searches for invisible  $Z'$  decays via missing-energy signatures. Even without extended dark sectors, invisible decay channels like  $Z' \rightarrow \nu\bar{\nu}$  to muon- or tau-neutrinos are guaranteed to have a large branching ratio. The two direct search bounds obtained by NA64-e [574] and NA64- $\mu$  [575] are shown in Fig. 5.4. These experiments measured the invisible decay rates of  $Z'$  bosons produced as bremsstrahlung in high-energy scattering of electron- or muon-beams off a fixed target. The resulting bounds apply similarly to a wide range of  $Z'$  scenarios with invisible decays. In the region with light  $M_{Z'}$  shown in the plot these bounds are stronger than the ones obtained from

the neutrino trident process discussed above. In combination these experiments already excluded most of the light  $Z'$  parameter space with large  $\Delta a_\mu$ , leaving only a small region around  $M_{Z'} \sim \mathcal{O}(1 \text{ MeV})$  where the deviation could have been as large as  $\Delta a_\mu^{\text{Exp-WP2020}}$ .

However, this region is mostly excluded by a number of constraints stemming from cosmology and astrophysics. Due to its properties, a light  $Z'$  can have a significant impact on both the thermal evolution of the universe as well as many astrophysical phenomena that have been observed and measured with great precision over the past decades.

For instance, the temperature of white dwarfs decreases over time resulting in characteristic luminosity functions that have been extracted from the Sloan Digital Sky Survey [576, 577]. The white dwarf cooling is well understood and simulations based on the SM are in good agreement with the data. The  $Z'$  contributes to this cooling through the decay of plasmons (electron excitations in the white dwarf plasma) into neutrinos [578]. This constraint is in particular relevant for small masses [573, 579]. For derivations and surveys of astrophysical limit from e.g. solar neutrinos, stellar cooling or the supernova 1987A neutrino burst we refer to Refs. [580–583].

Another very strong cosmological constraint on  $Z'$  bosons with masses in the MeV-range stems from its interactions with the neutrinos in the early universe. In this case the  $Z'$  is still present in the thermal bath around the time of neutrino decoupling and can have a significant impact on the evolution of the radiation energy density. This density is usually parametrised in terms of the effective number of neutrinos  $N_{\text{eff}}$  which is determined from observations of the cosmic microwave background [584] and given by

$$N_{\text{eff}} = 2.99 \pm 0.17 \quad (5.21)$$

The  $Z'$  results in a small positive correction  $\Delta N_{\text{eff}}$  that in turn translates into a stringent lower bound on  $M_{Z'} \gtrsim 10 \text{ GeV}$  [582]<sup>45</sup>. In Fig. 5.4 this constraint excludes most of the remaining parameter space with a deviation as large as  $\Delta a_\mu^{\text{Exp-WP2020}}$ . We refer to Refs. [585, 587–599] for further phenomenological studies of  $a_\mu$  in the  $U(1)_{L_\mu-L_\tau}$ -model, partially including also additional fields to describe dark matter.

Taking into account the above constraints the maximum value of  $\Delta a_\mu$  allowed in the plot is

$$\Delta a_\mu^{Z', \text{max}} \approx 20 \times 10^{-10} \quad \text{for} \quad M_{Z'} \approx 20 \text{ MeV} \quad \text{and} \quad g_{\mu\tau} \approx 5 \times 10^{-4}. \quad (5.22)$$

Smaller values of the mass  $M_{Z'}$  are excluded by cosmology, for the relevant coupling strength; for larger masses than shown in the plot the neutrino trident and further collider constraints take over, see Eq. (5.20) and Refs. [600, 601] for further collider investigations of the model.

The plot confirms that in this  $U(1)_{L_\mu-L_\tau}$  model the contributions to  $a_\mu$  can be larger than for the dark photon in the mass region below  $m_\mu$ . The new result  $\Delta a_\mu^{\text{Exp-WP2025}}$  therefore now disfavors the parameter region given in Eq. (5.22) and thus constitutes an important novel constraint on the model. Still, the parameter region where such large  $\Delta a_\mu$  is possible is very narrow and specific. For all other values of the  $Z'$  mass, the constraints from NA64- $e, \mu$  and from cosmology are stronger than the one from  $\Delta a_\mu^{\text{Exp-WP2025}}$ .

The plot and its discussion cover the basic (*vanilla*)  $L_\mu - L_\tau$  model. As stated in the beginning, the gauge group and its properties are appealing, and the model can be extended in many motivated ways. In such a larger framework, the interplay between the various bounds can also change. Like for dark photons, an obvious extension is to include a dark

---

<sup>45</sup>Interestingly, for small shifts around  $\Delta N_{\text{eff}} \sim 0.2 \dots 0.5$  this correction might help alleviate the Hubble tension [582, 585, 586], but larger  $\Delta N_{\text{eff}}$  are excluded.

matter candidate particle  $\chi$  to the theory, where  $\chi$  can interact with the  $Z'$ . Here constraints arise from the need to have sufficiently high dark matter annihilation cross section to avoid overabundance of dark matter while avoiding too large  $\Delta a_\mu$ . A naive estimate of the scaling for the dark matter annihilation cross section (see Sec. 3.6) and  $\Delta a_\mu$  gives

$$\langle\sigma v\rangle\propto\frac{g_\chi^4}{m_\chi^2}\quad\text{while}\quad\Delta a_\mu\propto g_\mu^2\quad(5.23)$$

where  $g_{\mu,\chi}$  denote the  $Z'$  couplings to the muon and the dark matter particle and  $m_\chi$  the dark matter mass. If one argues that in a gauge theory it is natural that  $g_{\mu,\chi}$  are of the same order of magnitude, typically the cross section is too low or  $\Delta a_\mu$  too high [602, 603]. Hence special regions of parameter space, and/or special dark matter models are needed. In Ref. [603], resonant annihilation is considered, which happens in the specific case where  $M_{Z'}\approx 2m_\chi$ . In Ref. [604] co-annihilation of two scalars with similar masses is considered. And Ref. [605] accepts strongly non-universal couplings  $g_\chi\gg g_\mu$  while allowing arbitrary dark matter masses. The cosmological bounds on the scenario with dark matter have also been evaluated [585], however, there is a subtle dependence on the value of the kinetic mixing which leads to small but non-zero couplings of the  $Z'$  to electrons [593].

Interestingly, the fact that  $\Delta a_\mu^{\text{Exp-WP2025}}$  is now compatible with zero and places a stringent upper limit on the coupling  $g_\mu$  (while  $\Delta a_\mu^{\text{Exp-WP2020}}$  preferred a non-vanishing value) exacerbates this tension between dark matter and  $a_\mu$  in this kind of models. For a viable explanation of dark matter in this context, the construction of special scenarios like in the mentioned references has therefore become even more important. Such a more involved scenario is considered in Ref. [203], where dark matter is self-interacting and the viable parameter space opens up.

It is also possible to extend the  $L_\mu-L_\tau$  model to include neutrino masses [567] in the parameter region of sizeable  $\Delta a_\mu$  [606–609], and such extensions lead also to additional constraints [610–617]. Here, Refs. [607, 609] propose variants of the tree-level seesaw mechanism to generate neutrino masses, where partially Majorana mass terms of the kind  $N_e N_\mu$  must be obtained from a *vev* of a  $U(1)_{L_\mu-L_\tau}$ -breaking new Higgs field which also gives mass to the  $Z'$ . These setups find no tension between explaining neutrino masses and  $\Delta a_\mu$ . In contrast, Ref. [612] combines the  $Z'$  with the scotogenic model for neutrino masses and finds a tension between  $\mu\rightarrow e\gamma$  and  $\Delta a_\mu$  of the kind discussed in Sec. 3.2, specifically the single-particle scenario.

#### 5.1.4. Axion-like particles and other light scalar particles

Here we discuss the phenomenology of light new spin-0 particles in view of  $a_\mu$ . Such spin-0 particles could couple to muons via renormalisable couplings of the form described in Sec. 2, such that the general statements of that section apply. Here we mainly focus on axion-like particles (ALPs), which are a particularly well motivated type of light dark sector particles with different kinds of couplings, and we will come back to generic scalars at the end of this section.

ALPs are excitations of a neutral pseudoscalar field  $a$  which has only effective (nonrenormalisable) interactions of the axion-portal type (5.5) with the SM. The properties are modelled after the original axion proposed to solve the strong CP problem by dynamically generating a vanishing coefficient in front of the  $G_{\mu\nu}\tilde{G}^{\mu\nu}$  term in the effective Lagrangian via a potential for the axion [394–396]. Since this proposal, many phenomenological models have been constructed and gained attention also in the context of  $\Delta a_\mu$ .

A crucial ingredient in the original formulation was the shift symmetry  $a(x)\rightarrow a(x)+\text{const.}$  The interaction terms allowed in the general ALP Lagrangian are required to have the same shift symmetry, even though the ALPs mass and coupling strengths are not required to solve the strong CP problem. Using the conventions of e.g. Refs. [618, 619], the

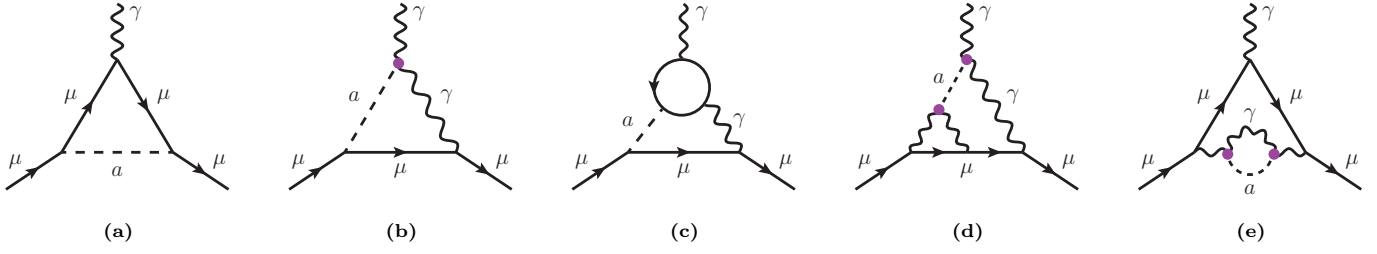


**Figure 5.5:** ALP one- and two-loop contributions to  $a_\mu$ . The purple vertex corresponds to the effective  $a\gamma\gamma$  coupling.

relevant low-energy Lagrangian can then be written as

$$\mathcal{L}_{\text{ALP}} \supset \frac{c_{ii}}{2} \frac{\partial_\mu a}{f_a} (\bar{e}_i \gamma^\mu \gamma_5 e_i) + c_{\gamma\gamma} \frac{\alpha}{4\pi} \frac{a}{f_a} F_{\mu\nu} \tilde{F}^{\mu\nu} - \frac{m_a^2 a^2}{2} + \dots \quad (5.24)$$

Here  $F^{\mu\nu}$  and  $\tilde{F}^{\mu\nu} = \frac{1}{2} \epsilon^{\mu\nu\rho\sigma} F_{\rho\sigma}$  are the photon field strength tensor and its dual. The hallmark of such theories are effective  $a\gamma\gamma$  interaction vertices and derivative interactions with the leptons. Similar terms involving other fermions or the gluon field strength tensor  $G^{\mu\nu}$  exist but are omitted here. All these terms correspond to non-renormalisable dimension-5 operators. By convention, the Wilson coefficients are written via dimensionless constants  $c_{\gamma\gamma}$  and  $c_{ii}$ , pulling out a mass scale  $f_a$ . Further, a loop factor has been pulled out of  $c_{\gamma\gamma}$ , taking into account that in fundamental theories the corresponding term will typically be loop-suppressed compared to the  $c_{ii}$  term, even though enhancements are possible [620]. Here we have neglected the possibility of lepton flavour violating axion couplings which we will come back to at the end of this section.

The Lagrangian in Eq. (5.24) can be simplified by using equations of motion of the renormalisable part of the theory [618, 621], such that the interaction terms can equivalently be written as

$$\mathcal{L}_{\text{int, ALP}} = -c_{ii} \frac{m_i}{f_a} a (\bar{e}_i i \gamma_5 e_i) + \tilde{c}_{\gamma\gamma} \frac{\alpha}{4\pi} \frac{a}{f_a} F_{\mu\nu} \tilde{F}^{\mu\nu} + \dots, \quad (5.25)$$

where the shifted  $a\gamma\gamma$  coupling parameter is given by  $\tilde{c}_{\gamma\gamma} = c_{\gamma\gamma} + \sum_i Q_i^2 c_{ii}$  [619]. The sum here extends over all SM fermions, although in the following we assume the quark couplings to vanish. The appearance of the lepton mass prefactors in the ALPs–lepton couplings arises naturally from the shift symmetry of the fundamental Lagrangian, combined with the equations of motion. Interestingly for discussing  $a_\mu$  and  $a_e$ , the conventions are such that naive scaling simply corresponds to flavour-independent Wilson coefficients  $c_{\mu\mu} \approx c_{ee}$ .

ALPs generally contribute to  $a_\mu$  via the diagrams of Fig. 5.5. Such contributions were discussed in Ref. [622], where diagrams (a,b,d,e) were computed. The calculations were then refined in Refs. [618–621, 623, 624]. Note that the EFT analyses used for the definition of the Lagrangian in Eq. (5.25) also suggested that the  $c_{\gamma\gamma}$ -term is loop suppressed; hence diagrams (b,c) should be treated of equal order and diagrams (d,e) as loop suppressed in comparison. The result for diagram (a) can be obtained from Eq. (5.8b), and the result for diagram (b) reads (using the form of Refs. [618, 622])

$$\Delta a_\mu^{a\gamma\gamma} = -\frac{m_\mu^2 c_{\mu\mu} \tilde{c}_{\gamma\gamma} \alpha}{8\pi^3 f_a^2} \left( \ln \frac{\Lambda^2}{m_\mu^2} + \frac{7}{2} - h_2(r) \right), \quad (5.26)$$

where the loop function is given in terms of  $r = m_a^2/m_\mu^2$  as

$$h_2(r) = 1 + \frac{r^2}{6} \ln r - \frac{r}{3} - \frac{r+2}{3} \sqrt{r(r-4)} \ln \left( \frac{\sqrt{r} + \sqrt{r-4}}{2} \right). \quad (5.27)$$

Since the  $a\gamma\gamma$  coupling is nonrenormalisable, the diagram is divergent. The result shown here is obtained using a momentum cutoff  $\Lambda$ , which is assumed to be of the order TeV. In a proper EFT setup, the logarithmic dependence can

be understood via renormalisation-group methods [619, 624]. The divergence is cancelled by the renormalisation of the dipole operator corresponding to  $a_\mu$ , and the cutoff-dependence is replaced by a dependence on an unknown further Wilson coefficient for the dipole operator [621].

The diagram (c) is a two-loop Barr-Zee diagram which however needs to be evaluated in the limit of very light  $a$ , which cannot be readily obtained from the formulas in Sec. 4.2. The results are provided in Refs. [618, 619]. Since diagrams (b) and (c) are formally of the same order, it is expected that two-loop diagram is important as well. This is indeed confirmed by the explicit calculations performed in Refs. [618, 619, 624]. However, the main effect of the Barr-Zee diagram (c) can be easily understood. In fact, the contribution of the Barr-Zee diagram (c) can essentially be absorbed in diagram (b) by replacing the  $a\gamma\gamma$  coupling  $\tilde{c}_{\gamma\gamma}$  with an effective coupling  $\tilde{c}_{\gamma\gamma}^{\text{eff}}$  that takes into account the inner fermion-loop correction to the  $a\gamma\gamma$  vertex [619]. The shift is not negligible and has been quantified in the same reference as a function of model parameters.

The interplay between the different contributions to  $a_\mu$  is important. The phenomenological behaviour of the diagrams (a) and (b+c) can be concisely summarised as [618, 625]

$$\Delta a_\mu^{a\mu\mu} \propto -\frac{c_{\mu\mu}^2}{16\pi^2}, \quad \Delta a_\mu^{a\gamma\gamma} \propto -\frac{c_{\mu\mu}\tilde{c}_{\gamma\gamma}^{\text{eff}}\alpha}{16\pi^3}. \quad (5.28)$$

As mentioned below Eq. (5.8a) the pseudoscalar FS-type one-loop diagram (a) with two ALP–muon couplings is always negative, whereas the diagrams (b) and (c) with effective  $a\gamma\gamma$ -coupling can have either sign depending on the relative sign of the two couplings. In particular, to obtain a positive contributions to  $a_\mu$  diagrams (b+c) involving the non-renormalisable  $\tilde{c}_{\gamma\gamma}^{\text{eff}}$ -term must be positive and dominate, which is possible for large logarithmic enhancements from  $\Lambda \gg m_\mu$  and large couplings  $|\tilde{c}_{\gamma\gamma}| \gtrsim |c_{\mu\mu}|$ .

The general scaling in Eq. (5.28) means that a large and positive contribution  $\Delta a_\mu$  as motivated in the past by  $\Delta a_\mu^{\text{Exp-WP2020}}$  is not trivial to achieve. In contrast, when the negative deviation  $\Delta a_e$  corresponding to Eq. (3.17a) was reported around 2018, one-loop ALP contributions were considered one of the plausible explanations. Combining this with positive contributions to  $a_\mu$  was possible via diagram (b) or via lepton-flavour violating couplings [625–628].

Now we turn to the phenomenology of ALP contributions to  $a_\mu$ , focusing on present constraints. For earlier studies for similar scenarios we refer to Refs. [543, 618, 621, 622, 625, 629–633], and for scenarios including dark matter to Ref. [634]. Similarly to the dark photon and the  $U(1)_{L_\mu-L_\tau}$  scenarios, a large number of experimental constraints restrict the viable parameter space  $(m_a, \tilde{c}_{\gamma\gamma}, c_{\mu\mu})$ . Fig. 5.6 from Ref. [530] shows constraints on the  $a\gamma\gamma$  coupling as a function of the mass  $m_a$ , where the coupling is normalised as

$$g_{a\gamma} = -\frac{c_{\gamma\gamma}\alpha}{f_a\pi} = -\frac{\tilde{c}_{\gamma\gamma} - \sum_i Q_i^2 c_{ii}}{f_a} \frac{\alpha}{\pi}. \quad (5.29)$$

For low masses, cosmological bounds essentially exclude ALPs unless the coupling is extremely tiny with negligible impact on  $\Delta a_\mu$ . For large  $m_a$ , collider constraints become restrictive. Intriguingly there is a window for  $m_a$  close to the muon mass  $m_\mu$  up to few GeV, where the largest couplings are viable.

In this mass region, the BESIII result [635] provides a strong constraint on  $g_{a\gamma}$ , based on the process  $J/\Psi \rightarrow \gamma^* \rightarrow \gamma a$  [636]. If the ALP also couples to the Higgs and the decay  $h \rightarrow aa$  is allowed, another important bound stems from the recent ATLAS search [637] for  $h \rightarrow aa \rightarrow 4\gamma$ . In fact, for sizeable couplings to the Higgs this search excludes most of the parameter region with large  $\Delta a_\mu$ . Equivalently, large  $g_{a\gamma}$  translate into a strong bound on the ALP–Higgs coupling. In the following we will not use this bound but only consider the bounds that directly depend on the ALPs couplings to photons and leptons, i.e. from the lepton dipole moments and BESIII.

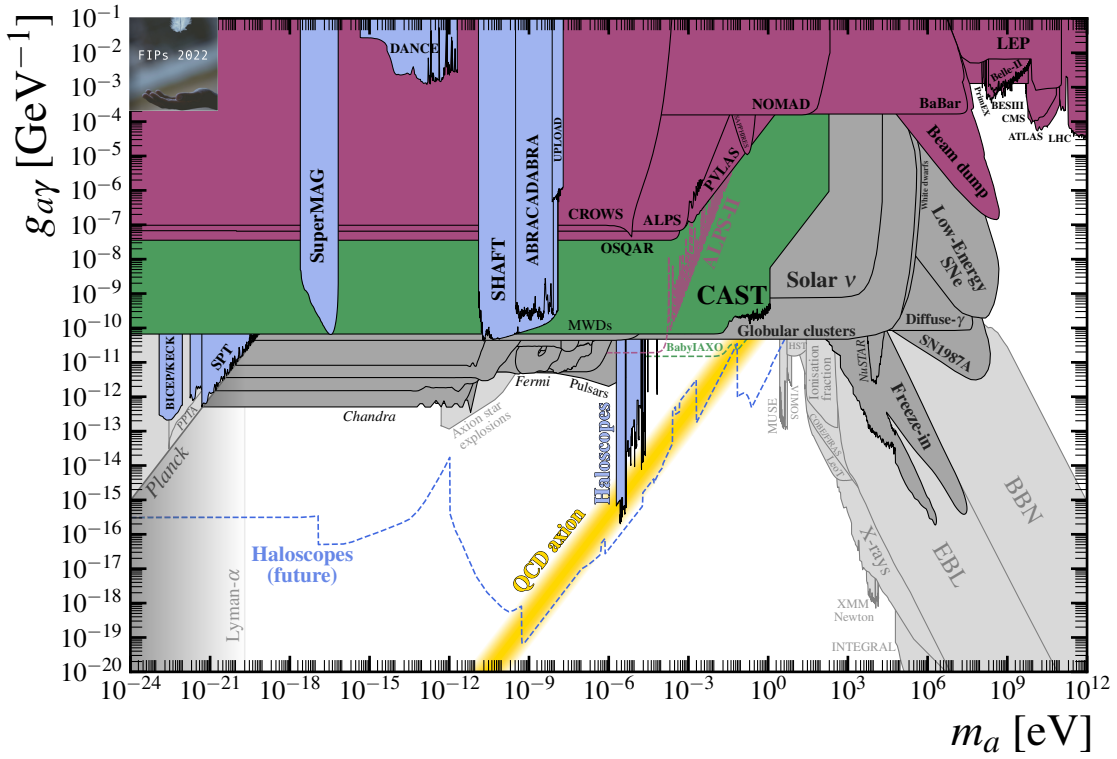


**Figure 5.6:** Fig. 50 from Ref. [530], displaying the bounds on the ALPs–photon coupling  $g_{a\gamma}$  as a function of the ALPs mass up to the TeV-scale. The coupling is related to the parameter  $c_{\gamma\gamma}$  as  $g_{a\gamma} = -\frac{c_{\gamma\gamma}}{f_a} \frac{\alpha}{\pi}$ . For original references and explanations we refer to Ref. [530].

In Fig. 5.7 we illustrate the current status of  $a_\mu$  contributions from an ALP  $a$ , following Ref. [632].<sup>46</sup> We fix  $m_a = 0.4$  GeV as a representative example in the mass window allowing largest couplings. For this particular ALP mass the BESIII measurements exclude couplings  $g_{a\gamma} > 6 \times 10^{-4} \text{ GeV}^{-1}$  which translate into a correlated bound on  $\tilde{c}_{\gamma\gamma}$  and  $c_{\mu\mu}$  due to Eq. (5.29). In this translation we assume the contribution of  $N_\ell$  equal lepton generations. Then notably the bound on  $c_{\mu\mu}$  depends on the number of leptons  $N_\ell$  coupling to the ALP and is weakest in the muon-specific scenario.

The  $\Delta a_\mu$  contour lines show a characteristic spike at large  $c_{\mu\mu}$  values, where the contributions of diagram (a) and (b) are both large but cancel, leaving a small fine-tuned region where  $\Delta a_\mu$  lies within the experimental bounds. Above this region the  $\tilde{c}_{\gamma\gamma} c_{\mu\mu}$  term dominates and  $\Delta a_\mu \gg 10^{-9}$  while below the  $c_{\mu\mu}^2$  term dominates resulting in a negative  $\Delta a_\mu < -10^{-9}$  which is also excluded. For smaller  $c_{\mu\mu}$  the region allowed by  $\Delta a_\mu^{\text{Exp-WP2025}}$  widens. We also show the bound from  $a_e$ , which is generally important in case of light new physics with couplings to electrons. Here, it applies only in the case  $N_\ell = 3$  where  $c_{ee} = c_{\mu\mu} = c_{\tau\tau}$ , while it does not apply in the muon-specific case. The experimental bound  $\Delta a_e \lesssim 10^{-12}$  is weaker than the BESIII exclusion limit, while a stronger potential future bound  $\Delta a_e \lesssim 10^{-13}$  would rule out most of the remaining region with large  $\Delta a_\mu$ .

We note that, similarly to Ref. [632], both  $\Delta a_\mu$  and  $\Delta a_e$  in Fig. 5.7 were computed taking into account only the contributions from diagram (a) and (b) in Fig. 5.5, while the Barr-Zee diagram (c) has been neglected. As mentioned above, this contribution can essentially be absorbed into  $\tilde{c}_{\gamma\gamma}^{\text{eff}}$ , such that the  $\Delta a_\ell$  contour lines in terms of this effective coupling would stay the same. On the other hand, the same loop corrections to the  $a\gamma\gamma$  vertex (see Eq. (3.1) in Ref. [619]) that enter into the two-loop Barr-Zee diagram for off-shell ALP momenta also enter  $g_{a\gamma}$  measured at BESIII. However,

<sup>46</sup>While finalising the review, Ref. [638] appeared, which constitutes an update of Ref. [632].

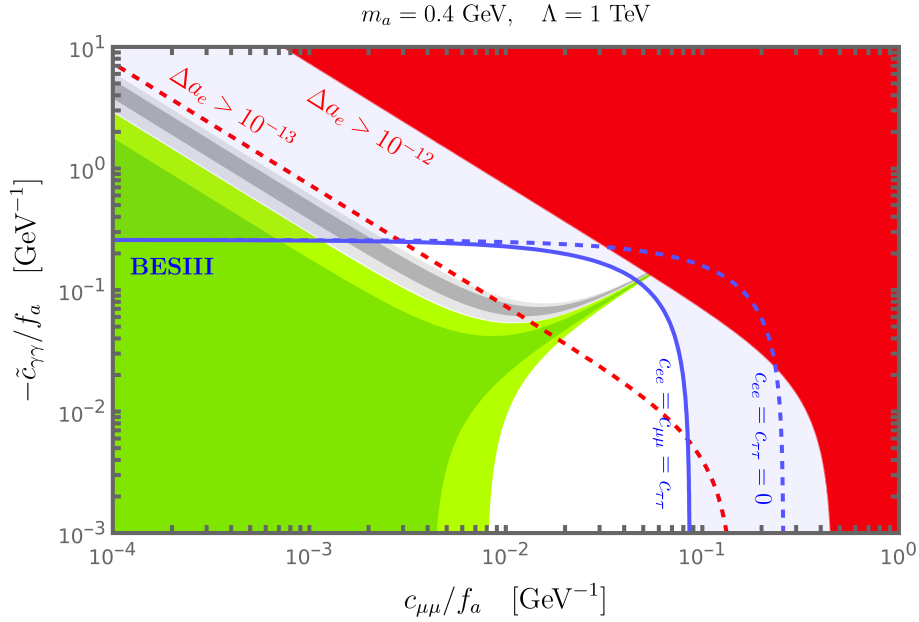


**Figure 5.7:** Plot of the  $1\sigma$  ( $2\sigma$ ) ranges for  $\Delta a_\mu$  in the ALP  $c_{\mu\mu} - \tilde{c}_{\gamma\gamma}$  plane for  $\Delta a_\mu^{\text{Exp-WP2025}}$  in (light) green and for  $\Delta a_\mu^{\text{Exp-WP2020}}$  in (light) grey. The ALP mass is fixed to  $m_a = 0.4 \text{ GeV}$  and the cutoff scale to  $\Lambda = 1 \text{ TeV}$ . The red contour shows the region excluded by  $\Delta a_e$  (assuming  $c_{ee} = c_{\mu\mu}$ ), while the blue contours show the BESIII bound on  $g_{a\gamma}$  for equal couplings  $c_{ee} = c_{\mu\mu} = c_{\tau\tau}$  to all leptons (solid) or muon specific couplings  $c_{ee} = c_{\tau\tau} = 0$  (dashed).

since this vertex is measured via  $a\gamma$  final states, the loop function must be evaluated for on-shell momenta of the ALP. Consequently, the effective coupling  $g_{a\gamma}$  constrained by BESIII corresponds to a different combination of the  $c_{ii}$  compared to  $\tilde{c}_{\gamma\gamma}^{\text{eff}}$ . It is plausible that in such a more detailed analysis the relation between the BESIII constraint and  $a_\mu$  shown in Fig. 5.7 would remain approximately the same, such a study is however beyond the scope of the present review.

Besides the current bounds discussed here, several experimental proposals to further scrutinise the ALP parameter space in the future have been put forward [633, 639–647].

We have highlighted the interplay between the ALPs couplings to photons and to leptons, expressed in the relationships  $c_{\gamma\gamma} \leftrightarrow \tilde{c}_{\gamma\gamma} \leftrightarrow \tilde{c}_{\gamma\gamma}^{\text{eff}}$ , which all differ by terms governed by  $c_{ii}$ . In light of this interplay one can consider more minimal setups, where the fundamental  $a\gamma\gamma$  coupling vanishes,  $c_{\gamma\gamma} = 0$ , as (partially) done in Ref. [625]. Even in this case, all contributions of Eq. (5.28) are present, and sizeable and positive contributions to  $a_\mu$  are possible. Similarly, Ref. [648] effectively sets  $\tilde{c}_{\gamma\gamma} = 0$  but takes into account the genuine 2-loop Barr-Zee diagrams of Fig. 5.5 (c). In particular, this reference shows that this setup is compatible with explaining dark matter by a light fermion which couples to  $a$  similarly as the leptons.

Finally, we comment on variations of the basic ALPs setup considered so far. While we have mainly focused on the case without lepton flavour violation, there is no fundamental necessity for the absence of CLFV ALPs couplings such as  $c_{\mu e}$ ,  $c_{\mu\tau}$  or  $c_{e\tau}$ . In the case these couplings are non-zero, new effects appear which show interesting differences to some of the generic cases discussed in Sec. 3.2. Within ALP scenarios with both quark and lepton flavour violation, also past  $B$ -physics anomalies could be accommodated together with large  $\Delta a_\mu$  [649, 650]. Generally, lepton flavour-violating ALPs couplings result in additional one-loop diagrams to  $a_\mu$  or  $a_e$ . If the loops contain an internal  $\tau$ -lepton there is strong chiral enhancement, which could lead to too large effects. Hence, there are upper limits on the related couplings, of the order [651]

$$\left| \frac{c_{\mu\tau}(m_\mu + m_\tau)}{2f_a} \right| \lesssim 10^{-3\dots-2} \quad \text{where} \quad m_a = 1 \dots 100 \text{ GeV}, \quad (5.30)$$

as well as similar limits on  $c_{e\tau}$ . In contradistinction, in an internal electron loop contributes to  $a_\mu$  there is no chiral enhancement, but the loop function changes sign [627] and positive  $\Delta a_e$  can result from the diagram type (a). In general, the current null results for deviations in  $a_\mu$  and  $a_e$  then lead to stringent constraints on such CLFV ALPs couplings [625, 627, 628, 651].

Regarding CLFV observables, ALPs scenarios with CLFV couplings typically do not follow the patterns of naive scaling and dipole dominance mentioned in Sec. 3.2 [625, 627, 652]. Instead, e.g. the ratio between  $\mu \rightarrow e$  conversion to  $\mu \rightarrow e\gamma$  is not given by Eq. (3.37) but can vary in the interval [625]

$$\text{BR}(\mu\text{Au} \rightarrow e\text{Au}) \simeq (1 \dots 4) \times 10^{-3} \times \text{BR}(\mu \rightarrow e\gamma), \quad (5.31)$$

if the coupling  $c_{\gamma\gamma}$  is varied from small to large values; for large ALP masses  $m_a \gtrsim 10$  GeV the dipole dominance value  $4 \times 10^{-3}$  is typically recovered unless the diagrams of type (b,c) are tuned to zero. In addition, new decay modes such as  $\mu \rightarrow ea$  can be possible, followed by  $a \rightarrow e^+e^-$  or  $a \rightarrow \gamma\gamma$  [627]. In this way, CLFV decays such as  $\mu \rightarrow 3e$  might be dominant CLFV decay modes, unrelated to  $\mu \rightarrow e\gamma$ .

As announced at the beginning of this section, we will now comment on the case of light, dark spin-0 particles which are not ALPs but which may have renormalisable couplings to muons or other SM particles. Such particles were studied in the light of recent experimental data in Refs. [533, 653–661].<sup>47</sup> Particularly Refs. [533, 655] provide very general analyses of wide classes of models with light scalars and relevant experimental constraints.

We highlight here that the new result  $\Delta a_\mu^{\text{Exp-WP2025}}$  impacts potential explanations of dark matter related to such light scalars. For instance, Refs. [656, 660] consider light fermionic dark matter, where a mediator particle is a light new Higgs doublet, which is shown to be viable. Similarly to the case of  $U(1)_{L_\mu-L_\tau}$  discussed earlier, there is a tension between  $\Delta a_\mu$  and the explanation of dark matter. Viable dark matter tends to require large annihilation cross sections which — in case of dark matter annihilating into muons — would lead to an even larger  $\Delta a_\mu$  value than the previous deviation  $\Delta a_\mu^{\text{Exp-WP2020}}$  in most of the parameter space.<sup>48</sup> An appealing way out of this tension is to assume that dark matter only annihilates into  $\tau$ -leptons. In this case,  $\Delta a_\mu$  vanishes, which is now compatible with the new  $\Delta a_\mu^{\text{Exp-WP2025}}$  and allows large couplings such that dark matter can be well accommodated in such models.

### 5.1.5. Models modifying $\sigma(e^+e^- \rightarrow \text{had})$

As discussed in Secs. 1.4 and 3.4, the SM hadronic vacuum polarisation contributions  $a_\mu^{\text{HVP}}$  are currently under intense scrutiny. Traditionally [2], the leading order HVP contributions were obtained from experimental  $e^+e^- \rightarrow \text{hadrons}$  data, leading to  $\Delta a_\mu^{\text{Exp-WP2020}}$ , while the current SM prediction for HVP,LO is purely based on computations in lattice gauge theory [3]. This caused a dramatic shift of the SM value, leading to  $\Delta a_\mu^{\text{Exp-WP2025}}$ . Between the two Theory Initiative White Papers Refs. [2, 3] several new lattice results appeared, which are internally very consistent and well cross-checked. Furthermore also the new  $e^+e^-$  measurement by CMD-3 appeared, which is more consistent with current lattice results than with earlier  $e^+e^-$  measurements.

While the new result  $\Delta a_\mu^{\text{Exp-WP2025}}$  shows full agreement between the experimentally measured  $a_\mu$  and the SM prediction, it remains unknown why the previous determinations of the HVP,LO contributions show such large discrepancies

<sup>47</sup>We mention that also the case of scalars that couple to muons only via dimension-6 operators have been considered in the context of  $a_\mu$  and spin-1 dark matter [662].

<sup>48</sup>In a similar investigation where a light CP-even scalar with lepton-flavour violating couplings is assumed to couple to electrons and muons, and to dark matter particles [659], no such tension was found, but the parameter region viable for dark matter is very tightly constrained.

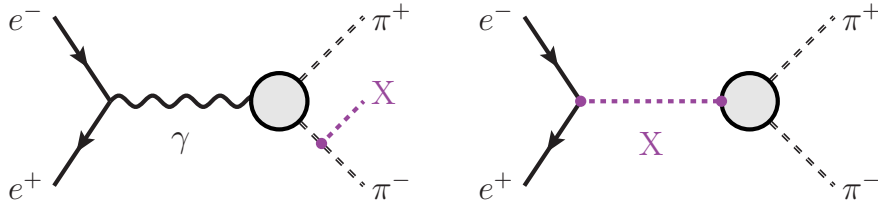


**Figure 5.8:** Direct BSM contributions to  $e^+e^- \rightarrow \pi^+\pi^-$ .

in comparison. Extensive analyses were performed in an effort to clarify the origin of inconsistencies between details of the various measurements and to produce the new SM prediction [3, 162, 169, 293, 294]. However, so far no clear sources of the discrepancies have been identified, and Ref. [3] concluded that no scientific grounds are known on which one may dismiss any of the data sets. Therefore, further scrutiny is required in order to satisfyingly resolve the current situation.

Meanwhile, this situation has motivated to ask whether physics beyond the SM could be the cause of the observed discrepancies. Most plausibly, light new particles of the kind discussed in the present section, with masses similar to hadron masses could be relevant. They might impact the  $e^+e^-$  cross section measurements, by contaminating the data or by affecting the data analysis [663–667]. In order to discuss this, it is useful to summarise the current situation in a coarse-grained way (for details see Sec. 1.4 and Refs. [2, 3]):

1. The  $e^+e^- \rightarrow$  hadrons data from before Ref. [2] yield low values for the cross section and the resulting  $a_\mu^{\text{HVP,LO}}$ .
  - (a) These data were taken by energy-scan experiments SND and CMD-2 as well as using initial-state radiation at KLOE, BaBar and BESIII.
  - (b) There are some internal discrepancies particularly between KLOE and BaBar.
2. The  $e^+e^- \rightarrow$  hadrons data from the CMD-3 experiment yield a higher cross section and higher  $a_\mu^{\text{HVP,LO}}$ .
3. The lattice results yield a higher  $a_\mu^{\text{HVP,LO}}$ .

To see how BSM physics could cause some of these discrepancies, we schematically write the experimentally determined cross section  $\sigma_{\text{had}}$  as

$$\frac{d\sigma_{\text{had}}}{ds} = \frac{N_{\text{had}} - N_{\text{bg}}}{\epsilon(s)L(s)}, \quad (5.32)$$

where  $N_{\text{had}}$  is the measured number of hadronic events,  $N_{\text{bg}}$  the estimated number of background events,  $\epsilon$  the detection efficiency and  $L(s)$  the luminosity for final states at c.o.m. energies  $\sqrt{s}$ . In particular the following two scenarios were considered:

- (i) BSM directly affects the hadronic production rates, lowering  $N_{\text{had}}$  [663, 666]. This could cause all  $e^+e^-$ -data based results to be systematically too low.
- (ii) BSM enters indirectly through other processes used to estimate  $N_{\text{bg}}$ ,  $\epsilon(s)$  or  $L(s)$  [664, 665]. This could cause different measured values depending on the details of the experiments.

In both cases the HVP contribution to  $a_\mu$  extracted from the data corresponds to

$$a_\mu^{\text{HVP,LO}} = \frac{1}{4\pi^3} \int_{s_{th}}^{\infty} ds K(s) \left( \sigma_{\text{had}}^{\text{SM}}(s) + \Delta\sigma_{\text{had}}^{\text{NP}}(s) \right). \quad (5.33)$$

Thus, if the NP contribution  $\Delta\sigma_{\text{had}}^{\text{NP}}(s) < 0$ , the resulting value of  $a_\mu^{\text{HVP,LO}}$  is decreased leading to a deviation from the experiment. Quantitatively, the correlation to the running finestructure constant  $\Delta\alpha$  discussed in Sec. 3.4, and detailed

comparisons with lattice computations show that the cross section should be modified mostly at low energies  $\sqrt{s} \lesssim 1$  GeV, and there the shift of the cross section must be of the order of a few percent. For simplicity in the following we focus on the  $2\pi$  channel that gives the dominant contribution to  $a_\mu^{\text{HVP,LO}}$ .<sup>49</sup>

Fig. 5.8 illustrates how  $N_{\text{had}}$  can be affected directly by initial- or final-state radiation (ISR,FSR) of a BSM particle, or by a new tree-level exchange diagram where the photon is replaced by a new particle  $X$ . As pointed out in Ref. [663], modifications of ISR or FSR alone are too small or too strongly constrained to account for the required few-percent effect. However, if the  $X$ -particle couples to both electrons and pions, the new  $s$ -channel diagram could in principle lead to a sizeable interference. Specifically, destructive interference is required to get a negative BSM contribution. Scalar, pseudoscalar, and axial vectors cannot destructively interfere with the photon diagram (or the interference is suppressed by the electron mass); hence the only plausible candidate is given by a light  $Z'$  boson with vector couplings to both the electron and light quarks [663], and a model Lagrangian can be written as

$$\mathcal{L} \supset (g_e \bar{e} \gamma^\mu e + g_u \bar{u} \gamma^\mu u + g_d \bar{d} \gamma^\mu d) Z'_\mu. \quad (5.34)$$

The interference then induces the following tree-level correction to the pion production cross section [663],

$$\Delta\sigma_{\pi\pi}^{\text{NP}}(s) = \sigma_{\pi\pi}^{\text{SM}}(s) \frac{2s(s - M_{Z'}^2)\epsilon + s^2\epsilon^2}{(s - M_{Z'}^2) + M_{Z'}^2\Gamma_{Z'}^2}, \quad \text{where} \quad \epsilon = \frac{g_e(g_u - g_d)}{e^2}. \quad (5.35)$$

This model therefore represents an explicit realisation of the scenarios discussed in the Refs. [286–288] mentioned in Sec. 3.4. It changes the extraction of the photon vacuum polarisation from  $e^+e^-$  data but itself does not contribute to  $a_\mu$  if the  $X$  particle does not couple to the muon. The required increase in the hadronic cross section then implies  $M_{Z'} < 1$  GeV and  $|\epsilon| \approx 0.01$ .

This basic idea has been investigated in detail in Refs. [663, 666] and further scrutinised in Ref. [668]. The relevant parameter space is already strongly constrained, in particular by LEP measurements of  $e^+e^- \rightarrow q\bar{q}$  which limit the overall coupling strengths as well as strong isospin-breaking observables like  $\Delta m_\pi = m_{\pi^\pm}^2 - m_{\pi^0}^2$  which limit the difference  $|g_u - g_d|$ . According to the calculations of Ref. [663], these constraints fully exclude the scenario. The LEP constraint was evaluated in more detail in Refs. [666, 668], finding slightly relaxed bounds. The  $\Delta m_\pi$ -constraint involves hadronic uncertainties and was evaluated using various arguments in all these references. Furthermore, the tree-level calculation leading to Eq. (5.35) can be improved in case of a large  $Z'$  width, leading to amplified effects [668]. Despite this, Ref. [668] confirms that the scenario is excluded, while the evaluation of Ref. [666] finds the constraints on the scenario with  $M_{Z'} \sim 700$  MeV to be strong but tolerable.

In total, the idea is strongly constrained and barely viable, even in generalised forms where the  $Z'$  can also decay invisibly or couple to muons and directly affect  $a_\mu$  [666]. Furthermore it is at odds with the more recent discrepancy between the CMD-3 and other  $e^+e^-$  measurements.

The second way BSM physics could affect the HVP discrepancies is via indirect effects, as illustrated in Fig. 5.9. If a BSM particle  $X$  does not couple to hadrons but to electrons and muons, the additional diagrams could still lead to a relevant modification of the hadronic cross section determined via Eq. (5.32) by modifying the luminosity measurement

<sup>49</sup>Although most likely the discrepancies cannot be explained by exclusively changing the  $2\pi$  channel at very low energies [292, 668]. In this context we note that the comparison between lattice computations and data-based results needs to be made on the level of integrals, since the cross section  $\sigma_{\text{had}}(s)$  with time-like momentum  $s > 0$  is not accessible on the lattice. A detailed comparison is facilitated by windowed integrals, isolating long-distance, short-distance, or intermediate contributions. These windows can be applied both to lattice computations [59] and to  $e^+e^-$  data [161].

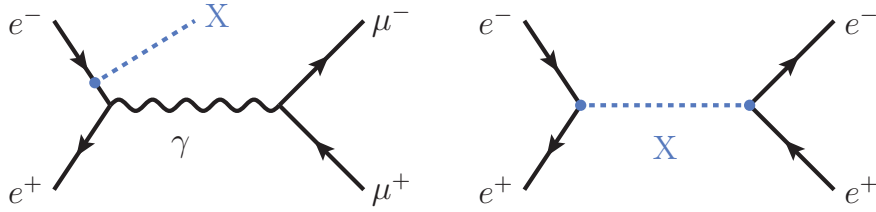


**Figure 5.9:** Indirect BSM contributions to the  $\sigma_{\text{had}}$  determination via normalisation processes.

[664, 665]. In detail, the luminosity for the KLOE08 and KLOE10 analyses [299, 669] was determined by measuring  $e^+e^-$  final states and comparing with the SM prediction for Bhabha scattering. Assuming a dark photon can be resonantly produced at KLOE and decays into  $e^+e^-$  pairs, the measured  $e^+e^-$  rate is higher than the actual SM Bhabha rate and the determined luminosity therefore larger than the true luminosity. Such a scenario could thus account for an underestimate of the hadronic cross section  $\sigma_{\text{had}}$  by KLOE08 and KLOE10.

In the measurements by KLOE12 [300] and BaBar [155], the luminosity dependence in Eq. (5.32) is effectively replaced by measuring the ratio of  $\pi^+\pi^-(\gamma)$  versus  $\mu^+\mu^-(\gamma)$  events, using SM theory predictions for the  $\mu^+\mu^-(\gamma)$  cross sections. These measurements are therefore highly sensitive to additional  $\mu^+\mu^-$  final states. The details depend on the experimental setup and are discussed in the literature; for instance KLOE12 reconstructed photons from the missing energy, hence any additional  $\mu^+\mu^-X$  events like in Fig. 5.9 would be included in the measured event number  $N_{\mu\mu\gamma}$ , decreasing the value of  $\sigma_{\pi\pi}$  estimated from Eq. (5.32). This again could happen e.g. in case of a dark photon or  $Z'$  at a mass close to 1 GeV. Refs. [664, 665] construct a working example of a dark photon of mass around 1 GeV with kinetic mixing and hence equal but weak couplings to electrons and muons. The scenario is accompanied by the idea of inelastic dark matter, such that the dark photon bounds are weakened as discussed in Sec. 5.1.2.

Because of the differing experimental setups, this scenario affects all ISR-based  $e^+e^-$  measurements differently. For example, the BaBar measurements are performed at a higher centre-of-mass energy compared to KLOE. Consequently a resonantly produced  $Z'$  leading to large effects at one of the experiments would be suppressed at the other. In turn this can alleviate some of the tensions between the ISR data sets. In contrast, the scenario does not affect the energy scan measurements. In this way, the tensions between KLOE and BaBar on the one hand, and lattice and CMD-3 on the other hand, can be significantly reduced. However, the tensions between CMD-3 and previous energy scan based measurements like CMD-2 and SND and minor tensions between KLOE and BaBar remain [665].

In summary, this scenario has not been excluded by other constraints, but it does not fully resolve the convoluted situation regarding the HVP determinations. An interesting lesson of this discussion is that BSM generally might not only affect the observables of primary interest like  $a_\mu$  but also experimental quantities such as luminosity measurements. In case of dark photons and similar particles, the impact on  $N_{\mu\mu\gamma}$  will actually be rather generic [664].

## 5.2. Supersymmetry

Here we consider supersymmetry (SUSY), one of the most promising ideas for extending the SM. SUSY is the unique symmetry that relates fermions and bosons in relativistic quantum field theories. SUSY at the TeV scale offers potential explanations of dark matter (DM) as the lightest SUSY particle (LSP), it explains the observed value of the Higgs-boson mass and improves electroweak naturalness. It is compatible with grand unification of gauge couplings, and local SUSY contains gravity and general relativity and can thus provide a link to ultra-high scale physics [670–672].

SUSY can be realised in different renormalizable models that are viable extensions of the SM. The best known option is the Minimal Supersymmetric Standard Model (MSSM), alternatives of interest for  $a_\mu$  include the Next-to-MSSM (NMSSM) and the Minimal R-symmetric Supersymmetric Standard Model (MRSSM). All these models contain the SM and enlarge the particle spectrum by superpartners (sparticles) to all SM fields whose quantum numbers and interactions are governed by SUSY. SUSY is explicitly broken by so-called soft-SUSY breaking terms [673], which are free parameters governing sparticle masses and mixings. The MSSM contains the minimal viable number of fields and extends the SM by a second Higgs doublet and all the superpartners. The MRSSM contains additional fields but also a higher degree of symmetry and hence a smaller number of free parameters, leading to dramatic changes of the  $a_\mu$  predictions. The NMSSM extends the MSSM by a scalar singlet and its superpartner, leading to interesting changes e.g. in dark matter phenomenology which can be correlated with  $a_\mu$ .

It is assumed that the soft-SUSY breaking terms are not fundamental but originate from some underlying mechanism involving spontaneous SUSY breaking. Corresponding setups typically involve spontaneous SUSY breaking in a hidden sector which is then mediated to the visible sector, effectively leading to soft-SUSY breaking terms at TeV-scale energies. Example mechanisms include gravity-mediated SUSY breaking, gauge-mediated SUSY breaking, anomaly-mediated SUSY breaking or gaugino-mediated SUSY breaking, see Ref. [672] and references therein. Especially in their simplest implementations, such as the Constrained MSSM (CMSSM) or minimal gauge-mediated SUSY breaking (mGMSB), they predict rigid patterns for the soft-SUSY breaking terms, often calculable as a function of few fundamental parameters. In this way models such as the CMSSM or mGMSB lead to specific predictions for  $a_\mu$  and strong correlations to other observables.

For the last two decades SUSY contributions to  $a_\mu$  were considered very promising explanations of the significant deviation  $\Delta a_\mu^{\text{Exp-WP2020}}$  in Eq. (1.6). Especially in the MSSM that deviation could be explained for values of parameters such as  $\tan\beta \sim 50$  and  $M_{\text{SUSY}} \sim 500$  GeV, which were attractive also for other reasons. For early reviews we refer to Refs. [4, 5]; a large number of phenomenological studies of SUSY and  $a_\mu$  were inspired by the first Brookhaven  $a_\mu$  measurement in 2001 [4, 674–705], and in the following years by improvements in the determination of  $a_\mu$  and in complementary measurements [149, 230, 469, 706–718].

Already before the dramatically shifted SM contributions led to the new value  $\Delta a_\mu^{\text{Exp-WP2025}}$ , SUSY scenarios have become constrained by other measurements, most importantly from dark matter searches and from LHC. In this review we first focus on the MSSM, its contributions to  $a_\mu$  and complementary constraints from dark matter, LHC and other considerations. We discuss several important standard scenarios and their current status, then provide a detailed account of the phenomenology of the general MSSM. Finally we also comment on alternative realisations of SUSY such as the MRSSM, the NMSSM and scenarios with unstable LSP.

### 5.2.1. Brief account of the MSSM

We begin with a brief introduction to the MSSM. We introduce the MSSM notation as well as the aspects of key importance for the phenomenological discussion. The MSSM contains the SM extended by a second Higgs doublet of opposite hypercharge, and by superpartner fields. The field content is illustrated in Tab. 5.1. The SM quarks and leptons of both chiralities receive spin-0 squark and slepton superpartners; the SM gauge and Higgs fields receive spin-1/2 gaugino and Higgsino superpartners. The two Higgs doublets are denoted  $\mathcal{H}_{u,d}$ , and supersymmetry only allows the tree-level coupling of  $\mathcal{H}_u$  to up-type quarks and of  $\mathcal{H}_d$  to down-type quarks and leptons. This corresponds to the two-Higgs doublet

		MSSM: Fermions			SUSY partners				MSSM: Bosons			SUSY partners	
		Rep.	Field	Spin	Field	Spin			Rep.	Field	Spin	Field	Spin
(s)leptons	( $\mathbf{1}, \mathbf{2}, -\frac{1}{2}$ )		$\begin{pmatrix} \nu_{Li} \\ e_{Li} \end{pmatrix}$	$\frac{1}{2}$	$\begin{pmatrix} \tilde{\nu}_{Li} \\ \tilde{e}_{Li} \end{pmatrix}$	0	Higgs(ino)	( $\mathbf{1}, \mathbf{2}, -\frac{1}{2}$ )	$\begin{pmatrix} \mathcal{H}_d^0 \\ \mathcal{H}_d^- \end{pmatrix}$	0	$\begin{pmatrix} \tilde{H}_d^0 \\ \tilde{H}_d^- \end{pmatrix}$	$\frac{1}{2}$	
	( $\mathbf{1}, \mathbf{1}, -1$ )		$e_{Ri}$	$\frac{1}{2}$	$\tilde{e}_{Ri}$	0		( $\mathbf{1}, \mathbf{2}, \frac{1}{2}$ )	$\begin{pmatrix} \mathcal{H}_u^0 \\ \mathcal{H}_u^- \end{pmatrix}$	0	$\begin{pmatrix} \tilde{H}_u^0 \\ \tilde{H}_u^- \end{pmatrix}$	$\frac{1}{2}$	
(s)quarks	( $\mathbf{3}, \mathbf{2}, \frac{1}{6}$ )		$\begin{pmatrix} u_{Li} \\ d_{Li} \end{pmatrix}$	$\frac{1}{2}$	$\begin{pmatrix} \tilde{u}_{Li} \\ \tilde{d}_{Li} \end{pmatrix}$	0	Gauge(ino)	( $\mathbf{1}, \mathbf{1}, 0$ )	$B_\mu$	1	$\tilde{B}$	$\frac{1}{2}$	
	( $\bar{\mathbf{3}}, \mathbf{1}, \frac{2}{3}$ )		$u_{Ri}$	$\frac{1}{2}$	$\tilde{u}_{Ri}$	0		( $\mathbf{1}, \mathbf{3}, 0$ )	$W_\mu^i$	1	$\tilde{W}^i$	$\frac{1}{2}$	
	( $\bar{\mathbf{3}}, \mathbf{1}, -\frac{1}{3}$ )		$d_{Ri}$	$\frac{1}{2}$	$\tilde{d}_{Ri}$	0		( $\mathbf{8}, \mathbf{1}, 0$ )	$G_\mu^a$	1	$\tilde{g}^a$	$\frac{1}{2}$	

$\left. \begin{array}{l} h, H, A, H^\pm, \gamma, Z, W^\pm \\ \chi_{1,2,3,4}^0, \chi_{1,2}^\pm \end{array} \right\}$

**Table 5.1:** The field/particle content of the MSSM. The table shows the gauge-eigenstate fields and their quantum numbers; next to the table the mass eigenstates corresponding to the electroweak gauge and Higgs bosons and their superpartners are indicated.

type II Yukawa structure, but in contrast to the non-SUSY two-Higgs doublet model, this Yukawa structure is modified by loop corrections.

Via electroweak symmetry breaking, the two Higgs doublets receive *vevs*  $v_{u,d}$ , and five physical Higgs fields  $h, H, A, H^\pm$  emerge, where  $h$  is assumed to be SM-like. The  $U(1)_Y$ ,  $SU(2)_L$  and  $SU(3)_c$  gauginos, called Bino  $\tilde{B}$ , Winos  $\tilde{W}^i$  and gluinos  $\tilde{g}^a$ , mix with the Higgsinos  $\tilde{H}_{u,d}$  to neutralino  $\chi_i^0$  and chargino  $\chi_i^\pm$  mass eigenstates, and also sfermions mix.

Two central MSSM parameters that are of particular importance for  $a_\mu$  are related to the two Higgs doublets. The first of these is the ratio of the two vacuum expectation values,

$$\tan \beta = \frac{v_u}{v_d}. \quad (5.36)$$

As mentioned above, only the doublet  $\mathcal{H}_d$  gives masses to down-type quarks and leptons such as the muon. As a result, the tree-level muon mass is given by  $m_\mu = y_\mu v_d / \sqrt{2}$ , and the tree-level muon Yukawa coupling  $y_\mu$  is enhanced compared to the SM-value by a factor  $1/\cos \beta$ , which becomes approximately an enhancement by  $\tan \beta$  for large  $\tan \beta$ . Similarly the up-type Yukawa couplings are enhanced by  $1/\sin \beta$ . In order to avoid non-perturbative values of all Yukawa couplings,  $\tan \beta$  is commonly restricted to the range between about 1 and 50, though this can be relaxed, which is discussed below. High values  $\tan \beta = \mathcal{O}(50)$  lead to similar top and bottom Yukawa couplings and are therefore favoured by the idea of top-bottom Yukawa coupling unification [719], see also Ref. [720] for a recent study in connection with  $a_\mu$ .

The second important parameter connecting the two Higgs doublets is the  $\mu$ -parameter, which appears in the MSSM Lagrangian in the terms

$$\mathcal{L}^{\text{MSSM}} \ni \mu \tilde{H}_d \tilde{H}_u - \mu F_{H_d} \mathcal{H}_u - \mu F_{H_u} \mathcal{H}_d + \text{h.c.} \quad (5.37)$$

The first term describes a Higgsino mass term, while in the other terms  $F_{H_{d,u}}$  are auxiliary fields whose elimination gives rise to interactions of  $\mathcal{H}_{d,u}$  with sfermions of the opposite type compared to the Yukawa couplings, producing e.g. mixing mass terms proportional to  $v_d \tilde{t}_L \tilde{t}_R^\dagger$  and  $v_u \tilde{\mu}_L \tilde{\mu}_R^\dagger$ .

In addition the MSSM contains a large number of parameters that parametrise soft SUSY breaking. The relevant soft parameters are

$$M_1, M_2, M_3; m_{\tilde{q}, \tilde{u}, \tilde{d}, \tilde{l}, \tilde{e}}^2; A_{u,d,e}, \quad (5.38)$$

where we follow the conventions of Refs. [721, 722], which are similar as e.g. in Refs. [5, 685, 723]. Here  $M_{1,2,3}$  are (Bino, Wino, gluino) gaugino mass parameters,  $m_i^2$  are  $3 \times 3$  hermitian matrices in generation space corresponding to the scalar masses in the sector  $i$ ;  $A_i$  are  $3 \times 3$  general matrices in generation space corresponding to trilinear interactions between Higgs doublets and sfermion doublets and singlets. Further parameters in the Higgs sector can be eliminated in favour of  $\tan \beta$  and e.g. the mass  $M_{H^\pm}$  of the charged Higgs boson. Except where explicitly stated we will restrict the number of the parameters by neglecting generation mixing and complex phases in the sfermion sectors, i.e. by assuming the corresponding matrices to be diagonal and real. Allowing off-diagonal or complex sfermion mass parameters would lead to sizeable predictions for flavour-violating processes and electric dipole moments in the quark and lepton sectors, and specifically the correlations between  $a_\mu$ , CLFV processes, and EDMs follow the general pattern described in Sec. 3.2 as will be discussed below.

Further, for the following phenomenological discussion it is common practice to use the term ‘‘sleptons’’ only for smuons and selectrons, while the ‘‘staus’’ are discussed separately. The reason is that in many respects, especially for LHC phenomenology, the staus behave very differently from the sleptons of the first two generations. Accordingly, we will use the following simplified notation for the slepton mass parameters,

$$m_L \equiv m_{\tilde{l},11} = m_{\tilde{l},22}, \quad m_{\tilde{\tau}_L} \equiv m_{\tilde{l},33}, \quad (5.39)$$

$$m_R \equiv m_{\tilde{e},11} = m_{\tilde{e},22}, \quad m_{\tilde{\tau}_R} \equiv m_{\tilde{e},33}. \quad (5.40)$$

Similarly, unless explicitly noted, we will assume that the MSSM conserves  $R$ -parity, where all SM-like states have positive  $R$ -parity and all SUSY partner states have negative  $R$ -parity.  $R$ -parity conservation implies that SUSY particles must be produced in pairs, and the decay of each SUSY particle ends up in a number of SM particles plus the LSP, and the LSP is stable.

To fix our notation for the most important parameters we provide the mass matrices of the charginos, the neutralinos and the smuons. They are given as

$$X = \begin{pmatrix} M_2 & M_W \sqrt{2} \sin \beta \\ M_W \sqrt{2} \cos \beta & \mu \end{pmatrix}, \quad (5.41)$$

$$Y = \begin{pmatrix} M_1 & 0 & -M_Z s_W \cos \beta & M_Z s_W \sin \beta \\ 0 & M_2 & M_Z c_W \cos \beta & -M_Z c_W \sin \beta \\ -M_Z s_W \cos \beta & M_Z c_W \cos \beta & 0 & -\mu \\ M_Z s_W \sin \beta & -M_Z c_W \sin \beta & -\mu & 0 \end{pmatrix}, \quad (5.42)$$

$$M_\mu^2 = \begin{pmatrix} m_\mu^2 + m_L^2 + M_Z^2 \cos 2\beta \left(-\frac{1}{2} + s_W^2\right) & m_\mu(-\mu \tan \beta + A_\mu^*) \\ m_\mu(-\mu^* \tan \beta + A_\mu) & m_\mu^2 + m_R^2 + M_Z^2 \cos 2\beta (-s_W^2) \end{pmatrix}, \quad (5.43)$$

where the fundamental SUSY parameters appearing in these expressions are  $\tan \beta$  and the two gaugino (Bino and Wino) mass parameters  $M_{1,2}$ , the Higgsino mass  $\mu$  and the left-/right-handed smuon masses  $m_{L,R}$ . The smuon mass matrix also involves the trilinear soft SUSY-breaking parameter  $A_\mu \equiv A_{e,22}$ , which however plays a subdominant role compared to the  $\mu \tan \beta$  term. The other appearing parameters are the SM parameters  $m_\mu, M_{W,Z}$  and  $s_W = \sqrt{1 - c_W^2}$ .

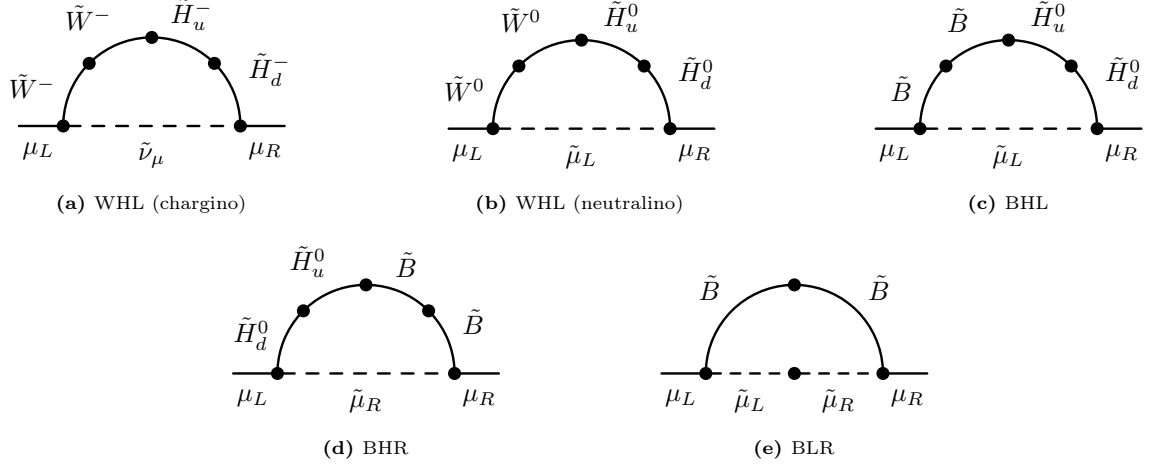


**Figure 5.10:** Mass-insertion diagrams of the MSSM contributing to  $a_\mu$  and to the muon self energy, see Eqs. (5.44) and (5.49). For contributions to  $a_\mu$ , an additional external photon couples to any of the charged particles in the loop.

### 5.2.2. MSSM contributions to $a_\mu$

The SUSY contributions to  $a_\mu$  are mainly generated by one-loop diagrams involving a smuon or sneutrino, together with a neutralino or chargino, i.e. the SUSY partners of the electroweak SM gauge and Higgs bosons. The diagrams are of the generic FS-type shown in Fig. 2.1a.

These one-loop contributions have been systematically and comprehensively studied for the MSSM in Ref. [207], for reviews see e.g. Refs. [5, 685, 723].

The MSSM one-loop contributions to  $a_\mu$  feature a very important chiral enhancement, which brings the possible values into the ballpark tested by the Fermilab experiment. Here we first focus on this dominant behaviour, using the mass-insertion approximation, which allows us to directly read off the main parameter dependences similarly to Sec. 2.3; then we comment on the full prediction in the MSSM.<sup>50</sup>

The relevant mass-insertion diagrams are shown in Fig. 5.10. Following the form given e.g. in Refs. [190, 228, 723] the corresponding contributions can be written as

$$\Delta a_\mu^{1\text{L}}{}^{\text{SUSY}} \approx \Delta a_\mu^{1\text{L}}(\text{WHL}) + \Delta a_\mu^{1\text{L}}(\text{BHL}) + \Delta a_\mu^{1\text{L}}(\text{BHR}) + \Delta a_\mu^{1\text{L}}(\text{BLR}),$$

with

$$\begin{aligned} \Delta a_\mu^{1\text{L}}(\text{WHL}) &= + m_\mu \left[ \frac{y_\mu v_u}{\sqrt{2}} \right] \frac{g_2^2}{8\pi^2} \frac{M_2 \mu}{m_L^4} F_a \left( \frac{M_2^2}{m_L^2}, \frac{\mu^2}{m_L^2} \right) \\ &\quad - m_\mu \left[ \frac{y_\mu v_u}{\sqrt{2}} \right] \frac{g_2^2}{16\pi^2} \frac{M_2 \mu}{m_L^4} F_b \left( \frac{M_2^2}{m_L^2}, \frac{1}{m_L^2} \right) \approx \pm 21 \times 10^{-10} \left( \frac{500 \text{ GeV}}{M_{\text{SUSY}}} \right)^2 \frac{\tan \beta^{\text{eff}}}{40}, \end{aligned} \quad (5.44a)$$

$$\Delta a_\mu^{1\text{L}}(\text{BHL}) = + m_\mu \left[ \frac{y_\mu v_u}{\sqrt{2}} \right] \frac{g_1^2}{16\pi^2} \frac{M_1 \mu}{m_L^4} F_b \left( \frac{M_1^2}{m_L^2}, \frac{\mu^2}{m_L^2} \right) \approx \pm 1.2 \times 10^{-10} \left( \frac{500 \text{ GeV}}{M_{\text{SUSY}}} \right)^2 \frac{\tan \beta^{\text{eff}}}{40}, \quad (5.44b)$$

$$\Delta a_\mu^{1\text{L}}(\text{BHR}) = - m_\mu \left[ \frac{y_\mu v_u}{\sqrt{2}} \right] \frac{g_1^2}{8\pi^2} \frac{M_1 \mu}{m_R^4} F_b \left( \frac{M_1^2}{m_R^2}, \frac{\mu^2}{m_R^2} \right) \approx \mp 2.4 \times 10^{-10} \left( \frac{500 \text{ GeV}}{M_{\text{SUSY}}} \right)^2 \frac{\tan \beta^{\text{eff}}}{40}, \quad (5.44c)$$

$$\Delta a_\mu^{1\text{L}}(\text{BLR}) = + m_\mu \left[ \frac{y_\mu v_u}{\sqrt{2}} \right] \frac{g_1^2}{8\pi^2} \frac{\mu}{M_1^3} F_b \left( \frac{m_L^2}{M_1^2}, \frac{m_R^2}{M_1^2} \right) \approx \pm 2.4 \times 10^{-10} \left( \frac{500 \text{ GeV}}{M_{\text{SUSY}}} \right)^3 \frac{\tan \beta^{\text{eff}}}{40} \frac{\mu}{500 \text{ GeV}}. \quad (5.44d)$$

<sup>50</sup>We note that this chiral enhancement is present also in many extensions of the MSSM, but e.g. not in the MRSSM, as will be discussed further below.

The appearing loop functions are normalised as  $F_a(1, 1) = 1/4$ ,  $F_b(1, 1) = 1/12$  and can be found in footnote 9. On the far right we provide numerical approximations valid if all SUSY mass parameters are equal, where the signs are given by the sign of the products  $M_{1,2}\mu$  and where  $\tan\beta^{\text{eff}} = \tan\beta$ +higher order corrections as explained further below. The letters B,W,H,L, and R are the abbreviations for Bino, Winos, Higgsinos, and Left- and Right-handed smuons/sneutrinos, respectively. As indicated and as visible in the Feynman diagrams, each contribution depends on three of these states and their respective masses. The factors  $y_\mu v_u$  in square brackets directly reflect the need for chirality flips and electroweak symmetry breaking discussed in Sec. 1.1.4, and generally the formulas are written analogously to Eq. (1.15). As an even simpler reference we provide an approximation if all relevant sparticle masses are equal to a common scale  $M_{\text{SUSY}}$ ,

$$\Delta a_\mu^{\text{SUSY}} \approx 22 \times 10^{-10} \left( \frac{500 \text{ GeV}}{M_{\text{SUSY}}} \right)^2 \frac{\tan\beta^{\text{eff}}}{40}. \quad (5.45)$$

There is a crucial chiral enhancement by the factor  $\tan\beta$  because the tree-level muon mass is given via the down-type  $vev$   $v_d$ , while the up-type  $vev$   $v_u$  can be larger, such that

$$\left[ \frac{y_\mu v_u}{\sqrt{2}} \right] \rightarrow m_\mu^{\text{tree}} \tan\beta \quad (5.46)$$

at lowest order. Diagrammatically, the chiral enhancement arises as follows. In the WHL, BHL and BHR contributions, the muon chirality is flipped at the Yukawa coupling to a Higgsino; the Higgsino is then converted to a gaugino via a Higgs vacuum expectation value. The appearance of the enhanced VEV is always accompanied by a factor of the Higgsino mass  $\mu$  which converts  $\tilde{H}_d$  into  $\tilde{H}_u$ . This explains the appearance of one Higgsino mass  $\mu$  in the numerators of all contributions. A gaugino (Bino or Wino) mass parameter  $M_{1,2}$  must also appear in each numerator. These contributions are very similar to the three-field models of Class II in Sec. 2.3, although the relevant Higgs doublet is different.<sup>51</sup>

The BLR contribution in the last line is special, and it behaves like the three-field model of Class III. Here the muon chirality is flipped at the smuon line via the insertion of a smuon-left-right flip, which is also governed by a product of the Higgsino mass  $\mu$  and the enhanced VEV in the smuon mixing matrix whose origin is explained below Eq. (5.37). In contrast to the other contributions, the BLR contribution is approximately linearly enhanced by the Higgsino mass  $\mu$  since this parameter does not appear as the mass of a virtual Higgsino. The signs of all contributions are determined by the signs of  $\mu$  and the gaugino masses  $M_{1,2}$ . Unless noted explicitly, in the following we will only consider positive signs of all these parameters, leading to positive MSSM contributions to  $a_\mu$ .

Specific constraints on this BLR-contribution have been very thoroughly investigated in Ref. [724–726]. Most importantly, vacuum stability requires that staus, the superpartners of  $\tau$ -leptons, do not receive a charge-breaking vacuum expectation value, and this provides a constraint on the relation between the off-diagonal and diagonal elements of the stau mass matrix similar to Eq. (5.43). As a quantitative example, Ref. [724] finds that in case of universal left- and right-handed stau masses  $m_{\tilde{\tau}_L} = m_{\tilde{\tau}_R} \equiv m_{\tilde{\tau}}$ , the Higgsino mass has an upper limit, specifically

$$\frac{\mu}{1 \text{ TeV}} \frac{\tan\beta}{40} \lesssim \frac{m_{\tilde{\tau}}}{300 \text{ GeV}}. \quad (5.47)$$

An analogous limit from the smuon mass matrix exists but is weaker because of the smaller muon mass; for a more accurate and general treatment we refer to Refs. [724–726].

It is illuminating to discuss a particular kind of higher-order corrections to  $a_\mu$  with the help of the same mass-insertion diagrams in Fig. 5.10. As explained in Secs. 1.1.4 and 3.1 there is a deep connection between contributions to  $a_\mu$  and

---

<sup>51</sup>Comparing e.g. the WHL case to the Class II behaviour in Eq. (2.19), the couplings  $\lambda_L \lambda_R \bar{\lambda}_H$  would correspond to  $g_2 y_\mu g_2$ , and the masses  $m_\psi m_\chi$  to  $M_2 \mu$ .

to the muon mass  $m_\mu$ . Interpreting the mass-insertion diagrams as contributions to the muon mass, they correspond to one-loop corrections to the relationship (5.46) between the muon mass and the muon Yukawa coupling. The decisive feature is that the loops generate a coupling of the muon to the larger  $vev$   $v_u$ . The result for the one-loop corrected muon mass can be written as

$$m_\mu = \frac{y_\mu v_d}{\sqrt{2}} + \frac{y_\mu v_u}{2} \Delta_\mu^{\text{red}}, \quad (5.48)$$

where the one-loop quantity  $\Delta_\mu^{\text{red}}$  can be approximated as [228]

$$\begin{aligned} \Delta_\mu^{\text{red}}(\text{WHL}) &= -\frac{g_2^2}{16\pi^2} M_2 \mu I(M_2, \mu, m_L) \\ &\quad -\frac{g_2^2}{32\pi^2} M_2 \mu I(M_2, \mu, m_L), \end{aligned} \quad (5.49a)$$

$$\Delta_\mu^{\text{red}}(\text{BHL}) = \frac{g_1^2}{32\pi^2} M_1 \mu I(M_1, \mu, m_L), \quad (5.49b)$$

$$\Delta_\mu^{\text{red}}(\text{BHR}) = -\frac{g_1^2}{16\pi^2} M_1 \mu I(M_1, \mu, m_R), \quad (5.49c)$$

$$\Delta_\mu^{\text{red}}(\text{BLR}) = \frac{g_1^2}{16\pi^2} M_1 \mu I(M_1, m_L, m_R), \quad (5.49d)$$

where the loop function is given by

$$I(a, b, c) = \frac{a^2 b^2 \ln \frac{a^2}{b^2} + b^2 c^2 \ln \frac{b^2}{c^2} + c^2 a^2 \ln \frac{c^2}{a^2}}{(a^2 - b^2)(b^2 - c^2)(a^2 - c^2)}, \quad (5.50)$$

with a scaling behaviour  $I \sim 1/M^2$ , where  $M$  denotes the largest of the three mass arguments.

The parallel structure of the one-loop contributions to  $a_\mu$  and for  $m_\mu$  via  $\Delta_\mu^{\text{red}}$  is apparent. This does not only illustrate and confirm the general discussions of Secs. 1.1.4 and 3.1. It also explains the possibility of an all-order resummation of large  $\tan\beta$ -enhanced effects, first analysed in Ref. [714] and further studied in Refs. [228, 727, 728]. The solution of Eq. (5.48) leads to the improved replacement for the Yukawa coupling  $y_\mu$ ,

$$\left[ \frac{y_\mu v_u}{\sqrt{2}} \right] \rightarrow \frac{m_\mu v_u}{v_d + v_u \Delta_\mu^{\text{red}}} \equiv m_\mu \tan\beta^{\text{eff}}, \quad (5.51)$$

where also an effective higher-order corrected  $\tan\beta^{\text{eff}} = \tan\beta/(1 + \tan\beta\Delta_\mu^{\text{red}})$  has been defined. If this replacement instead of the tree-level Eq. (5.46) is applied to the result for  $a_\mu$ , all  $n$ -loop corrections enhanced by  $\tan^n\beta$  are taken into account [714]. The resummed formula also allows the limit  $v_d \rightarrow 0$ ,  $\tan\beta \rightarrow \infty$  [228, 727, 728], in which case the muon mass vanishes at tree level and is generated radiatively as in the examples of Sec. 3.1.

Now we turn to the best available MSSM prediction for  $a_\mu$ . Given the importance of the model, significant effort has been invested in obtaining an accurate and reliable computation. The one-loop diagrams for  $a_\mu$  have been computed exactly in the general MSSM in Ref. [207], and the explicit formulas can be found there and in all other references mentioned above. In addition, a wide range of higher-precision calculations of 2-loop contributions is available. The known SUSY contributions (i.e. the difference between MSSM and SM contributions) to  $a_\mu$  can be summarised as

$$\Delta a_\mu^{\text{SUSY}} = \left[ \Delta a_\mu^{1\text{L,SUSY}} + \Delta a_\mu^{2\text{L(a)}} + \Delta a_\mu^{2\text{L, photonic}} + \Delta a_\mu^{2\text{L,ff}} \right]_{t_\beta\text{-resummed}}. \quad (5.52)$$

Here  $\Delta a_\mu^{2\text{L(a)}}$  corresponds 2-loop diagrams in which a SUSY loop is inserted into a SM-like loop, including Barr-Zee diagrams discussed in Sec. 4.2 where charginos or sfermions run in the inner loop. These were computed and evaluated in Refs. [149, 692, 693, 713, 716], and reviewed in detail in Ref. [5]; given today's experimental constraints these diagrams

must be negligibly small. The full 2-loop QED corrections  $\Delta a_\mu^{2L, \text{photonic}}$ , see Refs. [152, 469], include the leading QED-logarithms discussed in Sec. 4.3.1. Refs. [190, 729] computed genuine SUSY 2-loop corrections  $\Delta a_\mu^{2L, f\bar{f}}$  to the SUSY 1-loop diagrams which include non-decoupling effects from e.g. heavy squarks. Finally, the inclusion of a  $\tan\beta$ -resummation, i.e. of  $n$ -loop higher-order terms enhanced by  $(\tan\beta)^n$ , was developed in Refs. [228, 714], where also the muon mass corrections  $\Delta_\mu^{\text{red}}$  are given without mass-insertion approximation. Interestingly, each of these three kinds of higher-order corrections can shift the 1-loop contributions by around 10%. All these 1-loop and 2-loop contributions are implemented in the code GM2Calc [730], which is used in many phenomenological analyses in the recent literature. Ref. [730] also contains a compact collection of explicit formulas of all contributions.<sup>52</sup>

To provide a first overview, Fig. 5.11 shows the theoretical maximum of the SUSY contributions  $\Delta a_\mu^{\text{SUSY,Max}}$  in the plane of  $m_{\chi_2^\pm}$  and  $m_{\tilde{\mu}_1}$ , where  $\chi_2^\pm$  is the heavier chargino and  $\tilde{\mu}_1$  the lighter smuon (a version of this plot was also shown in Ref. [9], and for similar plots in different planes see Refs. [5, 709, 737]). It fixes  $\tan\beta = 40$  and allows all SUSY masses to vary independently between 100 GeV and 4 TeV.<sup>53</sup> The red dashed lines and the green/grey coloured regions correspond to the indicated values of  $\Delta a_\mu^{\text{SUSY,Max}}$ ; specifically the green and grey colours correspond to the  $1/2\sigma$  regions for the current result  $\Delta a_\mu^{\text{Exp-WP2025}}$  and the previous value  $\Delta a_\mu^{\text{Exp-WP2020}}$  from Eqs. (1.5) and (1.6), respectively. As indicated on the right of the legend plot, an alternative interpretation of the contour lines and regions is possible. Thanks to the approximate linearity in  $\tan\beta$ , each value for  $\Delta a_\mu^{\text{SUSY}}$  with  $\tan\beta = 40$  can be translated into approximate  $\tan\beta$ -values for which other values of  $\Delta a_\mu^{\text{SUSY}}$  can be obtained. In the legend plot this translation is done for  $\Delta a_\mu^{\text{SUSY}} = 17 \times 10^{-10}$ , the new  $2\sigma$  upper limit. For further details on the plot see the caption.

The figure and the previous formulas show that large contributions are in principle possible, but these are now strongly constrained by the new result  $\Delta a_\mu^{\text{Exp-WP2025}}$ . Using the plot we can read off how the current constraint can be satisfied if  $\tan\beta = 40$ :

- Masses  $\gtrsim 900 \dots 1000$  GeV tend to be in the green  $1\sigma$  region, which is “safe”, i.e. in this region  $\Delta a_\mu^{\text{SUSY}}$  with  $\tan\beta = 40$  is guaranteed to be sufficiently small.
- Smaller masses below the green region can still be possible, since  $\Delta a_\mu^{\text{SUSY,Max}}$  is shown, but they are strongly constrained and their viability depends on further details of SUSY masses and parameters.

Using the legend plot we can read off further viable parameter regions:

- For any value of the masses, the legend plot shows which  $\tan\beta$  is “safe” (to the extent that the rescaling is exact), i.e. it shows the value of  $\tan\beta$  for which  $\Delta a_\mu^{\text{SUSY,Max}}$  is definitely below the current  $2\sigma$  upper limit. E.g. for  $m_{\chi_2^\pm} = m_{\tilde{\mu}_1} = 400$  GeV,  $\tan\beta \leq 14$  is “safe”.
- Again, larger values of  $\tan\beta$  can be possible, depending on details of SUSY masses and parameters.

The plot also shows in which mass region larger values of  $\Delta a_\mu^{\text{SUSY}}$  are possible. E.g.  $\Delta a_\mu^{\text{SUSY}} > 20 \times 10^{-10}$  can only occur (for  $\tan\beta = 40$  and  $\mu \leq 4$  TeV) if

- either both chargino masses are lighter than around 1.1 TeV (vertical black line in Fig. 5.11)

<sup>52</sup>For higher-order calculations in extensions of the MSSM see Refs. [731–736].

<sup>53</sup>We note that the choice of the mass interval is not crucial because the maximum  $\Delta a_\mu^{\text{SUSY}}$  is obtained in the bulk of the mass range, not at its boundary. This is a reflection of the fact that the leading contributions approximated in Eq. (5.44) are suppressed if Bino, Wino or Higgsino masses are too large or too small.

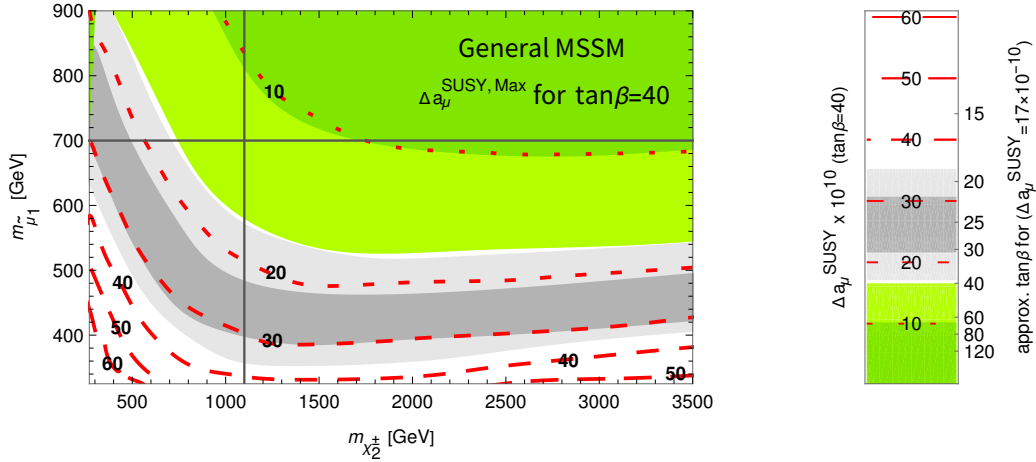


**Figure 5.11:** The theoretical maximum MSSM contribution  $a_\mu^{\text{SUSY,Max}}$  for  $\tan\beta = 40$  in the plane of the heaviest chargino and the lightest smuon mass. (For each point in the plane, the actual value of the MSSM contribution can take any value between 0 and  $\pm\Delta a_\mu^{\text{SUSY,Max}}$ , depending on the signs of parameters and details such as other masses and mixings.) The (light) green coloured regions show where  $\Delta a_\mu^{\text{SUSY,Max}}$  (for  $\tan\beta = 40$ ) is within the  $1\sigma$  ( $2\sigma$ ) bands corresponding to  $\Delta a_\mu^{\text{Exp-WP2025}}$ , see Eq. (1.5). The (light) grey regions correspond to the value  $\Delta a_\mu^{\text{Exp-WP2020}}$  in Eq. (1.6). The red dashed contour lines can be interpreted in two ways. Firstly, they directly correspond to certain values of  $\Delta a_\mu^{\text{SUSY,Max}}$  for  $\tan\beta = 40$ , as indicated in the left axis of the legend plot. Secondly, thanks to the approximate linearity in  $\tan\beta$ , each contour can be used to estimate the  $\tan\beta$  value for which  $\Delta a_\mu^{\text{SUSY,Max}}$  just reaches the upper limit of the  $2\sigma$  band around Eq. (1.5) (keeping other input parameters fixed). These  $\tan\beta$  values can be read off from the right axis of the legend plot (the values are approximate since the linearity is not exact). As an example of the reinterpretation we take the point  $m_{\chi_2^\pm} = 1100$  GeV and  $m_{\tilde{\rho}_1} = 400$  GeV. For  $\tan\beta = 40$  we get  $\Delta a_\mu^{\text{SUSY,Max}} = 30 \times 10^{-10}$ . The legend plot then shows that  $\Delta a_\mu^{\text{SUSY,Max}} < 17 \times 10^{-10}$  if  $\tan\beta \lesssim 23$ . The results for  $\Delta a_\mu^{\text{SUSY,Max}}$  were obtained from a scan using GM2Calc [730] in which all relevant SUSY masses are varied independently between 100 GeV and 4 TeV. The black lines indicate the approximate maximum LHC reach for charginos and sleptons of 1100 and 700 GeV.

- or one smuon is lighter than around 700 GeV (horizontal black line in Fig. 5.11).

While this mass region is of interest also for other reasons, it is in potential tension with LHC and other data, as discussed below. This tension was analysed in a large part of the literature in the past years.

To explain the behaviour of Fig. 5.11 in more detail, we note that the WHL contributions (5.44a) are by far most important in the largest part of parameter space. These are generically suppressed if any of the SUSY masses become large. However for large  $\mu$ , the BLR contribution can become sizable and even dominant due to its approximately linear  $\mu$ -dependence. In Fig. 5.11 the slight rise of  $\Delta a_\mu^{\text{SUSY,Max}}$  with increasing  $m_{\chi_2^\pm}$  is due to the BLR contribution. In contrast, the BHR and particularly the BHL contributions are not important for the maximum value  $\Delta a_\mu^{\text{SUSY,Max}}$ , and in general they are subdominant unless there are extremely large mass splittings between left- and right-handed smuons.<sup>54</sup>

### 5.2.3. Complementary constraints on MSSM parameters

The above formulas, in particular Eq. (5.45), and Fig. 5.11 illustrate that SUSY contributions to  $a_\mu$  can be sizeable if the relevant SUSY masses are in the few-hundred GeV range and  $\tan\beta$  is large. This general parameter region is motivated also independently as a realisation of SUSY. Accordingly, it has been investigated extensively, and the possibility of

<sup>54</sup>Specifically the BHR contribution can be decisive if  $\tan\beta \gg 50$  and if  $m_L \gg m_R$  [228]. For further dedicated investigations focusing on parameter situations in which the BHL or BHR contributions dominate we refer to Refs. [738, 739].

sizeable  $\Delta a_\mu$  in the MSSM has been scrutinised using complementary constraints on the parameter space. Earlier studies of the MSSM phenomenology of  $a_\mu$  of the LHC run-I era can be found in Refs. [228, 723, 724, 737, 740–769], more recent studies using detailed recasting of LHC run-II and/or dark matter data have been done in Refs. [9, 738, 739, 770–785]. In particular, the (series of) works in Refs. [739, 750, 776, 783], Refs. [777, 778, 780–782], Ref. [9] have systematically analysed the general MSSM parameter space coherently against LHC and dark matter data. These latter works are complementary in that they organise the discussions differently, according to dominant  $\Delta a_\mu$  contributions [739, 750, 776, 783], according to dark matter scenarios [777, 778, 780–782], or according to sparticle mass patterns, allowing all possible dark matter realisations [9]; Refs. [9, 739, 750, 776, 782, 783] allow  $\tilde{\tau}$  masses different from other slepton masses, Refs. [739, 750, 776–778, 780–783] allow different left-handed and right-handed slepton masses.

It has turned out that although the LHC strongly constrains the relevant parameter space, the dark matter constraints are at least as important. The latter have further strengthened through recent experimental progress, evaluated first in Ref. [785]. Here we briefly summarise the most important constraints. We begin with dark matter and LHC constraints, then we briefly mention constraints from the Higgs-boson mass, EDMs and CLFV and related observables.

Dark matter provides a strong motivation to consider SUSY. As long as there is no R-parity violation the lightest SUSY particle (LSP) is stable. If the LSP is a neutralino it constitutes a viable dark matter candidate, but constraints arise both from the dark matter relic density (DMRD) of 0.120, see Eq. (3.85), and from dark matter direct detection (DMDD) experiments. The DMDD experiments place upper limits on the possible cross section for dark matter–nucleon scattering, and the limits have substantially improved in recent years in a series of experiments such as PandaX, LUX, XENON1T and most recently LZ, see Fig. 3.7 and particularly Ref. [350].

Like in the general discussion of Sec. 3.6, the strong constraints on dark matter and thus on neutralinos significantly impact the parameter space of interest for  $a_\mu$ . Neutralino dark matter has been extensively reviewed in Ref. [343], and Refs. [785, 786] provide recent updates relevant for discussing  $a_\mu$ , see also Ref. [787] for a computation of higher-order corrections for dark matter direct detection. Here we provide a brief summary of the impact of the dark matter constraints on the SUSY parameter space of interest. Depending on the order of the gaugino and Higgsino masses  $M_{1,2}$ ,  $\mu$  entering the neutralino mass matrix in Eq. (5.42), the nature of the LSP can be dominantly Bino-like, Wino-like or Higgsino-like, with sizeable or negligible subdominant admixtures. In the following we briefly comment on these cases.

- Bino-like LSP: In the case of a Bino-like LSP in the considered mass range, the relic density is typically too large unless a specific mechanism acts to enhance the dark matter annihilation and to suppress the relic density. In the mass range of Bino masses of around 200...600 GeV there are three promising possibilities: stau-coannihilation, other slepton-coannihilation, and Wino-coannihilation [343, 788–791]. For higher masses, a Bino-like LSP can also explain the correct DMRD if there is coannihilation with coloured sparticles, squarks or gluinos [343, 792]. These coannihilation mechanisms are active if the masses between the LSP and the coannihilation partner are nearly degenerate.

If a Bino-like LSP explains the observed relic density, the most recent DMDD experiments provide very strong upper limits on neutralino–nucleon scattering. A Bino-like LSP can interact with nucleons via its Higgsino admixture. Hence strong gaugino–Higgsino mixing of the LSP is not viable, except in “blind spots” which are characterised by particular ratios  $\mu/m_{\text{LSP}}$ , require negative  $\mu$  and depend on  $\tan\beta$  and the CP-odd Higgs boson mass  $M_A$  [793–795].

For positive  $\mu$  we find the approximate bound

$$\mu \gtrsim 520 \text{ GeV} + M_1, \quad (5.53)$$

based on the analytical approximations of Ref. [785] and the latest LZ result [350] in the parameter space where  $\tan\beta \approx 40$  and the extra Higgs masses are large (the dependence of the bound on these parameters is mild). This bound supersedes the bounds found in Refs. [9, 739, 750, 776–778, 780–783] and is used in the following plots, though it is not based on full simulations and thus has an intrinsic uncertainty.

- Higgsino- and Wino-like LSP: If the LSP is Higgsino-like, there are automatically three almost degenerate states  $\chi_{1,2}^0$  and  $\chi_1^\pm$ . Without any other states close in mass, a Higgsino-like LSP generates the correct relic density for  $M_{\text{LSP}} \approx \mu \approx 1 \text{ TeV}$ . In case of Wino-like LSP without any other degenerate states, the relic density can be explained for  $M_{\text{LSP}} \approx M_2 \approx 2 \dots 3 \text{ TeV}$ . Higgsino-like or Wino-like LSPs with smaller masses typically lead to a relic density which is too small. For relevant discussions, including exceptions due to coannihilation effects, and for additional dark matter candidates we refer to Refs. [343, 796–800].

Scenarios with underabundant DMRD are viable (if additional dark matter candidates from beyond the MSSM are assumed), but still the DMDD constraints limit the gaugino–Higgsino mixing. For the particularly interesting case of Higgsino-like LSP without additional coannihilation or non-thermal effects, the results of Ref. [786] imply the approximate bounds (derived for large  $\tan\beta = 50$ , again with mild  $\tan\beta$ -dependence)

$$\text{for } M_1 \gg M_2 > \mu: \quad M_2 \gtrsim 1420 \text{ GeV} + 3\mu, \quad (5.54a)$$

$$\text{for } M_2 \gg M_1 > \mu: \quad M_1 \gtrsim 1100 \text{ GeV} + 2.3\mu. \quad (5.54b)$$

Now we turn to collider constraints on the MSSM. Particularly the non-observation of sparticles at the LHC excludes large parts of the MSSM parameter space. Here we summarise the major conclusions of the studies mentioned at the beginning of this subsection. The relevant LHC constraints can be grouped into “standard” searches for electroweak sparticles and searches optimised for compressed spectra. The standard searches assume the production of heavy electroweak SUSY particles (charginos/neutralinos or sleptons), followed by decay into SM particles and the LSP, which corresponds to missing energy. For instance, the strongest chargino/neutralino mass limits are obtained from the pair production channel  $pp \rightarrow \chi_1^\pm \chi_2^0$  with subsequent decay via on-shell sleptons into three charged leptons and two LSPs. Here the produced charginos/neutralinos could be Wino-like, while the LSP is a significantly lighter Bino-like neutralino and the slepton mass is in between. In simplified-model interpretations, in which 100% decay branching ratios are assumed and the slepton mass is halfway between the LSP- and the chargino mass, the limits extend up to

$$m_{\chi_1^\pm}(\text{max. limit [424, 801]}) \approx 1100 \text{ GeV}, \quad (5.55)$$

which is shown in Fig. 5.11 as an illustration of the maximum LHC reach. Direct searches for slepton pairs  $\tilde{l}\tilde{l}$ , ( $\tilde{l} = \tilde{e}, \tilde{\mu}$ ) with subsequent decay into leptons plus LSP have a mass reach up to

$$m_{\tilde{l}}(\text{max. limit [423, 424, 802]}) \approx 700 \text{ GeV}, \quad (5.56)$$

which is also shown in the Figure.

Further LHC limits arise on charginos/neutralinos from decays into other final states which can be available if decays into sleptons are impossible or subdominant. Searches dedicated to compressed spectra, i.e. the case where mass splittings

are less than around 100 GeV exist for a variety of scenarios, such as pairs of charginos/neutralinos, or a pair of neutralino and slepton. The mass reach of these searches, however, extends only up to around 200 GeV; they are thus only relevant for very light sparticle masses. We refer to the original literature, particularly Refs. [9, 739, 776–778, 780–783] for further discussions, references, and the recasting tools used to obtain LHC limits for realistic spectra.<sup>55</sup> <sup>56</sup> There are three general ways to evade the LHC constraints in MSSM parameter space.

1. Sufficiently heavy masses. Clearly, in this case the bounds are trivially evaded without considering further details. Heavy SUSY with e.g.  $m_{\chi_{1\pm}} \gtrsim 1100$  GeV and  $m_{\tilde{t}} \gtrsim 700$  GeV can be attractive for several reasons, including dark matter explanations via Higgsino- or Wino-like LSP, or in view of certain more fundamental models of SUSY breaking.
2. Compressed spectra. If the mass splitting between two relevant sparticles is too small typically below around 100 GeV, the standard searches become insensitive. In this case, dedicated searches for scenarios with compressed spectra are important. Interestingly, the coannihilation mechanisms for dark matter, which rely on small mass splittings, are not strongly constrained by LHC. The mentioned references find that in the region of 100...500 GeV for dark matter masses, the LHC constraints are easily evaded, dark matter can be explained and sizeable contributions to  $a_\mu$  are possible.
3. Different decay modes. If the SUSY particle in question decays into final states that are hard to detect at the LHC, the LHC limits weaken. An important example of this kind are Higgsino-like charginos. Even in case of the mass hierarchy assumed by the search of Refs. [424, 801], where the chargino is much heavier than the LSP and the slepton mass is in between, the Higgsino is essentially invisible and the Higgsino mass is unconstrained by this search.

In total, the discussion shows that a number of attractive MSSM scenarios emerge, where dark matter constraints and LHC constraints can be simultaneously satisfied and, partially, sizeable contributions to  $a_\mu$  are possible. They are summarised in Tab. 5.2.

Another crucial constraint on the SUSY parameter space results from the LHC measurement of the SM-like Higgs boson mass [104]

$$M_H = 125.20(11) \text{ GeV.} \tag{5.57}$$

The constraint is in general unrelated to  $a_\mu$ , except in the important class of scenarios where a fundamental mechanism is assumed to cause a correlation between SUSY parameters of the different strongly and weakly interacting sectors. In the MSSM, the prediction for the SM-like Higgs-boson mass has been developed to a high precision; for details and a summary of recent efforts on high-precision computations we refer to Refs. [820, 821]. For the purposes here it can be approximated in terms of only leading tree-level and one-loop effects for  $\tan\beta \gg 1$ . The leading one-loop quantum corrections are governed by top-quarks and their stop superpartners and dominantly depend on the mass scale of the

---

<sup>55</sup>For an up-to-date list of LHC SUSY searches and results see the web pages <https://twiki.cern.ch/twiki/bin/view/AtlasPublic/SupersymmetryPublicResults> and <https://twiki.cern.ch/twiki/bin/view/CMSPublic/PhysicsResultsSUS>.

<sup>56</sup>The plots with MSSM results shown in the following are based on updates of plots in Ref. [9], which in turn uses the `MSSMEFTiggs_mAmu` spectrum generator, created with `FlexibleSUSY` [803–808]. `FlexibleSUSY` also uses some numerical routines originally from [809, 810] and uses `sarah4.14.1` [811–814]. It is incorporated in the `GAMBIT-1.3` framework [405, 815–819]; for LHC recasting, `ColliderBit` within `GAMBIT` [405] was used. The fundamental SUSY parameters are treated as running  $\overline{\text{DR}}$ -parameters at the scale 1 TeV.

Scenario	Number	Mass range (GeV)	$\Delta a_\mu > 5 \times 10^{-10}$ possible	Comments
$\tilde{B}$ - $\tilde{W}$ -coann.	1	100...500	yes	$\mu$ : DMDD, (vacstab)
$\tilde{B}$ - $\tilde{I}$ -coann.	2	100...500	yes	$\mu$ : DMDD, (vacstab)
$\tilde{B}$ - $\tilde{\tau}$ -coann.	3	100...500	yes	$\mu$ : DMDD, vacstab
$\tilde{B}$ -various	4	up to several TeV	no	$\mu$ : DMDD, vacstab
$\tilde{H}$ -LSP full DM	5	1000	no	$M_{1,2}$ : DMDD
$\tilde{H}$ -LSP partial DM	6	< 1000	yes	$M_{1,2}$ : DMDD
$\tilde{W}$ -LSP full DM	7	2000...3000	no	$\mu$ : DMDD, (vacstab)
$\tilde{W}$ -LSP partial DM	8	< 2000	yes	$\mu$ : DMDD, (vacstab)

**Table 5.2:** Example MSSM scenarios of particular interest for  $a_\mu$ , with characteristic mass patterns which are generically compatible with constraints from dark matter and LHC. For Bino-like LSP the coannihilation partner is indicated where appropriate, and for Higgsino- or Wino-like LSP the two cases where the dark matter relic density is fully or partially explained are distinguished. In the given mass ranges it is easy to satisfy all constraints; the last column indicates whether constraints from dark matter direct detection are relevant for gaugino or Higgsino masses, and whether the constraint Eq. (5.47) from vacuum stability is relevant. The latter constraint is most relevant in case of light staus, which is optionally the case in some scenarios. Exceptions to the estimate for  $\Delta a_\mu$  can arise in cases with ultra-large  $\tan\beta$  or  $\mu$ , as discussed in Sec. 5.2.5.

stops  $m_{\tilde{t}}$  and the left-right stop mixing parameter  $x_t = (A_t - \mu^* / \tan\beta) / m_{\tilde{t}}$ . The approximation reads

$$M_h^2 \approx M_Z^2 + \frac{1}{8\pi^2} \frac{m_t^4}{v^2} \left[ 24 \ln \left( \frac{M_S}{m_t} \right) + x_t^2 (12 - x_t^2) \right]. \quad (5.58)$$

First, the formula illustrates a unique hallmark of SUSY theories in that the Higgs-boson mass becomes a prediction instead of an input parameter, and the prediction is of the order of  $M_Z$ , in agreement with observation. Second, in order to obtain quantitative agreement between experiment and the MSSM prediction, the tree-level value  $M_Z$  must be shifted by very large quantum corrections. It turns out that Eq. (5.58), improved using state-of-the-art calculations, reproduces the measurement in Eq. (5.57) e.g. if either the stop masses are as heavy as  $\mathcal{O}(10 \text{ TeV})$  leading to a large logarithm, or if the stop masses are approximately  $\mathcal{O}(3 \text{ TeV})$  and there is large stop mixing,  $|x_t| \approx \sqrt{6}$ , maximising the polynomial in  $x_t$ . In specific models of SUSY breaking there exist relations between smuon masses and stop masses. In such models, the constraints on the Higgs mass can imply lower mass limits on smuons and thus impact the possible values of  $a_\mu$ . We will discuss examples e.g. in Secs. 5.2.4, 5.2.5 below.

Observables which are more directly connected to  $a_\mu$  are leptonic dipole observables such as electric dipole moments and CLFV processes like  $\mu \rightarrow e\gamma$ . In the MSSM, the relationship between  $a_\mu$  and these other dipole observables is a prime example of the general discussion of Sec. 3.2: either  $\Delta a_\mu^{\text{SUSY}}$  must be tiny or the SUSY parameters must be CP and flavour conserving to a high degree. For this reason we will set such CPV and CLFV parameters to zero in most of the subsequent discussions but provide a short summary here.

In the MSSM, the dipole operators are chirally enhanced and satisfy naive scaling unless the slepton mass terms are very hierarchical [235, 252]. In principle, CP can be violated by complex phases of the Higgsino and gaugino masses  $\mu$ ,  $M_{1,2,3}$  in a flavour-independent way, and lepton flavour can be violated by off-diagonal elements of the mass matrices  $m_{i,\tilde{e}}^2$  or the trilinear interactions  $A_e$ . The MSSM correlations between  $a_\mu$  and the electron EDM and  $\mu \rightarrow e\gamma$  have been

investigated in detail in Refs. [237, 716, 822, 823] and [690, 752, 824–827], and the results are fully in line with the general discussion of Sec. 3.2: e.g. Ref. [823] finds (using a slightly weaker EDM bound than the one in Eq. (3.20a)) the implication

$$\text{if } \Delta a_\mu^{\text{SUSY}} \approx 10 \times 10^{-10} \quad \text{then } d_e \text{ and Eq. (3.20a) imply} \quad |\arg(\mu M_{1,2})| \lesssim 10^{-5} \quad (5.59)$$

under rather wide conditions. Similarly, e.g. Fig. 13 of Ref. [752] can be used to read off the constraint

$$\text{if } \Delta a_\mu^{\text{SUSY}} \approx 10 \times 10^{-10} \quad \text{then } \mu \rightarrow e\gamma \text{ and Eq. (3.21a) imply} \quad \left| \frac{m_{i,12}^2}{\sqrt{m_{i,11}^2 m_{i,22}^2}} \right| \lesssim 2 \times 10^{-4} \quad (5.60)$$

on the left-handed slepton mixing matrix, provided all relevant SUSY masses are approximately within a factor 2 of each other. Similarly rescaled results hold for other values of  $\Delta a_\mu^{\text{SUSY}}$ , and complex phases and flavour mixing of  $\mathcal{O}(1)$  are only possible if  $\Delta a_\mu^{\text{SUSY}}$  is many orders of magnitude below the experimental sensitivity.

Similar analyses have been applied to the specific case where the MSSM is extended to include neutrino masses and mixings, and slepton mixing is correlated to neutrino mixing [828–831]. These references find concrete SUSY models where neutrino mixing and bounds require only small slepton mass mixing and small CP violating phases. Nevertheless, they also show that in many particularly straightforward scenarios the non-observation of CLFV implies small  $\Delta a_\mu$ , hence the current result  $\Delta a_\mu^{\text{Exp-WP2025}}$  significantly opens up the parameter space of such models.

Finally we briefly mention that several studies [832–840] investigated whether the MSSM can accommodate simultaneously the significant previous deviation  $\Delta a_\mu^{\text{Exp-WP2020}}$  and the deviation in  $a_e$  between Eqs. (3.16) and (3.17a) present at the time before the appearance of Ref. [55]. Explaining both is challenging in the MSSM because the signs of the two deviations was opposite and the magnitudes did not follow naive scaling, hence sfermion mass parameters would have to be chosen in a very non-universal way. Similarly, it was investigated whether sizeable contributions  $a_\mu$  and positive shifts of the  $W$ -boson mass  $M_W$  are compatible. Under broad conditions, the MSSM was found to be unable [841–843] to accommodate the CDF measurement of the  $W$ -boson mass with the very high value  $M_W^{\text{CDF}} = 80.4335(94)$  GeV [844], which is however in tension with other measurements and excluded from the global average in Ref. [104], see also the discussion in Sec. 3.4.

#### 5.2.4. Baseline SUSY scenarios

If the MSSM is realised in nature, it is expected that the soft SUSY breaking parameters are effectively generated from some underlying dynamics involving spontaneous SUSY breaking. In this case the soft breaking parameters become correlated and functions of more fundamental parameters. Here we collect a few of the most discussed and simplest such scenarios. They are interesting in their own right and provide a baseline for phenomenological discussions and for understanding the literature. It is, however, important to note that each of them could be modified and generalised, and that SUSY could also be realised in quite different ways. Our discussion follows the review Ref. [672], where further details and original references can be found.

One well known scenario is called the Constrained MSSM (CMSSM) or minimal supergravity (mSUGRA), see e.g. Ref. [670]. Here the fundamental theory is assumed to be supergravity, where local SUSY is spontaneously broken in a hidden sector and where gravitational interactions mediate the SUSY breaking into the MSSM sector, leading to effective soft SUSY breaking terms. In the minimal setup it is assumed that the running soft parameters become universal

at a high scale around the GUT or Planck scale. The CMSSM thus has the free SUSY parameters

$$m_0, m_{1/2}, A_0, \tan \beta, \quad (5.61)$$

where  $m_{0,1/2}$  correspond to the unified scalar and gaugino masses at the high scale, and  $A_0$  to the unified  $A$ -parameters. Further parameters such as the Higgsino mass  $\mu$  and the Higgs mass spectrum are then predicted. As an example, the running soft parameters at the TeV-scale can then be approximated as [845]

$$m_l^2 \approx m_0^2 + 0.5m_{1/2}^2, \quad (5.62)$$

$$m_e^2 \approx m_0^2 + 0.15m_{1/2}^2, \quad (5.63)$$

$$m_{\bar{q}}^2 \approx m_0^2 + 6.5m_{1/2}^2, \quad (5.64)$$

$$m_{\bar{u}}^2 \approx m_0^2 + 6m_{1/2}^2, \quad (5.65)$$

$$m_{\bar{d}}^2 \approx m_0^2 + 6m_{1/2}^2, \quad (5.66)$$

$$M_{1,2,3} \approx \frac{\alpha_{1,2,3}}{\alpha_{\text{GUT}}} m_{1/2}, \quad (5.67)$$

where the  $\alpha_i$  in the last equation are GUT-normalised finestructure constants, which result in the gaugino mass pattern

$$M_1 : M_2 : M_3 \approx (1 : 2 : 6) 0.4 m_{1/2}. \quad (5.68)$$

This means that a pattern emerges between the different gaugino and scalar masses, where the coloured gluinos and squarks are the heaviest sparticles, while the sleptons, Bino and Wino are lighter by fixed factors.

Phenomenologically, the CMSSM is constrained by the very strong LHC mass limits on gluinos and squarks, where particularly the gluino mass limits imply robust lower limits on the Bino and Wino masses of the order  $M_2 \approx 2M_1 \gtrsim 1$  TeV. Further, the Higgs-boson mass  $M_h \approx 125$  GeV requires heavy stops or large mixing, and the  $\mu$ -parameter is a dependent quantity. All of these constraints imply rather large masses and thus constraints on the contributions to  $a_\mu$ , see Fig. 5.11 as well as on the possibilities to accommodate the dark matter relic density (DMRD). The remaining CMSSM parameter space corresponds to scenarios 4, 5 or 6 in Tab. 5.2. As a result, the CMSSM is incompatible with very large contributions to  $a_\mu$ , as already found in global fits after the first LHC runs [846–849]. The more recent update [850] finds the maximum values

$$\Delta a_\mu^{\text{CMSSM}} \begin{cases} < 2 \times 10^{-10} & \text{(DMRD fully explained),} \\ < 4 \times 10^{-10} & \text{(DMRD not overabundant).} \end{cases} \quad (5.69)$$

In view of the progress on  $a_\mu$  leading to the result  $\Delta a_\mu^{\text{Exp-WP2025}}$  in Eq. (1.5), the CMSSM prediction is actually well in agreement with observations and thus constitutes a viable scenario for SUSY.

In the literature, many extensions of the CMSSM were proposed and investigated. Some of them were partially motivated by the previous large deviation  $\Delta a_\mu^{\text{Exp-WP2020}}$ . For instance, a simple generalisation is to relax only the unification between the three gaugino masses, such that  $M_{1,2,3}$  become a independent input parameters while other GUT constraints still apply. This is sufficient to allow large values of  $\Delta a_\mu^{\text{SUSY}} \sim 20 \times 10^{-10}$  together with explaining the dark matter via Bino-like LSP with slepton coannihilation in the few-100 GeV mass region [747, 753, 761, 850–857], even in the “no-scale” special case where  $m_0$  is negligible [858]. The LHC and DMDD constraints can also be fulfilled [850, 853–855, 858], and some scenarios can also be augmented to SO(10) GUTs where even 3rd generation Yukawa couplings unify [720]. Similarly, relaxing the unification between  $M_1$  and  $M_2$  also allows the cases of Higgsino-like or Wino-like LSP [859].

Interestingly, relaxing only the unification between the scalar masses is not always sufficient to open the parameter space and allow sizeable  $\Delta a_\mu^{\text{SUSY}}$ . E.g. the SU(5) GUT motivated unification into four different scalar masses  $m_{10}$ ,  $m_5$ ,  $m_{H_u}$ ,  $m_{H_d}$  for each kind of GUT multiplet is not sufficient [860]. In contrast, again sizeable contributions to  $a_\mu$  are possible provided at least the 3rd-generation sfermions are disunified from the other sfermions [749, 765, 857, 861–863], though Ref. [863] finds strong constraints from dark matter unless also gaugino masses are disunified. Similarly, the gaugino and scalar mass patterns corresponding to so-called flipped SU(5) allow sizeable  $\Delta a_\mu^{\text{SUSY}}$  [864–866]. Further GUT-inspired extensions of the CMSSM with sizeable  $\Delta a_\mu$  are based on the left-right symmetric Pati-Salam gauge group [766] (here, also flavour symmetry is considered and light Winos are preferred), or Pati-Salam symmetry with specific Higgs sector [831, 867] (which is compatible with Bino-like LSP explaining the dark matter relic density).

A second class of basic scenarios is gauge-mediated SUSY breaking [868]. Though this also assumes an underlying supergravity theory and a hidden sector, the interactions producing the soft SUSY breaking terms are the known and renormalizable  $SU(3)_c \times SU(2)_L \times U(1)_Y$  gauge interactions. In the minimal setup (mGMSB), a set of  $N_5$  messenger fields which form complete SU(5) GUT multiplets and thus couple to all quark, lepton and gauge fields is assumed. The basic parameters are then

$$N_5, M_{\text{mess}}, F_Z/A_Z, \tan \beta, \quad (5.70)$$

where  $M_{\text{mess}}$  is the messenger mass,  $F_Z, A_Z$  are *vevs* relevant for SUSY breaking in the hidden sector. Computing the effective MSSM soft SUSY breaking parameters in mGMSB leads to patterns of scalar masses which differ from the CMSSM case, while the gaugino mass pattern turns out to be the same,

$$m_{\tilde{F}}^2 = 2 \left( \frac{F_Z}{A_Z} \right)^2 N_5 \sum_{i=1,2,3} C_i(F) \left( \frac{\alpha_i}{4\pi} \right)^2 \quad (\tilde{F} \in \{\tilde{q}, \tilde{u}, \tilde{d}, \tilde{l}, \tilde{e}\}), \quad (5.71)$$

$$M_{1,2,3} = \frac{\alpha_{1,2,3}}{4\pi} \frac{F_Z}{A_Z} N_5. \quad (5.72)$$

The values of the Casimir invariants  $C_i(F)$  can be found e.g. in Ref. [672]. The above equation is imposed for the running parameters at the scale  $M_{\text{mess}}$ , and running according to MSSM  $\beta$  functions is used to compute the final values of the soft breaking parameters at the TeV scale.

A big advantage of mGMSB is that the flavour universality of the gauge interactions automatically implies that the scalar masses are flavour universal, thus avoiding large unobserved flavour violating effects, see Sec. 5.2.3. This is in contrast to the CMSSM scenario where the assumption of flavour universality, leading to the parameter  $m_0$ , is ad hoc. At the same time, the  $A$ -parameters turn out to vanish in the mGMSB scenario. Because of this, however, the mixing left-right mixing in the stop sector is very small, and the Higgs-boson mass  $M_h \approx 125$  GeV can only be accommodated for stop masses of at least around 10 TeV. As a result the slepton masses are very large and contributions to  $a_\mu$  are tiny in mGMSB. A broad parameter scan in Ref. [869] shows that

$$\Delta a_\mu^{\text{mGMSB}} < 0.5 \times 10^{-10} \quad (5.73)$$

if the Higgs-boson mass is correctly accommodated in the mGMSB scenario. This upper limit is even smaller than the one in the CMSSM in Eq. (5.69), but it is also in agreement with the current status given in Eq. (1.5). Hence the mGMSB scenario is viable in view of  $a_\mu$ , and we refer to the literature for further properties of the scenario with respect to dark matter and LHC data.

Given the very rigid correlations in mGMSB and the tiny prediction (5.73) it might seem less promising to obtain larger values in generalisations of the mGMSB setup. Still, Refs. [869–871] have considered generalisations of mGMSB where

the messenger sector is non-minimal, leading to an increased freedom in the relationships between squark, slepton and gaugino masses. The resulting SUSY breaking mechanisms are viable, can explain the absence of observed CP-violating or CLFV effects, can lead to rather light Wino and Higgsino. The scenarios can also lead to significant  $\Delta a_\mu^{\text{SUSY}}$  and are thus constrained by the small current value  $\Delta a_\mu^{\text{Exp-WP2025}}$ . Also, Ref. [872] uses standard SU(5) GUT unification conditions in conjunction with gauge-mediated SUSY breaking and finds viable parameter space and also potentially sizeable  $\Delta a_\mu^{\text{SUSY}}$ . However, it also quantifies a tension between proton decay constraints and  $a_\mu$  where smaller values of  $\Delta a_\mu$  as preferred now widen the allowed parameter space for the fundamental SUSY breaking mechanism.

A third basic scenario of SUSY breaking is called anomaly-mediated SUSY breaking (AMSB) [873, 874]. Here the mediation mechanisms present in the CMSSM and mGMSB are assumed to be absent, and what remains are universally present contributions governed by the superconformal anomaly, i.e. by the existence of non-vanishing  $\beta$  functions. As a result, the gaugino masses satisfy the pattern

$$M_1 : M_2 : M_3 = \beta_1 : \beta_2 : \beta_3 \approx 3.3 : 1 : 9. \quad (5.74)$$

The importance of the modified gaugino mass patterns has also been stressed in Ref. [875]. In the very minimal AMSB setup, the slepton masses turn out to be tachyonic, which rules out the setup [672]. Extended models have been constructed, however, and these can lead to interesting spectra where the phenomenology differs substantially from the cases of the CMSSM or mGMSB. For instance, in Ref. [876], AMSB with the gaugino relation Eq. (5.74) and resulting Wino-like LSP is analysed. Changing the minimal setup for the scalars generates a viable scenario, where the Wino-LSP and the sleptons can have masses as low as about 700 GeV and  $\Delta a_\mu^{\text{SUSY}}$  can reach more than  $20 \times 10^{-10}$ . A further generalisation allowing modified gaugino mass patterns is considered in Ref. [877], such that also a Bino-like LSP and very large  $\mu$  becomes possible, again leading to sizeable  $\Delta a_\mu^{\text{SUSY}}$ .

In what follows, we will comment on the phenomenology in scenarios motivated by these and further model-building efforts, but also on the general MSSM phenomenology.

### 5.2.5. Phenomenological results for heavy sparticles in the MSSM

Here and in the following subsections we discuss the SUSY  $a_\mu$  phenomenology in more detail. We will consider models with high-scale constraints as discussed in Sec. 5.2.4 as well as the general MSSM, where we only impose assumptions on parameters mentioned in Sec. 5.2.1. Here we will begin with heavy SUSY, essentially corresponding to the upper right quadrant of the plot in Fig. 5.11, delineated by the black lines. For smuon masses above 700 GeV and chargino masses above 1100 GeV the LHC limits are trivially fulfilled for arbitrary mass splittings, see Sec. 5.2.3. As a simple guideline, Fig. 5.11 shows that

$$\Delta a_\mu^{\text{SUSY,max}}(\tan \beta = 40, m_{\text{LSP}} \geq 1 \text{ TeV}) < 10 \times 10^{-10}. \quad (5.75)$$

As mentioned in Sec. 5.2.4, several of the well-known SUSY scenarios such as the CMSSM or mGMSB can accommodate the current LHC and  $M_h$  constraints only for rather heavy SUSY particles, and they thus predict small  $\Delta a_\mu^{\text{SUSY}}$ ; concrete values are given in Eqs. (5.69,5.73). These small values are now compatible with the small current  $\Delta a_\mu^{\text{Exp-WP2025}}$ . The observed dark matter can also be accommodated in such scenarios, such as the CMSSM with Bino-like LSP with in a so-called funnel region where the Higgs mass  $M_A \approx 2m_{\text{LSP}}$  or with Higgsino-like LSP with  $m_{\text{LSP}} \approx 1 \text{ TeV}$  [343, 798, 878]. In this way, such simple scenarios re-emerge as well motivated potential realisations of SUSY, although the recent DMDD

bounds from the LZ experiment exclude significant portions of the parameter space [350].<sup>57</sup>

In general, even independently of the CMSSM or similar setups, the scenarios with Higgsino-like LSP with mass around 1 TeV or Wino-like LSP with mass around 2–3 TeV are very attractive: These scenarios lead to explanations of the observed dark matter relic density without further tuning of masses or mass splittings and can be realised in the constrained MSSM or in more general variants of the MSSM (see e.g. Ref. [343]). They are listed as scenarios 5, 7 in Tab. 5.2. However, all such scenarios restrict  $\Delta a_\mu^{\text{SUSY}}$  to very small values (actually much smaller than visible in Eq. (5.75) because of dark matter constraints) and are thus compatible with observation but not constrained by  $\Delta a_\mu^{\text{Exp-WP2025}}$ .

It is interesting to note that there exist heavy SUSY scenarios with rather large contributions to  $a_\mu$ . They are not visible in the plot of Fig. 5.11, but they involve ultra-high values of  $\tan\beta$  or of  $\mu$ . In both cases the linearity in  $\tan\beta$  and  $\mu$  visible in Eqs. (5.44) is replaced by a saturation resulting from resummed higher-order effects as illustrated in Eq. (5.51). And the vacuum stability constraint related to the off-diagonal slepton mass matrix elements and illustrated in Eq. (5.47) implies upper limits on the combination  $\mu \tan\beta$ . Such extreme parameter regions have been studied in several directions.

First, by increasing primarily the Higgsino mass parameter  $\mu$ , the BLR contribution to  $a_\mu$  becomes dominant since it is the only one without Higgsino propagators. It is then possible to analyse the overall maximum possible value of the BLR contribution by maximising  $\mu$  for any given value of the smuon and Bino masses [724–726]. It turns out that  $\Delta a_\mu^{\text{SUSY}}$  as large as  $25 \times 10^{-10}$  is possible even if the LSP mass is around 1 TeV. More generally, Ref. [726] finds e.g.

$$\Delta a_\mu^{\text{SUSY,BLR,max}} = \begin{cases} 25 \times 10^{-10} & \text{for } m_{L,R} = M_1 = 1 \text{ TeV} \\ 25 \times 10^{-10} & \text{for } m_{L,R} = 1.2 \text{ TeV}, M_1 = 600 \text{ GeV} \\ 25 \times 10^{-10} & \text{for } m_{L,R} = m_{\tilde{\tau}} = M_1 = 250 \text{ GeV} \end{cases} \quad (5.76)$$

where in the first two lines the stau masses are assumed to be large and irrelevant for vacuum stability and the last line is included as a contrast in case of degenerate stau/slepton masses. It has also been found that a ratio  $m_L = m_R$  is optimal for large contributions; similar limits also exist in the NMSSM [879]. Such a scenario with ultra-large  $\mu$  and TeV-scale Bino has also been investigated in Ref. [880], which showed that dark matter can be accommodated if— as motivated by gauge-mediated SUSY breaking — the MSSM neutralinos decay into a lighter gravitino which constitutes dark matter.

Second, by increasing  $\tan\beta$  to ultra-large values a similar behaviour can be obtained, provided  $\tan\beta$  becomes large enough to compensate a loop factor such that the muon mass correction  $\Delta_\mu$  becomes of  $\mathcal{O}(1)$ , see Eqs. (5.49) [228, 727, 728]. The limit  $\tan\beta \rightarrow \infty$  exists if the resummation Eq. (5.51) is taken into account, but it leads to a larger variety of contributions than the large- $\mu$  limit.

The actual  $\tan\beta \rightarrow \infty$  limit is appealing since it corresponds to  $v_d = 0$  and vanishing tree-level muon mass, and thus to one way to realise radiative muon mass generation in the MSSM [228]. The mass is generated via the one-loop coupling of the muon to the “wrong” Higgs  $vev v_u$ , described by the quantity  $\Delta_\mu$ . Thanks to the resummation in Eqs. (5.51,5.52), the final result for  $\Delta a_\mu^{\text{SUSY}}$  in this scenario becomes a ratio of the form 1-loop/1-loop, like the generic examples of Sec. 3.1. Many factors and sign dependences cancel between numerator and denominator, and the final result mainly depends on

---

<sup>57</sup>Comparing the CMSSM predictions in Ref. [798] with the LZ limit appears to essentially exclude the entire Higgsino-like dark matter region of the CMSSM, although a detailed analysis is lacking.

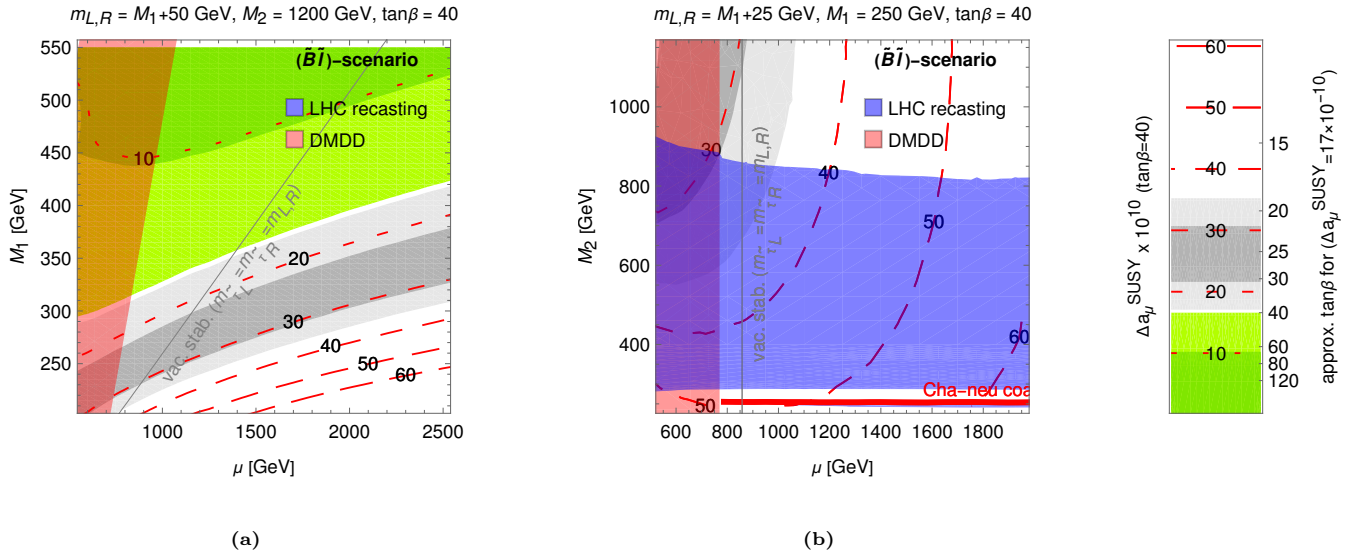


**Figure 5.12:** MSSM in the  $(\tilde{B}I)$ -scenario with Bino-like LSP and light sleptons. In the plots either  $M_2 = 1200$  GeV is fixed or  $M_1 = 250$  GeV is fixed, and the remaining chargino and slepton masses are varied. For the exact parameter values see the plots. The meaning of the red dashed lines, the green/grey coloured  $\Delta a_\mu^{\text{SUSY}}$  regions, and the reinterpretation in the legend plot are as in Fig. 5.11. The red shaded regions are excluded by dark matter direct detection if the LSP is assumed stable; the blue shaded region corresponds to LHC limits, see text for details. The red thick solid line in the right plot corresponds to the parameter strip where chargino–neutralino coannihilation is possible; directly below this strip a tiny region is excluded by the LHC-constraint from compressed masses, Ref. [449], but we verified that this does not exclude the chargino–neutralino coannihilation region. The grey thin line corresponds to the vacuum stability constraint of Ref. [724], see Eq. (5.47); it applies in case the left- and right-handed stau-masses are set equal to the smuon/selectron masses and excludes the points to the right, i.e. with larger  $\mu$ .

which of the contributions dominate. Ref. [228] finds e.g. the approximations

$$\Delta a_\mu^{\text{SUSY}, \tan \beta \rightarrow \infty} \approx \begin{cases} -72 \times 10^{-10} \left( \frac{1 \text{ TeV}}{M_{\text{SUSY}}} \right)^2 & \text{for } |\mu| = |M_2| = |M_1| = m_L = m_R \equiv M_{\text{SUSY}}, \\ +37 \times 10^{-10} \left( \frac{1 \text{ TeV}}{M_{\text{SUSY}}} \right)^2 & \text{for } m_L \gg |\mu| = |M_1| = m_R \equiv M_{\text{SUSY}}. \end{cases} \quad (5.77)$$

Here the first result corresponds to universally equal SUSY masses and is negative definite, the second case is positive definite and corresponds to heavy  $m_L$ , where the BHR contribution to  $a_\mu$  dominates. For heavy  $\mu$  and  $\tan \beta \rightarrow \infty$ , the result of Eq. (5.76) is recovered.

The common feature of both the large- $\mu$  and  $\tan \beta \rightarrow \infty$  limits is the strong modification of the muon mass generation mechanism. Two further scenarios with different modifications which also allow large  $\Delta a_\mu^{\text{SUSY}}$  for heavy SUSY masses are proposed in Refs. [229–231, 881, 882]. The first of these ideas is to realise radiative muon mass generation by setting the Yukawa coupling  $y_\mu = 0$  while keeping  $v_d \neq 0$  [229–231] and generating  $m_\mu$  via loops involving non-standard soft SUSY breaking parameters. The second idea is to introduce additional Higgs doublets into the theory [881]. In this way the  $\tau$ -lepton mass is obtained from a different  $vev$  than the muon mass, hence effectively different  $\tan \beta$ 's apply in the two sectors, which allows having larger effective  $\tan \beta_\mu^{\text{eff}}$  in the muon sector than in the tau sector, alleviating e.g. vacuum stability constraints while keeping agreement with the observed Higgs-boson mass [882]. All of these proposals can lead to contributions to  $a_\mu$  of similar magnitude as Eqs. (5.76, 5.77).

### 5.2.6. Phenomenological results with light Bino-like LSP in the MSSM

Next we consider the  $a_\mu$  phenomenology of lighter SUSY particles in connection with LHC and dark matter data, here focusing on the case of a Bino-like neutralino LSP. Mass spectra with Bino-like LSP are frequently studied and well motivated by the gaugino mass constraint  $M_1 \approx M_2/2$  of the CMSSM, mGMSB or many of their extensions, see Sec. 5.2.4. In particular, the case of Bino-like LSP has been analysed in view of LHC run-II data and the significant  $a_\mu$  deviation already before the Fermilab  $g-2$  experiment in Refs. [770, 774–778], in Refs. [774, 775, 777, 778] also including dark matter; after the Fermilab  $g-2$  Run-1 result, Refs. [9, 739, 779–785] presented further very detailed general analyses, partially also including other scenarios.<sup>58</sup> Here we summarise the status.

The mass range of interest is  $M_1$  in the few-100 GeV region, while some slepton and/or chargino masses are below the 700 and 1100 GeV limits used in Sec. 5.2.5 to characterise heavy SUSY. The Bino-like LSP is neutral and stable, hence a dark matter candidate. In general, the considered mass region leads to small annihilation cross sections and thus to a relic density which is too large, unless one of the following coannihilation mechanisms is possible [343], see also scenarios 1, 2, 3 in Tab. 5.2:

- Slepton coannihilation, where one or several sleptons (possibly also staus) are very close in mass to the LSP;
- Stau coannihilation, where one or two staus are very close in mass (but the sleptons significantly heavier) to the LSP;
- Wino coannihilation, where the Wino-like neutralino and chargino are very close in mass to the LSP.

Intriguingly, in each case the coannihilation partner is hidden from LHC because of the small mass splitting (exceptions may arise in the very-low mass region below around 200 GeV where dedicated compressed-mass searches are relevant). Hence the coannihilation mechanisms are essentially unconstrained by LHC. The masses of further SUSY particles, however, are important for  $a_\mu$  and constrained by LHC, dark matter and other considerations.

The interplay of constraints is illustrated in Fig 5.12, which updates results of Ref. [9] for the Bino-LSP scenario with additionally light sleptons evading LHC limits. The left plot Fig. 5.12a shows results in the  $\mu$ - $M_1$ -plane. The Wino mass is fixed to the rather high value  $M_2 = 1200$  GeV, safely but not too far above the maximum LHC chargino mass limit (5.55); the mass splitting is fixed to the reference value  $m_{L,R} - M_1 = 50$  GeV. The right plot Fig. 5.12b shows results in the  $\mu$ - $M_2$ -plane, while the Bino and slepton masses are fixed to the rather light values  $M_1 = 250$  GeV and  $m_{L,R} = 275$  GeV. The plots are evaluated for  $\tan\beta = 40$ , but most quantities except  $a_\mu$  do not strongly depend on  $\tan\beta$ .

Along the thick red strip in the right plot, Wino-coannihilation takes place and generates the correct DMRD. Outside of this strip, both plots are not very sensitive to the precise choice of the slepton and stau masses, so the plots are representative for a wider range of values for  $m_{L,R} - M_1$ ; in particular it would be possible to finetune the values of the slepton and stau masses to fit the correct DMRD everywhere (but the finetuning is not unique and hence not done [9]).

Assuming now that the relic density is correctly explained, the constraints from direct detection experiments are shown as the (light) red shaded bands; they exclude a large portion of the parameter space with small  $\mu$ , corresponding to the bound given in Eq. (5.53) in Sec. 5.2.3. Hence the Higgsino mass must be rather large. There is, however, also a potential upper limit on the Higgsino mass, shown as the thin solid grey line in the plots. It corresponds to the vacuum stability constraint of Ref. [724] on stau-mixing already explained around Eq. (5.47). It excludes the large- $\mu$  region to

<sup>58</sup>We refer to Ref. [9] for more detailed comments on comparisons between these studies.

its right under the condition that both left- and right-handed stau masses are as light as the smuon/selectron masses. This upper limit on  $\mu$  thus applies in particular if stau-coannihilation and  $m_{\tilde{\tau}_L} \approx m_{\tilde{\tau}_R}$  is assumed. Conversely, the region to the right of the grey line is allowed provided at least one stau is significantly heavier. Further, in interpreting the interplay between the DMDD limit and the vacuum stability limit on  $\mu$  one should note that the vacuum stability limit essentially constrains  $\mu \tan \beta$ , while the DMDD limit has a mild sensitivity on  $\tan \beta$ . Hence for smaller  $\tan \beta$ , the allowed region for  $\mu$  widens considerably even in case of light staus.

This discussion also changes in case of negative sign of  $M_1$ , where there are cancellations in the DMDD cross section, also allowing smaller  $\mu$  [793–795]. The parameter space considered in these references corresponds to the Wino-coannihilation region of Fig. 5.12b, but with smaller allowed  $\mu$ , which can alleviate electroweak finetuning. We also refer to Ref. [883] for a study of the Bino-slepton scenario in a simplified setup without the additional MSSM fields.

LHC-constraints obtained as described in Ref. [9] are displayed by the blue shaded region in the plots. The parameter space of the left plot Fig. 5.12a is entirely allowed. The right plot Fig. 5.12b shows a large excluded region approximately for  $300 \text{ GeV} < M_2 < 900 \text{ GeV}$ . Here the channel of Wino-like chargino/neutralino production with decay into sleptons is relevant. An additional strip of parameter space at around  $M_2 \approx M_1 - 5 \text{ GeV}$  (in which case the mass eigenvalues satisfy  $m_{\chi_1^\pm} - m_{\chi_1^0} \approx 15 \text{ GeV}$ ) is excluded by dedicated compressed-mass searches.

Before discussing  $a_\mu$  constraints, we highlight that in the plots we can identify the three generally viable parameter regions mentioned above, corresponding to the three ways to accommodate dark matter (scenarios 1, 2, 3 in Tab. 5.2): Wino coannihilation is possible along the thick red strip; stau/slepton coannihilation with equal stau and slepton masses is possible to the left of the grey vacuum stability constraint, with either very light or very heavy Wino, and slepton coannihilation with heavy staus is the only option to the right of the vacuum stability constraint at very large  $\mu$ .

On this parameter space, the red dashed lines and the green coloured regions show the contours of  $a_\mu$  for  $\tan \beta = 40$  and the allowed region corresponding to the new result  $\Delta a_\mu^{\text{Exp-WP2025}}$ . To guide the eye, the  $1/2\sigma$  regions corresponding to the old result  $\Delta a_\mu^{\text{Exp-WP2020}}$  are shown in grey. The behaviour of  $a_\mu$  in this Bino-LSP scenario with light sleptons is dominated by the WHL and BLR contributions of Eqs. (5.44) and can be well understood via these approximations. The WHL contributions dominate in the left plot at large  $M_1$  and very small  $\mu$  and in the right plot at  $\mu \lesssim 1 \text{ TeV}$ ; in these regions  $\Delta a_\mu^{\text{SUSY}}$  decreases with increasing  $\mu$ . The BLR contributions are linearly enhanced by  $\mu$  and dominate at large  $\mu$  in both plots. As the plots show very large  $\Delta a_\mu^{\text{SUSY}}$  can be obtained both for large  $\mu$ , where the BLR-contribution dominates, and for small  $\mu$  with WHL-dominance.

The results for  $a_\mu$  illustrate why this parameter region was considered a promising explanation of the old deviation (1.6). Now, the small value of  $\Delta a_\mu^{\text{Exp-WP2025}}$  places tight bounds on the parameter space. For fixed  $\tan \beta = 40$ , the masses must be rather large; smaller masses are allowed for smaller values of  $\tan \beta$ . For instance, the Wino-coannihilation region in the right plot is compatible with  $\Delta a_\mu^{\text{Exp-WP2025}}$  only for small  $\tan \beta \lesssim 15$  at the  $2\sigma$  level, as can be read off with the help of the legend plot.

As mentioned above, the same parameter region is investigated in a number of further references, with similar results. From large scans of the parameter space, Refs. [777, 780, 781] find that slepton as well as Wino coannihilation is possible for LSP masses in the wider range around

$$m_{\chi_1^0} \approx 130 \dots 500 \text{ GeV}, \tag{5.78}$$

and Ref. [784] argues that the scenario leads to moderate electroweak finetuning.

If sleptons are heavier than considered in Fig. 5.12, there are several relevant considerations. First, the LHC constraints

become stronger and exclude sleptons up to about 600 GeV for realistic scenarios [783], slightly less than the limit obtained by LHC for simplified models and quoted in Sec. 5.2.3. Second, there are significant dark matter constraints. A viable way to explain dark matter in the general parameter region with Bino-like LSP and heavier sleptons is Wino coannihilation [9, 780, 781]. An alternative way can be stau coannihilation in case the stau masses are not unified with the slepton masses. However, there are significant LHC constraints on chargino masses [783], which in case of stau coannihilation and light stau require at least one rather heavy chargino [9, 782]. The case where the left- and right-handed slepton masses are different has been considered in several references, and particularly Refs. [739, 783] have considered the extreme case where one of the two slepton chiralities decouples,  $m_L \rightarrow \infty$  or  $m_R \rightarrow \infty$ , such that only the BHL or BHR contributions to  $a_\mu$  survive. They find that dark matter data already excludes such scenarios with Bino-like LSP and significant  $a_\mu$ .

The recent model-building literature has put forward a variety of constructions leading to potentially large  $a_\mu$  with mass spectra of the kind of Fig. 5.12. First, simple extensions of baseline scenarios such as the CMSSM [747, 749, 753, 761, 765, 850–858, 861, 862, 864–867] or AMSB [877], mentioned in Sec. 5.2.4, can often lead to Bino-like LSP in combination with light sleptons and very heavy  $\mu$ , thus allowing large contributions to  $a_\mu$  via BLR- and WHL-contributions. Also, going beyond the baseline scenarios, dedicated constructions of SUSY breaking and mediation mechanisms were proposed in Refs. [863, 884–887]. The common feature of these constructions is the motivation to naturally explain heavy coloured SUSY particles and the heavy Higgs mass  $M_h$ , while allowing light sleptons and light Bino. A by-product of these constructions tends to be very large  $\mu$  in the multi-TeV region, which can lead to large BLR contributions to  $a_\mu$ .

The scenario with large  $\mu$  in the multi-TeV region also appears in the context of various specific model constructions, such as models based on Pati-Salam symmetry [766, 831, 867] or on SO(10) [720], or models with usual GUT constraints but extra vector-like matter fields [772, 888]. All mentioned scenarios are intrinsically motivated; the current constraint  $\Delta a_\mu^{\text{Exp-WP2025}}$  then imposes stringent lower mass limits, or equivalently stringent upper  $\tan\beta$  limits of the kind visible in Fig. 5.12.

Quite different scenarios with Bino-like LSP but small  $\mu$ , small  $M_2$  and heavier sleptons have been considered e.g. in Refs. [770, 889, 890]. Given the dark matter constraints, these scenarios are now strongly constrained.

### 5.2.7. Phenomenological results with light Higgsino- or Wino-like LSP in the MSSM

Now we focus on the  $a_\mu$  phenomenology in the MSSM with Wino- or Higgsino-like LSP. For masses above 2 TeV or 1 TeV, respectively, the full DMRD can be explained, see Sec. 5.2.3. Here we consider lighter masses considered here, such that the DMRD is below the observed one, see scenarios 6, 8 in Tab. 5.2. The underabundant DMRD is compatible with observations, although additional dark matter candidates from beyond the MSSM are required.

We illustrate the scenarios in Fig. 5.13. To discuss the parameter choices and results we first note that Wino- or Higgsino-like LSP are neutralinos which are accompanied by at least one chargino close in mass. Hence the LSP mass is directly constrained by dedicated LHC searches for such compressed neutralino–chargino pairs; above around 200 GeV such constraints become ineffective.

For the sleptons, the LHC constraints exclude a triangular  $m_{\tilde{t}}-m_{\chi_1^0}$  region; for LSP masses below around 200 GeV, either slepton masses above around 400–500 GeV or close to the LSP are allowed, and for LSP masses above 200 GeV, the slepton mass limits become weak [778]. Hence the plots in Fig. 5.13 show LSP mass parameters  $M_2, \mu$  above 200 GeV and choose the slepton masses  $m_{L,R}$  very close, just 50 GeV above  $M_2$  or  $\mu$ , respectively, in order to maximise the contributions to  $a_\mu$ . Among all mass hierarchies between the Wino, the Higgsino and the sleptons, the hierarchy

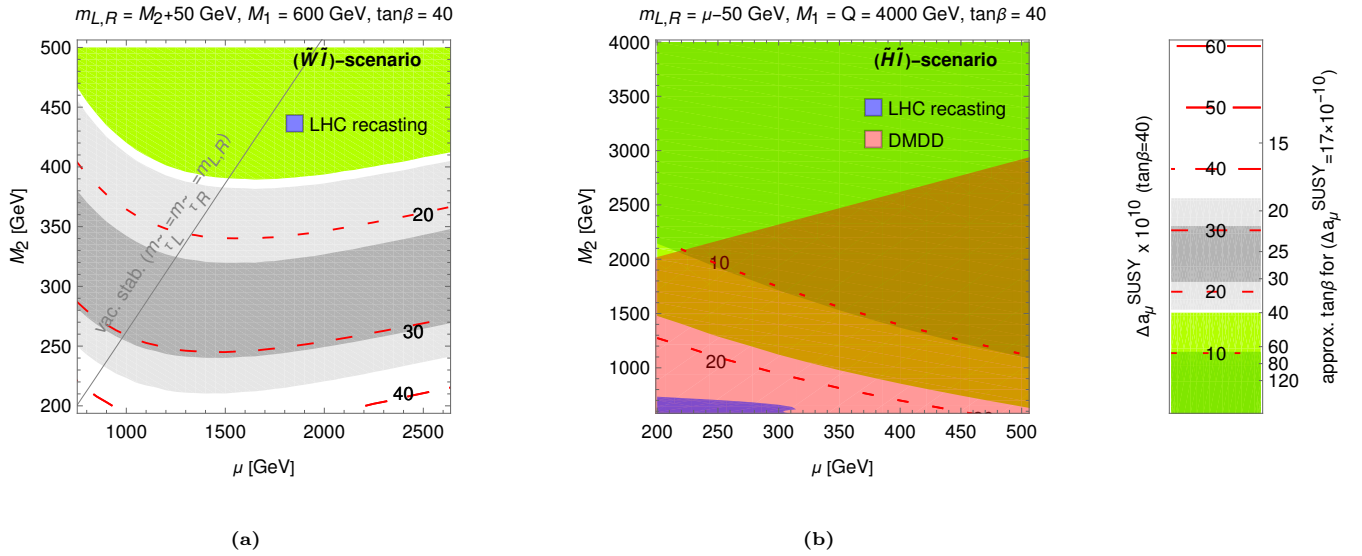


**Figure 5.13:** MSSM in the (a)  $(\tilde{W}\tilde{l})$ - and (b)  $(\tilde{H}\tilde{l})$ -scenarios with either Wino- or Higgsino-like LSP and light sleptons. For parameter values see the plots and the text. The meaning of the red dashed lines, the green/grey coloured  $\Delta a_\mu^{\text{SUSY}}$  regions, and the reinterpretation in the legend plot are as in Fig. 5.11. The red shaded region in the  $(\tilde{H}\tilde{l})$ -scenario is excluded by dark matter direct detection if the LSP is assumed stable; the blue shaded region corresponds to LHC limits. The thin solid grey line corresponds to the vacuum stability constraint of Ref. [724]; it applies in case the left- and right-handed stau-masses are set equal to the smuon/selectron masses and excludes the points to its right, i.e. with larger  $\mu$ . Different from the other plots, the plot (b) has been updated from Ref. [9] with modified input parameters to include higher gaugino masses: the running parameters at  $Q = 4$  TeV are  $M_1 = 4$  TeV, all squark mass parameters are set to 4 TeV, and the slepton mass parameter is set 50 GeV lower than the Higgsino mass. The loop-corrected pole masses then correspond to Higgsino-like LSP with slightly heavier sleptons.

“Wino>sleptons>Higgsino” leads to the strongest additional LHC limits on the Wino-like heavier chargino mass, which extends up to around 700 GeV in the plot [9]; otherwise the chargino masses in these scenarios are not strongly constrained by LHC [425].<sup>59</sup>

However, the LHC limits generally have far less impact on these scenarios than the DMDD limits from the most recent LZ data, see Eq. (5.54). For the Higgsino-like LSP case, these limits allow only values of  $M_2 > 2$  TeV in the plot; in the Wino-like LSP case, the limits are not evaluated but by comparison to previous calculations [9, 778] are expected not to affect the displayed parameter region.

In the allowed parameter regions, the SUSY contributions to  $a_\mu$  are dominated by the WHL contributions, and for very large  $\mu$  in case of Wino-like LSP also the BLR contributions are relevant. In the Wino-like LSP case the general behaviour is similar to the Bino-like LSP case shown in Fig. 5.12, and the displayed parameter region focuses on the turnover point where the BLR contributions start becoming important. As is visible, the Wino-like LSP parameter space is now strongly restricted by the new small result  $\Delta a_\mu^{\text{Exp-WP2025}}$ . For  $\tan\beta = 40$ , agreement at the  $2\sigma$ -level can be obtained for  $M_2 > 400$  GeV. For smaller  $\mu$  and also for larger  $\mu$  than shown in the plot,  $\Delta a_\mu^{\text{SUSY}}$  increases further;<sup>60</sup> hence heavier Wino masses (or smaller  $\tan\beta$ ) are required by  $\Delta a_\mu^{\text{Exp-WP2025}}$ . Another parameter region which is consistent with the new  $\Delta a_\mu$  constraint is light Wino-like LSP in conjunction with significantly heavier sleptons.

<sup>59</sup>The most recent LHC analyses from after the appearance of Refs. [9, 425] have not been used for this statement, and their evaluation is beyond the scope of the present review. However, their impact is not expected to change the viable parameter space considered here.

<sup>60</sup>The DMDD constraints will exclude too small  $\mu$ , similarly to the case of the Bino-like LSP shown in Fig. 5.12.

In case of Higgsino-like LSP, only rather small contributions to  $a_\mu$  remain possible for  $\tan\beta = 40$ . This used to be different but is now caused by the LZ DMDD constraint which forces  $M_2$  to be huge. This strong constraint is in line with expectations in Refs. [781, 891]. Hence the entire Higgsino-like LSP parameter region allowed by DMDD constraints is automatically in agreement with the  $a_\mu$  constraints (as long as  $\tan\beta \lesssim 40$ , see Sec. 5.2.2 for the limit  $\tan\beta \rightarrow \infty$ ). Interestingly, in this parameter scenario it is also possible to explain a slight excess seen at the LHC in  $\chi_2^0\chi_1^\pm$  channels [892].

In the model-building literature, scenarios with Wino- or Higgsino-like LSP have been widely considered. Specifically light Higgsinos can be generally motivated by electroweak finetuning [762, 764, 799] and according models have been constructed as simple CMSSM extensions [859] or based on gauge-mediated [869–871], anomaly-mediated [763], gaugino- and/or Higgs-mediated [760, 833, 893], or based on gravity-mediated SUSY breaking and focus-point behaviour [759]. The models of these references tend to also produce small Wino masses and allow either Higgsino-like or Wino-like LSP. Now the Higgsino-like LSP case with small Wino mass is excluded by the LZ DMDD data (unless one assumes the LSP to be unstable and not to contribute to dark matter which can be motivated in gauge-mediated SUSY breaking with light gravitino). The Wino-like LSP regions of those models can remain viable but are now constrained by DMDD and by  $a_\mu$ .

In contrast, Ref. [828] has considered a Higgsino-like LSP scenario with significant mass gap between the Higgsino-LSP and the two gauginos, motivated within the context of a model with seesaw mechanism and SO(10) GUT constraints on the gaugino masses but non-universal scalar masses. This reference finds only small viable contributions to  $a_\mu$ , which now turns out to be in agreement with observations.

The scenario with Wino-like LSP but very large  $\mu$  has been constructed in Ref. [876, 886] based on Higgs-anomaly mediated SUSY-breaking [748, 886, 894]; such scenarios are now strongly constrained by  $a_\mu$ , restricting essentially the maximum product of  $\mu \tan\beta$  as a function of the LSP and slepton masses.

### 5.2.8. SUSY beyond the R-parity conserving MSSM

Now we focus on the phenomenology of SUSY models different from the R-parity conserving MSSM. We will discuss the MRSSM, a distinct minimal model without  $\tan\beta$  enhancement, the NMSSM and further non-minimal models which can change the LHC and dark matter phenomenology, and return to the MSSM but without assuming a stable neutralino-LSP.

The Minimal R-symmetric Supersymmetric Standard Model (MRSSM) is defined as the minimal model with continuous unbroken  $U(1)_R$  symmetry [895]. This symmetry does not commute with SUSY and it assigns R-charges 0 to SM-like fields and R-charges  $\pm 1, \pm 2$  to the additional fields. R-symmetry implies R-parity conservation but goes beyond it. Importantly, the different squarks  $\tilde{q}_{L,R}$  have charges  $\pm 1$  such that the LHC production of e.g.  $\tilde{q}_L\tilde{q}_L^\dagger$  and  $\tilde{q}_L\tilde{q}_R$  is allowed while  $\tilde{q}_L\tilde{q}_L$  and  $\tilde{q}_L\tilde{q}_R^\dagger$  are forbidden. This reduces the LHC squark production cross section and alleviates LHC limits [896–899], and the MRSSM also has additional virtues with respect to dark matter and Higgs phenomenology [900–903]. The MRSSM also dramatically modifies the  $a_\mu$  and the related CLFV phenomenology [895, 904]. The R-symmetry forbids the MSSM-like Higgsino and gaugino mass parameters  $\mu, M_1$  and  $M_2$  but introduces Dirac mass terms involving additional degrees of freedom. As a result, all  $\tan\beta$ -enhanced MSSM contributions illustrated in Eqs. (5.44) vanish.<sup>61</sup>

Overall, there is no  $\tan\beta$  enhancement in the MRSSM contributions to leptonic dipole operators relevant for  $a_\mu$  or  $\mu \rightarrow e\gamma$  and similar processes [904]. There is an enhancement by MRSSM-specific Yukawa-like couplings, which is however

<sup>61</sup>This is different in models which Dirac gauginos without the restrictions of unbroken R-symmetry [905].

much weaker. As a result, the MRSSM contributions to  $a_\mu$  are generally small, and in a wide parameter scan, Ref. [904] found at most

$$\Delta a_\mu^{\text{MRSSM,max}} < 10 \times 10^{-10} \quad \text{if } M_{\text{LOSP}} > 300 \text{ GeV}, \quad (5.79)$$

where  $M_{\text{LOSP}}$  is the mass of the lightest electrically charged SUSY particle. Hence the MRSSM was no promising explanation of the previous deviation  $\Delta a_\mu^{\text{Exp-WP2020}}$ , but it now emerges as a model which is generically in full agreement with the new result  $\Delta a_\mu^{\text{Exp-WP2025}}$ . Since the dipole operator has at most a moderate enhancement, the corresponding correlations of CLFV observables  $\mu \rightarrow e\gamma$ ,  $\mu \rightarrow 3e$ ,  $\mu \rightarrow e$  conversion mentioned in Eqs. (3.36,3.37) are not valid. This means that the MRSSM might lead to visible signals in the upcoming  $\mu \rightarrow e$  experiments.

The Next-to-Minimal Supersymmetric Standard Model (NMSSM) extends the MSSM by a Higgs singlet and its superpartner, a singlino. Although the singlino can mix with the Bino, Wino and Higgsinos to form neutralino mass eigenstates, the additional fields do not modify the contributions to  $a_\mu$  significantly, though non-negligible modifications can occur if also right-handed neutrino and sneutrino fields are added [906]. Hence, the NMSSM can generally also accommodate sizeable contributions to  $a_\mu$  of similar behaviour as in the MSSM [879, 907–916]. Interestingly, the NMSSM contains several intriguing possibilities to explain dark matter which are distinct from the MSSM and which lead to different SUSY mass patterns. These can evade LHC limits and lead to sizeable contributions to  $a_\mu$ . First, a singlino-like LSP can accommodate the DMRD for rather small masses and allow e.g. Wino- or Higgsino-like neutralinos or even sneutrinos as the lightest MSSM-like sparticles. In these cases, LHC searches for electroweak sparticles become less effective and many sparticles can be light, leading to large contributions to  $a_\mu$  via the WHL diagram [911–915, 917]. Second, if also right-handed neutrinos are introduced, the sneutrino can be the LSP and constitute dark matter, and again small masses and large WHL contributions to  $a_\mu$  are possible [916]. These scenarios are attractive from the dark matter and LHC point of view, but the new result  $\Delta a_\mu^{\text{Exp-WP2025}}$  imposes constraints such as lower mass limits and/or upper  $\tan\beta$  limits. The MSSM plots in Figs. 5.12, 5.13 can be used as an illustration: compared to these plots, in the mentioned NMSSM scenarios  $a_\mu$  would behave similarly while LHC and DMDD constraints would be weakened.

Going beyond even the NMSSM, it is often motivated to consider SUSY models with extended gauge groups, which lead to  $Z'$  gauge bosons and additional neutralino states, which may have stronger interactions than the NMSSM singlino. In a series of works [732–734, 736, 918–925] models of this kind with an extra  $U(1)$  gauge group were considered, and additional possibilities for dark matter were found, as well as additional two-loop Barr-Zee contributions to  $a_\mu$ , which are now constrained. Similarly, an  $SO(10)$ -inspired left-right symmetric model with extra  $U(1)_R \times U(1)_{B-L}$  gauge group there are non-MSSM-like dark matter candidates such as a Bino corresponding to one of the extra  $U(1)$  gauge groups [926]. Again this changes the correlation between LHC, dark matter and  $a_\mu$  phenomenology, and interestingly, the model of Ref. [926] tends to prefer small contributions to  $a_\mu$ .

Within the MSSM and its extensions, we have so far mostly assumed the LSP to be neutral and stable and to contribute to dark matter. This does not need to be true, e.g. under two motivated conditions, reviewed e.g. in Ref. [927]: if R-parity is not conserved, or if the gravitino, the spin-3/2 superpartner of the graviton in supergravity, is lighter than all MSSM sparticles and therefore forms a dark matter candidate.

In case of R-parity violation (RPV), there can be vertices such as muon–electron–sneutrino, or muon–bottom–quark–stop, and accordingly there can be additional one-loop contributions to  $a_\mu$ . These, however, must be small given existing constraints on such lepton-number violating vertices [928, 929]. The major impact on phenomenology derives from modified correlations with other sectors. For instance, Refs. [930–933] considered models where the RPV couplings

explained deviations observed in B-physics, which however have been excluded in the meantime. The studies in Refs. [934, 935] describe how RPV can loosen the LHC limits on electroweak sparticles, and the so-called  $\mu\nu$ SSM can explain all neutrino masses, can explain dark matter via gravitinos or axinos, and can dynamically generate the MSSM  $\mu$ -parameter. However, interestingly in all these mentioned references, the motivation for RPV leads to specific viable mass ranges; these tend to prefer small  $a_\mu$ , hence in particular the  $\mu\nu$ SSM remains a viable model in view of  $\Delta a_\mu^{\text{Exp-WP2025}}$ .

In a more general context, Ref. [739] has investigated the impact of RPV or light gravitino on the MSSM parameter space of interest for  $a_\mu$ . Neither RPV nor a gravitino LSP changes  $a_\mu$  as such, but complementary constraints from dark matter and LHC can be significantly modified. In case of RPV, the LSP is unstable; hence in the simplest case it does not contribute to dark matter and all the strong constraints from DMDD as well as requirements for coannihilation and particular mass splittings are absent. Similarly, in the worst case the neutralino LSP can decay into three quarks, forming three jets which are hard to identify at the LHC, and LHC SUSY search limits are significantly weakened. Hence RPV can significantly open up the parameter space of the kind visible e.g. in Figs. 5.12, 5.13. In general, therefore, RPV SUSY could be a way to accommodate very large  $\Delta a_\mu$ , however, the small current value  $\Delta a_\mu^{\text{Exp-WP2025}}$  does not provide a strong motivation to consider such scenarios.

In the MSSM with additional light gravitino, the MSSM-like LSP (which is then the NLSP) is unstable since it can decay into the gravitino, which is then the true LSP. In contrast to the RPV case, the decay into gravitinos is seriously constrained by dedicated LHC searches, hence the parameter space of interest for  $a_\mu$  remains strongly constrained [739]. For instance, gravitino LSP with Higgsino- or Wino-like NLSP requires very heavy Higgsino and Wino masses above 650–750 GeV. Importantly, a light gravitino LSP also allows the case where charged particles such as sleptons or staus are the NLSP, i.e. the lightest MSSM-like sparticles. These cases are distinct from what is possible in the ordinary MSSM, and they allow lighter slepton and Higgsino masses [739]. An example embedding of such a scenario into a full SU(5) SUSY GUT with gauge-mediated SUSY breaking is presented in Ref. [872]. This reference finds viable parameter space and also potentially sizeable  $\Delta a_\mu^{\text{SUSY}}$ . However it also quantifies a tension between proton decay constraints and  $a_\mu$ ; smaller values of  $a_\mu$  as preferred by the new  $\Delta a_\mu^{\text{Exp-WP2025}}$  widen the allowed parameter space for the fundamental SUSY breaking mechanism.

### 5.2.9. Summary

In summary, the phenomenology of  $a_\mu$  in SUSY models is very rich and has led to a vast body of literature. SUSY extensions of the SM are well motivated in a number of ways, and for many years they have been considered as some of the most plausible explanations of the large deviation  $\Delta a_\mu^{\text{Exp-WP2020}}$ . The new  $a_\mu$  result, together with recent improvements in dark matter and LHC searches, now sheds a different light on possible realisations of SUSY.

Heavy SUSY, where all sparticle masses are  $\gtrsim 1$  TeV, almost inevitably leads to small  $\Delta a_\mu$  (exceptions such as radiative muon mass generation are discussed above). This was not preferred by the previous result but is now fully compatible with  $\Delta a_\mu^{\text{Exp-WP2025}}$ . Many scenarios such as the CMSSM, mGMSB and many of their generalisations or the generic scenarios with Higgsino- or Wino-like dark matter require heavy sparticles, either in view of LHC,  $M_h$ , or dark matter data. These motivated, and often rather simple scenarios thus re-emerge as attractive viable SUSY models (to the extent allowed by other constraints). In the future, they could only be challenged if an improved SM prediction of  $a_\mu$  firmly deviates from the experimental value.

The MSSM with lighter masses is constrained by LHC and dark matter data. Interestingly, the three scenarios to

explain the dark matter relic density with Bino-like LSP and coannihilation with sleptons, staus, or Winos, all evade LHC limits rather generically in the mass range 200...500 GeV, and even lower LSP masses are possible. For this case, the LZ dark matter experiment dramatically constrains the parameter space, preferring very large values of the Higgsino mass  $\mu$ . In this way, the BLR contributions to  $a_\mu$  actually increase, leading to stringent constraints on the parameter space from  $\Delta a_\mu^{\text{Exp-WP2025}}$ . As discussed and illustrated in the plots, the current  $a_\mu$  constraints translate into lower mass limits and/or upper  $\tan\beta$  limits on the scenarios with Bino-like LSP.

Scenarios with Higgsino- or Wino-like LSP with mass in the few-100 GeV range are also viable, though strongly constrained. The Higgsino-like LSP scenario, though the dark matter relic density is underabundant, is very strongly constrained by the LZ experiment. As a result, Higgsino-like LSP with  $\tan\beta \lesssim 40$  now automatically predicts small  $\Delta a_\mu$  in agreement with  $\Delta a_\mu^{\text{Exp-WP2025}}$ . In contrast, the Wino-like LSP scenario could lead to very large  $\Delta a_\mu$ ; it is therefore very strongly constrained by  $\Delta a_\mu^{\text{Exp-WP2025}}$ .

SUSY beyond the R-parity conserving MSSM can be well motivated and can change the  $a_\mu$  phenomenology. For instance, the MRSSM has an additional symmetry, fewer free parameters and automatically predicts small  $\Delta a_\mu$ . The MRSSM, but even more so the NMSSM, also enable additional options to accommodate dark matter via singlinos; in this way the strict MSSM interplay between  $a_\mu$  and dark matter is loosened. Similarly, if the LSP in the MSSM is unstable because of R-parity violation, the parameter space with small SUSY masses is opened up, while the case of LSP-decay into light gravitinos is strongly constrained and prefers small  $\Delta a_\mu$  in line with the new result  $\Delta a_\mu^{\text{Exp-WP2025}}$ .

### 5.3. Two-Higgs-doublet models

The 2HDM is among the most studied and best motivated extensions of the SM. It replaces the single SM Higgs doublet  $\Phi$  by two Higgs doublets  $\Phi_1, \Phi_2$  with  $Y = \frac{1}{2}$ . It represents one of the simplest ways to extend the scalar field content and allows to study Higgs boson properties, the nature of electroweak symmetry breaking and the origin of mass. In fact, the 2HDM changes two SM sectors in important ways. First, it modifies the Higgs sector and the Higgs potential, leading to a more complex vacuum structure, additional physical Higgs bosons, and modified couplings of the Higgs bosons to gauge bosons and Higgs self couplings. Second, the 2HDM also strongly alters the Yukawa sector, leading to a modified fermion mass generation mechanism, and to potentially enhanced couplings of fermions to Higgs bosons and resulting large effects in flavour physics. For reviews of the theory of the 2HDM we refer to Refs. [936, 937].

As analysed in Secs. 1.1.4 and 3.1, a modified muon mass generation mechanism is typically accompanied by contributions to muon  $g - 2$ . Indeed it has been known for a long time [463, 464, 467, 468, 938, 939] that the 2HDM could provide an explanation of deviations as large as  $\Delta a_\mu^{\text{Exp-WP2020}}$  in Eq. (1.6) reported at the time of the FNAL Run-1 or the earlier BNL measurement. Since then the 2HDM parameter space has been scrutinised by measurements at the LHC, by  $a_\mu$  and by a multitude of complementary constraints, with important recent new developments. Especially the complementary constraints have changed the 2HDM  $a_\mu$  phenomenology significantly in recent years, even before the new result  $\Delta a_\mu^{\text{Exp-WP2025}}$  appeared. Here we review the current status, focusing mainly on the scenarios within the 2HDM with the potential for sizeable  $\Delta a_\mu$ . These were motivated and considered in view of the previous result  $\Delta a_\mu^{\text{Exp-WP2020}}$  and are now constrained by  $\Delta a_\mu^{\text{Exp-WP2025}}$ . For recent in-depth analyses and fits of the parameter 2HDM space in scenarios with large or small  $\Delta a_\mu$  we refer to Refs. [940–945].

The Higgs potential of the 2HDM in general contains three quadratic and seven quartic terms in the Higgs doublets

$\Phi_{1,2}$  and can be written as [937, 946]

$$\begin{aligned}
V(\Phi_1, \Phi_2) &= m_{11}^2 \Phi_1^\dagger \Phi_1 + m_{22}^2 \Phi_2^\dagger \Phi_2 - \left( m_{12}^2 \Phi_1^\dagger \Phi_2 + h.c. \right) \\
&+ \frac{\lambda_1}{2} (\Phi_1^\dagger \Phi_1)^2 + \frac{\lambda_2}{2} (\Phi_2^\dagger \Phi_2)^2 + \lambda_3 (\Phi_1^\dagger \Phi_1) (\Phi_2^\dagger \Phi_2) + \lambda_4 (\Phi_1^\dagger \Phi_2) (\Phi_2^\dagger \Phi_1) \\
&+ \left( \frac{\lambda_5}{2} (\Phi_1^\dagger \Phi_2)^2 + \lambda_6 (\Phi_1^\dagger \Phi_1) (\Phi_1^\dagger \Phi_2) + \lambda_7 (\Phi_1^\dagger \Phi_2) (\Phi_2^\dagger \Phi_2) + h.c. \right).
\end{aligned} \tag{5.80}$$

If the potential contains a global minimum, both scalar doublets will acquire a vacuum expectation value ( $vev$ )  $\langle \Phi_i \rangle = \frac{1}{\sqrt{2}}(0, v_i)$ . Non-zero complex phases of the parameters  $m_{12}^2, \lambda_{5,6,7}$  and  $v_{1,2}$  are in general possible and correspond to CP violation in the scalar sector [947]. However, the  $a_\mu$  phenomenology is not strongly sensitive to this possibility and we therefore assume real parameters and real  $vevs$   $v_{1,2}$  in the following.

It is convenient to introduce the *Higgs basis* by rotating the scalar fields with  $\tan \beta = v_2/v_1$  into two doublets  $\Phi_v, \Phi_\perp$ , such that the  $vev$  and the unphysical Goldstone bosons are contained entirely in the doublet  $\Phi_v$ . The rotation and the field components read

$$\begin{pmatrix} \Phi_v \\ \Phi_\perp \end{pmatrix} = \begin{pmatrix} \cos \beta & \sin \beta \\ -\sin \beta & \cos \beta \end{pmatrix} \begin{pmatrix} \Phi_1 \\ \Phi_2 \end{pmatrix}, \quad \Phi_v = \begin{pmatrix} G^+ \\ \frac{1}{\sqrt{2}}(v + S_1 + iG^0) \end{pmatrix}, \quad \Phi_\perp = \begin{pmatrix} H^+ \\ \frac{1}{\sqrt{2}}(S_2 + iS_3) \end{pmatrix}, \tag{5.81}$$

where  $v \approx 246$  GeV is related to the  $vevs$  by  $v_1^2 + v_2^2 = v^2$ . The physical Higgs spectrum of the 2HDM consists of a charged scalar  $H^\pm$  as well as three neutral scalars  $h, H$  and  $A$  related to  $S_i$  by an orthogonal transformation. In the CP conserving case assumed here, the physical CP-odd Higgs  $A = S_3$  and the two physical CP-even Higgs bosons are

$$\begin{pmatrix} H \\ h \end{pmatrix} = \begin{pmatrix} \cos(\alpha - \beta) & \sin(\alpha - \beta) \\ -\sin(\alpha - \beta) & \cos(\alpha - \beta) \end{pmatrix} \begin{pmatrix} S_1 \\ S_2 \end{pmatrix}. \tag{5.82}$$

After introducing these mass-eigenstates, the Higgs potential can equivalently be parametrised in terms of the 4 scalar masses  $M_{h,H,A,H^\pm}$ , the mixing angles  $\tan \beta$  and  $\cos(\alpha - \beta)$  and three of the quartic Higgs couplings  $\lambda_1, \lambda_6$  and  $\lambda_7$ . In the so-called alignment limit [948] where either  $\sin(\alpha - \beta) = 0$  or  $\cos(\alpha - \beta) = 0$ , the doublet  $\Phi_v$  becomes purely SM-like and the field  $S_1$  becomes equal to either  $H$  or  $h$ , which then exactly correspond to the SM Higgs boson. In the following we will assume that  $h$  is approximately or exactly SM-like, such that  $\cos(\alpha - \beta)$  is small or zero.

If no further symmetries are imposed, all SM fermions are allowed to couple to both of the Higgs doublets, resulting in the most general possible 2HDM Yukawa Lagrangian

$$\mathcal{L} \supset - \sum_{a=v,\perp} \left[ \bar{l}_L Y_a^l e_R \Phi_a + \bar{q}_L Y_a^d d_R \Phi_a + \bar{q}_L Y_a^u u_R \tilde{\Phi}_a \right] + h.c. \tag{5.83}$$

The Yukawa Lagrangian can be equivalently written in terms of the general basis or the Higgs basis; the corresponding Yukawa matrices  $Y_{v,\perp}^f$  and  $Y_{1,2}^f$  are related similarly to the fields as in Eq. (5.81). The Yukawa couplings to  $\Phi_v$  in the Higgs basis are related to the tree-level fermion mass matrices as  $Y_v^f = \sqrt{2}M_f/v$ . The (approximately) SM-like Higgs boson  $h$  couples to fermions via  $Y_v^f$ , up to corrections of order  $\cos(\alpha - \beta)$ . In contrast, the physical Higgs bosons  $H, A$  and  $H^\pm$  couple via the additional Yukawa matrices  $Y_\perp^f$  (in case of  $H$  up to  $\cos(\alpha - \beta)$  corrections). These  $Y_\perp^f$  are in general unrelated to the fermion masses and can therefore result in large effects in flavour physics. This includes potentially significant contributions to  $a_\mu$ , but also flavour-changing neutral currents (FCNC) that are strongly constrained by experiment. We refer to the review [937] for a survey of ways to avoid too large FCNC contributions. Broadly speaking, one can impose exact or softly broken symmetries which force  $Y_\perp^f$  to be diagonal in the fermion mass basis (such as the

Model	type I	type II	type X	type Y	inert	FA
$\zeta_l$	$\cot \beta$	$-\tan \beta$	$-\tan \beta$	$\cot \beta$	0	$\lesssim 300$
$\zeta_d$	$\cot \beta$	$-\tan \beta$	$\cot \beta$	$-\tan \beta$	0	$\lesssim 1$
$\zeta_u$	$\cot \beta$	$\cot \beta$	$\cot \beta$	$\cot \beta$	0	$\lesssim 1$

**Table 5.3:** Values of the Yukawa alignment parameters  $\zeta_f$  in the Type-I,II,X,Y and inert 2HDM.

Type I, II, X, Y models or the muon-specific model) or one can postulate more general patterns of flavour textures of  $Y_2^f$  where FCNC are either completely absent (such as the flavour-aligned 2HDM) or strongly suppressed (such as various forms of the so-called Type-III model as discussed in Ref. [937]). In the following we focus on scenarios without FCNC.

### 5.3.1. Type I, II, X, Y and Flavour-aligned 2HDM

The most widely discussed way to avoid FCNC is to introduce a discrete  $\mathbb{Z}_2$  symmetry under which the general-basis fields  $\Phi_1$  and  $\Phi_2$  transform differently.<sup>62</sup> This forces each of the fermion fields to couple to only one of these scalar doublets, depending on the choice of charge assignment. Without loss of generality one can assume that the up-type quarks always couple to  $\Phi_2$ . There are then four distinct possibilities classified as type I (all fermions couple to  $\Phi_2$ ), type II ( $d$  and  $l$  couple to  $\Phi_1$ ,  $u$  to  $\Phi_2$ ), type X (or lepton-specific:  $l$  couples to  $\Phi_1$ ,  $u$  and  $d$  to  $\Phi_2$ ) and type Y ( $d$  couples to  $\Phi_1$ ,  $u$  and  $l$  to  $\Phi_2$ ). In all these cases, the Yukawa matrices corresponding to the Higgs basis  $Y_v^f$  and  $Y_\perp^f$  are then proportional to each other for each  $f = l, d, u$ , i.e. one can write

$$Y_\perp^l = \zeta_l Y_v^l, \quad Y_\perp^d = \zeta_d Y_v^d, \quad Y_\perp^u = \zeta_u Y_v^u, \quad (5.84)$$

where the values of the proportionality factors  $\zeta_{l,d,u}$  for the different types depend on  $\tan \beta$  and  $\cot \beta$  and are listed in Tab. 5.3.

A generalisation of the type I, II, X, Y models is given by the flavour-aligned 2HDM (FA2HDM), proposed and explored in Refs. [949, 950]. In the FA2HDM one assumes the validity of Eq. (5.84) with arbitrary, in general complex, values of the coefficients  $\zeta_{l,d,u}$ . Such general values are not necessarily governed by symmetries, and the general FA2HDM Yukawa structure is not guaranteed to be stable under renormalisation. But it provides a very useful unified framework which contains all types with discrete symmetries as special cases.

We mention in passing that there is a special case of the scenarios with discrete symmetries where one of the two Higgs doublets receives no  $vev$ , i.e. where  $\cot \beta = 0$ . This is only compatible with the type I Yukawa couplings in order for all fermions to receive mass. The resulting model is called the Inert Doublet model. The lightest BSM scalar is guaranteed to be stable thanks to the unbroken  $\mathbb{Z}_2$  symmetry. The Inert Doublet model is therefore of high interest in view of dark matter. However, since the BSM scalars do not couple to fermions (unless in generalisations [951–953]) it provides only tiny contributions to  $a_\mu$ , and  $a_\mu$  does not constrain the Inert Doublet model parameter space. Hence we will not discuss this case further.

For reference we also provide the Yukawa Lagrangian written in terms of mass-eigenstate fields. It follows from

<sup>62</sup>This also forces  $m_{12}^2$  and  $\lambda_{6,7}$  to vanish. However,  $m_{12}^2 \neq 0$  breaks the discrete symmetry only softly (leading to finite FCNC at one-loop order) and is therefore often included [936].

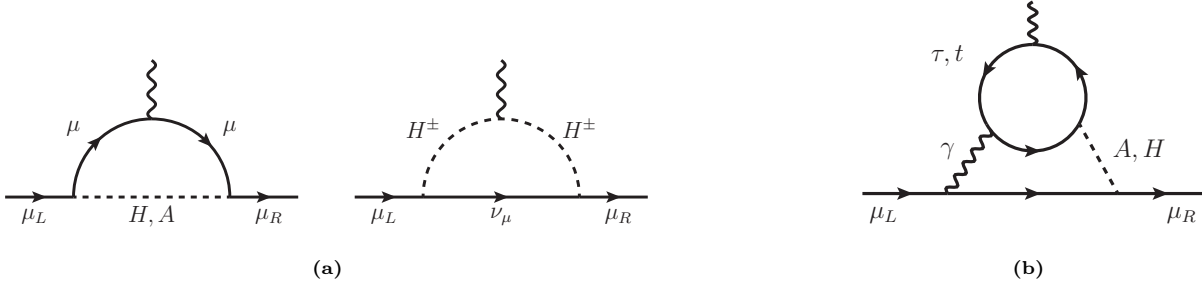


**Figure 5.14:** Example of one- and two-loop contributions of the heavy scalars  $H, A$  and  $H^\pm$  to  $a_\mu$  in the FA2HDM.

Eqs. (5.83), (5.84) and (5.81) and reads

$$\begin{aligned} \mathcal{L} \supset & - \sum_{f,S} \left[ Y_f^S \mathcal{S} \bar{f} \frac{M_f}{v} P_{R,f} \right] + \sqrt{2} H^+ Y_l^{H^\pm} \bar{\nu} \frac{M_e}{v} P_R e \\ & + \sqrt{2} H^+ \bar{u} \left[ Y_d^{H^\pm} V_{CKM} \frac{M_d}{v} P_R + Y_u^{H^\pm} \frac{M_u}{v} V_{CKM} P_L \right] d + h.c., \end{aligned} \quad (5.85)$$

where  $\mathcal{S} \in \{h, iA, H\}$ . The sum over fermion fields runs over the mass eigenstates  $f = e, u$  and  $d$ , where  $M_{e,u,d}$  denote the diagonal fermion mass matrices and generation indices are suppressed. The Yukawa modifier parameters appearing in the Lagrangian are given by

$$Y_f^h = \sin(\beta - \alpha) + \cos(\beta - \alpha) \zeta_f \quad (5.86a)$$

$$Y_f^H = \cos(\beta - \alpha) - \sin(\beta - \alpha) \zeta_f \quad (5.86b)$$

$$Y_{d,l}^A = Y_{d,l}^{H^\pm} = -\zeta_{d,l}, \quad Y_u^A = Y_u^{H^\pm} = \zeta_u, \quad (5.86c)$$

such that the couplings to the BSM Higgs states  $H, A, H^\pm$  are potentially enhanced by the  $\zeta_f$ , where important values are collected in Tab. 5.3 and the Higgs alignment limit is given by  $\cos(\beta - \alpha) \rightarrow 0$ .

### 5.3.2. 2HDM contributions to $a_\mu$

In the 2HDM significant corrections to the muon magnetic moment can arise at both the one-loop and two-loop order. The one-loop diagrams with the exchange of the new Higgs states  $H, A, H^\pm$  shown in Fig. 5.14a are of the generic form given in Eq. (2.3a)

$$\Delta a_\mu^{1l} \simeq \frac{1}{8\pi^2} \frac{m_\mu^2}{v^2} \left\{ (Y_\mu^A)^2 \frac{m_\mu^2}{M_A^2} \left[ \ln\left(\frac{m_\mu^2}{M_A^2}\right) + \frac{11}{6} \right] - (Y_\mu^H)^2 \frac{m_\mu^2}{M_H^2} \left[ \ln\left(\frac{m_\mu^2}{M_H^2}\right) + \frac{7}{6} \right] - (Y_\mu^{H^\pm})^2 \frac{m_\mu^2}{6M_{H^\pm}^2} \right\}. \quad (5.87a)$$

In the absence of lepton-flavour violating Higgs couplings, these one-loop diagrams are suppressed by two powers of the muon mass and two additional powers of the muon Yukawa couplings. Therefore, even if the BSM muon Yukawa coupling is enhanced by a large value of  $\zeta_l$ , the one-loop diagrams are typically subdominant.

References [463, 464, 467, 468, 938, 939] have stressed that the two-loop Barr-Zee diagrams discussed in Sec. 4.2 are chirally enhanced relative to the one-loop contributions and can dominate in large parts of the 2HDM parameter space. The simplest such diagram shown in Fig. 5.14b involves a one-loop  $\gamma\gamma$ -Higgs subdiagram with a heavy fermion loop, where one photon and the neutral Higgs boson connects to the muon line; it results in the contribution (cf. sec. 4.2)

$$\Delta a_\mu^{2l,f} \simeq \frac{\alpha}{8\pi^3} \frac{m_\mu^2}{v^2} N_c^f Q_f^2 \left\{ Y_\mu^H Y_f^H \frac{m_f^2}{M_H^2} \mathcal{F}_1\left(\frac{m_f^2}{M_H^2}\right) + Y_\mu^A Y_f^A \frac{m_f^2}{M_A^2} \mathcal{F}_2\left(\frac{m_f^2}{M_A^2}\right) \right\}, \quad (5.88)$$

where the loop-functions are given in Eq. (4.15).

Though the above formulas could be generalised, we continue to focus on the framework of the FA2HDM, which contains the well-known type I, II, X, Y models as special cases. In this general setup the qualitative behaviour of the most important contributions can be well understood in terms of the scalings

$$\Delta a_\mu^{1l} \sim \mp \frac{\zeta_l^2}{8\pi^2} \frac{m_\mu^4}{v^2 M_S^2}, \quad \Delta a_\mu^{2l,\tau} \sim \pm \zeta_l^2 \frac{m_\tau^2}{v^2} \times \frac{\alpha}{8\pi^3} \frac{m_\mu^2}{M_S^2}, \quad \Delta a_\mu^{2l,t} \sim -\zeta_l \zeta_u \frac{m_t^2}{v^2} \times \frac{N_c Q_t^2 \alpha}{8\pi^3} \frac{m_\mu^2}{M_S^2}. \quad (5.89)$$

Here  $\Delta a_\mu^{1l}$  is the one-loop contribution from one of the neutral scalars  $A, H$ , and  $\Delta a_\mu^{2l,\tau}$  and  $\Delta a_\mu^{2l,t}$  correspond to the Barr-Zee diagrams with a  $\tau$ -loop and top-loop, and we have explicitly inserted the expressions Eq. (5.86) for the Yukawa couplings in the flavour-alignment limit. Furthermore, the behaviour of the loop functions has been approximated by  $1/M_S^2$ , ignoring logarithmic enhancements. The signs correspond to  $S = A$  or  $H$ , respectively.

These scalings can also be understood in terms of the discussion of chirality flips presented in sec. 1.1.4. In particular, the factors before  $\times$  correspond to the chiral enhancement factor  $R_\chi$  of Eq. (1.10) (see also Tab. 1.1). For the one-loop contribution, regardless of whether the chirality is flipped at the external muon or the internal muon, there always appears an explicit factor of  $m_\mu^2$  and two additional powers of BSM muon Yukawa couplings and consequently  $\Delta a_\mu^{1l} \propto m_\mu^4$ . For the Barr-Zee diagrams, the muon chirality is flipped via the single coupling of the muon to the BSM Higgs, contributing one power of  $\zeta_l m_\mu/v$ . The BSM Higgs also couples to the inner fermion loop, yielding a factor of the BSM Yukawa coupling of the inner fermion. As explained in Sec. 1.1.4, any contribution to  $a_\mu$  must be proportional to the EWSB  $vev$ . In the Barr-Zee diagrams, the  $vev$  enters via the fermion mass of the inner fermion loop,  $m_\tau$  or  $m_t$ . Taken together, these considerations fully explain the factors appearing in  $\Delta a_\mu^{2l,\tau}$  and  $\Delta a_\mu^{2l,t}$ .

The estimate in Eq. (5.89) demonstrates how the Barr-Zee diagrams can dominate over the one-loop diagrams. The Barr-Zee  $\tau$ -loop diagram depends on the same Yukawa parameters, is suppressed by an additional loop factor but enhanced by  $m_\tau^2/m_\mu^2$ . The detailed calculations show that it dominates over the one-loop contribution provided that the Higgs masses  $M_{A,H}$  are larger than around  $M_A \gtrsim 3$  GeV and  $M_H \gtrsim 5$  GeV [463, 464, 467, 468, 938, 939]. For lower masses, the one-loop diagram is relatively enhanced by the logarithm  $\ln(M_S/m_\mu)$  and dominates, see also the limit of the loop function in Eq. (2.10). For Higgs masses above these values, the total sign of the one-loop plus the Barr-Zee  $\tau$ -loop contribution is positive for  $A$ -exchange and negative for  $H$ -exchange. The Barr-Zee top-loop contribution involves the even larger enhancement factor  $m_t^2/m_\mu^2$  compared to the one-loop contribution. But it depends on the Yukawa parameter  $\zeta_u$ , which is severely constrained as discussed below.

For the following phenomenological discussion in the present section we only consider BSM Higgs boson masses above around 5 GeV. For contributions of lighter particles to  $a_\mu$  we refer to the discussion in Sec. 5.1. Specifically for the 2HDM, the few-GeV mass range of scalars with significant Yukawa couplings is strongly constrained by  $B$  physics, see e.g. [954–956]. For large Higgs masses  $M_A \approx M_H \approx M_{H^\pm} \gtrsim 500$  GeV the following simple seminumerical formulas hold

$$\Delta a_\mu^{2l,\tau} \simeq + \left( \frac{\zeta_l}{100} \right)^2 \left\{ \frac{5.3 + \ln(x_s)}{x_s^2} \right\} \cdot 7.4 \times 10^{-13} \quad (5.90a)$$

$$\Delta a_\mu^{2l,t} \simeq - \left( \frac{\zeta_u \zeta_l}{100} \right) \left\{ \frac{3.5 + 3 \ln(x_s) + \ln(x_s)^2}{x_s^2} \right\} \cdot 1.9 \times 10^{-10}, \quad (5.90b)$$

with  $x_s = M_S/1000$  GeV. In contrast to the similar seminumerical results for small  $M_A \ll M_{H,H^\pm}$  obtained in Ref. [957], here the equal scalar mass limit implies a cancellation of the  $\ln^2(x_s)$  enhanced terms in the  $\tau$ -loop contribution, which is consequently even more suppressed compared to the top-loop correction  $\Delta a_\mu^{2l,t}$ .

Finally, besides the dominant contributions from the fermionic Barr-Zee diagrams there are also bosonic contributions to  $\Delta a_\mu$  at two-loop order. These do not give rise to additional chiral enhancements and are therefore generally small.

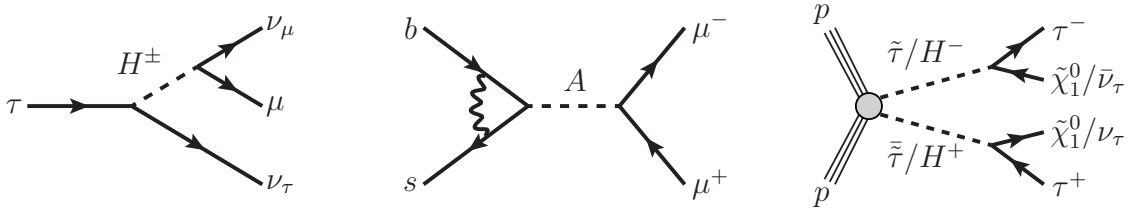


**Figure 5.15:** Illustration of diagrams contributing to low-energy flavour observables and Higgs production at the LHC in the 2HDM. *left:* tree-level correction of  $H^\pm$  to the  $\tau$  decay. *middle:* contribution of  $A$  to  $B_s^0 \rightarrow \mu^+ \mu^-$  with virtual  $W$ -boson and top-quark in the loop. *right:* stau ( $H^\pm$ ) pair production and subsequent decay searched for at the LHC.

The general class of all Barr-Zee type diagrams has been evaluated in Ref. [465]. A complete two-loop calculation of  $a_\mu$  in the 2HDM has been obtained and discussed in Refs. [957, 958], and a corresponding numerical computer code has been published in Ref. [959]. For a detailed discussion of the behaviour of the full two-loop result as a function of all parameters in the FA2HDM see Refs. [957, 958]. In general, the additional bosonic corrections can be noticeable if  $\cos(\beta - \alpha)$  differs from the SM-limit and  $\zeta_l$  and  $M_{H^\pm} - M_H$  become large; but given existing constraints the bosonic corrections are typically  $\lesssim \mathcal{O}(10^{-10})$ .

### 5.3.3. Constraints from $a_\mu$ and other observables on the Type I, II, X, Y and Flavour-aligned 2HDM

The estimate Eq. (5.89) illustrates in which parameter regions of the 2HDM sizeable contributions to  $a_\mu$  are generated. In particular, a large value of  $|\zeta_l| \gg 1$  (equivalently large  $\tan \beta$  in type II or type X) is required, and small Higgs masses as well as large  $|\zeta_u|$  are additionally preferred. In the past decade, after the Higgs discovery at the LHC and in anticipation of the Fermilab  $g-2$  measurement, this parameter space has been extensively scrutinised [9, 181, 957, 958, 960–975]. Here we discuss the most relevant constraints identified in the literature, see Fig. 5.15 for sample diagrams, then we discuss the phenomenological results, see Fig. 5.16.

First, the possible spectrum of Higgs masses compatible with  $m_h \approx 125$  GeV is restricted by theoretical constraints on the Higgs potential Eq. (5.80). The existence of a global minimum requires [976]

$$m_{12}^2 (m_{11}^2 - m_{22}^2 \sqrt{\lambda_1/\lambda_2}) (\tan \beta - \sqrt[4]{\lambda_1/\lambda_2}) > 0, \quad (5.91)$$

and the stability of the vacuum (i.e.  $V$  should be bounded from below) implies [946]

$$\lambda_{1,2} > 0, \quad \lambda_3 > -\sqrt{\lambda_1 \lambda_2}, \quad \text{and} \quad \lambda_3 + \lambda_4 - |\lambda_5| > -\sqrt{\lambda_1 \lambda_2}. \quad (5.92)$$

The quartic couplings must also be (approximately) bounded by  $|\lambda_i| \lesssim 4\pi$  in order to fulfil the tree-level unitarity constraints [977, 978]. In addition, an important experimental constraint on the 2HDM spectrum arises from requiring consistency with the  $\rho$ -parameter and electroweak precision observables. Ref. [960] showed that these basic constraints restrict the mass splittings between the three BSM Higgs states  $A, H, H^\pm$ . At least two out of the three masses must be similar, and the difference  $|M_A - M_{H^\pm}|$  is generally restricted. Two allowed mass patterns therefore are:

- A light  $M_A \lesssim 100$  GeV requires not too heavy  $M_H \approx M_{H^\pm} \lesssim 300$  GeV. This pattern is exemplified in our Fig. 5.16 (*left, middle*). Here the Barr-Zee diagrams with  $\tau$ -loop can dominate and potentially lead to sizeable, positive  $\Delta a_\mu$ .
- For  $M_H \approx M_{H^\pm} \gtrsim 300$  GeV,  $M_A$  must be of the same order as  $M_{H^\pm}$ . This mass pattern is exemplified in our Fig. 5.16 (*right*), where we set  $M_A = M_H = M_{H^\pm} = 1000$  GeV. Here all 2HDM contributions to  $a_\mu$  are suppressed, though  $\Delta a_\mu^{2l,t}$  can still reach values up to  $\mathcal{O}(10^{-9})$ .

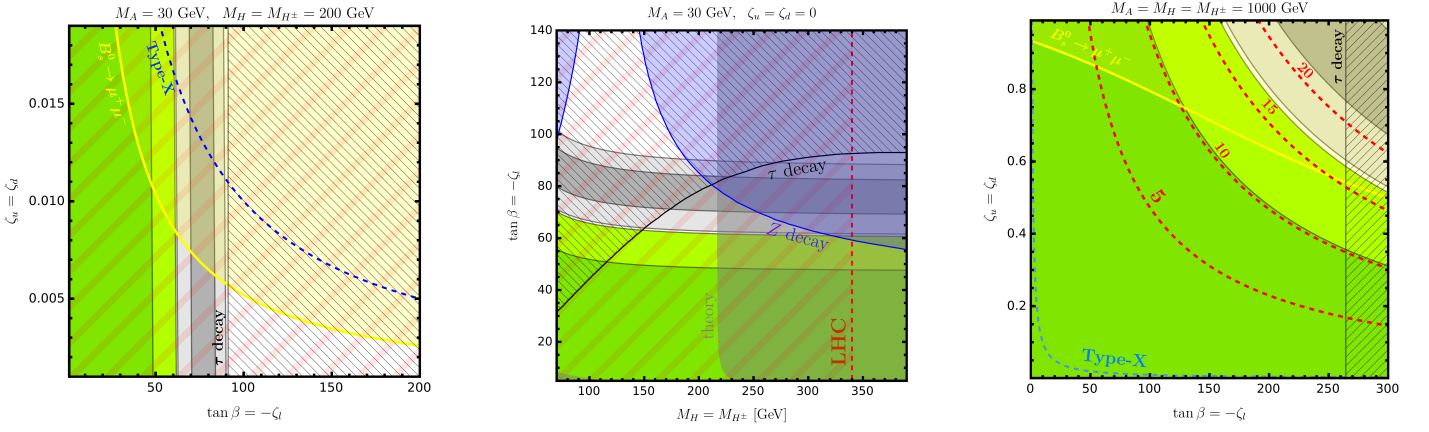


**Figure 5.16:**  $\Delta a_\mu$  contour plots for the FA2HDM in the  $\tan\beta - \zeta_u$  plane with light  $M_A$  (left), the  $M_{H^\pm} - \tan\beta$  plane with light  $M_A$  (middle) and the  $\tan\beta - \zeta_u$  plane with large scalar masses (right). The (light) green region corresponds to the  $1\sigma$  ( $2\sigma$ ) range of  $\Delta a_\mu^{\text{Exp-WP2025}}$ , and the (light) grey region to the  $1\sigma$  ( $2\sigma$ ) range around  $\Delta a_\mu^{\text{Exp-WP2020}}$ . In the right plot we have included (red, dashed) contour lines for  $\Delta a_\mu \times 10^{10}$ . The excluded regions are indicated by their corresponding constraints and were obtained using the formulas given in Refs. [943, 965]. In particular, the red hatched regions are excluded by the  $\tilde{\tau}$  search recasting of Ref. [943].

While Ref. [960] assumed the quartic potential terms to be  $\mathbb{Z}_2$  symmetric, a similar conclusion with slightly larger mass windows was also obtained for the general Higgs potential [962].

For each pattern of Higgs masses, the values of Yukawa couplings are constrained by flavour and collider physics. In the FA2HDM, the important coupling parameter  $\zeta_l$  is mainly restricted particularly by  $\tau$ -physics, in particular by lepton flavour universality measurements in  $\tau$ -decays [979], studied in Refs. [943, 957, 961, 963, 965, 966, 980]. The main 2HDM contribution stems from tree-level exchange of the charged Higgs  $H^\pm$  shown in Fig. 5.15 (left), as well as one-loop diagrams where all new scalars contribute, yielding a correction

$$\Gamma_{\tau \rightarrow l\nu\nu} \simeq \Gamma_{\tau \rightarrow l\nu\nu}^{\text{SM}} (1 + 2\delta_{\text{tree}} + 2\delta_{\text{loop}}), \quad (5.93)$$

where the explicit expressions for  $\delta_{\text{tree,loop}}$  together with the current experimental bounds are summarised in Ref. [943]. Complementary constraints arise also from  $Z \rightarrow \tau\tau$  decays [943, 957, 963, 965, 966, 981] and, for  $M_A \lesssim 20$  GeV,  $\tau\tau$ -production [957] both of which were measured at LEP [281, 982]. The resulting upper limits on  $|\zeta_l|$  range from around 100 (for  $M_A = 20 \dots 100$ ) to around 250 (for  $M_A = 1000$  GeV). The excluded regions are shown in Fig. 5.16 as the hatched and the blue regions, where Fig. 5.16 (left, right) only show the stronger of the two limits, while Fig. 5.16 (middle) shows both to illustrate their complementarity.

The quark Yukawa couplings are severely restricted by  $B$ -physics, see Fig. 5.15 (middle), and by LHC Higgs physics. For the models with discrete symmetry listed in Tab. 5.3 this has immediate conclusions [960]. Obviously, in the type I and Y models,  $\zeta_l$  and  $\zeta_u$  are equal and constraints on the top Yukawa coupling translate into a strong suppression of  $\zeta_l$  and hence of  $\Delta a_\mu$ . In the type II model, a strong constraint on the charged Higgs mass  $M_{H^\pm} \gtrsim 580$  GeV arises from  $\text{BR}(b \rightarrow s\gamma)$  [983].

As a result, Ref. [960] concluded that the type X model is the only of the  $\mathbb{Z}_2$ -symmetric models which has any potential of significant contributions to  $a_\mu$ . The type X model was then investigated in more detail also in view of CP violation and the electron electric dipole moment [968], and highly sensitive modest-energy lepton collider tests via the Yukawa process  $e^+e^- \rightarrow \gamma^*/Z^* \rightarrow \tau\tau A$  were proposed [984]. Within the type X model, also the “wrong-sign” Yukawa coupling is

of interest, where the SM-like Higgs coupling modifier  $Y_e^h \approx -1$  in Eq. (5.86), and the impact of this difference has been investigated in this context in Refs. [964, 965, 967, 971, 985].

In the more general FA2HDM scenario, constraints on the quark Yukawa parameters  $\zeta_{d,u}$  can be quantified individually. This was done in Refs. [9, 957, 958, 962] and more recently, based on important experimental updates, in Ref. [943]. The recent measurements of  $B_s^0 \rightarrow \mu^+\mu^-$  by LHCb [986] and CMS [987] have shifted the world average from  $\text{BR}(B_s^0 \rightarrow \mu^+\mu^-)^{2014} = (2.8 \pm 0.7) \times 10^{-9}$  [988] to [104]

$$\text{BR}(B_s^0 \rightarrow \mu^+\mu^-)^{2023} = (3.34 \pm 0.27) \times 10^{-9}, \quad (5.94)$$

in significantly better agreement with the SM prediction [989, 990]. As shown in Ref. [943], this measurement by far supersedes all previously considered constraints on the up-type Yukawa couplings. In Fig. 5.16 (*left*) the corresponding constraint is shown as the yellow region. For the Higgs masses chosen in this plot,  $B_s^0 \rightarrow \mu^+\mu^-$  limits  $\zeta_u$  to around 0.01 and even excludes the type X model where  $\zeta_u = -1/\zeta_l$ .

There also exist a number of direct searches at the LHC that dramatically restrict the possible range of BSM Higgs masses. As pointed out in Refs. [964, 967], in case of large  $\zeta_l$  the heavy Higgs bosons decay dominantly into  $\tau$  leptons, resulting in a significant excess in  $\tau$ -rich signatures. Resulting signatures closely resemble those of stau  $\tilde{\tau}$  production in the context of supersymmetric models, which have been studied extensively. The similarity is illustrated in Fig. 5.15 (*right*). In fact, the CMS search for  $\tilde{\tau}_L$  pair production [448] can be directly adapted to the FA2HDM and excludes charged scalar masses in the range of  $115 \leq M_{H^\pm} \leq 340$  GeV, assuming  $\text{BR}(H^\pm \rightarrow \tau^\pm \bar{\nu}) \simeq 1$  [943]. In Fig. 5.16 (*left, middle*) this constraint is shown as the red hatched region. In the (*middle*) plot, it is overlaid on top of the parameter space for  $M_A = 30$  GeV allowed by the  $B$ -physics,  $Z$  and  $\tau$  constraints, covering precisely the gap where large  $\Delta a_\mu$  was still possible. In the (*left*) plot, it excludes the entire shown region. A proper recasting of the updated stau analyses performed by ATLAS and CMS [448, 991–993] using the full Run-2 data set was also presented in Ref. [943] and excludes charged scalar masses up to more than 500 GeV and also excludes the region with small scalar masses that is still allowed in Fig. 5.16 (*middle*).

These recent additional  $B$ -physics and LHC search constraints change the viable 2HDM parameter space strongly. To illustrate the difference we note that prior to these constraints, Refs. [9, 957] evaluated the overall maximum possible contribution  $\Delta a_\mu$  in the type X and FA2HDM and found values around  $(30 \dots 50) \times 10^{-10}$ , respectively. In order to achieve such values,  $M_A$  around 30 GeV and maximised  $\zeta_{l,u}$  were needed. Now, with the recent additional constraints this entire region with light pseudo-scalar, large  $|\zeta_l|$  and  $\Delta a_\mu \sim \mathcal{O}(10^{-9})$  considered in Refs. [181, 957, 958, 960–975] is excluded [943].

In a recent global fit of the FA2HDM focusing on light new Higgs bosons, the model parameter space was extensively investigated [945]. This reference finds allowed parameter regions where light  $M_A$  is viable, and it even finds larger allowed  $\zeta_{l,u}$  than in Ref. [943] and visible in the plots of Fig. 5.16 (*left, middle*). However, it also confirms that there is no viable possibility for sizeable contributions to  $a_\mu$  within all its investigated FA2HDM parameter space where at least one of the BSM Higgs masses is below  $M_h \approx 125$  GeV.

This negative result is further complemented by a recent dedicated search for the light pseudo-scalar  $A$  with masses in the range of  $M_A = 20 \dots 90$  GeV performed by ATLAS [994], where no significant excess above the SM background was found. This search considered the process  $gg \rightarrow A \rightarrow \tau\tau$  with single production of  $A$  via gluon fusion and subsequent decay into a  $\tau$  pair and provides both a model-independent upper limit on the production cross-section as well as a FA2HDM-specific bound on  $|\zeta_u| \lesssim 0.2$  in the relevant parameter region.

We are thus led to focus on the remaining parameter space for the 2HDM in case of large lepton Yukawa couplings  $\zeta_l$ , which is characterised by large Higgs masses where the theoretical constraints enforce smaller (relative) mass splittings such that we consider  $M_A \approx M_H \approx M_{H^\pm} \gtrsim 500$  GeV. Since the FA2HDM contributions to the  $Z$  decay vanish for degenerate masses and the corrections to the  $\tau$  decay scale as  $\zeta_l^2/M_S^2$ , larger values of  $\zeta_l \sim 250$  are allowed in this region. At the same time thanks to the heavy masses,  $B$ -physics constraints are much weaker and allow up to  $\zeta_u \lesssim 0.8$ . In Fig. 5.16 (right) we show contours for  $\Delta a_\mu$  in the  $\zeta_l$ - $\zeta_u$  plane in this heavy mass region, fixing  $M_A = M_H = M_{H^\pm} = 1000$  GeV. Following Eq. (5.90) the dominant corrections to  $\Delta a_\mu$  stem from the top loop, while the  $\tau$  contributions are strongly suppressed. Particularly, if both couplings  $\zeta_{l,u}$  are maximised,  $\Delta a_\mu$  can still reach values up to  $10^{-9}$  in the FA2HDM even for Higgs masses as heavy as 1 TeV. A similar result has been obtained in a recent global fit [944] with focus on the heavy-mass region of the FA2HDM. Although  $a_\mu$  was not included as a constraint in the fit, significant contributions  $\Delta a_\mu$  were found to be possible. Conversely, this means that the current result  $\Delta a_\mu^{\text{Exp-WP2025}}$  constrains the FA2HDM parameter space in this region of very large  $\zeta_l \zeta_u$  in a non-trivial way. In contrast, in the type X scenario the small value of  $\zeta_u$  prevents significant contributions to  $a_\mu$ , such that the small value  $\Delta a_\mu^{\text{Exp-WP2025}}$  does not provide additional constraints on the type X model any more.

### 5.3.4. General 2HDM and summary

Although the FA2HDM is already a very general framework, it is of interest to study the range of possibilities of more general Yukawa structures in the 2HDM, for reviews focusing on  $a_\mu$  in this context see Refs. [943, 995]. The major limiting feature of the FA2HDM is the equality between the muon and  $\tau$ -lepton Yukawa enhancements via the common factor  $\zeta_l$ . Removing this equality immediately relaxes the constraints related to  $\tau$ -physics and LHC searches involving  $\tau$  final states.

Refs. [996, 997] consider the obvious generalisation where effectively, the single quantity  $\zeta_l$  in the lepton sector is generalised to three parameters  $\zeta_{e,\mu,\tau}$  (equivalent to  $n_{e,\mu,\tau}$  in Refs. [996, 997] and  $\kappa_{e,\mu,\tau}$  in Ref. [998]; the so-called power-alignment of Ref. [999] can be considered as a special case of this idea). This does not introduce FCNC but it allows for greater freedom in the Yukawa sector. In this way,  $\tau$ -constraints can be relaxed by smaller  $\zeta_\tau$ , which in turn allows significantly larger  $\zeta_\mu$ . Translating to our conventions, Ref. [997] finds 2HDM scenarios with  $\Delta a_\mu \sim 10^{-9}$  of several kinds:

- All  $A, H, H^\pm$  Higgs masses of order 1 TeV and similar, with very large  $\zeta_\mu \sim 1000$  and significant  $\zeta_u$ : this region is similar to the FA2HDM region shown in Fig. 5.16 (right) and allows sizeable  $\Delta a_\mu$  via top-loop Barr-Zee diagrams.
- All  $A, H, H^\pm$  Higgs masses of order 1 TeV,  $M_H < M_A$ , with very large  $\zeta_\mu$ : if the mass gap between  $M_H$  and  $M_A$  is sufficiently large, the one-loop diagram with  $H$ -exchange can provide a significant, positive contribution to  $a_\mu$ .
- All  $A, H, H^\pm$  Higgs masses between 500...1000 GeV, with  $M_H < M_A$  and opposite signs for  $\zeta_\mu$  and  $\zeta_\tau$ : in this case the  $\tau$ -loop Barr-Zee diagram with  $H$ -exchange is positive and can provide a relevant contribution to  $a_\mu$ .

In addition, Ref. [1000] finds viable parameter regions for additional 2HDM Higgs bosons with very light masses  $M_H \lesssim 1$  GeV if only Yukawa couplings to electron and muon are sizeable.

The so-called  $\mu$ -specific 2HDM [1001] can be regarded as a special case of the scenario of Refs. [996, 997], where the Yukawa pattern follows a discrete symmetry singling out the muon. In contrast to the usual type I, II, X, Y models, the  $\mu$ -specific model features a  $\mathbb{Z}_4$  symmetry, which effectively implies type I Yukawa couplings with the exception that

the muon couples to  $\Phi_1$  instead of  $\Phi_2$ , such that  $\zeta_\mu = -\tan\beta$ . For  $\tan\beta$  of order 1000, and a sufficient mass splitting  $M_H < M_A$ , the one-loop diagrams with  $H$ -exchange can provide a positive and sizeable contribution to  $a_\mu$  [1001]. The recent update in Ref. [943] however finds that the required Higgs mass splitting is strongly constrained by perturbativity of the Higgs potential, in particular if perturbativity up to higher energy scales is required.

A different variant of the 2HDM is given by the  $\mu$ - $\tau$ -specific model, where the BSM Higgs-lepton Yukawa coupling mediates a  $\mu$ - $\tau$  transition. It is possible to control charged lepton flavour violation while obtaining sizeable contributions to  $a_\mu$ . We refer to Refs. [943, 1002–1010] for discussions of this case and its generalisations.

In summary, the 2HDM  $a_\mu$  phenomenology has changed significantly in recent years. The parameter region with low pseudoscalar mass  $M_A$  in the type-X or more general FA2HDM with large  $\tan\beta$ /large  $\zeta_l$  has been scrutinised and is now excluded as a viable region with large  $\Delta a_\mu$ . Generally now, most viable 2HDM scenarios predict small contributions to  $a_\mu$  within the  $1\sigma$  band around the new value  $\Delta a_\mu^{\text{Exp-WP2025}}$ .

Still, in exceptional parameter regions the 2HDM can accommodate sizeable contributions to  $a_\mu$ ; e.g. the FA2HDM can reach  $\Delta a_\mu \sim 10^{-9}$  in the heavy-mass region with maximised  $\zeta_l\zeta_u$  as illustrated in Fig. 5.16 (*right*), or the models with generalised Yukawa patterns mentioned in the previous paragraphs can reach even larger values. We stress again that here we have mainly focused on those 2HDM scenarios which have the potential of sizeable contributions to  $a_\mu$ . These are now constrained in non-trivial ways by the new result  $\Delta a_\mu^{\text{Exp-WP2025}}$ , but could also have the potential of accommodating discrepancies, should such discrepancies emerge in the future.

Independently of  $a_\mu$ , there are motivated and simple variants such as the 2HDM type I or type II which are very well studied, and we refer to Refs. [940–942, 944, 945, 1011, 1012] for recent in-depth 2HDM analyses in the light of current experimental data. These references carry out systematic and general global fits of various types of 2HDM parameter spaces without including  $a_\mu$  as a constraint in the fits. They find viable regions in the FA2HDM with light new Higgs states [945] or heavy new Higgs states [940, 944], viable parameter regions in the general 2HDM [1011, 1012] and best-fit regions with Higgs masses around 1.7...2 TeV in the type I [942] and type II [941] models. Except for the FA2HDM region mentioned earlier, all viable regions found in these references predict negligible contributions to  $a_\mu$ , which is now in agreement with the new result  $\Delta a_\mu^{\text{Exp-WP2025}}$ .

Finally, we remark that the 2HDM is frequently considered not in isolation but as part of a larger framework, e.g. together with additional very light new physics [1013–1017] or further scalars [660, 1018–1022], where also dark matter may be explained, together with vector-like fermions [1023–1031] (see also Sec. 5.5.4) or neutrinos [1031], extra U(1) gauge bosons [1032, 1033] or more complicated extensions [1034–1045]. The 2HDM can also be extended to the 3HDM which offers a variety of potential mechanisms, including radiative muon mass generation, such that  $\Delta a_\mu$  behaves as discussed generically in Sec. 3.1 [1046]. All mentioned references focus on  $a_\mu$  in connection with complementary constraints, and we refer to the literature for details of these investigations.

## 5.4. Leptoquark models

Leptoquarks by definition are particles with direct couplings to quarks and leptons that can be assigned baryon and lepton number. Leptoquarks naturally arise both in the Higgs and the gauge sectors of unified theories where quarks and leptons are combined into larger gauge multiplets. More generally leptoquark models can be viewed as simple extensions of the SM by one or few new fields which are motivated by the structure of the quark and lepton sectors and their relationships.

Ref. [1047] has identified 10 possible types of leptoquarks with renormalizable and gauge invariant couplings.<sup>63</sup> The 10 types have either spin 0 or spin 1, and they differ by their electroweak gauge quantum numbers and the resulting possible couplings to up- or down-type left- or right-handed quark and lepton fields.

Adding leptoquarks to the SM dramatically modifies the flavour structure and introduces a large number of free parameters governing the interactions with quarks and leptons of all generations. Depending on these couplings and on the leptoquark mass, many flavour observables can be affected, including  $a_\mu$  but also CLFV and quark flavour observables. In addition, all leptoquarks are strongly interacting and hence can be produced at the LHC, provided their masses are accessible. The LHC experiments therefore obtained lower limits on viable leptoquark masses with values in the range 1 TeV... 5 TeV, see the discussion of Sec. 3.7 and the summary Sec. 94 of Ref. [104]. The values of the limits depend on the assumed flavour patterns of couplings and resulting decay modes. For the scenarios relevant for  $a_\mu$ , leptoquark couplings to muons and heavy quarks are needed, and the appropriate limits are around 2 TeV. Compared to other scenarios of interest for  $a_\mu$ , these are very high mass limits, but the  $a_\mu$  phenomenology is not very sensitive to the precise values; hence in the following we focus on leptoquark masses above 2 TeV.

For an extensive review covering collider and quark and lepton flavour physics of leptoquarks we refer to Ref. [1048]. Since the appearance of that review, leptoquark models have been intensely studied in view of experimental progress on  $a_\mu$  and also on  $B$ -physics where several results hinted at a violation of lepton flavour universality [1049]. It turned out that leptoquark models were particularly promising and intensely studied for combined explanations of deviations from the SM in  $a_\mu$  and  $B$ -physics [271, 608, 1050–1074].<sup>64</sup> However, more recent experimental results have not confirmed those hints for lepton flavour universality violation in  $B$ -physics [1078, 1079]. In the following we explain the possible leptoquark contributions to  $a_\mu$  and how leptoquark models are constrained by  $a_\mu$  and the most directly connected observables. At the end of the subsection we also survey important recent developments related to  $B$ -physics.

#### 5.4.1. Leptoquark types with and without chiral enhancements

The phenomenology of leptoquarks strongly depends on the type [1047] and the assumed flavour structure of couplings. For  $a_\mu$  it is particularly important whether couplings to left-handed and right-handed leptons are simultaneously possible. It has been known for a long time [1080–1082] that in this case very large, chirally enhanced contributions to  $a_\mu$  exist. Three out of the 10 types of leptoquarks allow for such chiral enhancements.<sup>65</sup> As an illustration we focus on one of them, denoted as  $S_1$  model in Ref. [1047]. The Lagrangian terms for the  $S_1$  couplings to quarks and leptons read

$$\mathcal{L}_{S_1} = -\lambda_L^{ij} \overline{q_{L_i}^C} i\sigma_2 l_{L_j} S_1 - \lambda_R^{ij} \overline{u_{R_i}^C} e_{R_j} S_1 + h.c.. \quad (5.95)$$

Here the leptoquark  $S_1$  has spin 0 and the  $SU(3)_c \times SU(2)_L \times U(1)_Y$  gauge quantum numbers  $(\overline{\mathbf{3}}, \mathbf{1}, 1/3)$ . It is thus a scalar  $SU(2)_L$  singlet with electric charge  $Q_{S_1} = 1/3$ . These quantum numbers allow gauge invariant couplings both to left-handed leptons (and left-handed quarks) and to right-handed leptons (and right-handed quarks). The couplings are described by two  $3 \times 3$  matrices in flavour space  $\lambda_{L,R}^{ij}$ . We omit here other gauge invariant operators such as diquark

<sup>63</sup>An additional two leptoquarks states were included in the review [1048], however these can only couple to right handed neutrinos that are not present in the standard model.

<sup>64</sup>Similarly, leptoquarks were considered as combined explanations of the deviations from the SM in  $a_\mu$  and the 2022 CDF measurement of  $M_W$  [290, 1073, 1075–1077]. The CDF measurement and more recent measurements of  $M_W$  were briefly discussed in Sec. 3.4.

<sup>65</sup>A fourth one, the spin-1 leptoquark  $V_1$  is constrained strongly when it is incorporated into an  $SU(5)$  ultraviolet completion and hence effectively cannot contribute to  $a_\mu$  with significant enhancement [194]; for phenomenological discussions of  $a_\mu$  in this model see Ref. [1083].

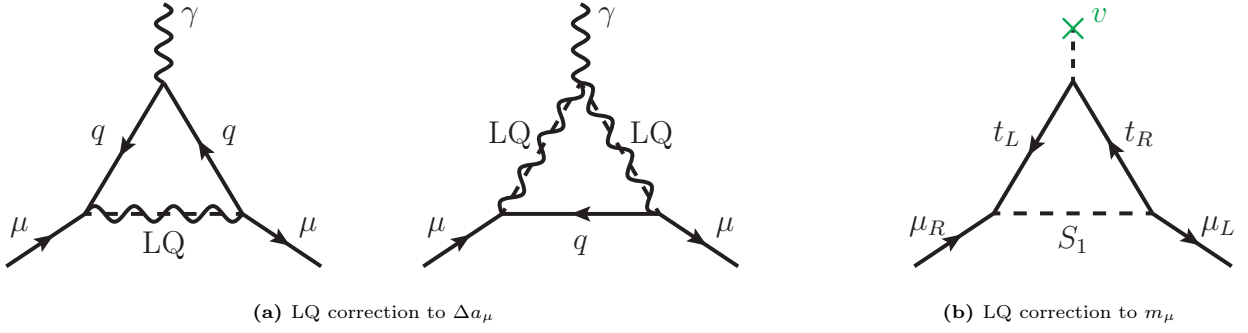


**Figure 5.17:** One-loop Feynman diagrams with leptoquarks (LQ). (a): Generic spin-0 or spin-1 LQ one-loop correction to  $\Delta a_\mu$ , (b):  $S_1$  one-loop contribution to  $m_\mu$  with top-quark mass insertion.

operators, which could mediate proton decay [1084, 1085].

In writing the Lagrangian above we have assumed that the lepton and up-type quark fields are already rotated to their mass basis, while the down-type quark fields inside the doublets need to be rotated to the mass basis using the CKM matrix  $V_{\text{CKM}}$ , such that the interactions with mass eigenstate fields become

$$\mathcal{L}_{S_1} \ni -\overline{u}_i^C (\lambda_L^{ij} P_L + \lambda_R^{ij} P_R) e_j S_1 + \overline{d}_i^C (\lambda_L^{kj} V_{\text{CKM}}^{ki} P_L) \nu_j S_1 + h.c. \quad (5.96)$$

In particular, the left-handed (right-handed) muon couples to the left-handed (right-handed) up-type quarks. Similarly, the so-called  $R_2$  is a scalar  $SU(2)_L$  doublet leptoquark which allows couplings of the left-handed (right-handed) muon to the right-handed (left-handed) up-type quarks; and the  $U_1$  leptoquark is a spin-1  $SU(2)_L$  singlet which allows couplings of the left-handed (right-handed) muon to the left-handed (right-handed) down-type quarks. For all other seven types of leptoquarks, only couplings to either left- or right-handed leptons are allowed, but not both.

The  $S_1$  leptoquark model, and similarly  $R_2$  and  $U_1$ , can be related to our previous discussion of 3-field models in Sec. 2.3 and chirality flips in Sec. 1.1.4. Together with the up-type quarks and their Yukawa couplings to the Higgs, the  $S_1$  model precisely represents a 3-field model of Class I. The left- and right-handed up-type quarks correspond to the fermions  $\psi$ ,  $\chi$ , and the up-type Yukawa couplings correspond to the Higgs coupling  $\lambda_H$  in the Lagrangian of Eq. (2.16a). In such models, the chiral symmetry related to the muon mass, see Eq. (1.12), is not only broken by the muon Yukawa coupling but also by the product of the additional couplings as shown in Eq. (2.22). Specifically for the  $S_1$  model, the relevant new sources of chirality flips are the combinations

$$\lambda_L^{32} \lambda_R^{32} (y_u)_{33}, \quad \lambda_L^{22} \lambda_R^{22} (y_u)_{22}, \quad (5.97)$$

which involve the top-quark and the charm-quark Yukawa coupling, respectively. They can be significantly larger than the muon Yukawa coupling even if the  $\lambda_{L,R}$ -couplings are perturbatively small.

#### 5.4.2. Leptoquark contributions to $a_\mu$

Leptoquarks can contribute to  $a_\mu$  via 1-loop Feynman diagrams as shown in Fig. 5.17a, with a leptoquark and a SM quark in the loop. For scalar leptoquarks, the diagrams correspond to the generic diagrams 2.1b, for vector leptoquarks to 2.1b. Specifically for the  $S_1$  leptoquark, the loop contains up-type quarks like the top quark, and the couplings allow a chiral enhancement as illustrated in Fig. 5.17b, where the chirality is flipped via the top-quark mass instead of the muon mass.

The resulting 1-loop contribution to  $a_\mu$  in the  $S_1$  model from a loop with the up-type quark  $u_i$  reads

$$\Delta a_\mu^{S_1} = \frac{N_C}{16\pi^2} \frac{m_\mu^2}{M_{S_1}^2} \left( \frac{m_{u_i}}{m_\mu} \operatorname{Re}\{\lambda_L^{i2*} \lambda_R^{i2}\} \mathcal{F}^{\text{FS}}(0, x; -1/3) + \{|\lambda_L^{i2}|^2 + |\lambda_R^{i2}|^2\} \mathcal{G}^{\text{FS}}(0, x; -1/3) \right), \quad (5.98)$$

where  $N_C = 3$  is the number of colours and  $M_{S_1}$  is the mass of the leptoquark. In the loop functions, the mass ratio  $x = m_{u_i}^2/M_{S_1}^2$  has been used, the charge  $-Q_{S_1} = -1/3$  needs to be inserted, while the muon mass has been neglected. The first term in Eq. (5.98) contains the chiral enhancement factor ratio  $m_{u_i}/m_\mu$ , resulting from the new sources of chiral symmetry breaking identified in Eq. (5.97). It is illuminating to compare this to Eqs. (3.1) and (3.2) and the discussion of the correlation to the muon mass. We can write the chirally enhanced contributions to  $m_\mu$  and to  $a_\mu$  in a uniform way as

$$\frac{\Delta m_\mu^{S_1}}{m_\mu} = -C_{\text{BSM}} \times B_0(0, m_{u_i}, M_{S_1}), \quad \Delta a_\mu^{S_1} = C_{\text{BSM}} \times \mathcal{F}^{\text{FS}}(0, x; -1/3) \frac{m_\mu^2}{M_{S_1}^2}, \quad (5.99)$$

where the coefficient governing the magnitude of the contributions can be written as

$$C_{\text{BSM}} = \frac{N_C [\operatorname{Re}\{\lambda_L^{i2*} \lambda_R^{i2}\} m_{u_i}]}{16\pi^2 m_\mu}. \quad (5.100)$$

The important factors related to chirality flips and electroweak symmetry breaking have been written between square brackets, as in Eqs. (1.14,1.15). Especially in case of the top-quark the ratio  $m_t/m_\mu \approx 1600$  can provide a huge chiral enhancement, which can lead to huge contributions to  $a_\mu$ , but also  $\mathcal{O}(1)$  corrections to  $m_\mu$ . Even in case of the charm-quark the chiral enhancement can be very large, if the LQ couplings are large.

The result in Eq. (5.98) can also be used to illustrate the behaviour of other types of leptoquarks different from  $S_1$ . For all three types with chiral enhancement,  $S_1$ ,  $R_2$ ,  $U_1$ , a term of the form  $m_{u_i, d_i} \lambda_L^{i2*} \lambda_R^{i2}$  exists which has a strong or very strong chiral enhancement in case the leptoquark couples muons to charm or top quarks (in case of  $S_1, R_2$ ) or bottom quarks (in case of  $U_1$ ). In case these chirally enhanced terms are present, they strongly dominate the result. In case they are zero, the  $|\lambda_L|^2$ - or  $|\lambda_R|^2$ -terms remain. These have no chiral enhancement, but at least one term of this structure exists for all types of leptoquarks.

The strongest chiral enhancement from the top quark is present if both coupling factors  $\lambda_L^{32}$  and  $\lambda_R^{32}$  connecting the muon to the top quark are non-vanishing. Similarly, the weaker chiral enhancement via the charm quark is invoked if both coupling factors  $\lambda_L^{22}$  and  $\lambda_R^{22}$  relating only 2nd-generation fields are non-vanishing. If either  $\lambda_L$  or  $\lambda_R$  vanishes, no chiral enhancement is possible.

Instructive seminumerical approximations for the most interesting contributions read

$$\text{top-loop: } \Delta a_\mu^{S_1} \approx 33 \times 10^{-10} \frac{1 + 0.64 \ln(M_{S_1}/2 \text{ TeV})}{(M_{S_1}/2 \text{ TeV})^2} \frac{\operatorname{Re}\{\lambda_L^{32*} \lambda_R^{32}\}}{0.01}, \quad (5.101)$$

$$\text{charm-loop: } \Delta a_\mu^{S_1} \approx 54 \times 10^{-10} \frac{1 + 0.14 \ln(M_{S_1}/2 \text{ TeV})}{(M_{S_1}/2 \text{ TeV})^2} \operatorname{Re}\{\lambda_L^{22*} \lambda_R^{22}\}, \quad (5.102)$$

$$\text{no chiral enhancement: } \Delta a_\mu^{S_1} \approx 8 \times 10^{-12} \frac{|\lambda_{L,R}^{i2}|^2}{(M_{S_1}/2 \text{ TeV})^2}. \quad (5.103)$$

Here the logarithmic terms arise from the limit of the loop function (2.10) for small fermion and large scalar mass; the numerical factors are from Ref. [1086], where the pure one-loop result (5.98) has been evaluated using running quark masses at the TeV-scale and improved by including the QED-logarithms as discussed in Sec. 4.3 and as implemented in FlexibleSUSY [803, 805].

These numbers show that large contributions of  $\Delta a_\mu \sim 20 \times 10^{-10}$  are easy to obtain in this model, for perturbative values of the couplings. Hence leptoquark models with such chiral enhancements were discussed as promising explanations

of  $\Delta a_\mu^{\text{Exp-WP2020}}$  in Eq. (1.6) in the literature in the Brookhaven era [1080–1082] and later, partially motivated by deviations from the SM in  $B$ -physics, [9, 193, 271–273, 1050–1072, 1074, 1086–1088]. More generally, the  $S_1$ ,  $R_2$  and  $U_1$  models are three of very few viable single-field explanations of  $\Delta a_\mu^{\text{Exp-WP2020}}$  [9, 192–194, 1089], where the spin-1 leptoquarks have been particularly considered in Refs. [192, 194].

In contrast, leptoquark models without chiral enhancements behave as Eq. (5.103), which fits to the generic result (2.15). Since the leptoquark masses are strongly constrained from below, the non-enhanced contributions to  $a_\mu$  are tiny, even if the couplings  $\lambda_{L,R}$  are as large as, e.g.  $\sqrt{4\pi}$ . Such leptoquarks could not explain any significant deviation  $\Delta a_\mu$ . Conversely, since the new result  $\Delta a_\mu^{\text{Exp-WP2025}}$  does not show a significant deviation, such leptoquark models are fully in agreement with  $a_\mu$  data but cannot be constrained by  $a_\mu$  in a non-trivial way.

### 5.4.3. Constraints on leptoquarks from $a_\mu$ and related observables

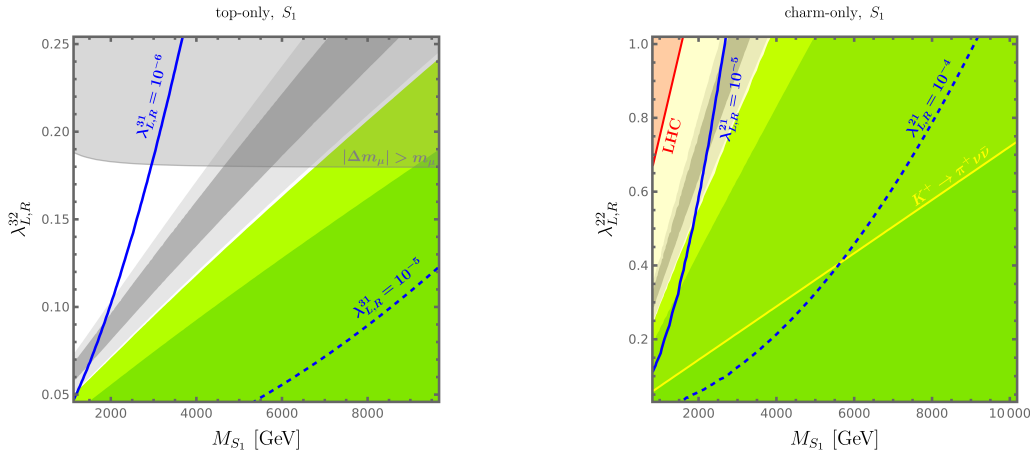


**Figure 5.18:** The leptoquark  $S_1$  parameter space in mass–coupling planes, in the case of couplings only to the top-quark (*left*) or only to the charm-quark (*right*). In both cases the left- and right-handed couplings are set equal,  $\lambda_{L,R}^2 = \lambda_{R,L}^2$ . The (light) green and grey contours correspond to the  $1\sigma$  ( $2\sigma$ ) ranges for  $\Delta a_\mu^{\text{Exp-WP2025}}$  and  $\Delta a_\mu^{\text{Exp-WP2020}}$ , respectively. In the top-only scenario, the transparent grey region shows the region where the LQ one-loop correction to the muon mass contributes more than 100%. In the charm-only scenario, the displayed exclusion regions correspond to  $\text{BR}(K^+ \rightarrow \pi^+ \nu \bar{\nu})$  (yellow) and LHC (red). In both cases, blue contour lines indicate the maximum values the corresponding electron-couplings  $\lambda_{L,R}^1$  can take given the bounds from  $\text{BR}(\mu \rightarrow e\gamma)$ .

As the above approximations show, leptoquark models without chiral enhancements cannot significantly modify  $a_\mu$ ; these models are in agreement with but not constrained by the current  $a_\mu$  results. In contrast, the  $S_1, R_2, U_1$  leptoquark models with chiral enhancements potentially lead to large contributions to  $a_\mu$ . In the following we discuss the relevant constraints derived from  $a_\mu$  and the most directly related complementary observables.

The three cases of leptoquark models with chiral enhancements behave quite similarly to each other [9, 192, 194, 271, 1057, 1088, 1090, 1091], where the  $S_1$  model is compatible with the largest contributions to  $a_\mu$ . Hence we provide explicit results here specifically for the  $S_1$  case. Representative results are shown in the plots in Fig. 5.18. The left plot shows the pure top-loop case (only  $\lambda_{L,R}^{32}$  are non-zero), the right plot shows the pure charm-loop case (only  $\lambda_{L,R}^{22}$  are non-zero).

The relevant parameters for the  $\Delta a_\mu^{S_1}$  contributions in Eqs. (5.101,5.102) are the leptoquark mass  $M_{S_1}$  and the leptoquark couplings between the muon and the top- or charm-quark,  $\lambda_{L,R}^{32}$  or  $\lambda_{L,R}^{22}$ . As mentioned in the beginning, direct LHC searches for leptoquarks are evaded for  $M_{S_1} \gtrsim 2$  TeV, which is what we focus on. In both plots the coupling values have been chosen such that  $\Delta a_\mu^{S_1}$  ranges from 0 to the ballpark of  $\Delta a_\mu^{\text{Exp-WP2020}}$ , while the LQ masses are well

above the basic LHC limit.

Two of the directly connected observables are the muon mass and the muon–Higgs coupling, as discussed in general in Secs. 3.1, 3.3. The muon mass is particularly interesting here because of the potentially very large chirality flipping parameter in Eq. (5.97). In terms of the coefficient  $C_{BSM}$  in Eq. (5.100) its one-loop correction in the  $\overline{\text{MS}}$  scheme at the scale  $\mu = M_{S_1}$  is

$$\left| \frac{\Delta m_\mu^{\text{fin}}}{m_\mu} \right| = C_{BSM} \times |B_0^{\text{fin}}(0; m_{u_i}^2, M_{S_1}^2)| \sim C_{BSM}. \quad (5.104)$$

In Fig. 5.18 the parameter region with  $|\Delta m_\mu| > m_\mu$  is indicated as the transparent grey region above around  $\lambda_{L,R}^{32} \gtrsim 0.18$  in the top-loop case. This region might be considered unphysical in view of finetuning in the muon mass, though this is not a strict bound [9, 105], see also Sec. 3.1. In line with the general relation (3.1) and in view of the lower LHC leptoquark mass limit, this consideration cuts off leptoquark contributions to  $\Delta a_\mu$  larger than  $\Delta a_\mu^{\text{Exp-WP2020}}$  for  $S_1$  masses above 5 TeV.<sup>66</sup>

The modification of the muon–Higgs coupling is generally correlated with contributions to  $a_\mu$  as explained in Sec. 3.3. Refs. [271, 273, 1087] and [202] specifically studied the correlation in case of leptoquark  $S_1$  and  $R_2$  models, and generalised 3-field models as defined in Sec. 2.3. In all these models, the muon–Higgs coupling is modified only at the loop level, and the resulting effects are below experimental sensitivities which can be reached at the LHC. Hence we do not show constraints from the muon–Higgs coupling in Fig. 5.18. Similarly, Z-boson couplings to leptons [272, 1092] and  $h \rightarrow \gamma\gamma$  decays [1093] can be modified by leptoquark loop contributions, but the constraints do not interfere significantly with the potential of large leptoquark contributions to  $a_\mu$ .

Very important constraints on the relevant parameters result from quark flavour-violating processes. Quark flavour violation is unavoidable because the coupling matrices acting in the up-/lepton sector and in the down-/neutrino sector, see Eq. (5.96), cannot be simultaneously diagonal. For general flavour constraints on leptoquarks we refer to Refs. [1094, 1095]. Here we follow Ref. [1088] and highlight several instructive minimal cases related to  $a_\mu$ :

- Charm-philic up-origin case: the muon–charm couplings  $\lambda_{L,R}^{22}$  are the only non-vanishing matrix elements of  $\lambda_{L,R}$ : in this case the muon-neutrino will inevitably couple to quarks of all generations, and the processes  $K^+ \rightarrow \pi^+ \nu \bar{\nu}$  [1088] and  $\bar{B} \rightarrow \bar{K} \nu \bar{\nu}$  [1050, 1087] are affected.
- Top-philic up-origin case: similarly for the muon–top couplings  $\lambda_{L,R}^{32}$ : the same processes are affected.
- Charm-philic down-origin case: the muon-neutrino–strange coupling  $(V_{\text{CKM}}^T \lambda_L)^{22}$  is assumed to be the only non-vanishing matrix element of  $(V_{\text{CKM}}^T \lambda_L)$ , and similarly for  $\lambda_R^{22}$ : in this case the coupling  $\lambda_L^{12}$  to the up-quark is generated and the  $D^0 \rightarrow \mu\mu$  [1050, 1088] and further charm-quark decays such as  $D^+ \rightarrow \pi^+ \mu\mu$  [1094] are affected.

One may also study an analogous top-philic down-origin case [1088] or a case where the leptoquark couples equally strongly to all lepton generations [1086], with analogous conclusions.

Quantitatively, the  $\bar{B} \rightarrow \bar{K} \nu \bar{\nu}$  process does not constrain the couplings relevant for  $\Delta a_\mu^{\text{LQ}} \lesssim 20 \times 10^{-10}$  at all [1050, 1087]. In contrast, the  $D^0 \rightarrow \mu\mu$  decay very significantly restricts the allowed ranges of the couplings to the charm- and

<sup>66</sup>The bound is only visible in the top-only case shown in the left panel of Fig. 5.18; essentially the same bound also exists in the charm-only case (right panel) but is located outside the region shown in the plot.

up-quarks [1050, 1088]. For instance, in the charm-philic down-origin case,  $\Delta a_\mu^{\text{LQ}}$  is bound to be smaller than around  $4 \times 10^{-10}$  [1088] in the  $S_1$  model, and similarly in the  $R_2$  model.

In the charm-philic up-origin case [1088], where  $\lambda_{L,R}^{22}$  are the only non-vanishing matrix elements, larger  $\Delta a_\mu^{\text{LQ}}$  are possible. Here, the  $K^+ \rightarrow \pi^+ \nu \bar{\nu}$  decay directly restricts the  $\lambda_L^{22}$  coupling. In an updated analysis, Refs. [1086, 1088] find

$$|\lambda_L^{22}| < 0.14 \left( \frac{M_{S_1}}{2 \text{ TeV}} \right). \quad (5.105)$$

This bound is shown as the yellow area in Fig. 5.18, but it is important to note that the bound in the plot relies on the equality  $\lambda_L^{22} = \lambda_R^{22}$  — larger  $\Delta a_\mu$  would be compatible with the  $K^+$  decay if  $\lambda_L^{22} < \lambda_R^{22}$ .

The muon–charm couplings  $\lambda_{L,R}^{22}$  are also constrained by LHC searches in a way that is relevant for  $a_\mu$  [1088, 1096]. Di-lepton or single-lepton production LHC processes at high  $p_T$  can be affected by leptoquark  $t$ -channel exchange even for very heavy leptoquark masses above the direct leptoquark search limit. Recasting LHC results for such processes results in constraints which essentially depend on the ratios  $\lambda_{L,R}^{22}/M_{S_1}$  to a good approximation and which are approximately equal for  $\lambda_L^{22}$  and  $\lambda_R^{22}$  [1088, 1096]. E.g. for  $M_{S_1} = 2 \text{ TeV}$ , these references find upper limits on the couplings between 1.2 and 1.8, depending on the employed LHC processes. As an approximation to the limits found in these references we take

$$|\lambda_{L,R}^{22}| < 0.3 + 0.9 \frac{M_{S_1}}{2 \text{ TeV}}. \quad (5.106)$$

In the plot this bound is weaker than the bound (5.105) from Kaon decay, but the LHC limits are still important since they independently apply onto the right-handed coupling  $\lambda_R^{22}$ . In Fig. 5.18 we show the LHC limit of Ref. [1088] as the red region.

Turning from quark to lepton flavour violation, Sec. 3.2 has explained the generic correlation between BSM contributions to  $a_\mu$  and to CLFV processes such as  $\mu \rightarrow e\gamma$ . This correlation is particularly acute in the case of leptoquarks, which can couple to all quark and all lepton generations with in principle arbitrary coupling matrices.<sup>67</sup>

While quark flavour violation is an unavoidable consequence of the leptoquark interactions, lepton flavour violation (in the limit of vanishing neutrino masses) can be avoided by specific choices of the interaction matrices. However, once all coupling matrix elements are allowed to be non-zero, the constraints are extremely strong.

The most important and most directly related CLFV process is the  $\mu \rightarrow e\gamma$  decay. Leptoquark contributions to  $\mu \rightarrow e\gamma$  have been computed and discussed in detail in Refs. [1048, 1053, 1084, 1086, 1098, 1099]. In line with the generic estimate (3.29) we can relate the leptoquark contributions to  $\mu \rightarrow e\gamma$  and  $a_\mu$  as

$$\text{top-loop:} \quad \text{BR}(\mu \rightarrow e\gamma)^{S_1} = 2 \times 10^{-4} \left( \frac{\Delta a_\mu^{S_1}}{10^{-9}} \right)^2 \left( \left| \frac{\lambda_L^{31}}{\lambda_L^{32}} \right|^2 + \left| \frac{\lambda_R^{31}}{\lambda_R^{32}} \right|^2 \right), \quad (5.107a)$$

$$\text{charm-loop:} \quad \text{BR}(\mu \rightarrow e\gamma)^{S_1} = 2 \times 10^{-4} \left( \frac{\Delta a_\mu^{S_1}}{10^{-9}} \right)^2 \left( \left| \frac{\lambda_L^{21}}{\lambda_L^{22}} \right|^2 + \left| \frac{\lambda_R^{21}}{\lambda_R^{22}} \right|^2 \right), \quad (5.107b)$$

where in each line we only allow either only couplings to the top- or to the charm-quark, respectively, like in Eq. (5.103). Here, in addition to the parameters contributing to  $a_\mu$ , also couplings to the electron, i.e.  $\lambda_{L,R}^{i1}$ , appear. The appearing ratios of couplings to electrons and muons are very strictly constrained because of the MEG-II limit on  $\text{BR}(\mu \rightarrow e\gamma)$ .

<sup>67</sup>Similarly, if complex couplings are allowed, there are strong correlations to electric dipole moments. As discussed in Sec. 3.2, this correlation is particularly constraining in case of naive scaling, which is not necessarily the case for leptoquark models due to the flavour structure of the couplings  $\lambda_{L,R}^{ij}$ , which is in general unknown. Here we assume real couplings and refer to the literature for EDM studies in the context of leptoquarks [1097].

In particular if the contributions to  $a_\mu$  are significant and of the order  $10^{-9}$ , the coupling ratios must be smaller than around  $10^{-5}$ .

This implies that significant leptoquark contributions to  $a_\mu$  are only tenable if the leptoquark couplings are highly non-universal — couplings to the muon must be many orders of magnitude larger than couplings to electrons. This result is illustrated in Fig. 5.18, where we show blue contours indicating where the maximum allowed values of leptoquark couplings to electrons are  $10^{-4,-5,-6}$ . Again, this is in line with the generic conclusions of Sec. 3.2.<sup>68</sup>

Next to  $\mu \rightarrow e\gamma$ , further CLFV processes such as  $\tau \rightarrow \mu\gamma$  and  $\mu \rightarrow e$  conversion provide important additional constraints on leptoquark couplings.  $\tau \rightarrow \mu\gamma$  constrains the couplings to the  $\tau$  lepton  $\lambda_{L,R}^{i3}$ , and  $\mu \rightarrow e$  conversion especially constrains the couplings to 1st-generation quarks,  $\lambda_{L,R}^{1i}$ . In all these cases, similar statements can be made as for  $\mu \rightarrow e\gamma$ : if leptoquarks lead to  $\Delta a_\mu \sim 10^{-9}$ , the leptoquark couplings mediating CLFV processes must be several orders of magnitude smaller than the ones to muons [1053, 1070, 1086].

It is instructive to summarise the main constraints on leptoquark couplings for the specific case of the  $S_1$  leptoquark with mass  $M_{S_1} \gtrsim 2$  TeV, as follows:

- $\Delta a_\mu^{S_1} \sim 10^{-9}$  is possible via muon–top couplings of order 0.1; the left- and right-handed couplings  $\lambda_{L,R}^{32}$  can be similar. CLFV constraints require the electron–top and  $\tau$ -lepton–top couplings to be several orders of magnitude smaller. This scenario predicts small effects e.g. in  $\bar{B} \rightarrow \bar{K}\nu\bar{\nu}$  and  $K^+ \rightarrow \pi^+\nu\bar{\nu}$  below the current sensitivity.
- Contributions of  $\Delta a_\mu^{S_1} \sim 10^{-9}$  are even possible for leptoquark masses in the multi-TeV region, however these are then accompanied by radiative corrections to the muon mass of order 100%, which may be considered unnatural.
- $\Delta a_\mu^{S_1} \sim 10^{-9}$  is also possible via muon–charm couplings. In this case,  $K^+ \rightarrow \pi^+\nu\bar{\nu}$  requires a strong hierarchy  $\lambda_L^{22} \ll \lambda_R^{22}$ , and again CLFV constraints require the couplings of electron and  $\tau$ -lepton to be much smaller.
- If only muon–charm couplings are allowed and equality  $\lambda_L^{22} \approx \lambda_R^{22}$  is assumed, the contributions to  $a_\mu$  are bound to be below around  $10^{-10}$  and thus negligible.
- If a generic flavour pattern is assumed where all leptoquark couplings  $\lambda_{L,R}^{ij}$  are of the same order of magnitude, the CLFV constraints from e.g. Eq. (5.107) limit contributions to  $a_\mu$  even stronger to below  $10^{-14}$ .

These statements illustrate why leptoquarks were considered so frequently in the literature as simple explanations of the old deviation  $\Delta a_\mu^{\text{Exp-WP2020}}$ . Still, the parameter regions which produce sizeable contributions to  $a_\mu$  are rather narrow, requiring specific types of leptoquark couplings and flavour patterns. The current result  $\Delta a_\mu^{\text{Exp-WP2025}}$  is compatible with smaller leptoquark contributions to  $a_\mu$ , which could allow e.g. anarchic leptoquark flavour patterns or small contributions to the muon mass.

#### 5.4.4. Brief survey of leptoquark scenarios with specific flavour structures

The summary above highlights that only leptoquark models with very non-generic flavour structure have the potential for significant contributions to  $a_\mu$ . In the past years, leptoquarks were very frequently considered also in view of several

<sup>68</sup>With respect to the correlation with other lepton dipole observables, we note that leptoquarks were also considered as a potential explanation of the deviation of the electron magnetic moment  $a_e$  resulting from the SM value in Eq. (3.17a) at the time [235, 629, 1090, 1091, 1100, 1101][1060], and that leptoquarks provide a slight variation of the “single particle contribution” explained in Sec. 3.2 with less constraints from  $\mu \rightarrow e\gamma$  because of the quark flavour structure allowed in the couplings [1091].

reported  $B$ -physics “anomalies”, i.e. deviations between SM predictions and measurements. The most prominent such anomalies were reported for the ratios of observables  $R(K^{(*)})$  and  $R(D^{(*)})$  related to  $b \rightarrow s$  and  $b \rightarrow c$  transitions, respectively. In the meantime, improved measurements show a reduced tension. Here we nevertheless provide a brief survey of the literature to illustrate the range of possible effects that can be caused by leptoquarks and how observables from other sectors can be related to  $a_\mu$ .

The ratios  $R(K^{(*)})$  are defined as  $R(K^{(*)}) = \Gamma(\bar{B} \rightarrow \bar{K}^{(*)}\mu\mu)/\Gamma(\bar{B} \rightarrow \bar{K}^{(*)}ee)$  and test lepton flavour universality (LFU) in  $b \rightarrow s$  transitions. As reviewed in 2021 e.g. in Ref. [1049], the SM predicts these ratios to be very close to unity, because gauge couplings to leptons are universal for all lepton generations, whereas experiments showed a  $> 3\sigma$  discrepancy from the SM prediction. The LHCb measurements published in 2022 [1078] supersede the previous ones and are in full agreement with the SM prediction, eliminating the hints for LFU violation [1079, 1102]. The ratios  $R(D^{(*)})$  are defined via  $b \rightarrow c$  decays  $R(D^{(*)}) = \Gamma(\bar{B} \rightarrow \bar{D}^{(*)}\tau\bar{\nu})/\Gamma(\bar{B} \rightarrow \bar{D}^{(*)}\ell\bar{\nu})$  where  $\ell = e, \mu$ . For these processes, there still is a certain disagreement between experiment and SM prediction [1103],

$$R(D)^{\text{SM}} = 0.296 \pm 0.004 \qquad R(D^*)^{\text{SM}} = 0.254 \pm 0.005, \qquad (5.108)$$

$$R(D)^{\text{Exp}} = 0.342 \pm 0.026 \qquad R(D^*)^{\text{Exp}} = 0.286 \pm 0.012. \qquad (5.109)$$

When the results for  $R(K^{(*)})$  and  $R(D^{(*)})$  were first reported to be anomalous, i.e. in tension between SM and experiment, Ref. [1050] showed that all these anomalies, and a significant contribution to  $a_\mu$  were simultaneously possible in the  $S_1$  leptoquark model, and it was also shown that this scenario could be embedded into a left-right symmetric gauge theory [1051] or into a model of radiative neutrino mass generation [1052, 1053]. Improved measurements and constraints from the  $B \rightarrow K\nu\bar{\nu}$  however ruled out simple explanations of the reported anomalies in  $R(K^{(*)})$ ,  $R(D^{(*)})$  and  $a_\mu$  at the time by just a single leptoquark [1054–1057].

Simultaneous explanations remained possible in more complicated models such as two leptoquarks  $S_1$  and  $S_3$  [1055, 1060, 1061], three different leptoquarks [1062], the  $S_1$  leptoquark plus a charged scalar singlet [1063]. Also simultaneous explanations of the anomalies at the time together with neutrino masses were considered with  $S_1$  and  $\tilde{R}_2$  [1064, 1070] or with  $S_1$ ,  $\tilde{R}_2$  and  $S_3$  [1068] or with  $R_2$  and  $S_3$  leptoquarks [1059], or with leptoquarks plus other BSM states [1065, 1066, 1071, 1072, 1074]. Reference [1067] also constructs elaborate models involving gauge symmetries related to flavour and include leptoquarks charged under that gauge symmetry to explain various observations, and Ref. [1104] uses such scenarios to even explain dark matter and neutrino masses at the same time. This exemplifies that one can build models with deep construction principles which can lead to large effects in all flavour observables — but it remains true that even within such symmetry-based models, large  $\Delta a_\mu$  and  $B$ -physics effects arise independently and are not connected. The need for such complicated constructions has been generalised into a no-go theorem [402] which states that at least four BSM fields are required to accommodate large  $\Delta a_\mu$ , the  $B$ -physics anomalies circa 2021, and dark matter.

The discussion shows that if leptoquarks exist in the few-TeV mass region, their flavour structure is likely highly non-generic. This point is also visualised graphically with best-fit points in Ref. [1070]. It motivates studies how non-generic flavour patterns could emerge from underlying mechanisms.

Basic ways to generate flavour patterns include the Froggatt-Nielsen mechanism [1105], which can be applied to single leptoquark models [1106] or models with  $S_1$  and  $S_3$  leptoquarks [1107], or generalisations of the Minimal Flavour Violation (MFV) paradigm [1108]. In all these cases the leptoquark couplings to muons, electrons and  $\tau$ -leptons depend on underlying parameters and are thus correlated. Huge coupling ratios such as the ones needed in the plots of Fig. 5.18 cannot occur. As a result, the bounds on CLFV processes imply that only negligibly small contributions to  $a_\mu$  are possible.

There exist, however, also leptoquark flavour constructions which allow significant contributions to  $a_\mu$ . An appealing example is provided by the combination of leptoquarks with a flavour-dependent gauge group such as  $U(1)_{L_\mu-L_\tau}$  discussed already in Sec. 5.1.3. Leptoquarks can be charged under this gauge group, thus allowing e.g. only couplings to muons but not to other leptons. Such leptoquarks, called muoquarks in Ref. [1067], cannot mediate CLFV processes and hence can have significant couplings to muons and lead to  $\Delta a_\mu$  contributions of the order  $10^{-9}$ .

In total, the current status of  $a_\mu$  as well as the flavour anomalies mentioned here do not show evidence for new physics. While the fundamental motivation for the existence of leptoquarks related e.g. to grand unification remains, current phenomenological constraints do not prefer particular parameter regions and do not require leptoquarks at the TeV-scale.

## 5.5. Vector-like fermion models

Over the past decade many properties of the Higgs boson have been measured with impressive precision and, consequently, reinforced our picture of the SM with exactly three generations of chiral fermions. The existence of a fourth, sequential chiral generation is conclusively ruled out [1109, 1110]. This statement, based mainly on measurements of  $h \rightarrow \gamma\gamma$ , however, does not rule out the existence of new fermions beyond the SM in general. Clearly, introducing new fermions is one of the obvious ways to extend the SM. For example, additional gauge singlet fermions (“right-handed neutrinos”) with large Majorana masses not only avoid the bounds from the Higgs signal strength but could also explain the observed tiny neutrino masses (cf. Sec. 3.5).

Another possibility, discussed in this section, is the existence of vector-like, or Dirac fermions. Unlike the chiral fermions in the SM, both the left- and right-handed chiralities of such fermions by definition transform in the same way under the SM gauge group, leading to vector-like interactions with the SM gauge bosons. Because of this, these *vector-like fermions* (VLF) can also possess a gauge invariant Dirac mass term before EWSB,

$$\mathcal{L} \supset \overline{F}_L M_F F_R + \overline{F}_R M_F^* F_L. \quad (5.110)$$

Consequently, the VLF can be arbitrarily heavy and again easily evade the Higgs signal strength bounds without violating perturbativity. Historically, VLF have gained attention in the context of Kaluza-Klein excitations [1111, 1112] in models with extra dimensions, mainly introduced in an attempt to address the hierarchy problem [1113, 1114]. Also anthropic arguments have been put forward to motivate that VLF should be the lightest BSM states, while new scalars should be much heavier [269, 1115]. At the same time, VLF have also been explored phenomenologically in the context of dark matter [1116, 1117], collider experiments [1118–1121] and, after the BNL measurement, also increasingly received interest in the context of  $\Delta a_\mu$  [191, 192, 269, 270, 1122].

In general, corrections from VLF first enter  $\Delta a_\mu$  at the two-loop level e.g. through Barr-Zee diagrams discussed in Sec. 4.2. Therefore, unless additional scalars are present that lead to further enhancements (see Sec. 5.5.4), their contributions are typically rather moderate. However, there is also a special class of VLF, the *vector-like leptons* (VLL), which can mix with the SM leptons at tree-level and can lead to new sources of chirality flips.

The phenomenology of such VLL is rich and distinctive, and the new tree-level chirality flips modify  $a_\mu$ ,  $m_\mu$ , Higgs decays and more generally the lepton mass-generation mechanism in unique ways which differ from other scenarios and can lead to large effects. Here we focus mainly on this case, first in the pure context of the SM extended by fermions, later by also allowing additional scalar fields in Sec. 5.5.4.

	$N$	$E$	$L$	$L_{\frac{3}{2}}$	$N^a$	$E^a$
<b>Repr.</b>	$(\mathbf{1}, 0)$	$(\mathbf{1}, -1)$	$(\mathbf{2}, -\frac{1}{2})$	$(\mathbf{2}, -\frac{3}{2})$	$(\mathbf{3}, 0)$	$(\mathbf{3}, -1)$
<b>Multiplet</b>	$N$	$E$	$\begin{pmatrix} L^0 \\ L^- \end{pmatrix}$	$\begin{pmatrix} L^- \\ L^{--} \end{pmatrix}$	$\begin{pmatrix} N^0 & \sqrt{2}N^+ \\ \sqrt{2}N^- & -N^0 \end{pmatrix}$	$\begin{pmatrix} E^- & \sqrt{2}E^0 \\ \sqrt{2}E^{--} & -E^- \end{pmatrix}$
$-\mathcal{L}_{\text{int}}$	$\lambda_L \bar{l}_L N \tilde{\Phi}$	$\lambda_L \bar{l}_L E \Phi$	$\lambda_R \bar{L} e_R \Phi$	$\lambda_R \bar{L}_{\frac{3}{2}} e_R \tilde{\Phi}$	$\lambda_L \bar{l}_L \sigma^a N^a \tilde{\Phi}$	$\lambda_L \bar{l}_L \sigma^a E^a \Phi$

**Table 5.4:**  $SU(2)_L \times U(1)_Y$  representation, multiplet structure ( $\sigma^a F^a$  for the triplets) and interaction terms for all possible vector-like fermions coupling to SM leptons and the Higgs doublet. The new Yukawa couplings follow the conventions from Sec. 2.3.

### 5.5.1. Vector-like lepton models and chiral enhancement

We define VLL as the subclass of VLF which can mix with the SM leptons via gauge invariant and renormalisable operators. Without the introduction of new scalars, this requirement of non-trivial mixing puts strong restrictions on their possible quantum numbers. The only allowed renormalisable kinds of mixing terms are either dimension-3 gauge invariant fermion mass terms, in which case the VLL is required to have the same quantum numbers as the SM counterpart, or dimension-4 Yukawa couplings of a VLL to a SM lepton and the Higgs doublet. Since the mass terms can be diagonalised (without breaking gauge invariance), the relevant mixing stems from the latter. Including the charge-conjugate Higgs field  $\tilde{\Phi} = i\sigma^2 \Phi^*$ , there are exactly 6 different possible such Yukawa terms (corresponding to model 10–15 in Tab. 2.1),

$$\bar{l}_L N \tilde{\Phi}, \quad \bar{l}_L E \Phi, \quad \bar{L} e_R \Phi, \quad \bar{L}_{\frac{3}{2}} e_R \tilde{\Phi}, \quad \bar{l}_L \sigma^a N^a \tilde{\Phi}, \quad \text{and} \quad \bar{l}_L \sigma^a E^a \Phi, \quad (5.111)$$

where the representations and hyper-charges of the Dirac fermion fields  $N, E, L, L_{\frac{3}{2}}, N^a, E^a$  are listed in Tab. 5.4 and we have suppressed the SM family indices. In the following we denote the couplings of VLL to the left-handed SM doublet by  $\lambda_L$  and to the right-handed singlet by  $\lambda_R$ .

In isolation, these new interactions can lead to Feynman diagrams as illustrated in Fig. 5.19a for the example of  $L$ . The left of the diagrams illustrates one-loop corrections to the muon–Higgs interaction, the muon mass and  $a_\mu$ . For instance, the correction to the muon mass and its correlation to the fundamental Yukawa coupling is of the form

$$m_\mu = \frac{y_\mu v}{\sqrt{2}} \left[ 1 + \mathcal{O}\left(\frac{\lambda_{L/R}^2 v^2}{M^2}\right) \right]. \quad (5.112)$$

This effect is obviously amplified if several VLL are present. However, there is no chiral enhancement since each of the terms in Eq. (5.111) on its own does not lead to an additional breaking of the SM lepton chiral symmetries.

In the case the SM is extended by several VLL at the same time, there is the possibility of a much stronger enhancement due to new sources of chiral symmetry breaking for the SM leptons. Concretely, this chiral enhancement emerges if Yukawa couplings between the VLL are allowed. In the minimal case of two VLL this is again allowed for precisely 6 different combinations, given by [269]

$$L \oplus E, \quad L \oplus N, \quad L_{\frac{3}{2}} \oplus E, \quad L \oplus E^a, \quad L \oplus N^a, \quad \text{and} \quad L_{\frac{3}{2}} \oplus E^a. \quad (5.113)$$

The corresponding Yukawa terms are given by<sup>69</sup>

$$L \oplus E : \quad \mathcal{L} \supset -\bar{L} \left( \lambda_\Phi P_R + \bar{\lambda}_\Phi P_L \right) E \Phi \quad + h.c. \quad (5.114a)$$

$$L \oplus N : \quad \mathcal{L} \supset -\bar{L} \left( \lambda_\Phi P_R + \bar{\lambda}_\Phi P_L \right) N \tilde{\Phi} \quad + h.c. \quad (5.114b)$$

$$L_{\frac{3}{2}} \oplus E : \quad \mathcal{L} \supset -\bar{L}_{\frac{3}{2}} \left( \lambda_\Phi P_R + \bar{\lambda}_\Phi P_L \right) E \tilde{\Phi} \quad + h.c. \quad (5.114c)$$

$$L \oplus E^a : \quad \mathcal{L} \supset -\bar{L} \left( \lambda_\Phi P_R + \bar{\lambda}_\Phi P_L \right) \sigma^a E^a \Phi \quad + h.c. \quad (5.114d)$$

$$L \oplus N^a : \quad \mathcal{L} \supset -\bar{L} \left( \lambda_\Phi P_R + \bar{\lambda}_\Phi P_L \right) \sigma^a N^a \tilde{\Phi} \quad + h.c. \quad (5.114e)$$

$$L_{\frac{3}{2}} \oplus E^a : \quad \mathcal{L} \supset -\bar{L}_{\frac{3}{2}} \left( \lambda_\Phi P_R + \bar{\lambda}_\Phi P_L \right) \sigma^a E^a \tilde{\Phi} \quad + h.c.. \quad (5.114f)$$

Fig. 5.19b shows sample diagrams involving these terms; the last of these contributes to the muon mass similarly to the seesaw mechanism for neutrino masses, hence the name charged-seesaw models [269]. Notably, the appearing coupling parameters  $\lambda_\Phi$  and  $\bar{\lambda}_\Phi$  for the two different chirality combinations are, in general, independent and in combination with  $\lambda_L$  and  $\lambda_R$  both lead to a new, separate breaking of the muon chiral symmetry of the kind discussed in Sec. 1.1.4. The two corresponding order parameters can be written as

$$\lambda_R \lambda_\Phi^* \lambda_L, \quad \text{and} \quad \lambda_R M_L^* \bar{\lambda}_\Phi^* M_{E/N}^* \lambda_L. \quad (5.115)$$

The appearance of the Dirac masses in the second product is noteworthy and in particular implies that the  $\bar{\lambda}_\Phi$ -term dominates the contributions to  $a_\mu$  in the limit of large VLL masses as discussed below.

The diagrams in Fig. 5.19b illustrate the correlated contributions of these VLL to the muon–Higgs coupling, and to  $a_\mu$ . Their analysis makes explicit the general arguments presented in Secs. 1.1.4, 3.1 and 3.3. Historically, the analysis of the correlations in VLL models of Refs. [269, 270] preceded the generic analysis presented already in Sec. 3.3. Here we first sketch the key observations, before providing detailed calculations and results.

Because of the new source of tree-level chirality flips, the muon mass receives two tree-level contributions

$$m_\mu^H = \frac{y_\mu v}{\sqrt{2}}, \quad m_\mu^{HHH} \sim -\frac{\lambda_{Li} \bar{\lambda}_\Phi^* \lambda_{Rj} v^3}{2\sqrt{2} M_E M_L}, \quad (5.116)$$

where the first one results from the fundamental Yukawa interaction and the second one from the diagram with three external Higgs fields in Fig. 5.19b. The exact form of its explicit result depends on the choice of the VLL model but is always of the generic form indicated in Eq. (5.116), involving the new chiral symmetry breaking parameter of Eq. (5.115) governed by  $\bar{\lambda}_\Phi$ . This second contribution corresponds to the Wilson coefficient for the dimension-6 operator introduced in Sec. 3.3 as  $m_\mu^{HHH} = -C_{e\Phi} v^3 / 2\sqrt{2}$ . With these two tree-level quantities representing the two origins of chirality flips,

---

<sup>69</sup> Though very similar, the VLL models do not all map directly onto the three-field models discussed in Sec. 2.3. Instead e.g. the  $L \oplus E$  model is more closely related to Model 6 discussed in Ref. [195] and mentioned in footnote 13, however, with the crucial difference that  $\phi \equiv \Phi$ . As a consequence the muon chiral symmetry cannot be extended to the scalar doublet and is indeed broken in the VLL models. For this reason, chiral enhancements are possible and the phenomenological behaviour is similar to the one of the three-field model of Class II. Similar comparisons can be made for all six cases listed in Eq. (5.113).

the physical results for the muon mass, the muon–Higgs coupling and for  $\Delta a_\mu$  can be written as

$$m_\mu = m_\mu^H + m_\mu^{HHH}, \quad (5.117a)$$

$$\frac{\lambda_{\mu\mu}}{\lambda_{\mu\mu}^{\text{SM}}} = \frac{m_\mu^H + 3m_\mu^{HHH}}{m_\mu} = 1 + \frac{2m_\mu^{HHH}}{m_\mu}, \quad (5.117b)$$

$$\Delta a_\mu = -\mathcal{Q} \frac{m_\mu m_\mu^{HHH}}{8\pi^2 v^2}, \quad (5.117c)$$

in full agreement with the discussions of Sec. 3.3 and Eq. (3.44). As announced there, the VLL models represent the important class of models, where there is a relative loop factor between the new chirality flips and the contributions to  $a_\mu$ , i.e. the prefactor  $\kappa = \frac{64\pi^2}{\mathcal{Q}}$  and  $\mathcal{Q}$  is of the order one. In the following we discuss the detailed computations of these and further related quantities, provide the explicit values of  $\mathcal{Q}$  and discuss the phenomenological behaviour. In that discussion, non-chirally enhanced corrections such as Eq. (5.112) will be neglected unless explicitly mentioned.

In order to determine the corrections more precisely one can either follow the EFT discussion presented in Sec. 3.3 or compute the exact results in the full theory, which we outline here. To start, performing the calculation in the full theory requires the introduction of unitary matrices  $U_L$  and  $U_R$  in order to diagonalise the lepton mass matrix. This matrix results on the one hand from the above Yukawa terms after EWSB, but also contains contributions from the Dirac mass terms of the VLL. For example, in the  $L \oplus E$  model it is given by (the analogous matrices in the other models are listed in Ref. [269])

$$\mathcal{M}^- = \begin{array}{c} \overline{e_{Li}} \\ \overline{L_L^-} \\ \overline{E_L} \end{array} \begin{array}{ccc} e_{Rj} & L_R^- & E_R \\ \left( \begin{array}{ccc} y_{ej} \frac{v}{\sqrt{2}} & 0 & \lambda_{Lj} \frac{v}{\sqrt{2}} \\ \lambda_{Rj} \frac{v}{\sqrt{2}} & M_L & \lambda_\Phi \frac{v}{\sqrt{2}} \\ 0 & \bar{\lambda}_\Phi \frac{v}{\sqrt{2}} & M_E \end{array} \right) & & \end{array}. \quad (5.118)$$

The unitary matrices are chosen such that  $U_L^\dagger \mathcal{M}^- U_R = \text{diag}(m_e, m_\mu, m_\tau, m_4, m_5) \equiv m_l$  and the corresponding mass-eigenstate lepton fields<sup>70</sup> are given by  $\hat{e}_{L/R} = U_{L/R}^\dagger (e_i, L^-, E)_{L/R}$ . Analytic expressions for  $U_{L/R}$  can be found e.g. in Ref. [270] up to order  $v^2$ , and in the other models similar diagonalisation matrices also need to be introduced for the neutral leptons  $\hat{\nu}_{L/R}$  and doubly charged fields  $\rho_{L/R}$ . As a result of going to the mass basis, the couplings to both the gauge bosons and the Higgs boson are changed by the unitary transformation. In particular, due to the presence of the Dirac masses, the lepton mass- and Yukawa matrices are no longer simultaneously diagonalised. In the above example we obtain for the coupling of lepton mass eigenstates to the physical Higgs

$$-\mathcal{L} \supset \bar{\hat{e}}_L U_L^\dagger \begin{pmatrix} y_e & 0 & \lambda_L \\ \lambda_R & 0 & \lambda_\Phi \\ 0 & \bar{\lambda}_\Phi & 0 \end{pmatrix} U_R \hat{e}_R \frac{h}{\sqrt{2}} = \bar{\hat{e}}_L \frac{1}{v} \left[ m_l - U_L^\dagger \text{diag}(0, M_L, M_E) U_R \right] \hat{e}_R h \equiv \bar{\hat{e}}_L^a \lambda_{ab} \hat{e}_R^b h. \quad (5.119)$$

This yields an enhanced tree-level correction to the effective (SM) lepton–Higgs couplings

$$\lambda_{ij} \approx \frac{m_i}{v} \delta_{ij} - \frac{\lambda_{Li} \bar{\lambda}_\Phi^* \lambda_{Rj} v^2}{\sqrt{2} M_E M_L} + \mathcal{O}(v^4), \quad (5.120)$$

<sup>70</sup>Because of the more complicated mixing structure than in the SM, we use modified conventions here compared to Appendix A: the fields  $\hat{e}^a$   $a = 1 \dots 5$  correspond to mass eigenstate fields, which are linear combinations of the SM lepton fields  $e_i$ ,  $i = 1 \dots 3$  and the new fields  $L^-$  and  $E$ . A similar notation can be used in the neutrino sector and in the other VLL models.

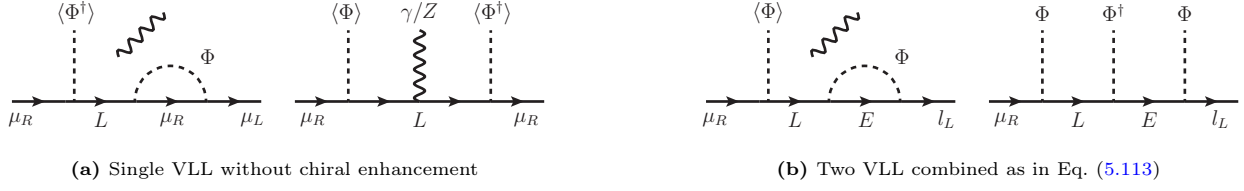


**Figure 5.19:** Sample VLL diagrams illustrating contributions to the muon mass,  $a_\mu$ , the muon–Higgs coupling and the dimension-6 operators defined in Sec. 3.3. The Higgs fields can either be interpreted as *vevs* or as physical Higgs bosons, and the gauge boson line can optionally be connected to the diagrams. (a): Single VLL contributes to e.g.  $\Delta a_\mu$  and the effective  $Z \rightarrow \mu\mu$  coupling with the same non-enhanced chiral structure. (b): Two VLL  $L \oplus E$  provide one-loop contributions to e.g.  $\Delta a_\mu$  and a tree-level correction to  $h \rightarrow \mu\mu$  with the same chirally enhanced structure.

in agreement with Eq. (3.44) and the announcement in Eq. (5.117b). As a side note, if one generation of VLL couples to multiple generations of SM leptons, LFV Higgs couplings are induced at tree-level which are already strongly constrained e.g. by LFV Higgs decays like  $h \rightarrow \tau\mu$  and low-energy LFV observables like  $\mu \rightarrow e$ . This behaviour is similar, though slightly more complex, to the single-field case discussed in Sec. 3.2 and Eq. (3.35).

Similarly, because of the mixing between leptons of different  $SU(2)_L$  representations, the couplings to the  $Z$ - and  $W$ -boson are also no longer diagonal,

$$\mathcal{L} \supset -\frac{g^2}{2c_W} \bar{e} \not{Z} \left( g_L^Z P_L + g_R^Z P_R \right) \hat{e} - \frac{g}{\sqrt{2}} \bar{\nu} W^+ \left( g_L^W P_L + g_R^W P_R \right) \hat{e} + h.c. \quad (5.121)$$

where  $(g_{L/R}^W)_{\nu_{ab}} = (U_{L/R})_{ab}$  and the  $Z$  coupling matrices are given by <sup>71</sup>

$$(g_L^Z)_{ab} = (s_W^2 - \frac{1}{2})\delta_{ab} + \frac{1}{2}(U_L^\dagger)_{a5}(U_L)_{5b}, \quad (5.122a)$$

$$(g_R^Z)_{ab} = s_W^2 \delta_{ab} - \frac{1}{2}(U_R^\dagger)_{a4}(U_R)_{4b}. \quad (5.122b)$$

Again the deviation from the SM coupling, in general, introduces LFV couplings at tree-level. However, unlike in the case of the chirality-flipping observables (in particular Eq. (5.120)) here the corrections are not proportional to either of the combinations in Eq. (5.115) but are instead given by

$$(\delta g_L^Z)_{ij} = +\frac{1}{2}(U_L^\dagger)_{i5}(U_L)_{5j} \approx +\frac{\lambda_{Li}^* \lambda_{Lj} v^2}{4M_E^2} + \mathcal{O}(v^4) \quad (5.123a)$$

$$(\delta g_R^Z)_{ij} = -\frac{1}{2}(U_R^\dagger)_{i4}(U_R)_{4j} \approx -\frac{\lambda_{Ri}^* \lambda_{Rj} v^2}{4M_L^2} + \mathcal{O}(v^4) \quad (5.123b)$$

This different structure compared to the corrections in the lepton–Higgs coupling is crucial to satisfy both the  $Z$ -pole precision observables and LHC constraints (discussed in more detail below) with non-zero Yukawa couplings to the VLL.

### 5.5.2. Vector-like lepton contributions to $a_\mu$

Thanks to the mixing, couplings between the muon and the VLL arise at tree level, and contributions to  $a_\mu$  arise at the one-loop level. They can be obtained immediately using the generic formulas given in Sec. 2.1 and the couplings computed above. The dominant contributions are generated by the diagrams with internal VLL and Higgs- or  $Z/W$ -boson, where

<sup>71</sup>Note that in the  $L \oplus E$  model diagonalisation matrices for the neutrino mass eigenstates are not required, such that  $\hat{\nu}_L = (\nu_{L,i}, L_L^0, 0)$  and  $\hat{\nu}_R = (0, L_R^0, 0)$ . For the other combinations this is usually not the case, such that e.g. the  $W$ -boson couplings also receive a contribution from the neutrino diagonalisation.

the chirality flip appears on the VLL line. For example, in the  $L \oplus E$  model these are given by<sup>72</sup>

$$\Delta a_\mu^h = \sum_{a=4,5} \frac{m_\mu m_a}{16\pi^2 M_h^2} \text{Re}\{\lambda_{\mu a} \lambda_{a\mu}\} \mathcal{F}^{\text{FS}}(0, \frac{m_a^2}{M_h^2}; 0) \quad (5.124a)$$

$$\Delta a_\mu^Z = \sum_{a=4,5} \frac{m_\mu m_a}{16\pi^2 M_Z^2} \text{Re}\{(g_L^Z)_{a\mu}^* (g_R^Z)_{a\mu}\} \mathcal{F}^{\text{FV}}(0, \frac{m_a^2}{M_Z^2}; 0) \quad (5.124b)$$

$$\Delta a_\mu^W = \frac{m_\mu M_L}{16\pi^2 M_W^2} \text{Re}\{(g_L^W)_{4\mu}^* (g_R^W)_{4\mu}\} \mathcal{F}^{\text{FV}}(0, \frac{M_L^2}{M_W^2}; -1). \quad (5.124c)$$

In addition, diagrams involving only SM fields are also different from the pure SM since, as discussed above, the mixing also affects the couplings between those fields. These effects are however strongly constrained and the resulting corrections to  $\Delta a_\mu$  therefore suppressed.

To gain qualitative insight into the above formulas for the case of  $M \gg v$  it is useful to consider the mass-insertion diagrams shown in Fig. 5.19. Fig. 5.19a illustrates the contribution of a single VLL to  $\Delta a_\mu$  (left) as well as a tree-level contribution to the muon- $Z$  coupling with the same chiral structure (right). For  $\Delta a_\mu$ , the required chirality flip and  $vev$  is provided by the SM muon Yukawa coupling and  $v$ , and the relevant mass scale in the loop is  $\mathcal{O}(v)$ . As a consequence, diagrams of this form do not result in chirally enhanced contributions to  $\Delta a_\mu$ , but instead give

$$\Delta a_\mu^{\text{VLL, non-enhanced}} \sim \frac{m_\mu y_\mu v}{16\pi^2 v^2} (\delta g_{L/R}^Z)_{\mu\mu}, \quad (5.125)$$

Since the constraints on deviations in the  $Z$ - $\mu$  coupling by electroweak precision data [1123, 1124] and  $Z$ -pole observables [191, 1125] are already rather stringent, such contributions can result at most in  $\Delta a_\mu^{\text{VLL, non-enhanced}} \lesssim \mathcal{O}(10^{-12})$ .

On the other hand, in Fig. 5.19b (left) we illustrate the contribution of two virtual VLL. Importantly, this diagram has the same chiral structure as the tree-level diagram Fig. 5.19b (right) that generates the  $\bar{l}_L \mu_R \Phi (\Phi^\dagger \Phi)$  operator discussed in Sec. 3.3 and which results in the chirally enhanced contributions to  $\lambda_{\mu\mu}$  in Eq. (5.120). This implies that such diagrams also generate the same chiral enhancement in  $\Delta a_\mu$ , and the full contributions can be estimated by multiplying with the required factors as discussed before and in Sec. 1.1.4,

$$\Delta a_\mu^{\text{VLL, enhanced}} \sim \frac{m_\mu}{16\pi^2} \frac{[\lambda_{L2} \bar{\lambda}_\Phi^* \lambda_{R2} v]}{\sqrt{2} M_E M_L}, \quad (5.126)$$

where the terms collected in the square brackets have the same meaning as in Eqs. (1.15), or equivalently

$$\Delta a_\mu^{\text{VLL, enhanced}} \sim \frac{m_\mu}{16\pi^2 v} \delta \lambda_{\mu\mu}, \quad (5.127)$$

where  $\delta \lambda_{\mu\mu}$  is the correction term on the r.h.s. of Eq. (5.120). This equation reproduces the announced result (5.117c). Compared to Eq. (5.125) this contribution is larger roughly by a chiral enhancement factor of  $\bar{\lambda}_\Phi / y_\mu \sim \mathcal{O}(1000)$  and can therefore comfortably reach large values such as  $\Delta a_\mu^{\text{Exp-WP2020}}$ .

Yet another useful way to understand the chirally enhanced VLL contributions to  $a_\mu$  is via the three-field models discussed in Sec. 2.3. As mentioned in footnote 69, the enhanced contribution in Eq. (5.126) behaves similarly to the one of the Class II three-field model, see also Eq. (2.19). A similar VLL contribution proportional to  $\lambda_\Phi$  exists as well and is similar to the Class I model. In the relevant limit where the VLL masses  $M_F$  are much larger than the SM Higgs-boson mass, the limiting behaviour of the three-field model analysed in Eq. (2.31) shows that the  $\lambda_\Phi$ -contribution has an additional  $v^2/M_F^2$ -suppression compared to the  $\bar{\lambda}_\Phi$ -term.

<sup>72</sup>In the models with  $L_{3/2}$  or  $E^a$  there will also be contributions from the doubly-charged VLL and  $W^+$ .

Model	$L \oplus E$	$L \oplus N$	$L_{\frac{3}{2}} \oplus E$	$L \oplus E^a$	$L \oplus N^a$	$L_{\frac{3}{2}} \oplus E^a$
$\mathcal{Q}$	1	–	5	9	1	5

**Table 5.5:** Correlation factors for the VLL models.

Now we turn to the correlation with the muon–Higgs coupling, which plays a unique role in VLL models as previewed in Eqs. (5.117). Indeed, combining the formula for  $\Delta a_\mu$  with the one for the muon–Higgs coupling in Eq. (5.120) results in a correlation like Eq. (3.47) (in the absence of CP violation) [269, 270, 274, 275, 1126],

$$R_{\mu\mu} \equiv \frac{\Gamma(h \rightarrow \mu\mu)}{\Gamma(h \rightarrow \mu\mu)_{\text{SM}}} \approx \left| \frac{\lambda_{\mu\mu}}{\lambda_{\mu\mu}^{\text{SM}}} \right|^2 = \left| 1 - 0.86 \left( \frac{\Delta a_\mu}{\mathcal{Q} \times 10^{-9}} \right) \right|^2, \quad (5.128)$$

where the constants  $\mathcal{Q}$  for the different models can be obtained from the full computation of all quantities and are listed in Tab. 5.5. As discussed in Sec. 3.3 a correlation of this form appears in any model where chirally enhanced contributions to  $\Delta a_\mu$  are present. However, in generic theories the corrections to  $\lambda_{\mu\mu}$  appear first at one-loop order [202] resulting in suppressions equivalent to  $\mathcal{Q} \sim \mathcal{O}(16\pi^2)$ .

As mentioned in Sec. 3.3, the VLL models are unique in that they predict much smaller values of  $\mathcal{Q} \sim \mathcal{O}(1)$  as a consequence of the fact that the chirally enhanced corrections to  $\lambda_{\mu\mu}$  arise already at tree level. Therefore, these models exhibit a strong correlation between  $R_{\mu\mu}$  and  $\Delta a_\mu$  which aids in discriminating between the different scenarios. The only exception is the  $L \oplus N$  model. In this case the operator  $(\bar{l}\tilde{\Phi}e)(\Phi^\dagger\tilde{\Phi})$  induced by the chiral structure in Fig. 5.19b vanishes due to the anti-symmetric  $SU(2)$  index contraction. Similarly, the leading-order corrections to  $\Delta a_\mu$  also vanish [1115], such that the model effectively behaves like one without any chiral enhancement. Hence, in this model the correlation is also accidentally weak. We note that allowing for complex couplings results in an additional contribution from  $d_\mu$  to the above correlation (cf. Sec. 3.3) and thus also a constraint on the possible CP violation [275, 1127, 1128].

The above correlation has an immediate, strong phenomenological consequence: In order to achieve  $R_{\mu\mu} \approx 1$  in agreement with LHC measurements,  $\Delta a_\mu$  is restricted, and numerically the restriction affects exactly the range of interest. One solution is sufficiently small  $\Delta a_\mu$ , a second solution is where the term involving  $\Delta a_\mu$  in Eq. (5.128) becomes  $\approx -2$ . This second, *flipped-sign* solution requires one specific non-vanishing and positive value of  $\Delta a_\mu$  in the ballpark of “a few”  $\times 10^{-9}$ . Here we point out that higher-order corrections to the correlation Eq. (5.128) can have a potentially significant effect on the predicted asymptotic value of  $\Delta a_\mu$  [1129]. Fig. 5.20 (left) shows a comparison between  $\Delta a_\mu$  (in the  $L \oplus E$  model) obtained for  $R_{\mu\mu} = 1$  at tree-level (red) and one-loop order<sup>73</sup> (blue). As predicted, for large masses the leading-order result converges to the fixed value  $\Delta a_\mu \approx 22 \times 10^{-10}$  dictated by Eq. (5.128), which is intriguingly close to the previous deviation  $\Delta a_\mu^{\text{Exp-WP2020}}$ . The one-loop corrected correlation predicts a significantly smaller value and no longer converges to a fixed value for increasing VLL masses due to the logarithmic enhancement present in the one-loop corrections. This effect is even stronger when non-zero values of  $\lambda_\Phi$  are allowed since at one-loop both combinations of chiral enhancement from Eq. (5.115) contribute in a similar way, as discussed in Ref. [1129].

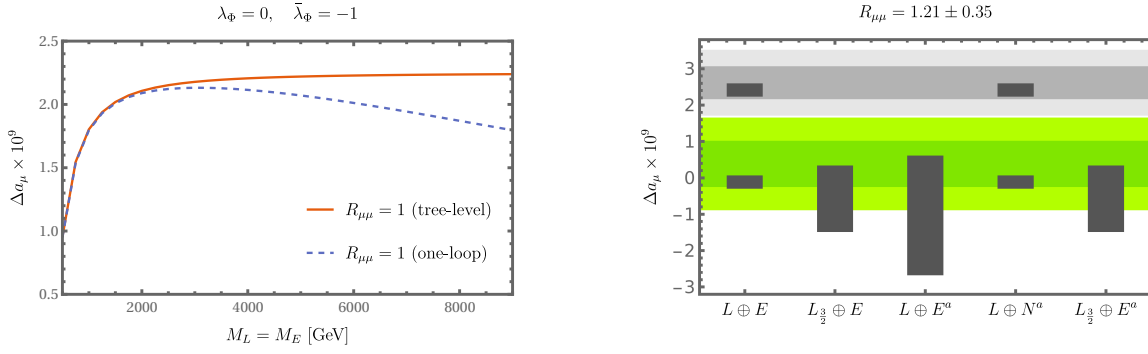


**Figure 5.20:** Correlation between  $\Delta a_\mu$  and the muon–Higgs coupling and its impact in the VLL model  $L \oplus E$ . *left:* Comparison between the value of  $\Delta a_\mu$  required to obtain  $R_{\mu\mu} = 1$  at tree-level (red) and one-loop (blue). *right:* Ranges of  $\Delta a_\mu$  allowed by Eq. 5.128 and the current experimental bounds. The (light) grey band shows the  $1\sigma$  ( $2\sigma$ ) range of  $\Delta a_\mu^{\text{Exp-WP2020}}$  while the (light) green band shows the  $1\sigma$  ( $2\sigma$ ) range for  $\Delta a_\mu^{\text{Exp-WP2025}}$ .

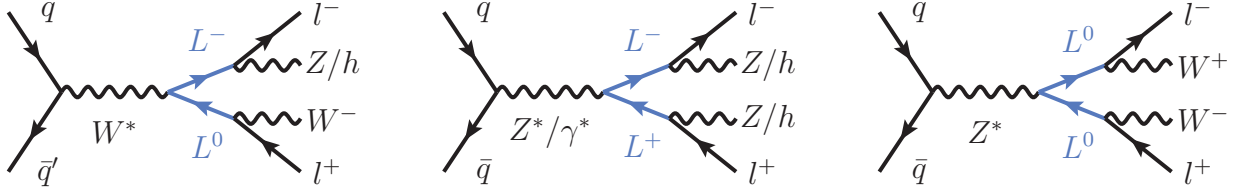


**Figure 5.21:** Illustration of pair-production and subsequent decay of a doublet VLL at the LHC.

### 5.5.3. Collider searches and precision constraints

Since the VLL have only a negligible impact on the Higgs production cross section, the experimental bounds on  $R_{\mu\mu}$  can immediately be obtained from the current measurements of the di-muon Higgs decay at the LHC resulting in [104, 276, 277]

$$R_{\mu\mu} = 1.21 \pm 0.35. \quad (5.129)$$

The resulting ranges of  $\Delta a_\mu$  allowed by Eq. (5.128) are shown for the different models in Fig. 5.20 (right). The grey band shows the ( $1$  and  $2\sigma$ ) region  $\Delta a_\mu = \Delta a_\mu^{\text{Exp-WP2020}}$  and the green band the new result  $\Delta a_\mu^{\text{Exp-WP2025}}$ , which is compatible with zero. As discussed, the correlation (5.128) for real parameters leads to two possible solutions. Agreement with the LHC data is achieved for either very small values of  $\Delta a_\mu$  or sufficiently large values such that the muon–Higgs coupling has the same magnitude but opposite sign (*flipped-sign* case) to the SM. Coincidentally, two of the models ( $L \oplus E$  and  $L \oplus N^a$ ) predict a large deviation very close to  $\Delta a_\mu^{\text{Exp-WP2020}}$  in this *flipped-sign* scenario, as already shown in Fig. 5.20 (left) in more detail. In contrast, the  $L_{\frac{3}{2}} \oplus E$ ,  $L \oplus E^a$  and  $L_{\frac{3}{2}} \oplus E^a$  models with  $\mathcal{Q} = 5$  or  $9$  would require a deviation much larger than  $\Delta a_\mu^{\text{Exp-WP2020}}$  to be compatible with  $R_{\mu\mu}$ . Consequently, for these last three models, the *flipped-sign* case had already been firmly excluded at the time of the previous result  $\Delta a_\mu^{\text{Exp-WP2020}}$ .

For the two  $L \oplus E$  and  $L \oplus N^a$  models, the previous result  $\Delta a_\mu^{\text{Exp-WP2020}}$  was very well compatible with the *flipped-sign* case; now, the new result  $\Delta a_\mu^{\text{Exp-WP2025}}$  disfavours this option. Even in the case where a future non-vanishing deviation is established, however of a smaller magnitude of order  $\lesssim 10^{-9}$ , the *flipped-sign* case would remain disfavoured or excluded

<sup>73</sup>These results are based on consistent one-loop calculations for both observables, but including two-loop (i.e. next-to-leading order) corrections to  $\Delta a_\mu$  could lead to further shifts of the correlation.

for all these VLL models.

For all the five models shown in Fig. 5.20 (right), on the other hand, the normal-sign case predicts small  $\Delta a_\mu$  and is thus compatible with  $\Delta a_\mu^{\text{Exp-WP2025}}$ . In this case the difference between the five models is the possible range of  $\Delta a_\mu$  values. In the two models with  $\mathcal{Q} = 1$ , the  $R_{\mu\mu}$  constraint is only compatible with very small  $\Delta a_\mu$ , while the models with  $\mathcal{Q} = 5$  or 9 still comfortably allow  $|\Delta a_\mu| \gtrsim \mathcal{O}(5 \times 10^{10})$  even in the normal-sign case. The current measurement of  $\Delta a_\mu^{\text{Exp-WP2025}}$  thus constrains the parameter space of the  $\mathcal{Q} = 5, 9$  models in a non-trivial way, and a future even more precise determination of  $\Delta a_\mu$  could be important to discriminate between the VLL models. We finally note that all models predict  $R_{\mu\mu} < 1$  for a positive deviation  $\Delta a_\mu$ , while the current measurement favours values larger than one. This leads to the asymmetric distribution around  $\Delta a_\mu = 0$  seen in Fig. 5.20.

Besides the indirect tests the LHC also provides very stringent exclusion limits on the VLL masses, significantly improving on the bound of  $M \gtrsim 100$  GeV set by LEP [426]. Several searches for direct production of VLL at the LHC were performed by ATLAS [428–430], CMS [431–433] and Refs. [191, 1130–1135] focused in particular on scenarios with the SM-like doublet and singlet VLL  $L$  and  $E$ . At the LHC these would mainly be pair-produced via exchange of a virtual gauge-boson, i.e.  $pp \rightarrow \gamma^*/Z^* \rightarrow L^+L^-$ ,  $pp \rightarrow Z^* \rightarrow L^0\bar{L}^0$  or  $pp \rightarrow W^* \rightarrow L^-\bar{L}^0$  in case of the doublet or  $pp \rightarrow \gamma^*/Z^* \rightarrow E^+E^-$  in case of the singlet. After production these VLL primarily decay into a SM lepton and gauge- or Higgs boson with branching ratios given by (in the limit of  $M \gg v$ )  $\text{BR}(L^\pm \rightarrow l^\pm + Z/h) \simeq 50\%$ ,  $\text{BR}(L^0 \rightarrow l^\pm + W^\mp) \simeq 100\%$  for the doublet as well as  $\text{BR}(E^\pm \rightarrow l^\pm Z/h) \simeq 25\%$  and  $\text{BR}(E^\pm \rightarrow \nu W^\pm) \simeq 50\%$  in case of the VLL singlet. The resulting processes relevant for the LHC analyses are shown in Fig. 5.21. Recently, searches for VLL in the full run-2 data set have been performed by ATLAS [430], CMS [433] and [1134], yielding the most stringent exclusion limits to date. For VLL coupling to exclusively to muons (electrons) [tau] [430, 433] these are given by<sup>74</sup>

$$\text{doublet : } \quad M_L > 1270 \text{ (1220) [1040] GeV} \quad (5.130)$$

$$\text{singlet : } \quad M_E > 400 \text{ (320) [170] GeV.} \quad (5.131)$$

The significantly weaker bounds on VLL singlets result from the smaller pair production cross section compared to the doublet scenario. So far, no dedicated searches for  $L_{3/2}$  or the triplet VLL have been performed, however, the similar type III see-saw triplet has already been excluded for masses below 1 TeV [1137]. Given that the pair production cross section is comparable to or even larger than in the doublet case [269], a recasting could further strengthen this bound.

Another important constraint on the VLL models stems from EWPO like  $Z$ -pole measurements [269, 270]. These result in bounds on the mixing between VLL and SM leptons, i.e. in particular the combination Eq. (5.123). For example, in case of the  $L \oplus E$  model the updated bounds on the  $\mu$ - $Z$  coupling from Ref. [1125] translate (at tree-level) into [1129]

$$\left| \frac{\lambda_R^\mu v}{M_L} \right| \lesssim 0.03, \quad \left( \frac{\lambda_L^\mu v}{M_E} \right)^2 + 1.16 \left( \frac{\lambda_R^\mu v}{M_L} \right)^2 \lesssim 0.001. \quad (5.132)$$

Similar constraints also hold for the other models. Notably, in combination with Eq. (5.115) and Eq. (5.128) these constraints require either  $\bar{\lambda}_\Phi \approx 0$  (with  $\Delta a_\mu \approx 0$ ) or  $|\bar{\lambda}_\Phi| \gtrsim 1.5$  (with  $\Delta a_\mu \approx \Delta a_\mu^{\text{Exp-WP2020}}$ ). While the latter case is consistent with perturbativity and other experimental bounds, it is potentially in conflict with the constraints from vacuum stability [1138–1140], which strengthens the conclusion that the *flipped-sign* case is now disfavoured. The technical

<sup>74</sup>It has been argued [1136] that searches for single production of VLL might be necessary to conclusively rule out VLL below the TeV scale.

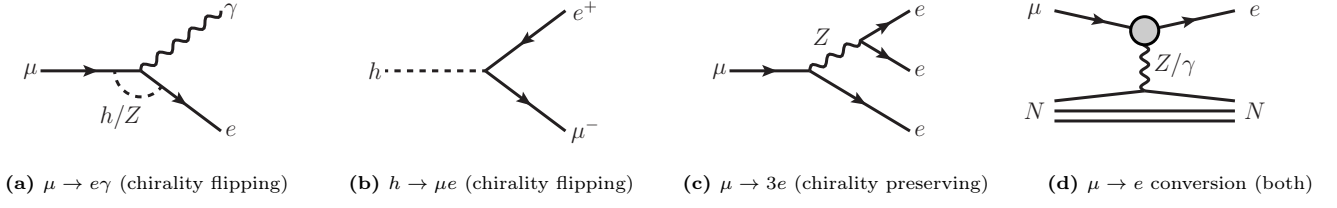


**Figure 5.22:** Illustration of the leading-order contributions to LFV observables in the VLL models.

reason is that VLF generically contribute in the same way as the top-quark to the RGE of the quartic Higgs coupling  $\lambda$

$$\beta(\lambda) \sim \frac{1}{4\pi^2} (2\bar{\lambda}_\Phi^2 \lambda - \bar{\lambda}_\Phi^4) \quad (5.133)$$

and thus further drive  $\lambda(\mu)$  to negative values as  $\mu$  increases. Requiring that the quartic Higgs coupling stays positive up to some scale  $\Lambda$  therefore translates into upper bounds on the VLL Yukawa couplings, which turn out to be rather stringent [1139]. In fact, already for moderate choices like  $\Lambda = 100$  TeV, values of  $\bar{\lambda}_\Phi \gtrsim 1$  are essentially excluded. This issue is potentially remedied by the introduction of additional scalars [1141] which will be discussed in the following subsection.

Lastly, if the VLL couple to multiple SM leptons simultaneously, constraints from LFV observables need to be taken into account. The impact of these constraints on the VLL models has already been studied in several different scenarios. Refs. [1142, 1143] considered in particular constraints from  $\mu \rightarrow e\gamma$  and  $\mu \rightarrow 3e$  on the  $L \oplus E$  model, Ref. [1144] also included a 4th generation of vector-like quarks and Refs. [235, 1122] considered extensions to 3 generations of VLL and with constraints from  $\mu \rightarrow e$  conversions and LFV processes involving also the 3rd generation. VLL besides the SM-like doublet and singlet have also been studied in Ref. [1145] with focus on models without chiral enhancement.

As discussed in Sec. 3.2, if  $a_\mu$  receives large contributions, the strongest LFV constraints typically stem from the dipole operators generated at one-loop through diagrams like Fig. 5.22a. In the VLL models the flavour mixing angles defined in Sec. 3.2 are given by

$$\theta_{2i} = \frac{\lambda_R^i}{\lambda_R^\mu}, \quad \text{and} \quad \theta_{i2} = \frac{\lambda_L^i}{\lambda_L^\mu}, \quad (5.134)$$

corresponding to the scenario of single particle contribution Eq. (3.34). The current CLFV bounds from  $\text{BR}(\mu \rightarrow e\gamma)$  and  $\text{BR}(\tau \rightarrow \mu\gamma)$  in Eq. (3.21) imply

$$|\theta_{i\mu}|^2 + |\theta_{\mu i}|^2 \lesssim \left( \frac{10^{-9}}{\Delta a_\mu} \right)^2 \begin{cases} 2.6 \times 10^{-9} & i = e \\ 0.4 & i = \tau \end{cases} \quad (5.135)$$

If the muon couplings are near the limits (5.132) for VLL masses around  $\mathcal{O}(1$  TeV) and sizeable  $\Delta a_\mu$ , the VLL must couple very weakly to the other generations  $|\lambda_{L/R}^e| \lesssim 10^{-5}$  and  $|\lambda_{L/R}^\tau| \lesssim 0.1$ .

It is also interesting to compare these processes to the Higgs decays  $\text{BR}(h \rightarrow \mu + \tau/e)$  induced by the tree-level diagram in Fig. 5.22b. Similar to Eq. (5.126), the LFV Higgs couplings are related to  $\Delta a_\mu$  by

$$\lambda_{ij} \approx -0.86 \frac{\theta_{ij} \Delta a_\mu}{\mathcal{Q} \times 10^{-9}} \frac{m_\mu}{v} \quad (5.136)$$

The relatively large Higgs decay width  $\Gamma_h \approx 4 \times 10^{-3}$  GeV combined with the current bounds [104]

$$\text{BR}(h \rightarrow \mu e) < 4.4 \times 10^{-5}, \quad \text{and} \quad \text{BR}(h \rightarrow \mu\tau) < 1.5 \times 10^{-3} \quad (5.137a)$$

lead to significantly weaker constraint (particularly in for the models with  $\mathcal{Q} = 9$  or 5) on the electron couplings compared to Eq. (3.21)

$$|\theta_{i\mu}|^2 + |\theta_{\mu i}|^2 \lesssim \left(\frac{10^{-9}}{\Delta a_\mu}\right)^2 \begin{cases} 0.5\mathcal{Q}^2 & i = e \\ 16\mathcal{Q}^2 & i = \tau \end{cases} \quad (5.138)$$

In scenarios without chiral enhancement strong LFV constraints result from  $\mu \rightarrow e$  conversion and  $\mu \rightarrow 3e$ . Numerically (again up to representation dependent  $\mathcal{O}(1)$  factors) we have [265, 266]

$$\begin{aligned} \text{BR}(\mu\text{Au} \rightarrow e\text{Au}) &= \frac{m_\mu^5}{8M_Z^4 \Gamma_{\text{capt}}^{\text{Au}} c_W^2} \left| (1 - 4s_W^2) V_{\text{Au}}^{(p)} - V_{\text{Au}}^{(n)} \right|^2 \left( |g_{L12}^Z|^2 + |g_{R12}^Z|^2 \right) \\ &\sim \frac{7 \times 10^{-13}}{(M/1 \text{ TeV})^4} \left( \left| \frac{\lambda_L^e \lambda_L^\mu}{10^{-5}} \right|^2 + \left| \frac{\lambda_R^e \lambda_R^\mu}{10^{-5}} \right|^2 \right) \end{aligned} \quad (5.139)$$

and similarly for  $\mu \rightarrow 3e$

$$\text{BR}(\mu \rightarrow 3e) = \frac{\alpha m_\mu^5}{128\pi^2 M_Z^4 \Gamma_\mu c_W^2} \left( |g_{L12}^Z|^2 + |g_{R12}^Z|^2 \right) \sim \frac{4.2 \times 10^{-13}}{(M/1 \text{ TeV})^4} \left( \left| \frac{\lambda_L^e \lambda_L^\mu}{5 \cdot 10^{-5}} \right|^2 + \left| \frac{\lambda_R^e \lambda_R^\mu}{5 \cdot 10^{-5}} \right|^2 \right). \quad (5.140)$$

Again, these require highly non-universal couplings to the SM leptons and, as mentioned in Sec. 3.2, the bounds for both  $\mu \rightarrow 3e$  and  $\mu \rightarrow e$  conversions are even expected to improve by several order of magnitude in the near future.

#### 5.5.4. Vector-like fermions with extended scalar sectors

So far, we have highlighted several motivations for studying extended fermion sectors and, e.g. in Sec. 5.3, also extended scalar sectors. Here we want to discuss how a combination of both VLF and new scalar sectors can lead to appealing BSM scenarios which can offer solutions to open questions and lead to a diverse phenomenology. Notably, there are several mutual benefits which motivate both extended scalar sectors from the perspective of VLF and vice versa. On the one hand, additional scalars help to weaken the strong bounds on VLF imposed by vacuum stability [1139–1141, 1146, 1147] which can significantly increase the high energy validity of such models. They also open up further possibilities for including dark matter [203, 545, 1148–1153], neutrino masses (e.g. in case of triplet scalar) [1150, 1154–1157] or even explanations of the entire SM flavour structure [1038, 1046, 1158, 1159]. On the other hand, additional fermions in theories with extended scalar sectors can free up otherwise excluded parameter space [1030, 1155, 1160] and aid in the explanation of tentative anomalies [1161–1163].

Among the examples above, one of the most well studied scenarios is the addition of new fermion content in the 2HDM. Such models not only fit naturally into the context of SUSY, where additional VLF can solve the little hierarchy problem and provide (at least in part) the large required corrections to the Higgs mass [1164–1166], but also offer a rich phenomenology, especially in the context of  $\Delta a_\mu$ . For simplicity we consider only the case of 2HDM+ $L \oplus E$  for concrete examples and results, although most of the discussion will also apply for other combinations of VLL and more generic VLF.

Similar to the usual Yukawa interaction terms in the 2HDM (cf. Eq. (5.83)), the VLF generically couple to both Higgs doublets

$$\mathcal{L} \supset - \sum_{a=1,2} \left\{ \bar{L}_L Y_a^l e_R + \bar{L} \lambda_R^a e_R + \bar{L}_L \lambda_L^a E + \bar{L} \left( \lambda_\Phi^a P_R + \bar{\lambda}_\Phi^a P_L \right) E \right\} \Phi_a + h.c., \quad (5.141)$$

In order to avoid large FCNC (in the limit  $\lambda_{L/R} \rightarrow 0$ ) one can impose a  $\mathbb{Z}_2$  symmetry under which  $\Phi_1 \rightarrow -\Phi_1$  and  $\Phi_2 \rightarrow \Phi_2$ . Like in the usual 2HDM, this also forces the VLF to couple exclusively to one of Higgs doublets, depending

on their charge assignments. Usually,  $L$  is chosen to transform like  $l_L$  and  $E$  like  $e_R$ , such that both the SM leptons and VLL couple only to  $\Phi_1$ . This scenario was extensively studied in Refs. [1023, 1024, 1026, 1028, 1029] and corresponds to type-II/X assignments for both the VLL and SM leptons. However, other choices are also possible. For example, taking the opposite charge assignments for the VLL implies that the VLL mix with the SM leptons only via  $\phi_2$ , leading to a relative  $\cot\beta$  suppression of these terms.

For the usual type-II/X assignments the resulting lepton mass matrix is given by

$$\mathcal{M}^- = \begin{array}{c} \overline{e_{Li}} \\ \overline{L_L} \\ \overline{E_L} \end{array} \begin{array}{ccc} e_{Rj} & L_R^- & E_R \\ \left( \begin{array}{ccc} (Y_1^l)_{ij} \frac{v_1}{\sqrt{2}} & 0 & \lambda_{Li}^1 \frac{v_1}{\sqrt{2}} \\ \lambda_{Rj}^1 \frac{v_1}{\sqrt{2}} & M_L & \lambda_\Phi^1 \frac{v_1}{\sqrt{2}} \\ 0 & \bar{\lambda}_\Phi^1 \frac{v_1}{\sqrt{2}} & M_E \end{array} \right) \end{array}. \quad (5.142)$$

It is the same matrix as in Eq. (5.118) except for the appearance of  $v_1$  instead of  $v$ . Introducing mass diagonalisation matrices  $U_{L/R}$  like in Sec. 5.5.1 therefore yields the same expressions for the gauge-coupling matrices with  $v$  replaced by  $v_1$ . The Yukawa Lagrangian in the mass basis is given by

$$\mathcal{L} \supset -\bar{\hat{e}}_a \left[ \lambda_{ab}^h h + \lambda_{ab}^H H + \lambda_{ab}^A iA \right] P_R \hat{e}_b - \sqrt{2} H^+ \bar{\hat{\nu}}_a \lambda_{ab}^{H^+} P_R \hat{e}_b - \sqrt{2} H^- \bar{\hat{e}}_a \lambda_{ab}^{H^-} P_R \hat{\nu}_b + h.c. \quad (5.143)$$

where the Yukawa coupling matrices are listed in Ref. [1029]. In the case where mixing between the VLL and SM leptons is neglected ( $\lambda_{L/R}^a = 0$ ), the SM couplings reduce to the expressions discussed for the pure 2HDM in Sec. 5.3.1.

Like in case of the usual 2HDM-II/X the couplings  $\lambda_{ab}^{H/A/H^\pm}$  to the new scalars are enhanced by a factor of  $\tan\beta$  compared to the coupling to the SM-like Higgs  $h$ . However, because  $v_1 = v \cos\beta$  the leading-order tree-level corrections to the coupling matrices are suppressed by additional factors of  $\cos\beta$  compared to Eq. (5.120) or (5.123). In particular, the tree-level correction to the muon-Higgs coupling is

$$\lambda_{\mu\mu}^h \simeq \frac{m_\mu}{v} - \frac{\lambda_{L\mu}^1 \bar{\lambda}_\Phi^1 \lambda_{R\mu}^1 v^2}{\sqrt{2} M_E M_L} \cos^3 \beta, \quad (5.144)$$

such that the correction term is multiplied by  $\cos^3\beta$  compared to its counterpart with SM Higgs sector in Eq. (5.120).

As discussed in Sec. 5.3, the dominant contributions to  $\Delta a_\mu$  in the 2HDM arise through Barr-Zee diagrams at the two-loop level. Therefore any additional charged fermion with significant couplings to the Higgs further increases  $\Delta a_\mu$ . This effect was studied e.g. in Refs. [1023, 1024, 1026] who considered additional VLL while neglecting mixing with the SM leptons. In this case, the VLF will contribute through Barr-Zee diagrams like those shown in Fig. 5.23a with either exchange of a neutral scalar and a photon discussed in Sec. 4.2 or charged scalar and  $W$ -boson. In both cases only the diagonal couplings  $\lambda_{aa}^S$  in mass-eigenstate basis contribute, such that the resulting  $\Delta a_\mu$  behaves similarly to the contribution from a heavier  $\tau$ -lepton with the difference that the VLL mass is unrelated to its Yukawa coupling thanks to the Dirac mass term. As a result, the  $\Delta a_\mu$  contribution is strongly suppressed unless there is significant mixing (i.e. large Yukawa coupling) between the VLL. Specifically, this requires not too heavy VLL with small mass splittings  $M_L \sim M_E \equiv M_F$ . At the same time, the flavour and LHC constraints on the scalar masses discussed in Sec. 5.3 still apply and require small mass splittings also between the scalars  $M_H \sim M_A \equiv M_S$ . Therefore, the dominant contribution

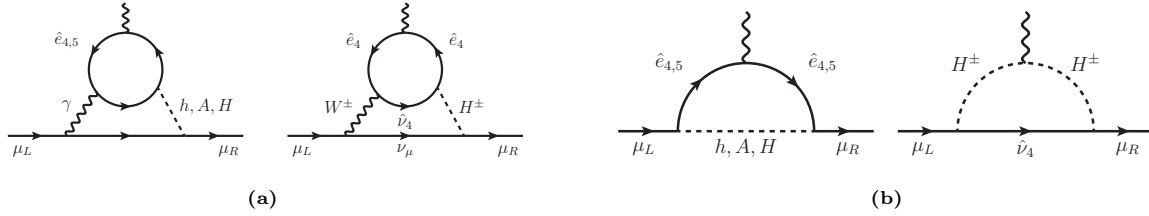


**Figure 5.23:** (a): Two-loop Barr-Zee contributions from generic charged VLF in the 2HDM+VLF. (b): One-loop contributions to  $\Delta a_\mu$  from VLL and scalars in the 2HDM+VLL.

from the neutral scalar exchange results in<sup>75</sup>

$$\Delta a_\mu^{\text{VLF,BZ}} = \frac{\sin^2 \beta}{(M_S/1000 \text{ GeV})^2} \left\{ (|\lambda_\Phi^1|^2 + |\bar{\lambda}_\Phi^1|^2) \mathcal{F}_1\left(\frac{M_F^2}{M_S^2}\right) + (|\lambda_\Phi^1|^2 - |\bar{\lambda}_\Phi^1|^2) \mathcal{F}_2\left(\frac{M_F^2}{M_S^2}\right) \right\} \cdot 3.3 \times 10^{-13} \quad (5.145)$$

Compared to the  $\tau$  contribution Eq. (5.90) this is enhanced roughly by a factor of  $500(\lambda_1^2 - 6\bar{\lambda}_1^2) \cos^2 \beta$ . However, because of the additional factor of  $\cos^2 \beta$  together with the theoretical constraints on the Yukawa couplings discussed in the previous section, the VLF Barr-Zee contribution is still smaller than that from the top-loop. Additionally, if  $\bar{\lambda}_\Phi^1$  is large enough the contribution will even be negative.

The situation changes once mixing between the VLL and the muon is permitted. In this case, both the VLF and new scalars will contribute to  $\Delta a_\mu$  already at one-loop order, resulting in a large effect from both the chiral and  $\tan \beta$  enhancement [1028, 1029]. The resulting correction can be obtained directly from the generic formulas in Sec. 2.1. In particular, to discuss the qualitative behaviour we can consider the simple case where  $M_F \sim M_S$ , in this case the contributions to  $\Delta a_\mu$  reduce to [1029]

$$\Delta a_\mu^{\text{VLF,1L}} \simeq -\frac{m_\mu v}{16\pi^2} \frac{\lambda_{L\mu}^1 \bar{\lambda}_\Phi^1 \lambda_{R\mu}^1}{\sqrt{2} M_E M_L} (1 + \tan^2 \beta) \cos^3 \beta. \quad (5.146)$$

Here the terms enhanced by  $\tan^2 \beta$  stem from the contributions of the VLF and new scalars shown in Fig. 5.23b, while the non-enhanced contributions stem from diagrams involving the VLF and the SM Higgs/gauge-bosons which are analogous to Eq. (5.126). Consequently, a similar correlation as in Eq. (5.128) arises

$$R_{\mu\mu} \approx \left| 1 - \frac{0.87}{1 + \tan^2 \beta} \left( \frac{\Delta a_\mu}{10^{-9}} \right) \right|^2. \quad (5.147)$$

Because of the additional  $\tan^2 \beta$  suppression, a much wider range of  $\Delta a_\mu$  is consistent with the current measurement on  $R_{\mu\mu}$ . Like Eq. (5.128) this correlation also generalises to the other VLL combinations with modified coefficients that were computed in Ref. [1025]. In conclusion, the combination of VLL and 2HDM allows larger  $\Delta a_\mu$  than either of the models on their own. Conversely, such models are now severely restricted by the new result  $\Delta a_\mu^{\text{Exp-WP2025}}$ .

## 5.6. Muon $g - 2$ and neutrino mass

In Sec. 3.5 we have already explained that neutrino masses and neutrino oscillations are firmly established. Together with dark matter, they constitute the strongest direct evidence for BSM physics, and the origin of neutrino masses remains one of the most pressing open questions in fundamental physics. In that section we also introduced and explained a large number of theoretical proposals to generate non-degenerate neutrino masses and a possible correlation between neutrino

<sup>75</sup>The analogous expression for the BZ diagram with  $H^\pm$  exchange is slightly more involved and can be found e.g. in Refs. [1023, 1026]

masses and  $a_\mu$  in the framework of SMEFT. Generically, there does not have to be a strong correlation between neutrino masses or neutrino mass mechanisms with contributions to  $a_\mu$ .

However, there is a subset of motivated neutrino mass models where correlations with  $a_\mu$  and sizeable corrections  $\Delta a_\mu \sim \mathcal{O}(10^{-9})$  can arise. These models were sometimes proposed as potential explanations of the previous deviation  $\Delta a_\mu^{\text{Exp-WP2020}}$ . Now the new result  $\Delta a_\mu^{\text{Exp-WP2025}}$  constitutes a constraint on the parameter space of such models. In this section we present a survey of a set of neutrino mass models of this kind, where sizeable contributions to  $a_\mu$  are in principle possible.

What makes this section particularly complementary to earlier sections is the diverse nature of the relevant BSM ideas. The models involve new scalars, new fermions, and/or new gauge bosons. Some of them are motivated not only by the quest to understand neutrino masses but also by dark matter or the desire to explain all quark and lepton masses simultaneously with neutrino masses. Many involve heavy BSM states, some very light new particles. For this reason the present section will make use of results and insights of many of the previous sections, but at the same time it will mostly limit the discussion to qualitative statements.

To set the stage, Sec. 3.5 has sketched six different well-known neutrino mass models. In all cases the tiny active neutrino masses are explained by heavy BSM particles that can be integrated out. These heavy particles are either fermions or bosons. Three of the models are the seesaw type I, II, III models, which generate the neutrino mass terms at tree level. In the Zee, Babu, and Ma (or scotogenic) models the Majorana mass terms are generated via one- or two-loop Feynman diagrams. The three seesaw models and the loop-generation models are summarised in Tab. 3.3 and 3.4, respectively. For general reviews of radiative neutrino mass generation we also refer to Refs. [1167–1169].

### 5.6.1. Extensions of the scotogenic model

We begin with the scotogenic model (or Ma model) [326] and extensions thereof and focus on five particular extensions that represent the wide range of possibilities for neutrino masses, particle content and  $\Delta a_\mu$  contributions. Tab. 5.6 collects the models and their most important properties. The key feature of these models is the simultaneous explanation of neutrino masses and dark matter via the same new states. All such models contain right-handed neutrino singlets  $N_i$ , where we suppress the chirality subscript  $R$ .<sup>76</sup> with gauge invariant Majorana mass terms, a scalar doublet  $\eta = (\eta^+, \eta^0)^T$  which may be assigned lepton number, and they involve a (fundamental or effective) quartic scalar interaction  $\lambda_5(\Phi^\dagger\eta)^2$  which breaks lepton number conservation and governs the magnitude of the loop-generated neutrino masses.<sup>77</sup> The new fields are odd under a  $\mathbb{Z}_2$  symmetry such that the lightest new state is a stable WIMP dark matter candidate.

The original scotogenic model has been described in Sec. 3.5 and approximations for the neutrino masses and  $\Delta a_\mu$  were given. Two simple numerical estimates are

$$M_\nu \sim 0.1 \frac{\lambda_5}{M/100 \text{ GeV}} \left( \frac{\mathbf{h}}{10^{-5}} \right)^2 \text{ eV}, \quad \Delta a_\mu \sim 10^{-19} \left( \frac{100 \text{ GeV}}{M} \right)^2 \left( \frac{\mathbf{h}}{10^{-5}} \right)^2, \quad (5.148)$$

where  $M$  is assumed to be the common mass scale of the new states. Hence the contributions to  $a_\mu$  are extremely tiny if the sub-eV neutrino masses are explained with  $\lambda_5 \sim 1$ . For very small  $\lambda_5$ , the Yukawa couplings  $\mathbf{h}$  and the resulting  $\Delta a_\mu$  could be larger, but constraints from lepton-flavour violating observables like  $\mu \rightarrow e\gamma$  rule out sizeable contributions

<sup>76</sup>Throughout this section, we always use a compact notation and identify  $N \equiv N_R$  for right-handed fermion singlets.

<sup>77</sup>The generalisation for an arbitrary number of sterile (right-handed) neutrinos and inert scalar doublets with zero vacuum expectation value has been discussed in Ref. [1170].

Model	Symmetry Groups	New Fields		Comments
		Fermions	Scalars	
S1	$\mathcal{G}_{EW}; \mathbb{Z}_2$	$N_{1,2,3}$ (1, 0; -)	$\eta$ (2, $\frac{1}{2}$ ; -) $h^+$ (1, 1; -)	Scotogenic-Zee model chirally enhanced $\Delta a_\mu$ [1171].
S2	$\mathcal{G}_{EW}; \mathbb{Z}_2,$ $U(1)_{L_\mu-L_\tau}$	$N_e$ (1, 0; -, 0) $N_\mu$ (1, 0; -, +1) $N_\tau$ (1, 0; -, -1)	$\eta$ (2, $\frac{1}{2}$ ; -, 0) $\Phi_1$ (1, 0; +, 1) $\Phi_2$ (1, 0; +, 2)	Scotogenic $U(1)_{L_\mu-L_\tau}$ model, $Z_{\mu\tau^-}$ and $\eta^+$ -contributions to $a_\mu$ . $\lambda_5 \geq 10^{-8}$ favoured by CLFV [612].
S3	$\mathcal{G}_{EW}; \mathbb{Z}_2,$ $U(1)_{L_\mu-L_\tau}$	$N_e$ (1, 0; -, 0) $N_\mu$ (1, 0; -, +1) $N_\tau$ (1, 0; -, -1) $L'$ (2, $-\frac{1}{2}$ ; -, 0)	$\eta$ (2, $\frac{1}{2}$ ; -, 0) $\varphi$ (1, 0; +, 1) $\chi^-$ (1, -1; -, 1)	scotogenic $U(1)_{L_\mu-L_\tau} + VLL$ . $\Delta a_\mu^{\text{Exp-WP2020}}$ obtained for $\mathbf{g}_\mu \sim 1.5$ , $\mathbf{h} \sim -1$ and $M_{\chi^\pm} \sim 160$ GeV [1172].
S4	$\mathcal{G}_{EW}; \mathbb{Z}_2,$ $U(1)_\chi$	$N_{1,2,3}$ (1, 0; -, 1) $N_0$ (1, 0; +, 2) $X$ (2, $-\frac{1}{2}$ ; -, 1)	$H_I$ (2, $\frac{1}{2}$ ; -, 1)	Two-loop generation of neutrino mass via vector-like fermion; chirally en- hanced $\Delta a_\mu$ [1173].
S5	$\mathcal{G}_{EW}; \mathbb{Z}_2,$ $U(1)'$	$N_{1,2}$ (1, 0; -, 0)	$\eta$ (2, $\frac{1}{2}$ ; -, 3) $\varphi$ (1, 0; -, 3) $\rho$ (1, 0; -, -1) $\zeta$ (1, 0; -, 0) $\sigma$ (1, 0; +, $\frac{1}{2}$ )	Three-loop generation of neutrino mass via extended Inert Doublet model [1174], non-enhanced $\Delta a_\mu$ like in minimal scotogenic model.

**Table 5.6:** List of extended scotogenic models discussed in this section, all of which explain neutrino masses and dark matter via the same new fields. Again, we identify  $N \equiv N_R$  for right-handed fermion singlets.  $\mathcal{G}_{EW} = SU(2)_L \times U(1)_Y$ . All fields here are singlets under  $SU(3)_c$ . In S2 and S3,  $U(1)_{L_\mu-L_\tau}$  is an additional gauge group, while  $\mathbb{Z}_2$ ,  $U(1)_\chi$  and  $U(1)'$  are only global symmetries of the respective models. The order of representation labels after each field corresponds to the order of the symmetry groups.

$\Delta a_\mu \sim 10^{-9}$ . Models S1-3 contain tree-level quartic coupling terms whereas  $\lambda_5$  is induced at the one- or two-loop level in S4 and S5 respectively.

The model S1 in Tab. 5.6 is called the scotogenic-Zee model [1171] and is the combination of two one-loop neutrino mass generation models. It combines the scalar doublet  $\eta$  and three singlet right-handed neutrinos  $N_{1,2,3}$  of the scotogenic model with one charged  $\mathbb{Z}_2$ -odd scalar singlet  $h^+$  as in the Zee model. The neutrino masses are generated as in the scotogenic model by the  $\mathbb{Z}_2$ -odd scalar doublet  $\eta$ , while  $\Delta a_\mu$  contributions arise from the charged scalar loops involving states that are mixtures of  $\eta^+$  and  $h^+$ . In terms of mass-insertion diagrams, the contributions to  $M_\nu$  and  $a_\mu$  in this model can be approximated as

$$M_\nu^{S1} \sim \nu \xrightarrow{h} \text{Loop}(N, \eta^0) \xrightarrow{h} \nu, \quad \Delta a_\mu^{S1} \sim \mu_L \xrightarrow{h} \text{Loop}(N, h^+) \xrightarrow{h} \mu_R + \gamma, \quad (5.149)$$

where the parameters and the external Higgs  $vev$  insertions are explicitly shown. The Feynman diagrams in (5.149)

are derived from the triple-scalar interaction term  $\mu\tilde{\Phi}^\dagger\eta h^-$  and the Yukawa interaction terms involving the right-chiral neutrinos like  $\mathbf{h}_{ij}^\dagger\overline{l_{Li}}\tilde{\eta}N_j$  and  $\mathbf{f}_{ij}\overline{e_{Ri}}h^-N_j^C$ , as well as the typical scotogenic  $\lambda_5$  interaction term.

In this model the  $\Delta a_\mu$  contributions are chirally enhanced and resemble the three-field model of Class III in Eq. (2.19), where the fermion mass insertion  $m_\psi$  is the Majorana neutrino mass term  $M_R$  and the scalar mixing term  $a_\Phi$  corresponds to the trilinear  $\eta$ - $h^+$ -Higgs interaction term. In this way the sign of  $\Delta a_\mu$  depends on the relative signs of the model parameters and can be positive or negative, and significant enhancements of  $\Delta a_\mu$  are possible. At the same time the neutrino masses depend on the additional lepton-number violating parameter  $\lambda_5$  which can be naturally small. Ref. [1171] finds indeed that this scenario can describe the neutrino masses and mixing, satisfy bounds from lepton flavour violation, but produce sizeable  $\Delta a_\mu$  as large as  $\Delta a_\mu^{\text{Exp-WP2020}}$ . Such scenarios are now constrained by the new result  $\Delta a_\mu^{\text{Exp-WP2025}}$  in a non-trivial way.

The two scotogenic extensions S2 and S3 of Tab. 5.6 both involve an additional gauge group and associated  $Z'$  gauge boson. The chosen gauge group in both cases is  $U(1)_{L_\mu-L_\tau}$  where the  $Q_{L_\mu-L_\tau}$  charges are  $(0, 1, -1)$  for both left- and right-handed  $(e, \mu, \tau)$  and also for the corresponding neutrinos, including the right-handed neutrinos  $N_{e,\mu,\tau}$ . This gauge group has already been discussed in Sec. 5.1.3 and it is one of the possible anomaly-free additional  $U(1)$  gauge groups and is compatible with a  $Z' \equiv Z_{\mu\tau}$  in the MeV–GeV mass region.

For neutrino-mass generation the gauge group is of particular interest since it imposes particular flavour patterns on the Majorana neutrino mass terms, such that  $N_e N_e$  and  $N_\mu N_\tau$  are allowed while other combinations are forbidden. Apart from these restrictions, the neutrino masses arise similarly to the original scotogenic model in Eqs. (5.148) and (3.79c), but the number of particles running inside the loop and their masses vary. The new Yukawa couplings and quartic couplings of the scalar fields play a crucial role.

Model S2 from Ref. [612] contains, apart from the scotogenic field content, two neutral scalar singlets which have different  $U(1)_{L_\mu-L_\tau}$  charges, are even under  $\mathbb{Z}_2$  and have non-vanishing vacuum expectation values,  $\langle\Phi_1\rangle = v_1$ ,  $\langle\Phi_2\rangle = v_2$ . These break  $U(1)_{L_\mu-L_\tau}$  symmetry and the gauge boson gains the mass  $M_{Z_{\mu\tau}} = g_{\mu\tau}\sqrt{2(v_1^2 + 4v_2^2)}$ . The neutrino mass takes the typical scotogenic neutrino mass form given in Eq. (3.79c). In contrast to model S1, in this model S2 the field quantum numbers prevent mass mixing of any of the new fields via couplings to the SM Higgs field. Hence there are no chirally enhanced contributions to  $a_\mu$ . The dominant  $\Delta a_\mu$  contributions arise from the Feynman diagram with the  $Z_{\mu\tau}$  and/or from the diagram with right-handed neutrinos and charged scalars, schematically

$$\Delta a_\mu^{\text{S2}} \sim \begin{array}{c} \text{Diagram 1: } Z_{\mu\tau} \text{ loop} \\ \text{Diagram 2: } \eta^+ N \eta^+ \text{ loop} \end{array} \quad (5.150)$$

where sample assignments of chiralities and the non-enhanced chirality flips at the external lines have also been indicated. The  $Z_{\mu\tau}$  contribution is positive and behaves as discussed in Sec. 5.1.3; the FS-type contribution is negative and behaves as the non-enhanced two-field models of Sec. 2.2 and Tab. 2.2. For this reason the model is automatically in agreement with the new result  $\Delta a_\mu^{\text{Exp-WP2025}}$  except in the small  $Z_{\mu\tau}$  parameter region disfavoured in the plot in Fig. 5.4, see also Eq. (5.22).

Model S3 [1172] realises the  $U(1)_{L_\mu-L_\tau}$  symmetry differently. In addition to the scotogenic field content it adds a vector-like fermion  $L'$ , a charged scalar  $\chi^-$  and one neutral scalar field with nonzero  $vev$ ,  $\langle\varphi\rangle \equiv \frac{v_\varphi}{\sqrt{2}}$  that gives mass to the  $Z_{\mu\tau}$ . All additional fields are odd under  $\mathbb{Z}_2$  except  $\varphi$ . The neutrino mass is generated in the same way as in

the scotogenic model, though there are now five instead of three neutral right-handed states. These are three singlet right-handed neutrinos and two new neutral right-handed fields from the vector-like fermions  $L'_L{}^C$  and  $L'_R$ . The  $5 \times 5$  mixing is constrained by the  $U(1)_{L_\mu-L_\tau}$ -charges of the fields and results in mass eigenvalues  $M_k$ . In this model S3, mass mixing via the SM Higgs  $vev$  is possible between specific fermions, e.g. between  $N_e$  and  $L'$ , such that contributions to  $a_\mu$  similar to the Class I/II three-field models of Sec. 2.3 are possible, see also Eq. (2.19). The corresponding mass-insertion diagram is

$$\Delta a_\mu^{\text{S3}} \sim \text{Diagram} \quad (5.151)$$

where the mass insertion is explicitly indicated. As discussed in Ref. [1172], these contributions can be sizeable and easily dominate over the non-chirally enhanced contributions from e.g. the  $Z_{\mu\tau}$ -loop. This reference identifies parameter regions where dark matter and neutrino masses are explained and bounds from CLFV are avoided. For normal hierarchy of neutrino masses,  $\Delta a_\mu$  could be as large as  $\mathcal{O}(10^{-9})$ . Hence the parameter regions with normal ordering are now constrained by the new result  $\Delta a_\mu^{\text{Exp-WP2025}}$ . For inverted hierarchy of neutrino masses, Ref. [1172] finds that  $\Delta a_\mu$  is at most of order  $\mathcal{O}(10^{-12})$ . Hence this case is not constrained by  $\Delta a_\mu^{\text{Exp-WP2025}}$  but automatically compatible with it.

The extended scotogenic models S4 and S5 do not involve an extra gauge group but represent a different idea. Since the neutrino masses are proportional to the quartic scalar coupling  $\lambda_5(\Phi^\dagger\eta)^2$ , their smallness might be related to the fact that this quartic scalar is forbidden at tree level but allowed only via loops.<sup>78</sup> In model S4, the quartic scalar coupling arises at one-loop order, resulting in two-loop neutrino masses; in model S5, the quartic scalar coupling arises at two-loop order and the neutrino masses are therefore three-loop suppressed. These models are thus well motivated by neutrino mass considerations, but the fields appearing in the loop generating the effective quartic scalar interactions might also enter diagrams that contribute to  $a_\mu$ .

Model S4 has been defined in Ref. [1173], and a representative diagram corresponding to the neutrino mass dimension-5 operator is given by

$$M_\nu^{\text{S4}} \sim \text{Diagram} \quad (5.152)$$

where again the Higgs  $vev$  insertions, the field assignments and the relevant model parameters are explicitly shown and the crosses denote fermion mass term insertions. In this model the typical scotogenic inert doublet is called  $H_I$ , and

<sup>78</sup>A different way to generate neutrino masses at the multiloop level is discussed in Ref. [1175], also in connection with  $a_\mu$ . In that reference, the neutrino masses are generated similarly to the scotogenic mechanism, however the right-handed neutrino Majorana masses are generated via one-loop diagrams. This leads to the so-called inverse seesaw mechanism. The model considered in Ref. [1175] is based on left-right symmetry and also contains vector-like leptons that can lead to sizeable corrections to  $a_\mu$ .



Model	Symmetry Groups	New Fields		Comments
		Fermions	Scalars	
E1	$\mathcal{G}_{EW}$		$h^+$ $(\mathbf{1}, 1)$ $\Phi_2$ $(\mathbf{2}, \frac{1}{2})$	Zee model, see Sec. 3.5, Eq. (3.78a). $\Delta a_\mu$ as in non-flavour-aligned 2HDM.
E2	$\mathcal{G}_{SM}; \mathbb{Z}_2$	$N$ $(\mathbf{1}, \mathbf{1}, 0; -)$	$\eta_{1,2}$ $(\mathbf{1}, \mathbf{2}, \frac{1}{2}; -)$ $S$ $(\mathbf{3}, \mathbf{2}, \frac{1}{6}; -)$ $\phi$ $(\mathbf{1}, \mathbf{1}, -1; -)$	Similar to scotogenic-Zee model plus leptoquarks (LQ); neutrino mass and dark matter as in scotogenic, $\Delta a_\mu$ as in scotogenic-Zee, LQ could accommodate $B$ -anomalies [1182].
E3	$\mathcal{G}_{SM}$		$S_1$ $(\bar{\mathbf{3}}, \mathbf{1}, \frac{1}{3})$ $\tilde{R}_2$ $(\mathbf{3}, \mathbf{2}, \frac{1}{6})$ $S_3$ $(\bar{\mathbf{3}}, \mathbf{3}, \frac{1}{3})$	Extension by three LQs, neutrino mass via LQ loop, chiral enhancement for $\Delta a_\mu$ via LQ/quark loops [1068].
E4	$\mathcal{G}_{EW}; \mathbb{Z}_2$	$F_{1,2,3}$ $(\mathbf{1}, -1; -)$	$\phi_1$ $(\mathbf{2}, \frac{1}{2}; -)$ $\phi_2$ $(\mathbf{2}, \frac{3}{2}; -)$ $\eta$ $(\mathbf{1}, 0; -)$	Neutrino mass via charged vector-like fermions $F_i$ , DM candidate and chiral enhancement for $\Delta a_\mu$ via new scalars [1150].
E5	$\mathcal{G}_{EW}; \mathbb{Z}_2$	$N_{1,2}$ $(\mathbf{1}, 0; -)$	$\varphi^+$ $(\mathbf{1}, 1; -)$ $\Phi_2$ $(\mathbf{2}, \frac{1}{2}; -)$	$\nu$ -philic 2HDM (or seesaw type IB) [1183], one-loop Majorana neutrino mass generation as in scotogenic model, chiral enhancement for $a_\mu$ as in E4 or S1.

**Table 5.7:** List of non-scotogenic models with radiative neutrino mass generation discussed in the text. We identify  $N \equiv N_R$  for right-handed fermion singlets.  $\mathcal{G}_{EW}$  denotes the EW gauge group as in Tab. 5.6 and  $\mathcal{G}_{SM}$  the full SM gauge group, and  $\Phi$  is the SM Higgs doublet. The representation label after each field corresponds to the order of the symmetry groups.

the one in the original scotogenic model, i.e. it is negative and has a small magnitude which is essentially automatically in agreement with the current  $\Delta a_\mu^{\text{Exp-WP2025}}$ . Ref. [1174] studies further extensions of the model by vector-like leptons. With such additional particles, the contributions to  $a_\mu$  could be larger, however the current result  $\Delta a_\mu^{\text{Exp-WP2025}}$  does not provide a motivation for such extensions. Rather, the model S5 exemplifies the idea that the neutrino masses could be small because of fundamental symmetries that prevent lower-order diagrams and lead to very strong loop suppressions of neutrino masses. In the model, the mass scale of the relevant particles can be  $\mathcal{O}(1 \text{ TeV})$  while the relevant couplings are unsuppressed and CLFV constraints are avoided, and dark matter can be explained via the new fermions or new scalars.

### 5.6.2. Neutrino mass models based on other mechanisms

Here we illustrate the wide range of possible neutrino mass models further. Tab. 5.7 provides an overview of selected examples, all of which differ in various ways from the examples of Tab. 5.6.

First, model E1 is the original Zee model already discussed in Sec. 3.5. Since this model actually is the 2HDM, further extended by an additional charged scalar singlet, the phenomenology of  $a_\mu$  can be obtained from studying the 2HDM. However, because of the desire to explain neutrino masses, the preferred and typically considered values of the Yukawa matrices by which the quarks and leptons couple to the second Higgs doublet are very different in the Zee model than in the usually considered 2HDM. Ref. [1184] has carried out an extensive study of  $a_\mu$  in the Zee model, taking into account

constraints from neutrino masses, lepton flavour violation and from collider searches. The investigated textures of the Yukawa matrices in generation space are very different from the ones of e.g. the flavour-aligned 2HDM of Sec. 5.3.3. Instead, the authors assume that the second Higgs doublet only couples to leptons but with different strengths to the electron, muon and tau, and lepton-flavour violating Yukawa couplings are allowed and needed to reproduce the neutrino masses. With such patterns, sizeable  $\Delta a_\mu$  contributions are possible [1184].

Models E2 and E3 in Tab. 5.7 are models with leptoquarks and thus contain coloured BSM particles. The structure of the two models is quite different, though. Model E2 [1182] may still be regarded as an extended scotogenic model, where the  $\mathbb{Z}_2$ -odd sector is enlarged substantially to a dark sector. The dark sector contains one right-handed neutrino (instead of three) and two inert scalar doublets (instead of one), and in addition it contains a scalar singlet  $\phi$  and a doublet leptoquark  $S$  with hypercharge  $\frac{1}{6}$  which is identical to  $\tilde{R}_2$  in model E3. Apart from the leptoquark it also has similarities to the scotogenic-Zee model S1. In Ref. [1182] the model was motivated as a potential explanation of a set of several hints for BSM physics from  $B$ -physics and from  $a_\mu$  that were present around 2020–2022 as already mentioned in Sec. 5.4.4. Though these hints have substantially reduced in the meantime it may be of interest to discuss model E2 as a representative example trying to accommodate neutrino masses, dark matter, and large effects in  $\Delta a_\mu$  and  $B$ -physics at the same time.

In model E2, the neutrino masses are explained as in the scotogenic or the scotogenic-Zee models, while  $\Delta a_\mu$  takes the same form as in the scotogenic-Zee model S1. The leptoquark plays a role for  $B$ -physics observables, and dark matter can be explained by the lightest  $\mathbb{Z}_2$ -odd particle which may be  $N$  or, more favourably, one of the neutral  $\eta_a$ -components. The fact that the model contains such a large number of new particles is a reflection of the no-go theorem of Ref. [402] also mentioned in Sec. 5.4.4 which states that at least four BSM fields are required to accommodate dark matter, sizeable  $\Delta a_\mu$  and the  $B$ -physics anomalies of the time.

Model E3 [1068] involves three different leptoquarks, one singlet  $S_1$ , one doublet  $\tilde{R}_2$  and one triplet  $S_3$ . Its key feature is that it does not introduce any other, non-leptoquark particles. Hence the neutrino masses are explained in a different way, via leptoquark–quark loops. A sample mass-insertion diagram is

(5.155)

which contains leptoquarks  $S_1^{\frac{1}{3}}$  and  $\tilde{R}_2^{-\frac{1}{3}}$  with electric charge  $\pm\frac{1}{3}$ . The loop diagrams generating  $M_\nu$  must involve lepton-number violating mass mixing of the different leptoquarks types induced by couplings to the SM Higgs  $vev$ , either  $S_1 - \tilde{R}_2$  as shown in Eq. (5.155) and/or  $S_3 - \tilde{R}_2$ . A second Higgs insertion happens at the down-quark line, such that Eq. (5.155) corresponds to neutrino mass generation via the dimension-5 operator in Eq. (3.71), like in the other neutrino mass models. This model E3 has already been discussed in Sec. 5.4.4, together with a variety of further models with similar goals where leptoquarks were used to explain flavour anomalies. Similarly to many other such models, model E3 can contribute to  $a_\mu$  particularly via the leptoquark  $S_1$ , which leads to chirally enhanced contributions. These contributions are now constrained by  $\Delta a_\mu^{\text{Exp-WP2025}}$ .

Model E4 is a model without leptoquarks and without right-handed neutrinos. It instead extends the fermion sector by three charged vector-like leptons  $F_i$  and the scalar sector by two scalar doublets  $\phi_{1,2}$  with different hypercharges and one neutral scalar singlet  $\eta_3$ . The model is one of the examples mentioned in Sec. 5.5.4 where vector-like fermions with

extended scalar sectors can lead to appealing phenomenology including explanations of neutrino masses and dark matter.

In model E4 specifically, the dark matter candidate is stable thanks to the unbroken  $\mathbb{Z}_2$  symmetry, like in the scotogenic model. The neutrino mass is generated from loop diagrams of the form

The diagram shows a loop diagram for the neutrino mass  $M_\nu^{E4}$ . It features a central loop with two scalar doublets  $\phi_1$  and  $\phi_2$  (indicated by dashed lines) and two vector-like leptons  $F_R$  and  $F_L$  (indicated by solid lines). The loop is connected to external neutrino lines  $\nu$ . The loop contains a Dirac mass  $M_D$  (green cross) and a quartic scalar coupling  $\lambda_5$  (red dot) between  $\phi_1$  and  $\phi_2$ . The diagram is labeled (5.156).

which contains the vector-like leptons  $F_i$  and the two scalar doublets  $\phi_{1,2}$  inside the loop. Here  $\phi_1$  couples with the SM lepton doublet  $l_L$  and  $F_R$ , while  $\phi_2$  couples with  $l_L$  and  $F_L^C$ . In the loop generating the neutrino-masses, the  $F_i$  undergo a chirality flip via their Dirac mass, and the  $\phi_1$ - $\phi_2$  transition is governed by a quartic scalar coupling between  $\phi_{1,2}$  and the SM Higgs field of the form  $\phi_1^\dagger \tilde{\Phi} \Phi^\dagger \phi_2$ , which is analogous to the  $\lambda_5$  coupling in the scotogenic model and which may be considered lepton-number violating. The entire structure of this loop diagram is thus similar to the one in the scotogenic model shown in Fig. 3.5c, except for the charges of the involved fields.

The singlet scalar  $\eta_3$  in the model can couple with the SM lepton singlet  $e_R$  and the left-chiral vector-like singlet fermion  $F_L$ , and a mass mixing of  $\eta_3$ - $\phi_1$  via a coupling to the SM Higgs  $vev$  is allowed by the quantum numbers. In this way, the contributions to  $a_\mu$  are dominated by the diagram

The diagram shows a loop diagram for the muon anomaly  $\Delta a_\mu^{E4}$ . It features a central loop with two scalar doublets  $\phi_1$  and  $\eta$  (indicated by dashed lines) and two vector-like leptons  $F_R$  and  $F_L$  (indicated by solid lines). The loop is connected to external muon lines  $\mu_L$  and  $\mu_R$ . The loop contains a Dirac mass  $M_D$  (green cross) and a quartic scalar coupling  $\mu_1$  (orange dot) between  $\phi_1$  and  $\eta$ . The diagram is labeled (5.157).

and are thus chirally enhanced. The structure of this diagram and the enhancement is analogous to the one in the Class III three-field model, see Eq. (2.19). Ref. [1150] shows that the model is representative of a wider class of models explaining the neutrino masses and dark matter. In each such model, there is a  $\mathbb{Z}_2$ -odd dark sector comprised of charged vector-like fermions and at least three different scalars. Two of the scalars appear in the neutrino-mass loop, and another set of two scalars appears in the  $a_\mu$ -loop. It is possible to accommodate neutrino masses and dark matter for BSM masses in the 100...1000 GeV region. Now, the new result  $\Delta a_\mu^{\text{Exp-WP2025}}$  restricts the values of the chirality-flipping parameters.

With model E5, we return to the simpler case of tree-level generation of neutrino masses. This model is an example of several variations of the original seesaw type I mechanism studied in Ref. [1183], which differ in the additional field content and the associated symmetries. The basic idea is that two Higgs doublets  $\Phi_{1,2}$  with non-vanishing  $vevs$  exist, where  $\Phi_2$  is SM-like but the neutrino masses can only arise due to coupling to  $\Phi_1$ , thanks to certain discrete symmetries. Our choice E5 corresponds to the neutrinophilic 2HDM considered in the reference, where the neutrino masses are given by

The diagram shows a tree-level diagram for the neutrino mass  $M_\nu^{E5}$ . It features a central neutrino line  $N$  (indicated by a solid line) and two Higgs doublets  $\Phi_1$  (indicated by dashed lines). The diagram is connected to external neutrino lines  $\nu$ . The diagram contains a Dirac mass  $M_R$  (green cross) and two Yukawa couplings  $\lambda^{(1)}$  (blue dots) between  $\Phi_1$  and  $N$ . The diagram is labeled (5.158).

and are therefore proportional to  $\langle \Phi_1 \rangle^2$ . In contrast, all other SM fermion masses arise from couplings to the SM-like  $\langle \Phi_2 \rangle$ . In another variant called type IB the neutrino masses are proportional to  $\langle \Phi_1 \rangle \langle \Phi_2 \rangle$ . The smallness of neutrino

masses is then related to the smallness of the  $vev$   $\langle \Phi_1 \rangle$ . Similarly to the scotogenic-Zee model S1, a charged singlet scalar  $\varphi^+$  is introduced which participates in a triple scalar coupling with the both Higgs doublets. Hence contributions to  $a_\mu$  arise via

$$\Delta a_\mu^{\text{E5}} \sim \begin{array}{c} \langle \Phi_2 \rangle \\ \uparrow \\ \Phi_1 \quad \mu_\varphi \\ \uparrow \quad \downarrow \\ \mu_L \quad N \quad N \quad \mu_R \\ \leftarrow \lambda^{(1)} \quad \leftarrow M_R \quad \leftarrow f \end{array} \quad (5.159)$$

which is essentially the same as in models S1 and E4 or in the Class III three-field models discussed before. The chiral enhancement is proportional to the Majorana neutrino mass term and the triple scalar coupling. This model can accommodate neutrino masses with TeV-scale  $M_R$  and can at the same time lead to sizeable  $\Delta a_\mu$  via the chiral enhancement. With the current  $\Delta a_\mu^{\text{Exp-WP2025}}$ , there is an upper limit on the chiral enhancement. CLFV constraints can also be important here. As is typical for neutrino mass models, contributions to  $a_\mu$  are inevitably linked to contributions to processes such as  $\mu \rightarrow e\gamma$ , see Sec. 3.2 and Eq. (3.29). For model E5, the CLFV constraints are strong if  $\Delta a_\mu \sim 10^{-9}$ . The constraints can be avoided by special regions in parameter space where e.g. orthogonality conditions between the Yukawa couplings such as  $(\mathbf{f}_{1\mu}, \mathbf{f}_{2\mu}) \propto (\lambda_{2e}, -\lambda_{1e})$  hold. If, on the other hand,  $\Delta a_\mu$  is much smaller, as allowed by the current  $\Delta a_\mu^{\text{Exp-WP2025}}$ , the CLFV relations between the Yukawa couplings are relaxed. In the type Ib model also investigated in Ref. [1183], it turns out that CLFV constraints entirely exclude sizeable contributions to  $a_\mu$  of the order  $10^{-9}$ .

In summary, the previous examples illustrate the great diversity of neutrino mass models and the richness of potential extensions of the SM, with new gauge bosons, new vector-like or chiral fermions, and/or new scalars, including leptoquarks. The models S1–S5, and E2, E4 can explain dark matter via some of the new fermions or bosons. The majority of the discussed models lead to chirally enhanced contributions to  $a_\mu$  often of the types discussed in previous sections; model S2 can contribute to  $a_\mu$  via a light  $Z_{\mu\tau}$  gauge boson. All of the discussed models explain neutrino masses via loops, some at the multi-loop level; they thus naturally allow smaller mass scales than tree-level neutrino mass models.

All neutrino mass models predict CLFV effects, although the correlations with  $a_\mu$ , expressed e.g. via Eq. (3.29), are highly model-specific. In several models, TeV-scale new particles and sizeable contributions to  $a_\mu$  are compatible with CLFV constraints. Such models are now non-trivially constrained by the current  $\Delta a_\mu^{\text{Exp-WP2025}}$ . Conversely, the current  $\Delta a_\mu^{\text{Exp-WP2025}}$  is generally compatible with neutrino mass models that can only produce small corrections to  $a_\mu$ , including the more straightforward models discussed in Sec. 3.5.

## 6. Summary

Recently, the Fermilab muon  $g - 2$  experiment has released its final result that surpasses its design precision and is in full agreement with earlier measurements, but with a significantly reduced uncertainty. Similarly, the muon  $g - 2$  Theory Initiative has published an updated SM prediction, however with a shifted value that dramatically transforms the implications of this measurement. After more than 20 years with a tantalising and persisting discrepancy, there is now instead full agreement between SM and experiment, leading to upper limits on possible BSM contributions. Nevertheless, BSM physics must exist, e.g. in view of dark matter, neutrino masses or other fundamental open questions.

The anomalous magnetic moment of the muon  $a_\mu$  is a key observable for studying BSM physics, with connections to many other observables and relevant effects in a large variety of scenarios. Through significant work in the past years, it is now very well understood how different BSM scenarios can contribute to  $a_\mu$  and how these contributions are related to other, complementary observables.

The present review aims to provide a comprehensive summary of the impact of  $a_\mu$  for BSM physics and a guide to the literature on the topic. It emphasises model-independent, qualitative and generic results and interrelations to other observables such as dark matter, neutrino masses and collider constraints but also more closely connected observables such as the muon mass, the muon–Higgs coupling and other dipole observables. It also presents quantitative evaluations in specific models, taking into account many constraints. With its brief but self-contained introductions to complementary observables and a range of BSM scenarios, the review may also be useful for researchers interested in BSM phenomenology independently of  $a_\mu$ .

Here we summarise a few examples that illustrate the range of possible results and interconnections.

- In many models with a light dark sector, there is a complementarity between constraints from  $a_\mu$ , direct searches and other low-energy constraints or even cosmology, see e.g. Fig. 5.7, where  $a_\mu$ ,  $a_e$  and BESIII constraints on the ALPs parameter space are shown.
- In SUSY models, there is a strong interplay between  $a_\mu$ , LHC and dark matter, see e.g. Fig. 5.12. LHC experiments allow the Bino–slepton and Bino–wino coannihilation regions, but dark matter constraints require large Higgsino mass, which enhances  $a_\mu$ ; the current  $a_\mu$  constraints then limit  $\tan\beta$  to be rather small.
- In leptoquark models with chiral enhancement,  $\Delta a_\mu$  is correlated with contributions to the muon mass and to CLFV processes, see e.g. Fig. 5.18. Large contributions to  $a_\mu$  require  $\mathcal{O}(1)$  corrections to the muon mass and are only viable in case of highly non-universal flavour patterns of leptoquark couplings. The current small  $\Delta a_\mu^{\text{Exp-WP2025}}$  allows leptoquark parameter regions with less extreme properties.
- In models with vector-like leptons and seesaw-like tree-level contributions to the muon mass,  $\Delta a_\mu$  is correlated with the muon–Higgs coupling. The combination of current constraints now conclusively rule out several such VLL scenarios, while for other scenarios the parameter space is strongly constrained, see e.g. Fig. 5.20 (*right*).
- In models with radiative muon mass generation, the correlation between  $\Delta m_\mu$  and  $\Delta a_\mu$  leads to a fixed contribution to  $a_\mu$ , see e.g. Eq. (3.4), which currently implies a lower mass limit of around 3 TeV on such models.

In addition to these examples we also refer to our summaries of many models in Table 1.1, the plot in Fig. 3.9, and the tables in Sec. 2.2. Furthermore, the sections on dark matter and neutrino masses, Secs. 3.5, 3.6 and 5.6 discuss many

minimal as well as highly elaborate scenarios that show a great diversity in their structure and in their contributions to  $a_\mu$ .

Generally, there are examples of BSM scenarios which inevitably predict large  $\Delta a_\mu$  and which are therefore now excluded by  $\Delta a_\mu^{\text{Exp-WP2025}}$ . There also exist many BSM models which can accommodate large or small  $\Delta a_\mu$ . Especially models with chiral enhancements and/or dark sector particles are often of this kind. The parameter spaces of such models are significantly constrained by  $a_\mu$ .

Finally, it is worth noting that several well-known BSM scenarios are not able to explain deviations as large as  $\Delta a_\mu^{\text{Exp-WP2020}}$  in view of constraints related to dark matter, direct searches,  $B$ -physics or other observables — many such scenarios now re-emerge as viable. Examples include minimal SUSY models such as the CMSSM or Higgsino-like LSP dark matter, the 2HDM of type I or II, the minimal dark photon, or many straightforward neutrino mass models. More generally, the connection to CLFV implies that models with generic BSM flavour patterns are only compatible with  $\Delta a_\mu \lesssim 10^{-14}$ , which is now viable.

The current agreement between the SM prediction and the final Fermilab measurement may mark a new era for  $a_\mu$  and BSM physics. However, the experimental precision of  $a_\mu$  is now about four times better than the current SM precision, which hopefully can be further improved. With such an improvement, the constraints on BSM physics might sharpen, or a discrepancy and signal for non-vanishing BSM contributions might re-emerge. At the same time, progress on complementary observables such as dark matter or CLFV searches and Higgs-coupling measurements is expected. The review was organised with these prospects in mind and should be a useful resource accompanying future developments.

## Acknowledgments

We thank our many collaborators on topics related to the muon magnetic moment and BSM physics, as well as many experimental and theory colleagues from the Fermilab muon  $g-2$  collaboration and the  $g-2$  Theory Initiative, for fruitful collaborations, stimulating discussions and insightful comments. We are particularly grateful to Rodolfo Capdevilla, Uwe Hernandez Acosta, Martin Hoferichter, Wojciech Kotlarski, Gordon Krnjaic, Alberto Lusiani, Stefan Müller, René Reimann, Enrico Sessolo and Adrian Signer for discussions on specific parts of the review. KM, DS and HSK acknowledge funding by DFG grants STO 876/7-2, 10-1, and by the EU Horizon 2020 Marie Skłodowska-Curie RISE Grant Agreement No. 101006726, and thank Fermilab, where part of this work was carried out, for the hospitality. The work of PA is supported by NNSFC Key Projects grant No. 12335005 and the supporting fund for foreign experts grant wgz2022021. The Feynman diagrams were created using Axodraw [1185].

Standard Model	Leptons		Quarks			Higgs
Field name	$l_{Li}$	$e_{Ri}$	$q_{Li}$	$u_{Ri}$	$d_{Ri}$	$\Phi$
Representation	$(\mathbf{1}, \mathbf{2}, -\frac{1}{2})$	$(\mathbf{1}, \mathbf{1}, -1)$	$(\mathbf{3}, \mathbf{2}, \frac{1}{6})$	$(\mathbf{3}, \mathbf{1}, \frac{2}{3})$	$(\mathbf{3}, \mathbf{1}, -\frac{1}{3})$	$(\mathbf{1}, \mathbf{2}, \frac{1}{2})$
Gauge Fields	$SU(3)_c : G_\mu^a$		$SU(2)_L : W_\mu^b$	$U(1)_Y : B_\mu$		

**Table A.1:** The definition of the Standard Model gauge multiplets.  $l_{Li}$  denote the left-handed lepton doublets and  $q_{Li}$  the left-handed quark doublets.  $u_{Ri}$  and  $d_{Ri}$  denote the right-handed up- and down-type quark singlets respectively, and  $e_{Ri}$  denote the right-handed charged lepton singlets.  $\Phi$  is the Higgs doublet. The index  $L/R$  denotes the chirality of the fermion field, the generation indices are denoted by  $i = 1, 2, 3$ . Colour and  $SU(2)_L$  indices are suppressed here and whenever possible without risk of confusion.

## Appendix A. Conventions

Here we collect the conventions used throughout the review.

We use the Minkowski metric tensor with mostly-minus metric  $(g^{\mu\nu}) = (g_{\mu\nu}) = \text{diag}(1, -1, -1, -1)$ . We denote 3-vectors by bold symbols, such that 4-vectors are combined as  $x^\mu = (x^0, \mathbf{x})$  and  $x_\mu = g_{\mu\nu}x^\nu = (x_0, -\mathbf{x})$ . The 4-gradient is defined as  $\partial_\mu = (\partial_0, \nabla)$ , such that  $\partial_\mu x_\nu = g_{\mu\nu}$ . The Minkowski-space Fourier transform is given by

$$A(x) = \int \frac{d^4q}{(2\pi)^4} \tilde{A}(q) e^{-iq \cdot x}. \quad (\text{A.1})$$

For convenience we list the Pauli matrices

$$\sigma^1 = \begin{pmatrix} 0 & 1 \\ 1 & 0 \end{pmatrix}, \quad \sigma^2 = \begin{pmatrix} 0 & -i \\ i & 0 \end{pmatrix}, \quad \sigma^3 = \begin{pmatrix} 1 & 0 \\ 0 & -1 \end{pmatrix}, \quad (\text{A.2})$$

which fulfil the (anti-)commutator relations  $[\sigma^i, \sigma^j] = 2i\epsilon_{ijk}\sigma^k$  and  $\{\sigma^i, \sigma^j\} = 2\delta^{ij}$ . The  $\gamma$ -matrices satisfy  $\{\gamma^\mu, \gamma^\nu\} = 2g^{\mu\nu}$ , and we use the usual notation  $\not{p} \equiv p_\mu \gamma^\mu$ . For 4-spinors  $\Psi$  we generally use the decomposition  $\Psi = \Psi_L + \Psi_R$  where  $\Psi_{L,R} = P_{L,R}\Psi$  with chiral projectors  $P_{L,R} = \frac{1}{2}(1 \mp \gamma_5)$ , and we denote charge conjugated spinors as  $\Psi^C = C\bar{\Psi}^T$  with  $C = i\gamma^0\gamma^2$ . In cases where explicit representations are needed we use the Weyl (chiral) representation. It can be written as

$$\gamma^\mu = \begin{pmatrix} 0 & \sigma^\mu \\ \bar{\sigma}^\mu & 0 \end{pmatrix}, \quad \gamma^5 = i\gamma^0\gamma^1\gamma^2\gamma^3 = \begin{pmatrix} -\mathbb{1} & 0 \\ 0 & \mathbb{1} \end{pmatrix} \quad (\text{A.3})$$

in terms of  $\sigma^\mu = (\mathbf{1}, \boldsymbol{\sigma})$  and  $\bar{\sigma}^\mu = (\mathbf{1}, -\boldsymbol{\sigma})$ . The 4-spinors  $\Psi$  in this representation could be written in terms of a left-handed Weyl 2-spinor  $\psi_{L,\alpha}$  and a right-handed Weyl 2-spinor  $\bar{\psi}_R^{\dot{\beta}}$  such that  $\Psi = \begin{pmatrix} \psi_{L,\alpha} \\ \bar{\psi}_R^{\dot{\beta}} \end{pmatrix}$ , where the corresponding charge-conjugated Dirac spinor becomes  $\Psi^C = \begin{pmatrix} \psi_{L,\alpha} \\ \bar{\psi}_R^{\dot{\beta}} \end{pmatrix}$  and we follow the notation of e.g. Ref. [1186] and refer to Ref. [1187] for a general review of 2-component spinors. We will however mostly use representation-independent 4-spinor notation.

For the Standard Model, our notation of the fundamental fields together with their quantum numbers is given in Tab. A.1. We refer to the review Ref. [1188] for details of the SM Lagrangian including its quantisation, renormalisation and applications, and we refer to Ref. [1189] for a useful comparison of different conventions. In our conventions, the  $SU(3)_c \times SU(2)_L \times U(1)_Y$  covariant derivative is given by

$$D_\mu = \partial_\mu + i(g_1 Y B_\mu + g_2 T^i W_\mu^i + g_3 t^a G_\mu^a) \quad (\text{A.4})$$

with the gauge couplings  $g_{1,2,3}$ , where we identify  $g_s \equiv g_3$ . In the fundamental representation, the  $SU(2)_L$  generators are given by  $T^i = \sigma^i/2$  and the  $SU(3)_c$  generators by  $t^a = \lambda^a/2$  where  $\lambda^a$  denotes the Gell-Mann matrices and fulfil the

commutation relation  $[\lambda^a, \lambda^b] = 2if_{abc}\lambda^c$ . The SM field-strength tensors are defined as

$$B_{\mu\nu} = \partial_\mu B_\nu - \partial_\nu B_\mu, \quad W_{\mu\nu}^i = \partial_\mu W_\nu^i - \partial_\nu W_\mu^i - g_2 \epsilon_{ijk} W_\mu^j W_\nu^k, \quad G_{\mu\nu}^a = \partial_\mu G_\nu^a - \partial_\nu G_\mu^a - g_s f_{abc} G_\mu^b G_\nu^c. \quad (\text{A.5})$$

The Lagrangian of the SM can be decomposed as

$$\mathcal{L}_{\text{SM}} = \mathcal{L}_{\text{gauge}} + \mathcal{L}_{\text{Fermion}} + \mathcal{L}_{\text{Higgs}} + \mathcal{L}_{\text{Yukawa}}. \quad (\text{A.6})$$

We specify the Higgs and Yukawa part as

$$\mathcal{L}_{\text{Higgs}} = (D_\mu \Phi)^\dagger (D^\mu \Phi) + \mu^2 |\Phi|^2 - \lambda |\Phi|^4, \quad (\text{A.7a})$$

$$\mathcal{L}_{\text{Yukawa}} = -(y_e)_{kj} \bar{l}_{Lk} \Phi e_{Rj} - (y_d)_{kj} \bar{q}_{Lk} \Phi d_{Rj} - (y_u)_{kj} \bar{q}_{Lk} \tilde{\Phi} u_{Rj} + \text{h.c.}, \quad (\text{A.7b})$$

while the remaining terms follow unambiguously from gauge invariance. Here, the  $\text{SU}(2)_L$  lepton, quark and Higgs doublets are decomposed as

$$l_{Li} = \begin{pmatrix} \nu_{Li} \\ e_{Li} \end{pmatrix}, \quad q_{Li} = \begin{pmatrix} u_{Li} \\ V_{\text{CKM}}^{ij} d_{Lj} \end{pmatrix}, \quad \Phi = \begin{pmatrix} G^+ \\ \frac{1}{\sqrt{2}}(v + h + iG^0) \end{pmatrix}, \quad \tilde{\Phi} = i\sigma^2 \Phi^* \equiv \begin{pmatrix} \frac{1}{\sqrt{2}}(v + h - iG) \\ -G^- \end{pmatrix} \quad (\text{A.8})$$

where  $G^- = (G^+)^\dagger$  and we have split off the  $vev$  of the Higgs field with the normalisation  $v \approx 246$  GeV. Furthermore, without loss of generality we take the lepton and up-type quark Yukawa matrices  $y_e$  and  $y_u$  to be diagonal, while the down-type Yukawa matrix  $y_d$  is diagonalised by the CKM matrix  $V_{\text{CKM}}$ .

If appropriate, we use explicit names

$$\nu_i = \{\nu_e, \nu_\mu, \nu_\tau\}, \quad e_i = \{e, \mu, \tau\}, \quad u_i = \{u, c, t\}, \quad d_i = \{d, s, b\} \quad (\text{A.9})$$

for the individual generations of fermion mass eigenstates  $f_i = f_{Li} + f_{Ri}$ . We also adopt corresponding short-hand notations with obvious meanings, such as  $y_\mu \equiv (y_e)_{22}$  or  $y_t \equiv (y_u)_{33}$ . In certain BSM scenarios, the Yukawa sector is modified, and in such cases the notation will be adapted as appropriate. The gauge boson mass-eigenstate fields are introduced as

$$\begin{pmatrix} A_\mu \\ Z_\mu \end{pmatrix} = \begin{pmatrix} c_W & s_W \\ -s_W & c_W \end{pmatrix} \begin{pmatrix} B_\mu \\ W_\mu^3 \end{pmatrix}, \quad W_\mu^\pm = \frac{1}{\sqrt{2}}(W_\mu^1 \mp iW_\mu^2) \quad (\text{A.10})$$

where  $c_W \equiv \cos \theta_W$  and  $s_W \equiv \sin \theta_W$  denote the cosine and sine of the weak mixing angle. For reference, the tree-level masses of the fermions, Higgs and gauge-bosons are given by

$$m_f = \frac{y_f v}{\sqrt{2}}, \quad M_h = \sqrt{2\lambda} v = \sqrt{2} \mu, \quad M_W = c_W M_Z = \frac{g_2 v}{2}. \quad (\text{A.11})$$

In terms of the mass-eigenstate fields the covariant derivative Eq. (A.4) becomes

$$D_\mu = \partial_\mu + ieQA_\mu + i\frac{g_2}{c_W}(T^3 - Qs_W^2)Z_\mu + i\frac{g_2}{\sqrt{2}}(T^+W_\mu^+ + T^-W_\mu^-) + ig_s t^a G_\mu^a, \quad (\text{A.12})$$

where  $T^\pm = T^1 \pm iT^2$ , and the electromagnetic gauge coupling and electric charge operator are given by

$$e = g_1 c_W = g_2 s_W, \quad Q = T^3 + Y. \quad (\text{A.13})$$

The electric charge eigenvalues of  $Q$  are  $\{0, -1, \frac{2}{3}, -\frac{1}{3}\}$  for neutrinos  $\nu_i$ , charged leptons  $e_i$ , up-type quarks  $u_i$  and down-type quarks  $d_i$ .

The SM covariant derivative contains the QED covariant derivative which, together with the electromagnetic field strength tensor, is given by

$$D_\mu^{\text{QED}} = \partial_\mu + ieQA_\mu, \quad (\text{A.14})$$

$$F_{\mu\nu} = \partial_\mu A_\nu - \partial_\nu A_\mu. \quad (\text{A.15})$$

## References

- [1] D. P. Aguillard et al. “Measurement of the Positive Muon Anomalous Magnetic Moment to 127 ppb”. In: (June 2025). arXiv: [2506.03069 \[hep-ex\]](#).
- [2] T. Aoyama et al. “The anomalous magnetic moment of the muon in the Standard Model”. In: *Phys. Rept.* 887 (2020), pp. 1–166. DOI: [10.1016/j.physrep.2020.07.006](#). arXiv: [2006.04822 \[hep-ph\]](#).
- [3] R. Aliberti et al. “The anomalous magnetic moment of the muon in the Standard Model: an update”. In: (May 2025). arXiv: [2505.21476 \[hep-ph\]](#).
- [4] Andrzej Czarnecki and William J. Marciano. “The Muon anomalous magnetic moment: A Harbinger for ‘new physics’”. In: *Phys. Rev. D* 64 (2001), p. 013014. DOI: [10.1103/PhysRevD.64.013014](#). arXiv: [hep-ph/0102122](#).
- [5] Dominik Stockinger. “The Muon Magnetic Moment and Supersymmetry”. In: *J. Phys. G* 34 (2007), R45–R92. DOI: [10.1088/0954-3899/34/2/R01](#). arXiv: [hep-ph/0609168](#).
- [6] Andrzej Czarnecki and William J. Marciano. “Electromagnetic dipole moments and new physics”. In: *Adv. Ser. Direct. High Energy Phys.* 20 (2009), pp. 11–67. DOI: [10.1142/9789814271844\\_0002](#).
- [7] Dominik Stöckinger. “Muon ( $g - 2$ ) and Physics Beyond the Standard Model”. In: *Adv. Ser. Direct. High Energy Phys.* 20 (2009), pp. 393–438. DOI: [10.1142/9789814271844\\_0012](#).
- [8] Manfred Lindner, Moritz Platscher, and Farinaldo S. Queiroz. “A Call for New Physics : The Muon Anomalous Magnetic Moment and Lepton Flavor Violation”. In: *Phys. Rept.* 731 (2018), pp. 1–82. DOI: [10.1016/j.physrep.2017.12.001](#). arXiv: [1610.06587 \[hep-ph\]](#).
- [9] Peter Athron, Csaba Balázs, Douglas H. J. Jacob, Wojciech Kotlarski, Dominik Stöckinger, and Hyejung Stöckinger-Kim. “New physics explanations of  $a_\mu$  in light of the FNAL muon  $g - 2$  measurement”. In: *JHEP* 09 (2021), p. 080. DOI: [10.1007/JHEP09\(2021\)080](#). arXiv: [2104.03691 \[hep-ph\]](#).
- [10] K. Melnikov and A. Vainshtein. *Theory of the muon anomalous magnetic moment*. Vol. 216. 2006. DOI: [10.1007/3-540-32807-6](#).
- [11] Friedrich Jegerlehner. *The Anomalous Magnetic Moment of the Muon*. Vol. 274. Cham: Springer, 2017. DOI: [10.1007/978-3-319-63577-4](#).
- [12] Fred Jegerlehner and Andreas Nyffeler. “The Muon  $g-2$ ”. In: *Phys. Rept.* 477 (2009), pp. 1–110. DOI: [10.1016/j.physrep.2009.04.003](#). arXiv: [0902.3360 \[hep-ph\]](#).
- [13] Alex Keshavarzi, Kim Siang Khaw, and Tamaki Yoshioka. “Muon  $g - 2$ : A review”. In: *Nucl. Phys. B* 975 (2022), p. 115675. DOI: [10.1016/j.nuclphysb.2022.115675](#). arXiv: [2106.06723 \[hep-ex\]](#).
- [14] Paul A. M. Dirac. “The quantum theory of the electron”. In: *Proc. Roy. Soc. Lond. A* 117 (1928), pp. 610–624. DOI: [10.1098/rspa.1928.0023](#).
- [15] Julian S. Schwinger. “On Quantum electrodynamics and the magnetic moment of the electron”. In: *Phys. Rev.* 73 (1948), pp. 416–417. DOI: [10.1103/PhysRev.73.416](#).
- [16] Julian S. Schwinger. “On gauge invariance and vacuum polarization”. In: *Phys. Rev.* 82 (1951). Ed. by K. A. Milton, pp. 664–679. DOI: [10.1103/PhysRev.82.664](#).

- [17] J. Bailey et al. “The Anomalous Magnetic Moment of Positive and Negative Muons”. In: *Phys. Lett. B* 67 (1977), p. 225. DOI: [10.1016/0370-2693\(77\)90199-X](https://doi.org/10.1016/0370-2693(77)90199-X).
- [18] J. Bailey et al. “Final Report on the CERN Muon Storage Ring Including the Anomalous Magnetic Moment and the Electric Dipole Moment of the Muon, and a Direct Test of Relativistic Time Dilation”. In: *Nucl. Phys. B* 150 (1979), pp. 1–75. DOI: [10.1016/0550-3213\(79\)90292-X](https://doi.org/10.1016/0550-3213(79)90292-X).
- [19] H. N. Brown et al. “Precise measurement of the positive muon anomalous magnetic moment”. In: *Phys. Rev. Lett.* 86 (2001), pp. 2227–2231. DOI: [10.1103/PhysRevLett.86.2227](https://doi.org/10.1103/PhysRevLett.86.2227). arXiv: [hep-ex/0102017](https://arxiv.org/abs/hep-ex/0102017).
- [20] G. W. Bennett et al. “Measurement of the positive muon anomalous magnetic moment to 0.7 ppm”. In: *Phys. Rev. Lett.* 89 (2002). [Erratum: *Phys.Rev.Lett.* 89, 129903 (2002)], p. 101804. DOI: [10.1103/PhysRevLett.89.101804](https://doi.org/10.1103/PhysRevLett.89.101804). arXiv: [hep-ex/0208001](https://arxiv.org/abs/hep-ex/0208001).
- [21] G. W. Bennett et al. “Measurement of the negative muon anomalous magnetic moment to 0.7 ppm”. In: *Phys. Rev. Lett.* 92 (2004), p. 161802. DOI: [10.1103/PhysRevLett.92.161802](https://doi.org/10.1103/PhysRevLett.92.161802). arXiv: [hep-ex/0401008](https://arxiv.org/abs/hep-ex/0401008).
- [22] G. W. Bennett et al. “Final Report of the Muon E821 Anomalous Magnetic Moment Measurement at BNL”. In: *Phys. Rev. D* 73 (2006), p. 072003. DOI: [10.1103/PhysRevD.73.072003](https://doi.org/10.1103/PhysRevD.73.072003). arXiv: [hep-ex/0602035](https://arxiv.org/abs/hep-ex/0602035).
- [23] B. Abi et al. “Measurement of the Positive Muon Anomalous Magnetic Moment to 0.46 ppm”. In: *Phys. Rev. Lett.* 126.14 (2021), p. 141801. DOI: [10.1103/PhysRevLett.126.141801](https://doi.org/10.1103/PhysRevLett.126.141801). arXiv: [2104.03281](https://arxiv.org/abs/2104.03281) [[hep-ex](#)].
- [24] D. P. Aguillard et al. “Measurement of the Positive Muon Anomalous Magnetic Moment to 0.20 ppm”. In: *Phys. Rev. Lett.* 131.16 (2023), p. 161802. DOI: [10.1103/PhysRevLett.131.161802](https://doi.org/10.1103/PhysRevLett.131.161802). arXiv: [2308.06230](https://arxiv.org/abs/2308.06230) [[hep-ex](#)].
- [25] D. P. Aguillard et al. “Detailed report on the measurement of the positive muon anomalous magnetic moment to 0.20 ppm”. In: *Phys. Rev. D* 110.3 (2024), p. 032009. DOI: [10.1103/PhysRevD.110.032009](https://doi.org/10.1103/PhysRevD.110.032009). arXiv: [2402.15410](https://arxiv.org/abs/2402.15410) [[hep-ex](#)].
- [26] Tatsumi Aoyama, Masashi Hayakawa, Toichiro Kinoshita, and Makiko Nio. “Complete Tenth-Order QED Contribution to the Muon  $g-2$ ”. In: *Phys. Rev. Lett.* 109 (2012), p. 111808. DOI: [10.1103/PhysRevLett.109.111808](https://doi.org/10.1103/PhysRevLett.109.111808). arXiv: [1205.5370](https://arxiv.org/abs/1205.5370) [[hep-ph](#)].
- [27] Tatsumi Aoyama, Toichiro Kinoshita, and Makiko Nio. “Theory of the Anomalous Magnetic Moment of the Electron”. In: *Atoms* 7.1 (2019), p. 28. DOI: [10.3390/atoms7010028](https://doi.org/10.3390/atoms7010028).
- [28] Andrzej Czarnecki, William J. Marciano, and Arkady Vainshtein. “Refinements in electroweak contributions to the muon anomalous magnetic moment”. In: *Phys. Rev. D* 67 (2003). [Erratum: *Phys.Rev.D* 73, 119901 (2006)], p. 073006. DOI: [10.1103/PhysRevD.67.073006](https://doi.org/10.1103/PhysRevD.67.073006). arXiv: [hep-ph/0212229](https://arxiv.org/abs/hep-ph/0212229).
- [29] C. Gnendiger, D. Stöckinger, and H. Stöckinger-Kim. “The electroweak contributions to  $(g-2)_\mu$  after the Higgs boson mass measurement”. In: *Phys. Rev. D* 88 (2013), p. 053005. DOI: [10.1103/PhysRevD.88.053005](https://doi.org/10.1103/PhysRevD.88.053005). arXiv: [1306.5546](https://arxiv.org/abs/1306.5546) [[hep-ph](#)].
- [30] Michel Davier, Andreas Hoecker, Bogdan Malaescu, and Zhiqing Zhang. “Reevaluation of the hadronic vacuum polarisation contributions to the Standard Model predictions of the muon  $g-2$  and  $\alpha(m_Z^2)$  using newest hadronic cross-section data”. In: *Eur. Phys. J. C* 77.12 (2017), p. 827. DOI: [10.1140/epjc/s10052-017-5161-6](https://doi.org/10.1140/epjc/s10052-017-5161-6). arXiv: [1706.09436](https://arxiv.org/abs/1706.09436) [[hep-ph](#)].

- [31] Alexander Keshavarzi, Daisuke Nomura, and Thomas Teubner. “Muon  $g - 2$  and  $\alpha(M_Z^2)$ : a new data-based analysis”. In: *Phys. Rev. D* 97.11 (2018), p. 114025. DOI: [10.1103/PhysRevD.97.114025](https://doi.org/10.1103/PhysRevD.97.114025). arXiv: [1802.02995](https://arxiv.org/abs/1802.02995) [hep-ph].
- [32] Gilberto Colangelo, Martin Hoferichter, and Peter Stoffer. “Two-pion contribution to hadronic vacuum polarization”. In: *JHEP* 02 (2019), p. 006. DOI: [10.1007/JHEP02\(2019\)006](https://doi.org/10.1007/JHEP02(2019)006). arXiv: [1810.00007](https://arxiv.org/abs/1810.00007) [hep-ph].
- [33] Martin Hoferichter, Bai-Long Hoid, and Bastian Kubis. “Three-pion contribution to hadronic vacuum polarization”. In: *JHEP* 08 (2019), p. 137. DOI: [10.1007/JHEP08\(2019\)137](https://doi.org/10.1007/JHEP08(2019)137). arXiv: [1907.01556](https://arxiv.org/abs/1907.01556) [hep-ph].
- [34] M. Davier, A. Hoecker, B. Malaescu, and Z. Zhang. “A new evaluation of the hadronic vacuum polarisation contributions to the muon anomalous magnetic moment and to  $\alpha(m_Z^2)$ ”. In: *Eur. Phys. J. C* 80.3 (2020). [Erratum: *Eur.Phys.J.C* 80, 410 (2020)], p. 241. DOI: [10.1140/epjc/s10052-020-7792-2](https://doi.org/10.1140/epjc/s10052-020-7792-2). arXiv: [1908.00921](https://arxiv.org/abs/1908.00921) [hep-ph].
- [35] Alexander Keshavarzi, Daisuke Nomura, and Thomas Teubner. “ $g - 2$  of charged leptons,  $\alpha(M_Z^2)$ , and the hyperfine splitting of muonium”. In: *Phys. Rev. D* 101.1 (2020), p. 014029. DOI: [10.1103/PhysRevD.101.014029](https://doi.org/10.1103/PhysRevD.101.014029). arXiv: [1911.00367](https://arxiv.org/abs/1911.00367) [hep-ph].
- [36] Alexander Kurz, Tao Liu, Peter Marquard, and Matthias Steinhauser. “Hadronic contribution to the muon anomalous magnetic moment to next-to-next-to-leading order”. In: *Phys. Lett. B* 734 (2014), pp. 144–147. DOI: [10.1016/j.physletb.2014.05.043](https://doi.org/10.1016/j.physletb.2014.05.043). arXiv: [1403.6400](https://arxiv.org/abs/1403.6400) [hep-ph].
- [37] Kirill Melnikov and Arkady Vainshtein. “Hadronic light-by-light scattering contribution to the muon anomalous magnetic moment revisited”. In: *Phys. Rev. D* 70 (2004), p. 113006. DOI: [10.1103/PhysRevD.70.113006](https://doi.org/10.1103/PhysRevD.70.113006). arXiv: [hep-ph/0312226](https://arxiv.org/abs/hep-ph/0312226).
- [38] Pere Masjuan and Pablo Sanchez-Puertas. “Pseudoscalar-pole contribution to the  $(g_\mu - 2)$ : a rational approach”. In: *Phys. Rev. D* 95.5 (2017), p. 054026. DOI: [10.1103/PhysRevD.95.054026](https://doi.org/10.1103/PhysRevD.95.054026). arXiv: [1701.05829](https://arxiv.org/abs/1701.05829) [hep-ph].
- [39] Gilberto Colangelo, Martin Hoferichter, Massimiliano Procura, and Peter Stoffer. “Dispersion relation for hadronic light-by-light scattering: two-pion contributions”. In: *JHEP* 04 (2017), p. 161. DOI: [10.1007/JHEP04\(2017\)161](https://doi.org/10.1007/JHEP04(2017)161). arXiv: [1702.07347](https://arxiv.org/abs/1702.07347) [hep-ph].
- [40] Martin Hoferichter, Bai-Long Hoid, Bastian Kubis, Stefan Leupold, and Sebastian P. Schneider. “Dispersion relation for hadronic light-by-light scattering: pion pole”. In: *JHEP* 10 (2018), p. 141. DOI: [10.1007/JHEP10\(2018\)141](https://doi.org/10.1007/JHEP10(2018)141). arXiv: [1808.04823](https://arxiv.org/abs/1808.04823) [hep-ph].
- [41] Antoine Gérardin, Harvey B. Meyer, and Andreas Nyffeler. “Lattice calculation of the pion transition form factor with  $N_f = 2 + 1$  Wilson quarks”. In: *Phys. Rev. D* 100.3 (2019), p. 034520. DOI: [10.1103/PhysRevD.100.034520](https://doi.org/10.1103/PhysRevD.100.034520). arXiv: [1903.09471](https://arxiv.org/abs/1903.09471) [hep-lat].
- [42] Johan Bijnens, Nils Hermansson-Truedsson, and Antonio Rodríguez-Sánchez. “Short-distance constraints for the HLbL contribution to the muon anomalous magnetic moment”. In: *Phys. Lett. B* 798 (2019), p. 134994. DOI: [10.1016/j.physletb.2019.134994](https://doi.org/10.1016/j.physletb.2019.134994). arXiv: [1908.03331](https://arxiv.org/abs/1908.03331) [hep-ph].
- [43] Gilberto Colangelo, Franziska Hagelstein, Martin Hoferichter, Laetitia Laub, and Peter Stoffer. “Longitudinal short-distance constraints for the hadronic light-by-light contribution to  $(g - 2)_\mu$  with large- $N_c$  Regge models”. In: *JHEP* 03 (2020), p. 101. DOI: [10.1007/JHEP03\(2020\)101](https://doi.org/10.1007/JHEP03(2020)101). arXiv: [1910.13432](https://arxiv.org/abs/1910.13432) [hep-ph].

- [44] Vladyslav Pauk and Marc Vanderhaeghen. “Single meson contributions to the muon’s anomalous magnetic moment”. In: *Eur. Phys. J. C* 74.8 (2014), p. 3008. DOI: [10.1140/epjc/s10052-014-3008-y](https://doi.org/10.1140/epjc/s10052-014-3008-y). arXiv: [1401.0832](https://arxiv.org/abs/1401.0832) [hep-ph].
- [45] Igor Danilkin and Marc Vanderhaeghen. “Light-by-light scattering sum rules in light of new data”. In: *Phys. Rev. D* 95.1 (2017), p. 014019. DOI: [10.1103/PhysRevD.95.014019](https://doi.org/10.1103/PhysRevD.95.014019). arXiv: [1611.04646](https://arxiv.org/abs/1611.04646) [hep-ph].
- [46] M. Knecht, S. Narison, A. Rabemananjara, and D. Rabetiariivony. “Scalar meson contributions to a  $\mu$  from hadronic light-by-light scattering”. In: *Phys. Lett. B* 787 (2018), pp. 111–123. DOI: [10.1016/j.physletb.2018.10.048](https://doi.org/10.1016/j.physletb.2018.10.048). arXiv: [1808.03848](https://arxiv.org/abs/1808.03848) [hep-ph].
- [47] Gernot Eichmann, Christian S. Fischer, and Richard Williams. “Kaon-box contribution to the anomalous magnetic moment of the muon”. In: *Phys. Rev. D* 101.5 (2020), p. 054015. DOI: [10.1103/PhysRevD.101.054015](https://doi.org/10.1103/PhysRevD.101.054015). arXiv: [1910.06795](https://arxiv.org/abs/1910.06795) [hep-ph].
- [48] Pablo Roig and Pablo Sanchez-Puertas. “Axial-vector exchange contribution to the hadronic light-by-light piece of the muon anomalous magnetic moment”. In: *Phys. Rev. D* 101.7 (2020), p. 074019. DOI: [10.1103/PhysRevD.101.074019](https://doi.org/10.1103/PhysRevD.101.074019). arXiv: [1910.02881](https://arxiv.org/abs/1910.02881) [hep-ph].
- [49] Thomas Blum, Norman Christ, Masashi Hayakawa, Taku Izubuchi, Luchang Jin, Chulwoo Jung, and Christoph Lehner. “Hadronic Light-by-Light Scattering Contribution to the Muon Anomalous Magnetic Moment from Lattice QCD”. In: *Phys. Rev. Lett.* 124.13 (2020), p. 132002. DOI: [10.1103/PhysRevLett.124.132002](https://doi.org/10.1103/PhysRevLett.124.132002). arXiv: [1911.08123](https://arxiv.org/abs/1911.08123) [hep-lat].
- [50] Gilberto Colangelo, Martin Hoferichter, Andreas Nyffeler, Massimo Passera, and Peter Stoffer. “Remarks on higher-order hadronic corrections to the muon  $g-2$ ”. In: *Phys. Lett. B* 735 (2014), pp. 90–91. DOI: [10.1016/j.physletb.2014.06.012](https://doi.org/10.1016/j.physletb.2014.06.012). arXiv: [1403.7512](https://arxiv.org/abs/1403.7512) [hep-ph].
- [51] Sergey Volkov. “Calculating the five-loop QED contribution to the electron anomalous magnetic moment: Graphs without lepton loops”. In: *Phys. Rev. D* 100.9 (2019), p. 096004. DOI: [10.1103/PhysRevD.100.096004](https://doi.org/10.1103/PhysRevD.100.096004). arXiv: [1909.08015](https://arxiv.org/abs/1909.08015) [hep-ph].
- [52] Sergey Volkov. “Calculation of the total 10th order QED contribution to the electron magnetic moment”. In: *Phys. Rev. D* 110.3 (2024), p. 036001. DOI: [10.1103/PhysRevD.110.036001](https://doi.org/10.1103/PhysRevD.110.036001). arXiv: [2404.00649](https://arxiv.org/abs/2404.00649) [hep-ph].
- [53] Tatsumi Aoyama, Masashi Hayakawa, Akira Hirayama, and Makiko Nio. “Verification of the tenth-order QED contribution to the anomalous magnetic moment of the electron from diagrams without fermion loops”. In: *Phys. Rev. D* 111.3 (2025), p. L031902. DOI: [10.1103/PhysRevD.111.L031902](https://doi.org/10.1103/PhysRevD.111.L031902). arXiv: [2412.06473](https://arxiv.org/abs/2412.06473) [hep-ph].
- [54] Richard H. Parker, Chenghui Yu, Weicheng Zhong, Brian Estey, and Holger Müller. “Measurement of the fine-structure constant as a test of the Standard Model”. In: *Science* 360 (2018), p. 191. DOI: [10.1126/science.aap7706](https://doi.org/10.1126/science.aap7706). arXiv: [1812.04130](https://arxiv.org/abs/1812.04130) [physics.atom-ph].
- [55] Léo Morel, Zhibin Yao, Pierre Cladé, and Saïda Guellati-Khélifa. “Determination of the fine-structure constant with an accuracy of 81 parts per trillion”. In: *Nature* 588.7836 (2020), pp. 61–65. DOI: [10.1038/s41586-020-2964-7](https://doi.org/10.1038/s41586-020-2964-7).

- [56] X. Fan, T. G. Myers, B. A. D. Sukra, and G. Gabrielse. “Measurement of the Electron Magnetic Moment”. In: *Phys. Rev. Lett.* 130.7 (2023), p. 071801. DOI: [10.1103/PhysRevLett.130.071801](https://doi.org/10.1103/PhysRevLett.130.071801). arXiv: [2209.13084](https://arxiv.org/abs/2209.13084) [[physics.atom-ph](https://arxiv.org/archive/physics)].
- [57] Jan Lüdtke, Massimiliano Procura, and Peter Stoffer. “Dispersion relations for the hadronic VVA correlator”. In: *JHEP* 04 (2025), p. 130. DOI: [10.1007/JHEP04\(2025\)130](https://doi.org/10.1007/JHEP04(2025)130). arXiv: [2410.11946](https://arxiv.org/abs/2410.11946) [[hep-ph](https://arxiv.org/archive/hep)].
- [58] Martin Hoferichter, Jan Lüdtke, Luca Naterop, Massimiliano Procura, and Peter Stoffer. “An improved evaluation of the electroweak contribution to  $(g - 2)_\mu$ ”. In: (Mar. 2025). arXiv: [2503.04883](https://arxiv.org/abs/2503.04883) [[hep-ph](https://arxiv.org/archive/hep)].
- [59] T. Blum, P. A. Boyle, V. Gülpers, T. Izubuchi, L. Jin, C. Jung, A. Jüttner, C. Lehner, A. Portelli, and J. T. Tsang. “Calculation of the hadronic vacuum polarization contribution to the muon anomalous magnetic moment”. In: *Phys. Rev. Lett.* 121.2 (2018), p. 022003. DOI: [10.1103/PhysRevLett.121.022003](https://doi.org/10.1103/PhysRevLett.121.022003). arXiv: [1801.07224](https://arxiv.org/abs/1801.07224) [[hep-lat](https://arxiv.org/archive/hep)].
- [60] D. Giusti, V. Lubicz, G. Martinelli, F. Sanfilippo, and S. Simula. “Electromagnetic and strong isospin-breaking corrections to the muon  $g - 2$  from Lattice QCD+QED”. In: *Phys. Rev. D* 99.11 (2019), p. 114502. DOI: [10.1103/PhysRevD.99.114502](https://doi.org/10.1103/PhysRevD.99.114502). arXiv: [1901.10462](https://arxiv.org/abs/1901.10462) [[hep-lat](https://arxiv.org/archive/hep)].
- [61] Sz. Borsanyi et al. “Leading hadronic contribution to the muon magnetic moment from lattice QCD”. In: *Nature* 593.7857 (2021), pp. 51–55. DOI: [10.1038/s41586-021-03418-1](https://doi.org/10.1038/s41586-021-03418-1). arXiv: [2002.12347](https://arxiv.org/abs/2002.12347) [[hep-lat](https://arxiv.org/archive/hep)].
- [62] Christoph Lehner and Aaron S. Meyer. “Consistency of hadronic vacuum polarization between lattice QCD and the R-ratio”. In: *Phys. Rev. D* 101 (2020), p. 074515. DOI: [10.1103/PhysRevD.101.074515](https://doi.org/10.1103/PhysRevD.101.074515). arXiv: [2003.04177](https://arxiv.org/abs/2003.04177) [[hep-lat](https://arxiv.org/archive/hep)].
- [63] Gen Wang, Terrence Draper, Keh-Fei Liu, and Yi-Bo Yang. “Muon  $g-2$  with overlap valence fermions”. In: *Phys. Rev. D* 107.3 (2023), p. 034513. DOI: [10.1103/PhysRevD.107.034513](https://doi.org/10.1103/PhysRevD.107.034513). arXiv: [2204.01280](https://arxiv.org/abs/2204.01280) [[hep-lat](https://arxiv.org/archive/hep)].
- [64] Christopher Aubin, Thomas Blum, Maarten Golterman, and Santiago Peris. “Muon anomalous magnetic moment with staggered fermions: Is the lattice spacing small enough?” In: *Phys. Rev. D* 106.5 (2022), p. 054503. DOI: [10.1103/PhysRevD.106.054503](https://doi.org/10.1103/PhysRevD.106.054503). arXiv: [2204.12256](https://arxiv.org/abs/2204.12256) [[hep-lat](https://arxiv.org/archive/hep)].
- [65] Marco Cè et al. “Window observable for the hadronic vacuum polarization contribution to the muon  $g-2$  from lattice QCD”. In: *Phys. Rev. D* 106.11 (2022), p. 114502. DOI: [10.1103/PhysRevD.106.114502](https://doi.org/10.1103/PhysRevD.106.114502). arXiv: [2206.06582](https://arxiv.org/abs/2206.06582) [[hep-lat](https://arxiv.org/archive/hep)].
- [66] C. Alexandrou et al. “Lattice calculation of the short and intermediate time-distance hadronic vacuum polarization contributions to the muon magnetic moment using twisted-mass fermions”. In: *Phys. Rev. D* 107.7 (2023), p. 074506. DOI: [10.1103/PhysRevD.107.074506](https://doi.org/10.1103/PhysRevD.107.074506). arXiv: [2206.15084](https://arxiv.org/abs/2206.15084) [[hep-lat](https://arxiv.org/archive/hep)].
- [67] T. Blum et al. “Update of Euclidean windows of the hadronic vacuum polarization”. In: *Phys. Rev. D* 108.5 (2023), p. 054507. DOI: [10.1103/PhysRevD.108.054507](https://doi.org/10.1103/PhysRevD.108.054507). arXiv: [2301.08696](https://arxiv.org/abs/2301.08696) [[hep-lat](https://arxiv.org/archive/hep)].
- [68] Simon Kuberski, Marco Cè, Georg von Hippel, Harvey B. Meyer, Konstantin Ottnad, Andreas Risch, and Hartmut Wittig. “Hadronic vacuum polarization in the muon  $g - 2$ : the short-distance contribution from lattice QCD”. In: *JHEP* 03 (2024), p. 172. DOI: [10.1007/JHEP03\(2024\)172](https://doi.org/10.1007/JHEP03(2024)172). arXiv: [2401.11895](https://arxiv.org/abs/2401.11895) [[hep-lat](https://arxiv.org/archive/hep)].
- [69] A. Boccaletti et al. “High precision calculation of the hadronic vacuum polarisation contribution to the muon anomaly”. In: (July 2024). arXiv: [2407.10913](https://arxiv.org/abs/2407.10913) [[hep-lat](https://arxiv.org/archive/hep)].

- [70] Sebastian Spiegel and Christoph Lehner. “A high-precision continuum limit study of the HVP short-distance window”. In: (Oct. 2024). arXiv: [2410.17053](https://arxiv.org/abs/2410.17053) [[hep-lat](#)].
- [71] T. Blum et al. “Long-Distance Window of the Hadronic Vacuum Polarization for the Muon  $g-2$ ”. In: *Phys. Rev. Lett.* 134.20 (2025), p. 201901. DOI: [10.1103/PhysRevLett.134.201901](https://doi.org/10.1103/PhysRevLett.134.201901). arXiv: [2410.20590](https://arxiv.org/abs/2410.20590) [[hep-lat](#)].
- [72] Dalibor Djukanovic, Georg von Hippel, Simon Kuberski, Harvey B. Meyer, Nolan Miller, Konstantin Ottnad, Julian Parrino, Andreas Risch, and Hartmut Wittig. “The hadronic vacuum polarization contribution to the muon  $g - 2$  at long distances”. In: *JHEP* 04 (2025), p. 098. DOI: [10.1007/JHEP04\(2025\)098](https://doi.org/10.1007/JHEP04(2025)098). arXiv: [2411.07969](https://arxiv.org/abs/2411.07969) [[hep-lat](#)].
- [73] C. Alexandrou et al. “Strange and charm quark contributions to the muon anomalous magnetic moment in lattice QCD with twisted-mass fermions”. In: *Phys. Rev. D* 111.5 (2025), p. 054502. DOI: [10.1103/PhysRevD.111.054502](https://doi.org/10.1103/PhysRevD.111.054502). arXiv: [2411.08852](https://arxiv.org/abs/2411.08852) [[hep-lat](#)].
- [74] Alexei Bazavov et al. “Hadronic vacuum polarization for the muon  $g-2$  from lattice QCD: Complete short and intermediate windows”. In: *Phys. Rev. D* 111.9 (2025), p. 094508. DOI: [10.1103/PhysRevD.111.094508](https://doi.org/10.1103/PhysRevD.111.094508). arXiv: [2411.09656](https://arxiv.org/abs/2411.09656) [[hep-lat](#)].
- [75] Alexei Bazavov et al. “Hadronic vacuum polarization for the muon  $g - 2$  from lattice QCD: Long-distance and full light-quark connected contribution”. In: (Dec. 2024). arXiv: [2412.18491](https://arxiv.org/abs/2412.18491) [[hep-lat](#)].
- [76] Luca Di Luzio, Alexander Keshavarzi, Antonio Masiero, and Paride Paradisi. “Model-Independent Tests of the Hadronic Vacuum Polarization Contribution to the Muon  $g-2$ ”. In: *Phys. Rev. Lett.* 134.1 (2025), p. 011902. DOI: [10.1103/PhysRevLett.134.011902](https://doi.org/10.1103/PhysRevLett.134.011902). arXiv: [2408.01123](https://arxiv.org/abs/2408.01123) [[hep-ph](#)].
- [77] Gilberto Colangelo, Martin Hoferichter, Massimiliano Procura, and Peter Stoffer. “Dispersion relation for hadronic light-by-light scattering: theoretical foundations”. In: *JHEP* 09 (2015), p. 074. DOI: [10.1007/JHEP09\(2015\)074](https://doi.org/10.1007/JHEP09(2015)074). arXiv: [1506.01386](https://arxiv.org/abs/1506.01386) [[hep-ph](#)].
- [78] Gernot Eichmann, Christian S. Fischer, Esther Weil, and Richard Williams. “Single pseudoscalar meson pole and pion box contributions to the anomalous magnetic moment of the muon”. In: *Phys. Lett. B* 797 (2019). [Erratum: *Phys.Lett.B* 799, 135029 (2019)], p. 134855. DOI: [10.1016/j.physletb.2019.134855](https://doi.org/10.1016/j.physletb.2019.134855). arXiv: [1903.10844](https://arxiv.org/abs/1903.10844) [[hep-ph](#)].
- [79] Josef Leutgeb and Anton Rebhan. “Axial vector transition form factors in holographic QCD and their contribution to the anomalous magnetic moment of the muon”. In: *Phys. Rev. D* 101.11 (2020), p. 114015. DOI: [10.1103/PhysRevD.101.114015](https://doi.org/10.1103/PhysRevD.101.114015). arXiv: [1912.01596](https://arxiv.org/abs/1912.01596) [[hep-ph](#)].
- [80] Luigi Cappiello, Oscar Catà, Giancarlo D’Ambrosio, David Greynat, and Abhishek Iyer. “Axial-vector and pseudoscalar mesons in the hadronic light-by-light contribution to the muon ( $g - 2$ )”. In: *Phys. Rev. D* 102.1 (2020), p. 016009. DOI: [10.1103/PhysRevD.102.016009](https://doi.org/10.1103/PhysRevD.102.016009). arXiv: [1912.02779](https://arxiv.org/abs/1912.02779) [[hep-ph](#)].
- [81] Pere Masjuan, Pablo Roig, and Pablo Sanchez-Puertas. “The interplay of transverse degrees of freedom and axial-vector mesons with short-distance constraints in  $g - 2$ ”. In: *J. Phys. G* 49.1 (2022), p. 015002. DOI: [10.1088/1361-6471/ac3892](https://doi.org/10.1088/1361-6471/ac3892). arXiv: [2005.11761](https://arxiv.org/abs/2005.11761) [[hep-ph](#)].

- [82] Johan Bijnens, Nils Hermansson-Truedsson, Laetitia Laub, and Antonio Rodríguez-Sánchez. “Short-distance HLbL contributions to the muon anomalous magnetic moment beyond perturbation theory”. In: *JHEP* 10 (2020), p. 203. DOI: [10.1007/JHEP10\(2020\)203](https://doi.org/10.1007/JHEP10(2020)203). arXiv: [2008.13487](https://arxiv.org/abs/2008.13487) [[hep-ph](#)].
- [83] Johan Bijnens, Nils Hermansson-Truedsson, Laetitia Laub, and Antonio Rodríguez-Sánchez. “The two-loop perturbative correction to the  $(g - 2)_\mu$  HLbL at short distances”. In: *JHEP* 04 (2021), p. 240. DOI: [10.1007/JHEP04\(2021\)240](https://doi.org/10.1007/JHEP04(2021)240). arXiv: [2101.09169](https://arxiv.org/abs/2101.09169) [[hep-ph](#)].
- [84] Igor Danilkin, Martin Hoferichter, and Peter Stoffer. “A dispersive estimate of scalar contributions to hadronic light-by-light scattering”. In: *Phys. Lett. B* 820 (2021), p. 136502. DOI: [10.1016/j.physletb.2021.136502](https://doi.org/10.1016/j.physletb.2021.136502). arXiv: [2105.01666](https://arxiv.org/abs/2105.01666) [[hep-ph](#)].
- [85] Dominik Stamen, Deepti Hariharan, Martin Hoferichter, Bastian Kubis, and Peter Stoffer. “Kaon electromagnetic form factors in dispersion theory”. In: *Eur. Phys. J. C* 82.5 (2022), p. 432. DOI: [10.1140/epjc/s10052-022-10348-3](https://doi.org/10.1140/epjc/s10052-022-10348-3). arXiv: [2202.11106](https://arxiv.org/abs/2202.11106) [[hep-ph](#)].
- [86] Josef Leutgeb, Jonas Mager, and Anton Rebhan. “Hadronic light-by-light contribution to the muon  $g-2$  from holographic QCD with solved U(1)<sub>A</sub> problem”. In: *Phys. Rev. D* 107.5 (2023), p. 054021. DOI: [10.1103/PhysRevD.107.054021](https://doi.org/10.1103/PhysRevD.107.054021). arXiv: [2211.16562](https://arxiv.org/abs/2211.16562) [[hep-ph](#)].
- [87] Martin Hoferichter, Bastian Kubis, and Marvin Zanke. “Axial-vector transition form factors and  $e^+e^- \rightarrow f_1\pi^+\pi^-$ ”. In: *JHEP* 08 (2023), p. 209. DOI: [10.1007/JHEP08\(2023\)209](https://doi.org/10.1007/JHEP08(2023)209). arXiv: [2307.14413](https://arxiv.org/abs/2307.14413) [[hep-ph](#)].
- [88] Martin Hoferichter, Peter Stoffer, and Maximilian Zillinger. “An optimized basis for hadronic light-by-light scattering”. In: *JHEP* 04 (2024), p. 092. DOI: [10.1007/JHEP04\(2024\)092](https://doi.org/10.1007/JHEP04(2024)092). arXiv: [2402.14060](https://arxiv.org/abs/2402.14060) [[hep-ph](#)].
- [89] Emilio J. Estrada, Sergi González-Solís, Adolfo Guevara, and Pablo Roig. “Improved  $\pi^0$ ,  $\eta$ ,  $\eta'$  transition form factors in resonance chiral theory and their  $a_\mu^{\text{HLbL}}$  contribution”. In: *JHEP* 12 (2024), p. 203. DOI: [10.1007/JHEP12\(2024\)203](https://doi.org/10.1007/JHEP12(2024)203). arXiv: [2409.10503](https://arxiv.org/abs/2409.10503) [[hep-ph](#)].
- [90] Oleksandra Deineka, Igor Danilkin, and Marc Vanderhaeghen. “Dispersive estimate of the  $a_0(980)$  contribution to  $(g-2)_\mu$ ”. In: *Phys. Rev. D* 111.3 (2025), p. 034009. DOI: [10.1103/PhysRevD.111.034009](https://doi.org/10.1103/PhysRevD.111.034009). arXiv: [2410.12894](https://arxiv.org/abs/2410.12894) [[hep-ph](#)].
- [91] Gernot Eichmann, Christian S. Fischer, Tim Haeuser, and Oliver Regenfelder. “Axial-vector and scalar contributions to hadronic light-by-light scattering”. In: *Eur. Phys. J. C* 85.4 (2025), p. 445. DOI: [10.1140/epjc/s10052-025-14055-7](https://doi.org/10.1140/epjc/s10052-025-14055-7). arXiv: [2411.05652](https://arxiv.org/abs/2411.05652) [[hep-ph](#)].
- [92] Johan Bijnens, Nils Hermansson-Truedsson, and Antonio Rodríguez-Sánchez. “Constraints on the hadronic light-by-light tensor in corner kinematics for the muon  $g - 2$ ”. In: *JHEP* 03 (2025), p. 094. DOI: [10.1007/JHEP03\(2025\)094](https://doi.org/10.1007/JHEP03(2025)094). arXiv: [2411.09578](https://arxiv.org/abs/2411.09578) [[hep-ph](#)].
- [93] Martin Hoferichter, Peter Stoffer, and Maximilian Zillinger. “Dispersion relation for hadronic light-by-light scattering: subleading contributions”. In: *JHEP* 02 (2025), p. 121. DOI: [10.1007/JHEP02\(2025\)121](https://doi.org/10.1007/JHEP02(2025)121). arXiv: [2412.00178](https://arxiv.org/abs/2412.00178) [[hep-ph](#)].
- [94] Simon Holz, Martin Hoferichter, Bai-Long Hoid, and Bastian Kubis. “Dispersion relation for hadronic light-by-light scattering:  $\eta$  and  $\eta'$  poles”. In: *JHEP* 04 (2025), p. 147. DOI: [10.1007/JHEP04\(2025\)147](https://doi.org/10.1007/JHEP04(2025)147). arXiv: [2412.16281](https://arxiv.org/abs/2412.16281) [[hep-ph](#)].

- [95] Luigi Cappiello, Josef Leutgeb, Jonas Mager, and Anton Rebhan. “Tensor meson transition form factors in holographic QCD and the muon  $g - 2$ ”. In: (Jan. 2025). arXiv: [2501.09699](https://arxiv.org/abs/2501.09699) [[hep-ph](#)].
- [96] En-Hung Chao, Renwick J. Hudspith, Antoine Gérardin, Jeremy R. Green, Harvey B. Meyer, and Konstantin Ottnad. “Hadronic light-by-light contribution to  $(g - 2)_\mu$  from lattice QCD: a complete calculation”. In: *Eur. Phys. J. C* 81.7 (2021), p. 651. DOI: [10.1140/epjc/s10052-021-09455-4](https://doi.org/10.1140/epjc/s10052-021-09455-4). arXiv: [2104.02632](https://arxiv.org/abs/2104.02632) [[hep-lat](#)].
- [97] En-Hung Chao, Renwick J. Hudspith, Antoine Gérardin, Jeremy R. Green, and Harvey B. Meyer. “The charm-quark contribution to light-by-light scattering in the muon  $(g - 2)$  from lattice QCD”. In: *Eur. Phys. J. C* 82.8 (2022), p. 664. DOI: [10.1140/epjc/s10052-022-10589-2](https://doi.org/10.1140/epjc/s10052-022-10589-2). arXiv: [2204.08844](https://arxiv.org/abs/2204.08844) [[hep-lat](#)].
- [98] Thomas Blum, Norman Christ, Masashi Hayakawa, Taku Izubuchi, Luchang Jin, Chulwoo Jung, Christoph Lehner, and Cheng Tu. “Hadronic light-by-light contribution to the muon anomaly from lattice QCD with infinite volume QED at physical pion mass”. In: *Phys. Rev. D* 111.1 (2025), p. 014501. DOI: [10.1103/PhysRevD.111.014501](https://doi.org/10.1103/PhysRevD.111.014501). arXiv: [2304.04423](https://arxiv.org/abs/2304.04423) [[hep-lat](#)].
- [99] Zoltan Fodor, Antoine Gerardin, Laurent Lellouch, Kalman K. Szabo, Balint C. Toth, and Christian Zimmermann. “Hadronic light-by-light scattering contribution to the anomalous magnetic moment of the muon at the physical pion mass”. In: (Nov. 2024). arXiv: [2411.11719](https://arxiv.org/abs/2411.11719) [[hep-lat](#)].
- [100] F. V. Ignatov et al. “Measurement of the  $e+e\rightarrow\pi+\pi^-$  cross section from threshold to 1.2 GeV with the CMD-3 detector”. In: *Phys. Rev. D* 109.11 (2024), p. 112002. DOI: [10.1103/PhysRevD.109.112002](https://doi.org/10.1103/PhysRevD.109.112002). arXiv: [2302.08834](https://arxiv.org/abs/2302.08834) [[hep-ex](#)].
- [101] F. V. Ignatov et al. “Measurement of the Pion Form Factor with CMD-3 Detector and its Implication to the Hadronic Contribution to Muon  $(g-2)$ ”. In: *Phys. Rev. Lett.* 132.23 (2024), p. 231903. DOI: [10.1103/PhysRevLett.132.231903](https://doi.org/10.1103/PhysRevLett.132.231903). arXiv: [2309.12910](https://arxiv.org/abs/2309.12910) [[hep-ex](#)].
- [102] G. Colangelo et al. “Prospects for precise predictions of  $a_\mu$  in the Standard Model”. In: (Mar. 2022). arXiv: [2203.15810](https://arxiv.org/abs/2203.15810) [[hep-ph](#)].
- [103] Gilberto Colangelo, Martin Hoferichter, and Peter Stoffer. “Puzzles in the hadronic contributions to the muon anomalous magnetic moment”. In: *PoS Muon4Future2023* (2024), p. 019. DOI: [10.22323/1.452.0019](https://doi.org/10.22323/1.452.0019).
- [104] S. Navas et al. “Review of particle physics”. In: *Phys. Rev. D* 110.3 (2024), p. 030001. DOI: [10.1103/PhysRevD.110.030001](https://doi.org/10.1103/PhysRevD.110.030001).
- [105] Dominik Stöckinger and Hyejung Stöckinger-Kim. “On the role of chirality flips for the muon magnetic moment and its relation to the muon mass”. In: *Front. in Phys.* 10 (2022), p. 944614. DOI: [10.3389/fphy.2022.944614](https://doi.org/10.3389/fphy.2022.944614).
- [106] Othmar Steinmann. “What is the magnetic moment of the electron?” In: *Commun. Math. Phys.* 237 (2003), pp. 181–201. DOI: [10.1007/s00220-003-0847-z](https://doi.org/10.1007/s00220-003-0847-z). arXiv: [hep-ph/0211187](https://arxiv.org/abs/hep-ph/0211187).
- [107] T. W. B. Kibble. “Frequency Shift in High-Intensity Compton Scattering”. In: *Phys. Rev.* 138 (3B 1965), B740–B753. DOI: [10.1103/PhysRev.138.B740](https://doi.org/10.1103/PhysRev.138.B740). URL: <https://link.aps.org/doi/10.1103/PhysRev.138.B740>.
- [108] Lee M. Frantz. “Compton Scattering of an Intense Photon Beam”. In: *Phys. Rev.* 139 (5B 1965), B1326–B1336. DOI: [10.1103/PhysRev.139.B1326](https://doi.org/10.1103/PhysRev.139.B1326). URL: <https://link.aps.org/doi/10.1103/PhysRev.139.B1326>.

- [109] Anton Ilderton and Daniel Seipt. “Backreaction on background fields: A coherent state approach”. In: *Phys. Rev. D* 97 (1 2018), p. 016007. DOI: [10.1103/PhysRevD.97.016007](https://doi.org/10.1103/PhysRevD.97.016007). URL: <https://link.aps.org/doi/10.1103/PhysRevD.97.016007>.
- [110] A. Fedotov, A. Ilderton, F. Karbstein, B. King, D. Seipt, H. Taya, and G. Torgrimsson. “Advances in QED with intense background fields”. In: *Phys. Rept.* 1010 (2023), pp. 1–138. DOI: [10.1016/j.physrep.2023.01.003](https://doi.org/10.1016/j.physrep.2023.01.003). arXiv: [2203.00019](https://arxiv.org/abs/2203.00019) [[hep-ph](#)].
- [111] Uwe Hernandez Acosta and Burkhard Kämpfer. “Strong-field QED in the Furry-picture momentum-space formulation: Ward identities and Feynman diagrams”. In: *Phys. Rev. D* 108.1 (2023), p. 016013. DOI: [10.1103/PhysRevD.108.016013](https://doi.org/10.1103/PhysRevD.108.016013). arXiv: [2303.12941](https://arxiv.org/abs/2303.12941) [[hep-ph](#)].
- [112] Anton Ilderton and Greger Torgrimsson. “Scattering in plane-wave backgrounds: infra-red effects and pole structure”. In: *Phys. Rev. D* 87 (2013), p. 085040. DOI: [10.1103/PhysRevD.87.085040](https://doi.org/10.1103/PhysRevD.87.085040). arXiv: [1210.6840](https://arxiv.org/abs/1210.6840) [[hep-th](#)].
- [113] James D. Bjorken and Sidney D. Drell. “Relativistic quantum fields”. In: (1965).
- [114] C. Itzykson and J. B. Zuber. *Quantum Field Theory*. International Series In Pure and Applied Physics. New York: McGraw-Hill, 1980. ISBN: 978-0-486-44568-7.
- [115] Michael E. Peskin and Daniel V. Schroeder. *An Introduction to quantum field theory*. Reading, USA: Addison-Wesley, 1995. ISBN: 978-0-201-50397-5, 978-0-429-50355-9, 978-0-429-49417-8. DOI: [10.1201/9780429503559](https://doi.org/10.1201/9780429503559).
- [116] Chris Quigg. *Gauge Theories of the Strong, Weak, and Electromagnetic Interactions: Second Edition*. USA: Princeton University Press, Sept. 2013. ISBN: 978-0-691-13548-9, 978-1-4008-4822-5. DOI: [10.1515/9781400848225](https://doi.org/10.1515/9781400848225).
- [117] Craig D. Roberts and Anthony G. Williams. “Dyson-Schwinger equations and their application to hadronic physics”. In: *Prog. Part. Nucl. Phys.* 33 (1994), pp. 477–575. DOI: [10.1016/0146-6410\(94\)90049-3](https://doi.org/10.1016/0146-6410(94)90049-3). arXiv: [hep-ph/9403224](https://arxiv.org/abs/hep-ph/9403224).
- [118] T. Albahri et al. “Measurement of the anomalous precession frequency of the muon in the Fermilab Muon  $g - 2$  Experiment”. In: *Phys. Rev. D* 103.7 (2021), p. 072002. DOI: [10.1103/PhysRevD.103.072002](https://doi.org/10.1103/PhysRevD.103.072002). arXiv: [2104.03247](https://arxiv.org/abs/2104.03247) [[hep-ex](#)].
- [119] T. Albahri et al. “Magnetic-field measurement and analysis for the Muon  $g - 2$  Experiment at Fermilab”. In: *Phys. Rev. A* 103.4 (2021), p. 042208. DOI: [10.1103/PhysRevA.103.042208](https://doi.org/10.1103/PhysRevA.103.042208). arXiv: [2104.03201](https://arxiv.org/abs/2104.03201) [[hep-ex](#)].
- [120] T. Albahri et al. “Beam dynamics corrections to the Run-1 measurement of the muon anomalous magnetic moment at Fermilab”. In: *Phys. Rev. Accel. Beams* 24.4 (2021), p. 044002. DOI: [10.1103/PhysRevAccelBeams.24.044002](https://doi.org/10.1103/PhysRevAccelBeams.24.044002). arXiv: [2104.03240](https://arxiv.org/abs/2104.03240) [[physics.acc-ph](#)].
- [121] W. E. Caswell and G. P. Lepage. “Effective Lagrangians for Bound State Problems in QED, QCD, and Other Field Theories”. In: *Phys. Lett. B* 167 (1986), pp. 437–442. DOI: [10.1016/0370-2693\(86\)91297-9](https://doi.org/10.1016/0370-2693(86)91297-9).
- [122] T. Kinoshita and M. Nio. “Radiative corrections to the muonium hyperfine structure. 1. The  $\alpha^2$  ( $Z\alpha$ ) correction”. In: *Phys. Rev. D* 53 (1996), pp. 4909–4929. DOI: [10.1103/PhysRevD.53.4909](https://doi.org/10.1103/PhysRevD.53.4909). arXiv: [hep-ph/9512327](https://arxiv.org/abs/hep-ph/9512327).
- [123] Aneesh V. Manohar. “The HQET / NRQCD Lagrangian to order  $\alpha / m^3$ ”. In: *Phys. Rev. D* 56 (1997), pp. 230–237. DOI: [10.1103/PhysRevD.56.230](https://doi.org/10.1103/PhysRevD.56.230). arXiv: [hep-ph/9701294](https://arxiv.org/abs/hep-ph/9701294).

- [124] Richard J. Hill, Gabriel Lee, Gil Paz, and Mikhail P. Solon. “NRQED Lagrangian at order  $1/M^4$ ”. In: *Phys. Rev. D* 87 (2013), p. 053017. DOI: [10.1103/PhysRevD.87.053017](https://doi.org/10.1103/PhysRevD.87.053017). arXiv: [1212.4508](https://arxiv.org/abs/1212.4508) [hep-ph].
- [125] Gil Paz. “An Introduction to NRQED”. In: *Mod. Phys. Lett. A* 30.26 (2015), p. 1550128. DOI: [10.1142/S021773231550128X](https://doi.org/10.1142/S021773231550128X). arXiv: [1503.07216](https://arxiv.org/abs/1503.07216) [hep-ph].
- [126] Steven Weinberg. *The Quantum theory of fields. Vol. 1: Foundations*. Cambridge University Press, June 2005. ISBN: 978-0-521-67053-1, 978-0-511-25204-4. DOI: [10.1017/CB09781139644167](https://doi.org/10.1017/CB09781139644167).
- [127] V. Bargmann, Louis Michel, and V. L. Telegdi. “Precession of the polarization of particles moving in a homogeneous electromagnetic field”. In: *Phys. Rev. Lett.* 2 (1959). Ed. by Thibault Damour, Ivan Todorov, and Boris Zhilinskii, pp. 435–436. DOI: [10.1103/PhysRevLett.2.435](https://doi.org/10.1103/PhysRevLett.2.435).
- [128] L. D. Landau and E. M. Lifshitz. *Course on Theoretical Physics, Vol. 4: Quantum Electrodynamics*. Ed. by E.M.Lifshitz V. B.Berestetskii L. P.Pitaevskii. 1987.
- [129] James P. Miller, Eduardo de Rafael, B. Lee Roberts, and Dominik Stöckinger. “Muon ( $g-2$ ): Experiment and Theory”. In: *Ann. Rev. Nucl. Part. Sci.* 62 (2012), pp. 237–264. DOI: [10.1146/annurev-nucl-031312-120340](https://doi.org/10.1146/annurev-nucl-031312-120340).
- [130] B. Lee Roberts. “The History of the Muon ( $g - 2$ ) Experiments”. In: *SciPost Phys. Proc.* 1 (2019), p. 032. DOI: [10.21468/SciPostPhysProc.1.032](https://doi.org/10.21468/SciPostPhysProc.1.032). arXiv: [1811.06974](https://arxiv.org/abs/1811.06974) [hep-ex].
- [131] R. L. Garwin, L. M. Lederman, and Marcel Weinrich. “Observations of the Failure of Conservation of Parity and Charge Conjugation in Meson Decays: The Magnetic Moment of the Free Muon”. In: *Phys. Rev.* 105 (1957), pp. 1415–1417. DOI: [10.1103/PhysRev.105.1415](https://doi.org/10.1103/PhysRev.105.1415).
- [132] J M Cassels, T W O’Keeffe, M Rigby, A M Wetherell, and J R Wormald. “Experiments with a Polarized Muon Beam”. In: *Proceedings of the Physical Society. Section A* 70.7 (1957), p. 543. DOI: [10.1088/0370-1298/70/7/412](https://doi.org/10.1088/0370-1298/70/7/412).
- [133] T. D. Lee and Chen-Ning Yang. “Question of Parity Conservation in Weak Interactions”. In: *Phys. Rev.* 104 (1956), pp. 254–258. DOI: [10.1103/PhysRev.104.254](https://doi.org/10.1103/PhysRev.104.254).
- [134] J. I. Friedman and V. L. Telegdi. “Nuclear Emulsion Evidence for Parity Nonconservation in the Decay Chain  $\pi^+ \rightarrow \mu^+ \rightarrow e^+$ ”. In: *Phys. Rev.* 106 (1957), pp. 1290–1293. DOI: [10.1103/PhysRev.106.1290](https://doi.org/10.1103/PhysRev.106.1290).
- [135] John David Jackson. *Classical Electrodynamics*. Wiley, 1998. ISBN: 978-0-471-30932-1.
- [136] R. L. Garwin, D. P. Hutchinson, S. Penman, and G. Shapiro. “Accurate Determination of the  $\mu^+$  Magnetic Moment”. In: *Phys. Rev.* 118 (1960), pp. 271–283. DOI: [10.1103/PhysRev.118.271](https://doi.org/10.1103/PhysRev.118.271).
- [137] Georges Charpak, F. J. M. Farley, R. L. Garwin, T. Muller, J. C. Sens, V. L. Telegdi, and A. Zichichi. “Measurement of the anomalous magnetic moment of the muon”. In: *Phys. Rev. Lett.* 6 (1961). Ed. by N. Cabibbo, pp. 128–132. DOI: [10.1103/PhysRevLett.6.128](https://doi.org/10.1103/PhysRevLett.6.128).
- [138] G. Charpak, F. J. M. Farley, and R. L. Garwin. “A New Measurement of the Anomalous Magnetic Moment of the Muon”. In: *Phys. Lett.* 1 (1962), p. 16. DOI: [10.1016/0031-9163\(62\)90263-9](https://doi.org/10.1016/0031-9163(62)90263-9).
- [139] G. Charpak, P. J. M. Farley, E. L. Garwin, T. Muller, J. C. Sens, and A. Zichichi. “The anomalous magnetic moment of the muon”. In: *Nuovo Cim.* 37 (1965), pp. 1241–1363. DOI: [10.1007/BF02783344](https://doi.org/10.1007/BF02783344).
- [140] F. Combley and E. Picasso. “The Muon ( $G-2$ ) Precession Experiments: Past, Present and Future”. In: *Phys. Rept.* 14 (1974), p. 1. DOI: [10.1016/0370-1573\(74\)90004-0](https://doi.org/10.1016/0370-1573(74)90004-0).

- [141] J. Grange et al. “Muon (g-2) Technical Design Report”. In: (Jan. 2015). arXiv: [1501.06858 \[physics.ins-det\]](#).
- [142] Tsutomu Mibe. “New g-2 experiment at J-PARC”. In: *Chin. Phys. C* 34 (2010). Ed. by Chang-Zheng Yuan, pp. 745–748. DOI: [10.1088/1674-1137/34/6/022](#).
- [143] Hiromi Iinuma. “New approach to the muon g-2 and EDM experiment at J-PARC”. In: *J. Phys. Conf. Ser.* 295 (2011). Ed. by Hans Stroher and Frank Rathmann, p. 012032. DOI: [10.1088/1742-6596/295/1/012032](#).
- [144] Tsutomu Mibe. “Measurement of muon g-2 and EDM with an ultra-cold muon beam at J-PARC”. In: *Nucl. Phys. B Proc. Suppl.* 218 (2011). Ed. by George Lafferty and Stefan Soldner-Rembold, pp. 242–246. DOI: [10.1016/j.nuclphysbps.2011.06.039](#).
- [145] Naohito Saito. “A novel precision measurement of muon g-2 and EDM at J-PARC”. In: *AIP Conf. Proc.* 1467 (2012). Ed. by Takeshi Fukuyama and Rabindra Nath Mohapatra, pp. 45–56. DOI: [10.1063/1.4742078](#).
- [146] M. Abe et al. “A New Approach for Measuring the Muon Anomalous Magnetic Moment and Electric Dipole Moment”. In: *PTEP* 2019.5 (2019), p. 053C02. DOI: [10.1093/ptep/ptz030](#). arXiv: [1901.03047 \[physics.ins-det\]](#).
- [147] S. Aritome et al. “Acceleration of positive muons by a radio-frequency cavity”. In: (Oct. 2024). arXiv: [2410.11367 \[physics.acc-ph\]](#).
- [148] Andrzej Czarnecki, Bernd Krause, and William J. Marciano. “Electroweak corrections to the muon anomalous magnetic moment”. In: *Phys. Rev. Lett.* 76 (1996), pp. 3267–3270. DOI: [10.1103/PhysRevLett.76.3267](#). arXiv: [hep-ph/9512369](#).
- [149] Sven Heinemeyer, Dominik Stockinger, and Georg Weiglein. “Electroweak and supersymmetric two-loop corrections to (g-2)(mu)”. In: *Nucl. Phys. B* 699 (2004), pp. 103–123. DOI: [10.1016/j.nuclphysb.2004.08.014](#). arXiv: [hep-ph/0405255](#).
- [150] T. Gribovk and A. Czarnecki. “Electroweak interactions and the muon g-2: Bosonic two-loop effects”. In: *Phys. Rev. D* 72 (2005), p. 053016. DOI: [10.1103/PhysRevD.72.053016](#). arXiv: [hep-ph/0509205](#).
- [151] Tadashi Ishikawa, Nobuya Nakazawa, and Yoshiaki Yasui. “Numerical calculation of the full two-loop electroweak corrections to muon (g-2)”. In: *Phys. Rev. D* 99.7 (2019), p. 073004. DOI: [10.1103/PhysRevD.99.073004](#). arXiv: [1810.13445 \[hep-ph\]](#).
- [152] G. Degrossi and G. F. Giudice. “QED logarithms in the electroweak corrections to the muon anomalous magnetic moment”. In: *Phys. Rev. D* 58 (1998), p. 053007. DOI: [10.1103/PhysRevD.58.053007](#). arXiv: [hep-ph/9803384](#).
- [153] Andrzej Czarnecki, Bernd Krause, and William J. Marciano. “Electroweak Fermion loop contributions to the muon anomalous magnetic moment”. In: *Phys. Rev. D* 52 (1995), R2619–R2623. DOI: [10.1103/PhysRevD.52.R2619](#). arXiv: [hep-ph/9506256](#).
- [154] A. Anastasi et al. “Combination of KLOE  $\sigma(e^+e^- \rightarrow \pi^+\pi^-\gamma(\gamma))$  measurements and determination of  $a_\mu^{\pi^+\pi^-}$  in the energy range  $0.10 < s < 0.95 \text{ GeV}^2$ ”. In: *JHEP* 03 (2018), p. 173. DOI: [10.1007/JHEP03\(2018\)173](#). arXiv: [1711.03085 \[hep-ex\]](#).
- [155] J. P. Lees et al. “Precise Measurement of the  $e^+e^- \rightarrow \pi^+\pi^-(\gamma)$  Cross Section with the Initial-State Radiation Method at BABAR”. In: *Phys. Rev. D* 86 (2012), p. 032013. DOI: [10.1103/PhysRevD.86.032013](#). arXiv: [1205.2228 \[hep-ex\]](#).

- [156] R. R. Akhmetshin et al. “Measurement of  $e^+ e^- \rightarrow \pi^+ \pi^-$  cross-section with CMD-2 around rho meson”. In: *Phys. Lett. B* 527 (2002), pp. 161–172. DOI: [10.1016/S0370-2693\(02\)01168-1](https://doi.org/10.1016/S0370-2693(02)01168-1). arXiv: [hep-ex/0112031](https://arxiv.org/abs/hep-ex/0112031).
- [157] R. R. Akhmetshin et al. “Reanalysis of hadronic cross-section measurements at CMD-2”. In: *Phys. Lett. B* 578 (2004), pp. 285–289. DOI: [10.1016/j.physletb.2003.10.108](https://doi.org/10.1016/j.physletb.2003.10.108). arXiv: [hep-ex/0308008](https://arxiv.org/abs/hep-ex/0308008).
- [158] M. N. Achasov et al. “Update of the  $e^+ e^- \rightarrow \pi^+ \pi^-$  cross-section measured by SND detector in the energy region  $400\text{-MeV} < s^{**}(1/2) < 1000\text{-MeV}$ ”. In: *J. Exp. Theor. Phys.* 103 (2006), pp. 380–384. DOI: [10.1134/S106377610609007X](https://doi.org/10.1134/S106377610609007X). arXiv: [hep-ex/0605013](https://arxiv.org/abs/hep-ex/0605013).
- [159] M. N. Achasov et al. “Measurement of the  $e^+ e^- \rightarrow \pi^+ \pi^-$  process cross section with the SND detector at the VEPP-2000 collider in the energy region  $0.525 < \sqrt{s} < 0.883$  GeV”. In: *JHEP* 01 (2021), p. 113. DOI: [10.1007/JHEP01\(2021\)113](https://doi.org/10.1007/JHEP01(2021)113). arXiv: [2004.00263](https://arxiv.org/abs/2004.00263) [[hep-ex](#)].
- [160] M. Ablikim et al. “Measurement of the  $e^+ e^- \rightarrow \pi^+ \pi^-$  cross section between 600 and 900 MeV using initial state radiation”. In: *Phys. Lett. B* 753 (2016). [Erratum: *Phys.Lett.B* 812, 135982 (2021)], pp. 629–638. DOI: [10.1016/j.physletb.2015.11.043](https://doi.org/10.1016/j.physletb.2015.11.043). arXiv: [1507.08188](https://arxiv.org/abs/1507.08188) [[hep-ex](#)].
- [161] G. Colangelo, A. X. El-Khadra, M. Hoferichter, A. Keshavarzi, C. Lehner, P. Stoffer, and T. Teubner. “Data-driven evaluations of Euclidean windows to scrutinize hadronic vacuum polarization”. In: *Phys. Lett. B* 833 (2022), p. 137313. DOI: [10.1016/j.physletb.2022.137313](https://doi.org/10.1016/j.physletb.2022.137313). arXiv: [2205.12963](https://arxiv.org/abs/2205.12963) [[hep-ph](#)].
- [162] Michel Davier, Andreas Hoecker, Anne-Marie Lutz, Bogdan Malaescu, and Zhiqing Zhang. “Tensions in  $e^+ e^- \rightarrow \pi^+ \pi^- (\gamma)$  measurements: the new landscape of data-driven hadronic vacuum polarization predictions for the muon  $g-2$ ”. In: *Eur. Phys. J. C* 84.7 (2024), p. 721. DOI: [10.1140/epjc/s10052-024-12964-7](https://doi.org/10.1140/epjc/s10052-024-12964-7). arXiv: [2312.02053](https://arxiv.org/abs/2312.02053) [[hep-ph](#)].
- [163] Michel Davier, Zoltan Fodor, Antoine Gerardin, Laurent Lellouch, Bogdan Malaescu, Finn M. Stokes, Kalman K. Szabo, Balint C. Toth, Lukas Varnhorst, and Zhiqing Zhang. “Hadronic vacuum polarization: Comparing lattice QCD and data-driven results in systematically improvable ways”. In: *Phys. Rev. D* 109.7 (2024), p. 076019. DOI: [10.1103/PhysRevD.109.076019](https://doi.org/10.1103/PhysRevD.109.076019). arXiv: [2308.04221](https://arxiv.org/abs/2308.04221) [[hep-ph](#)].
- [164] Genessa Benton, Diogo Boito, Maarten Golterman, Alexander Keshavarzi, Kim Maltman, and Santiago Peris. “Data-Driven Determination of the Light-Quark Connected Component of the Intermediate-Window Contribution to the Muon  $g-2$ ”. In: *Phys. Rev. Lett.* 131.25 (2023), p. 251803. DOI: [10.1103/PhysRevLett.131.251803](https://doi.org/10.1103/PhysRevLett.131.251803). arXiv: [2306.16808](https://arxiv.org/abs/2306.16808) [[hep-ph](#)].
- [165] Pere Masjuan, Alejandro Miranda, and Pablo Roig. “ $\tau$  data-driven evaluation of Euclidean windows for the hadronic vacuum polarization”. In: *Phys. Lett. B* 850 (2024), p. 138492. DOI: [10.1016/j.physletb.2024.138492](https://doi.org/10.1016/j.physletb.2024.138492). arXiv: [2305.20005](https://arxiv.org/abs/2305.20005) [[hep-ph](#)].
- [166] Joaquim Prades, Eduardo de Rafael, and Arkady Vainshtein. “The Hadronic Light-by-Light Scattering Contribution to the Muon and Electron Anomalous Magnetic Moments”. In: *Adv. Ser. Direct. High Energy Phys.* 20 (2009), pp. 303–317. DOI: [10.1142/9789814271844\\_0009](https://doi.org/10.1142/9789814271844_0009). arXiv: [0901.0306](https://arxiv.org/abs/0901.0306) [[hep-ph](#)].
- [167] Simon Holz, Martin Hoferichter, Bai-Long Hoid, and Bastian Kubis. “Precision Evaluation of the  $\eta$ - and  $\eta'$ -Pole Contributions to Hadronic Light-by-Light Scattering in the Anomalous Magnetic Moment of the Muon”. In: *Phys. Rev. Lett.* 134.17 (2025), p. 171902. DOI: [10.1103/PhysRevLett.134.171902](https://doi.org/10.1103/PhysRevLett.134.171902). arXiv: [2411.08098](https://arxiv.org/abs/2411.08098) [[hep-ph](#)].

- [168] Johan Bijnens, Nils Hermansson-Truedsson, and Antonio Rodríguez-Sánchez. “Constraints on the hadronic light-by-light in the Melnikov-Vainshtein regime”. In: *JHEP* 02 (2023), p. 167. DOI: [10.1007/JHEP02\(2023\)167](https://doi.org/10.1007/JHEP02(2023)167). arXiv: [2211.17183](https://arxiv.org/abs/2211.17183) [hep-ph].
- [169] Riccardo Aliberti et al. “Radiative corrections and Monte Carlo tools for low-energy hadronic cross sections in  $e^+e^-$  collisions”. In: (Oct. 2024). arXiv: [2410.22882](https://arxiv.org/abs/2410.22882) [hep-ph].
- [170] Ricard Alemany, Michel Davier, and Andreas Hocker. “Improved determination of the hadronic contribution to the muon ( $g-2$ ) and to alpha ( $M(z)$ ) using new data from hadronic tau decays”. In: *Eur. Phys. J. C* 2 (1998), pp. 123–135. DOI: [10.1007/s100520050127](https://doi.org/10.1007/s100520050127). arXiv: [hep-ph/9703220](https://arxiv.org/abs/hep-ph/9703220).
- [171] C. M. Carloni Calame, M. Passera, L. Trentadue, and G. Venanzoni. “A new approach to evaluate the leading hadronic corrections to the muon  $g-2$ ”. In: *Phys. Lett. B* 746 (2015), pp. 325–329. DOI: [10.1016/j.physletb.2015.05.020](https://doi.org/10.1016/j.physletb.2015.05.020). arXiv: [1504.02228](https://arxiv.org/abs/1504.02228) [hep-ph].
- [172] G. Abbiendi et al. “Measuring the leading hadronic contribution to the muon  $g-2$  via  $\mu e$  scattering”. In: *Eur. Phys. J. C* 77.3 (2017), p. 139. DOI: [10.1140/epjc/s10052-017-4633-z](https://doi.org/10.1140/epjc/s10052-017-4633-z). arXiv: [1609.08987](https://arxiv.org/abs/1609.08987) [hep-ex].
- [173] “Letter of Intent: the MUonE project”. In: (June 2019).
- [174] Pulak Banerjee et al. “Theory for muon-electron scattering @ 10 ppm: A report of the MUonE theory initiative”. In: *Eur. Phys. J. C* 80.6 (2020), p. 591. DOI: [10.1140/epjc/s10052-020-8138-9](https://doi.org/10.1140/epjc/s10052-020-8138-9). arXiv: [2004.13663](https://arxiv.org/abs/2004.13663) [hep-ph].
- [175] Giovanni Abbiendi. “Status of the MUonE experiment”. In: *Phys. Scripta* 97.5 (2022), p. 054007. DOI: [10.1088/1402-4896/ac6297](https://doi.org/10.1088/1402-4896/ac6297). arXiv: [2201.13177](https://arxiv.org/abs/2201.13177) [physics.ins-det].
- [176] Fedor Ignatov, Riccardo Nunzio Pilato, Thomas Teubner, and Graziano Venanzoni. “An alternative evaluation of the leading-order hadronic contribution to the muon  $g - 2$  with MUonE”. In: *Phys. Lett. B* 848 (2024), p. 138344. DOI: [10.1016/j.physletb.2023.138344](https://doi.org/10.1016/j.physletb.2023.138344). arXiv: [2309.14205](https://arxiv.org/abs/2309.14205) [hep-ph].
- [177] P. S. Bhupal Dev, Werner Rodejohann, Xun-Jie Xu, and Yongchao Zhang. “MUonE sensitivity to new physics explanations of the muon anomalous magnetic moment”. In: *JHEP* 05 (2020), p. 053. DOI: [10.1007/JHEP05\(2020\)053](https://doi.org/10.1007/JHEP05(2020)053). arXiv: [2002.04822](https://arxiv.org/abs/2002.04822) [hep-ph].
- [178] A. Masiero, P. Paradisi, and M. Passera. “New physics at the MUonE experiment at CERN”. In: *Phys. Rev. D* 102.7 (2020), p. 075013. DOI: [10.1103/PhysRevD.102.075013](https://doi.org/10.1103/PhysRevD.102.075013). arXiv: [2002.05418](https://arxiv.org/abs/2002.05418) [hep-ph].
- [179] Kento Asai, Koichi Hamaguchi, Natsumi Nagata, Shih-Yen Tseng, and Juntaro Wada. “Probing the  $L_\mu-L_\tau$  gauge boson at the MUonE experiment”. In: *Phys. Rev. D* 106.5 (2022), p. L051702. DOI: [10.1103/PhysRevD.106.L051702](https://doi.org/10.1103/PhysRevD.106.L051702). arXiv: [2109.10093](https://arxiv.org/abs/2109.10093) [hep-ph].
- [180] Giovanni Grilli di Cortona and Enrico Nardi. “Probing light mediators at the MUonE experiment”. In: *Phys. Rev. D* 105.11 (2022), p. L111701. DOI: [10.1103/PhysRevD.105.L111701](https://doi.org/10.1103/PhysRevD.105.L111701). arXiv: [2204.04227](https://arxiv.org/abs/2204.04227) [hep-ph].
- [181] Oliver Atkinson, Matthew Black, Christoph Englert, Alexander Lenz, and Aleksey Rusov. “MUonE, muon  $g-2$  and electroweak precision constraints within 2HDMS”. In: *Phys. Rev. D* 106.11 (2022), p. 115031. DOI: [10.1103/PhysRevD.106.115031](https://doi.org/10.1103/PhysRevD.106.115031). arXiv: [2207.02789](https://arxiv.org/abs/2207.02789) [hep-ph].
- [182] Duc Ninh Le, Van Dung Le, Duc Truyen Le, and Van Cuong Le. “Unparticle effects at the MUonE experiment”. In: *Eur. Phys. J. C* 83.11 (2023), p. 1037. DOI: [10.1140/epjc/s10052-023-12213-3](https://doi.org/10.1140/epjc/s10052-023-12213-3). arXiv: [2304.04439](https://arxiv.org/abs/2304.04439) [hep-ph].

- [183] Jacques P. Leveille. “The Second Order Weak Correction to  $(G-2)$  of the Muon in Arbitrary Gauge Models”. In: *Nucl. Phys. B* 137 (1978), pp. 63–76. DOI: [10.1016/0550-3213\(78\)90051-2](https://doi.org/10.1016/0550-3213(78)90051-2).
- [184] Bingrong Yu and Shun Zhou. “General remarks on the one-loop contributions to the muon anomalous magnetic moment”. In: *Nucl. Phys. B* 975 (2022), p. 115674. DOI: [10.1016/j.nuclphysb.2022.115674](https://doi.org/10.1016/j.nuclphysb.2022.115674). arXiv: [2106.11291](https://arxiv.org/abs/2106.11291) [[hep-ph](#)].
- [185] L. T. Hue, H. N. Long, V. H. Binh, H. L. T. Mai, and T. Phong Nguyen. “One-loop contributions to decays  $eb \rightarrow e\alpha\gamma$  and  $(g-2)ea$  anomalies, and Ward identity”. In: *Nucl. Phys. B* 992 (2023), p. 116244. DOI: [10.1016/j.nuclphysb.2023.116244](https://doi.org/10.1016/j.nuclphysb.2023.116244). arXiv: [2301.05407](https://arxiv.org/abs/2301.05407) [[hep-ph](#)].
- [186] Kevin R. Lynch. “A Note on one loop electroweak contributions to  $g-2$ : A Companion to BUHEP-01-16”. In: (Aug. 2001). arXiv: [hep-ph/0108081](https://arxiv.org/abs/hep-ph/0108081).
- [187] L. Lavoura. “General formulae for  $f(1) \rightarrow f(2) \gamma$ ”. In: *Eur. Phys. J. C* 29 (2003), pp. 191–195. DOI: [10.1140/epjc/s2003-01212-7](https://doi.org/10.1140/epjc/s2003-01212-7). arXiv: [hep-ph/0302221](https://arxiv.org/abs/hep-ph/0302221).
- [188] Juan C. Criado, Abdelhak Djouadi, Niko Koivunen, Kristjan Mürsepp, Martti Raidal, and Hardi Veermäe. “Confronting spin-3/2 and other new fermions with the muon  $g-2$  measurement”. In: *Phys. Lett. B* 820 (2021), p. 136491. DOI: [10.1016/j.physletb.2021.136491](https://doi.org/10.1016/j.physletb.2021.136491). arXiv: [2104.03231](https://arxiv.org/abs/2104.03231) [[hep-ph](#)].
- [189] M. L. Graesser. “Extra dimensions and the muon anomalous magnetic moment”. In: *Phys. Rev. D* 61 (2000), p. 074019. DOI: [10.1103/PhysRevD.61.074019](https://doi.org/10.1103/PhysRevD.61.074019). arXiv: [hep-ph/9902310](https://arxiv.org/abs/hep-ph/9902310).
- [190] Helvecio Fagnoli, Christoph Gnendiger, Sebastian Paßehr, Dominik Stöckinger, and Hyejung Stöckinger-Kim. “Two-loop corrections to the muon magnetic moment from fermion/sfermion loops in the MSSM: detailed results”. In: *JHEP* 02 (2014), p. 070. DOI: [10.1007/JHEP02\(2014\)070](https://doi.org/10.1007/JHEP02(2014)070). arXiv: [1311.1775](https://arxiv.org/abs/1311.1775) [[hep-ph](#)].
- [191] Ayres Freitas, Joseph Lykken, Stefan Kell, and Susanne Westhoff. “Testing the Muon  $g-2$  Anomaly at the LHC”. In: *JHEP* 05 (2014). [Erratum: *JHEP* 09, 155 (2014)], p. 145. DOI: [10.1007/JHEP09\(2014\)155](https://doi.org/10.1007/JHEP09(2014)155). arXiv: [1402.7065](https://arxiv.org/abs/1402.7065) [[hep-ph](#)].
- [192] Farinaldo S. Queiroz and William Shepherd. “New Physics Contributions to the Muon Anomalous Magnetic Moment: A Numerical Code”. In: *Phys. Rev. D* 89.9 (2014), p. 095024. DOI: [10.1103/PhysRevD.89.095024](https://doi.org/10.1103/PhysRevD.89.095024). arXiv: [1403.2309](https://arxiv.org/abs/1403.2309) [[hep-ph](#)].
- [193] Carla Biggio and Marzia Bordone. “Minimal muon anomalous magnetic moment”. In: *JHEP* 02 (2015), p. 099. DOI: [10.1007/JHEP02\(2015\)099](https://doi.org/10.1007/JHEP02(2015)099). arXiv: [1411.6799](https://arxiv.org/abs/1411.6799) [[hep-ph](#)].
- [194] Carla Biggio, Marzia Bordone, Luca Di Luzio, and Giovanni Ridolfi. “Massive vectors and loop observables: the  $g - 2$  case”. In: *JHEP* 10 (2016), p. 002. DOI: [10.1007/JHEP10\(2016\)002](https://doi.org/10.1007/JHEP10(2016)002). arXiv: [1607.07621](https://arxiv.org/abs/1607.07621) [[hep-ph](#)].
- [195] Kamila Kowalska and Enrico Maria Sessolo. “Expectations for the muon  $g-2$  in simplified models with dark matter”. In: *JHEP* 09 (2017), p. 112. DOI: [10.1007/JHEP09\(2017\)112](https://doi.org/10.1007/JHEP09(2017)112). arXiv: [1707.00753](https://arxiv.org/abs/1707.00753) [[hep-ph](#)].
- [196] Lorenzo Calibbi, Robert Ziegler, and Jure Zupan. “Minimal models for dark matter and the muon  $g-2$  anomaly”. In: *JHEP* 07 (2018), p. 046. DOI: [10.1007/JHEP07\(2018\)046](https://doi.org/10.1007/JHEP07(2018)046). arXiv: [1804.00009](https://arxiv.org/abs/1804.00009) [[hep-ph](#)].
- [197] Guilherme Guedes and Pablo Ogoso. “A bridge to new physics: proposing new — and reviving old — explanations of  $a_\mu$ ”. In: *JHEP* 09 (2022), p. 181. DOI: [10.1007/JHEP09\(2022\)181](https://doi.org/10.1007/JHEP09(2022)181). arXiv: [2205.04480](https://arxiv.org/abs/2205.04480) [[hep-ph](#)].

- [198] F. Pisano and V. Pleitez. “An  $SU(3) \times U(1)$  model for electroweak interactions”. In: *Phys. Rev. D* 46 (1992), pp. 410–417. DOI: [10.1103/PhysRevD.46.410](https://doi.org/10.1103/PhysRevD.46.410). arXiv: [hep-ph/9206242](https://arxiv.org/abs/hep-ph/9206242).
- [199] Michael J. Baker, Peter Cox, and Raymond R. Volkas. “Has the Origin of the Third-Family Fermion Masses been Determined?” In: *JHEP* 04 (2021), p. 151. DOI: [10.1007/JHEP04\(2021\)151](https://doi.org/10.1007/JHEP04(2021)151). arXiv: [2012.10458](https://arxiv.org/abs/2012.10458) [[hep-ph](#)].
- [200] Michael J. Baker, Peter Cox, and Raymond R. Volkas. “Radiative muon mass models and  $(g - 2)_\mu$ ”. In: *JHEP* 05 (2021), p. 174. DOI: [10.1007/JHEP05\(2021\)174](https://doi.org/10.1007/JHEP05(2021)174). arXiv: [2103.13401](https://arxiv.org/abs/2103.13401) [[hep-ph](#)].
- [201] Rodolfo Capdevilla, David Curtin, Yonatan Kahn, and Gordan Krnjaic. “No-lose theorem for discovering the new physics of  $(g - 2)_\mu$  at muon colliders”. In: *Phys. Rev. D* 105.1 (2022), p. 015028. DOI: [10.1103/PhysRevD.105.015028](https://doi.org/10.1103/PhysRevD.105.015028). arXiv: [2101.10334](https://arxiv.org/abs/2101.10334) [[hep-ph](#)].
- [202] Andreas Crivellin and Martin Hoferichter. “Consequences of chirally enhanced explanations of  $(g - 2)_\mu$  for  $h \rightarrow \mu\mu$  and  $Z \rightarrow \mu\mu$ ”. In: *JHEP* 07 (2021). [Erratum: *JHEP* 10, 030 (2022)], p. 135. DOI: [10.1007/JHEP07\(2021\)135](https://doi.org/10.1007/JHEP07(2021)135). arXiv: [2104.03202](https://arxiv.org/abs/2104.03202) [[hep-ph](#)].
- [203] Junichiro Kawamura, Shohei Okawa, and Yuji Omura. “Current status and muon  $g - 2$  explanation of lepton portal dark matter”. In: *JHEP* 08 (2020), p. 042. DOI: [10.1007/JHEP08\(2020\)042](https://doi.org/10.1007/JHEP08(2020)042). arXiv: [2002.12534](https://arxiv.org/abs/2002.12534) [[hep-ph](#)].
- [204] Gudrun Hiller, Clara Hormigos-Feliu, Daniel F. Litim, and Tom Steudtner. “Anomalous magnetic moments from asymptotic safety”. In: *Phys. Rev. D* 102.7 (2020), p. 071901. DOI: [10.1103/PhysRevD.102.071901](https://doi.org/10.1103/PhysRevD.102.071901). arXiv: [1910.14062](https://arxiv.org/abs/1910.14062) [[hep-ph](#)].
- [205] Gudrun Hiller, Clara Hormigos-Feliu, Daniel F. Litim, and Tom Steudtner. “Model Building from Asymptotic Safety with Higgs and Flavor Portals”. In: *Phys. Rev. D* 102.9 (2020), p. 095023. DOI: [10.1103/PhysRevD.102.095023](https://doi.org/10.1103/PhysRevD.102.095023). arXiv: [2008.08606](https://arxiv.org/abs/2008.08606) [[hep-ph](#)].
- [206] Kamila Kowalska and Enrico Maria Sessolo. “Minimal models for  $g-2$  and dark matter confront asymptotic safety”. In: *Phys. Rev. D* 103.11 (2021), p. 115032. DOI: [10.1103/PhysRevD.103.115032](https://doi.org/10.1103/PhysRevD.103.115032). arXiv: [2012.15200](https://arxiv.org/abs/2012.15200) [[hep-ph](#)].
- [207] Takeo Moroi. “The Muon anomalous magnetic dipole moment in the minimal supersymmetric standard model”. In: *Phys. Rev. D* 53 (1996). [Erratum: *Phys.Rev.D* 56, 4424 (1997)], pp. 6565–6575. DOI: [10.1103/PhysRevD.53.6565](https://doi.org/10.1103/PhysRevD.53.6565). arXiv: [hep-ph/9512396](https://arxiv.org/abs/hep-ph/9512396).
- [208] A. Dedes, M. Paraskevas, J. Rosiek, K. Suxho, and K. Tamvakis. “Mass Insertions vs. Mass Eigenstates calculations in Flavour Physics”. In: *JHEP* 06 (2015), p. 151. DOI: [10.1007/JHEP06\(2015\)151](https://doi.org/10.1007/JHEP06(2015)151). arXiv: [1504.00960](https://arxiv.org/abs/1504.00960) [[hep-ph](#)].
- [209] Andreas Crivellin, Zofia Fabisiewicz, Weronika Materkowska, Ulrich Nierste, Stefan Pokorski, and Janusz Rosiek. “Lepton flavour violation in the MSSM: exact diagonalization vs mass expansion”. In: *JHEP* 06 (2018), p. 003. DOI: [10.1007/JHEP06\(2018\)003](https://doi.org/10.1007/JHEP06(2018)003). arXiv: [1802.06803](https://arxiv.org/abs/1802.06803) [[hep-ph](#)].
- [210] Gino Isidori, Felix Wilsch, and Daniel Wyler. “The standard model effective field theory at work”. In: *Rev. Mod. Phys.* 96.1 (2024), p. 015006. DOI: [10.1103/RevModPhys.96.015006](https://doi.org/10.1103/RevModPhys.96.015006). arXiv: [2303.16922](https://arxiv.org/abs/2303.16922) [[hep-ph](#)].
- [211] Lukas Allwicher, Luca Di Luzio, Marco Fedele, Federico Mescia, and Marco Nardecchia. “What is the scale of new physics behind the muon  $g-2$ ?” In: *Phys. Rev. D* 104.5 (2021), p. 055035. DOI: [10.1103/PhysRevD.104.055035](https://doi.org/10.1103/PhysRevD.104.055035). arXiv: [2105.13981](https://arxiv.org/abs/2105.13981) [[hep-ph](#)].

- [212] Jason Aebischer, Wouter Dekens, Elizabeth E. Jenkins, Aneesh V. Manohar, Dipan Sengupta, and Peter Stoffer. “Effective field theory interpretation of lepton magnetic and electric dipole moments”. In: *JHEP* 07 (2021), p. 107. DOI: [10.1007/JHEP07\(2021\)107](https://doi.org/10.1007/JHEP07(2021)107). arXiv: [2102.08954](https://arxiv.org/abs/2102.08954) [hep-ph].
- [213] Elizabeth E. Jenkins, Aneesh V. Manohar, and Peter Stoffer. “Low-Energy Effective Field Theory below the Electroweak Scale: Operators and Matching”. In: *JHEP* 03 (2018). [Erratum: *JHEP* 12, 043 (2023)], p. 016. DOI: [10.1007/JHEP03\(2018\)016](https://doi.org/10.1007/JHEP03(2018)016). arXiv: [1709.04486](https://arxiv.org/abs/1709.04486) [hep-ph].
- [214] Gerhard Buchalla, Andrzej J. Buras, and Markus E. Lautenbacher. “Weak decays beyond leading logarithms”. In: *Rev. Mod. Phys.* 68 (1996), pp. 1125–1144. DOI: [10.1103/RevModPhys.68.1125](https://doi.org/10.1103/RevModPhys.68.1125). arXiv: [hep-ph/9512380](https://arxiv.org/abs/hep-ph/9512380).
- [215] C. Gnendiger et al. “To  $d$ , or not to  $d$ : recent developments and comparisons of regularization schemes”. In: *Eur. Phys. J. C* 77.7 (2017), p. 471. DOI: [10.1140/epjc/s10052-017-5023-2](https://doi.org/10.1140/epjc/s10052-017-5023-2). arXiv: [1705.01827](https://arxiv.org/abs/1705.01827) [hep-ph].
- [216] Wouter Dekens, Elizabeth E. Jenkins, Aneesh V. Manohar, and Peter Stoffer. “Non-perturbative effects in  $\mu \rightarrow e\gamma$ ”. In: *JHEP* 01 (2019), p. 088. DOI: [10.1007/JHEP01\(2019\)088](https://doi.org/10.1007/JHEP01(2019)088). arXiv: [1810.05675](https://arxiv.org/abs/1810.05675) [hep-ph].
- [217] W. Buchmuller and D. Wyler. “Effective Lagrangian Analysis of New Interactions and Flavor Conservation”. In: *Nucl. Phys. B* 268 (1986), pp. 621–653. DOI: [10.1016/0550-3213\(86\)90262-2](https://doi.org/10.1016/0550-3213(86)90262-2).
- [218] B. Grzadkowski, M. Iskrzynski, M. Misiak, and J. Rosiek. “Dimension-Six Terms in the Standard Model Lagrangian”. In: *JHEP* 10 (2010), p. 085. DOI: [10.1007/JHEP10\(2010\)085](https://doi.org/10.1007/JHEP10(2010)085). arXiv: [1008.4884](https://arxiv.org/abs/1008.4884) [hep-ph].
- [219] Wouter Dekens and Peter Stoffer. “Low-energy effective field theory below the electroweak scale: matching at one loop”. In: *JHEP* 10 (2019). [Erratum: *JHEP* 11, 148 (2022)], p. 197. DOI: [10.1007/JHEP10\(2019\)197](https://doi.org/10.1007/JHEP10(2019)197). arXiv: [1908.05295](https://arxiv.org/abs/1908.05295) [hep-ph].
- [220] Dario Buttazzo and Paride Paradisi. “Probing the muon  $g - 2$  anomaly with the Higgs boson at a muon collider”. In: *Phys. Rev. D* 104.7 (2021), p. 075021. DOI: [10.1103/PhysRevD.104.075021](https://doi.org/10.1103/PhysRevD.104.075021). arXiv: [2012.02769](https://arxiv.org/abs/2012.02769) [hep-ph].
- [221] Vincenzo Cirigliano, Wouter Dekens, Jordy de Vries, Kaori Fuyuto, Emanuele Mereghetti, and Richard Ruiz. “Leptonic anomalous magnetic moments in  $\nu$  SMEFT”. In: *JHEP* 08 (2021), p. 103. DOI: [10.1007/JHEP08\(2021\)103](https://doi.org/10.1007/JHEP08(2021)103). arXiv: [2105.11462](https://arxiv.org/abs/2105.11462) [hep-ph].
- [222] Akanksha Bhardwaj, Christoph Englert, and Panagiotis Stylianou. “Implications of the muon anomalous magnetic moment for the LHC and MUonE”. In: *Phys. Rev. D* 106.7 (2022), p. 075031. DOI: [10.1103/PhysRevD.106.075031](https://doi.org/10.1103/PhysRevD.106.075031). arXiv: [2206.14640](https://arxiv.org/abs/2206.14640) [hep-ph].
- [223] Fabiola Fortuna, Juan Manuel Márquez, and Pablo Roig. “HEFT approach to investigate the muon  $g-2$  anomaly at a muon collider”. In: *Phys. Rev. D* 111.7 (2025), p. 075012. DOI: [10.1103/PhysRevD.111.075012](https://doi.org/10.1103/PhysRevD.111.075012). arXiv: [2408.16954](https://arxiv.org/abs/2408.16954) [hep-ph].
- [224] Wen Yin. “Radiative lepton mass and muon  $g - 2$  with suppressed lepton flavor and CP violations”. In: *JHEP* 08 (2021), p. 043. DOI: [10.1007/JHEP08\(2021\)043](https://doi.org/10.1007/JHEP08(2021)043). arXiv: [2103.14234](https://arxiv.org/abs/2103.14234) [hep-ph].
- [225] Cheng-Wei Chiang and Kei Yagyu. “Radiative Seesaw Mechanism for Charged Leptons”. In: *Phys. Rev. D* 103.11 (2021), p. L111302. DOI: [10.1103/PhysRevD.103.L111302](https://doi.org/10.1103/PhysRevD.103.L111302). arXiv: [2104.00890](https://arxiv.org/abs/2104.00890) [hep-ph].
- [226] Cheng-Wei Chiang, Ryomei Obuchi, and Kei Yagyu. “Dark sector as origin of light lepton mass and its phenomenology”. In: *JHEP* 05 (2022), p. 070. DOI: [10.1007/JHEP05\(2022\)070](https://doi.org/10.1007/JHEP05(2022)070). arXiv: [2202.07784](https://arxiv.org/abs/2202.07784) [hep-ph].

- [227] Cesar Bonilla, A. E. Carcamo Hernandez, Sergey Kovalenko, H. Lee, R. Pasechnik, and Ivan Schmidt. “Fermion mass hierarchy in an extended left-right symmetric model”. In: *JHEP* 12 (2023), p. 075. DOI: [10.1007/JHEP12\(2023\)075](https://doi.org/10.1007/JHEP12(2023)075). arXiv: [2305.11967](https://arxiv.org/abs/2305.11967) [[hep-ph](#)].
- [228] Markus Bach, Jae-hyeon Park, Dominik Stöckinger, and Hyejung Stöckinger-Kim. “Large muon  $(g - 2)$  with TeV-scale SUSY masses for  $\tan \beta \rightarrow \infty$ ”. In: *JHEP* 10 (2015), p. 026. DOI: [10.1007/JHEP10\(2015\)026](https://doi.org/10.1007/JHEP10(2015)026). arXiv: [1504.05500](https://arxiv.org/abs/1504.05500) [[hep-ph](#)].
- [229] Francesca Borzumati, Glennys R. Farrar, Nir Polonsky, and Scott D. Thomas. “Soft Yukawa couplings in supersymmetric theories”. In: *Nucl. Phys. B* 555 (1999), pp. 53–115. DOI: [10.1016/S0550-3213\(99\)00328-4](https://doi.org/10.1016/S0550-3213(99)00328-4). arXiv: [hep-ph/9902443](https://arxiv.org/abs/hep-ph/9902443).
- [230] Andreas Crivellin, Jennifer Girsch, and Ulrich Nierste. “Yukawa coupling and anomalous magnetic moment of the muon: an update for the LHC era”. In: *Phys. Rev. D* 83 (2011), p. 055009. DOI: [10.1103/PhysRevD.83.055009](https://doi.org/10.1103/PhysRevD.83.055009). arXiv: [1010.4485](https://arxiv.org/abs/1010.4485) [[hep-ph](#)].
- [231] Arun Thalappilil and Scott Thomas. “Higgs Boson Yukawa Form Factors from Supersymmetric Radiative Fermion Masses”. In: (Nov. 2014). arXiv: [1411.7362](https://arxiv.org/abs/1411.7362) [[hep-ph](#)].
- [232] Lorenzo Calibbi, M. L. López-Ibáñez, Aurora Melis, and Oscar Vives. “Muon and electron  $g - 2$  and lepton masses in flavor models”. In: *JHEP* 06 (2020), p. 087. DOI: [10.1007/JHEP06\(2020\)087](https://doi.org/10.1007/JHEP06(2020)087). arXiv: [2003.06633](https://arxiv.org/abs/2003.06633) [[hep-ph](#)].
- [233] Rodolfo Capdevilla, David Curtin, Yonatan Kahn, and Gordan Krnjaic. “Discovering the physics of  $(g - 2)_\mu$  at future muon colliders”. In: *Phys. Rev. D* 103.7 (2021), p. 075028. DOI: [10.1103/PhysRevD.103.075028](https://doi.org/10.1103/PhysRevD.103.075028). arXiv: [2006.16277](https://arxiv.org/abs/2006.16277) [[hep-ph](#)].
- [234] Paride Paradisi, Olcyr Sumensari, and Alessandro Valenti. “High-energy frontier of the muon  $g-2$  at a muon collider”. In: *Phys. Rev. D* 106.11 (2022), p. 115038. DOI: [10.1103/PhysRevD.106.115038](https://doi.org/10.1103/PhysRevD.106.115038). arXiv: [2203.06103](https://arxiv.org/abs/2203.06103) [[hep-ph](#)].
- [235] Andreas Crivellin, Martin Hoferichter, and Philipp Schmidt-Wellenburg. “Combined explanations of  $(g - 2)_{\mu,e}$  and implications for a large muon EDM”. In: *Phys. Rev. D* 98.11 (2018), p. 113002. DOI: [10.1103/PhysRevD.98.113002](https://doi.org/10.1103/PhysRevD.98.113002). arXiv: [1807.11484](https://arxiv.org/abs/1807.11484) [[hep-ph](#)].
- [236] Michael J. Booth. “The Electric dipole moment of the W and electron in the Standard Model”. In: (Jan. 1993). arXiv: [hep-ph/9301293](https://arxiv.org/abs/hep-ph/9301293).
- [237] Maxim Pospelov and Adam Ritz. “Electric dipole moments as probes of new physics”. In: *Annals Phys.* 318 (2005), pp. 119–169. DOI: [10.1016/j.aop.2005.04.002](https://doi.org/10.1016/j.aop.2005.04.002). arXiv: [hep-ph/0504231](https://arxiv.org/abs/hep-ph/0504231).
- [238] Yasuhiro Yamaguchi and Nodoka Yamanaka. “Large long-distance contributions to the electric dipole moments of charged leptons in the standard model”. In: *Phys. Rev. Lett.* 125 (2020), p. 241802. DOI: [10.1103/PhysRevLett.125.241802](https://doi.org/10.1103/PhysRevLett.125.241802). arXiv: [2003.08195](https://arxiv.org/abs/2003.08195) [[hep-ph](#)].
- [239] Yasuhiro Yamaguchi and Nodoka Yamanaka. “Quark level and hadronic contributions to the electric dipole moment of charged leptons in the standard model”. In: *Phys. Rev. D* 103.1 (2021), p. 013001. DOI: [10.1103/PhysRevD.103.013001](https://doi.org/10.1103/PhysRevD.103.013001). arXiv: [2006.00281](https://arxiv.org/abs/2006.00281) [[hep-ph](#)].

- [240] S. T. Petcov. “The Processes  $\mu \rightarrow e + \gamma, \mu \rightarrow e + \bar{e}, \nu' \rightarrow \nu + \gamma$  in the Weinberg-Salam Model with Neutrino Mixing”. In: *Sov. J. Nucl. Phys.* 25 (1977). [Erratum: *Sov.J.Nucl.Phys.* 25, 698 (1977), Erratum: *Yad.Fiz.* 25, 1336 (1977)], p. 340.
- [241] W. J. Marciano and A. I. Sanda. “Exotic Decays of the Muon and Heavy Leptons in Gauge Theories”. In: *Phys. Lett. B* 67 (1977), pp. 303–305. DOI: [10.1016/0370-2693\(77\)90377-X](https://doi.org/10.1016/0370-2693(77)90377-X).
- [242] Benjamin W. Lee and Robert E. Shrock. “Natural Suppression of Symmetry Violation in Gauge Theories: Muon - Lepton and Electron Lepton Number Nonconservation”. In: *Phys. Rev. D* 16 (1977), p. 1444. DOI: [10.1103/PhysRevD.16.1444](https://doi.org/10.1103/PhysRevD.16.1444).
- [243] Tanya S. Roussy et al. “An improved bound on the electron’s electric dipole moment”. In: *Science* 381.6653 (2023), adg4084. DOI: [10.1126/science.adg4084](https://doi.org/10.1126/science.adg4084). arXiv: [2212.11841](https://arxiv.org/abs/2212.11841) [[physics.atom-ph](#)].
- [244] G. W. Bennett et al. “An Improved Limit on the Muon Electric Dipole Moment”. In: *Phys. Rev. D* 80 (2009), p. 052008. DOI: [10.1103/PhysRevD.80.052008](https://doi.org/10.1103/PhysRevD.80.052008). arXiv: [0811.1207](https://arxiv.org/abs/0811.1207) [[hep-ex](#)].
- [245] K. Afanaciev et al. “A search for  $\mu^+ \rightarrow e^+\gamma$  with the first dataset of the MEG II experiment”. In: *Eur. Phys. J. C* 84.3 (2024). [Erratum: *Eur.Phys.J.C* 84, 1042 (2024)], p. 216. DOI: [10.1140/epjc/s10052-024-12416-2](https://doi.org/10.1140/epjc/s10052-024-12416-2). arXiv: [2310.12614](https://arxiv.org/abs/2310.12614) [[hep-ex](#)].
- [246] Bernard Aubert et al. “Searches for Lepton Flavor Violation in the Decays  $\tau_{+-} \rightarrow e_{+-} \gamma$  and  $\tau_{+-} \rightarrow \mu_{+-} \gamma$ ”. In: *Phys. Rev. Lett.* 104 (2010), p. 021802. DOI: [10.1103/PhysRevLett.104.021802](https://doi.org/10.1103/PhysRevLett.104.021802). arXiv: [0908.2381](https://arxiv.org/abs/0908.2381) [[hep-ex](#)].
- [247] A. Abdesselam et al. “Search for lepton-flavor-violating tau-lepton decays to  $\ell\gamma$  at Belle”. In: *JHEP* 10 (2021), p. 19. DOI: [10.1007/JHEP10\(2021\)019](https://doi.org/10.1007/JHEP10(2021)019). arXiv: [2103.12994](https://arxiv.org/abs/2103.12994) [[hep-ex](#)].
- [248] B. Lee Roberts and William J. Marciano, eds. *Lepton dipole moments*. Vol. 20. 2009. ISBN: 978-981-4271-83-7, 978-981-4468-08-4. DOI: [10.1142/7273](https://doi.org/10.1142/7273).
- [249] Oscar Vives and Nicola Valori. “Beyond the Standard Model contributions to dipole moments”. In: (May 2025). arXiv: [2505.06345](https://arxiv.org/abs/2505.06345) [[hep-ph](#)].
- [250] Andreas Crivellin, Saereh Najjari, and Janusz Rosiek. “Lepton Flavor Violation in the Standard Model with general Dimension-Six Operators”. In: *JHEP* 04 (2014), p. 167. DOI: [10.1007/JHEP04\(2014\)167](https://doi.org/10.1007/JHEP04(2014)167). arXiv: [1312.0634](https://arxiv.org/abs/1312.0634) [[hep-ph](#)].
- [251] Giovanni Marco Pruna and Adrian Signer. “The  $\mu \rightarrow e\gamma$  decay in a systematic effective field theory approach with dimension 6 operators”. In: *JHEP* 10 (2014), p. 014. DOI: [10.1007/JHEP10\(2014\)014](https://doi.org/10.1007/JHEP10(2014)014). arXiv: [1408.3565](https://arxiv.org/abs/1408.3565) [[hep-ph](#)].
- [252] G. F. Giudice, P. Paradisi, and M. Passera. “Testing new physics with the electron g-2”. In: *JHEP* 11 (2012), p. 113. DOI: [10.1007/JHEP11\(2012\)113](https://doi.org/10.1007/JHEP11(2012)113). arXiv: [1208.6583](https://arxiv.org/abs/1208.6583) [[hep-ph](#)].
- [253] Lorenzo Calibbi, M. L. López-Ibáñez, Aurora Melis, and Oscar Vives. “Implications of the Muon g-2 result on the flavour structure of the lepton mass matrix”. In: *Eur. Phys. J. C* 81.10 (2021), p. 929. DOI: [10.1140/epjc/s10052-021-09741-1](https://doi.org/10.1140/epjc/s10052-021-09741-1). arXiv: [2104.03296](https://arxiv.org/abs/2104.03296) [[hep-ph](#)].

- [254] M. L. López-Ibáñez, Aurora Melis, M. Jay Pérez, Moinul Hossain Rahat, and Oscar Vives. “Constraining low-scale flavor models with  $(g-2)_\mu$  and lepton flavor violation”. In: *Phys. Rev. D* 105.3 (2022), p. 035021. DOI: [10.1103/PhysRevD.105.035021](https://doi.org/10.1103/PhysRevD.105.035021). arXiv: [2112.11455](https://arxiv.org/abs/2112.11455) [hep-ph].
- [255] Gino Isidori, Julie Pagès, and Felix Wilsch. “Flavour alignment of New Physics in light of the  $(g - 2)_\mu$  anomaly”. In: *JHEP* 03 (2022), p. 011. DOI: [10.1007/JHEP03\(2022\)011](https://doi.org/10.1007/JHEP03(2022)011). arXiv: [2111.13724](https://arxiv.org/abs/2111.13724) [hep-ph].
- [256] Vincenzo Cirigliano, Benjamin Grinstein, Gino Isidori, and Mark B. Wise. “Minimal flavor violation in the lepton sector”. In: *Nucl. Phys. B* 728 (2005), pp. 121–134. DOI: [10.1016/j.nuclphysb.2005.08.037](https://doi.org/10.1016/j.nuclphysb.2005.08.037). arXiv: [hep-ph/0507001](https://arxiv.org/abs/hep-ph/0507001).
- [257] A. M. Baldini et al. “The design of the MEG II experiment”. In: *Eur. Phys. J. C* 78.5 (2018), p. 380. DOI: [10.1140/epjc/s10052-018-5845-6](https://doi.org/10.1140/epjc/s10052-018-5845-6). arXiv: [1801.04688](https://arxiv.org/abs/1801.04688) [physics.ins-det].
- [258] K. Arndt et al. “Technical design of the phase I Mu3e experiment”. In: *Nucl. Instrum. Meth. A* 1014 (2021), p. 165679. DOI: [10.1016/j.nima.2021.165679](https://doi.org/10.1016/j.nima.2021.165679). arXiv: [2009.11690](https://arxiv.org/abs/2009.11690) [physics.ins-det].
- [259] R. Abramishvili et al. “COMET Phase-I Technical Design Report”. In: *PTEP* 2020.3 (2020), p. 033C01. DOI: [10.1093/ptep/ptz125](https://doi.org/10.1093/ptep/ptz125). arXiv: [1812.09018](https://arxiv.org/abs/1812.09018) [physics.ins-det].
- [260] L. Bartoszek et al. “Mu2e Technical Design Report”. In: (Oct. 2014). DOI: [10.2172/1172555](https://doi.org/10.2172/1172555). arXiv: [1501.05241](https://arxiv.org/abs/1501.05241) [physics.ins-det].
- [261] W. Altmannshofer et al. “The Belle II Physics Book”. In: *PTEP* 2019.12 (2019). Ed. by E. Kou and P. Urquijo. [Erratum: *PTEP* 2020, 029201 (2020)], p. 123C01. DOI: [10.1093/ptep/ptz106](https://doi.org/10.1093/ptep/ptz106). arXiv: [1808.10567](https://arxiv.org/abs/1808.10567) [hep-ex].
- [262] Marco Ardu, Sacha Davidson, and Stéphane Lavignac. “Distinguishing models with  $\mu \rightarrow e$  observables”. In: *JHEP* 11 (2023), p. 101. DOI: [10.1007/JHEP11\(2023\)101](https://doi.org/10.1007/JHEP11(2023)101). arXiv: [2308.16897](https://arxiv.org/abs/2308.16897) [hep-ph].
- [263] Marco Ardu, Sacha Davidson, and Stéphane Lavignac. “Constraining new physics models from  $\mu \rightarrow e$  observables in bottom-up EFT”. In: *Eur. Phys. J. C* 84.5 (2024), p. 458. DOI: [10.1140/epjc/s10052-024-12782-x](https://doi.org/10.1140/epjc/s10052-024-12782-x). arXiv: [2401.06214](https://arxiv.org/abs/2401.06214) [hep-ph].
- [264] Yoshitaka Kuno and Yasuhiro Okada. “Muon decay and physics beyond the standard model”. In: *Rev. Mod. Phys.* 73 (2001), pp. 151–202. DOI: [10.1103/RevModPhys.73.151](https://doi.org/10.1103/RevModPhys.73.151). arXiv: [hep-ph/9909265](https://arxiv.org/abs/hep-ph/9909265).
- [265] Ryuichiro Kitano, Masafumi Koike, and Yasuhiro Okada. “Detailed calculation of lepton flavor violating muon electron conversion rate for various nuclei”. In: *Phys. Rev. D* 66 (2002). [Erratum: *Phys.Rev.D* 76, 059902 (2007)], p. 096002. DOI: [10.1103/PhysRevD.76.059902](https://doi.org/10.1103/PhysRevD.76.059902). arXiv: [hep-ph/0203110](https://arxiv.org/abs/hep-ph/0203110).
- [266] Andreas Crivellin, Sacha Davidson, Giovanni Marco Pruna, and Adrian Signer. “Renormalisation-group improved analysis of  $\mu \rightarrow e$  processes in a systematic effective-field-theory approach”. In: *JHEP* 05 (2017), p. 117. DOI: [10.1007/JHEP05\(2017\)117](https://doi.org/10.1007/JHEP05(2017)117). arXiv: [1702.03020](https://arxiv.org/abs/1702.03020) [hep-ph].
- [267] U. Bellgardt et al. “Search for the Decay  $\mu^+ \rightarrow e^+e^+e^-$ ”. In: *Nucl. Phys. B* 299 (1988), pp. 1–6. DOI: [10.1016/0550-3213\(88\)90462-2](https://doi.org/10.1016/0550-3213(88)90462-2).
- [268] Wilhelm H. Bertl et al. “A Search for muon to electron conversion in muonic gold”. In: *Eur. Phys. J. C* 47 (2006), pp. 337–346. DOI: [10.1140/epjc/s2006-02582-x](https://doi.org/10.1140/epjc/s2006-02582-x).

- [269] Kristjan Kannike, Martti Raidal, David M. Straub, and Alessandro Strumia. “Anthropic solution to the magnetic muon anomaly: the charged see-saw”. In: *JHEP* 02 (2012). [Erratum: *JHEP* 10, 136 (2012)], p. 106. DOI: [10.1007/JHEP02\(2012\)106](https://doi.org/10.1007/JHEP02(2012)106). arXiv: [1111.2551](https://arxiv.org/abs/1111.2551) [[hep-ph](#)].
- [270] Radovan Dermisek and Aditi Raval. “Explanation of the Muon  $g-2$  Anomaly with Vectorlike Leptons and its Implications for Higgs Decays”. In: *Phys. Rev. D* 88 (2013), p. 013017. DOI: [10.1103/PhysRevD.88.013017](https://doi.org/10.1103/PhysRevD.88.013017). arXiv: [1305.3522](https://arxiv.org/abs/1305.3522) [[hep-ph](#)].
- [271] Andreas Crivellin, Dario Mueller, and Francesco Saturnino. “Correlating  $h \rightarrow \mu + \mu^-$  to the Anomalous Magnetic Moment of the Muon via Leptoquarks”. In: *Phys. Rev. Lett.* 127.2 (2021), p. 021801. DOI: [10.1103/PhysRevLett.127.021801](https://doi.org/10.1103/PhysRevLett.127.021801). arXiv: [2008.02643](https://arxiv.org/abs/2008.02643) [[hep-ph](#)].
- [272] Andreas Crivellin, Christoph Greub, Dario Müller, and Francesco Saturnino. “Scalar Leptoquarks in Leptonic Processes”. In: *JHEP* 02 (2021), p. 182. DOI: [10.1007/JHEP02\(2021\)182](https://doi.org/10.1007/JHEP02(2021)182). arXiv: [2010.06593](https://arxiv.org/abs/2010.06593) [[hep-ph](#)].
- [273] Svjetlana Fajfer, Jernej F. Kamenik, and Michele Tammaro. “Interplay of New Physics effects in  $(g - 2)_\ell$  and  $h \rightarrow \ell^+ \ell^-$  — lessons from SMEFT”. In: *JHEP* 06 (2021), p. 099. DOI: [10.1007/JHEP06\(2021\)099](https://doi.org/10.1007/JHEP06(2021)099). arXiv: [2103.10859](https://arxiv.org/abs/2103.10859) [[hep-ph](#)].
- [274] Radovan Dermisek, Keith Hermanek, Navin McGinnis, and Sangsik Yoon. “Ellipse of Muon Dipole Moments”. In: *Phys. Rev. Lett.* 129.22 (2022), p. 221801. DOI: [10.1103/PhysRevLett.129.221801](https://doi.org/10.1103/PhysRevLett.129.221801). arXiv: [2205.14243](https://arxiv.org/abs/2205.14243) [[hep-ph](#)].
- [275] Radovan Dermisek, Keith Hermanek, Navin McGinnis, and Sangsik Yoon. “Effective field theory of chirally enhanced muon mass and dipole operators”. In: *Phys. Rev. D* 107.9 (2023), p. 095043. DOI: [10.1103/PhysRevD.107.095043](https://doi.org/10.1103/PhysRevD.107.095043). arXiv: [2302.14144](https://arxiv.org/abs/2302.14144) [[hep-ph](#)].
- [276] Georges Aad et al. “A search for the dimuon decay of the Standard Model Higgs boson with the ATLAS detector”. In: *Phys. Lett. B* 812 (2021), p. 135980. DOI: [10.1016/j.physletb.2020.135980](https://doi.org/10.1016/j.physletb.2020.135980). arXiv: [2007.07830](https://arxiv.org/abs/2007.07830) [[hep-ex](#)].
- [277] Armen Tumasyan et al. “A portrait of the Higgs boson by the CMS experiment ten years after the discovery.” In: *Nature* 607.7917 (2022). [Erratum: *Nature* 623, (2023)], pp. 60–68. DOI: [10.1038/s41586-022-04892-x](https://doi.org/10.1038/s41586-022-04892-x). arXiv: [2207.00043](https://arxiv.org/abs/2207.00043) [[hep-ex](#)].
- [278] Kim Siang Khaw, Cheng Chen, Massimo Giovannozzi, Tianqi Hu, Meng Lv, Jun Kai Ng, Angela Papa, Philipp Schmidt-Wellenburg, Bastiano Vitali, and Guan Ming Wong. “Status of the muEDM Experiment at PSI †”. In: *Phys. Sci. Forum* 8.1 (2023), p. 50. DOI: [10.3390/psf2023008050](https://doi.org/10.3390/psf2023008050). arXiv: [2307.01535](https://arxiv.org/abs/2307.01535) [[hep-ex](#)].
- [279] M. Benedikt et al. “Future Circular Hadron Collider FCC-hh: Overview and Status”. In: (Mar. 2022). arXiv: [2203.07804](https://arxiv.org/abs/2203.07804) [[physics.acc-ph](#)].
- [280] P. Sikivie, Leonard Susskind, Mikhail B. Voloshin, and Valentin I. Zakharov. “Isospin Breaking in Technicolor Models”. In: *Nucl. Phys. B* 173 (1980), pp. 189–207. DOI: [10.1016/0550-3213\(80\)90214-X](https://doi.org/10.1016/0550-3213(80)90214-X).
- [281] S. Schael et al. “Precision electroweak measurements on the  $Z$  resonance”. In: *Phys. Rept.* 427 (2006), pp. 257–454. DOI: [10.1016/j.physrep.2005.12.006](https://doi.org/10.1016/j.physrep.2005.12.006). arXiv: [hep-ex/0509008](https://arxiv.org/abs/hep-ex/0509008).
- [282] M. J. G. Veltman. “Limit on Mass Differences in the Weinberg Model”. In: *Nucl. Phys. B* 123 (1977), pp. 89–99. DOI: [10.1016/0550-3213\(77\)90342-X](https://doi.org/10.1016/0550-3213(77)90342-X).

- [283] Michael E. Peskin and Tatsu Takeuchi. “Estimation of oblique electroweak corrections”. In: *Phys. Rev. D* 46 (1992), pp. 381–409. DOI: [10.1103/PhysRevD.46.381](https://doi.org/10.1103/PhysRevD.46.381).
- [284] Loyal Durand. “Pionic Contributions to the Magnetic Moment of the Muon”. In: *Phys. Rev.* 128 (1962), pp. 441–448. DOI: [10.1103/PhysRev.128.441](https://doi.org/10.1103/PhysRev.128.441).
- [285] M. Gourdin and E. De Rafael. “Hadronic contributions to the muon g-factor”. In: *Nucl. Phys. B* 10 (1969), pp. 667–674. DOI: [10.1016/0550-3213\(69\)90333-2](https://doi.org/10.1016/0550-3213(69)90333-2).
- [286] M. Passera, W. J. Marciano, and A. Sirlin. “The Muon g-2 and the bounds on the Higgs boson mass”. In: *Phys. Rev. D* 78 (2008), p. 013009. DOI: [10.1103/PhysRevD.78.013009](https://doi.org/10.1103/PhysRevD.78.013009). arXiv: [0804.1142](https://arxiv.org/abs/0804.1142) [[hep-ph](#)].
- [287] Andreas Crivellin, Martin Hoferichter, Claudio Andrea Manzari, and Marc Montull. “Hadronic Vacuum Polarization:  $(g - 2)_\mu$  versus Global Electroweak Fits”. In: *Phys. Rev. Lett.* 125.9 (2020), p. 091801. DOI: [10.1103/PhysRevLett.125.091801](https://doi.org/10.1103/PhysRevLett.125.091801). arXiv: [2003.04886](https://arxiv.org/abs/2003.04886) [[hep-ph](#)].
- [288] Alexander Keshavarzi, William J. Marciano, Massimo Passera, and Alberto Sirlin. “Muon  $g - 2$  and  $\Delta\alpha$  connection”. In: *Phys. Rev. D* 102.3 (2020), p. 033002. DOI: [10.1103/PhysRevD.102.033002](https://doi.org/10.1103/PhysRevD.102.033002). arXiv: [2006.12666](https://arxiv.org/abs/2006.12666) [[hep-ph](#)].
- [289] Bogdan Malaescu and Matthias Schott. “Impact of correlations between  $a_\mu$  and  $\alpha_{\text{QED}}$  on the EW fit”. In: *Eur. Phys. J. C* 81.1 (2021), p. 46. DOI: [10.1140/epjc/s10052-021-08848-9](https://doi.org/10.1140/epjc/s10052-021-08848-9). arXiv: [2008.08107](https://arxiv.org/abs/2008.08107) [[hep-ph](#)].
- [290] Peter Athron, Andrew Fowlie, Chih-Ting Lu, Lei Wu, Yongcheng Wu, and Bin Zhu. “Hadronic uncertainties versus new physics for the W boson mass and Muon  $g - 2$  anomalies”. In: *Nature Commun.* 14 (2023), p. 659. DOI: [10.1038/s41467-023-36366-7](https://doi.org/10.1038/s41467-023-36366-7). arXiv: [2204.03996](https://arxiv.org/abs/2204.03996) [[hep-ph](#)].
- [291] Eduardo de Rafael. “Constraints between  $\Delta\alpha_{\text{had}}(M_Z^2)$  and  $(g_\mu - 2)_{\text{HVP}}$ ”. In: *Phys. Rev. D* 102.5 (2020), p. 056025. DOI: [10.1103/PhysRevD.102.056025](https://doi.org/10.1103/PhysRevD.102.056025). arXiv: [2006.13880](https://arxiv.org/abs/2006.13880) [[hep-ph](#)].
- [292] Gilberto Colangelo, Martin Hoferichter, and Peter Stoffer. “Constraints on the two-pion contribution to hadronic vacuum polarization”. In: *Phys. Lett. B* 814 (2021), p. 136073. DOI: [10.1016/j.physletb.2021.136073](https://doi.org/10.1016/j.physletb.2021.136073). arXiv: [2010.07943](https://arxiv.org/abs/2010.07943) [[hep-ph](#)].
- [293] Francisco Campanario, Henryk Czyż, Janusz Gluza, Tomasz Jeliński, Germán Rodrigo, Szymon Tracz, and Dmitry Zhuridov. “Standard model radiative corrections in the pion form factor measurements do not explain the  $a_\mu$  anomaly”. In: *Phys. Rev. D* 100.7 (2019), p. 076004. DOI: [10.1103/PhysRevD.100.076004](https://doi.org/10.1103/PhysRevD.100.076004). arXiv: [1903.10197](https://arxiv.org/abs/1903.10197) [[hep-ph](#)].
- [294] J. P. Lees et al. “Measurement of additional radiation in the initial-state-radiation processes  $e+e\rightarrow\mu+\mu-\gamma$  and  $e+e\rightarrow\pi+\pi-\gamma$  at BABAR”. In: *Phys. Rev. D* 108.11 (2023), p. L111103. DOI: [10.1103/PhysRevD.108.L111103](https://doi.org/10.1103/PhysRevD.108.L111103). arXiv: [2308.05233](https://arxiv.org/abs/2308.05233) [[hep-ex](#)].
- [295] Georges Aad et al. “Measurement of the W-boson mass and width with the ATLAS detector using proton–proton collisions at  $\sqrt{s} = 7$  TeV”. In: *Eur. Phys. J. C* 84.12 (2024), p. 1309. DOI: [10.1140/epjc/s10052-024-13190-x](https://doi.org/10.1140/epjc/s10052-024-13190-x). arXiv: [2403.15085](https://arxiv.org/abs/2403.15085) [[hep-ex](#)].
- [296] Vladimir Chekhovsky et al. “High-precision measurement of the W boson mass with the CMS experiment at the LHC”. In: (Dec. 2024). arXiv: [2412.13872](https://arxiv.org/abs/2412.13872) [[hep-ex](#)].

- [297] T. Aaltonen et al. “High-precision measurement of the  $W$  boson mass with the CDF II detector”. In: *Science* 376.6589 (2022), pp. 170–176. DOI: [10.1126/science.abk1781](https://doi.org/10.1126/science.abk1781).
- [298] Simone Amoroso et al. “Compatibility and combination of world  $W$ -boson mass measurements”. In: *Eur. Phys. J. C* 84.5 (2024), p. 451. DOI: [10.1140/epjc/s10052-024-12532-z](https://doi.org/10.1140/epjc/s10052-024-12532-z). arXiv: [2308.09417 \[hep-ex\]](https://arxiv.org/abs/2308.09417).
- [299] F. Ambrosino et al. “Measurement of  $\sigma(e^+e^- \rightarrow \pi^+\pi^-)$  from threshold to  $0.85 \text{ GeV}^2$  using Initial State Radiation with the KLOE detector”. In: *Phys. Lett. B* 700 (2011), pp. 102–110. DOI: [10.1016/j.physletb.2011.04.055](https://doi.org/10.1016/j.physletb.2011.04.055). arXiv: [1006.5313 \[hep-ex\]](https://arxiv.org/abs/1006.5313).
- [300] D. Babusci et al. “Precision measurement of  $\sigma(e^+e^- \rightarrow \pi^+\pi^-\gamma)/\sigma(e^+e^- \rightarrow \mu^+\mu^-\gamma)$  and determination of the  $\pi^+\pi^-$  contribution to the muon anomaly with the KLOE detector”. In: *Phys. Lett. B* 720 (2013), pp. 336–343. DOI: [10.1016/j.physletb.2013.02.029](https://doi.org/10.1016/j.physletb.2013.02.029). arXiv: [1212.4524 \[hep-ex\]](https://arxiv.org/abs/1212.4524).
- [301] Jens Erler and Rodolfo Ferro-Hernandez. “Perturbative contributions to  $\Delta\alpha^{(5)}(M_Z^2)$ ”. In: *JHEP* 12 (2023), p. 131. DOI: [10.1007/JHEP12\(2023\)131](https://doi.org/10.1007/JHEP12(2023)131). arXiv: [2308.05740 \[hep-ph\]](https://arxiv.org/abs/2308.05740).
- [302] Johannes Haller, Andreas Hoecker, Roman Kogler, Klaus Mönig, Thomas Peiffer, and Jörg Stelzer. “Update of the global electroweak fit and constraints on two-Higgs-doublet models”. In: *Eur. Phys. J. C* 78.8 (2018), p. 675. DOI: [10.1140/epjc/s10052-018-6131-3](https://doi.org/10.1140/epjc/s10052-018-6131-3). arXiv: [1803.01853 \[hep-ph\]](https://arxiv.org/abs/1803.01853).
- [303] Y. Fukuda et al. “Measurements of the solar neutrino flux from Super-Kamiokande’s first 300 days”. In: *Phys. Rev. Lett.* 81 (1998). [Erratum: *Phys.Rev.Lett.* 81, 4279 (1998)], pp. 1158–1162. DOI: [10.1103/PhysRevLett.81.1158](https://doi.org/10.1103/PhysRevLett.81.1158). arXiv: [hep-ex/9805021](https://arxiv.org/abs/hep-ex/9805021).
- [304] Q. R. Ahmad et al. “Measurement of the rate of  $\nu_e + d \rightarrow p + p + e^-$  interactions produced by  $^8\text{B}$  solar neutrinos at the Sudbury Neutrino Observatory”. In: *Phys. Rev. Lett.* 87 (2001), p. 071301. DOI: [10.1103/PhysRevLett.87.071301](https://doi.org/10.1103/PhysRevLett.87.071301). arXiv: [nucl-ex/0106015](https://arxiv.org/abs/nucl-ex/0106015).
- [305] Ivan Esteban, M. C. Gonzalez-Garcia, Michele Maltoni, Ivan Martinez-Soler, João Paulo Pinheiro, and Thomas Schwetz. “NuFit-6.0: updated global analysis of three-flavor neutrino oscillations”. In: *JHEP* 12 (2024), p. 216. DOI: [10.1007/JHEP12\(2024\)216](https://doi.org/10.1007/JHEP12(2024)216). arXiv: [2410.05380 \[hep-ph\]](https://arxiv.org/abs/2410.05380).
- [306] Samuel Brieden, Héctor Gil-Marín, and Licia Verde. “Model-agnostic interpretation of 10 billion years of cosmic evolution traced by BOSS and eBOSS data”. In: *JCAP* 08.08 (2022), p. 024. DOI: [10.1088/1475-7516/2022/08/024](https://doi.org/10.1088/1475-7516/2022/08/024). arXiv: [2204.11868 \[astro-ph.CO\]](https://arxiv.org/abs/2204.11868).
- [307] M. Aker et al. “Direct neutrino-mass measurement with sub-electronvolt sensitivity”. In: *Nature Phys.* 18.2 (2022), pp. 160–166. DOI: [10.1038/s41567-021-01463-1](https://doi.org/10.1038/s41567-021-01463-1). arXiv: [2105.08533 \[hep-ex\]](https://arxiv.org/abs/2105.08533).
- [308] Kazuo Fujikawa and Robert Shrock. “The Magnetic Moment of a Massive Neutrino and Neutrino Spin Rotation”. In: *Phys. Rev. Lett.* 45 (1980), p. 963. DOI: [10.1103/PhysRevLett.45.963](https://doi.org/10.1103/PhysRevLett.45.963).
- [309] S. Abe et al. “Search for the Majorana Nature of Neutrinos in the Inverted Mass Ordering Region with KamLAND-Zen”. In: *Phys. Rev. Lett.* 130.5 (2023), p. 051801. DOI: [10.1103/PhysRevLett.130.051801](https://doi.org/10.1103/PhysRevLett.130.051801). arXiv: [2203.02139 \[hep-ex\]](https://arxiv.org/abs/2203.02139).
- [310] M. Agostini et al. “Final Results of GERDA on the Search for Neutrinoless Double- $\beta$  Decay”. In: *Phys. Rev. Lett.* 125.25 (2020), p. 252502. DOI: [10.1103/PhysRevLett.125.252502](https://doi.org/10.1103/PhysRevLett.125.252502). arXiv: [2009.06079 \[nucl-ex\]](https://arxiv.org/abs/2009.06079).

- [311] Peter Minkowski. “ $\mu \rightarrow e\gamma$  at a Rate of One Out of  $10^9$  Muon Decays?” In: *Phys. Lett. B* 67 (1977), pp. 421–428. DOI: [10.1016/0370-2693\(77\)90435-X](https://doi.org/10.1016/0370-2693(77)90435-X).
- [312] Murray Gell-Mann, Pierre Ramond, and Richard Slansky. “Complex Spinors and Unified Theories”. In: *Conf. Proc. C* 790927 (1979), pp. 315–321. arXiv: [1306.4669 \[hep-th\]](https://arxiv.org/abs/1306.4669).
- [313] Tsutomu Yanagida. “Horizontal gauge symmetry and masses of neutrinos”. In: *Conf. Proc. C* 7902131 (1979). Ed. by Osamu Sawada and Akio Sugamoto, pp. 95–99.
- [314] J. Schechter and J. W. F. Valle. “Neutrino Masses in  $SU(2) \times U(1)$  Theories”. In: *Phys. Rev. D* 22 (1980), p. 2227. DOI: [10.1103/PhysRevD.22.2227](https://doi.org/10.1103/PhysRevD.22.2227).
- [315] Steven Weinberg. “Baryon and Lepton Nonconserving Processes”. In: *Phys. Rev. Lett.* 43 (1979), pp. 1566–1570. DOI: [10.1103/PhysRevLett.43.1566](https://doi.org/10.1103/PhysRevLett.43.1566).
- [316] Robert Foot, H. Lew, X. G. He, and Girish C. Joshi. “Seesaw Neutrino Masses Induced by a Triplet of Leptons”. In: *Z. Phys. C* 44 (1989), p. 441. DOI: [10.1007/BF01415558](https://doi.org/10.1007/BF01415558).
- [317] Rabindra N. Mohapatra and Goran Senjanovic. “Neutrino Masses and Mixings in Gauge Models with Spontaneous Parity Violation”. In: *Phys. Rev. D* 23 (1981), p. 165. DOI: [10.1103/PhysRevD.23.165](https://doi.org/10.1103/PhysRevD.23.165).
- [318] Apostolos Pilaftsis. “Radiatively induced neutrino masses and large Higgs neutrino couplings in the standard model with Majorana fields”. In: *Z. Phys. C* 55 (1992), pp. 275–282. DOI: [10.1007/BF01482590](https://doi.org/10.1007/BF01482590). arXiv: [hep-ph/9901206](https://arxiv.org/abs/hep-ph/9901206).
- [319] K. S. Babu and Ernest Ma. “Natural Hierarchy of Radiatively Induced Majorana Neutrino Masses”. In: *Phys. Rev. Lett.* 61 (1988), p. 674. DOI: [10.1103/PhysRevLett.61.674](https://doi.org/10.1103/PhysRevLett.61.674).
- [320] R. N. Mohapatra and J. W. F. Valle. “Neutrino Mass and Baryon Number Nonconservation in Superstring Models”. In: *Phys. Rev. D* 34 (1986), p. 1642. DOI: [10.1103/PhysRevD.34.1642](https://doi.org/10.1103/PhysRevD.34.1642).
- [321] M. C. Gonzalez-Garcia and J. W. F. Valle. “Fast Decaying Neutrinos and Observable Flavor Violation in a New Class of Majoron Models”. In: *Phys. Lett. B* 216 (1989), pp. 360–366. DOI: [10.1016/0370-2693\(89\)91131-3](https://doi.org/10.1016/0370-2693(89)91131-3).
- [322] S. M. Barr. “A Different seesaw formula for neutrino masses”. In: *Phys. Rev. Lett.* 92 (2004), p. 101601. DOI: [10.1103/PhysRevLett.92.101601](https://doi.org/10.1103/PhysRevLett.92.101601). arXiv: [hep-ph/0309152](https://arxiv.org/abs/hep-ph/0309152).
- [323] Michal Malinsky, J. C. Romao, and J. W. F. Valle. “Novel supersymmetric  $SO(10)$  seesaw mechanism”. In: *Phys. Rev. Lett.* 95 (2005), p. 161801. DOI: [10.1103/PhysRevLett.95.161801](https://doi.org/10.1103/PhysRevLett.95.161801). arXiv: [hep-ph/0506296](https://arxiv.org/abs/hep-ph/0506296).
- [324] A. Zee. “A Theory of Lepton Number Violation, Neutrino Majorana Mass, and Oscillation”. In: *Phys. Lett. B* 93 (1980). [Erratum: *Phys.Lett.B* 95, 461 (1980)], p. 389. DOI: [10.1016/0370-2693\(80\)90349-4](https://doi.org/10.1016/0370-2693(80)90349-4).
- [325] K. S. Babu. “Model of ‘Calculable’ Majorana Neutrino Masses”. In: *Phys. Lett. B* 203 (1988), pp. 132–136. DOI: [10.1016/0370-2693\(88\)91584-5](https://doi.org/10.1016/0370-2693(88)91584-5).
- [326] Ernest Ma. “Verifiable radiative seesaw mechanism of neutrino mass and dark matter”. In: *Phys. Rev. D* 73 (2006), p. 077301. DOI: [10.1103/PhysRevD.73.077301](https://doi.org/10.1103/PhysRevD.73.077301). arXiv: [hep-ph/0601225](https://arxiv.org/abs/hep-ph/0601225).
- [327] W. Grimus and H. Neufeld. “Radiative Neutrino Masses in an  $SU(2) \times U(1)$  Model”. In: *Nucl. Phys. B* 325 (1989), pp. 18–32. DOI: [10.1016/0550-3213\(89\)90370-2](https://doi.org/10.1016/0550-3213(89)90370-2).

- [328] K. S. Babu, Sudip Jana, Manfred Lindner, and Vishnu P. K. “Muon  $g - 2$  anomaly and neutrino magnetic moments”. In: *JHEP* 10 (2021), p. 240. DOI: [10.1007/JHEP10\(2021\)240](https://doi.org/10.1007/JHEP10(2021)240). arXiv: [2104.03291](https://arxiv.org/abs/2104.03291) [[hep-ph](#)].
- [329] Ernest Ma and Martti Raidal. “Neutrino mass, muon anomalous magnetic moment, and lepton flavor nonconservation”. In: *Phys. Rev. Lett.* 87 (2001). [Erratum: *Phys.Rev.Lett.* 87, 159901 (2001)], p. 011802. DOI: [10.1103/PhysRevLett.87.011802](https://doi.org/10.1103/PhysRevLett.87.011802). arXiv: [hep-ph/0102255](https://arxiv.org/abs/hep-ph/0102255).
- [330] C. Biggio. “The Contribution of fermionic seesaws to the anomalous magnetic moment of leptons”. In: *Phys. Lett. B* 668 (2008), pp. 378–384. DOI: [10.1016/j.physletb.2008.09.004](https://doi.org/10.1016/j.physletb.2008.09.004). arXiv: [0806.2558](https://arxiv.org/abs/0806.2558) [[hep-ph](#)].
- [331] Vera C. Rubin and W. Kent Ford Jr. “Rotation of the Andromeda Nebula from a Spectroscopic Survey of Emission Regions”. In: *Astrophys. J.* 159 (1970), pp. 379–403. DOI: [10.1086/150317](https://doi.org/10.1086/150317).
- [332] V. C. Rubin, N. Thonnard, and W. K. Ford Jr. “Rotational properties of 21 SC galaxies with a large range of luminosities and radii, from NGC 4605 / $R = 4\text{kpc}$ / to UGC 2885 / $R = 122\text{kpc}$ /”. In: *Astrophys. J.* 238 (1980), p. 471. DOI: [10.1086/158003](https://doi.org/10.1086/158003).
- [333] Douglas Clowe, Marusa Bradac, Anthony H. Gonzalez, Maxim Markevitch, Scott W. Randall, Christine Jones, and Dennis Zaritsky. “A direct empirical proof of the existence of dark matter”. In: *Astrophys. J. Lett.* 648 (2006), pp. L109–L113. DOI: [10.1086/508162](https://doi.org/10.1086/508162). arXiv: [astro-ph/0608407](https://arxiv.org/abs/astro-ph/0608407).
- [334] R. Gavazzi, C. Adami, F. Durret, J. C. Cuillandre, O. Ilbert, A. Mazure, R. Pelló, and M. P. Ulmer. “A weak lensing study of the Coma cluster”. In: *Astronomy and Astrophysics* 498.2 (2009), pp. L33–L36. DOI: [10.1051/0004-6361/200911841](https://doi.org/10.1051/0004-6361/200911841). arXiv: [0904.0220](https://arxiv.org/abs/0904.0220) [[astro-ph.CO](#)].
- [335] N. Aghanim et al. “Planck 2018 results. VI. Cosmological parameters”. In: (July 2018). arXiv: [1807.06209](https://arxiv.org/abs/1807.06209) [[astro-ph.CO](#)].
- [336] Gianfranco Bertone and Dan Hooper. “History of dark matter”. In: *Rev. Mod. Phys.* 90.4 (2018), p. 045002. DOI: [10.1103/RevModPhys.90.045002](https://doi.org/10.1103/RevModPhys.90.045002). arXiv: [1605.04909](https://arxiv.org/abs/1605.04909) [[astro-ph.CO](#)].
- [337] Marco Cirelli, Alessandro Strumia, and Jure Zupan. “Dark Matter”. In: (June 2024). arXiv: [2406.01705](https://arxiv.org/abs/2406.01705) [[hep-ph](#)].
- [338] Csaba Balazs, Torsten Bringmann, Felix Kahlhoefer, and Martin White. “A Primer on Dark Matter”. In: (Nov. 2024). arXiv: [2411.05062](https://arxiv.org/abs/2411.05062) [[astro-ph.CO](#)].
- [339] Haim Goldberg and Lawrence J. Hall. “A New Candidate for Dark Matter”. In: *Phys. Lett. B* 174 (1986). Ed. by J. Tran Thanh Van, p. 151. DOI: [10.1016/0370-2693\(86\)90731-8](https://doi.org/10.1016/0370-2693(86)90731-8).
- [340] Kingman Cheung and Tzu-Chiang Yuan. “Hidden fermion as milli-charged dark matter in Stueckelberg  $Z'$ -prime model”. In: *JHEP* 03 (2007), p. 120. DOI: [10.1088/1126-6708/2007/03/120](https://doi.org/10.1088/1126-6708/2007/03/120). arXiv: [hep-ph/0701107](https://arxiv.org/abs/hep-ph/0701107).
- [341] Ji-Haeng Huh, Jihn E. Kim, Jong-Chul Park, and Seong Chan Park. “Galactic 511 keV line from MeV milli-charged dark matter”. In: *Phys. Rev. D* 77 (2008), p. 123503. DOI: [10.1103/PhysRevD.77.123503](https://doi.org/10.1103/PhysRevD.77.123503). arXiv: [0711.3528](https://arxiv.org/abs/0711.3528) [[astro-ph](#)].
- [342] Samuel D. McDermott, Hai-Bo Yu, and Kathryn M. Zurek. “Turning off the Lights: How Dark is Dark Matter?” In: *Phys. Rev. D* 83 (2011), p. 063509. DOI: [10.1103/PhysRevD.83.063509](https://doi.org/10.1103/PhysRevD.83.063509). arXiv: [1011.2907](https://arxiv.org/abs/1011.2907) [[hep-ph](#)].
- [343] Leszek Roszkowski, Enrico Maria Sessolo, and Sebastian Trojanowski. “WIMP dark matter candidates and searches—current status and future prospects”. In: *Rept. Prog. Phys.* 81.6 (2018), p. 066201. DOI: [10.1088/1361-6633/aab913](https://doi.org/10.1088/1361-6633/aab913). arXiv: [1707.06277](https://arxiv.org/abs/1707.06277) [[hep-ph](#)].

- [344] Jonathan L. Feng. “The WIMP paradigm: Theme and variations”. In: *SciPost Phys. Lect. Notes* 71 (2023), p. 1. DOI: [10.21468/SciPostPhysLectNotes.71](https://doi.org/10.21468/SciPostPhysLectNotes.71). arXiv: [2212.02479](https://arxiv.org/abs/2212.02479) [hep-ph].
- [345] G. Belanger, F. Boudjema, A. Pukhov, and A. Semenov. “MicrOMEGAs: A Program for calculating the relic density in the MSSM”. In: *Comput. Phys. Commun.* 149 (2002), pp. 103–120. DOI: [10.1016/S0010-4655\(02\)00596-9](https://doi.org/10.1016/S0010-4655(02)00596-9). arXiv: [hep-ph/0112278](https://arxiv.org/abs/hep-ph/0112278).
- [346] P. Gondolo, J. Edsjo, P. Ullio, L. Bergstrom, Mia Schelke, and E. A. Baltz. “DarkSUSY: Computing supersymmetric dark matter properties numerically”. In: *JCAP* 07 (2004), p. 008. DOI: [10.1088/1475-7516/2004/07/008](https://doi.org/10.1088/1475-7516/2004/07/008). arXiv: [astro-ph/0406204](https://arxiv.org/abs/astro-ph/0406204).
- [347] A. Arbey, F. Mahmoudi, and G. Robbins. “SuperIso Relic v4: A program for calculating dark matter and flavour physics observables in Supersymmetry”. In: *Comput. Phys. Commun.* 239 (2019), pp. 238–264. DOI: [10.1016/j.cpc.2019.01.014](https://doi.org/10.1016/j.cpc.2019.01.014). arXiv: [1806.11489](https://arxiv.org/abs/1806.11489) [hep-ph].
- [348] Giorgio Arcadi, Maíra Dutra, Pradipta Ghosh, Manfred Lindner, Yann Mambrini, Mathias Pierre, Stefano Profumo, and Farinaldo S. Queiroz. “The waning of the WIMP? A review of models, searches, and constraints”. In: *Eur. Phys. J. C* 78.3 (2018), p. 203. DOI: [10.1140/epjc/s10052-018-5662-y](https://doi.org/10.1140/epjc/s10052-018-5662-y). arXiv: [1703.07364](https://arxiv.org/abs/1703.07364) [hep-ph].
- [349] S. P. Ahlen, F. T. Avignone, R. L. Brodzinski, A. K. Drukier, G. Gelmini, and D. N. Spergel. “Limits on Cold Dark Matter Candidates from an Ultralow Background Germanium Spectrometer”. In: *Phys. Lett. B* 195 (1987). Ed. by M. A. Srednicki, pp. 603–608. DOI: [10.1016/0370-2693\(87\)91581-4](https://doi.org/10.1016/0370-2693(87)91581-4).
- [350] J. Aalbers et al. “Dark Matter Search Results from 4.2 Tonne-Years of Exposure of the LUX-ZEPLIN (LZ) Experiment”. In: (Oct. 2024). arXiv: [2410.17036](https://arxiv.org/abs/2410.17036) [hep-ex].
- [351] D. Baxter et al. “Recommended conventions for reporting results from direct dark matter searches”. In: *Eur. Phys. J. C* 81.10 (2021), p. 907. DOI: [10.1140/epjc/s10052-021-09655-y](https://doi.org/10.1140/epjc/s10052-021-09655-y). arXiv: [2105.00599](https://arxiv.org/abs/2105.00599) [hep-ex].
- [352] Tracy R. Slatyer. “Indirect detection of dark matter.” In: *Theoretical Advanced Study Institute in Elementary Particle Physics: Anticipating the Next Discoveries in Particle Physics*. 2018, pp. 297–353. DOI: [10.1142/9789813233348\\_0005](https://doi.org/10.1142/9789813233348_0005). arXiv: [1710.05137](https://arxiv.org/abs/1710.05137) [hep-ph].
- [353] Marco Cirelli, Gennaro Corcella, Andi Hektor, Gert Hutsi, Mario Kadastik, Paolo Panci, Martti Raidal, Filippo Sala, and Alessandro Strumia. “PPPC 4 DM ID: A Poor Particle Physicist Cookbook for Dark Matter Indirect Detection”. In: *JCAP* 03 (2011). [Erratum: *JCAP* 10, E01 (2012)], p. 051. DOI: [10.1088/1475-7516/2012/10/E01](https://doi.org/10.1088/1475-7516/2012/10/E01). arXiv: [1012.4515](https://arxiv.org/abs/1012.4515) [hep-ph].
- [354] M. Ackermann et al. “Searching for Dark Matter Annihilation from Milky Way Dwarf Spheroidal Galaxies with Six Years of Fermi Large Area Telescope Data”. In: *Phys. Rev. Lett.* 115.23 (2015), p. 231301. DOI: [10.1103/PhysRevLett.115.231301](https://doi.org/10.1103/PhysRevLett.115.231301). arXiv: [1503.02641](https://arxiv.org/abs/1503.02641) [astro-ph.HE].
- [355] M. L. Ahnen et al. “Limits to Dark Matter Annihilation Cross-Section from a Combined Analysis of MAGIC and Fermi-LAT Observations of Dwarf Satellite Galaxies”. In: *JCAP* 02 (2016), p. 039. DOI: [10.1088/1475-7516/2016/02/039](https://doi.org/10.1088/1475-7516/2016/02/039). arXiv: [1601.06590](https://arxiv.org/abs/1601.06590) [astro-ph.HE].
- [356] S. Archambault et al. “Dark Matter Constraints from a Joint Analysis of Dwarf Spheroidal Galaxy Observations with VERITAS”. In: *Phys. Rev. D* 95.8 (2017), p. 082001. DOI: [10.1103/PhysRevD.95.082001](https://doi.org/10.1103/PhysRevD.95.082001). arXiv: [1703.04937](https://arxiv.org/abs/1703.04937) [astro-ph.HE].

- [357] M. G. Aartsen et al. “Search for annihilating dark matter in the Sun with 3 years of IceCube data”. In: *Eur. Phys. J. C* 77.3 (2017). [Erratum: *Eur.Phys.J.C* 79, 214 (2019)], p. 146. DOI: [10.1140/epjc/s10052-017-4689-9](https://doi.org/10.1140/epjc/s10052-017-4689-9). arXiv: [1612.05949](https://arxiv.org/abs/1612.05949) [[astro-ph.HE](#)].
- [358] S. Adrian-Martinez et al. “Limits on Dark Matter Annihilation in the Sun using the ANTARES Neutrino Telescope”. In: *Phys. Lett. B* 759 (2016), pp. 69–74. DOI: [10.1016/j.physletb.2016.05.019](https://doi.org/10.1016/j.physletb.2016.05.019). arXiv: [1603.02228](https://arxiv.org/abs/1603.02228) [[astro-ph.HE](#)].
- [359] M. Aguilar et al. “Antiproton Flux, Antiproton-to-Proton Flux Ratio, and Properties of Elementary Particle Fluxes in Primary Cosmic Rays Measured with the Alpha Magnetic Spectrometer on the International Space Station”. In: *Phys. Rev. Lett.* 117.9 (2016), p. 091103. DOI: [10.1103/PhysRevLett.117.091103](https://doi.org/10.1103/PhysRevLett.117.091103).
- [360] O. Adriani et al. “Cosmic-Ray Positron Energy Spectrum Measured by PAMELA”. In: *Phys. Rev. Lett.* 111 (2013), p. 081102. DOI: [10.1103/PhysRevLett.111.081102](https://doi.org/10.1103/PhysRevLett.111.081102). arXiv: [1308.0133](https://arxiv.org/abs/1308.0133) [[astro-ph.HE](#)].
- [361] Jennifer M. Gaskins. “A review of indirect searches for particle dark matter”. In: *Contemp. Phys.* 57.4 (2016), pp. 496–525. DOI: [10.1080/00107514.2016.1175160](https://doi.org/10.1080/00107514.2016.1175160). arXiv: [1604.00014](https://arxiv.org/abs/1604.00014) [[astro-ph.HE](#)].
- [362] J. Aalbers et al. “First Dark Matter Search Results from the LUX-ZEPLIN (LZ) Experiment”. In: *Phys. Rev. Lett.* 131.4 (2023), p. 041002. DOI: [10.1103/PhysRevLett.131.041002](https://doi.org/10.1103/PhysRevLett.131.041002). arXiv: [2207.03764](https://arxiv.org/abs/2207.03764) [[hep-ex](#)].
- [363] Yue Meng et al. “Dark Matter Search Results from the PandaX-4T Commissioning Run”. In: *Phys. Rev. Lett.* 127.26 (2021), p. 261802. DOI: [10.1103/PhysRevLett.127.261802](https://doi.org/10.1103/PhysRevLett.127.261802). arXiv: [2107.13438](https://arxiv.org/abs/2107.13438) [[hep-ex](#)].
- [364] D. S. Akerib et al. “Results from a search for dark matter in the complete LUX exposure”. In: *Phys. Rev. Lett.* 118.2 (2017), p. 021303. DOI: [10.1103/PhysRevLett.118.021303](https://doi.org/10.1103/PhysRevLett.118.021303). arXiv: [1608.07648](https://arxiv.org/abs/1608.07648) [[astro-ph.CO](#)].
- [365] E. Aprile et al. “First Dark Matter Search with Nuclear Recoils from the XENONnT Experiment”. In: *Phys. Rev. Lett.* 131.4 (2023), p. 041003. DOI: [10.1103/PhysRevLett.131.041003](https://doi.org/10.1103/PhysRevLett.131.041003). arXiv: [2303.14729](https://arxiv.org/abs/2303.14729) [[hep-ex](#)].
- [366] E. Aprile et al. “Dark Matter Search Results from a One Ton-Year Exposure of XENON1T”. In: *Phys. Rev. Lett.* 121.11 (2018), p. 111302. DOI: [10.1103/PhysRevLett.121.111302](https://doi.org/10.1103/PhysRevLett.121.111302). arXiv: [1805.12562](https://arxiv.org/abs/1805.12562) [[astro-ph.CO](#)].
- [367] R. Ajaj et al. “Search for dark matter with a 231-day exposure of liquid argon using DEAP-3600 at SNOLAB”. In: *Phys. Rev. D* 100.2 (2019), p. 022004. DOI: [10.1103/PhysRevD.100.022004](https://doi.org/10.1103/PhysRevD.100.022004). arXiv: [1902.04048](https://arxiv.org/abs/1902.04048) [[astro-ph.CO](#)].
- [368] Lawrence J. Hall, Karsten Jedamzik, John March-Russell, and Stephen M. West. “Freeze-In Production of FIMP Dark Matter”. In: *JHEP* 03 (2010), p. 080. DOI: [10.1007/JHEP03\(2010\)080](https://doi.org/10.1007/JHEP03(2010)080). arXiv: [0911.1120](https://arxiv.org/abs/0911.1120) [[hep-ph](#)].
- [369] Bernard Carr, Kazunori Kohri, Yuuiti Sendouda, and Jun’ichi Yokoyama. “Constraints on primordial black holes”. In: *Rept. Prog. Phys.* 84.11 (2021), p. 116902. DOI: [10.1088/1361-6633/ac1e31](https://doi.org/10.1088/1361-6633/ac1e31). arXiv: [2002.12778](https://arxiv.org/abs/2002.12778) [[astro-ph.CO](#)].
- [370] Bernard Carr and Florian Kuhnel. “Primordial black holes as dark matter candidates”. In: *SciPost Phys. Lect. Notes* 48 (2022), p. 1. DOI: [10.21468/SciPostPhysLectNotes.48](https://doi.org/10.21468/SciPostPhysLectNotes.48). arXiv: [2110.02821](https://arxiv.org/abs/2110.02821) [[astro-ph.CO](#)].
- [371] Vanda Silveira and A. Zee. “SCALAR PHANTOMS”. In: *Phys. Lett. B* 161 (1985), pp. 136–140. DOI: [10.1016/0370-2693\(85\)90624-0](https://doi.org/10.1016/0370-2693(85)90624-0).
- [372] John McDonald. “Gauge singlet scalars as cold dark matter”. In: *Phys. Rev. D* 50 (1994), pp. 3637–3649. DOI: [10.1103/PhysRevD.50.3637](https://doi.org/10.1103/PhysRevD.50.3637). arXiv: [hep-ph/0702143](https://arxiv.org/abs/hep-ph/0702143).

- [373] Laura Lopez Honorez, Emmanuel Nezri, Josep F. Oliver, and Michel H. G. Tytgat. “The Inert Doublet Model: An Archetype for Dark Matter”. In: *JCAP* 02 (2007), p. 028. DOI: [10.1088/1475-7516/2007/02/028](https://doi.org/10.1088/1475-7516/2007/02/028). arXiv: [hep-ph/0612275](https://arxiv.org/abs/hep-ph/0612275).
- [374] Marco Cirelli, Nicolao Fornengo, and Alessandro Strumia. “Minimal dark matter”. In: *Nucl. Phys. B* 753 (2006), pp. 178–194. DOI: [10.1016/j.nuclphysb.2006.07.012](https://doi.org/10.1016/j.nuclphysb.2006.07.012). arXiv: [hep-ph/0512090](https://arxiv.org/abs/hep-ph/0512090).
- [375] S. Tremaine and J. E. Gunn. “Dynamical Role of Light Neutral Leptons in Cosmology”. In: *Phys. Rev. Lett.* 42 (1979). Ed. by M. A. Srednicki, pp. 407–410. DOI: [10.1103/PhysRevLett.42.407](https://doi.org/10.1103/PhysRevLett.42.407).
- [376] James Alvey, Nashwan Sabti, Victoria Tiki, Diego Blas, Kyrylo Bondarenko, Alexey Boyarsky, Miguel Escudero, Malcolm Fairbairn, Matthew Orkney, and Justin I. Read. “New constraints on the mass of fermionic dark matter from dwarf spheroidal galaxies”. In: *Mon. Not. Roy. Astron. Soc.* 501.1 (2021), pp. 1188–1201. DOI: [10.1093/mnras/staa3640](https://doi.org/10.1093/mnras/staa3640). arXiv: [2010.03572 \[hep-ph\]](https://arxiv.org/abs/2010.03572).
- [377] Hooman Davoudiasl, Peter B. Denton, and David A. McGady. “Ultralight fermionic dark matter”. In: *Phys. Rev. D* 103.5 (2021), p. 055014. DOI: [10.1103/PhysRevD.103.055014](https://doi.org/10.1103/PhysRevD.103.055014). arXiv: [2008.06505 \[hep-ph\]](https://arxiv.org/abs/2008.06505).
- [378] Bob Holdom. “Two U(1)’s and Epsilon Charge Shifts”. In: *Phys. Lett. B* 166 (1986), pp. 196–198. DOI: [10.1016/0370-2693\(86\)91377-8](https://doi.org/10.1016/0370-2693(86)91377-8).
- [379] Maxim Pospelov, Adam Ritz, and Mikhail B. Voloshin. “Secluded WIMP Dark Matter”. In: *Phys. Lett. B* 662 (2008), pp. 53–61. DOI: [10.1016/j.physletb.2008.02.052](https://doi.org/10.1016/j.physletb.2008.02.052). arXiv: [0711.4866 \[hep-ph\]](https://arxiv.org/abs/0711.4866).
- [380] Nima Arkani-Hamed, Douglas P. Finkbeiner, Tracy R. Slatyer, and Neal Weiner. “A Theory of Dark Matter”. In: *Phys. Rev. D* 79 (2009), p. 015014. DOI: [10.1103/PhysRevD.79.015014](https://doi.org/10.1103/PhysRevD.79.015014). arXiv: [0810.0713 \[hep-ph\]](https://arxiv.org/abs/0810.0713).
- [381] Maxim Pospelov. “Secluded U(1) below the weak scale”. In: *Phys. Rev. D* 80 (2009), p. 095002. DOI: [10.1103/PhysRevD.80.095002](https://doi.org/10.1103/PhysRevD.80.095002). arXiv: [0811.1030 \[hep-ph\]](https://arxiv.org/abs/0811.1030).
- [382] Ann E. Nelson and Jakub Scholtz. “Dark Light, Dark Matter and the Misalignment Mechanism”. In: *Phys. Rev. D* 84 (2011), p. 103501. DOI: [10.1103/PhysRevD.84.103501](https://doi.org/10.1103/PhysRevD.84.103501). arXiv: [1105.2812 \[hep-ph\]](https://arxiv.org/abs/1105.2812).
- [383] Paola Arias, Davide Cadamuro, Mark Goodsell, Joerg Jaeckel, Javier Redondo, and Andreas Ringwald. “WISPy Cold Dark Matter”. In: *JCAP* 06 (2012), p. 013. DOI: [10.1088/1475-7516/2012/06/013](https://doi.org/10.1088/1475-7516/2012/06/013). arXiv: [1201.5902 \[hep-ph\]](https://arxiv.org/abs/1201.5902).
- [384] Peter W. Graham, Jeremy Mardon, and Surjeet Rajendran. “Vector Dark Matter from Inflationary Fluctuations”. In: *Phys. Rev. D* 93.10 (2016), p. 103520. DOI: [10.1103/PhysRevD.93.103520](https://doi.org/10.1103/PhysRevD.93.103520). arXiv: [1504.02102 \[hep-ph\]](https://arxiv.org/abs/1504.02102).
- [385] Prateek Agrawal, Naoya Kitajima, Matthew Reece, Toyokazu Sekiguchi, and Fuminobu Takahashi. “Relic Abundance of Dark Photon Dark Matter”. In: *Phys. Lett. B* 801 (2020), p. 135136. DOI: [10.1016/j.physletb.2019.135136](https://doi.org/10.1016/j.physletb.2019.135136). arXiv: [1810.07188 \[hep-ph\]](https://arxiv.org/abs/1810.07188).
- [386] Mar Bastero-Gil, Jose Santiago, Lorenzo Ubaldi, and Roberto Vega-Morales. “Vector dark matter production at the end of inflation”. In: *JCAP* 04 (2019), p. 015. DOI: [10.1088/1475-7516/2019/04/015](https://doi.org/10.1088/1475-7516/2019/04/015). arXiv: [1810.07208 \[hep-ph\]](https://arxiv.org/abs/1810.07208).
- [387] James M. Cline. “Status of Dark Photons”. In: *58th Rencontres de Moriond on Electroweak Interactions and Unified Theories*. May 2024. arXiv: [2405.08534 \[hep-ph\]](https://arxiv.org/abs/2405.08534).

- [388] Hooman Davoudiasl, Hye-Sung Lee, and William J. Marciano. “‘Dark’ Z implications for Parity Violation, Rare Meson Decays, and Higgs Physics”. In: *Phys. Rev. D* 85 (2012), p. 115019. DOI: [10.1103/PhysRevD.85.115019](https://doi.org/10.1103/PhysRevD.85.115019). arXiv: [1203.2947 \[hep-ph\]](https://arxiv.org/abs/1203.2947).
- [389] Hooman Davoudiasl, Hye-Sung Lee, and William J. Marciano. “Muon Anomaly and Dark Parity Violation”. In: *Phys. Rev. Lett.* 109 (2012), p. 031802. DOI: [10.1103/PhysRevLett.109.031802](https://doi.org/10.1103/PhysRevLett.109.031802). arXiv: [1205.2709 \[hep-ph\]](https://arxiv.org/abs/1205.2709).
- [390] Hooman Davoudiasl, Hye-Sung Lee, and William J. Marciano. “Dark Side of Higgs Diphoton Decays and Muon  $g-2$ ”. In: *Phys. Rev. D* 86 (2012), p. 095009. DOI: [10.1103/PhysRevD.86.095009](https://doi.org/10.1103/PhysRevD.86.095009). arXiv: [1208.2973 \[hep-ph\]](https://arxiv.org/abs/1208.2973).
- [391] Hooman Davoudiasl, Hye-Sung Lee, and William J. Marciano. “Muon  $g-2$ , rare kaon decays, and parity violation from dark bosons”. In: *Phys. Rev. D* 89.9 (2014), p. 095006. DOI: [10.1103/PhysRevD.89.095006](https://doi.org/10.1103/PhysRevD.89.095006). arXiv: [1402.3620 \[hep-ph\]](https://arxiv.org/abs/1402.3620).
- [392] M. Cadeddu, N. Cargioli, F. Dordei, C. Giunti, and E. Picciau. “Muon and electron  $g-2$  and proton and cesium weak charges implications on dark Zd models”. In: *Phys. Rev. D* 104.1 (2021), p. 011701. DOI: [10.1103/PhysRevD.104.L011701](https://doi.org/10.1103/PhysRevD.104.L011701). arXiv: [2104.03280 \[hep-ph\]](https://arxiv.org/abs/2104.03280).
- [393] Francesca Chadha-Day, John Ellis, and David J. E. Marsh. “Axion dark matter: What is it and why now?” In: *Sci. Adv.* 8.8 (2022), abj3618. DOI: [10.1126/sciadv.abj3618](https://doi.org/10.1126/sciadv.abj3618). arXiv: [2105.01406 \[hep-ph\]](https://arxiv.org/abs/2105.01406).
- [394] R. D. Peccei and Helen R. Quinn. “CP Conservation in the Presence of Instantons”. In: *Phys. Rev. Lett.* 38 (1977), pp. 1440–1443. DOI: [10.1103/PhysRevLett.38.1440](https://doi.org/10.1103/PhysRevLett.38.1440).
- [395] Frank Wilczek. “Problem of Strong  $P$  and  $T$  Invariance in the Presence of Instantons”. In: *Phys. Rev. Lett.* 40 (1978), pp. 279–282. DOI: [10.1103/PhysRevLett.40.279](https://doi.org/10.1103/PhysRevLett.40.279).
- [396] Steven Weinberg. “A New Light Boson?” In: *Phys. Rev. Lett.* 40 (1978), pp. 223–226. DOI: [10.1103/PhysRevLett.40.223](https://doi.org/10.1103/PhysRevLett.40.223).
- [397] John Preskill, Mark B. Wise, and Frank Wilczek. “Cosmology of the Invisible Axion”. In: *Phys. Lett. B* 120 (1983). Ed. by M. A. Srednicki, pp. 127–132. DOI: [10.1016/0370-2693\(83\)90637-8](https://doi.org/10.1016/0370-2693(83)90637-8).
- [398] L. F. Abbott and P. Sikivie. “A Cosmological Bound on the Invisible Axion”. In: *Phys. Lett. B* 120 (1983). Ed. by M. A. Srednicki, pp. 133–136. DOI: [10.1016/0370-2693\(83\)90638-X](https://doi.org/10.1016/0370-2693(83)90638-X).
- [399] Michael Dine and Willy Fischler. “The Not So Harmless Axion”. In: *Phys. Lett. B* 120 (1983). Ed. by M. A. Srednicki, pp. 137–141. DOI: [10.1016/0370-2693\(83\)90639-1](https://doi.org/10.1016/0370-2693(83)90639-1).
- [400] Masahiro Kawasaki, Ken’ichi Saikawa, and Toyokazu Sekiguchi. “Axion dark matter from topological defects”. In: *Phys. Rev. D* 91.6 (2015), p. 065014. DOI: [10.1103/PhysRevD.91.065014](https://doi.org/10.1103/PhysRevD.91.065014). arXiv: [1412.0789 \[hep-ph\]](https://arxiv.org/abs/1412.0789).
- [401] Prateek Agrawal, Zackaria Chacko, and Christopher B. Verhaaren. “Leptophilic Dark Matter and the Anomalous Magnetic Moment of the Muon”. In: *JHEP* 08 (2014), p. 147. DOI: [10.1007/JHEP08\(2014\)147](https://doi.org/10.1007/JHEP08(2014)147). arXiv: [1402.7369 \[hep-ph\]](https://arxiv.org/abs/1402.7369).
- [402] Giorgio Arcadi, Lorenzo Calibbi, Marco Fedele, and Federico Mescia. “Muon  $g-2$  and  $B$ -anomalies from Dark Matter”. In: *Phys. Rev. Lett.* 127.6 (2021), p. 061802. DOI: [10.1103/PhysRevLett.127.061802](https://doi.org/10.1103/PhysRevLett.127.061802). arXiv: [2104.03228 \[hep-ph\]](https://arxiv.org/abs/2104.03228).
- [403] Nicole F. Bell, Yi Cai, Rebecca K. Leane, and Anibal D. Medina. “Leptophilic dark matter with  $Z'$  interactions”. In: *Phys. Rev. D* 90.3 (2014), p. 035027. DOI: [10.1103/PhysRevD.90.035027](https://doi.org/10.1103/PhysRevD.90.035027). arXiv: [1407.3001 \[hep-ph\]](https://arxiv.org/abs/1407.3001).

- [404] Salvatore Bottaro, Dario Buttazzo, Marco Costa, Roberto Franceschini, Paolo Panci, Diego Redigolo, and Ludovico Vittorio. “The last complex WIMPs standing”. In: *Eur. Phys. J. C* 82.11 (2022), p. 992. DOI: [10.1140/epjc/s10052-022-10918-5](https://doi.org/10.1140/epjc/s10052-022-10918-5). arXiv: [2205.04486](https://arxiv.org/abs/2205.04486) [hep-ph].
- [405] Csaba Balázs et al. “ColliderBit: a GAMBIT module for the calculation of high-energy collider observables and likelihoods”. In: *Eur. Phys. J. C* 77.11 (2017), p. 795. DOI: [10.1140/epjc/s10052-017-5285-8](https://doi.org/10.1140/epjc/s10052-017-5285-8). arXiv: [1705.07919](https://arxiv.org/abs/1705.07919) [hep-ph].
- [406] Sabine Kraml, Suchita Kulkarni, Ursula Laa, Andre Lessa, Wolfgang Magerl, Doris Proschofsky-Spindler, and Wolfgang Waltenberger. “SModelS: a tool for interpreting simplified-model results from the LHC and its application to supersymmetry”. In: *Eur. Phys. J. C* 74 (2014), p. 2868. DOI: [10.1140/epjc/s10052-014-2868-5](https://doi.org/10.1140/epjc/s10052-014-2868-5). arXiv: [1312.4175](https://arxiv.org/abs/1312.4175) [hep-ph].
- [407] Jamie Tattersall, Daniel Dercks, Nishita Desai, Jong Soo Kim, Frederic Poncza, Krzysztof Rolbiecki, and Torsten Weber. “CheckMATE: Checkmating new physics at the LHC”. In: *PoS ICHEP2016* (2016), p. 120. DOI: [10.22323/1.282.0120](https://doi.org/10.22323/1.282.0120).
- [408] Georges Aad et al. “Search for new phenomena in final states with photons, jets and missing transverse momentum in pp collisions at  $\sqrt{s} = 13$  TeV with the ATLAS detector”. In: *JHEP* 07 (2023), p. 021. DOI: [10.1007/JHEP07\(2023\)021](https://doi.org/10.1007/JHEP07(2023)021). arXiv: [2206.06012](https://arxiv.org/abs/2206.06012) [hep-ex].
- [409] Georges Aad et al. “Search for supersymmetry in final states with missing transverse momentum and three or more b-jets in  $139 \text{ fb}^{-1}$  of proton–proton collisions at  $\sqrt{s} = 13$  TeV with the ATLAS detector”. In: *Eur. Phys. J. C* 83.7 (2023), p. 561. DOI: [10.1140/epjc/s10052-023-11543-6](https://doi.org/10.1140/epjc/s10052-023-11543-6). arXiv: [2211.08028](https://arxiv.org/abs/2211.08028) [hep-ex].
- [410] Albert M Sirunyan et al. “Search for top squark production in fully-hadronic final states in proton-proton collisions at  $\sqrt{s} = 13$  TeV”. In: *Phys. Rev. D* 104.5 (2021), p. 052001. DOI: [10.1103/PhysRevD.104.052001](https://doi.org/10.1103/PhysRevD.104.052001). arXiv: [2103.01290](https://arxiv.org/abs/2103.01290) [hep-ex].
- [411] Albert M Sirunyan et al. “Searches for physics beyond the standard model with the  $M_{T2}$  variable in hadronic final states with and without disappearing tracks in proton-proton collisions at  $\sqrt{s} = 13$  TeV”. In: *Eur. Phys. J. C* 80.1 (2020), p. 3. DOI: [10.1140/epjc/s10052-019-7493-x](https://doi.org/10.1140/epjc/s10052-019-7493-x). arXiv: [1909.03460](https://arxiv.org/abs/1909.03460) [hep-ex].
- [412] Morad Aaboud et al. “Search for photonic signatures of gauge-mediated supersymmetry in 13 TeV  $pp$  collisions with the ATLAS detector”. In: *Phys. Rev. D* 97.9 (2018), p. 092006. DOI: [10.1103/PhysRevD.97.092006](https://doi.org/10.1103/PhysRevD.97.092006). arXiv: [1802.03158](https://arxiv.org/abs/1802.03158) [hep-ex].
- [413] The Cms Collaboration et al. “Search for supersymmetry in proton-proton collisions at 13 TeV in final states with jets and missing transverse momentum”. In: *JHEP* 10 (2019), p. 244. DOI: [10.1007/JHEP10\(2019\)244](https://doi.org/10.1007/JHEP10(2019)244). arXiv: [1908.04722](https://arxiv.org/abs/1908.04722) [hep-ex].
- [414] Georges Aad et al. “Search for pair-produced scalar and vector leptoquarks decaying into third-generation quarks and first- or second-generation leptons in pp collisions with the ATLAS detector”. In: *JHEP* 2306 (2023), p. 188. DOI: [10.1007/JHEP06\(2023\)188](https://doi.org/10.1007/JHEP06(2023)188). arXiv: [2210.04517](https://arxiv.org/abs/2210.04517) [hep-ex].
- [415] Aram Hayrapetyan et al. “Search for pair production of scalar and vector leptoquarks decaying to muons and bottom quarks in proton-proton collisions at  $s=13$  TeV”. In: *Phys. Rev. D* 109.11 (2024), p. 112003. DOI: [10.1103/PhysRevD.109.112003](https://doi.org/10.1103/PhysRevD.109.112003). arXiv: [2402.08668](https://arxiv.org/abs/2402.08668) [hep-ex].

- [416] Aram Hayrapetyan et al. “Search for Scalar Leptoquarks Produced via  $\tau$ -Lepton–Quark Scattering in pp Collisions at  $s=13$  TeV”. In: *Phys. Rev. Lett.* 132.6 (2024), p. 061801. DOI: [10.1103/PhysRevLett.132.061801](https://doi.org/10.1103/PhysRevLett.132.061801). arXiv: [2308.06143](https://arxiv.org/abs/2308.06143) [hep-ex].
- [417] Aram Hayrapetyan et al. “Search for  $t$ -channel scalar and vector leptoquark exchange in the high-mass dimuon and dielectron spectra in proton-proton collisions at  $\sqrt{s} = 13$  TeV”. In: (Mar. 2025). arXiv: [2503.20023](https://arxiv.org/abs/2503.20023) [hep-ex].
- [418] Georges Aad et al. “Search for a scalar partner of the top quark in the all-hadronic  $t\bar{t}$  plus missing transverse momentum final state at  $\sqrt{s} = 13$  TeV with the ATLAS detector”. In: *Eur. Phys. J. C* 80.8 (2020), p. 737. DOI: [10.1140/epjc/s10052-020-8102-8](https://doi.org/10.1140/epjc/s10052-020-8102-8). arXiv: [2004.14060](https://arxiv.org/abs/2004.14060) [hep-ex].
- [419] Armen Tumasyan et al. “Combined searches for the production of supersymmetric top quark partners in proton–proton collisions at  $\sqrt{s} = 13$  TeV”. In: *Eur. Phys. J. C* 81.11 (2021), p. 970. DOI: [10.1140/epjc/s10052-021-09721-5](https://doi.org/10.1140/epjc/s10052-021-09721-5). arXiv: [2107.10892](https://arxiv.org/abs/2107.10892) [hep-ex].
- [420] Aram Hayrapetyan et al. “Search for heavy neutral resonances decaying to tau lepton pairs in proton-proton collisions at  $\sqrt{s} = 13$  TeV”. In: (Dec. 2024). arXiv: [2412.04357](https://arxiv.org/abs/2412.04357) [hep-ex].
- [421] Armen Tumasyan et al. “Measurement of the Drell-Yan forward-backward asymmetry at high dilepton masses in proton-proton collisions at  $\sqrt{s} = 13$  TeV”. In: *JHEP* 2022.08 (2022), p. 063. DOI: [10.1007/JHEP08\(2022\)063](https://doi.org/10.1007/JHEP08(2022)063). arXiv: [2202.12327](https://arxiv.org/abs/2202.12327) [hep-ex].
- [422] Serguei Chatrchyan et al. “Search for Resonances in the Dijet Mass Spectrum from 7 TeV pp Collisions at CMS”. In: *Phys. Lett. B* 704 (2011), pp. 123–142. DOI: [10.1016/j.physletb.2011.09.015](https://doi.org/10.1016/j.physletb.2011.09.015). arXiv: [1107.4771](https://arxiv.org/abs/1107.4771) [hep-ex].
- [423] Georges Aad et al. “Search for electroweak production of charginos and sleptons decaying into final states with two leptons and missing transverse momentum in  $\sqrt{s} = 13$  TeV  $pp$  collisions using the ATLAS detector”. In: *Eur. Phys. J. C* 80.2 (2020), p. 123. DOI: [10.1140/epjc/s10052-019-7594-6](https://doi.org/10.1140/epjc/s10052-019-7594-6). arXiv: [1908.08215](https://arxiv.org/abs/1908.08215) [hep-ex].
- [424] M. Aaboud et al. “Search for electroweak production of supersymmetric particles in final states with two or three leptons at  $\sqrt{s} = 13$  TeV with the ATLAS detector”. In: *Eur. Phys. J. C* 78.12 (2018), p. 995. DOI: [10.1140/epjc/s10052-018-6423-7](https://doi.org/10.1140/epjc/s10052-018-6423-7). arXiv: [1803.02762](https://arxiv.org/abs/1803.02762) [hep-ex].
- [425] Peter Athron et al. “Combined collider constraints on neutralinos and charginos”. In: *Eur. Phys. J. C* 79.5 (2019), p. 395. DOI: [10.1140/epjc/s10052-019-6837-x](https://doi.org/10.1140/epjc/s10052-019-6837-x). arXiv: [1809.02097](https://arxiv.org/abs/1809.02097) [hep-ph].
- [426] P. Achard et al. “Search for heavy neutral and charged leptons in  $e^+e^-$  annihilation at LEP”. In: *Phys. Lett. B* 517 (2001), pp. 75–85. DOI: [10.1016/S0370-2693\(01\)01005-X](https://doi.org/10.1016/S0370-2693(01)01005-X). arXiv: [hep-ex/0107015](https://arxiv.org/abs/hep-ex/0107015).
- [427] A. Heister et al. “Search for scalar leptons in  $e^+e^-$  collisions at center-of-mass energies up to 209-GeV”. In: *Phys. Lett. B* 526 (2002), pp. 206–220. DOI: [10.1016/S0370-2693\(01\)01494-0](https://doi.org/10.1016/S0370-2693(01)01494-0). arXiv: [hep-ex/0112011](https://arxiv.org/abs/hep-ex/0112011).
- [428] Georges Aad et al. “Search for heavy lepton resonances decaying to a  $Z$  boson and a lepton in  $pp$  collisions at  $\sqrt{s} = 8$  TeV with the ATLAS detector”. In: *JHEP* 09 (2015), p. 108. DOI: [10.1007/JHEP09\(2015\)108](https://doi.org/10.1007/JHEP09(2015)108). arXiv: [1506.01291](https://arxiv.org/abs/1506.01291) [hep-ex].
- [429] Georges Aad et al. “Search for third-generation vector-like leptons in  $pp$  collisions at  $\sqrt{s} = 13$  TeV with the ATLAS detector”. In: *JHEP* 07 (2023), p. 118. DOI: [10.1007/JHEP07\(2023\)118](https://doi.org/10.1007/JHEP07(2023)118). arXiv: [2303.05441](https://arxiv.org/abs/2303.05441) [hep-ex].
- [430] Georges Aad et al. “Search for vector-like leptons coupling to first- and second-generation Standard Model leptons in  $pp$  collisions at  $\sqrt{s} = 13$  TeV with the ATLAS detector”. In: (Nov. 2024). arXiv: [2411.07143](https://arxiv.org/abs/2411.07143) [hep-ex].

- [431] Albert M Sirunyan et al. “Search for vector-like leptons in multilepton final states in proton-proton collisions at  $\sqrt{s} = 13$  TeV”. In: *Phys. Rev. D* 100.5 (2019), p. 052003. DOI: [10.1103/PhysRevD.100.052003](https://doi.org/10.1103/PhysRevD.100.052003). arXiv: [1905.10853](https://arxiv.org/abs/1905.10853) [hep-ex].
- [432] “Search for long-lived heavy neutral leptons decaying in the CMS muon detectors in proton-proton collisions at  $\sqrt{s} = 13$  TeV”. In: (2023).
- [433] Aram Hayrapetyan et al. “Review of searches for vector-like quarks, vector-like leptons, and heavy neutral leptons in proton-proton collisions at  $\sqrt{s} = 13$  TeV at the CMS experiment”. In: (May 2024). arXiv: [2405.17605](https://arxiv.org/abs/2405.17605) [hep-ex].
- [434] Albert M Sirunyan et al. “Search for pair production of first-generation scalar leptoquarks at  $\sqrt{s} = 13$  TeV”. In: *Phys. Rev. D* 99.5 (2019), p. 052002. DOI: [10.1103/PhysRevD.99.052002](https://doi.org/10.1103/PhysRevD.99.052002). arXiv: [1811.01197](https://arxiv.org/abs/1811.01197) [hep-ex].
- [435] Albert M Sirunyan et al. “Search for pair production of second-generation leptoquarks at  $\sqrt{s} = 13$  TeV”. In: *Phys. Rev. D* 99.3 (2019), p. 032014. DOI: [10.1103/PhysRevD.99.032014](https://doi.org/10.1103/PhysRevD.99.032014). arXiv: [1808.05082](https://arxiv.org/abs/1808.05082) [hep-ex].
- [436] Albert M Sirunyan et al. “Search for leptoquarks coupled to third-generation quarks in proton-proton collisions at  $\sqrt{s} = 13$  TeV”. In: *Phys. Rev. Lett.* 121.24 (2018), p. 241802. DOI: [10.1103/PhysRevLett.121.241802](https://doi.org/10.1103/PhysRevLett.121.241802). arXiv: [1809.05558](https://arxiv.org/abs/1809.05558) [hep-ex].
- [437] Albert M Sirunyan et al. “Search for singly and pair-produced leptoquarks coupling to third-generation fermions in proton-proton collisions at  $s=13$  TeV”. In: *Phys. Lett. B* 819 (2021), p. 136446. DOI: [10.1016/j.physletb.2021.136446](https://doi.org/10.1016/j.physletb.2021.136446). arXiv: [2012.04178](https://arxiv.org/abs/2012.04178) [hep-ex].
- [438] Morad Aaboud et al. “Searches for scalar leptoquarks and differential cross-section measurements in dilepton-dijet events in proton-proton collisions at a centre-of-mass energy of  $\sqrt{s} = 13$  TeV with the ATLAS experiment”. In: *Eur. Phys. J. C* 79.9 (2019), p. 733. DOI: [10.1140/epjc/s10052-019-7181-x](https://doi.org/10.1140/epjc/s10052-019-7181-x). arXiv: [1902.00377](https://arxiv.org/abs/1902.00377) [hep-ex].
- [439] Morad Aaboud et al. “Searches for third-generation scalar leptoquarks in  $\sqrt{s} = 13$  TeV pp collisions with the ATLAS detector”. In: *JHEP* 06 (2019), p. 144. DOI: [10.1007/JHEP06\(2019\)144](https://doi.org/10.1007/JHEP06(2019)144). arXiv: [1902.08103](https://arxiv.org/abs/1902.08103) [hep-ex].
- [440] Georges Aad et al. “Search for new phenomena in  $pp$  collisions in final states with tau leptons, b-jets, and missing transverse momentum with the ATLAS detector”. In: *Phys. Rev. D* 104.11 (2021), p. 112005. DOI: [10.1103/PhysRevD.104.112005](https://doi.org/10.1103/PhysRevD.104.112005). arXiv: [2108.07665](https://arxiv.org/abs/2108.07665) [hep-ex].
- [441] Georges Aad et al. “Search for pair production of third-generation leptoquarks decaying into a bottom quark and a  $\tau$ -lepton with the ATLAS detector”. In: *Eur. Phys. J. C* 83.11 (2023), p. 1075. DOI: [10.1140/epjc/s10052-023-12104-7](https://doi.org/10.1140/epjc/s10052-023-12104-7). arXiv: [2303.01294](https://arxiv.org/abs/2303.01294) [hep-ex].
- [442] Georges Aad et al. “Search for pair production of third-generation scalar leptoquarks decaying into a top quark and a  $\tau$ -lepton in  $pp$  collisions at  $\sqrt{s} = 13$  TeV with the ATLAS detector”. In: *JHEP* 06 (2021), p. 179. DOI: [10.1007/JHEP06\(2021\)179](https://doi.org/10.1007/JHEP06(2021)179). arXiv: [2101.11582](https://arxiv.org/abs/2101.11582) [hep-ex].
- [443] Georges Aad et al. “Search for pairs of scalar leptoquarks decaying into quarks and electrons or muons in  $\sqrt{s} = 13$  TeV  $pp$  collisions with the ATLAS detector”. In: *JHEP* 10 (2020), p. 112. DOI: [10.1007/JHEP10\(2020\)112](https://doi.org/10.1007/JHEP10(2020)112). arXiv: [2006.05872](https://arxiv.org/abs/2006.05872) [hep-ex].
- [444] Georges Aad et al. “Search for pair production of scalar leptoquarks decaying into first- or second-generation leptons and top quarks in proton-proton collisions at  $\sqrt{s} = 13$  TeV with the ATLAS detector”. In: *Eur. Phys. J. C* 81.4 (2021), p. 313. DOI: [10.1140/epjc/s10052-021-09009-8](https://doi.org/10.1140/epjc/s10052-021-09009-8). arXiv: [2010.02098](https://arxiv.org/abs/2010.02098) [hep-ex].

- [445] Georges Aad et al. “Search for leptoquark pair production decaying into  $te^{-}\bar{t}e^{+}$  or  $t\mu^{-}\bar{t}\mu^{+}$  in multi-lepton final states in pp collisions at  $\sqrt{s} = 13$  TeV with the ATLAS detector”. In: *Eur. Phys. J. C* 84.8 (2024), p. 818. DOI: [10.1140/epjc/s10052-024-12975-4](https://doi.org/10.1140/epjc/s10052-024-12975-4). arXiv: [2306.17642](https://arxiv.org/abs/2306.17642) [hep-ex].
- [446] Georges Aad et al. “Search for new phenomena in final states with  $b$ -jets and missing transverse momentum in  $\sqrt{s} = 13$  TeV  $pp$  collisions with the ATLAS detector”. In: *JHEP* 05 (2021), p. 093. DOI: [10.1007/JHEP05\(2021\)093](https://doi.org/10.1007/JHEP05(2021)093). arXiv: [2101.12527](https://arxiv.org/abs/2101.12527) [hep-ex].
- [447] Armen Tumasyan et al. “Inclusive nonresonant multilepton probes of new phenomena at  $\sqrt{s}=13$  TeV”. In: *Phys. Rev. D* 105.11 (2022), p. 112007. DOI: [10.1103/PhysRevD.105.112007](https://doi.org/10.1103/PhysRevD.105.112007). arXiv: [2202.08676](https://arxiv.org/abs/2202.08676) [hep-ex].
- [448] Armen Tumasyan et al. “Search for direct pair production of supersymmetric partners of  $\tau$  leptons in the final state with two hadronically decaying  $\tau$  leptons and missing transverse momentum in proton-proton collisions at  $\sqrt{s} = 13$  TeV”. In: *Phys. Rev. D* 108.1 (2023), p. 012011. DOI: [10.1103/PhysRevD.108.012011](https://doi.org/10.1103/PhysRevD.108.012011). arXiv: [2207.02254](https://arxiv.org/abs/2207.02254) [hep-ex].
- [449] Albert M Sirunyan et al. “Search for new physics in events with two soft oppositely charged leptons and missing transverse momentum in proton-proton collisions at  $\sqrt{s} = 13$  TeV”. In: *Phys. Lett. B* 782 (2018), pp. 440–467. DOI: [10.1016/j.physletb.2018.05.062](https://doi.org/10.1016/j.physletb.2018.05.062). arXiv: [1801.01846](https://arxiv.org/abs/1801.01846) [hep-ex].
- [450] Georges Aad et al. “Search for direct pair production of sleptons and charginos decaying to two leptons and neutralinos with mass splittings near the W-boson mass in  $\sqrt{s} = 13$  TeV  $pp$  collisions with the ATLAS detector”. In: *JHEP* 06 (2023), p. 031. DOI: [10.1007/JHEP06\(2023\)031](https://doi.org/10.1007/JHEP06(2023)031). arXiv: [2209.13935](https://arxiv.org/abs/2209.13935) [hep-ex].
- [451] Georges Aad et al. “Searches for electroweak production of supersymmetric particles with compressed mass spectra in  $\sqrt{s} = 13$  TeV  $pp$  collisions with the ATLAS detector”. In: *Phys. Rev. D* 101.5 (2020), p. 052005. DOI: [10.1103/PhysRevD.101.052005](https://doi.org/10.1103/PhysRevD.101.052005). arXiv: [1911.12606](https://arxiv.org/abs/1911.12606) [hep-ex].
- [452] Georges Aad et al. “Searches for direct slepton production in the compressed-mass corridor in  $\sqrt{s} = 13$  TeV  $pp$  collisions with the ATLAS detector”. In: (Mar. 2025). arXiv: [2503.17186](https://arxiv.org/abs/2503.17186) [hep-ex].
- [453] Albert M Sirunyan et al. “Search for Supersymmetry with a Compressed Mass Spectrum in Events with a Soft  $\tau$  Lepton, a Highly Energetic Jet, and Large Missing Transverse Momentum in Proton-Proton Collisions at  $\sqrt{s} = 13$  TeV”. In: *Phys. Rev. Lett.* 124.4 (2020), p. 041803. DOI: [10.1103/PhysRevLett.124.041803](https://doi.org/10.1103/PhysRevLett.124.041803). arXiv: [1910.01185](https://arxiv.org/abs/1910.01185) [hep-ex].
- [454] Aram Hayrapetyan et al. “Combined search for electroweak production of winos, binos, higgsinos, and sleptons in proton-proton collisions at  $s=13$  TeV”. In: *Phys. Rev. D* 109.11 (2024), p. 112001. DOI: [10.1103/PhysRevD.109.112001](https://doi.org/10.1103/PhysRevD.109.112001). arXiv: [2402.01888](https://arxiv.org/abs/2402.01888) [hep-ex].
- [455] Albert M Sirunyan et al. “Search for top squarks in final states with two top quarks and several light-flavor jets in proton-proton collisions at  $\sqrt{s} = 13$  TeV”. In: *Phys. Rev. D* 104.3 (2021), p. 032006. DOI: [10.1103/PhysRevD.104.032006](https://doi.org/10.1103/PhysRevD.104.032006). arXiv: [2102.06976](https://arxiv.org/abs/2102.06976) [hep-ex].
- [456] Stanley J. Brodsky and Jeremiah D. Sullivan. “W BOSON CONTRIBUTION TO THE ANOMALOUS MAGNETIC MOMENT OF THE MUON”. In: *Phys. Rev.* 156 (1967), pp. 1644–1647. DOI: [10.1103/PhysRev.156.1644](https://doi.org/10.1103/PhysRev.156.1644).

- [457] Janis Aldins, Toichiro Kinoshita, Stanley J. Brodsky, and A. J. Dufner. “PHOTON - PHOTON SCATTERING CONTRIBUTION TO THE SIXTH ORDER MAGNETIC MOMENTS OF THE MUON AND ELECTRON”. In: *Phys. Rev. D* 1 (1970), p. 2378. DOI: [10.1103/PhysRevD.1.2378](https://doi.org/10.1103/PhysRevD.1.2378).
- [458] Riccardo Barbieri, J. A. Mignaco, and E. Remiddi. “Electron form-factors up to fourth order. 1.” In: *Nuovo Cim. A* 11 (1972), pp. 824–864. DOI: [10.1007/BF02728545](https://doi.org/10.1007/BF02728545).
- [459] Riccardo Barbieri and E. Remiddi. “Electron and Muon  $1/2(g-2)$  from Vacuum Polarization Insertions”. In: *Nucl. Phys. B* 90 (1975), pp. 233–266. DOI: [10.1016/0550-3213\(75\)90645-8](https://doi.org/10.1016/0550-3213(75)90645-8).
- [460] Riccardo Barbieri, Michele Caffo, and E. Remiddi. “A Sixth Order Contribution to the electron Anomalous Magnetic Moment”. In: *Phys. Lett. B* 57 (1975), pp. 460–462. DOI: [10.1016/0370-2693\(75\)90268-3](https://doi.org/10.1016/0370-2693(75)90268-3).
- [461] Andrzej Czarnecki and Bernd Krause. “Electroweak corrections to the muon anomalous magnetic moment”. In: *Nucl. Phys. B Proc. Suppl.* 51 (1996). Ed. by J. Blumlein, F. Jegerlehner, and T. Riemann, pp. 148–153. DOI: [10.1016/S0920-5632\(96\)90019-5](https://doi.org/10.1016/S0920-5632(96)90019-5). arXiv: [hep-ph/9606393](https://arxiv.org/abs/hep-ph/9606393).
- [462] Stephen M. Barr and A. Zee. “Electric Dipole Moment of the Electron and of the Neutron”. In: *Phys. Rev. Lett.* 65 (1990). [Erratum: *Phys.Rev.Lett.* 65, 2920 (1990)], pp. 21–24. DOI: [10.1103/PhysRevLett.65.21](https://doi.org/10.1103/PhysRevLett.65.21).
- [463] Darwin Chang, We-Fu Chang, Chung-Hsien Chou, and Wai-Yee Keung. “Large two loop contributions to  $g-2$  from a generic pseudoscalar boson”. In: *Phys. Rev. D* 63 (2001), p. 091301. DOI: [10.1103/PhysRevD.63.091301](https://doi.org/10.1103/PhysRevD.63.091301). arXiv: [hep-ph/0009292](https://arxiv.org/abs/hep-ph/0009292).
- [464] King-man Cheung, Chung-Hsien Chou, and Otto C. W. Kong. “Muon anomalous magnetic moment, two Higgs doublet model, and supersymmetry”. In: *Phys. Rev. D* 64 (2001), p. 111301. DOI: [10.1103/PhysRevD.64.111301](https://doi.org/10.1103/PhysRevD.64.111301). arXiv: [hep-ph/0103183](https://arxiv.org/abs/hep-ph/0103183).
- [465] Victor Ilisie. “New Barr-Zee contributions to  $(g - 2)_\mu$  in two-Higgs-doublet models”. In: *JHEP* 04 (2015), p. 077. DOI: [10.1007/JHEP04\(2015\)077](https://doi.org/10.1007/JHEP04(2015)077). arXiv: [1502.04199](https://arxiv.org/abs/1502.04199) [[hep-ph](https://arxiv.org/abs/hep-ph)].
- [466] Tomohiro Abe, Junji Hisano, Teppei Kitahara, and Kohsaku Tobioka. “Gauge invariant Barr-Zee type contributions to fermionic EDMs in the two-Higgs doublet models”. In: *JHEP* 01 (2014). [Erratum: *JHEP* 04, 161 (2016)], p. 106. DOI: [10.1007/JHEP01\(2014\)106](https://doi.org/10.1007/JHEP01(2014)106). arXiv: [1311.4704](https://arxiv.org/abs/1311.4704) [[hep-ph](https://arxiv.org/abs/hep-ph)].
- [467] Yue-Liang Wu and Yu-Feng Zhou. “Muon anomalous magnetic moment in the standard model with two Higgs doublets”. In: *Phys. Rev. D* 64 (2001), p. 115018. DOI: [10.1103/PhysRevD.64.115018](https://doi.org/10.1103/PhysRevD.64.115018). arXiv: [hep-ph/0104056](https://arxiv.org/abs/hep-ph/0104056).
- [468] Maria Krawczyk. “Precision muon  $g-2$  results and light Higgs bosons in the 2HDM(II)”. In: *Acta Phys. Polon. B* 33 (2002), pp. 2621–2634. arXiv: [hep-ph/0208076](https://arxiv.org/abs/hep-ph/0208076).
- [469] P. von Weitershausen, M. Schafer, H. Stockinger-Kim, and D. Stockinger. “Photonic SUSY Two-Loop Corrections to the Muon Magnetic Moment”. In: *Phys. Rev. D* 81 (2010), p. 093004. DOI: [10.1103/PhysRevD.81.093004](https://doi.org/10.1103/PhysRevD.81.093004). arXiv: [1003.5820](https://arxiv.org/abs/1003.5820) [[hep-ph](https://arxiv.org/abs/hep-ph)].
- [470] Elizabeth E. Jenkins, Aneesh V. Manohar, and Peter Stoffer. “Low-Energy Effective Field Theory below the Electroweak Scale: Anomalous Dimensions”. In: *JHEP* 01 (2018). [Erratum: *JHEP* 12, 042 (2023)], p. 084. DOI: [10.1007/JHEP01\(2018\)084](https://doi.org/10.1007/JHEP01(2018)084). arXiv: [1711.05270](https://arxiv.org/abs/1711.05270) [[hep-ph](https://arxiv.org/abs/hep-ph)].

- [471] Elizabeth E. Jenkins, Aneesh V. Manohar, and Michael Trott. “Renormalization Group Evolution of the Standard Model Dimension Six Operators I: Formalism and lambda Dependence”. In: *JHEP* 10 (2013), p. 087. DOI: [10.1007/JHEP10\(2013\)087](https://doi.org/10.1007/JHEP10(2013)087). arXiv: [1308.2627](https://arxiv.org/abs/1308.2627) [[hep-ph](#)].
- [472] Elizabeth E. Jenkins, Aneesh V. Manohar, and Michael Trott. “Renormalization Group Evolution of the Standard Model Dimension Six Operators II: Yukawa Dependence”. In: *JHEP* 01 (2014), p. 035. DOI: [10.1007/JHEP01\(2014\)035](https://doi.org/10.1007/JHEP01(2014)035). arXiv: [1310.4838](https://arxiv.org/abs/1310.4838) [[hep-ph](#)].
- [473] Rodrigo Alonso, Elizabeth E. Jenkins, Aneesh V. Manohar, and Michael Trott. “Renormalization Group Evolution of the Standard Model Dimension Six Operators III: Gauge Coupling Dependence and Phenomenology”. In: *JHEP* 04 (2014), p. 159. DOI: [10.1007/JHEP04\(2014\)159](https://doi.org/10.1007/JHEP04(2014)159). arXiv: [1312.2014](https://arxiv.org/abs/1312.2014) [[hep-ph](#)].
- [474] Marco Ciuchini, E. Franco, L. Reina, and L. Silvestrini. “Leading order QCD corrections to  $b \rightarrow s \gamma$  and  $b \rightarrow s g$  decays in three regularization schemes”. In: *Nucl. Phys. B* 421 (1994), pp. 41–64. DOI: [10.1016/0550-3213\(94\)90223-2](https://doi.org/10.1016/0550-3213(94)90223-2). arXiv: [hep-ph/9311357](https://arxiv.org/abs/hep-ph/9311357).
- [475] T. Huang, Z. H. Lin, L. Y. Shan, and X. Zhang. “Muon anomalous magnetic moment and lepton flavor violation”. In: *Phys. Rev. D* 64 (2001), p. 071301. DOI: [10.1103/PhysRevD.64.071301](https://doi.org/10.1103/PhysRevD.64.071301). arXiv: [hep-ph/0102193](https://arxiv.org/abs/hep-ph/0102193).
- [476] S. N. Gninenko and N. V. Krasnikov. “The Muon anomalous magnetic moment and a new light gauge boson”. In: *Phys. Lett. B* 513 (2001), p. 119. DOI: [10.1016/S0370-2693\(01\)00693-1](https://doi.org/10.1016/S0370-2693(01)00693-1). arXiv: [hep-ph/0102222](https://arxiv.org/abs/hep-ph/0102222).
- [477] Brandon Murakami. “The Impact of lepton flavor violating Z-prime bosons on muon g-2 and other muon observables”. In: *Phys. Rev. D* 65 (2002), p. 055003. DOI: [10.1103/PhysRevD.65.055003](https://doi.org/10.1103/PhysRevD.65.055003). arXiv: [hep-ph/0110095](https://arxiv.org/abs/hep-ph/0110095).
- [478] Jae Ho Heo. “About a peculiar  $U(1) : Z'$  discovery limit, Muon anomalous magnetic moment, Electron electric dipole moment”. In: *Phys. Rev. D* 80 (2009), p. 033001. DOI: [10.1103/PhysRevD.80.033001](https://doi.org/10.1103/PhysRevD.80.033001). arXiv: [0811.0298](https://arxiv.org/abs/0811.0298) [[hep-ph](#)].
- [479] Geneviève Bélanger, Cédric Delaunay, and Susanne Westhoff. “A Dark Matter Relic From Muon Anomalies”. In: *Phys. Rev. D* 92 (2015), p. 055021. DOI: [10.1103/PhysRevD.92.055021](https://doi.org/10.1103/PhysRevD.92.055021). arXiv: [1507.06660](https://arxiv.org/abs/1507.06660) [[hep-ph](#)].
- [480] Arnab Dasgupta, P. S. Bhupal Dev, Tao Han, Rojalin Padhan, Si Wang, and Keping Xie. “Searching for heavy leptophilic  $Z'$ : from lepton colliders to gravitational waves”. In: *JHEP* 12 (2023), p. 011. DOI: [10.1007/JHEP12\(2023\)011](https://doi.org/10.1007/JHEP12(2023)011). arXiv: [2308.12804](https://arxiv.org/abs/2308.12804) [[hep-ph](#)].
- [481] J. Kriewald, J. Orloff, E. Pinsard, and A. M. Teixeira. “Prospects for a flavour violating  $Z'$  explanation of  $\Delta a_{\mu,e}$ ”. In: *Eur. Phys. J. C* 82.9 (2022), p. 844. DOI: [10.1140/epjc/s10052-022-10776-1](https://doi.org/10.1140/epjc/s10052-022-10776-1). arXiv: [2204.13134](https://arxiv.org/abs/2204.13134) [[hep-ph](#)].
- [482] Anirban Biswas and Sarif Khan. “ $(g - 2)_{e,\mu}$  and strongly interacting dark matter with collider implications”. In: *JHEP* 07 (2022), p. 037. DOI: [10.1007/JHEP07\(2022\)037](https://doi.org/10.1007/JHEP07(2022)037). arXiv: [2112.08393](https://arxiv.org/abs/2112.08393) [[hep-ph](#)].
- [483] M. Ashry, K. Ezzat, and S. Khalil. “Muon g-2 anomaly in a left-right model with an inverse seesaw mechanism”. In: *Phys. Rev. D* 107.5 (2023), p. 055044. DOI: [10.1103/PhysRevD.107.055044](https://doi.org/10.1103/PhysRevD.107.055044). arXiv: [2207.05828](https://arxiv.org/abs/2207.05828) [[hep-ph](#)].
- [484] Ritu Dcruz. “Flavor physics constraints on left-right symmetric models with universal seesaw”. In: *Nucl. Phys. B* 1001 (2024), p. 116519. DOI: [10.1016/j.nuclphysb.2024.116519](https://doi.org/10.1016/j.nuclphysb.2024.116519). arXiv: [2301.10786](https://arxiv.org/abs/2301.10786) [[hep-ph](#)].
- [485] João Paulo Pinheiro, C. A. de S. Pires, Farinaldo S. Queiroz, and Yoxara S. Villamizar. “Confronting the inverse seesaw mechanism with the recent muon g-2 result”. In: *Phys. Lett. B* 823 (2021), p. 136764. DOI: [10.1016/j.physletb.2021.136764](https://doi.org/10.1016/j.physletb.2021.136764). arXiv: [2107.01315](https://arxiv.org/abs/2107.01315) [[hep-ph](#)].

- [486] Tianjun Li, Junle Pei, and Wenxing Zhang. “Muon anomalous magnetic moment and Higgs potential stability in the 331 model from SU(6)”. In: *Eur. Phys. J. C* 81.7 (2021), p. 671. DOI: [10.1140/epjc/s10052-021-09474-1](https://doi.org/10.1140/epjc/s10052-021-09474-1). arXiv: [2104.03334](https://arxiv.org/abs/2104.03334) [hep-ph].
- [487] L. T. Hue, H. T. Hung, N. T. Tham, H. N. Long, and T. Phong Nguyen. “Large  $(g-2)_\mu$  and signals of decays  $eb \rightarrow ea\gamma$  in a 3-3-1 model with inverse seesaw neutrinos”. In: *Phys. Rev. D* 104.3 (2021), p. 033007. DOI: [10.1103/PhysRevD.104.033007](https://doi.org/10.1103/PhysRevD.104.033007). arXiv: [2104.01840](https://arxiv.org/abs/2104.01840) [hep-ph].
- [488] L. T. Hue, Khiem Hong Phan, T. Phong Nguyen, H. N. Long, and H. T. Hung. “An explanation of experimental data of  $(g-2)_{e,\mu}$  in 3-3-1 models with inverse seesaw neutrinos”. In: *Eur. Phys. J. C* 82.8 (2022), p. 722. DOI: [10.1140/epjc/s10052-022-10691-5](https://doi.org/10.1140/epjc/s10052-022-10691-5). arXiv: [2109.06089](https://arxiv.org/abs/2109.06089) [hep-ph].
- [489] T. T. Hong, N. H. T. Nha, T. Phong Nguyen, L. T. T. Phuong, and L. T. Hue. “Decays  $h \rightarrow eaeb$ ,  $eb \rightarrow ea\gamma$ , and  $(g-2)_{e,\mu}$  in a 3-3-1 model with inverse seesaw neutrinos”. In: *PTEP* 2022.9 (2022), 093B05. DOI: [10.1093/ptep/ptac109](https://doi.org/10.1093/ptep/ptac109). arXiv: [2206.08028](https://arxiv.org/abs/2206.08028) [hep-ph].
- [490] A. L. Cherchiglia and O. L. G. Peres. “On the viability of a light scalar spectrum for 3-3-1 models”. In: *JHEP* 04 (2023), p. 017. DOI: [10.1007/JHEP04\(2023\)017](https://doi.org/10.1007/JHEP04(2023)017). arXiv: [2209.12063](https://arxiv.org/abs/2209.12063) [hep-ph].
- [491] A. E. Cárcamo Hernández, Sergey Kovalenko, Farinaldo S. Queiroz, and Yoxara S. Villamizar. “An extended 3-3-1 model with radiative linear seesaw mechanism”. In: *Phys. Lett. B* 829 (2022), p. 137082. DOI: [10.1016/j.physletb.2022.137082](https://doi.org/10.1016/j.physletb.2022.137082). arXiv: [2105.01731](https://arxiv.org/abs/2105.01731) [hep-ph].
- [492] V. H. Binh, Cesar Bonilla, A. E. Cárcamo Hernández, D. T. Huong, Vishnudath K. N., H. N. Long, P. N. Thu, and Iván Schmidt. “Phenomenology of 3-3-1 models with a radiative inverse seesaw mechanism”. In: *Phys. Rev. D* 110.7 (2024), p. 075022. DOI: [10.1103/PhysRevD.110.075022](https://doi.org/10.1103/PhysRevD.110.075022). arXiv: [2404.13373](https://arxiv.org/abs/2404.13373) [hep-ph].
- [493] A. E. Cárcamo Hernández, Hoang Ngoc Long, M. L. Mora-Urrutia, N. H. Thao, and V. V. Vien. “Fermion masses and mixings and  $g-2$  muon anomaly in a 3-3-1 model with  $D_4$  family symmetry”. In: *Eur. Phys. J. C* 82.8 (2022), p. 769. DOI: [10.1140/epjc/s10052-022-10639-9](https://doi.org/10.1140/epjc/s10052-022-10639-9). arXiv: [2104.04559](https://arxiv.org/abs/2104.04559) [hep-ph].
- [494] T. T. Hong, L. T. T. Phuong, T. Phong Nguyen, N. H. T. Nha, and L. T. Hue. “ $(g-2)_{e,\mu}$  anomalies and decays  $h, Z \rightarrow ebea$  in 3-3-1 models with inverse seesaw neutrinos”. In: *Phys. Rev. D* 110.7 (2024), p. 075010. DOI: [10.1103/PhysRevD.110.075010](https://doi.org/10.1103/PhysRevD.110.075010). arXiv: [2404.05524](https://arxiv.org/abs/2404.05524) [hep-ph].
- [495] A. Doff and C. A. de S. Pires. “Introducing scalar leptoquarks into a 3-3-1 model to solve the  $(g-2)_\mu$  puzzle”. In: *Phys. Lett. B* 854 (2024), p. 138733. DOI: [10.1016/j.physletb.2024.138733](https://doi.org/10.1016/j.physletb.2024.138733). arXiv: [2403.19338](https://arxiv.org/abs/2403.19338) [hep-ph].
- [496] Kai-Feng Chen, Cheng-Wei Chiang, and Kei Yagyu. “An explanation for the muon and electron  $g-2$  anomalies and dark matter”. In: *JHEP* 09 (2020), p. 119. DOI: [10.1007/JHEP09\(2020\)119](https://doi.org/10.1007/JHEP09(2020)119). arXiv: [2006.07929](https://arxiv.org/abs/2006.07929) [hep-ph].
- [497] Shun-Ichi Horigome, Taisuke Katayose, Shigeki Matsumoto, and Ipsita Saha. “Leptophilic fermion WIMP: Role of future lepton colliders”. In: *Phys. Rev. D* 104.5 (2021), p. 055001. DOI: [10.1103/PhysRevD.104.055001](https://doi.org/10.1103/PhysRevD.104.055001). arXiv: [2102.08645](https://arxiv.org/abs/2102.08645) [hep-ph].
- [498] Debasish Borah, Satyabrata Mahapatra, Dibyendu Nanda, Sujit Kumar Sahoo, and Narendra Sahu. “Singlet-doublet fermion Dark Matter with Dirac neutrino mass,  $(g-2)_\mu$  and  $\Delta N_{eff}$ ”. In: *JHEP* 05 (2024), p. 096. DOI: [10.1007/JHEP05\(2024\)096](https://doi.org/10.1007/JHEP05(2024)096). arXiv: [2310.03721](https://arxiv.org/abs/2310.03721) [hep-ph].

- [499] Talal Ahmed Chowdhury and Shaikh Saad. “Non-Abelian vector dark matter and lepton  $g-2$ ”. In: *JCAP* 10 (2021), p. 014. DOI: [10.1088/1475-7516/2021/10/014](https://doi.org/10.1088/1475-7516/2021/10/014). arXiv: [2107.11863](https://arxiv.org/abs/2107.11863) [[hep-ph](#)].
- [500] Gerrit Bickendorf and Manuel Drees. “Constraints on light leptophilic dark matter mediators from decay experiments”. In: *Eur. Phys. J. C* 82.12 (2022), p. 1163. DOI: [10.1140/epjc/s10052-022-11128-9](https://doi.org/10.1140/epjc/s10052-022-11128-9). arXiv: [2206.05038](https://arxiv.org/abs/2206.05038) [[hep-ph](#)].
- [501] Seong Chan Park and H. S. Song. “Muon anomalous magnetic moment and the stabilized Randall-Sundrum scenario”. In: *Phys. Lett. B* 506 (2001), pp. 99–102. DOI: [10.1016/S0370-2693\(01\)00417-8](https://doi.org/10.1016/S0370-2693(01)00417-8). arXiv: [hep-ph/0103072](https://arxiv.org/abs/hep-ph/0103072).
- [502] C. S. Kim, J. D. Kim, and Jeong-Hyeon Song. “Muon anomalous magnetic moment ( $g-2$ )(muon) and the Randall-Sundrum model”. In: *Phys. Lett. B* 511 (2001), pp. 251–256. DOI: [10.1016/S0370-2693\(01\)00635-9](https://doi.org/10.1016/S0370-2693(01)00635-9). arXiv: [hep-ph/0103127](https://arxiv.org/abs/hep-ph/0103127).
- [503] K. Agashe, N. G. Deshpande, and G. H. Wu. “Can extra dimensions accessible to the SM explain the recent measurement of anomalous magnetic moment of the muon?” In: *Phys. Lett. B* 511 (2001), pp. 85–91. DOI: [10.1016/S0370-2693\(01\)00488-9](https://doi.org/10.1016/S0370-2693(01)00488-9). arXiv: [hep-ph/0103235](https://arxiv.org/abs/hep-ph/0103235).
- [504] Xavier Calmet and Andrey Neronov. “Kaluza-Klein theories and the anomalous magnetic moment of the muon”. In: *Phys. Rev. D* 65 (2002), p. 067702. DOI: [10.1103/PhysRevD.65.067702](https://doi.org/10.1103/PhysRevD.65.067702). arXiv: [hep-ph/0104278](https://arxiv.org/abs/hep-ph/0104278).
- [505] Zhao-Hua Xiong and Jin Min Yang. “Muon anomalous magnetic moment in technicolor models”. In: *Phys. Lett. B* 508 (2001), pp. 295–300. DOI: [10.1016/S0370-2693\(01\)00521-4](https://doi.org/10.1016/S0370-2693(01)00521-4). arXiv: [hep-ph/0102259](https://arxiv.org/abs/hep-ph/0102259).
- [506] Xavier Calmet, Harald Fritzsch, and Dirk Holtmannspotter. “The Anomalous magnetic moment of the muon and radiative lepton decays”. In: *Phys. Rev. D* 64 (2001), p. 037701. DOI: [10.1103/PhysRevD.64.037701](https://doi.org/10.1103/PhysRevD.64.037701). arXiv: [hep-ph/0103012](https://arxiv.org/abs/hep-ph/0103012).
- [507] Yuan-Ben Dai, Chao-Shang Huang, and Ailin Zhang. “ $g-2$  in composite models of leptons”. In: *J. Phys. G* 28 (2002), pp. 139–150. DOI: [10.1088/0954-3899/28/1/310](https://doi.org/10.1088/0954-3899/28/1/310). arXiv: [hep-ph/0103317](https://arxiv.org/abs/hep-ph/0103317).
- [508] Chong-xing Yue, Qing-jun Xu, and Guo-li Liu. “Topcolor assisted technicolor models and muon anomalous magnetic moment”. In: *J. Phys. G* 27 (2001), pp. 1807–1812. DOI: [10.1088/0954-3899/27/8/310](https://doi.org/10.1088/0954-3899/27/8/310). arXiv: [hep-ph/0103084](https://arxiv.org/abs/hep-ph/0103084).
- [509] Thomas Appelquist and Bogdan A. Dobrescu. “Universal extra dimensions and the muon magnetic moment”. In: *Phys. Lett. B* 516 (2001). Ed. by Paul Frampton and Jack Ng, pp. 85–91. DOI: [10.1016/S0370-2693\(01\)00901-7](https://doi.org/10.1016/S0370-2693(01)00901-7). arXiv: [hep-ph/0106140](https://arxiv.org/abs/hep-ph/0106140).
- [510] Prasanta Kumar Das. “Muon anomalous magnetic moment and a lower bound on Higgs mass due to stabilized radion in the Randall-Sundrum model”. In: *Int. J. Mod. Phys. A* 21 (2006), pp. 5205–5220. DOI: [10.1142/S0217751X06033222](https://doi.org/10.1142/S0217751X06033222). arXiv: [hep-ph/0407041](https://arxiv.org/abs/hep-ph/0407041).
- [511] F. Tabbakh, Jing-Jing Liu, and Wen-Gan Ma. “Muon  $g-2$  in the littlest Higgs model”. In: *Commun. Theor. Phys.* 45 (2006), pp. 894–900. DOI: [10.1088/0253-6102/45/5/026](https://doi.org/10.1088/0253-6102/45/5/026).
- [512] Monika Blanke, Andrzej J. Buras, Bjoern Duling, Anton Poschenrieder, and Cecilia Tarantino. “Charged Lepton Flavour Violation and ( $g-2$ )( $\mu$ ) in the Littlest Higgs Model with T-Parity: A Clear Distinction from Supersymmetry”. In: *JHEP* 05 (2007), p. 013. DOI: [10.1088/1126-6708/2007/05/013](https://doi.org/10.1088/1126-6708/2007/05/013). arXiv: [hep-ph/0702136](https://arxiv.org/abs/hep-ph/0702136).

- [513] Andi Hektor, Yuji Kajiyama, and Kristjan Kannike. “Muon Anomalous Magnetic Moment and Lepton Flavor Violating Tau Decay in Unparticle Physics”. In: *Phys. Rev. D* 78 (2008), p. 053008. DOI: [10.1103/PhysRevD.78.053008](https://doi.org/10.1103/PhysRevD.78.053008). arXiv: [0802.4015 \[hep-ph\]](https://arxiv.org/abs/0802.4015).
- [514] R. S. Hundi, Sourov Roy, and Soumitra SenGupta. “Muon ( $g-2$ ) from the bulk neutrino field in a warped extra dimensional model”. In: *Phys. Rev. D* 86 (2012), p. 036014. DOI: [10.1103/PhysRevD.86.036014](https://doi.org/10.1103/PhysRevD.86.036014). arXiv: [1206.5137 \[hep-ph\]](https://arxiv.org/abs/1206.5137).
- [515] A. Doff and Clarissa Siqueira. “Composite Higgs Models, Technicolor and The Muon Anomalous Magnetic Moment”. In: *Phys. Lett. B* 754 (2016), pp. 294–301. DOI: [10.1016/j.physletb.2016.01.043](https://doi.org/10.1016/j.physletb.2016.01.043). arXiv: [1512.03256 \[hep-ph\]](https://arxiv.org/abs/1512.03256).
- [516] Deog Ki Hong and Du Hwan Kim. “Composite (pseudo) scalar contributions to muon  $g - 2$ ”. In: *Phys. Lett. B* 758 (2016), pp. 370–372. DOI: [10.1016/j.physletb.2016.05.034](https://doi.org/10.1016/j.physletb.2016.05.034). arXiv: [1602.06628 \[hep-ph\]](https://arxiv.org/abs/1602.06628).
- [517] Eugenio Megias, Mariano Quiros, and Lindber Salas. “ $g_\mu - 2$  from Vector-Like Leptons in Warped Space”. In: *JHEP* 05 (2017), p. 016. DOI: [10.1007/JHEP05\(2017\)016](https://doi.org/10.1007/JHEP05(2017)016). arXiv: [1701.05072 \[hep-ph\]](https://arxiv.org/abs/1701.05072).
- [518] Luis A. Anchordoqui, Ignatios Antoniadis, Xing Huang, Dieter Lüster, François Rondeau, and Tomasz R. Taylor. “Leptophilic U(1) Massive Vector Bosons from Large Extra Dimensions: Reexamination of Constraints from LEP Data”. In: *Phys. Lett. B* 828 (2022), p. 137014. DOI: [10.1016/j.physletb.2022.137014](https://doi.org/10.1016/j.physletb.2022.137014). arXiv: [2110.01247 \[hep-ph\]](https://arxiv.org/abs/2110.01247).
- [519] Luis A. Anchordoqui, Ignatios Antoniadis, Xing Huang, Dieter Lust, and Tomasz R. Taylor. “Leptophilic U(1) massive vector bosons from large extra dimensions”. In: *Phys. Lett. B* 820 (2021), p. 136585. DOI: [10.1016/j.physletb.2021.136585](https://doi.org/10.1016/j.physletb.2021.136585). arXiv: [2105.02630 \[hep-ph\]](https://arxiv.org/abs/2105.02630).
- [520] Giacomo Cacciapaglia, Corentin Cot, and Francesco Sannino. “Naturalness of lepton non-universality and muon  $g-2$ ”. In: *Phys. Lett. B* 825 (2022), p. 136864. DOI: [10.1016/j.physletb.2021.136864](https://doi.org/10.1016/j.physletb.2021.136864). arXiv: [2104.08818 \[hep-ph\]](https://arxiv.org/abs/2104.08818).
- [521] Shuai Xu and Sibor Zheng. “Resolving muon  $g-2$  anomaly with partial compositeness”. In: *Eur. Phys. J. C* 82.10 (2022), p. 969. DOI: [10.1140/epjc/s10052-022-10949-y](https://doi.org/10.1140/epjc/s10052-022-10949-y). arXiv: [2204.05456 \[hep-ph\]](https://arxiv.org/abs/2204.05456).
- [522] Andreas Crivellin, Fiona Kirk, and Marco Schreck. “Impact of Lorentz violation on anomalous magnetic moments of charged leptons”. In: *JHEP* 11 (2022), p. 109. DOI: [10.1007/JHEP11\(2022\)109](https://doi.org/10.1007/JHEP11(2022)109). arXiv: [2208.11420 \[hep-ph\]](https://arxiv.org/abs/2208.11420).
- [523] Hai-Xing Lin, Jian Tang, Sampsa Vihonen, and Pedro Pasquini. “Nonminimal Lorentz invariance violation in light of the muon anomalous magnetic moment and long-baseline neutrino oscillation data”. In: *Phys. Rev. D* 105.9 (2022), p. 096029. DOI: [10.1103/PhysRevD.105.096029](https://doi.org/10.1103/PhysRevD.105.096029). arXiv: [2111.14336 \[hep-ph\]](https://arxiv.org/abs/2111.14336).
- [524] Da Huang, Chao-Qiang Geng, and Jiajun Wu. “Muon  $g-2$  anomaly from a massive spin-2 particle”. In: *Phys. Rev. D* 107.3 (2023), p. 035008. DOI: [10.1103/PhysRevD.107.035008](https://doi.org/10.1103/PhysRevD.107.035008). arXiv: [2207.13421 \[hep-ph\]](https://arxiv.org/abs/2207.13421).
- [525] Da Huang, Chao-Qiang Geng, and Jiajun Wu. “Unitarity bounds on the massive spin-2 particle explanation of muon  $g - 2$  anomaly”. In: *Eur. Phys. J. C* 84.3 (2024), p. 246. DOI: [10.1140/epjc/s10052-024-12569-0](https://doi.org/10.1140/epjc/s10052-024-12569-0). arXiv: [2208.01097 \[hep-ph\]](https://arxiv.org/abs/2208.01097).
- [526] Joerg Jaeckel and Andreas Ringwald. “The Low-Energy Frontier of Particle Physics”. In: *Ann. Rev. Nucl. Part. Sci.* 60 (2010), pp. 405–437. DOI: [10.1146/annurev.nucl.012809.104433](https://doi.org/10.1146/annurev.nucl.012809.104433). arXiv: [1002.0329 \[hep-ph\]](https://arxiv.org/abs/1002.0329).

- [527] Rouven Essig et al. “Working Group Report: New Light Weakly Coupled Particles”. In: *Snowmass 2013: Snowmass on the Mississippi*. Oct. 2013. arXiv: [1311.0029 \[hep-ph\]](#).
- [528] J. Beacham et al. “Physics Beyond Colliders at CERN: Beyond the Standard Model Working Group Report”. In: *J. Phys. G* 47.1 (2020), p. 010501. DOI: [10.1088/1361-6471/ab4cd2](#). arXiv: [1901.09966 \[hep-ex\]](#).
- [529] Prateek Agrawal et al. “Feebly-interacting particles: FIPs 2020 workshop report”. In: *Eur. Phys. J. C* 81.11 (2021), p. 1015. DOI: [10.1140/epjc/s10052-021-09703-7](#). arXiv: [2102.12143 \[hep-ph\]](#).
- [530] C. Antel et al. “Feebly-interacting particles: FIPs 2022 Workshop Report”. In: *Eur. Phys. J. C* 83.12 (2023), p. 1122. DOI: [10.1140/epjc/s10052-023-12168-5](#). arXiv: [2305.01715 \[hep-ph\]](#).
- [531] Jorge Martin Camalich and Robert Ziegler. “Flavor phenomenology of light dark sectors”. In: (Mar. 2025). DOI: [10.1146/annurev-nucl-121423-100931](#). arXiv: [2503.17323 \[hep-ph\]](#).
- [532] Marco Ardu, Moinul Hossain Rahat, Nicola Valori, and Oscar Vives. “Electric Dipole Moments as indirect probes of dark sectors”. In: *JHEP* 11 (2024), p. 049. DOI: [10.1007/JHEP11\(2024\)049](#). arXiv: [2407.21100 \[hep-ph\]](#).
- [533] Rodolfo Capdevilla, David Curtin, Yonatan Kahn, and Gordan Krnjaic. “Systematically testing singlet models for  $(g - 2)_\mu$ ”. In: *JHEP* 04 (2022), p. 129. DOI: [10.1007/JHEP04\(2022\)129](#). arXiv: [2112.08377 \[hep-ph\]](#).
- [534] Luc Darmé, Marco Fedele, Kamila Kowalska, and Enrico Maria Sessolo. “Flavour anomalies and the muon  $g - 2$  from feebly interacting particles”. In: *JHEP* 03 (2022), p. 085. DOI: [10.1007/JHEP03\(2022\)085](#). arXiv: [2106.12582 \[hep-ph\]](#).
- [535] Jorge Gamboa, Justo López-Sarrión, Fernando Méndez, and Natalia Tapia Arellano. “Corrections of  $Z'$  to the magnetic moment of the muon”. In: *Phys. Rev. D* 108.9 (2023), p. 095042. DOI: [10.1103/PhysRevD.108.095042](#). arXiv: [2305.00073 \[hep-ph\]](#).
- [536] Motoi Endo, Koichi Hamaguchi, and Go Mishima. “Constraints on Hidden Photon Models from Electron  $g-2$  and Hydrogen Spectroscopy”. In: *Phys. Rev. D* 86 (2012), p. 095029. DOI: [10.1103/PhysRevD.86.095029](#). arXiv: [1209.2558 \[hep-ph\]](#).
- [537] Philip Ilten, Yotam Soreq, Mike Williams, and Wei Xue. “Serendipity in dark photon searches”. In: *JHEP* 06 (2018), p. 004. DOI: [10.1007/JHEP06\(2018\)004](#). arXiv: [1801.04847 \[hep-ph\]](#).
- [538] D. Banerjee et al. “Search for a Hypothetical 16.7 MeV Gauge Boson and Dark Photons in the NA64 Experiment at CERN”. In: *Phys. Rev. Lett.* 120.23 (2018), p. 231802. DOI: [10.1103/PhysRevLett.120.231802](#). arXiv: [1803.07748 \[hep-ex\]](#).
- [539] J. R. Batley et al. “Search for the dark photon in  $\pi^0$  decays”. In: *Phys. Lett. B* 746 (2015), pp. 178–185. DOI: [10.1016/j.physletb.2015.04.068](#). arXiv: [1504.00607 \[hep-ex\]](#).
- [540] Chien-Yi Chen, Hooman Davoudiasl, William J. Marciano, and Cen Zhang. “Implications of a light “dark Higgs” solution to the  $g_\mu-2$  discrepancy”. In: *Phys. Rev. D* 93.3 (2016), p. 035006. DOI: [10.1103/PhysRevD.93.035006](#). arXiv: [1511.04715 \[hep-ph\]](#).
- [541] Gopolang Mohlabeng. “Revisiting the dark photon explanation of the muon anomalous magnetic moment”. In: *Phys. Rev. D* 99.11 (2019), p. 115001. DOI: [10.1103/PhysRevD.99.115001](#). arXiv: [1902.05075 \[hep-ph\]](#).

- [542] Yu-Dai Tsai, Patrick deNiverville, and Ming Xiong Liu. “Dark Photon and Muon  $g - 2$  Inspired Inelastic Dark Matter Models at the High-Energy Intensity Frontier”. In: *Phys. Rev. Lett.* 126.18 (2021), p. 181801. DOI: [10.1103/PhysRevLett.126.181801](https://doi.org/10.1103/PhysRevLett.126.181801). arXiv: [1908.07525](https://arxiv.org/abs/1908.07525) [hep-ph].
- [543] Shao-Feng Ge, Xiao-Dong Ma, and Pedro Pasquini. “Probing the dark axion portal with muon anomalous magnetic moment”. In: *Eur. Phys. J. C* 81.9 (2021), p. 787. DOI: [10.1140/epjc/s10052-021-09571-1](https://doi.org/10.1140/epjc/s10052-021-09571-1). arXiv: [2104.03276](https://arxiv.org/abs/2104.03276) [hep-ph].
- [544] Alakabha Datta, A. Hammad, Danny Marfatia, Lopamudra Mukherjee, and Ahmed Rashed. “Dark photon and dark Z mediated B meson decays”. In: *JHEP* 03 (2023), p. 108. DOI: [10.1007/JHEP03\(2023\)108](https://doi.org/10.1007/JHEP03(2023)108). arXiv: [2210.15662](https://arxiv.org/abs/2210.15662) [hep-ph].
- [545] George N. Wojcik, Lisa L. Everett, Shu Tian Eu, and Ricardo Ximenes. “Portal matter, kinetic mixing, and muon  $g - 2$ ”. In: *Phys. Lett. B* 841 (2023), p. 137931. DOI: [10.1016/j.physletb.2023.137931](https://doi.org/10.1016/j.physletb.2023.137931). arXiv: [2211.09918](https://arxiv.org/abs/2211.09918) [hep-ph].
- [546] Waleed Abdallah, Mustafa Ashry, Junichiro Kawamura, and Ahmad Moursy. “Semivisible dark photon in a model with vectorlike leptons for the  $(g-2)_e, \mu$  and W-boson mass anomalies”. In: *Phys. Rev. D* 109.1 (2024), p. 015031. DOI: [10.1103/PhysRevD.109.015031](https://doi.org/10.1103/PhysRevD.109.015031). arXiv: [2308.05691](https://arxiv.org/abs/2308.05691) [hep-ph].
- [547] Asli M. Abdullahi, Matheus Hostert, Daniele Massaro, and Silvia Pascoli. “Semi-Visible Dark Photon Phenomenology at the GeV Scale”. In: *Phys. Rev. D* 108.1 (2023), p. 015032. DOI: [10.1103/PhysRevD.108.015032](https://doi.org/10.1103/PhysRevD.108.015032). arXiv: [2302.05410](https://arxiv.org/abs/2302.05410) [hep-ph].
- [548] Keisuke Harigaya, Evan Petrosky, and Aaron Pierce. “Precision electroweak tensions and a dark photon”. In: *JHEP* 07 (2024), p. 201. DOI: [10.1007/JHEP07\(2024\)201](https://doi.org/10.1007/JHEP07(2024)201). arXiv: [2307.13045](https://arxiv.org/abs/2307.13045) [hep-ph].
- [549] Alexey S. Zhevlakov, Dmitry V. Kirpichnikov, and Valery E. Lyubovitskij. “Lepton flavor violating dark photon”. In: *Phys. Rev. D* 109.1 (2024), p. 015015. DOI: [10.1103/PhysRevD.109.015015](https://doi.org/10.1103/PhysRevD.109.015015). arXiv: [2307.10771](https://arxiv.org/abs/2307.10771) [hep-ph].
- [550] Yu. M. Andreev et al. “Search for Light Dark Matter with NA64 at CERN”. In: *Phys. Rev. Lett.* 131.16 (2023), p. 161801. DOI: [10.1103/PhysRevLett.131.161801](https://doi.org/10.1103/PhysRevLett.131.161801). arXiv: [2307.02404](https://arxiv.org/abs/2307.02404) [hep-ex].
- [551] Asli Abdullahi, Matheus Hostert, and Silvia Pascoli. “A dark seesaw solution to low energy anomalies: MiniBooNE, the muon  $(g - 2)$ , and BaBar”. In: *Phys. Lett. B* 820 (2021), p. 136531. DOI: [10.1016/j.physletb.2021.136531](https://doi.org/10.1016/j.physletb.2021.136531). arXiv: [2007.11813](https://arxiv.org/abs/2007.11813) [hep-ph].
- [552] Zhaofeng Kang and Yoshihiro Shigekami. “ $(g - 2)_\mu$  versus  $K \rightarrow \pi + E_{miss}$  induced by the  $(B - L)_{23}$  boson”. In: *JHEP* 04 (2021), p. 238. DOI: [10.1007/JHEP04\(2021\)238](https://doi.org/10.1007/JHEP04(2021)238). arXiv: [2008.09793](https://arxiv.org/abs/2008.09793) [hep-ph].
- [553] Jian-Yong Cen, Yu Cheng, Xiao-Gang He, and Jin Sun. “Flavor specific  $U(1)_{Bq-L\mu}$  gauge model for muon  $g - 2$  and  $b \rightarrow s\mu^-\mu$  anomalies”. In: *Nucl. Phys. B* 978 (2022), p. 115762. DOI: [10.1016/j.nuclphysb.2022.115762](https://doi.org/10.1016/j.nuclphysb.2022.115762). arXiv: [2104.05006](https://arxiv.org/abs/2104.05006) [hep-ph].
- [554] Talal Ahmed Chowdhury, Md. Ehsanuzzaman, and Shaikh Saad. “Dark Matter and  $(g - 2)_{\mu,e}$  in radiative Dirac neutrino mass models”. In: *JCAP* 08 (2022), p. 076. DOI: [10.1088/1475-7516/2022/08/076](https://doi.org/10.1088/1475-7516/2022/08/076). arXiv: [2203.14983](https://arxiv.org/abs/2203.14983) [hep-ph].
- [555] P. M. Ferreira, B. L. Gonçalves, and F. R. Joaquim. “A closer look at the  $U(1)_{B-L}$  explanation of the ATOMKI nuclear anomalies”. In: *JHEP* 04 (2024), p. 003. DOI: [10.1007/JHEP04\(2024\)003](https://doi.org/10.1007/JHEP04(2024)003). arXiv: [2311.18004](https://arxiv.org/abs/2311.18004) [hep-ph].

- [556] Sumit Ghosh and Pyungwon Ko. “Explaining ATOMKI,  $(g-2)_\mu$ , and MiniBooNE anomalies with light mediators in  $U(1)_H$  extended model”. In: (Nov. 2023). arXiv: [2311.14099 \[hep-ph\]](#).
- [557] Hye-Sung Lee. “Muon  $g-2$  anomaly and dark leptonic gauge boson”. In: *Phys. Rev. D* 90.9 (2014), p. 091702. DOI: [10.1103/PhysRevD.90.091702](#). arXiv: [1408.4256 \[hep-ph\]](#).
- [558] Takaaki Nomura, Hiroshi Okada, and Yuichi Uesaka. “A two-loop induced neutrino mass model, dark matter, and LFV processes  $\ell_i \rightarrow \ell_j \gamma$ , and  $\mu e \rightarrow ee$  in a hidden local  $U(1)$  symmetry”. In: *Nucl. Phys. B* 962 (2021), p. 115236. DOI: [10.1016/j.nuclphysb.2020.115236](#). arXiv: [2008.02673 \[hep-ph\]](#).
- [559] Dan Hooper, Joaquim Iguaz Juan, and Pasquale D. Serpico. “Signals of a new gauge boson from IceCube and the muon  $g-2$ ”. In: *Phys. Rev. D* 108.2 (2023), p. 023007. DOI: [10.1103/PhysRevD.108.023007](#). arXiv: [2302.03571 \[astro-ph.HE\]](#).
- [560] Rishu Verma, Ankush, and B. C. Chauhan. “Electron and Muon  $(g-2)_{e,\mu}$  Anomalous Magnetic Moment in  $U(1)_{L_e-L_\mu}$  Symmetry Model”. In: (Apr. 2024). arXiv: [2404.13546 \[hep-ph\]](#).
- [561] Admir Greljo, Peter Stangl, Anders Eller Thomsen, and Jure Zupan. “On  $(g-2)_\mu$  from gauged  $U(1)_X$ ”. In: *JHEP* 07 (2022), p. 098. DOI: [10.1007/JHEP07\(2022\)098](#). arXiv: [2203.13731 \[hep-ph\]](#).
- [562] Robert Foot. “New Physics From Electric Charge Quantization?” In: *Mod. Phys. Lett. A* 6 (1991), pp. 527–530. DOI: [10.1142/S0217732391000543](#).
- [563] Takeshi Araki, Fumihiro Kaneko, Toshihiko Ota, Joe Sato, and Takashi Shimomura. “MeV scale leptonic force for cosmic neutrino spectrum and muon anomalous magnetic moment”. In: *Phys. Rev. D* 93.1 (2016), p. 013014. DOI: [10.1103/PhysRevD.93.013014](#). arXiv: [1508.07471 \[hep-ph\]](#).
- [564] Wolfgang Altmannshofer, Chien-Yi Chen, P. S. Bhupal Dev, and Amarjit Soni. “Lepton flavor violating  $Z'$  explanation of the muon anomalous magnetic moment”. In: *Phys. Lett. B* 762 (2016), pp. 389–398. DOI: [10.1016/j.physletb.2016.09.046](#). arXiv: [1607.06832 \[hep-ph\]](#).
- [565] Seungwon Baek, N. G. Deshpande, X. G. He, and P. Ko. “Muon anomalous  $g-2$  and gauged  $L(\mu) - L(\tau)$  models”. In: *Phys. Rev. D* 64 (2001), p. 055006. DOI: [10.1103/PhysRevD.64.055006](#). arXiv: [hep-ph/0104141](#).
- [566] Ernest Ma, D. P. Roy, and Sourov Roy. “Gauged  $L(\mu) - L(\tau)$  with large muon anomalous magnetic moment and the bimaximal mixing of neutrinos”. In: *Phys. Lett. B* 525 (2002), pp. 101–106. DOI: [10.1016/S0370-2693\(01\)01428-9](#). arXiv: [hep-ph/0110146](#).
- [567] Julian Heeck and Werner Rodejohann. “Gauged  $L_\mu - L_\tau$  Symmetry at the Electroweak Scale”. In: *Phys. Rev. D* 84 (2011), p. 075007. DOI: [10.1103/PhysRevD.84.075007](#). arXiv: [1107.5238 \[hep-ph\]](#).
- [568] Wolfgang Altmannshofer, Stefania Gori, Maxim Pospelov, and Itay Yavin. “Quark flavor transitions in  $L_\mu - L_\tau$  models”. In: *Phys. Rev. D* 89 (2014), p. 095033. DOI: [10.1103/PhysRevD.89.095033](#). arXiv: [1403.1269 \[hep-ph\]](#).
- [569] Wolfgang Altmannshofer, Stefania Gori, Maxim Pospelov, and Itay Yavin. “Neutrino Trident Production: A Powerful Probe of New Physics with Neutrino Beams”. In: *Phys. Rev. Lett.* 113 (2014), p. 091801. DOI: [10.1103/PhysRevLett.113.091801](#). arXiv: [1406.2332 \[hep-ph\]](#).
- [570] D. Geiregat et al. “First observation of neutrino trident production”. In: *Phys. Lett. B* 245 (1990), pp. 271–275. DOI: [10.1016/0370-2693\(90\)90146-W](#).

- [571] S. R. Mishra et al. “Neutrino Tridents and W Z Interference”. In: *Phys. Rev. Lett.* 66 (1991), pp. 3117–3120. DOI: [10.1103/PhysRevLett.66.3117](https://doi.org/10.1103/PhysRevLett.66.3117).
- [572] T. Adams et al. “Neutrino trident production from NuTeV”. In: *29th International Conference on High-Energy Physics*. July 1998, pp. 631–634. arXiv: [hep-ex/9811012](https://arxiv.org/abs/hep-ex/9811012).
- [573] Martin Bauer, Patrick Foldenauer, and Joerg Jaeckel. “Hunting All the Hidden Photons”. In: *JHEP* 07 (2018), p. 094. DOI: [10.1007/JHEP07\(2018\)094](https://doi.org/10.1007/JHEP07(2018)094). arXiv: [1803.05466](https://arxiv.org/abs/1803.05466) [[hep-ph](#)].
- [574] Yu. M. Andreev et al. “First constraints on the  $L_\mu - L_\tau$  explanation of the muon  $g-2$  anomaly from NA64-e at CERN”. In: *JHEP* 07 (2024), p. 212. DOI: [10.1007/JHEP07\(2024\)212](https://doi.org/10.1007/JHEP07(2024)212). arXiv: [2404.06982](https://arxiv.org/abs/2404.06982) [[hep-ex](#)].
- [575] Yu. M. Andreev et al. “Shedding light on dark sectors with high-energy muons at the NA64 experiment at the CERN SPS”. In: *Phys. Rev. D* 110.11 (2024), p. 112015. DOI: [10.1103/PhysRevD.110.112015](https://doi.org/10.1103/PhysRevD.110.112015). arXiv: [2409.10128](https://arxiv.org/abs/2409.10128) [[hep-ex](#)].
- [576] Hugh C. Harris et al. “The white dwarf luminosity function from sdss imaging data”. In: *Astron. J.* 131 (2006), pp. 571–581. DOI: [10.1086/497966](https://doi.org/10.1086/497966). arXiv: [astro-ph/0510820](https://arxiv.org/abs/astro-ph/0510820).
- [577] Steven DeGennaro, Ted von Hippel, D. E. Winget, S. O. Kepler, Atsuko Nitta, Detlev Koester, and Leandro Althaus. “White Dwarf Luminosity and Mass Functions from Sloan Digital Sky Survey Spectra”. In: *Astron. J.* 135 (2008), pp. 1–9. DOI: [10.1088/0004-6256/135/1/1](https://doi.org/10.1088/0004-6256/135/1/1). arXiv: [0709.2190](https://arxiv.org/abs/0709.2190) [[astro-ph](#)].
- [578] Herbert K. Dreiner, Jean-François Fortin, Jordi Isern, and Lorenzo Ubaldi. “White Dwarfs constrain Dark Forces”. In: *Phys. Rev. D* 88 (2013), p. 043517. DOI: [10.1103/PhysRevD.88.043517](https://doi.org/10.1103/PhysRevD.88.043517). arXiv: [1303.7232](https://arxiv.org/abs/1303.7232) [[hep-ph](#)].
- [579] Patrick Foldenauer and Jaime Hoefken Zink. “How to rule out  $(g - 2)_\mu$  in  $U(1)_{L_\mu - L_\tau}$  with white dwarf cooling”. In: *JHEP* 07 (2024), p. 096. DOI: [10.1007/JHEP07\(2024\)096](https://doi.org/10.1007/JHEP07(2024)096). arXiv: [2405.00094](https://arxiv.org/abs/2405.00094) [[hep-ph](#)].
- [580] Dorian Warren Praia do Amaral, David G. Cerdeno, Patrick Foldenauer, and Elliott Reid. “Solar neutrino probes of the muon anomalous magnetic moment in the gauged  $U(1)_{L_\mu - L_\tau}$ ”. In: *JHEP* 12 (2020), p. 155. DOI: [10.1007/JHEP12\(2020\)155](https://doi.org/10.1007/JHEP12(2020)155). arXiv: [2006.11225](https://arxiv.org/abs/2006.11225) [[hep-ph](#)].
- [581] D. W. P. Amaral, D. G. Cerdeno, A. Cheek, and P. Foldenauer. “Confirming  $U(1)_{L_\mu - L_\tau}$  as a solution for  $(g - 2)_\mu$  with neutrinos”. In: *Eur. Phys. J. C* 81.10 (2021), p. 861. DOI: [10.1140/epjc/s10052-021-09670-z](https://doi.org/10.1140/epjc/s10052-021-09670-z). arXiv: [2104.03297](https://arxiv.org/abs/2104.03297) [[hep-ph](#)].
- [582] Miguel Escudero, Dan Hooper, Gordan Krnjaic, and Mathias Pierre. “Cosmology with A Very Light  $L_\mu - L_\tau$  Gauge Boson”. In: *JHEP* 03 (2019), p. 071. DOI: [10.1007/JHEP03\(2019\)071](https://doi.org/10.1007/JHEP03(2019)071). arXiv: [1901.02010](https://arxiv.org/abs/1901.02010) [[hep-ph](#)].
- [583] Claudio Andrea Manzari, Jorge Martin Camalich, Jonas Spinner, and Robert Ziegler. “Supernova limits on muonic dark forces”. In: *Phys. Rev. D* 108.10 (2023), p. 103020. DOI: [10.1103/PhysRevD.108.103020](https://doi.org/10.1103/PhysRevD.108.103020). arXiv: [2307.03143](https://arxiv.org/abs/2307.03143) [[hep-ph](#)].
- [584] N. Aghanim et al. “Planck 2018 results. VI. Cosmological parameters”. In: *Astron. Astrophys.* 641 (2020). [Erratum: *Astron. Astrophys.* 652, C4 (2021)], A6. DOI: [10.1051/0004-6361/201833910](https://doi.org/10.1051/0004-6361/201833910). arXiv: [1807.06209](https://arxiv.org/abs/1807.06209) [[astro-ph.CO](#)].
- [585] Manuel Drees and Wenbin Zhao. “ $U(1)_{L_\mu - L_\tau}$  for light dark matter,  $g\mu - 2$ , the 511 keV excess and the Hubble tension”. In: *Phys. Lett. B* 827 (2022), p. 136948. DOI: [10.1016/j.physletb.2022.136948](https://doi.org/10.1016/j.physletb.2022.136948). arXiv: [2107.14528](https://arxiv.org/abs/2107.14528) [[hep-ph](#)].

- [586] Eleonora Di Valentino, Olga Mena, Supriya Pan, Luca Visinelli, Weiqiang Yang, Alessandro Melchiorri, David F. Mota, Adam G. Riess, and Joseph Silk. “In the realm of the Hubble tension—a review of solutions”. In: *Class. Quant. Grav.* 38.15 (2021), p. 153001. DOI: [10.1088/1361-6382/ac086d](https://doi.org/10.1088/1361-6382/ac086d). arXiv: [2103.01183](https://arxiv.org/abs/2103.01183) [[astro-ph.CO](#)].
- [587] S. N. Gninenko, N. V. Krasnikov, and V. A. Matveev. “Muon  $g-2$  and searches for a new leptophobic sub-GeV dark boson in a missing-energy experiment at CERN”. In: *Phys. Rev. D* 91 (2015), p. 095015. DOI: [10.1103/PhysRevD.91.095015](https://doi.org/10.1103/PhysRevD.91.095015). arXiv: [1412.1400](https://arxiv.org/abs/1412.1400) [[hep-ph](#)].
- [588] Wolfgang Altmannshofer, Marcela Carena, and Andreas Crivellin. “ $L_\mu - L_\tau$  theory of Higgs flavor violation and  $(g - 2)_\mu$ ”. In: *Phys. Rev. D* 94.9 (2016), p. 095026. DOI: [10.1103/PhysRevD.94.095026](https://doi.org/10.1103/PhysRevD.94.095026). arXiv: [1604.08221](https://arxiv.org/abs/1604.08221) [[hep-ph](#)].
- [589] Sudhanwa Patra, Soumya Rao, Nirakar Sahoo, and Narendra Sahu. “Gauged  $U(1)_{L_\mu-L_\tau}$  model in light of muon  $g - 2$  anomaly, neutrino mass and dark matter phenomenology”. In: *Nucl. Phys. B* 917 (2017), pp. 317–336. DOI: [10.1016/j.nuclphysb.2017.02.010](https://doi.org/10.1016/j.nuclphysb.2017.02.010). arXiv: [1607.04046](https://arxiv.org/abs/1607.04046) [[hep-ph](#)].
- [590] Anirban Biswas, Sandhya Choubey, and Sarif Khan. “FIMP and Muon  $(g - 2)$  in a  $U(1)_{L_\mu-L_\tau}$  Model”. In: *JHEP* 02 (2017), p. 123. DOI: [10.1007/JHEP02\(2017\)123](https://doi.org/10.1007/JHEP02(2017)123). arXiv: [1612.03067](https://arxiv.org/abs/1612.03067) [[hep-ph](#)].
- [591] S. N. Gninenko and N. V. Krasnikov. “Probing the muon  $g_\mu - 2$  anomaly,  $L_\mu - L_\tau$  gauge boson and Dark Matter in dark photon experiments”. In: *Phys. Lett. B* 783 (2018), pp. 24–28. DOI: [10.1016/j.physletb.2018.06.043](https://doi.org/10.1016/j.physletb.2018.06.043). arXiv: [1801.10448](https://arxiv.org/abs/1801.10448) [[hep-ph](#)].
- [592] Jose Alonso Carpio, Kohta Murase, Ian M. Shoemaker, and Zahra Tabrizi. “High-energy cosmic neutrinos as a probe of the vector mediator scenario in light of the muon  $g-2$  anomaly and Hubble tension”. In: *Phys. Rev. D* 107.10 (2023), p. 103057. DOI: [10.1103/PhysRevD.107.103057](https://doi.org/10.1103/PhysRevD.107.103057). arXiv: [2104.15136](https://arxiv.org/abs/2104.15136) [[hep-ph](#)].
- [593] Timothy Hapitas, Douglas Tuckler, and Yue Zhang. “General kinetic mixing in gauged  $U(1)_{L_\mu-L_\tau}$  model for muon  $g-2$  and dark matter”. In: *Phys. Rev. D* 105.1 (2022), p. 016014. DOI: [10.1103/PhysRevD.105.016014](https://doi.org/10.1103/PhysRevD.105.016014). arXiv: [2108.12440](https://arxiv.org/abs/2108.12440) [[hep-ph](#)].
- [594] Yu Cheng, Xiao-Gang He, and Jin Sun. “Widening the  $U(1)_{L_\mu-L_\tau Z}$  mass range for resolving the muon  $g - 2$  anomaly”. In: *Phys. Lett. B* 827 (2022), p. 136989. DOI: [10.1016/j.physletb.2022.136989](https://doi.org/10.1016/j.physletb.2022.136989). arXiv: [2112.09920](https://arxiv.org/abs/2112.09920) [[hep-ph](#)].
- [595] Keiko I. Nagao, Takaaki Nomura, Hiroshi Okada, and Takashi Shimomura. “Neutrinophilic dark-matter annihilation in a model with  $U(1)_{L_\mu-L_\tau} \times U(1)_H$  gauge symmetry”. In: *Phys. Rev. D* 108.5 (2023), p. 055032. DOI: [10.1103/PhysRevD.108.055032](https://doi.org/10.1103/PhysRevD.108.055032). arXiv: [2212.14528](https://arxiv.org/abs/2212.14528) [[hep-ph](#)].
- [596] Sougata Ganguly, Sourov Roy, and Ananya Tapadar. “Secluded dark sector and muon  $(g-2)$  in the light of fast expanding Universe”. In: *JCAP* 02 (2023), p. 044. DOI: [10.1088/1475-7516/2023/02/044](https://doi.org/10.1088/1475-7516/2023/02/044). arXiv: [2208.13608](https://arxiv.org/abs/2208.13608) [[hep-ph](#)].
- [597] Jie Wang, Jinghong Ma, Jing Gao, Xiao-Fang Han, and Lei Wang. “ $U(1)_{L_\mu-L_\tau}$  breaking phase transition, muon  $g-2$ , dark matter, collider, and gravitational wave<sup>\*</sup>”. In: *Chin. Phys. C* 48.2 (2024), p. 023101. DOI: [10.1088/1674-1137/ad0f89](https://doi.org/10.1088/1674-1137/ad0f89). arXiv: [2309.09210](https://arxiv.org/abs/2309.09210) [[hep-ph](#)].
- [598] Arnab Paul, Sourov Roy, and Abhijit Kumar Saha. “Gauged  $L_\mu-L_\tau$  Model: Satisfying Cosmic Inflation and Anomalous  $(g - 2)_\mu$ ”. In: *Springer Proc. Phys.* 304 (2024), pp. 1138–1140. DOI: [10.1007/978-981-97-0289-3\\_315](https://doi.org/10.1007/978-981-97-0289-3_315).

- [599] Kento Asai, Coh Miyao, Shohei Okawa, and Koji Tsumura. “New constraints on gauged  $U(1)_{L_\mu-L_\tau}$  models via  $Z - Z'$  mixing”. In: *JHEP* 12 (2024), p. 018. DOI: [10.1007/JHEP12\(2024\)018](https://doi.org/10.1007/JHEP12(2024)018). arXiv: [2401.17613](https://arxiv.org/abs/2401.17613) [hep-ph].
- [600] Guo-yuan Huang, Farinaldo S. Queiroz, and Werner Rodejohann. “Gauged  $L_\mu-L_\tau$  at a muon collider”. In: *Phys. Rev. D* 103.9 (2021), p. 095005. DOI: [10.1103/PhysRevD.103.095005](https://doi.org/10.1103/PhysRevD.103.095005). arXiv: [2101.04956](https://arxiv.org/abs/2101.04956) [hep-ph].
- [601] Connor Brown, Juri Fiaschi, Oliver Fischer, and Thomas Teubner. “Systematic analysis of search strategies for  $L_\mu - L_\tau$  gauge bosons at Belle II”. In: *JHEP* 10 (2024), p. 233. DOI: [10.1007/JHEP10\(2024\)233](https://doi.org/10.1007/JHEP10(2024)233). arXiv: [2406.10204](https://arxiv.org/abs/2406.10204) [hep-ph].
- [602] Patrick Foldenauer. “Light dark matter in a gauged  $U(1)_{L_\mu-L_\tau}$  model”. In: *Phys. Rev. D* 99.3 (2019), p. 035007. DOI: [10.1103/PhysRevD.99.035007](https://doi.org/10.1103/PhysRevD.99.035007). arXiv: [1808.03647](https://arxiv.org/abs/1808.03647) [hep-ph].
- [603] Ian Holst, Dan Hooper, and Gordan Krnjaic. “Simplest and Most Predictive Model of Muon  $g-2$  and Thermal Dark Matter”. In: *Phys. Rev. Lett.* 128.14 (2022), p. 141802. DOI: [10.1103/PhysRevLett.128.141802](https://doi.org/10.1103/PhysRevLett.128.141802). arXiv: [2107.09067](https://arxiv.org/abs/2107.09067) [hep-ph].
- [604] XinXin Qi, AiGeng Yang, Wei Liu, and Hao Sun. “Scalar dark matter and muon  $g-2$  in a model \*”. In: *Chin. Phys. C* 46.8 (2022), p. 083102. DOI: [10.1088/1674-1137/ac67d0](https://doi.org/10.1088/1674-1137/ac67d0). arXiv: [2106.14134](https://arxiv.org/abs/2106.14134) [hep-ph].
- [605] Pablo Figueroa, Gonzalo Herrera, and Fredy Ochoa. “Direct detection of light dark matter charged under a  $L_\mu-L_\tau$  symmetry”. In: *Phys. Rev. D* 110.9 (2024), p. 095018. DOI: [10.1103/PhysRevD.110.095018](https://doi.org/10.1103/PhysRevD.110.095018). arXiv: [2404.03090](https://arxiv.org/abs/2404.03090) [hep-ph].
- [606] Anirban Biswas, Sandhya Choubey, and Sarif Khan. “Neutrino Mass, Dark Matter and Anomalous Magnetic Moment of Muon in a  $U(1)_{L_\mu-L_\tau}$  Model”. In: *JHEP* 09 (2016), p. 147. DOI: [10.1007/JHEP09\(2016\)147](https://doi.org/10.1007/JHEP09(2016)147). arXiv: [1608.04194](https://arxiv.org/abs/1608.04194) [hep-ph].
- [607] Kento Asai, Koichi Hamaguchi, Natsumi Nagata, Shih-Yen Tseng, and Koji Tsumura. “Minimal Gauged  $U(1)_{L_\alpha-L_\beta}$  Models Driven into a Corner”. In: *Phys. Rev. D* 99.5 (2019), p. 055029. DOI: [10.1103/PhysRevD.99.055029](https://doi.org/10.1103/PhysRevD.99.055029). arXiv: [1811.07571](https://arxiv.org/abs/1811.07571) [hep-ph].
- [608] Admir Greljo, Yotam Soreq, Peter Stangl, Anders Eller Thomsen, and Jure Zupan. “Muonic force behind flavor anomalies”. In: *JHEP* 04 (2022), p. 151. DOI: [10.1007/JHEP04\(2022\)151](https://doi.org/10.1007/JHEP04(2022)151). arXiv: [2107.07518](https://arxiv.org/abs/2107.07518) [hep-ph].
- [609] Francesco Costa, Sarif Khan, and Jinsu Kim. “A two-component dark matter model and its associated gravitational waves”. In: *JHEP* 06 (2022), p. 026. DOI: [10.1007/JHEP06\(2022\)026](https://doi.org/10.1007/JHEP06(2022)026). arXiv: [2202.13126](https://arxiv.org/abs/2202.13126) [hep-ph].
- [610] Debasish Borah, Satyabrata Mahapatra, Dibyendu Nanda, and Narendra Sahu. “Inelastic fermion dark matter origin of XENON1T excess with muon  $(g-2)$  and light neutrino mass”. In: *Phys. Lett. B* 811 (2020), p. 135933. DOI: [10.1016/j.physletb.2020.135933](https://doi.org/10.1016/j.physletb.2020.135933). arXiv: [2007.10754](https://arxiv.org/abs/2007.10754) [hep-ph].
- [611] Debasish Borah, Lopamudra Mukherjee, and Soumitra Nandi. “Low scale  $U(1)_X$  gauge symmetry as an origin of dark matter, neutrino mass and flavour anomalies”. In: *JHEP* 12 (2020), p. 052. DOI: [10.1007/JHEP12\(2020\)052](https://doi.org/10.1007/JHEP12(2020)052). arXiv: [2007.13778](https://arxiv.org/abs/2007.13778) [hep-ph].
- [612] Debasish Borah, Manoranjan Dutta, Satyabrata Mahapatra, and Narendra Sahu. “Lepton anomalous magnetic moment with singlet-doublet fermion dark matter in a scotogenic  $U(1)_{L_\mu-L_\tau}$  model”. In: *Phys. Rev. D* 105.1 (2022), p. 015029. DOI: [10.1103/PhysRevD.105.015029](https://doi.org/10.1103/PhysRevD.105.015029). arXiv: [2109.02699](https://arxiv.org/abs/2109.02699) [hep-ph].

- [613] Debasish Borah, Manoranjan Dutta, Satyabrata Mahapatra, and Narendra Sahu. “Muon ( $g - 2$ ) and XENON1T excess with boosted dark matter in  $L_\mu - L_\tau$  model”. In: *Phys. Lett. B* 820 (2021), p. 136577. DOI: [10.1016/j.physletb.2021.136577](https://doi.org/10.1016/j.physletb.2021.136577). arXiv: [2104.05656](https://arxiv.org/abs/2104.05656) [hep-ph].
- [614] Debasish Borah, Arnab Dasgupta, and Devabrat Mahanta. “TeV scale resonant leptogenesis with  $L_\mu-L_\tau$  gauge symmetry in light of the muon  $g-2$ ”. In: *Phys. Rev. D* 104.7 (2021), p. 075006. DOI: [10.1103/PhysRevD.104.075006](https://doi.org/10.1103/PhysRevD.104.075006). arXiv: [2106.14410](https://arxiv.org/abs/2106.14410) [hep-ph].
- [615] Labh Singh, Monal Kashav, and Surender Verma. “Gauged  $U(1)_{L_\mu-L_\tau}$  symmetry and two-zero textures of inverse neutrino mass matrix in light of muon ( $g - 2$ )”. In: *Mod. Phys. Lett. A* 37.30 (2022), p. 2250202. DOI: [10.1142/S0217732322502029](https://doi.org/10.1142/S0217732322502029). arXiv: [2207.08415](https://arxiv.org/abs/2207.08415) [hep-ph].
- [616] Shintaro Eijima, Masahiro Ibe, and Kai Murai. “Muon  $g - 2$  and non-thermal leptogenesis in  $U(1)_{L_\mu-L_\tau}$  model”. In: *JHEP* 05 (2023), p. 010. DOI: [10.1007/JHEP05\(2023\)010](https://doi.org/10.1007/JHEP05(2023)010). arXiv: [2303.09751](https://arxiv.org/abs/2303.09751) [hep-ph].
- [617] Masahiro Ibe, Satoshi Shirai, and Keiichi Watanabe. “Global Neutrino Constraints on the Minimal  $U(1)_{L_\mu-L_\tau}$  Model”. In: (Mar. 2025). arXiv: [2503.01399](https://arxiv.org/abs/2503.01399) [hep-ph].
- [618] Manuel A. Buen-Abad, JiJi Fan, Matthew Reece, and Chen Sun. “Challenges for an axion explanation of the muon  $g - 2$  measurement”. In: *JHEP* 09 (2021), p. 101. DOI: [10.1007/JHEP09\(2021\)101](https://doi.org/10.1007/JHEP09(2021)101). arXiv: [2104.03267](https://arxiv.org/abs/2104.03267) [hep-ph].
- [619] Matthias Neubert and Marvin Schnubel. “Two-loop contributions of axion-like particles to electromagnetic and chromomagnetic form factors”. In: *Eur. Phys. J. C* 84.6 (2024), p. 571. DOI: [10.1140/epjc/s10052-024-12881-9](https://doi.org/10.1140/epjc/s10052-024-12881-9). arXiv: [2403.00913](https://arxiv.org/abs/2403.00913) [hep-ph].
- [620] Martin Bauer, Matthias Neubert, Sophie Renner, Marvin Schnubel, and Andrea Thamm. “The Low-Energy Effective Theory of Axions and ALPs”. In: *JHEP* 04 (2021), p. 063. DOI: [10.1007/JHEP04\(2021\)063](https://doi.org/10.1007/JHEP04(2021)063). arXiv: [2012.12272](https://arxiv.org/abs/2012.12272) [hep-ph].
- [621] Martin Bauer, Matthias Neubert, and Andrea Thamm. “Collider Probes of Axion-Like Particles”. In: *JHEP* 12 (2017), p. 044. DOI: [10.1007/JHEP12\(2017\)044](https://doi.org/10.1007/JHEP12(2017)044). arXiv: [1708.00443](https://arxiv.org/abs/1708.00443) [hep-ph].
- [622] W. J. Marciano, A. Masiero, P. Paradisi, and M. Passera. “Contributions of axionlike particles to lepton dipole moments”. In: *Phys. Rev. D* 94.11 (2016), p. 115033. DOI: [10.1103/PhysRevD.94.115033](https://doi.org/10.1103/PhysRevD.94.115033). arXiv: [1607.01022](https://arxiv.org/abs/1607.01022) [hep-ph].
- [623] Martin Bauer, Matthias Neubert, Sophie Renner, Marvin Schnubel, and Andrea Thamm. “Flavor probes of axion-like particles”. In: *JHEP* 09 (2022), p. 056. DOI: [10.1007/JHEP09\(2022\)056](https://doi.org/10.1007/JHEP09(2022)056). arXiv: [2110.10698](https://arxiv.org/abs/2110.10698) [hep-ph].
- [624] Anne Mareike Galda and Matthias Neubert. “ALP-LEFT Interference and the Muon ( $g-2$ )”. In: *JHEP* 11 (2023), p. 015. DOI: [10.1007/JHEP11\(2023\)015](https://doi.org/10.1007/JHEP11(2023)015). arXiv: [2308.01338](https://arxiv.org/abs/2308.01338) [hep-ph].
- [625] Claudia Cornella, Paride Paradisi, and Olcyr Sumensari. “Hunting for ALPs with Lepton Flavor Violation”. In: *JHEP* 01 (2020), p. 158. DOI: [10.1007/JHEP01\(2020\)158](https://doi.org/10.1007/JHEP01(2020)158). arXiv: [1911.06279](https://arxiv.org/abs/1911.06279) [hep-ph].
- [626] Hooman Davoudiasl and William J. Marciano. “Tale of two anomalies”. In: *Phys. Rev. D* 98.7 (2018), p. 075011. DOI: [10.1103/PhysRevD.98.075011](https://doi.org/10.1103/PhysRevD.98.075011). arXiv: [1806.10252](https://arxiv.org/abs/1806.10252) [hep-ph].

- [627] Martin Bauer, Matthias Neubert, Sophie Renner, Marvin Schnubel, and Andrea Thamm. “Axionlike Particles, Lepton-Flavor Violation, and a New Explanation of  $a_\mu$  and  $a_e$ ”. In: *Phys. Rev. Lett.* 124.21 (2020), p. 211803. DOI: [10.1103/PhysRevLett.124.211803](https://doi.org/10.1103/PhysRevLett.124.211803). arXiv: [1908.00008](https://arxiv.org/abs/1908.00008) [hep-ph].
- [628] Dario Buttazzo, Paolo Panci, Daniele Teresi, and Robert Ziegler. “Xenon1T excess from electron recoils of non-relativistic Dark Matter”. In: *Phys. Lett. B* 817 (2021), p. 136310. DOI: [10.1016/j.physletb.2021.136310](https://doi.org/10.1016/j.physletb.2021.136310). arXiv: [2011.08919](https://arxiv.org/abs/2011.08919) [hep-ph].
- [629] Wai-Yee Keung, Danny Marfatia, and Po-Yan Tseng. “Axion-Like Particles, Two-Higgs-Doublet Models, Leptoquarks, and the Electron and Muon  $g - 2$ ”. In: *LHEP 2021* (2021), p. 209. DOI: [10.31526/lhep.2021.209](https://doi.org/10.31526/lhep.2021.209). arXiv: [2104.03341](https://arxiv.org/abs/2104.03341) [hep-ph].
- [630] Vedran Brdar, Sudip Jana, Jisuke Kubo, and Manfred Lindner. “Semi-secretly interacting Axion-like particle as an explanation of Fermilab muon  $g - 2$  measurement”. In: *Phys. Lett. B* 820 (2021), p. 136529. DOI: [10.1016/j.physletb.2021.136529](https://doi.org/10.1016/j.physletb.2021.136529). arXiv: [2104.03282](https://arxiv.org/abs/2104.03282) [hep-ph].
- [631] Sougata Ganguly, Biswarup Mukhopadhyaya, and Sourov Roy. “Can leptophilic-ALP be a solution to the muon ( $g - 2$ ) anomaly?” In: (Apr. 2022). arXiv: [2204.07920](https://arxiv.org/abs/2204.07920) [hep-ph].
- [632] Aleksandr Pustyntsev and Marc Vanderhaeghen. “Constraints for scalars and pseudoscalars from  $(g-2)_l$  and existing  $e^+e^-$  colliders”. In: *Phys. Rev. D* 110.7 (2024), p. 075027. DOI: [10.1103/PhysRevD.110.075027](https://doi.org/10.1103/PhysRevD.110.075027). arXiv: [2407.20202](https://arxiv.org/abs/2407.20202) [hep-ph].
- [633] Pramod Sharma, Soham Singh, Mukesh Kumar, and Ashok Goyal. “Comprehensive Constraints on ALP Couplings from future  $e^+e^-$  Colliders, Muon  $g - 2$ , Thermal Dark Matter and Higgs Measurements”. In: (May 2025). arXiv: [2505.12466](https://arxiv.org/abs/2505.12466) [hep-ph].
- [634] Luc Darmé, Federica Giacchino, Enrico Nardi, and Mauro Raggi. “Invisible decays of axion-like particles: constraints and prospects”. In: *JHEP* 06 (2021), p. 009. DOI: [10.1007/JHEP06\(2021\)009](https://doi.org/10.1007/JHEP06(2021)009). arXiv: [2012.07894](https://arxiv.org/abs/2012.07894) [hep-ph].
- [635] Medina Ablikim et al. “Search for an axion-like particle in radiative  $J/\psi$  decays”. In: *Phys. Lett. B* 838 (2023), p. 137698. DOI: [10.1016/j.physletb.2023.137698](https://doi.org/10.1016/j.physletb.2023.137698). arXiv: [2211.12699](https://arxiv.org/abs/2211.12699) [hep-ex].
- [636] L. Merlo, F. Pobbe, S. Rigolin, and O. Sumensari. “Revisiting the production of ALPs at B-factories”. In: *JHEP* 06 (2019), p. 091. DOI: [10.1007/JHEP06\(2019\)091](https://doi.org/10.1007/JHEP06(2019)091). arXiv: [1905.03259](https://arxiv.org/abs/1905.03259) [hep-ph].
- [637] Georges Aad et al. “Search for short- and long-lived axion-like particles in  $H \rightarrow aa \rightarrow 4\gamma$  decays with the ATLAS experiment at the LHC”. In: *Eur. Phys. J. C* 84.7 (2024), p. 742. DOI: [10.1140/epjc/s10052-024-12979-0](https://doi.org/10.1140/epjc/s10052-024-12979-0). arXiv: [2312.03306](https://arxiv.org/abs/2312.03306) [hep-ex].
- [638] Aleksandr Pustyntsev and Marc Vanderhaeghen. “Implications of recent  $(g - 2)_\mu$  measurements for MeV-GeV dark sector searches”. In: (June 2025). arXiv: [2506.17750](https://arxiv.org/abs/2506.17750) [hep-ph].
- [639] Chuan-Xin Cui, Hiroyuki Ishida, Shinya Matsuzaki, and Yoshihiro Shigekami. “Probing an intrinsically flavorful ALP via tau-lepton flavor physics”. In: *Phys. Rev. D* 105.9 (2022), p. 095033. DOI: [10.1103/PhysRevD.105.095033](https://doi.org/10.1103/PhysRevD.105.095033). arXiv: [2110.11640](https://arxiv.org/abs/2110.11640) [hep-ph].

- [640] Kingman Cheung, Abner Soffer, Zeren Simon Wang, and Yu-Heng Wu. “Probing charged lepton flavor violation with axion-like particles at Belle II”. In: *JHEP* 11 (2021), p. 218. DOI: [10.1007/JHEP11\(2021\)218](https://doi.org/10.1007/JHEP11(2021)218). arXiv: [2108.11094](https://arxiv.org/abs/2108.11094) [hep-ph].
- [641] Hooman Davoudiasl, Roman Marcarelli, Nicholas Miesch, and Ethan T. Neil. “Searching for flavor-violating ALPs in Higgs boson decays”. In: *Phys. Rev. D* 104.5 (2021), p. 055022. DOI: [10.1103/PhysRevD.104.055022](https://doi.org/10.1103/PhysRevD.104.055022). arXiv: [2105.05866](https://arxiv.org/abs/2105.05866) [hep-ph].
- [642] Kingman Cheung, Jui-Lin Kuo, Po-Yan Tseng, and Zeren Simon Wang. “Atmospheric axionlike particles at Super-Kamiokande”. In: *Phys. Rev. D* 106.9 (2022), p. 095029. DOI: [10.1103/PhysRevD.106.095029](https://doi.org/10.1103/PhysRevD.106.095029). arXiv: [2208.05111](https://arxiv.org/abs/2208.05111) [hep-ph].
- [643] Anke Biekötter, Mikael Chala, and Michael Spannowsky. “New Higgs decays to axion-like particles”. In: *Phys. Lett. B* 834 (2022), p. 137465. DOI: [10.1016/j.physletb.2022.137465](https://doi.org/10.1016/j.physletb.2022.137465). arXiv: [2203.14984](https://arxiv.org/abs/2203.14984) [hep-ph].
- [644] Lorenzo Calibbi, Zijie Huang, Shaoyang Qin, Yiming Yang, and Xiaoyue Yin. “Testing axion couplings to leptons in Z decays at future e+e- colliders”. In: *Phys. Rev. D* 108.1 (2023), p. 015002. DOI: [10.1103/PhysRevD.108.015002](https://doi.org/10.1103/PhysRevD.108.015002). arXiv: [2212.02818](https://arxiv.org/abs/2212.02818) [hep-ph].
- [645] Prateek Agrawal, David E. Kaplan, On Kim, Surjeet Rajendran, and Mario Reig. “Searching for axion forces with precision precession in storage rings”. In: *Phys. Rev. D* 108.1 (2023), p. 015017. DOI: [10.1103/PhysRevD.108.015017](https://doi.org/10.1103/PhysRevD.108.015017). arXiv: [2210.17547](https://arxiv.org/abs/2210.17547) [hep-ph].
- [646] Jia Liu, Xiaolin Ma, Lian-Tao Wang, and Xiao-Ping Wang. “ALP explanation to the muon (g-2) and its test at future Tera-Z and Higgs factories”. In: *Phys. Rev. D* 107.9 (2023), p. 095016. DOI: [10.1103/PhysRevD.107.095016](https://doi.org/10.1103/PhysRevD.107.095016). arXiv: [2210.09335](https://arxiv.org/abs/2210.09335) [hep-ph].
- [647] Simon Knapen, Kevin Langhoff, Toby Opferkuch, and Diego Redigolo. “Angling for insights: illuminating light new physics at Mu3e through angular correlations”. In: *JHEP* 07 (2024), p. 194. DOI: [10.1007/JHEP07\(2024\)194](https://doi.org/10.1007/JHEP07(2024)194). arXiv: [2311.17913](https://arxiv.org/abs/2311.17913) [hep-ph].
- [648] Giovanni Armando, Paolo Panci, Joachim Weiss, and Robert Ziegler. “Leptonic ALP portal to the dark sector”. In: *Phys. Rev. D* 109.5 (2024), p. 055029. DOI: [10.1103/PhysRevD.109.055029](https://doi.org/10.1103/PhysRevD.109.055029). arXiv: [2310.05827](https://arxiv.org/abs/2310.05827) [hep-ph].
- [649] Bhuvanajyoti Bhattacharya, Alakabha Datta, Danny Marfatia, Soumitra Nandi, and John Waite. “Axion-like particles resolve the  $B \rightarrow \pi K$  and  $g - 2$  anomalies”. In: *Phys. Rev. D* 104.5 (2021), p. L051701. DOI: [10.1103/PhysRevD.104.L051701](https://doi.org/10.1103/PhysRevD.104.L051701). arXiv: [2104.03947](https://arxiv.org/abs/2104.03947) [hep-ph].
- [650] J. Bonilla, A. de Giorgi, B. Gavela, L. Merlo, and M. Ramos. “The cost of an ALP solution to the neutral B-anomalies”. In: *JHEP* 02 (2023), p. 138. DOI: [10.1007/JHEP02\(2023\)138](https://doi.org/10.1007/JHEP02(2023)138). arXiv: [2209.11247](https://arxiv.org/abs/2209.11247) [hep-ph].
- [651] Lorenzo Calibbi, Tong Li, Lopamudra Mukherjee, and Yiming Yang. “Probing ALP lepton flavor violation at  $\mu$ TRISTAN”. In: *Phys. Rev. D* 110.11 (2024), p. 115009. DOI: [10.1103/PhysRevD.110.115009](https://doi.org/10.1103/PhysRevD.110.115009). arXiv: [2406.13234](https://arxiv.org/abs/2406.13234) [hep-ph].
- [652] Lorenzo Calibbi, Diego Redigolo, Robert Ziegler, and Jure Zupan. “Looking forward to lepton-flavor-violating ALPs”. In: *JHEP* 09 (2021), p. 173. DOI: [10.1007/JHEP09\(2021\)173](https://doi.org/10.1007/JHEP09(2021)173). arXiv: [2006.04795](https://arxiv.org/abs/2006.04795) [hep-ph].
- [653] Jia Liu, Carlos E. M. Wagner, and Xiao-Ping Wang. “A light complex scalar for the electron and muon anomalous magnetic moments”. In: *JHEP* 03 (2019), p. 008. DOI: [10.1007/JHEP03\(2019\)008](https://doi.org/10.1007/JHEP03(2019)008). arXiv: [1810.11028](https://arxiv.org/abs/1810.11028) [hep-ph].

- [654] Waleed Abdallah, Raj Gandhi, and Samiran Roy. “Understanding the MiniBooNE and the muon and electron  $g - 2$  anomalies with a light  $Z'$  and a second Higgs doublet”. In: *JHEP* 12 (2020), p. 188. DOI: [10.1007/JHEP12\(2020\)188](https://doi.org/10.1007/JHEP12(2020)188). arXiv: [2006.01948](https://arxiv.org/abs/2006.01948) [hep-ph].
- [655] Pablo Escribano and Avelino Vicente. “Ultralight scalars in leptonic observables”. In: *JHEP* 03 (2021), p. 240. DOI: [10.1007/JHEP03\(2021\)240](https://doi.org/10.1007/JHEP03(2021)240). arXiv: [2008.01099](https://arxiv.org/abs/2008.01099) [hep-ph].
- [656] Lian-Bao Jia. “A dark leptophilic scalar with the updated muon  $g - 2$  anomaly”. In: *Eur. Phys. J. C* 82.4 (2022), p. 321. DOI: [10.1140/epjc/s10052-022-10207-1](https://doi.org/10.1140/epjc/s10052-022-10207-1). arXiv: [2105.13805](https://arxiv.org/abs/2105.13805) [hep-ph].
- [657] Andrea Caputo, Georg Raffelt, and Edoardo Vitagliano. “Muonic boson limits: Supernova redux”. In: *Phys. Rev. D* 105.3 (2022), p. 035022. DOI: [10.1103/PhysRevD.105.035022](https://doi.org/10.1103/PhysRevD.105.035022). arXiv: [2109.03244](https://arxiv.org/abs/2109.03244) [hep-ph].
- [658] Reuven Balkin, Cedric Delaunay, Michael Geller, Enrique Kajomovitz, Gilad Perez, Yogev Shpilman, and Yotam Soreq. “Custodial symmetry for muon  $g-2$ ”. In: *Phys. Rev. D* 104.5 (2021), p. 053009. DOI: [10.1103/PhysRevD.104.053009](https://doi.org/10.1103/PhysRevD.104.053009). arXiv: [2104.08289](https://arxiv.org/abs/2104.08289) [hep-ph].
- [659] S. N. Gninenko and N. V. Krasnikov. “Leptonic scalar portal: Origin of muon  $g - 2$  anomaly and dark matter?” In: *Phys. Rev. D* 106.1 (2022), p. 015003. DOI: [10.1103/PhysRevD.106.015003](https://doi.org/10.1103/PhysRevD.106.015003). arXiv: [2202.04410](https://arxiv.org/abs/2202.04410) [hep-ph].
- [660] Johannes Herms, Sudip Jana, Vishnu P. K., and Shaikh Saad. “Minimal Realization of Light Thermal Dark Matter”. In: *Phys. Rev. Lett.* 129.9 (2022), p. 091803. DOI: [10.1103/PhysRevLett.129.091803](https://doi.org/10.1103/PhysRevLett.129.091803). arXiv: [2203.05579](https://arxiv.org/abs/2203.05579) [hep-ph].
- [661] Yohei Ema, Zhen Liu, Kun-Feng Lyu, and Maxim Pospelov. “Flavor-changing light bosons with accidental longevity”. In: *JHEP* 02 (2023), p. 135. DOI: [10.1007/JHEP02\(2023\)135](https://doi.org/10.1007/JHEP02(2023)135). arXiv: [2211.00664](https://arxiv.org/abs/2211.00664) [hep-ph].
- [662] Karim Ghorbani. “Light vector dark matter with scalar mediator and muon  $g-2$  anomaly”. In: *Phys. Rev. D* 104.11 (2021), p. 115008. DOI: [10.1103/PhysRevD.104.115008](https://doi.org/10.1103/PhysRevD.104.115008). arXiv: [2104.13810](https://arxiv.org/abs/2104.13810) [hep-ph].
- [663] Luca Di Luzio, Antonio Masiero, Paride Paradisi, and Massimo Passera. “New physics behind the new muon  $g-2$  puzzle?” In: *Phys. Lett. B* 829 (2022), p. 137037. DOI: [10.1016/j.physletb.2022.137037](https://doi.org/10.1016/j.physletb.2022.137037). arXiv: [2112.08312](https://arxiv.org/abs/2112.08312) [hep-ph].
- [664] Luc Darmé, Giovanni Grilli di Cortona, and Enrico Nardi. “The muon  $g - 2$  anomaly confronts new physics in  $e$  and  $\mu$  final states scattering”. In: *JHEP* 06 (2022), p. 122. DOI: [10.1007/JHEP06\(2022\)122](https://doi.org/10.1007/JHEP06(2022)122). arXiv: [2112.09139](https://arxiv.org/abs/2112.09139) [hep-ph].
- [665] Luc Darmé, Giovanni Grilli di Cortona, and Enrico Nardi. “Indirect new physics effects on  $\sigma_{had}$  confront the  $(g-2)_\mu$  window discrepancies and the CMD-3 result”. In: *Phys. Rev. D* 108.9 (2023), p. 095056. DOI: [10.1103/PhysRevD.108.095056](https://doi.org/10.1103/PhysRevD.108.095056). arXiv: [2212.03877](https://arxiv.org/abs/2212.03877) [hep-ph].
- [666] Nina M. Coyle and Carlos E. M. Wagner. “Resolving the muon  $g - 2$  tension through  $Z'$ -induced modifications to  $\sigma_{had}$ ”. In: *JHEP* 12 (2023), p. 071. DOI: [10.1007/JHEP12\(2023\)071](https://doi.org/10.1007/JHEP12(2023)071). arXiv: [2305.02354](https://arxiv.org/abs/2305.02354) [hep-ph].
- [667] Kaustubh Agashe, Abhishek Banerjee, Minuyan Jiang, Shmuel Nussinov, Kushan Panchal, Srijit Paul, Gilad Perez, and Yotam Soreq. “Searching for hadronic scale baryonic and dark forces at  $(g - 2)_\mu$ ’s lattice-vs-dispersion front”. In: (Dec. 2024). arXiv: [2412.12266](https://arxiv.org/abs/2412.12266) [hep-ph].

- [668] Andreas Crivellin and Martin Hoferichter. “Width effects of broad new resonances in loop observables and application to  $(g-2)\mu$ ”. In: *Phys. Rev. D* 108.1 (2023), p. 013005. DOI: [10.1103/PhysRevD.108.013005](https://doi.org/10.1103/PhysRevD.108.013005). arXiv: [2211.12516](https://arxiv.org/abs/2211.12516) [hep-ph].
- [669] F. Ambrosino et al. “Measurement of  $\sigma(e^+e^- \rightarrow \pi^+\pi^-\gamma(\gamma))$  and the dipion contribution to the muon anomaly with the KLOE detector”. In: *Phys. Lett. B* 670 (2009), pp. 285–291. DOI: [10.1016/j.physletb.2008.10.060](https://doi.org/10.1016/j.physletb.2008.10.060). arXiv: [0809.3950](https://arxiv.org/abs/0809.3950) [hep-ex].
- [670] Hans Peter Nilles. “Supersymmetry, Supergravity and Particle Physics”. In: *Phys. Rept.* 110 (1984), pp. 1–162. DOI: [10.1016/0370-1573\(84\)90008-5](https://doi.org/10.1016/0370-1573(84)90008-5).
- [671] Howard E. Haber and Gordon L. Kane. “The Search for Supersymmetry: Probing Physics Beyond the Standard Model”. In: *Phys. Rept.* 117 (1985), pp. 75–263. DOI: [10.1016/0370-1573\(85\)90051-1](https://doi.org/10.1016/0370-1573(85)90051-1).
- [672] Stephen P. Martin. “A Supersymmetry primer”. In: *Adv. Ser. Direct. High Energy Phys.* 18 (1998). Ed. by Gordon L. Kane, pp. 1–98. DOI: [10.1142/9789812839657\\_0001](https://doi.org/10.1142/9789812839657_0001). arXiv: [hep-ph/9709356](https://arxiv.org/abs/hep-ph/9709356).
- [673] L. Girardello and Marcus T. Grisaru. “Soft Breaking of Supersymmetry”. In: *Nucl. Phys. B* 194 (1982), p. 65. DOI: [10.1016/0550-3213\(82\)90512-0](https://doi.org/10.1016/0550-3213(82)90512-0).
- [674] Richard L. Arnowitt, Bhaskar Dutta, B. Hu, and Y. Santoso. “Muon  $g-2$ , dark matter detection and accelerator physics”. In: *Phys. Lett. B* 505 (2001), pp. 177–183. DOI: [10.1016/S0370-2693\(01\)00370-7](https://doi.org/10.1016/S0370-2693(01)00370-7). arXiv: [hep-ph/0102344](https://arxiv.org/abs/hep-ph/0102344).
- [675] E. A. Baltz and P. Gondolo. “Implications of muon anomalous magnetic moment for supersymmetric dark matter”. In: *Phys. Rev. Lett.* 86 (2001), p. 5004. DOI: [10.1103/PhysRevLett.86.5004](https://doi.org/10.1103/PhysRevLett.86.5004). arXiv: [hep-ph/0102147](https://arxiv.org/abs/hep-ph/0102147).
- [676] Lisa L. Everett, Gordon L. Kane, Stefano Rigolin, and Lian-Tao Wang. “Implications of muon  $g-2$  for supersymmetry and for discovering superpartners directly”. In: *Phys. Rev. Lett.* 86 (2001), pp. 3484–3487. DOI: [10.1103/PhysRevLett.86.3484](https://doi.org/10.1103/PhysRevLett.86.3484). arXiv: [hep-ph/0102145](https://arxiv.org/abs/hep-ph/0102145).
- [677] Jonathan L. Feng and Konstantin T. Matchev. “Supersymmetry and the anomalous magnetic moment of the muon”. In: *Phys. Rev. Lett.* 86 (2001), pp. 3480–3483. DOI: [10.1103/PhysRevLett.86.3480](https://doi.org/10.1103/PhysRevLett.86.3480). arXiv: [hep-ph/0102146](https://arxiv.org/abs/hep-ph/0102146).
- [678] Utpal Chattopadhyay and Pran Nath. “Upper limits on sparticle masses from  $g-2$  and the possibility for discovery of SUSY at colliders and in dark matter searches”. In: *Phys. Rev. Lett.* 86 (2001), pp. 5854–5857. DOI: [10.1103/PhysRevLett.86.5854](https://doi.org/10.1103/PhysRevLett.86.5854). arXiv: [hep-ph/0102157](https://arxiv.org/abs/hep-ph/0102157).
- [679] Shinji Komine, Takeo Moroi, and Masahiro Yamaguchi. “Recent result from E821 experiment on muon  $g-2$  and unconstrained minimal supersymmetric standard model”. In: *Phys. Lett. B* 506 (2001), pp. 93–98. DOI: [10.1016/S0370-2693\(01\)00381-1](https://doi.org/10.1016/S0370-2693(01)00381-1). arXiv: [hep-ph/0102204](https://arxiv.org/abs/hep-ph/0102204).
- [680] Junji Hisano and Kazuhiro Tobe. “Neutrino masses, muon  $g-2$ , and lepton flavor violation in the supersymmetric seesaw model”. In: *Phys. Lett. B* 510 (2001), pp. 197–204. DOI: [10.1016/S0370-2693\(01\)00494-4](https://doi.org/10.1016/S0370-2693(01)00494-4). arXiv: [hep-ph/0102315](https://arxiv.org/abs/hep-ph/0102315).
- [681] Tarek Ibrahim, Utpal Chattopadhyay, and Pran Nath. “Constraints on explicit CP violation from the Brookhaven muon  $g-2$  experiment”. In: *Phys. Rev. D* 64 (2001), p. 016010. DOI: [10.1103/PhysRevD.64.016010](https://doi.org/10.1103/PhysRevD.64.016010). arXiv: [hep-ph/0102324](https://arxiv.org/abs/hep-ph/0102324).

- [682] John R. Ellis, Dimitri V. Nanopoulos, and Keith A. Olive. “Combining the muon anomalous magnetic moment with other constraints on the CMSSM”. In: *Phys. Lett. B* 508 (2001), pp. 65–73. DOI: [10.1016/S0370-2693\(01\)00480-4](https://doi.org/10.1016/S0370-2693(01)00480-4). arXiv: [hep-ph/0102331](https://arxiv.org/abs/hep-ph/0102331).
- [683] Kiwoon Choi, Kyuwan Hwang, Sin Kyu Kang, Kang Young Lee, and Wan Young Song. “Probing the messenger of supersymmetry breaking by the muon anomalous magnetic moment”. In: *Phys. Rev. D* 64 (2001), p. 055001. DOI: [10.1103/PhysRevD.64.055001](https://doi.org/10.1103/PhysRevD.64.055001). arXiv: [hep-ph/0103048](https://arxiv.org/abs/hep-ph/0103048).
- [684] Jihn E. Kim, Bumseok Kyae, and Hyun Min Lee. “Effective supersymmetric theory and  $(g-2)$ (muon with R-parity violation)”. In: *Phys. Lett. B* 520 (2001), pp. 298–306. DOI: [10.1016/S0370-2693\(01\)01134-0](https://doi.org/10.1016/S0370-2693(01)01134-0). arXiv: [hep-ph/0103054](https://arxiv.org/abs/hep-ph/0103054).
- [685] Stephen P. Martin and James D. Wells. “Muon Anomalous Magnetic Dipole Moment in Supersymmetric Theories”. In: *Phys. Rev. D* 64 (2001), p. 035003. DOI: [10.1103/PhysRevD.64.035003](https://doi.org/10.1103/PhysRevD.64.035003). arXiv: [hep-ph/0103067](https://arxiv.org/abs/hep-ph/0103067).
- [686] Shinji Komine, Takeo Moroi, and Masahiro Yamaguchi. “No scale scenarios in the light of new measurement of muon anomalous magnetic moment”. In: *Phys. Lett. B* 507 (2001), pp. 224–230. DOI: [10.1016/S0370-2693\(01\)00452-X](https://doi.org/10.1016/S0370-2693(01)00452-X). arXiv: [hep-ph/0103182](https://arxiv.org/abs/hep-ph/0103182).
- [687] Seungwon Baek, P. Ko, and Hong Seok Lee. “Muon anomalous magnetic moment,  $B \rightarrow X(s)$  gamma and dark matter detection in the string models with dilaton domination”. In: *Phys. Rev. D* 65 (2002), p. 035004. DOI: [10.1103/PhysRevD.65.035004](https://doi.org/10.1103/PhysRevD.65.035004). arXiv: [hep-ph/0103218](https://arxiv.org/abs/hep-ph/0103218).
- [688] D. F. Carvalho, John R. Ellis, M. E. Gomez, and S. Lola. “Charged lepton flavor violation in the CMSSM in view of the muon anomalous magnetic moment”. In: *Phys. Lett. B* 515 (2001), pp. 323–332. DOI: [10.1016/S0370-2693\(01\)00835-8](https://doi.org/10.1016/S0370-2693(01)00835-8). arXiv: [hep-ph/0103256](https://arxiv.org/abs/hep-ph/0103256).
- [689] Howard Baer, Csaba Balazs, Javier Ferrandis, and Xerxes Tata. “Impact of muon anomalous magnetic moment on supersymmetric models”. In: *Phys. Rev. D* 64 (2001), p. 035004. DOI: [10.1103/PhysRevD.64.035004](https://doi.org/10.1103/PhysRevD.64.035004). arXiv: [hep-ph/0103280](https://arxiv.org/abs/hep-ph/0103280).
- [690] Z. Chacko and Graham D. Kribs. “Constraints on lepton flavor violation in the MSSM from the muon anomalous magnetic moment measurement”. In: *Phys. Rev. D* 64 (2001), p. 075015. DOI: [10.1103/PhysRevD.64.075015](https://doi.org/10.1103/PhysRevD.64.075015). arXiv: [hep-ph/0104317](https://arxiv.org/abs/hep-ph/0104317).
- [691] Seungwon Baek, Toru Goto, Yasuhiro Okada, and Ken-ichi Okumura. “Muon anomalous magnetic moment, lepton flavor violation, and flavor changing neutral current processes in SUSY GUT with right-handed neutrino”. In: *Phys. Rev. D* 64 (2001), p. 095001. DOI: [10.1103/PhysRevD.64.095001](https://doi.org/10.1103/PhysRevD.64.095001). arXiv: [hep-ph/0104146](https://arxiv.org/abs/hep-ph/0104146).
- [692] Chuan-Hung Chen and C. Q. Geng. “The Muon anomalous magnetic moment from a generic charged Higgs with SUSY”. In: *Phys. Lett. B* 511 (2001), pp. 77–84. DOI: [10.1016/S0370-2693\(01\)00651-7](https://doi.org/10.1016/S0370-2693(01)00651-7). arXiv: [hep-ph/0104151](https://arxiv.org/abs/hep-ph/0104151).
- [693] Abdesslam Arhrib and Seungwon Baek. “Two loop Barr-Zee type contributions to  $(g-2)$ (muon) in the MSSM”. In: *Phys. Rev. D* 65 (2002), p. 075002. DOI: [10.1103/PhysRevD.65.075002](https://doi.org/10.1103/PhysRevD.65.075002). arXiv: [hep-ph/0104225](https://arxiv.org/abs/hep-ph/0104225).
- [694] Kari Enqvist, Emidio Gabrielli, and Katri Huitu. “ $g-2$  of the muon in SUSY models with gauge multiplets in the bulk of extra dimensions”. In: *Phys. Lett. B* 512 (2001), pp. 107–114. DOI: [10.1016/S0370-2693\(01\)00662-1](https://doi.org/10.1016/S0370-2693(01)00662-1). arXiv: [hep-ph/0104174](https://arxiv.org/abs/hep-ph/0104174).

- [695] D. G. Cerdeno, E. Gabrielli, S. Khalil, C. Munoz, and E. Torrente-Lujan. “Muon anomalous magnetic moment in supersymmetric scenarios with an intermediate scale and nonuniversality”. In: *Phys. Rev. D* 64 (2001), p. 093012. DOI: [10.1103/PhysRevD.64.093012](https://doi.org/10.1103/PhysRevD.64.093012). arXiv: [hep-ph/0104242](https://arxiv.org/abs/hep-ph/0104242).
- [696] Yeong Gyun Kim and Mihoko M. Nojiri. “Implications of muon anomalous magnetic moment for direct detection of neutralino dark matter”. In: *Prog. Theor. Phys.* 106 (2001), pp. 561–575. DOI: [10.1143/PTP.106.561](https://doi.org/10.1143/PTP.106.561). arXiv: [hep-ph/0104258](https://arxiv.org/abs/hep-ph/0104258).
- [697] Gi-Chol Cho and Kaoru Hagiwara. “Supersymmetric contributions to muon  $g-2$  and the electroweak precision measurements”. In: *Phys. Lett. B* 514 (2001), pp. 123–130. DOI: [10.1016/S0370-2693\(01\)00815-2](https://doi.org/10.1016/S0370-2693(01)00815-2). arXiv: [hep-ph/0105037](https://arxiv.org/abs/hep-ph/0105037).
- [698] Richard L. Arnowitt, Bhaskar Dutta, and Y. Santoso. “SUSY phases, the electron electric dipole moment and the muon magnetic moment”. In: *Phys. Rev. D* 64 (2001), p. 113010. DOI: [10.1103/PhysRevD.64.113010](https://doi.org/10.1103/PhysRevD.64.113010). arXiv: [hep-ph/0106089](https://arxiv.org/abs/hep-ph/0106089).
- [699] G. Belanger, F. Boudjema, A. Cottrant, R. M. Godbole, and A. Semenov. “The MSSM invisible Higgs in the light of dark matter and  $g-2$ ”. In: *Phys. Lett. B* 519 (2001), pp. 93–102. DOI: [10.1016/S0370-2693\(01\)00976-5](https://doi.org/10.1016/S0370-2693(01)00976-5). arXiv: [hep-ph/0106275](https://arxiv.org/abs/hep-ph/0106275).
- [700] W. de Boer, M. Huber, C. Sander, and D. I. Kazakov. “A Global fit to the anomalous magnetic moment,  $b \rightarrow X(s)$  ( $\gamma$ ) and Higgs limits in the constrained MSSM”. In: (June 2001). arXiv: [hep-ph/0106311](https://arxiv.org/abs/hep-ph/0106311).
- [701] Leszek Roszkowski, Roberto Ruiz de Austri, and Takeshi Nihei. “New cosmological and experimental constraints on the CMSSM”. In: *JHEP* 08 (2001), p. 024. DOI: [10.1088/1126-6708/2001/08/024](https://doi.org/10.1088/1126-6708/2001/08/024). arXiv: [hep-ph/0106334](https://arxiv.org/abs/hep-ph/0106334).
- [702] Rathin Adhikari, Ernest Ma, and G. Rajasekaran. “Supersymmetric model of muon anomalous magnetic moment and neutrino masses”. In: *Phys. Rev. D* 65 (2002), p. 077703. DOI: [10.1103/PhysRevD.65.077703](https://doi.org/10.1103/PhysRevD.65.077703). arXiv: [hep-ph/0108167](https://arxiv.org/abs/hep-ph/0108167).
- [703] W. de Boer, M. Huber, C. Sander, and D. I. Kazakov. “A global fit to the anomalous magnetic moment,  $b \rightarrow X/s$   $\gamma$  and Higgs limits in the constrained MSSM”. In: *Phys. Lett. B* 515 (2001), pp. 283–290. DOI: [10.1016/S0370-2693\(01\)00895-4](https://doi.org/10.1016/S0370-2693(01)00895-4).
- [704] Motoi Endo and Takeo Moroi. “Muon magnetic dipole moment and Higgs mass in supersymmetric SU(5) models”. In: *Phys. Lett. B* 525 (2002), pp. 121–129. DOI: [10.1016/S0370-2693\(01\)01417-4](https://doi.org/10.1016/S0370-2693(01)01417-4). arXiv: [hep-ph/0110383](https://arxiv.org/abs/hep-ph/0110383).
- [705] Gi-Chol Cho, Naoyuki Haba, and Junji Hisano. “The Stau exchange contribution to muon  $g-2$  in the decoupling solution”. In: *Phys. Lett. B* 529 (2002), pp. 117–123. DOI: [10.1016/S0370-2693\(02\)01252-2](https://doi.org/10.1016/S0370-2693(02)01252-2). arXiv: [hep-ph/0112163](https://arxiv.org/abs/hep-ph/0112163).
- [706] Chao-Shang Huang and Wei Liao. “ $(g-2)$  ( $\mu$ ) and CP asymmetries in  $B_0(d, s) \rightarrow l^+ l^-$  and  $b \rightarrow s$   $\gamma$  in SUSY models”. In: *Phys. Lett. B* 538 (2002), pp. 301–308. DOI: [10.1016/S0370-2693\(02\)02034-8](https://doi.org/10.1016/S0370-2693(02)02034-8). arXiv: [hep-ph/0201121](https://arxiv.org/abs/hep-ph/0201121).
- [707] Seungwon Baek, P. Ko, and Jae-hyeon Park. “Muon anomalous magnetic moment from effective supersymmetry”. In: *Eur. Phys. J. C* 24 (2002), pp. 613–618. DOI: [10.1007/s10052-002-0971-5](https://doi.org/10.1007/s10052-002-0971-5). arXiv: [hep-ph/0203251](https://arxiv.org/abs/hep-ph/0203251).
- [708] Utpal Chattopadhyay and Pran Nath. “Interpreting the new Brookhaven muon ( $g-2$ ) result”. In: *Phys. Rev. D* 66 (2002), p. 093001. DOI: [10.1103/PhysRevD.66.093001](https://doi.org/10.1103/PhysRevD.66.093001). arXiv: [hep-ph/0208012](https://arxiv.org/abs/hep-ph/0208012).

- [709] Mark Byrne, Christopher Kolda, and Jason E. Lennon. “Updated implications of the muon anomalous magnetic moment for supersymmetry”. In: *Phys. Rev. D* 67 (2003), p. 075004. DOI: [10.1103/PhysRevD.67.075004](https://doi.org/10.1103/PhysRevD.67.075004). arXiv: [hep-ph/0208067](https://arxiv.org/abs/hep-ph/0208067).
- [710] Yeong Gyun Kim, Takeshi Nihei, Leszek Roszkowski, and Roberto Ruiz de Austri. “Upper and lower limits on neutralino WIMP mass and spin independent scattering cross-section, and impact of new  $(g-2)(\mu)$  measurement”. In: *JHEP* 12 (2002), p. 034. DOI: [10.1088/1126-6708/2002/12/034](https://doi.org/10.1088/1126-6708/2002/12/034). arXiv: [hep-ph/0208069](https://arxiv.org/abs/hep-ph/0208069).
- [711] Seungwon Baek, P. Ko, and Wan Young Song. “SUSY breaking mediation mechanisms and  $(g-2)(\mu)$ ,  $B \rightarrow X_s \gamma$ ,  $B \rightarrow X_s \ell^+ \ell^-$  and  $B_s \rightarrow \mu^+ \mu^-$ ”. In: *JHEP* 03 (2003), p. 054. DOI: [10.1088/1126-6708/2003/03/054](https://doi.org/10.1088/1126-6708/2003/03/054). arXiv: [hep-ph/0208112](https://arxiv.org/abs/hep-ph/0208112).
- [712] Stephen P. Martin and James D. Wells. “Superconservative Interpretation of Muon G-2 Results Applied to Supersymmetry”. In: *Phys. Rev. D* 67 (2003), p. 015002. DOI: [10.1103/PhysRevD.67.015002](https://doi.org/10.1103/PhysRevD.67.015002). arXiv: [hep-ph/0209309](https://arxiv.org/abs/hep-ph/0209309).
- [713] S. Heinemeyer, D. Stockinger, and G. Weiglein. “Two loop SUSY corrections to the anomalous magnetic moment of the muon”. In: *Nucl. Phys. B* 690 (2004), pp. 62–80. DOI: [10.1016/j.nuclphysb.2004.04.017](https://doi.org/10.1016/j.nuclphysb.2004.04.017). arXiv: [hep-ph/0312264](https://arxiv.org/abs/hep-ph/0312264).
- [714] Sedar Marchetti, Susanne Mertens, Ulrich Nierste, and Dominik Stockinger. “Tan(beta)-enhanced supersymmetric corrections to the anomalous magnetic moment of the muon”. In: *Phys. Rev. D* 79 (2009), p. 013010. DOI: [10.1103/PhysRevD.79.013010](https://doi.org/10.1103/PhysRevD.79.013010). arXiv: [0808.1530 \[hep-ph\]](https://arxiv.org/abs/0808.1530).
- [715] Florian Domingo and Ulrich Ellwanger. “Constraints from the Muon  $g-2$  on the Parameter Space of the NMSSM”. In: *JHEP* 07 (2008), p. 079. DOI: [10.1088/1126-6708/2008/07/079](https://doi.org/10.1088/1126-6708/2008/07/079). arXiv: [0806.0733 \[hep-ph\]](https://arxiv.org/abs/0806.0733).
- [716] Kingman Cheung, Otto C. W. Kong, and Jae Sik Lee. “Electric and anomalous magnetic dipole moments of the muon in the MSSM”. In: *JHEP* 06 (2009), p. 020. DOI: [10.1088/1126-6708/2009/06/020](https://doi.org/10.1088/1126-6708/2009/06/020). arXiv: [0904.4352 \[hep-ph\]](https://arxiv.org/abs/0904.4352).
- [717] Lars Hofer, Ulrich Nierste, and Dominik Scherer. “Resummation of tan-beta-enhanced supersymmetric loop corrections beyond the decoupling limit”. In: *JHEP* 10 (2009), p. 081. DOI: [10.1088/1126-6708/2009/10/081](https://doi.org/10.1088/1126-6708/2009/10/081). arXiv: [0907.5408 \[hep-ph\]](https://arxiv.org/abs/0907.5408).
- [718] K. S. Babu, Ilia Gogoladze, Qaisar Shafi, and Cem Salih Ün. “Muon  $g-2$ , 125 GeV Higgs boson, and neutralino dark matter in a flavor symmetry-based MSSM”. In: *Phys. Rev. D* 90.11 (2014), p. 116002. DOI: [10.1103/PhysRevD.90.116002](https://doi.org/10.1103/PhysRevD.90.116002). arXiv: [1406.6965 \[hep-ph\]](https://arxiv.org/abs/1406.6965).
- [719] B. Ananthanarayan, George Lazarides, and Q. Shafi. “Top mass prediction from supersymmetric guts”. In: *Phys. Rev. D* 44 (1991), pp. 1613–1615. DOI: [10.1103/PhysRevD.44.1613](https://doi.org/10.1103/PhysRevD.44.1613).
- [720] Amin Aboubrahim, Pran Nath, and Raza M. Syed. “Yukawa coupling unification in an SO(10) model consistent with Fermilab  $(g-2)_\mu$  result”. In: *JHEP* 06 (2021), p. 002. DOI: [10.1007/JHEP06\(2021\)002](https://doi.org/10.1007/JHEP06(2021)002). arXiv: [2104.10114 \[hep-ph\]](https://arxiv.org/abs/2104.10114).
- [721] B. C. Allanach et al. “The Snowmass Points and Slopes: Benchmarks for SUSY Searches”. In: *Eur. Phys. J. C* 25 (2002). Ed. by Norman Graf, pp. 113–123. DOI: [10.1007/s10052-002-0949-3](https://doi.org/10.1007/s10052-002-0949-3). arXiv: [hep-ph/0202233](https://arxiv.org/abs/hep-ph/0202233).

- [722] Juan Antonio Aguilar-Saavedra et al. “Supersymmetry parameter analysis: SPA convention and project”. In: *Eur. Phys. J. C* 46 (2006), pp. 43–60. DOI: [10.1140/epjc/s2005-02460-1](https://doi.org/10.1140/epjc/s2005-02460-1). arXiv: [hep-ph/0511344](https://arxiv.org/abs/hep-ph/0511344).
- [723] Gi-Chol Cho, Kaoru Hagiwara, Yu Matsumoto, and Daisuke Nomura. “The MSSM confronts the precision electroweak data and the muon  $g-2$ ”. In: *JHEP* 11 (2011), p. 068. DOI: [10.1007/JHEP11\(2011\)068](https://doi.org/10.1007/JHEP11(2011)068). arXiv: [1104.1769](https://arxiv.org/abs/1104.1769) [[hep-ph](https://arxiv.org/abs/hep-ph)].
- [724] Motoi Endo, Koichi Hamaguchi, Teppei Kitahara, and Takahiro Yoshinaga. “Probing Bino contribution to muon  $g - 2$ ”. In: *JHEP* 11 (2013), p. 013. DOI: [10.1007/JHEP11\(2013\)013](https://doi.org/10.1007/JHEP11(2013)013). arXiv: [1309.3065](https://arxiv.org/abs/1309.3065) [[hep-ph](https://arxiv.org/abs/hep-ph)].
- [725] So Chigusa, Takeo Moroi, and Yutaro Shoji. “Upper bound on the smuon mass from vacuum stability in the light of muon  $g - 2$  anomaly”. In: *Phys. Lett. B* 831 (2022), p. 137163. DOI: [10.1016/j.physletb.2022.137163](https://doi.org/10.1016/j.physletb.2022.137163). arXiv: [2203.08062](https://arxiv.org/abs/2203.08062) [[hep-ph](https://arxiv.org/abs/hep-ph)].
- [726] So Chigusa, Takeo Moroi, and Yutaro Shoji. “Stability of electroweak vacuum and supersymmetric contribution to muon  $g - 2$ ”. In: *JHEP* 11 (2023), p. 027. DOI: [10.1007/JHEP11\(2023\)027](https://doi.org/10.1007/JHEP11(2023)027). arXiv: [2306.16596](https://arxiv.org/abs/2306.16596) [[hep-ph](https://arxiv.org/abs/hep-ph)].
- [727] Bogdan A. Dobrescu and Patrick J. Fox. “Uplifted Supersymmetric Higgs Region”. In: *Eur. Phys. J. C* 70 (2010), pp. 263–270. DOI: [10.1140/epjc/s10052-010-1399-y](https://doi.org/10.1140/epjc/s10052-010-1399-y). arXiv: [1001.3147](https://arxiv.org/abs/1001.3147) [[hep-ph](https://arxiv.org/abs/hep-ph)].
- [728] Wolfgang Altmannshofer and David M. Straub. “Viability of MSSM scenarios at very large  $\tan\beta$ ”. In: *JHEP* 09 (2010), p. 078. DOI: [10.1007/JHEP09\(2010\)078](https://doi.org/10.1007/JHEP09(2010)078). arXiv: [1004.1993](https://arxiv.org/abs/1004.1993) [[hep-ph](https://arxiv.org/abs/hep-ph)].
- [729] H. G. Fargnoli, C. Gnendiger, S. Paßehr, D. Stöckinger, and H. Stöckinger-Kim. “Non-decoupling two-loop corrections to  $(g - 2)_\mu$  from fermion/sfermion loops in the MSSM”. In: *Phys. Lett. B* 726 (2013), pp. 717–724. DOI: [10.1016/j.physletb.2013.09.034](https://doi.org/10.1016/j.physletb.2013.09.034). arXiv: [1309.0980](https://arxiv.org/abs/1309.0980) [[hep-ph](https://arxiv.org/abs/hep-ph)].
- [730] Peter Athron, Markus Bach, Helvecio G. Fargnoli, Christoph Gnendiger, Robert Greifenhagen, Jae-hyeon Park, Sebastian Paßehr, Dominik Stöckinger, Hyejung Stöckinger-Kim, and Alexander Voigt. “GM2Calc: Precise MSSM prediction for  $(g - 2)$  of the muon”. In: *Eur. Phys. J. C* 76.2 (2016), p. 62. DOI: [10.1140/epjc/s10052-015-3870-2](https://doi.org/10.1140/epjc/s10052-015-3870-2). arXiv: [1510.08071](https://arxiv.org/abs/1510.08071) [[hep-ph](https://arxiv.org/abs/hep-ph)].
- [731] Shu-Min Zhao, Tai-Fu Feng, Hai-Bin Zhang, Ben Yan, and Xi-Jie Zhan. “The corrections from one loop and two-loop Barr-Zee type diagrams to muon MDM in BLMSSM”. In: *JHEP* 11 (2014), p. 119. DOI: [10.1007/JHEP11\(2014\)119](https://doi.org/10.1007/JHEP11(2014)119). arXiv: [1405.7561](https://arxiv.org/abs/1405.7561) [[hep-ph](https://arxiv.org/abs/hep-ph)].
- [732] Jin-Lei Yang, Tai-Fu Feng, Yu-Li Yan, Wei Li, Shu-Min Zhao, and Hai-Bin Zhang. “Lepton-flavor violation and two loop electroweak corrections to  $(g - 2)_\mu$  in the B-L symmetric SSM”. In: *Phys. Rev. D* 99.1 (2019), p. 015002. DOI: [10.1103/PhysRevD.99.015002](https://doi.org/10.1103/PhysRevD.99.015002). arXiv: [1812.03860](https://arxiv.org/abs/1812.03860) [[hep-ph](https://arxiv.org/abs/hep-ph)].
- [733] Xing-Xing Dong, Shu-Min Zhao, Hai-Bin Zhang, and Tai-Fu Feng. “The two-loop corrections to lepton MDMs and EDMs in the EBLMSSM”. In: *J. Phys. G* 47.4 (2020), p. 045002. DOI: [10.1088/1361-6471/ab5f8f](https://doi.org/10.1088/1361-6471/ab5f8f). arXiv: [1901.07701](https://arxiv.org/abs/1901.07701) [[hep-ph](https://arxiv.org/abs/hep-ph)].
- [734] Lu-Hao Su, Shu-Min Zhao, Xing-Xing Dong, Dan-Dan Cui, Tai-Fu Feng, and Hai-Bin Zhang. “The two-loop contributions to muon MDM in  $U(1)_X$  SSM”. In: *Eur. Phys. J. C* 81.5 (2021), p. 433. DOI: [10.1140/epjc/s10052-021-09219-0](https://doi.org/10.1140/epjc/s10052-021-09219-0). arXiv: [2012.04824](https://arxiv.org/abs/2012.04824) [[hep-ph](https://arxiv.org/abs/hep-ph)].

- [735] Chang-Xin Liu, Hai-Bin Zhang, Jin-Lei Yang, Shu-Min Zhao, Yu-Bin Liu, and Tai-Fu Feng. “Higgs boson decay  $h \rightarrow Z\gamma$  and muon magnetic dipole moment in the  $\mu\nu$ SSM”. In: *JHEP* 04 (2020), p. 002. DOI: [10.1007/JHEP04\(2020\)002](https://doi.org/10.1007/JHEP04(2020)002). arXiv: [2002.04370](https://arxiv.org/abs/2002.04370) [[hep-ph](#)].
- [736] Shu-Min Zhao, Lu-Hao Su, Xing-Xing Dong, Tong-Tong Wang, and Tai-Fu Feng. “Study muon  $g - 2$  at two-loop level in the  $U(1)_X$ SSM”. In: *JHEP* 03 (2022), p. 101. DOI: [10.1007/JHEP03\(2022\)101](https://doi.org/10.1007/JHEP03(2022)101). arXiv: [2107.03571](https://arxiv.org/abs/2107.03571) [[hep-ph](#)].
- [737] Marcin Badziak, Zygmunt Lalak, Marek Lewicki, Marek Olechowski, and Stefan Pokorski. “Upper bounds on sparticle masses from muon  $g - 2$  and the Higgs mass and the complementarity of future colliders”. In: *JHEP* 03 (2015), p. 003. DOI: [10.1007/JHEP03\(2015\)003](https://doi.org/10.1007/JHEP03(2015)003). arXiv: [1411.1450](https://arxiv.org/abs/1411.1450) [[hep-ph](#)].
- [738] Motoi Endo, Koichi Hamaguchi, Sho Iwamoto, and Keisuke Yanagi. “Probing minimal SUSY scenarios in the light of muon  $g - 2$  and dark matter”. In: *JHEP* 06 (2017), p. 031. DOI: [10.1007/JHEP06\(2017\)031](https://doi.org/10.1007/JHEP06(2017)031). arXiv: [1704.05287](https://arxiv.org/abs/1704.05287) [[hep-ph](#)].
- [739] Manimala Chakraborti, Sho Iwamoto, Jong Soo Kim, Rafał Maselek, and Kazuki Sakurai. “Supersymmetric explanation of the muon  $g - 2$  anomaly with and without stable neutralino”. In: *JHEP* 08 (2022), p. 124. DOI: [10.1007/JHEP08\(2022\)124](https://doi.org/10.1007/JHEP08(2022)124). arXiv: [2202.12928](https://arxiv.org/abs/2202.12928) [[hep-ph](#)].
- [740] Motoi Endo, Koichi Hamaguchi, Sho Iwamoto, Kazunori Nakayama, and Norimi Yokozaki. “Higgs mass and muon anomalous magnetic moment in the  $U(1)$  extended MSSM”. In: *Phys. Rev. D* 85 (2012), p. 095006. DOI: [10.1103/PhysRevD.85.095006](https://doi.org/10.1103/PhysRevD.85.095006). arXiv: [1112.6412](https://arxiv.org/abs/1112.6412) [[hep-ph](#)].
- [741] Motoi Endo, Koichi Hamaguchi, Sho Iwamoto, and Norimi Yokozaki. “Higgs mass, muon  $g-2$ , and LHC prospects in gauge mediation models with vector-like matters”. In: *Phys. Rev. D* 85 (2012), p. 095012. DOI: [10.1103/PhysRevD.85.095012](https://doi.org/10.1103/PhysRevD.85.095012). arXiv: [1112.5653](https://arxiv.org/abs/1112.5653) [[hep-ph](#)].
- [742] Motoi Endo, Koichi Hamaguchi, Sho Iwamoto, and Norimi Yokozaki. “Higgs Mass and Muon Anomalous Magnetic Moment in Supersymmetric Models with Vector-Like Matters”. In: *Phys. Rev. D* 84 (2011), p. 075017. DOI: [10.1103/PhysRevD.84.075017](https://doi.org/10.1103/PhysRevD.84.075017). arXiv: [1108.3071](https://arxiv.org/abs/1108.3071) [[hep-ph](#)].
- [743] Jihn E. Kim. “Inverted effective supersymmetry with combined  $Z'$  and gravity mediation, and muon anomalous magnetic moment”. In: *Phys. Rev. D* 87.1 (2013), p. 015004. DOI: [10.1103/PhysRevD.87.015004](https://doi.org/10.1103/PhysRevD.87.015004). arXiv: [1208.5484](https://arxiv.org/abs/1208.5484) [[hep-ph](#)].
- [744] Masahiro Ibe, Shigeki Matsumoto, Tsutomu T. Yanagida, and Norimi Yokozaki. “Heavy Squarks and Light Sleptons in Gauge Mediation ~From the viewpoint of 125 GeV Higgs Boson and Muon  $g-2$ ~”. In: *JHEP* 03 (2013), p. 078. DOI: [10.1007/JHEP03\(2013\)078](https://doi.org/10.1007/JHEP03(2013)078). arXiv: [1210.3122](https://arxiv.org/abs/1210.3122) [[hep-ph](#)].
- [745] Hai-Bin Zhang, Tai-Fu Feng, Shu-Min Zhao, and Tie-Jun Gao. “Lepton-flavor violation and  $(g - 2)_\mu$  in the  $\mu\nu$ SSM”. In: *Nucl. Phys. B* 873 (2013). [Erratum: *Nucl.Phys.B* 879, 235 (2014)], pp. 300–324. DOI: [10.1016/j.nuclphysb.2013.04.018](https://doi.org/10.1016/j.nuclphysb.2013.04.018). arXiv: [1304.6248](https://arxiv.org/abs/1304.6248) [[hep-ph](#)].
- [746] Gautam Bhattacharyya, Biplob Bhattacharjee, Tsutomu T. Yanagida, and Norimi Yokozaki. “A practical GMSB model for explaining the muon  $(g-2)$  with gauge coupling unification”. In: *Phys. Lett. B* 730 (2014), pp. 231–235. DOI: [10.1016/j.physletb.2013.12.064](https://doi.org/10.1016/j.physletb.2013.12.064). arXiv: [1311.1906](https://arxiv.org/abs/1311.1906) [[hep-ph](#)].

- [747] Sujeet Akula and Pran Nath. “Gluino-driven radiative breaking, Higgs boson mass, muon  $g-2$ , and the Higgs diphoton decay in supergravity unification”. In: *Phys. Rev. D* 87.11 (2013), p. 115022. DOI: [10.1103/PhysRevD.87.115022](https://doi.org/10.1103/PhysRevD.87.115022). arXiv: [1304.5526](https://arxiv.org/abs/1304.5526) [hep-ph].
- [748] Jason L. Evans, Masahiro Ibe, Keith A. Olive, and Tsutomu T. Yanagida. “One-loop anomaly mediated scalar masses and  $(g-2)_{\mu}$  in pure gravity mediation”. In: *Eur. Phys. J. C* 74.2 (2014), p. 2775. DOI: [10.1140/epjc/s10052-014-2775-9](https://doi.org/10.1140/epjc/s10052-014-2775-9). arXiv: [1312.1984](https://arxiv.org/abs/1312.1984) [hep-ph].
- [749] Masahiro Ibe, Tsutomu T. Yanagida, and Norimi Yokozaki. “Muon  $g-2$  and 125 GeV Higgs in Split-Family Supersymmetry”. In: *JHEP* 08 (2013), p. 067. DOI: [10.1007/JHEP08\(2013\)067](https://doi.org/10.1007/JHEP08(2013)067). arXiv: [1303.6995](https://arxiv.org/abs/1303.6995) [hep-ph].
- [750] Motoi Endo, Koichi Hamaguchi, Sho Iwamoto, and Takahiro Yoshinaga. “Muon  $g-2$  vs LHC in Supersymmetric Models”. In: *JHEP* 01 (2014), p. 123. DOI: [10.1007/JHEP01\(2014\)123](https://doi.org/10.1007/JHEP01(2014)123). arXiv: [1303.4256](https://arxiv.org/abs/1303.4256) [hep-ph].
- [751] Sho Iwamoto, Tsutomu T. Yanagida, and Norimi Yokozaki. “CP-safe gravity mediation and muon  $g-2$ ”. In: *PTEP* 2015 (2015), 073B01. DOI: [10.1093/ptep/ptv084](https://doi.org/10.1093/ptep/ptv084). arXiv: [1407.4226](https://arxiv.org/abs/1407.4226) [hep-ph].
- [752] Jörn Kersten, Jae-hyeon Park, Dominik Stöckinger, and Liliana Velasco-Sevilla. “Understanding the correlation between  $(g-2)_{\mu}$  and  $\mu \rightarrow e\gamma$  in the MSSM”. In: *JHEP* 08 (2014), p. 118. DOI: [10.1007/JHEP08\(2014\)118](https://doi.org/10.1007/JHEP08(2014)118). arXiv: [1405.2972](https://arxiv.org/abs/1405.2972) [hep-ph].
- [753] Ilia Gogoladze, Fariha Nasir, Qaisar Shafi, and Cem Salih Un. “Nonuniversal Gaugino Masses and Muon  $g-2$ ”. In: *Phys. Rev. D* 90.3 (2014), p. 035008. DOI: [10.1103/PhysRevD.90.035008](https://doi.org/10.1103/PhysRevD.90.035008). arXiv: [1403.2337](https://arxiv.org/abs/1403.2337) [hep-ph].
- [754] M. Adeel Ajaib, Bhaskar Dutta, Tathagata Ghosh, Ilia Gogoladze, and Qaisar Shafi. “Neutralinos and sleptons at the LHC in light of muon  $(g-2)_{\mu}$ ”. In: *Phys. Rev. D* 92.7 (2015), p. 075033. DOI: [10.1103/PhysRevD.92.075033](https://doi.org/10.1103/PhysRevD.92.075033). arXiv: [1505.05896](https://arxiv.org/abs/1505.05896) [hep-ph].
- [755] Kamila Kowalska, Leszek Roszkowski, Enrico Maria Sessolo, and Andrew J. Williams. “GUT-inspired SUSY and the muon  $g-2$  anomaly: prospects for LHC 14 TeV”. In: *JHEP* 06 (2015), p. 020. DOI: [10.1007/JHEP06\(2015\)020](https://doi.org/10.1007/JHEP06(2015)020). arXiv: [1503.08219](https://arxiv.org/abs/1503.08219) [hep-ph].
- [756] Shaaban Khalil and Cem Salih Un. “Muon Anomalous Magnetic Moment in SUSY B-L Model with Inverse Seesaw”. In: *Phys. Lett. B* 763 (2016), pp. 164–168. DOI: [10.1016/j.physletb.2016.10.035](https://doi.org/10.1016/j.physletb.2016.10.035). arXiv: [1509.05391](https://arxiv.org/abs/1509.05391) [hep-ph].
- [757] Ilia Gogoladze, Qaisar Shafi, and Cem Salih Ün. “Reconciling the muon  $g-2$ , a 125 GeV Higgs boson, and dark matter in gauge mediation models”. In: *Phys. Rev. D* 92.11 (2015), p. 115014. DOI: [10.1103/PhysRevD.92.115014](https://doi.org/10.1103/PhysRevD.92.115014). arXiv: [1509.07906](https://arxiv.org/abs/1509.07906) [hep-ph].
- [758] F. V. Flores-Baez, M. Gómez Bock, and M. Mondragón. “Muon  $g-2$  through a flavor structure on soft SUSY terms”. In: *Eur. Phys. J. C* 76.10 (2016), p. 561. DOI: [10.1140/epjc/s10052-016-4402-4](https://doi.org/10.1140/epjc/s10052-016-4402-4). arXiv: [1512.00902](https://arxiv.org/abs/1512.00902) [hep-ph].
- [759] Keisuke Harigaya, Tsutomu T. Yanagida, and Norimi Yokozaki. “Muon  $g-2$  in focus point SUSY”. In: *Phys. Rev. D* 92.3 (2015), p. 035011. DOI: [10.1103/PhysRevD.92.035011](https://doi.org/10.1103/PhysRevD.92.035011). arXiv: [1505.01987](https://arxiv.org/abs/1505.01987) [hep-ph].
- [760] Keisuke Harigaya, Tsutomu T. Yanagida, and Norimi Yokozaki. “Higgs boson mass of 125 GeV and  $g-2$  of the muon in a gaugino mediation model”. In: *Phys. Rev. D* 91.7 (2015), p. 075010. DOI: [10.1103/PhysRevD.91.075010](https://doi.org/10.1103/PhysRevD.91.075010). arXiv: [1501.07447](https://arxiv.org/abs/1501.07447) [hep-ph].

- [761] Joydeep Chakrabortty, Arghya Choudhury, and Subhadeep Mondal. “Non-universal Gaugino mass models under the lamppost of muon ( $g-2$ )”. In: *JHEP* 07 (2015), p. 038. DOI: [10.1007/JHEP07\(2015\)038](https://doi.org/10.1007/JHEP07(2015)038). arXiv: [1503.08703](https://arxiv.org/abs/1503.08703) [[hep-ph](#)].
- [762] B. Paul Padley, Kuver Sinha, and Kechen Wang. “Natural Supersymmetry, Muon  $g - 2$ , and the Last Crevices for the Top Squark”. In: *Phys. Rev. D* 92.5 (2015), p. 055025. DOI: [10.1103/PhysRevD.92.055025](https://doi.org/10.1103/PhysRevD.92.055025). arXiv: [1505.05877](https://arxiv.org/abs/1505.05877) [[hep-ph](#)].
- [763] Debtosh Chowdhury and Norimi Yokozaki. “Muon  $g - 2$  in anomaly mediated SUSY breaking”. In: *JHEP* 08 (2015), p. 111. DOI: [10.1007/JHEP08\(2015\)111](https://doi.org/10.1007/JHEP08(2015)111). arXiv: [1505.05153](https://arxiv.org/abs/1505.05153) [[hep-ph](#)].
- [764] Tianjun Li, Shabbar Raza, and Kechen Wang. “Constraining Natural SUSY via the Higgs Coupling and the Muon Anomalous Magnetic Moment Measurements”. In: *Phys. Rev. D* 93.5 (2016), p. 055040. DOI: [10.1103/PhysRevD.93.055040](https://doi.org/10.1103/PhysRevD.93.055040). arXiv: [1601.00178](https://arxiv.org/abs/1601.00178) [[hep-ph](#)].
- [765] Nobuchika Okada and Hieu Minh Tran. “125 GeV Higgs boson mass and muon  $g - 2$  in 5D MSSM”. In: *Phys. Rev. D* 94.7 (2016), p. 075016. DOI: [10.1103/PhysRevD.94.075016](https://doi.org/10.1103/PhysRevD.94.075016). arXiv: [1606.05329](https://arxiv.org/abs/1606.05329) [[hep-ph](#)].
- [766] Alexander S. Belyaev, Jose E. Camargo-Molina, Steve F. King, David J. Miller, António P. Morais, and Patrick B. Schaefers. “A to Z of the Muon Anomalous Magnetic Moment in the MSSM with Pati-Salam at the GUT scale”. In: *JHEP* 06 (2016), p. 142. DOI: [10.1007/JHEP06\(2016\)142](https://doi.org/10.1007/JHEP06(2016)142). arXiv: [1605.02072](https://arxiv.org/abs/1605.02072) [[hep-ph](#)].
- [767] Archil Kobakhidze, Matthew Talia, and Lei Wu. “Probing the MSSM explanation of the muon  $g-2$  anomaly in dark matter experiments and at a 100 TeV  $pp$  collider”. In: *Phys. Rev. D* 95.5 (2017), p. 055023. DOI: [10.1103/PhysRevD.95.055023](https://doi.org/10.1103/PhysRevD.95.055023). arXiv: [1608.03641](https://arxiv.org/abs/1608.03641) [[hep-ph](#)].
- [768] Geneviève Bélanger, Jonathan Da Silva, and Hieu Minh Tran. “Dark matter in U(1) extensions of the MSSM with gauge kinetic mixing”. In: *Phys. Rev. D* 95.11 (2017), p. 115017. DOI: [10.1103/PhysRevD.95.115017](https://doi.org/10.1103/PhysRevD.95.115017). arXiv: [1703.03275](https://arxiv.org/abs/1703.03275) [[hep-ph](#)].
- [769] Takeshi Fukuyama, Nobuchika Okada, and Hieu Minh Tran. “Sparticle spectroscopy of the minimal SO(10) model”. In: *Phys. Lett. B* 767 (2017), pp. 295–302. DOI: [10.1016/j.physletb.2017.02.021](https://doi.org/10.1016/j.physletb.2017.02.021). arXiv: [1611.08341](https://arxiv.org/abs/1611.08341) [[hep-ph](#)].
- [770] Kaoru Hagiwara, Kai Ma, and Satyanarayan Mukhopadhyay. “Closing in on the chargino contribution to the muon  $g-2$  in the MSSM: current LHC constraints”. In: *Phys. Rev. D* 97.5 (2018), p. 055035. DOI: [10.1103/PhysRevD.97.055035](https://doi.org/10.1103/PhysRevD.97.055035). arXiv: [1706.09313](https://arxiv.org/abs/1706.09313) [[hep-ph](#)].
- [771] E. Bagnaschi et al. “Likelihood Analysis of the pMSSM11 in Light of LHC 13-TeV Data”. In: *Eur. Phys. J. C* 78.3 (2018), p. 256. DOI: [10.1140/epjc/s10052-018-5697-0](https://doi.org/10.1140/epjc/s10052-018-5697-0). arXiv: [1710.11091](https://arxiv.org/abs/1710.11091) [[hep-ph](#)].
- [772] Arghya Choudhury, Soumya Rao, and Leszek Roszkowski. “Impact of LHC data on muon  $g - 2$  solutions in a vectorlike extension of the constrained MSSM”. In: *Phys. Rev. D* 96.7 (2017), p. 075046. DOI: [10.1103/PhysRevD.96.075046](https://doi.org/10.1103/PhysRevD.96.075046). arXiv: [1708.05675](https://arxiv.org/abs/1708.05675) [[hep-ph](#)].
- [773] Kun Wang, Fei Wang, Jingya Zhu, and Quanlin Jie. “The semi-constrained NMSSM in light of muon  $g-2$ , LHC, and dark matter constraints”. In: *Chin. Phys. C* 42.10 (2018), pp. 103109–103109. DOI: [10.1088/1674-1137/42/10/103109](https://doi.org/10.1088/1674-1137/42/10/103109). arXiv: [1811.04435](https://arxiv.org/abs/1811.04435) [[hep-ph](#)].

- [774] Peter Cox, Chengcheng Han, and Tsutomu T. Yanagida. “Muon  $g - 2$  and dark matter in the minimal supersymmetric standard model”. In: *Phys. Rev. D* 98.5 (2018), p. 055015. DOI: [10.1103/PhysRevD.98.055015](https://doi.org/10.1103/PhysRevD.98.055015). arXiv: [1805.02802](https://arxiv.org/abs/1805.02802) [hep-ph].
- [775] Murat Abdughani, Ken-Ichi Hikasa, Lei Wu, Jin Min Yang, and Jun Zhao. “Testing electroweak SUSY for muon  $g - 2$  and dark matter at the LHC and beyond”. In: *JHEP* 11 (2019), p. 095. DOI: [10.1007/JHEP11\(2019\)095](https://doi.org/10.1007/JHEP11(2019)095). arXiv: [1909.07792](https://arxiv.org/abs/1909.07792) [hep-ph].
- [776] Motoi Endo, Koichi Hamaguchi, Sho Iwamoto, and Teppei Kitahara. “Muon  $g-2$  vs LHC Run 2 in supersymmetric models”. In: *JHEP* 04 (2020), p. 165. DOI: [10.1007/JHEP04\(2020\)165](https://doi.org/10.1007/JHEP04(2020)165). arXiv: [2001.11025](https://arxiv.org/abs/2001.11025) [hep-ph].
- [777] Manimala Chakraborti, Sven Heinemeyer, and Ipsita Saha. “Improved  $(g - 2)_\mu$  Measurements and Supersymmetry”. In: *Eur. Phys. J. C* 80.10 (2020), p. 984. DOI: [10.1140/epjc/s10052-020-08504-8](https://doi.org/10.1140/epjc/s10052-020-08504-8). arXiv: [2006.15157](https://arxiv.org/abs/2006.15157) [hep-ph].
- [778] Manimala Chakraborti, Sven Heinemeyer, and Ipsita Saha. “Improved  $(g - 2)_\mu$  measurements and wino/higgsino dark matter”. In: *Eur. Phys. J. C* 81.12 (2021), p. 1069. DOI: [10.1140/epjc/s10052-021-09814-1](https://doi.org/10.1140/epjc/s10052-021-09814-1). arXiv: [2103.13403](https://arxiv.org/abs/2103.13403) [hep-ph].
- [779] Peter Cox, Chengcheng Han, and Tsutomu T. Yanagida. “Muon  $g-2$  and coannihilating dark matter in the minimal supersymmetric standard model”. In: *Phys. Rev. D* 104.7 (2021), p. 075035. DOI: [10.1103/PhysRevD.104.075035](https://doi.org/10.1103/PhysRevD.104.075035). arXiv: [2104.03290](https://arxiv.org/abs/2104.03290) [hep-ph].
- [780] Manimala Chakraborti, Sven Heinemeyer, and Ipsita Saha. “The new “MUON G-2” result and supersymmetry”. In: *Eur. Phys. J. C* 81.12 (2021), p. 1114. DOI: [10.1140/epjc/s10052-021-09900-4](https://doi.org/10.1140/epjc/s10052-021-09900-4). arXiv: [2104.03287](https://arxiv.org/abs/2104.03287) [hep-ph].
- [781] Manimala Chakraborti, Sven Heinemeyer, Ipsita Saha, and Christian Schappacher. “ $(g - 2)_\mu$  and SUSY dark matter: direct detection and collider search complementarity”. In: *Eur. Phys. J. C* 82.5 (2022), p. 483. DOI: [10.1140/epjc/s10052-022-10414-w](https://doi.org/10.1140/epjc/s10052-022-10414-w). arXiv: [2112.01389](https://arxiv.org/abs/2112.01389) [hep-ph].
- [782] Manimala Chakraborti, Sven Heinemeyer, and Ipsita Saha. “ $(g - 2)_\mu$  and stau coannihilation: dark matter and collider analysis”. In: *Eur. Phys. J. C* 84.2 (2024), p. 165. DOI: [10.1140/epjc/s10052-024-12497-z](https://doi.org/10.1140/epjc/s10052-024-12497-z). arXiv: [2308.05723](https://arxiv.org/abs/2308.05723) [hep-ph].
- [783] Motoi Endo, Koichi Hamaguchi, Sho Iwamoto, and Teppei Kitahara. “Supersymmetric interpretation of the muon  $g - 2$  anomaly”. In: *JHEP* 07 (2021), p. 075. DOI: [10.1007/JHEP07\(2021\)075](https://doi.org/10.1007/JHEP07(2021)075). arXiv: [2104.03217](https://arxiv.org/abs/2104.03217) [hep-ph].
- [784] Melissa Van Beekveld, Wim Beenakker, Marrit Schutten, and Jeremy De Wit. “Dark matter, fine-tuning and  $(g - 2)_\mu$  in the pMSSM”. In: *SciPost Phys.* 11.3 (2021), p. 049. DOI: [10.21468/SciPostPhys.11.3.049](https://doi.org/10.21468/SciPostPhys.11.3.049). arXiv: [2104.03245](https://arxiv.org/abs/2104.03245) [hep-ph].
- [785] Yangle He, Lei Meng, Yuanfang Yue, and Di Zhang. “Impact of the recent measurement of  $(g-2)_\mu$ , the LHC search for supersymmetry, and the LZ experiment on the minimal supersymmetric standard model”. In: *Phys. Rev. D* 108.11 (2023), p. 115010. DOI: [10.1103/PhysRevD.108.115010](https://doi.org/10.1103/PhysRevD.108.115010). arXiv: [2303.02360](https://arxiv.org/abs/2303.02360) [hep-ph].
- [786] Stephen P. Martin. “Curtain lowers on directly detectable higgsino dark matter”. In: *Phys. Rev. D* 111.7 (2025), p. 075004. DOI: [10.1103/PhysRevD.111.075004](https://doi.org/10.1103/PhysRevD.111.075004). arXiv: [2412.08958](https://arxiv.org/abs/2412.08958) [hep-ph].

- [787] Subhadip Bisal, Arindam Chatterjee, Debottam Das, and Syed Adil Pasha. “Confronting electroweak MSSM through one-loop renormalized neutralino-Higgs interactions for dark matter direct detection and the muon  $g-2$ ”. In: *Phys. Rev. D* 110.1 (2024), p. 015021. DOI: [10.1103/PhysRevD.110.015021](https://doi.org/10.1103/PhysRevD.110.015021). arXiv: [2311.09938](https://arxiv.org/abs/2311.09938) [hep-ph].
- [788] John R. Ellis, Toby Falk, and Keith A. Olive. “Neutralino - Stau coannihilation and the cosmological upper limit on the mass of the lightest supersymmetric particle”. In: *Phys. Lett. B* 444 (1998), pp. 367–372. DOI: [10.1016/S0370-2693\(98\)01392-6](https://doi.org/10.1016/S0370-2693(98)01392-6). arXiv: [hep-ph/9810360](https://arxiv.org/abs/hep-ph/9810360).
- [789] John R. Ellis, Toby Falk, Keith A. Olive, and Mark Srednicki. “Calculations of neutralino-stau coannihilation channels and the cosmologically relevant region of MSSM parameter space”. In: *Astropart. Phys.* 13 (2000). [Erratum: *Astropart. Phys.* 15, 413–414 (2001)], pp. 181–213. DOI: [10.1016/S0927-6505\(99\)00104-8](https://doi.org/10.1016/S0927-6505(99)00104-8). arXiv: [hep-ph/9905481](https://arxiv.org/abs/hep-ph/9905481).
- [790] Takeshi Nihei, Leszek Roszkowski, and Roberto Ruiz de Austri. “Exact cross-sections for the neutralino slepton coannihilation”. In: *JHEP* 07 (2002), p. 024. DOI: [10.1088/1126-6708/2002/07/024](https://doi.org/10.1088/1126-6708/2002/07/024). arXiv: [hep-ph/0206266](https://arxiv.org/abs/hep-ph/0206266).
- [791] Keisuke Harigaya, Kunio Kaneta, and Shigeki Matsumoto. “Gaugino coannihilations”. In: *Phys. Rev. D* 89.11 (2014), p. 115021. DOI: [10.1103/PhysRevD.89.115021](https://doi.org/10.1103/PhysRevD.89.115021). arXiv: [1403.0715](https://arxiv.org/abs/1403.0715) [hep-ph].
- [792] Celine Boehm, Abdelhak Djouadi, and Manuel Drees. “Light scalar top quarks and supersymmetric dark matter”. In: *Phys. Rev. D* 62 (2000), p. 035012. DOI: [10.1103/PhysRevD.62.035012](https://doi.org/10.1103/PhysRevD.62.035012). arXiv: [hep-ph/9911496](https://arxiv.org/abs/hep-ph/9911496).
- [793] Peisi Huang and Carlos E. M. Wagner. “Blind Spots for neutralino Dark Matter in the MSSM with an intermediate  $m_A$ ”. In: *Phys. Rev. D* 90.1 (2014), p. 015018. DOI: [10.1103/PhysRevD.90.015018](https://doi.org/10.1103/PhysRevD.90.015018). arXiv: [1404.0392](https://arxiv.org/abs/1404.0392) [hep-ph].
- [794] Sebastian Baum, Marcela Carena, Nausheen R. Shah, and Carlos E. M. Wagner. “The tiny ( $g-2$ ) muon wobble from small- $\mu$  supersymmetry”. In: *JHEP* 01 (2022), p. 025. DOI: [10.1007/JHEP01\(2022\)025](https://doi.org/10.1007/JHEP01(2022)025). arXiv: [2104.03302](https://arxiv.org/abs/2104.03302) [hep-ph].
- [795] Sebastian Baum, Marcela Carena, Tong Ou, Duncan Rocha, Nausheen R. Shah, and Carlos E. M. Wagner. “Lighting up the LHC with Dark Matter”. In: *JHEP* 11 (2023), p. 037. DOI: [10.1007/JHEP11\(2023\)037](https://doi.org/10.1007/JHEP11(2023)037). arXiv: [2303.01523](https://arxiv.org/abs/2303.01523) [hep-ph].
- [796] Joseph Bramante, Nishita Desai, Patrick Fox, Adam Martin, Bryan Ostdiek, and Tilman Plehn. “Towards the Final Word on Neutralino Dark Matter”. In: *Phys. Rev. D* 93.6 (2016), p. 063525. DOI: [10.1103/PhysRevD.93.063525](https://doi.org/10.1103/PhysRevD.93.063525). arXiv: [1510.03460](https://arxiv.org/abs/1510.03460) [hep-ph].
- [797] Manimala Chakraborti, Utpal Chattopadhyay, and Sujoy Poddar. “How light a higgsino or a wino dark matter can become in a compressed scenario of MSSM”. In: *JHEP* 09 (2017), p. 064. DOI: [10.1007/JHEP09\(2017\)064](https://doi.org/10.1007/JHEP09(2017)064). arXiv: [1702.03954](https://arxiv.org/abs/1702.03954) [hep-ph].
- [798] Kamila Kowalska and Enrico Maria Sessolo. “The discreet charm of higgsino dark matter - a pocket review”. In: *Adv. High Energy Phys.* 2018 (2018), p. 6828560. DOI: [10.1155/2018/6828560](https://doi.org/10.1155/2018/6828560). arXiv: [1802.04097](https://arxiv.org/abs/1802.04097) [hep-ph].
- [799] Howard Baer, Vernon Barger, Dibyashree Sengupta, and Xerxes Tata. “Is natural higgsino-only dark matter excluded?” In: *Eur. Phys. J. C* 78.10 (2018), p. 838. DOI: [10.1140/epjc/s10052-018-6306-y](https://doi.org/10.1140/epjc/s10052-018-6306-y). arXiv: [1803.11210](https://arxiv.org/abs/1803.11210) [hep-ph].

- [800] Martin Beneke, Robert Szafron, and Kai Urban. “Sommerfeld-corrected relic abundance of wino dark matter with NLO electroweak potentials”. In: *JHEP* 02 (2021), p. 020. DOI: [10.1007/JHEP02\(2021\)020](https://doi.org/10.1007/JHEP02(2021)020). arXiv: [2009.00640](https://arxiv.org/abs/2009.00640) [[hep-ph](#)].
- [801] A. M. Sirunyan et al. “Search for electroweak production of charginos and neutralinos in multilepton final states in proton-proton collisions at  $\sqrt{s} = 13$  TeV”. In: *JHEP* 03 (2018), p. 166. DOI: [10.1007/JHEP03\(2018\)166](https://doi.org/10.1007/JHEP03(2018)166). arXiv: [1709.05406](https://arxiv.org/abs/1709.05406) [[hep-ex](#)].
- [802] Albert M. Sirunyan et al. “Search for supersymmetric partners of electrons and muons in proton-proton collisions at  $\sqrt{s} = 13$  TeV”. In: *Phys. Lett. B* 790 (2019), pp. 140–166. DOI: [10.1016/j.physletb.2019.01.005](https://doi.org/10.1016/j.physletb.2019.01.005). arXiv: [1806.05264](https://arxiv.org/abs/1806.05264) [[hep-ex](#)].
- [803] Peter Athron, Jae-hyeon Park, Dominik Stöckinger, and Alexander Voigt. “FlexibleSUSY—A spectrum generator generator for supersymmetric models”. In: *Comput. Phys. Commun.* 190 (2015), pp. 139–172. DOI: [10.1016/j.cpc.2014.12.020](https://doi.org/10.1016/j.cpc.2014.12.020). arXiv: [1406.2319](https://arxiv.org/abs/1406.2319) [[hep-ph](#)].
- [804] Peter Athron, Jae-hyeon Park, Tom Steudtner, Dominik Stöckinger, and Alexander Voigt. “Precise Higgs mass calculations in (non-)minimal supersymmetry at both high and low scales”. In: *JHEP* 01 (2017), p. 079. DOI: [10.1007/JHEP01\(2017\)079](https://doi.org/10.1007/JHEP01(2017)079). arXiv: [1609.00371](https://arxiv.org/abs/1609.00371) [[hep-ph](#)].
- [805] Peter Athron, Markus Bach, Dylan Harries, Thomas Kwasnitza, Jae-hyeon Park, Dominik Stöckinger, Alexander Voigt, and Jobst Ziebell. “FlexibleSUSY 2.0: Extensions to investigate the phenomenology of SUSY and non-SUSY models”. In: *Comput. Phys. Commun.* 230 (2018), pp. 145–217. DOI: [10.1016/j.cpc.2018.04.016](https://doi.org/10.1016/j.cpc.2018.04.016). arXiv: [1710.03760](https://arxiv.org/abs/1710.03760) [[hep-ph](#)].
- [806] Thomas Kwasnitza, Dominik Stöckinger, and Alexander Voigt. “Improved MSSM Higgs mass calculation using the 3-loop FlexibleEFTHiggs approach including  $x_t$ -resummation”. In: *JHEP* 07.07 (2020), p. 197. DOI: [10.1007/JHEP06\(2023\)201](https://doi.org/10.1007/JHEP06(2023)201). arXiv: [2003.04639](https://arxiv.org/abs/2003.04639) [[hep-ph](#)].
- [807] Peter Athron, Adam Büchner, Dylan Harries, Wojciech Kotlarski, Dominik Stöckinger, and Alexander Voigt. “FlexibleDecay: An automated calculator of scalar decay widths”. In: *Comput. Phys. Commun.* 283 (2023), p. 108584. DOI: [10.1016/j.cpc.2022.108584](https://doi.org/10.1016/j.cpc.2022.108584). arXiv: [2106.05038](https://arxiv.org/abs/2106.05038) [[hep-ph](#)].
- [808] Uladzimir Khasianevich, Wojciech Kotlarski, Dominik Stöckinger, and Alexander Voigt. “FlexibleSUSY extended to automatically compute physical quantities in any beyond the standard model theory: Charged lepton flavor violation processes, Higgs decays, and user-defined observables”. In: *Comput. Phys. Commun.* 302 (2024), p. 109244. DOI: [10.1016/j.cpc.2024.109244](https://doi.org/10.1016/j.cpc.2024.109244). arXiv: [2402.14630](https://arxiv.org/abs/2402.14630) [[hep-ph](#)].
- [809] B. C. Allanach. “SOFTSUSY: a program for calculating supersymmetric spectra”. In: *Comput. Phys. Commun.* 143 (2002), pp. 305–331. DOI: [10.1016/S0010-4655\(01\)00460-X](https://doi.org/10.1016/S0010-4655(01)00460-X). arXiv: [hep-ph/0104145](https://arxiv.org/abs/hep-ph/0104145).
- [810] B. C. Allanach, P. Athron, Lewis C. Tunstall, A. Voigt, and A. G. Williams. “Next-to-Minimal SOFTSUSY”. In: *Comput. Phys. Commun.* 185 (2014). [Erratum: *Comput.Phys.Comm.* 250, 107044 (2020)], pp. 2322–2339. DOI: [10.1016/j.cpc.2014.04.015](https://doi.org/10.1016/j.cpc.2014.04.015). arXiv: [1311.7659](https://arxiv.org/abs/1311.7659) [[hep-ph](#)].
- [811] Florian Staub. “From Superpotential to Model Files for FeynArts and CalcHep/CompHep”. In: *Comput. Phys. Commun.* 181 (2010), pp. 1077–1086. DOI: [10.1016/j.cpc.2010.01.011](https://doi.org/10.1016/j.cpc.2010.01.011). arXiv: [0909.2863](https://arxiv.org/abs/0909.2863) [[hep-ph](#)].

- [812] Florian Staub. “Automatic Calculation of supersymmetric Renormalization Group Equations and Self Energies”. In: *Comput. Phys. Commun.* 182 (2011), pp. 808–833. DOI: [10.1016/j.cpc.2010.11.030](https://doi.org/10.1016/j.cpc.2010.11.030). arXiv: [1002.0840](https://arxiv.org/abs/1002.0840) [hep-ph].
- [813] Florian Staub. “SARAH 3.2: Dirac Gauginos, UFO output, and more”. In: *Comput. Phys. Commun.* 184 (2013), pp. 1792–1809. DOI: [10.1016/j.cpc.2013.02.019](https://doi.org/10.1016/j.cpc.2013.02.019). arXiv: [1207.0906](https://arxiv.org/abs/1207.0906) [hep-ph].
- [814] Florian Staub. “SARAH 4 : A tool for (not only SUSY) model builders”. In: *Comput. Phys. Commun.* 185 (2014), pp. 1773–1790. DOI: [10.1016/j.cpc.2014.02.018](https://doi.org/10.1016/j.cpc.2014.02.018). arXiv: [1309.7223](https://arxiv.org/abs/1309.7223) [hep-ph].
- [815] Peter Athron et al. “GAMBIT: The Global and Modular Beyond-the-Standard-Model Inference Tool”. In: *Eur. Phys. J. C* 77.11 (2017). [Addendum: *Eur.Phys.J.C* 78, 98 (2018)], p. 784. DOI: [10.1140/epjc/s10052-017-5321-8](https://doi.org/10.1140/epjc/s10052-017-5321-8). arXiv: [1705.07908](https://arxiv.org/abs/1705.07908) [hep-ph].
- [816] Peter Athron et al. “SpecBit, DecayBit and PrecisionBit: GAMBIT modules for computing mass spectra, particle decay rates and precision observables”. In: *Eur. Phys. J. C* 78.1 (2018), p. 22. DOI: [10.1140/epjc/s10052-017-5390-8](https://doi.org/10.1140/epjc/s10052-017-5390-8). arXiv: [1705.07936](https://arxiv.org/abs/1705.07936) [hep-ph].
- [817] Torsten Bringmann et al. “DarkBit: A GAMBIT module for computing dark matter observables and likelihoods”. In: *Eur. Phys. J. C* 77.12 (2017), p. 831. DOI: [10.1140/epjc/s10052-017-5155-4](https://doi.org/10.1140/epjc/s10052-017-5155-4). arXiv: [1705.07920](https://arxiv.org/abs/1705.07920) [hep-ph].
- [818] Gregory D. Martinez, James McKay, Ben Farmer, Pat Scott, Elinore Roebber, Antje Putze, and Jan Conrad. “Comparison of statistical sampling methods with ScannerBit, the GAMBIT scanning module”. In: *Eur. Phys. J. C* 77.11 (2017), p. 761. DOI: [10.1140/epjc/s10052-017-5274-y](https://doi.org/10.1140/epjc/s10052-017-5274-y). arXiv: [1705.07959](https://arxiv.org/abs/1705.07959) [hep-ph].
- [819] Florian U. Bernlochner et al. “FlavBit: A GAMBIT module for computing flavour observables and likelihoods”. In: *Eur. Phys. J. C* 77.11 (2017), p. 786. DOI: [10.1140/epjc/s10052-017-5157-2](https://doi.org/10.1140/epjc/s10052-017-5157-2). arXiv: [1705.07933](https://arxiv.org/abs/1705.07933) [hep-ph].
- [820] Patrick Draper and Heidi Rzehak. “A Review of Higgs Mass Calculations in Supersymmetric Models”. In: *Phys. Rept.* 619 (2016), pp. 1–24. DOI: [10.1016/j.physrep.2016.01.001](https://doi.org/10.1016/j.physrep.2016.01.001). arXiv: [1601.01890](https://arxiv.org/abs/1601.01890) [hep-ph].
- [821] P. Slavich et al. “Higgs-mass predictions in the MSSM and beyond”. In: *Eur. Phys. J. C* 81.5 (2021). Ed. by P. Slavich and S. Heinemeyer, p. 450. DOI: [10.1140/epjc/s10052-021-09198-2](https://doi.org/10.1140/epjc/s10052-021-09198-2). arXiv: [2012.15629](https://arxiv.org/abs/2012.15629) [hep-ph].
- [822] John R. Ellis, Jae Sik Lee, and Apostolos Pilaftsis. “Electric Dipole Moments in the MSSM Reloaded”. In: *JHEP* 10 (2008), p. 049. DOI: [10.1088/1126-6708/2008/10/049](https://doi.org/10.1088/1126-6708/2008/10/049). arXiv: [0808.1819](https://arxiv.org/abs/0808.1819) [hep-ph].
- [823] Chengcheng Han. “Muon g-2 and CP violation in MSSM”. In: (Apr. 2021). arXiv: [2104.03292](https://arxiv.org/abs/2104.03292) [hep-ph].
- [824] Michael Graesser and Scott D. Thomas. “Supersymmetric relations among electromagnetic dipole operators”. In: *Phys. Rev. D* 65 (2002), p. 075012. DOI: [10.1103/PhysRevD.65.075012](https://doi.org/10.1103/PhysRevD.65.075012). arXiv: [hep-ph/0104254](https://arxiv.org/abs/hep-ph/0104254).
- [825] Gino Isidori, Federico Mescia, Paride Paradisi, and David Temes. “Flavour physics at large  $\tan(\beta)$  with a Bino-like LSP”. In: *Phys. Rev. D* 75 (2007), p. 115019. DOI: [10.1103/PhysRevD.75.115019](https://doi.org/10.1103/PhysRevD.75.115019). arXiv: [hep-ph/0703035](https://arxiv.org/abs/hep-ph/0703035).
- [826] Lorenzo Calibbi, Paride Paradisi, and Robert Ziegler. “Lepton Flavor Violation in Flavored Gauge Mediation”. In: *Eur. Phys. J. C* 74.12 (2014), p. 3211. DOI: [10.1140/epjc/s10052-014-3211-x](https://doi.org/10.1140/epjc/s10052-014-3211-x). arXiv: [1408.0754](https://arxiv.org/abs/1408.0754) [hep-ph].
- [827] Lorenzo Calibbi, Iftah Galon, Antonio Masiero, Paride Paradisi, and Yael Shadmi. “Charged Slepton Flavor post the 8 TeV LHC: A Simplified Model Analysis of Low-Energy Constraints and LHC SUSY Searches”. In: *JHEP* 10 (2015), p. 043. DOI: [10.1007/JHEP10\(2015\)043](https://doi.org/10.1007/JHEP10(2015)043). arXiv: [1502.07753](https://arxiv.org/abs/1502.07753) [hep-ph].

- [828] Chengcheng Han, M. L. López-Ibañez, Aurora Melis, Óscar Vives, Lei Wu, and Jin Min Yang. “LFV and  $(g-2)$  in non-universal SUSY models with light higgsinos”. In: *JHEP* 05 (2020), p. 102. DOI: [10.1007/JHEP05\(2020\)102](https://doi.org/10.1007/JHEP05(2020)102). arXiv: [2003.06187 \[hep-ph\]](https://arxiv.org/abs/2003.06187).
- [829] Ryo Nagai and Norimi Yokozaki. “Lepton flavor violations in SUSY models for muon  $g - 2$  with right-handed neutrinos”. In: *JHEP* 01 (2021), p. 099. DOI: [10.1007/JHEP01\(2021\)099](https://doi.org/10.1007/JHEP01(2021)099). arXiv: [2007.00943 \[hep-ph\]](https://arxiv.org/abs/2007.00943).
- [830] Yuichiro Nakai, Matthew Reece, and Motoo Suzuki. “Supersymmetric alignment models for  $(g - 2)_\mu$ ”. In: *JHEP* 10 (2021), p. 068. DOI: [10.1007/JHEP10\(2021\)068](https://doi.org/10.1007/JHEP10(2021)068). arXiv: [2107.10268 \[hep-ph\]](https://arxiv.org/abs/2107.10268).
- [831] Mario E. Gomez, Smaragda Lola, Qaisar Shafi, and Cem Salih Un. “Muon  $g-2$  and lepton flavor violation in supersymmetric GUTs”. In: *Phys. Rev. D* 110.9 (2024), p. 095003. DOI: [10.1103/PhysRevD.110.095003](https://doi.org/10.1103/PhysRevD.110.095003). arXiv: [2404.02337 \[hep-ph\]](https://arxiv.org/abs/2404.02337).
- [832] Marcin Badziak and Kazuki Sakurai. “Explanation of electron and muon  $g - 2$  anomalies in the MSSM”. In: *JHEP* 10 (2019), p. 024. DOI: [10.1007/JHEP10\(2019\)024](https://doi.org/10.1007/JHEP10(2019)024). arXiv: [1908.03607 \[hep-ph\]](https://arxiv.org/abs/1908.03607).
- [833] Motoi Endo and Wen Yin. “Explaining electron and muon  $g - 2$  anomaly in SUSY without lepton-flavor mixings”. In: *JHEP* 08 (2019), p. 122. DOI: [10.1007/JHEP08\(2019\)122](https://doi.org/10.1007/JHEP08(2019)122). arXiv: [1906.08768 \[hep-ph\]](https://arxiv.org/abs/1906.08768).
- [834] Md. Isha Ali, Manimala Chakraborti, Utpal Chattopadhyay, and Samadrita Mukherjee. “Muon and electron  $(g - 2)$  anomalies with non-holomorphic interactions in MSSM”. In: *Eur. Phys. J. C* 83.1 (2023), p. 60. DOI: [10.1140/epjc/s10052-023-11216-4](https://doi.org/10.1140/epjc/s10052-023-11216-4). arXiv: [2112.09867 \[hep-ph\]](https://arxiv.org/abs/2112.09867).
- [835] Mariana Frank, Yaşar Hiçyılmaz, Subhadeep Mondal, Özer Özdal, and Cem Salih Ün. “Electron and muon magnetic moments and implications for dark matter and model characterisation in non-universal  $U(1)$ ’ supersymmetric models”. In: *JHEP* 10 (2021), p. 063. DOI: [10.1007/JHEP10\(2021\)063](https://doi.org/10.1007/JHEP10(2021)063). arXiv: [2107.04116 \[hep-ph\]](https://arxiv.org/abs/2107.04116).
- [836] Song Li, Yang Xiao, and Jin Min Yang. “Constraining CP-phases in SUSY: An interplay of muon/electron  $g - 2$  and electron EDM”. In: *Nucl. Phys. B* 974 (2022), p. 115629. DOI: [10.1016/j.nuclphysb.2021.115629](https://doi.org/10.1016/j.nuclphysb.2021.115629). arXiv: [2108.00359 \[hep-ph\]](https://arxiv.org/abs/2108.00359).
- [837] Song Li, Yang Xiao, and Jin Min Yang. “Can electron and muon  $g - 2$  anomalies be jointly explained in SUSY?”. In: *Eur. Phys. J. C* 82.3 (2022), p. 276. DOI: [10.1140/epjc/s10052-022-10242-y](https://doi.org/10.1140/epjc/s10052-022-10242-y). arXiv: [2107.04962 \[hep-ph\]](https://arxiv.org/abs/2107.04962).
- [838] Junjie Cao, Lei Meng, and Yuanfang Yue. “Electron and muon anomalous magnetic moments in the  $Z_3$ -NMSSM”. In: *Phys. Rev. D* 108.3 (2023), p. 035043. DOI: [10.1103/PhysRevD.108.035043](https://doi.org/10.1103/PhysRevD.108.035043). arXiv: [2306.06854 \[hep-ph\]](https://arxiv.org/abs/2306.06854).
- [839] Junjie Cao, Yangle He, Jingwei Lian, Di Zhang, and Pengxuan Zhu. “Electron and muon anomalous magnetic moments in the inverse seesaw extended NMSSM”. In: *Phys. Rev. D* 104.5 (2021), p. 055009. DOI: [10.1103/PhysRevD.104.055009](https://doi.org/10.1103/PhysRevD.104.055009). arXiv: [2102.11355 \[hep-ph\]](https://arxiv.org/abs/2102.11355).
- [840] Li-Jun Jia, Zhuang Li, and Fei Wang. “Explaining the Muon  $g - 2$  Anomaly in Deflected AMSB for NMSSM”. In: *Universe* 9.5 (2023), p. 214. DOI: [10.3390/universe9050214](https://doi.org/10.3390/universe9050214). arXiv: [2305.04623 \[hep-ph\]](https://arxiv.org/abs/2305.04623).
- [841] Jin Min Yang and Yang Zhang. “Low energy SUSY confronted with new measurements of W-boson mass and muon  $g-2$ ”. In: *Sci. Bull.* 67.14 (2022), pp. 1430–1436. DOI: [10.1016/j.scib.2022.06.007](https://doi.org/10.1016/j.scib.2022.06.007). arXiv: [2204.04202 \[hep-ph\]](https://arxiv.org/abs/2204.04202).

- [842] Emanuele Bagnaschi, Manimala Chakraborti, Sven Heinemeyer, Ipsita Saha, and Georg Weiglein. “Interdependence of the new “MUON G-2” result and the W-boson mass”. In: *Eur. Phys. J. C* 82.5 (2022), p. 474. DOI: [10.1140/epjc/s10052-022-10402-0](https://doi.org/10.1140/epjc/s10052-022-10402-0). arXiv: [2203.15710](https://arxiv.org/abs/2203.15710) [hep-ph].
- [843] Peter Athron, Markus Bach, Douglas H. J. Jacob, Wojciech Kotlarski, Dominik Stöckinger, and Alexander Voigt. “Precise calculation of the W boson pole mass beyond the standard model with FlexibleSUSY”. In: *Phys. Rev. D* 106.9 (2022), p. 095023. DOI: [10.1103/PhysRevD.106.095023](https://doi.org/10.1103/PhysRevD.106.095023). arXiv: [2204.05285](https://arxiv.org/abs/2204.05285) [hep-ph].
- [844] T. Aaltonen et al. “High-precision measurement of the  $\langle i \rangle W \langle /i \rangle$  boson mass with the CDF II detector”. In: *Science* 376.6589 (2022), pp. 170–176. DOI: [10.1126/science.abk1781](https://doi.org/10.1126/science.abk1781). eprint: <https://www.science.org/doi/pdf/10.1126/science.abk1781>. URL: <https://www.science.org/doi/abs/10.1126/science.abk1781>.
- [845] Manuel Drees and Stephen P. Martin. “Implications of SUSY model building”. In: *Electroweak symmetry breaking and new physics at the TeV scale*. Ed. by T. L. Barklow, S. Dawson, H. E. Haber, and J. L. Siegrist. Mar. 1995, pp. 146–215. DOI: [10.1142/9789812830265\\_0003](https://doi.org/10.1142/9789812830265_0003). arXiv: [hep-ph/9504324](https://arxiv.org/abs/hep-ph/9504324).
- [846] O. Buchmueller et al. “The CMSSM and NUHM1 after LHC Run 1”. In: *Eur. Phys. J. C* 74.6 (2014), p. 2922. DOI: [10.1140/epjc/s10052-014-2922-3](https://doi.org/10.1140/epjc/s10052-014-2922-3). arXiv: [1312.5250](https://arxiv.org/abs/1312.5250) [hep-ph].
- [847] Philip Bechtle et al. “Killing the cMSSM softly”. In: *Eur. Phys. J. C* 76.2 (2016), p. 96. DOI: [10.1140/epjc/s10052-015-3864-0](https://doi.org/10.1140/epjc/s10052-015-3864-0). arXiv: [1508.05951](https://arxiv.org/abs/1508.05951) [hep-ph].
- [848] Chengcheng Han, Ken-ichi Hikasa, Lei Wu, Jin Min Yang, and Yang Zhang. “Status of CMSSM in light of current LHC Run-2 and LUX data”. In: *Phys. Lett. B* 769 (2017), pp. 470–476. DOI: [10.1016/j.physletb.2017.04.026](https://doi.org/10.1016/j.physletb.2017.04.026). arXiv: [1612.02296](https://arxiv.org/abs/1612.02296) [hep-ph].
- [849] Peter Athron et al. “Global fits of GUT-scale SUSY models with GAMBIT”. In: *Eur. Phys. J. C* 77.12 (2017), p. 824. DOI: [10.1140/epjc/s10052-017-5167-0](https://doi.org/10.1140/epjc/s10052-017-5167-0). arXiv: [1705.07935](https://arxiv.org/abs/1705.07935) [hep-ph].
- [850] Manimala Chakraborti, Leszek Roszkowski, and Sebastian Trojanowski. “GUT-constrained supersymmetry and dark matter in light of the new  $(g-2)_\mu$  determination”. In: *JHEP* 05 (2021), p. 252. DOI: [10.1007/JHEP05\(2021\)252](https://doi.org/10.1007/JHEP05(2021)252). arXiv: [2104.04458](https://arxiv.org/abs/2104.04458) [hep-ph].
- [851] Fei Wang, Kun Wang, Jin Min Yang, and Jingya Zhu. “Solving the muon g-2 anomaly in CMSSM extension with non-universal gaugino masses”. In: *JHEP* 12 (2018), p. 041. DOI: [10.1007/JHEP12\(2018\)041](https://doi.org/10.1007/JHEP12(2018)041). arXiv: [1808.10851](https://arxiv.org/abs/1808.10851) [hep-ph].
- [852] Amin Aboubrahim, Michael Klasen, and Pran Nath. “What the Fermilab muon  $g-2$  experiment tells us about discovering supersymmetry at high luminosity and high energy upgrades to the LHC”. In: *Phys. Rev. D* 104.3 (2021), p. 035039. DOI: [10.1103/PhysRevD.104.035039](https://doi.org/10.1103/PhysRevD.104.035039). arXiv: [2104.03839](https://arxiv.org/abs/2104.03839) [hep-ph].
- [853] Zhuang Li, Guo-Li Liu, Fei Wang, Jin Min Yang, and Yang Zhang. “Gluino-SUGRA scenarios in light of FNAL muon  $g-2$  anomaly”. In: *JHEP* 12 (2021), p. 219. DOI: [10.1007/JHEP12\(2021\)219](https://doi.org/10.1007/JHEP12(2021)219). arXiv: [2106.04466](https://arxiv.org/abs/2106.04466) [hep-ph].
- [854] Waqas Ahmed, Imtiaz Khan, Jinmian Li, Tianjun Li, Shabbar Raza, and Wenxing Zhang. “The natural explanation of the muon anomalous magnetic moment via the electroweak supersymmetry from the GmSUGRA in the MSSM”. In: *Phys. Lett. B* 827 (2022), p. 136879. DOI: [10.1016/j.physletb.2022.136879](https://doi.org/10.1016/j.physletb.2022.136879). arXiv: [2104.03491](https://arxiv.org/abs/2104.03491) [hep-ph].

- [855] Fei Wang, Lei Wu, Yang Xiao, Jin Min Yang, and Yang Zhang. “GUT-scale constrained SUSY in light of new muon  $g-2$  measurement”. In: *Nucl. Phys. B* 970 (2021), p. 115486. DOI: [10.1016/j.nuclphysb.2021.115486](https://doi.org/10.1016/j.nuclphysb.2021.115486). arXiv: [2104.03262](https://arxiv.org/abs/2104.03262) [hep-ph].
- [856] Fei Wang, Wenyu Wang, Jinmin Yang, Yang Zhang, and Bin Zhu. “Low Energy Supersymmetry Confronted with Current Experiments: An Overview”. In: *Universe* 8.3 (2022), p. 178. DOI: [10.3390/universe8030178](https://doi.org/10.3390/universe8030178). arXiv: [2201.00156](https://arxiv.org/abs/2201.00156) [hep-ph].
- [857] John Ellis, Keith A. Olive, and Vassilis C. Spanos. “Non-universal SUSY models,  $g_\mu - 2$ ,  $m_H$  and dark matter”. In: *Eur. Phys. J. C* 84.10 (2024), p. 1121. DOI: [10.1140/epjc/s10052-024-13499-7](https://doi.org/10.1140/epjc/s10052-024-13499-7). arXiv: [2407.08679](https://arxiv.org/abs/2407.08679) [hep-ph].
- [858] Adam K. Forster and Stephen F. King. “Muon  $g-2$ , dark matter and the Higgs mass in no-scale supergravity”. In: *Nucl. Phys. B* 976 (2022), p. 115700. DOI: [10.1016/j.nuclphysb.2022.115700](https://doi.org/10.1016/j.nuclphysb.2022.115700). arXiv: [2109.10802](https://arxiv.org/abs/2109.10802) [hep-ph].
- [859] Sho Iwamoto, Tsutomu T. Yanagida, and Norimi Yokozaki. “Wino-Higgsino dark matter in MSSM from the  $g - 2$  anomaly”. In: *Phys. Lett. B* 823 (2021), p. 136768. DOI: [10.1016/j.physletb.2021.136768](https://doi.org/10.1016/j.physletb.2021.136768). arXiv: [2104.03223](https://arxiv.org/abs/2104.03223) [hep-ph].
- [860] E. Bagnaschi et al. “Likelihood Analysis of Supersymmetric SU(5) GUTs”. In: *Eur. Phys. J. C* 77.2 (2017), p. 104. DOI: [10.1140/epjc/s10052-017-4639-6](https://doi.org/10.1140/epjc/s10052-017-4639-6). arXiv: [1610.10084](https://arxiv.org/abs/1610.10084) [hep-ph].
- [861] Mureed Hussain and Rizwan Khalid. “Understanding the muon anomalous magnetic moment in light of a flavor symmetry-based Minimal Supersymmetric Standard Model”. In: *PTEP* 2018.8 (2018), 083B06. DOI: [10.1093/ptep/pty087](https://doi.org/10.1093/ptep/pty087). arXiv: [1704.04085](https://arxiv.org/abs/1704.04085) [hep-ph].
- [862] Hieu Minh Tran and Huong Thu Nguyen. “GUT-inspired MSSM in light of muon  $g - 2$  and LHC results at  $\sqrt{s} = 13$  TeV”. In: *Phys. Rev. D* 99.3 (2019), p. 035040. DOI: [10.1103/PhysRevD.99.035040](https://doi.org/10.1103/PhysRevD.99.035040). arXiv: [1812.11757](https://arxiv.org/abs/1812.11757) [hep-ph].
- [863] Masahiro Ibe, Motoo Suzuki, Tsutomu T. Yanagida, and Norimi Yokozaki. “Muon  $g - 2$  in Split-Family SUSY in light of LHC Run II”. In: *Eur. Phys. J. C* 79.8 (2019), p. 688. DOI: [10.1140/epjc/s10052-019-7186-5](https://doi.org/10.1140/epjc/s10052-019-7186-5). arXiv: [1903.12433](https://arxiv.org/abs/1903.12433) [hep-ph].
- [864] John Ellis, Jason L. Evans, Natsumi Nagata, Dimitri V. Nanopoulos, and Keith A. Olive. “Flipped  $\mathbf{g}_\mu - \mathbf{2}$ ”. In: *Eur. Phys. J. C* 81.12 (2021), p. 1079. DOI: [10.1140/epjc/s10052-021-09829-8](https://doi.org/10.1140/epjc/s10052-021-09829-8). arXiv: [2107.03025](https://arxiv.org/abs/2107.03025) [hep-ph].
- [865] Joseph L. Lamborn, Tianjun Li, James A. Maxin, and Dimitri V. Nanopoulos. “Resolving the  $(g - 2)_\mu$  discrepancy with  $\mathcal{F}$ -SU(5) intersecting D-branes”. In: *JHEP* 11 (2021), p. 081. DOI: [10.1007/JHEP11\(2021\)081](https://doi.org/10.1007/JHEP11(2021)081). arXiv: [2108.08084](https://arxiv.org/abs/2108.08084) [hep-ph].
- [866] John Ellis, Jason L. Evans, Natsumi Nagata, Dimitri V. Nanopoulos, and Keith A. Olive. “Flipped SU(5) GUT phenomenology: proton decay and  $\mathbf{g}_\mu - \mathbf{2}$ ”. In: *Eur. Phys. J. C* 81.12 (2021), p. 1109. DOI: [10.1140/epjc/s10052-021-09896-x](https://doi.org/10.1140/epjc/s10052-021-09896-x). arXiv: [2110.06833](https://arxiv.org/abs/2110.06833) [hep-ph].
- [867] Mario E. Gomez, Qaisar Shafi, Amit Tiwari, and Cem Salih Un. “Muon  $\mathbf{g} - \mathbf{2}$ , neutralino dark matter and stau NLSP”. In: *Eur. Phys. J. C* 82.6 (2022), p. 561. DOI: [10.1140/epjc/s10052-022-10507-6](https://doi.org/10.1140/epjc/s10052-022-10507-6). arXiv: [2202.06419](https://arxiv.org/abs/2202.06419) [hep-ph].
- [868] G. F. Giudice and R. Rattazzi. “Theories with gauge mediated supersymmetry breaking”. In: *Phys. Rept.* 322 (1999), pp. 419–499. DOI: [10.1016/S0370-1573\(99\)00042-3](https://doi.org/10.1016/S0370-1573(99)00042-3). arXiv: [hep-ph/9801271](https://arxiv.org/abs/hep-ph/9801271).

- [869] Masahiro Ibe, Shin Kobayashi, Yuhei Nakayama, and Satoshi Shirai. “Muon  $g - 2$  in gauge mediation without SUSY CP problem”. In: *JHEP* 07 (2021), p. 098. DOI: [10.1007/JHEP07\(2021\)098](https://doi.org/10.1007/JHEP07(2021)098). arXiv: [2104.03289](https://arxiv.org/abs/2104.03289) [[hep-ph](#)].
- [870] Gautam Bhattacharyya, Tsutomu T. Yanagida, and Norimi Yokozaki. “An extended gauge mediation for muon ( $g - 2$ ) explanation”. In: *Phys. Lett. B* 784 (2018), pp. 118–121. DOI: [10.1016/j.physletb.2018.07.037](https://doi.org/10.1016/j.physletb.2018.07.037). arXiv: [1805.01607](https://arxiv.org/abs/1805.01607) [[hep-ph](#)].
- [871] Jason L. Evans, Tsutomu T. Yanagida, and Norimi Yokozaki. “Flavor- and CP-safe explanation of  $g_\mu - 2$  anomaly”. In: *JHEP* 03 (2023), p. 024. DOI: [10.1007/JHEP03\(2023\)024](https://doi.org/10.1007/JHEP03(2023)024). arXiv: [2205.14906](https://arxiv.org/abs/2205.14906) [[hep-ph](#)].
- [872] Seong-Sik Kim, Hyun Min Lee, and Sung-Bo Sim. “Muon  $g-2$  and proton lifetime in SUSY SU(5) GUTs with split superpartners”. In: *Phys. Rev. D* 109.7 (2024), p. 075035. DOI: [10.1103/PhysRevD.109.075035](https://doi.org/10.1103/PhysRevD.109.075035). arXiv: [2402.04850](https://arxiv.org/abs/2402.04850) [[hep-ph](#)].
- [873] Lisa Randall and Raman Sundrum. “Out of this world supersymmetry breaking”. In: *Nucl. Phys. B* 557 (1999), pp. 79–118. DOI: [10.1016/S0550-3213\(99\)00359-4](https://doi.org/10.1016/S0550-3213(99)00359-4). arXiv: [hep-th/9810155](https://arxiv.org/abs/hep-th/9810155).
- [874] Gian F. Giudice, Markus A. Luty, Hitoshi Murayama, and Riccardo Rattazzi. “Gaugino mass without singlets”. In: *JHEP* 12 (1998), p. 027. DOI: [10.1088/1126-6708/1998/12/027](https://doi.org/10.1088/1126-6708/1998/12/027). arXiv: [hep-ph/9810442](https://arxiv.org/abs/hep-ph/9810442).
- [875] Kiwoon Choi and Hans Peter Nilles. “The Gaugino code”. In: *JHEP* 04 (2007), p. 006. DOI: [10.1088/1126-6708/2007/04/006](https://doi.org/10.1088/1126-6708/2007/04/006). arXiv: [hep-ph/0702146](https://arxiv.org/abs/hep-ph/0702146).
- [876] Wen Yin. “Muon  $g - 2$  anomaly in anomaly mediation”. In: *JHEP* 06 (2021), p. 029. DOI: [10.1007/JHEP06\(2021\)029](https://doi.org/10.1007/JHEP06(2021)029). arXiv: [2104.03259](https://arxiv.org/abs/2104.03259) [[hep-ph](#)].
- [877] Kwang Sik Jeong, Junichiro Kawamura, and Chan Beom Park. “Mixed modulus and anomaly mediation in light of the muon  $g - 2$  anomaly”. In: *JHEP* 10 (2021), p. 064. DOI: [10.1007/JHEP10\(2021\)064](https://doi.org/10.1007/JHEP10(2021)064). arXiv: [2106.04238](https://arxiv.org/abs/2106.04238) [[hep-ph](#)].
- [878] K. Kowalska, L. Roszkowski, E. M. Sessolo, S. Trojanowski, and A. J. Williams. “Looking for supersymmetry:  $\sim 1$  TeV WIMP and the power of complementarity in LHC and dark matter searches”. In: *50th Rencontres de Moriond on QCD and High Energy Interactions*. July 2015, pp. 195–198. arXiv: [1507.07446](https://arxiv.org/abs/1507.07446) [[hep-ph](#)].
- [879] Kun Wang and Jingya Zhu. “Smuon in the NMSSM confronted with the muon  $g-2$  anomaly and SUSY searches\*”. In: *Chin. Phys. C* 47.1 (2023), p. 013107. DOI: [10.1088/1674-1137/ac9896](https://doi.org/10.1088/1674-1137/ac9896). arXiv: [2112.14576](https://arxiv.org/abs/2112.14576) [[hep-ph](#)].
- [880] Yuchao Gu, Ning Liu, Liangliang Su, and Daohan Wang. “Heavy bino and slepton for muon  $g - 2$  anomaly”. In: *Nucl. Phys. B* 969 (2021), p. 115481. DOI: [10.1016/j.nuclphysb.2021.115481](https://doi.org/10.1016/j.nuclphysb.2021.115481). arXiv: [2104.03239](https://arxiv.org/abs/2104.03239) [[hep-ph](#)].
- [881] Wolfgang Altmannshofer, Sri Aditya Gadam, Stefania Gori, and Nick Hamer. “Explaining  $(g - 2)_\mu$  with multi-TeV sleptons”. In: *JHEP* 07 (2021), p. 118. DOI: [10.1007/JHEP07\(2021\)118](https://doi.org/10.1007/JHEP07(2021)118). arXiv: [2104.08293](https://arxiv.org/abs/2104.08293) [[hep-ph](#)].
- [882] Wenqi Ke and Pietro Slavich. “Higgs-mass constraints on a supersymmetric solution of the muon  $g - 2$  anomaly”. In: *Eur. Phys. J. C* 82.1 (2022), p. 89. DOI: [10.1140/epjc/s10052-022-10004-w](https://doi.org/10.1140/epjc/s10052-022-10004-w). arXiv: [2109.15277](https://arxiv.org/abs/2109.15277) [[hep-ph](#)].
- [883] Jan Tristram Acuña, Patrick Stengel, and Piero Ullio. “Minimal dark matter model for muon  $g-2$  with scalar lepton partners up to the TeV scale”. In: *Phys. Rev. D* 105.7 (2022), p. 075007. DOI: [10.1103/PhysRevD.105.075007](https://doi.org/10.1103/PhysRevD.105.075007). arXiv: [2112.08992](https://arxiv.org/abs/2112.08992) [[hep-ph](#)].

- [884] Bin Zhu, Ran Ding, and Tianjun Li. “Higgs mass and muon anomalous magnetic moment in the MSSM with gauge-gravity hybrid mediation”. In: *Phys. Rev. D* 96.3 (2017), p. 035029. DOI: [10.1103/PhysRevD.96.035029](https://doi.org/10.1103/PhysRevD.96.035029). arXiv: [1610.09840 \[hep-ph\]](https://arxiv.org/abs/1610.09840).
- [885] Tsutomu T. Yanagida and Norimi Yokozaki. “Muon  $g - 2$  in MSSM gauge mediation revisited”. In: *Phys. Lett. B* 772 (2017), pp. 409–414. DOI: [10.1016/j.physletb.2017.07.002](https://doi.org/10.1016/j.physletb.2017.07.002). arXiv: [1704.00711 \[hep-ph\]](https://arxiv.org/abs/1704.00711).
- [886] Tsutomu T. Yanagida, Wen Yin, and Norimi Yokozaki. “Muon  $g - 2$  in Higgs-anomaly mediation”. In: *JHEP* 06 (2020), p. 154. DOI: [10.1007/JHEP06\(2020\)154](https://doi.org/10.1007/JHEP06(2020)154). arXiv: [2001.02672 \[hep-ph\]](https://arxiv.org/abs/2001.02672).
- [887] Kaustubh Agashe, Majid Ekhterachian, Zhen Liu, and Raman Sundrum. “Sleptonic SUSY: from UV framework to IR phenomenology”. In: *JHEP* 09 (2022), p. 142. DOI: [10.1007/JHEP09\(2022\)142](https://doi.org/10.1007/JHEP09(2022)142). arXiv: [2203.01796 \[hep-ph\]](https://arxiv.org/abs/2203.01796).
- [888] Arghya Choudhury, Luc Darmé, Leszek Roszkowski, Enrico Maria Sessolo, and Sebastian Trojanowski. “Muon  $g - 2$  and related phenomenology in constrained vector-like extensions of the MSSM”. In: *JHEP* 05 (2017), p. 072. DOI: [10.1007/JHEP05\(2017\)072](https://doi.org/10.1007/JHEP05(2017)072). arXiv: [1701.08778 \[hep-ph\]](https://arxiv.org/abs/1701.08778).
- [889] Zafer Altın, Özer Özdal, and Cem Salih Ün. “Muon  $g-2$  in an alternative quasi-Yukawa unification with a less fine-tuned seesaw mechanism”. In: *Phys. Rev. D* 97.5 (2018), p. 055007. DOI: [10.1103/PhysRevD.97.055007](https://doi.org/10.1103/PhysRevD.97.055007). arXiv: [1703.00229 \[hep-ph\]](https://arxiv.org/abs/1703.00229).
- [890] Giancarlo Pozzo and Yang Zhang. “Constraining resonant dark matter with combined LHC electroweakino searches”. In: *Phys. Lett. B* 789 (2019), pp. 582–591. DOI: [10.1016/j.physletb.2018.12.062](https://doi.org/10.1016/j.physletb.2018.12.062). arXiv: [1807.01476 \[hep-ph\]](https://arxiv.org/abs/1807.01476).
- [891] Jun Zhao, Jingya Zhu, Pengxuan Zhu, and Rui Zhu. “Light Higgsino scenario confronted with the muon  $g-2$ ”. In: *Phys. Rev. D* 107.5 (2023), p. 055030. DOI: [10.1103/PhysRevD.107.055030](https://doi.org/10.1103/PhysRevD.107.055030). arXiv: [2211.14587 \[hep-ph\]](https://arxiv.org/abs/2211.14587).
- [892] Manimala Chakraborti, Sven Heinemeyer, and Ipsita Saha. “Consistent excesses in the search for  $\tilde{\chi}_2^0 \tilde{\chi}_1^\pm$ : wino/bino vs. Higgsino dark matter”. In: *Eur. Phys. J. C* 84.8 (2024), p. 812. DOI: [10.1140/epjc/s10052-024-13180-z](https://doi.org/10.1140/epjc/s10052-024-13180-z). arXiv: [2403.14759 \[hep-ph\]](https://arxiv.org/abs/2403.14759).
- [893] Peter Cox, Chengcheng Han, Tsutomu T. Yanagida, and Norimi Yokozaki. “Gaugino mediation scenarios for muon  $g - 2$  and dark matter”. In: *JHEP* 08 (2019), p. 097. DOI: [10.1007/JHEP08\(2019\)097](https://doi.org/10.1007/JHEP08(2019)097). arXiv: [1811.12699 \[hep-ph\]](https://arxiv.org/abs/1811.12699).
- [894] Wen Yin and Norimi Yokozaki. “Splitting mass spectra and muon  $g - 2$  in Higgs-anomaly mediation”. In: *Phys. Lett. B* 762 (2016), pp. 72–79. DOI: [10.1016/j.physletb.2016.09.024](https://doi.org/10.1016/j.physletb.2016.09.024). arXiv: [1607.05705 \[hep-ph\]](https://arxiv.org/abs/1607.05705).
- [895] Graham D. Kribs, Erich Poppitz, and Neal Weiner. “Flavor in supersymmetry with an extended R-symmetry”. In: *Phys. Rev. D* 78 (2008), p. 055010. DOI: [10.1103/PhysRevD.78.055010](https://doi.org/10.1103/PhysRevD.78.055010). arXiv: [0712.2039 \[hep-ph\]](https://arxiv.org/abs/0712.2039).
- [896] Matti Heikinheimo, Moshe Kellerstein, and Veronica Sanz. “How Many Supersymmetries?” In: *JHEP* 04 (2012), p. 043. DOI: [10.1007/JHEP04\(2012\)043](https://doi.org/10.1007/JHEP04(2012)043). arXiv: [1111.4322 \[hep-ph\]](https://arxiv.org/abs/1111.4322).
- [897] Graham D. Kribs and Adam Martin. “Dirac Gauginos in Supersymmetry – Suppressed Jets + MET Signals: A Snowmass Whitepaper”. In: (Aug. 2013). arXiv: [1308.3468 \[hep-ph\]](https://arxiv.org/abs/1308.3468).
- [898] Philip Diessner, Wojciech Kotlarski, Sebastian Liebschner, and Dominik Stöckinger. “Squark production in R-symmetric SUSY with Dirac gluinos: NLO corrections”. In: *JHEP* 10 (2017), p. 142. DOI: [10.3204/PUBDB-2017-10328](https://doi.org/10.3204/PUBDB-2017-10328). arXiv: [1707.04557 \[hep-ph\]](https://arxiv.org/abs/1707.04557).

- [899] Philip Diessner, Jan Kalinowski, Wojciech Kotlarski, and Dominik Stöckinger. “Confronting the coloured sector of the MRSSM with LHC data”. In: *JHEP* 09 (2019), p. 120. DOI: [10.1007/JHEP09\(2019\)120](https://doi.org/10.1007/JHEP09(2019)120). arXiv: [1907.11641](https://arxiv.org/abs/1907.11641) [[hep-ph](#)].
- [900] Enrico Bertuzzo, Claudia Frugiuele, Thomas Gregoire, and Eduardo Ponton. “Dirac gauginos, R symmetry and the 125 GeV Higgs”. In: *JHEP* 04 (2015), p. 089. DOI: [10.1007/JHEP04\(2015\)089](https://doi.org/10.1007/JHEP04(2015)089). arXiv: [1402.5432](https://arxiv.org/abs/1402.5432) [[hep-ph](#)].
- [901] Philip Dießner, Jan Kalinowski, Wojciech Kotlarski, and Dominik Stöckinger. “Higgs boson mass and electroweak observables in the MRSSM”. In: *JHEP* 12 (2014), p. 124. DOI: [10.1007/JHEP12\(2014\)124](https://doi.org/10.1007/JHEP12(2014)124). arXiv: [1410.4791](https://arxiv.org/abs/1410.4791) [[hep-ph](#)].
- [902] Philip Diessner, Jan Kalinowski, Wojciech Kotlarski, and Dominik Stöckinger. “Exploring the Higgs sector of the MRSSM with a light scalar”. In: *JHEP* 03 (2016), p. 007. DOI: [10.1007/JHEP03\(2016\)007](https://doi.org/10.1007/JHEP03(2016)007). arXiv: [1511.09334](https://arxiv.org/abs/1511.09334) [[hep-ph](#)].
- [903] Jan Kalinowski and Wojciech Kotlarski. “Interpreting 95 GeV di-photon/ $b\bar{b}$  excesses as a lightest Higgs boson of the MRSSM”. In: *JHEP* 07 (2024), p. 037. DOI: [10.1007/JHEP07\(2024\)037](https://doi.org/10.1007/JHEP07(2024)037). arXiv: [2403.08720](https://arxiv.org/abs/2403.08720) [[hep-ph](#)].
- [904] Wojciech Kotlarski, Dominik Stöckinger, and Hyejung Stöckinger-Kim. “Low-energy lepton physics in the MRSSM:  $(g - 2)_\mu$ ,  $\mu \rightarrow e\gamma$  and  $\mu \rightarrow e$  conversion”. In: *JHEP* 08 (2019), p. 082. DOI: [10.1007/JHEP08\(2019\)082](https://doi.org/10.1007/JHEP08(2019)082). arXiv: [1902.06650](https://arxiv.org/abs/1902.06650) [[hep-ph](#)].
- [905] Chuang Li, Bin Zhu, and Tianjun Li. “Naturalness, dark matter, and the muon anomalous magnetic moment in supersymmetric extensions of the standard model with a pseudo-Dirac gluino”. In: *Nucl. Phys. B* 927 (2018), pp. 255–273. DOI: [10.1016/j.nuclphysb.2017.12.012](https://doi.org/10.1016/j.nuclphysb.2017.12.012). arXiv: [1704.05584](https://arxiv.org/abs/1704.05584) [[hep-ph](#)].
- [906] Thi Nhung Dao, Duc Ninh Le, and Margarete Mühlleitner. “Leptonic anomalous magnetic and electric dipole moments in the CP-violating NMSSM with and without inverse seesaw mechanism”. In: *Eur. Phys. J. C* 82.10 (2022), p. 954. DOI: [10.1140/epjc/s10052-022-10928-3](https://doi.org/10.1140/epjc/s10052-022-10928-3). arXiv: [2207.12618](https://arxiv.org/abs/2207.12618) [[hep-ph](#)].
- [907] Tian-Peng Tang, Murat Abdughani, Lei Feng, Yue-Lin Sming Tsai, Jian Wu, and Yi-Zhong Fan. “NMSSM neutralino dark matter for CDF II W-boson mass and muon  $g - 2$  and the promising prospect of direct detection”. In: *Sci. China Phys. Mech. Astron.* 66.3 (2023), p. 239512. DOI: [10.1007/s11433-022-2046-y](https://doi.org/10.1007/s11433-022-2046-y). arXiv: [2204.04356](https://arxiv.org/abs/2204.04356) [[hep-ph](#)].
- [908] Ming Xia Huang, Fei Wang, and Ying Kai Zhang. “Interplay between the muon  $g-2$  anomaly and the PTA nHz gravitational waves from domain walls in the next-to-minimal supersymmetric standard model”. In: *Phys. Rev. D* 109.7 (2024), p. 075032. DOI: [10.1103/PhysRevD.109.075032](https://doi.org/10.1103/PhysRevD.109.075032). arXiv: [2309.06378](https://arxiv.org/abs/2309.06378) [[hep-ph](#)].
- [909] Murat Abdughani, Yi-Zhong Fan, Lei Feng, Yue-Lin Sming Tsai, Lei Wu, and Qiang Yuan. “A common origin of muon  $g-2$  anomaly, Galaxy Center GeV excess and AMS-02 anti-proton excess in the NMSSM”. In: *Sci. Bull.* 66 (2021), pp. 2170–2174. DOI: [10.1016/j.scib.2021.07.029](https://doi.org/10.1016/j.scib.2021.07.029). arXiv: [2104.03274](https://arxiv.org/abs/2104.03274) [[hep-ph](#)].
- [910] Junjie Cao, Jingwei Lian, Lei Meng, Yuanfang Yue, and Pengxuan Zhu. “Anomalous muon magnetic moment in the inverse seesaw extended next-to-minimal supersymmetric standard model”. In: *Phys. Rev. D* 101.9 (2020), p. 095009. DOI: [10.1103/PhysRevD.101.095009](https://doi.org/10.1103/PhysRevD.101.095009). arXiv: [1912.10225](https://arxiv.org/abs/1912.10225) [[hep-ph](#)].

- [911] Junjie Cao, Jingwei Lian, Yusi Pan, Di Zhang, and Pengxuan Zhu. “Improved  $(g - 2)_\mu$  measurement and singlino dark matter in  $\mu$ -term extended  $\mathbb{Z}_3$ -NMSSM”. In: *JHEP* 09 (2021), p. 175. DOI: [10.1007/JHEP09\(2021\)175](https://doi.org/10.1007/JHEP09(2021)175). arXiv: [2104.03284](https://arxiv.org/abs/2104.03284) [hep-ph].
- [912] Junjie Cao, Xinglong Jia, Lei Meng, Yuanfang Yue, and Di Zhang. “Status of the singlino-dominated dark matter in general Next-to-Minimal Supersymmetric Standard Model”. In: *JHEP* 03 (2023), p. 198. DOI: [10.1007/JHEP03\(2023\)198](https://doi.org/10.1007/JHEP03(2023)198). arXiv: [2210.08769](https://arxiv.org/abs/2210.08769) [hep-ph].
- [913] Junjie Cao, Jingwei Lian, Yusi Pan, Yuanfang Yue, and Di Zhang. “Impact of recent  $(g - 2)_\mu$  measurement on the light CP-even Higgs scenario in general Next-to-Minimal Supersymmetric Standard Model”. In: *JHEP* 03 (2022), p. 203. DOI: [10.1007/JHEP03\(2022\)203](https://doi.org/10.1007/JHEP03(2022)203). arXiv: [2201.11490](https://arxiv.org/abs/2201.11490) [hep-ph].
- [914] Junjie Cao, Xinglong Jia, and Jingwei Lian. “Unified interpretation of the muon  $g-2$  anomaly, the 95 GeV diphoton, and  $bb^-$  excesses in the general next-to-minimal supersymmetric standard model”. In: *Phys. Rev. D* 110.11 (2024), p. 115039. DOI: [10.1103/PhysRevD.110.115039](https://doi.org/10.1103/PhysRevD.110.115039). arXiv: [2402.15847](https://arxiv.org/abs/2402.15847) [hep-ph].
- [915] Florian Domingo, Ulrich Ellwanger, and Cyril Hugonie. “ $M_W$ , dark matter and  $a_\mu$  in the NMSSM”. In: *Eur. Phys. J. C* 82.11 (2022), p. 1074. DOI: [10.1140/epjc/s10052-022-11059-5](https://doi.org/10.1140/epjc/s10052-022-11059-5). arXiv: [2209.03863](https://arxiv.org/abs/2209.03863) [hep-ph].
- [916] Jong Soo Kim, Daniel E. Lopez-Fogliani, Andres D. Perez, and Roberto Ruiz de Austri. “The new  $(g-2)_\mu$  and right-handed sneutrino dark matter”. In: *Nucl. Phys. B* 974 (2022), p. 115637. DOI: [10.1016/j.nuclphysb.2021.115637](https://doi.org/10.1016/j.nuclphysb.2021.115637). arXiv: [2107.02285](https://arxiv.org/abs/2107.02285) [hep-ph].
- [917] Haijing Zhou and Guangning Ban. “Status of  $\mathbb{Z}_3$ -NMSSM featuring a light bino-dominated LSP and a light singlet-like scalar under the LZ Experiment”. In: (Feb. 2025). arXiv: [2502.14664](https://arxiv.org/abs/2502.14664) [hep-ph].
- [918] Mariana Frank and Özer Özdal. “Exploring the supersymmetric  $U(1)_{B-L} \times U(1)_R$  model with dark matter, muon  $g - 2$  and  $Z'$  mass limits”. In: *Phys. Rev. D* 97.1 (2018), p. 015012. DOI: [10.1103/PhysRevD.97.015012](https://doi.org/10.1103/PhysRevD.97.015012). arXiv: [1709.04012](https://arxiv.org/abs/1709.04012) [hep-ph].
- [919] Jin-Lei Yang, Tai-Fu Feng, and Hai-Bin Zhang. “Electron and muon  $(g - 2)$  in the B-LSSM”. In: *J. Phys. G* 47.5 (2020), p. 055004. DOI: [10.1088/1361-6471/ab7986](https://doi.org/10.1088/1361-6471/ab7986). arXiv: [2003.09781](https://arxiv.org/abs/2003.09781) [hep-ph].
- [920] Shu-Min Zhao, Guo-Zhu Ning, Jing-Jing Feng, Hai-Bin Zhang, Tai-Fu Feng, and Xing-Xing Dong. “Light neutralino dark matter in  $U(1)_X$ SSTM”. In: *Nucl. Phys. B* 969 (2021), p. 115469. DOI: [10.1016/j.nuclphysb.2021.115469](https://doi.org/10.1016/j.nuclphysb.2021.115469). arXiv: [2008.06209](https://arxiv.org/abs/2008.06209) [hep-ph].
- [921] Hai-Bin Zhang, Chang-Xin Liu, Jin-Lei Yang, and Tai-Fu Feng. “Muon anomalous magnetic dipole moment in the  $\mu$   $\nu$ SSTM<sup>\*</sup>”. In: *Chin. Phys. C* 46.9 (2022), p. 093107. DOI: [10.1088/1674-1137/ac71a6](https://doi.org/10.1088/1674-1137/ac71a6). arXiv: [2104.03489](https://arxiv.org/abs/2104.03489) [hep-ph].
- [922] Jin-Lei Yang, Hai-Bin Zhang, Chang-Xin Liu, Xing-Xing Dong, and Tai-Fu Feng. “Muon  $(g - 2)$  in the B-LSSM”. In: *JHEP* 08 (2021), p. 086. DOI: [10.1007/JHEP08\(2021\)086](https://doi.org/10.1007/JHEP08(2021)086). arXiv: [2104.03542](https://arxiv.org/abs/2104.03542) [hep-ph].
- [923] Tong-Tong Wang, Shu-Min Zhao, Jian-Fei Zhang, Xing-Xing Dong, and Tai-Fu Feng. “Lepton flavor violating decays  $l_j \rightarrow l_i \gamma$  in the  $U(1)_X$ SSTM model within the mass insertion approximation”. In: *Eur. Phys. J. C* 82.7 (2022), p. 639. DOI: [10.1140/epjc/s10052-022-10613-5](https://doi.org/10.1140/epjc/s10052-022-10613-5). arXiv: [2205.10485](https://arxiv.org/abs/2205.10485) [hep-ph].

- [924] Xi Wang, Xin-Xin Long, Yi-Tong Wang, Tong-Tong Wang, Hai-Bin Zhang, Tai-Fu Feng, Rong-Xiang Zhang, and Shu-Min Zhao. “Study on muon MDM and lepton EDM in BLMSSM via the mass insertion approximation”. In: *J. Phys. G* 51.1 (2024), p. 015004. DOI: [10.1088/1361-6471/ad06c8](https://doi.org/10.1088/1361-6471/ad06c8). arXiv: [2211.10848](https://arxiv.org/abs/2211.10848) [hep-ph].
- [925] Jin-Lei Yang, Zhong-Jun Yang, Xiu-Yi Yang, Hai-Bin Zhang, and Tai-Fu Feng. “New dark matter candidate in the  $B-L$  symmetric SSM”. In: *Eur. Phys. J. C* 83.11 (2023), p. 1073. DOI: [10.1140/epjc/s10052-023-12235-x](https://doi.org/10.1140/epjc/s10052-023-12235-x).
- [926] Parham Dehghani and Mariana Frank. “Reconciling collider signals, dark matter, and the muon anomalous magnetic moment in the supersymmetric  $U(1)_R \times U(1)_{B-L}$  model”. In: *JHEP* 06 (2023), p. 001. DOI: [10.1007/JHEP06\(2023\)001](https://doi.org/10.1007/JHEP06(2023)001). arXiv: [2301.05959](https://arxiv.org/abs/2301.05959) [hep-ph].
- [927] R. Barbier et al. “R-parity violating supersymmetry”. In: *Phys. Rept.* 420 (2005), pp. 1–202. DOI: [10.1016/j.physrep.2005.08.006](https://doi.org/10.1016/j.physrep.2005.08.006). arXiv: [hep-ph/0406039](https://arxiv.org/abs/hep-ph/0406039).
- [928] Arghya Choudhury, Sourav Mitra, Arpita Mondal, and Subhadeep Mondal. “Bilinear R-parity violating supersymmetry under the light of neutrino oscillation, Higgs and flavor data”. In: *JHEP* 02 (2024), p. 004. DOI: [10.1007/JHEP02\(2024\)004](https://doi.org/10.1007/JHEP02(2024)004). arXiv: [2305.15211](https://arxiv.org/abs/2305.15211) [hep-ph].
- [929] Arghya Choudhury, Arpita Mondal, and Subhadeep Mondal. “Status of R-parity violating SUSY”. In: (Feb. 2024). DOI: [10.1140/epjs/s11734-024-01100-x](https://doi.org/10.1140/epjs/s11734-024-01100-x). arXiv: [2402.04040](https://arxiv.org/abs/2402.04040) [hep-ph].
- [930] Min-Di Zheng and Hong-Hao Zhang. “Studying the  $b \rightarrow s\ell^+\ell^-$  anomalies and  $(g-2)_\mu$  in R-parity violating MSSM framework with the inverse seesaw mechanism”. In: *Phys. Rev. D* 104.11 (2021), p. 115023. DOI: [10.1103/PhysRevD.104.115023](https://doi.org/10.1103/PhysRevD.104.115023). arXiv: [2105.06954](https://arxiv.org/abs/2105.06954) [hep-ph].
- [931] Min-Di Zheng, Feng-Zhi Chen, and Hong-Hao Zhang. “Explaining anomalies of B-physics, muon  $g-2$  and W mass in R-parity violating MSSM with seesaw mechanism”. In: *Eur. Phys. J. C* 82.10 (2022), p. 895. DOI: [10.1140/epjc/s10052-022-10822-y](https://doi.org/10.1140/epjc/s10052-022-10822-y). arXiv: [2207.07636](https://arxiv.org/abs/2207.07636) [hep-ph].
- [932] P. S. Bhupal Dev, Amarjit Soni, and Fang Xu. “Hints of natural supersymmetry in flavor anomalies?” In: *Phys. Rev. D* 106.1 (2022), p. 015014. DOI: [10.1103/PhysRevD.106.015014](https://doi.org/10.1103/PhysRevD.106.015014). arXiv: [2106.15647](https://arxiv.org/abs/2106.15647) [hep-ph].
- [933] Yoav Afik, P. S. Bhupal Dev, Amarjit Soni, and Fang Xu. “Probing the muon  $(g-2)$  anomaly at the LHC in final states with two muons and two taus”. In: *Phys. Lett. B* 843 (2023), p. 138032. DOI: [10.1016/j.physletb.2023.138032](https://doi.org/10.1016/j.physletb.2023.138032). arXiv: [2212.06160](https://arxiv.org/abs/2212.06160) [hep-ph].
- [934] Essodjolo Kpatcha, Iñaki Lara, Daniel E. López-Fogliani, Carlos Muñoz, and Natsumi Nagata. “Explaining muon  $g-2$  data in the  $\mu\nu$ SSM”. In: *Eur. Phys. J. C* 81.2 (2021), p. 154. DOI: [10.1140/epjc/s10052-021-08938-8](https://doi.org/10.1140/epjc/s10052-021-08938-8). arXiv: [1912.04163](https://arxiv.org/abs/1912.04163) [hep-ph].
- [935] Sven Heinemeyer, Essodjolo Kpatcha, Iñaki Lara, Daniel E. López-Fogliani, Carlos Muñoz, and Natsumi Nagata. “The new  $(g-2)_\mu$  result and the  $\mu\nu$ SSM”. In: *Eur. Phys. J. C* 81.9 (2021), p. 802. DOI: [10.1140/epjc/s10052-021-09601-y](https://doi.org/10.1140/epjc/s10052-021-09601-y). arXiv: [2104.03294](https://arxiv.org/abs/2104.03294) [hep-ph].
- [936] John F. Gunion, Howard E. Haber, Gordon L. Kane, and Sally Dawson. *The Higgs Hunter’s Guide*. Vol. 80. 2000. ISBN: 978-0-429-49644-8. DOI: [10.1201/9780429496448](https://doi.org/10.1201/9780429496448).
- [937] G. C. Branco, P. M. Ferreira, L. Lavoura, M. N. Rebelo, Marc Sher, and Joao P. Silva. “Theory and phenomenology of two-Higgs-doublet models”. In: *Phys. Rept.* 516 (2012), pp. 1–102. DOI: [10.1016/j.physrep.2012.02.002](https://doi.org/10.1016/j.physrep.2012.02.002). arXiv: [1106.0034](https://arxiv.org/abs/1106.0034) [hep-ph].

- [938] Maria Krawczyk. “The New  $(g-2)$  for muon measurement and limits on the light Higgs bosons in 2HDM (II)”. In: (Mar. 2001). arXiv: [hep-ph/0103223](https://arxiv.org/abs/hep-ph/0103223).
- [939] F. Larios, G. Tavares-Velasco, and C. P. Yuan. “A Very light CP odd scalar in the two Higgs doublet model”. In: *Phys. Rev. D* 64 (2001), p. 055004. DOI: [10.1103/PhysRevD.64.055004](https://doi.org/10.1103/PhysRevD.64.055004). arXiv: [hep-ph/0103292](https://arxiv.org/abs/hep-ph/0103292).
- [940] Otto Eberhardt, Ana Peñuelas Martínez, and Antonio Pich. “Global fits in the Aligned Two-Higgs-Doublet model”. In: *JHEP* 05 (2021), p. 005. DOI: [10.1007/JHEP05\(2021\)005](https://doi.org/10.1007/JHEP05(2021)005). arXiv: [2012.09200](https://arxiv.org/abs/2012.09200) [[hep-ph](https://arxiv.org/abs/hep-ph)].
- [941] Oliver Atkinson, Matthew Black, Alexander Lenz, Aleksey Rusov, and James Wynne. “Cornering the Two Higgs Doublet Model Type II”. In: *JHEP* 04 (2022), p. 172. DOI: [10.1007/JHEP04\(2022\)172](https://doi.org/10.1007/JHEP04(2022)172). arXiv: [2107.05650](https://arxiv.org/abs/2107.05650) [[hep-ph](https://arxiv.org/abs/hep-ph)].
- [942] Oliver Atkinson, Matthew Black, Christoph Englert, Alexander Lenz, Aleksey Rusov, and James Wynne. “The flavourful present and future of 2HDMs at the collider energy frontier”. In: *JHEP* 11 (2022), p. 139. DOI: [10.1007/JHEP11\(2022\)139](https://doi.org/10.1007/JHEP11(2022)139). arXiv: [2202.08807](https://arxiv.org/abs/2202.08807) [[hep-ph](https://arxiv.org/abs/hep-ph)].
- [943] Syuhei Iguro, Teppei Kitahara, Martin S. Lang, and Michihisa Takeuchi. “Current status of the muon  $g-2$  interpretations within two-Higgs-doublet models”. In: *Phys. Rev. D* 108.11 (2023), p. 115012. DOI: [10.1103/PhysRevD.108.115012](https://doi.org/10.1103/PhysRevD.108.115012). arXiv: [2304.09887](https://arxiv.org/abs/2304.09887) [[hep-ph](https://arxiv.org/abs/hep-ph)].
- [944] Anirban Karan, Víctor Miralles, and Antonio Pich. “Updated global fit of the aligned two-Higgs-doublet model with heavy scalars”. In: *Phys. Rev. D* 109.3 (2024), p. 035012. DOI: [10.1103/PhysRevD.109.035012](https://doi.org/10.1103/PhysRevD.109.035012). arXiv: [2307.15419](https://arxiv.org/abs/2307.15419) [[hep-ph](https://arxiv.org/abs/hep-ph)].
- [945] Antonio M. Coutinho, Anirban Karan, Víctor Miralles, and Antonio Pich. “Light scalars within the  $\mathcal{CP}$ -conserving Aligned-two-Higgs-doublet model”. In: *JHEP* 02 (2025), p. 057. DOI: [10.1007/JHEP02\(2025\)057](https://doi.org/10.1007/JHEP02(2025)057). arXiv: [2412.14906](https://arxiv.org/abs/2412.14906) [[hep-ph](https://arxiv.org/abs/hep-ph)].
- [946] John F. Gunion and Howard E. Haber. “The CP conserving two Higgs doublet model: The Approach to the decoupling limit”. In: *Phys. Rev. D* 67 (2003), p. 075019. DOI: [10.1103/PhysRevD.67.075019](https://doi.org/10.1103/PhysRevD.67.075019). arXiv: [hep-ph/0207010](https://arxiv.org/abs/hep-ph/0207010).
- [947] T. D. Lee. “A Theory of Spontaneous T Violation”. In: *Phys. Rev. D* 8 (1973). Ed. by G. Feinberg, pp. 1226–1239. DOI: [10.1103/PhysRevD.8.1226](https://doi.org/10.1103/PhysRevD.8.1226).
- [948] Jérémy Bernon, John F. Gunion, Howard E. Haber, Yun Jiang, and Sabine Kraml. “Scrutinizing the alignment limit in two-Higgs-doublet models:  $m_h=125$  GeV”. In: *Phys. Rev. D* 92.7 (2015), p. 075004. DOI: [10.1103/PhysRevD.92.075004](https://doi.org/10.1103/PhysRevD.92.075004). arXiv: [1507.00933](https://arxiv.org/abs/1507.00933) [[hep-ph](https://arxiv.org/abs/hep-ph)].
- [949] Antonio Pich and Paula Tuzon. “Yukawa Alignment in the Two-Higgs-Doublet Model”. In: *Phys. Rev. D* 80 (2009), p. 091702. DOI: [10.1103/PhysRevD.80.091702](https://doi.org/10.1103/PhysRevD.80.091702). arXiv: [0908.1554](https://arxiv.org/abs/0908.1554) [[hep-ph](https://arxiv.org/abs/hep-ph)].
- [950] Martin Jung, Antonio Pich, and Paula Tuzon. “Charged-Higgs phenomenology in the Aligned two-Higgs-doublet model”. In: *JHEP* 11 (2010), p. 003. DOI: [10.1007/JHEP11\(2010\)003](https://doi.org/10.1007/JHEP11(2010)003). arXiv: [1006.0470](https://arxiv.org/abs/1006.0470) [[hep-ph](https://arxiv.org/abs/hep-ph)].
- [951] Hong-Xin Wang, Lei Wang, and Yang Zhang. “Muon  $g - 2$  anomaly and  $\mu$ - $\tau$ -philic Higgs doublet with a light CP-even component”. In: *Eur. Phys. J. C* 81.11 (2021), p. 1007. DOI: [10.1140/epjc/s10052-021-09778-2](https://doi.org/10.1140/epjc/s10052-021-09778-2). arXiv: [2104.03242](https://arxiv.org/abs/2104.03242) [[hep-ph](https://arxiv.org/abs/hep-ph)].

- [952] Xiao-Fang Han, Tianjun Li, Hong-Xin Wang, Lei Wang, and Yang Zhang. “Lepton-specific inert two-Higgs-doublet model confronted with the new results for muon and electron  $g-2$  anomalies and multilepton searches at the LHC”. In: *Phys. Rev. D* 104.11 (2021), p. 115001. DOI: [10.1103/PhysRevD.104.115001](https://doi.org/10.1103/PhysRevD.104.115001). arXiv: [2104.03227](https://arxiv.org/abs/2104.03227) [[hep-ph](#)].
- [953] Xiao-Fang Han, Fei Wang, Lei Wang, Jin Min Yang, and Yang Zhang. “Joint explanation of W-mass and muon  $g-2$  in the 2HDM\*”. In: *Chin. Phys. C* 46.10 (2022), p. 103105. DOI: [10.1088/1674-1137/ac7c63](https://doi.org/10.1088/1674-1137/ac7c63). arXiv: [2204.06505](https://arxiv.org/abs/2204.06505) [[hep-ph](#)].
- [954] Athanasios Dedes and Howard E. Haber. “Can the Higgs sector contribute significantly to the muon anomalous magnetic moment?” In: *JHEP* 05 (2001), p. 006. DOI: [10.1088/1126-6708/2001/05/006](https://doi.org/10.1088/1126-6708/2001/05/006). arXiv: [hep-ph/0102297](https://arxiv.org/abs/hep-ph/0102297).
- [955] A. Dedes and H. E. Haber. “A Light Higgs boson explanation for the  $g-2$  crisis”. In: *36th Rencontres de Moriond on Electroweak Interactions and Unified Theories*. Mar. 2001. arXiv: [hep-ph/0105014](https://arxiv.org/abs/hep-ph/0105014).
- [956] Kai Schmidt-Hoberg, Florian Staub, and Martin Wolfgang Winkler. “Constraints on light mediators: confronting dark matter searches with B physics”. In: *Phys. Lett. B* 727 (2013), pp. 506–510. DOI: [10.1016/j.physletb.2013.11.015](https://doi.org/10.1016/j.physletb.2013.11.015). arXiv: [1310.6752](https://arxiv.org/abs/1310.6752) [[hep-ph](#)].
- [957] Adriano Cherchiglia, Dominik Stöckinger, and Hyejung Stöckinger-Kim. “Muon  $g-2$  in the 2HDM: maximum results and detailed phenomenology”. In: *Phys. Rev. D* 98 (2018), p. 035001. DOI: [10.1103/PhysRevD.98.035001](https://doi.org/10.1103/PhysRevD.98.035001). arXiv: [1711.11567](https://arxiv.org/abs/1711.11567) [[hep-ph](#)].
- [958] Adriano Cherchiglia, Patrick Kneschke, Dominik Stöckinger, and Hyejung Stöckinger-Kim. “The muon magnetic moment in the 2HDM: complete two-loop result”. In: *JHEP* 01 (2017). [Erratum: *JHEP* 10, 242 (2021)], p. 007. DOI: [10.1007/JHEP10\(2021\)242](https://doi.org/10.1007/JHEP10(2021)242). arXiv: [1607.06292](https://arxiv.org/abs/1607.06292) [[hep-ph](#)].
- [959] Peter Athron, Csaba Balazs, Adriano Cherchiglia, Douglas H. J. Jacob, Dominik Stöckinger, Hyejung Stöckinger-Kim, and Alexander Voigt. “Two-loop prediction of the anomalous magnetic moment of the muon in the Two-Higgs Doublet Model with GM2Calc 2”. In: *Eur. Phys. J. C* 82.3 (2022), p. 229. DOI: [10.1140/epjc/s10052-022-10148-9](https://doi.org/10.1140/epjc/s10052-022-10148-9). arXiv: [2110.13238](https://arxiv.org/abs/2110.13238) [[hep-ph](#)].
- [960] Alessandro Broggio, Eung Jin Chun, Massimo Passera, Ketan M. Patel, and Sudhir K. Vempati. “Limiting two-Higgs-doublet models”. In: *JHEP* 11 (2014), p. 058. DOI: [10.1007/JHEP11\(2014\)058](https://doi.org/10.1007/JHEP11(2014)058). arXiv: [1409.3199](https://arxiv.org/abs/1409.3199) [[hep-ph](#)].
- [961] Lei Wang and Xiao-Fang Han. “A light pseudoscalar of 2HDM confronted with muon  $g-2$  and experimental constraints”. In: *JHEP* 05 (2015), p. 039. DOI: [10.1007/JHEP05\(2015\)039](https://doi.org/10.1007/JHEP05(2015)039). arXiv: [1412.4874](https://arxiv.org/abs/1412.4874) [[hep-ph](#)].
- [962] Tao Han, Sin Kyu Kang, and Joshua Sayre. “Muon  $g-2$  in the aligned two Higgs doublet model”. In: *JHEP* 02 (2016), p. 097. DOI: [10.1007/JHEP02\(2016\)097](https://doi.org/10.1007/JHEP02(2016)097). arXiv: [1511.05162](https://arxiv.org/abs/1511.05162) [[hep-ph](#)].
- [963] Tomohiro Abe, Ryosuke Sato, and Kei Yagyu. “Lepton-specific two Higgs doublet model as a solution of muon  $g-2$  anomaly”. In: *JHEP* 07 (2015), p. 064. DOI: [10.1007/JHEP07\(2015\)064](https://doi.org/10.1007/JHEP07(2015)064). arXiv: [1504.07059](https://arxiv.org/abs/1504.07059) [[hep-ph](#)].
- [964] Eung Jin Chun, Zhaofeng Kang, Michihisa Takeuchi, and Yue-Lin Sming Tsai. “LHC  $\tau$ -rich tests of lepton-specific 2HDM for  $(g-2)_\mu$ ”. In: *JHEP* 11 (2015), p. 099. DOI: [10.1007/JHEP11\(2015\)099](https://doi.org/10.1007/JHEP11(2015)099). arXiv: [1507.08067](https://arxiv.org/abs/1507.08067) [[hep-ph](#)].

- [965] Eung Jin Chun and Jinsu Kim. “Leptonic Precision Test of Leptophilic Two-Higgs-Doublet Model”. In: *JHEP* 07 (2016), p. 110. DOI: [10.1007/JHEP07\(2016\)110](https://doi.org/10.1007/JHEP07(2016)110). arXiv: [1605.06298](https://arxiv.org/abs/1605.06298) [[hep-ph](#)].
- [966] Lei Wang, Jin Min Yang, Mengchao Zhang, and Yang Zhang. “Revisiting lepton-specific 2HDM in light of muon  $g - 2$  anomaly”. In: *Phys. Lett. B* 788 (2019), pp. 519–529. DOI: [10.1016/j.physletb.2018.11.045](https://doi.org/10.1016/j.physletb.2018.11.045). arXiv: [1809.05857](https://arxiv.org/abs/1809.05857) [[hep-ph](#)].
- [967] Syuhei Iguro, Yuji Omura, and Michihisa Takeuchi. “Testing the 2HDM explanation of the muon  $g - 2$  anomaly at the LHC”. In: *JHEP* 11 (2019), p. 130. DOI: [10.1007/JHEP11\(2019\)130](https://doi.org/10.1007/JHEP11(2019)130). arXiv: [1907.09845](https://arxiv.org/abs/1907.09845) [[hep-ph](#)].
- [968] Eung Jin Chun, Jongkuk Kim, and Tanmoy Mondal. “Electron EDM and Muon anomalous magnetic moment in Two-Higgs-Doublet Models”. In: *JHEP* 12 (2019), p. 068. DOI: [10.1007/JHEP12\(2019\)068](https://doi.org/10.1007/JHEP12(2019)068). arXiv: [1906.00612](https://arxiv.org/abs/1906.00612) [[hep-ph](#)].
- [969] Danielle Sabatta, Alan S. Cornell, Ashok Goyal, Mukesh Kumar, Bruce Mellado, and Xifeng Ruan. “Connecting muon anomalous magnetic moment and multi-lepton anomalies at LHC”. In: *Chin. Phys. C* 44.6 (2020), p. 063103. DOI: [10.1088/1674-1137/44/6/063103](https://doi.org/10.1088/1674-1137/44/6/063103). arXiv: [1909.03969](https://arxiv.org/abs/1909.03969) [[hep-ph](#)].
- [970] Luigi Delle Rose, Shaaban Khalil, and Stefano Moretti. “Explaining electron and muon  $g - 2$  anomalies in an Aligned 2-Higgs Doublet Model with right-handed neutrinos”. In: *Phys. Lett. B* 816 (2021), p. 136216. DOI: [10.1016/j.physletb.2021.136216](https://doi.org/10.1016/j.physletb.2021.136216). arXiv: [2012.06911](https://arxiv.org/abs/2012.06911) [[hep-ph](#)].
- [971] Nivedita Ghosh and Jayita Lahiri. “Generalized 2HDM with wrong-sign lepton-Yukawa coupling, in light of  $g_\mu - 2$  and lepton flavor violation at the future LHC”. In: *Eur. Phys. J. C* 81.12 (2021), p. 1074. DOI: [10.1140/epjc/s10052-021-09844-9](https://doi.org/10.1140/epjc/s10052-021-09844-9). arXiv: [2103.10632](https://arxiv.org/abs/2103.10632) [[hep-ph](#)].
- [972] Adil Jueid, Jinheung Kim, Soojin Lee, and Jeonghyeon Song. “Type-X two-Higgs-doublet model in light of the muon  $g-2$ : Confronting Higgs boson and collider data”. In: *Phys. Rev. D* 104.9 (2021), p. 095008. DOI: [10.1103/PhysRevD.104.095008](https://doi.org/10.1103/PhysRevD.104.095008). arXiv: [2104.10175](https://arxiv.org/abs/2104.10175) [[hep-ph](#)].
- [973] Atri Dey, Jayita Lahiri, and Biswarup Mukhopadhyaya. “Muon  $g-2$  and a type-X two-Higgs-doublet scenario: Some studies in high-scale validity”. In: *Phys. Rev. D* 106.5 (2022), p. 055023. DOI: [10.1103/PhysRevD.106.055023](https://doi.org/10.1103/PhysRevD.106.055023). arXiv: [2106.01449](https://arxiv.org/abs/2106.01449) [[hep-ph](#)].
- [974] Jongkuk Kim. “Compatibility of muon  $g - 2$ ,  $W$  mass anomaly in type-X 2HDM”. In: *Phys. Lett. B* 832 (2022), p. 137220. DOI: [10.1016/j.physletb.2022.137220](https://doi.org/10.1016/j.physletb.2022.137220). arXiv: [2205.01437](https://arxiv.org/abs/2205.01437) [[hep-ph](#)].
- [975] Jinheung Kim, Soojin Lee, Prasenjit Sanyal, and Jeonghyeon Song. “CDF  $W$ -boson mass and muon  $g-2$  in a type-X two-Higgs-doublet model with a Higgs-phobic light pseudoscalar”. In: *Phys. Rev. D* 106.3 (2022), p. 035002. DOI: [10.1103/PhysRevD.106.035002](https://doi.org/10.1103/PhysRevD.106.035002). arXiv: [2205.01701](https://arxiv.org/abs/2205.01701) [[hep-ph](#)].
- [976] A. Barroso, P. M. Ferreira, I. P. Ivanov, and Rui Santos. “Metastability bounds on the two Higgs doublet model”. In: *JHEP* 06 (2013), p. 045. DOI: [10.1007/JHEP06\(2013\)045](https://doi.org/10.1007/JHEP06(2013)045). arXiv: [1303.5098](https://arxiv.org/abs/1303.5098) [[hep-ph](#)].
- [977] Shinya Kanemura, Takahiro Kubota, and Eiichi Takasugi. “Lee-Quigg-Thacker bounds for Higgs boson masses in a two doublet model”. In: *Phys. Lett. B* 313 (1993), pp. 155–160. DOI: [10.1016/0370-2693\(93\)91205-2](https://doi.org/10.1016/0370-2693(93)91205-2). arXiv: [hep-ph/9303263](https://arxiv.org/abs/hep-ph/9303263).
- [978] I. F. Ginzburg and I. P. Ivanov. “Tree-level unitarity constraints in the most general 2HDM”. In: *Phys. Rev. D* 72 (2005), p. 115010. DOI: [10.1103/PhysRevD.72.115010](https://doi.org/10.1103/PhysRevD.72.115010). arXiv: [hep-ph/0508020](https://arxiv.org/abs/hep-ph/0508020).

- [979] Yasmine Sara Amhis et al. “Averages of b-hadron, c-hadron, and  $\tau$ -lepton properties as of 2021”. In: *Phys. Rev. D* 107.5 (2023), p. 052008. DOI: [10.1103/PhysRevD.107.052008](https://doi.org/10.1103/PhysRevD.107.052008). arXiv: [2206.07501](https://arxiv.org/abs/2206.07501) [[hep-ex](#)].
- [980] Maria Krawczyk and David Temes. “2HDM(II) radiative corrections in leptonic tau decays”. In: *Eur. Phys. J. C* 44 (2005), pp. 435–446. DOI: [10.1140/epjc/s2005-02370-2](https://doi.org/10.1140/epjc/s2005-02370-2). arXiv: [hep-ph/0410248](https://arxiv.org/abs/hep-ph/0410248).
- [981] Ansgar Denner, R. J. Guth, W. Hollik, and Johann H. Kuhn. “The Z width in the two Higgs doublet model”. In: *Z. Phys. C* 51 (1991), pp. 695–705. DOI: [10.1007/BF01565598](https://doi.org/10.1007/BF01565598).
- [982] J. Abdallah et al. “Searches for neutral higgs bosons in extended models”. In: *Eur. Phys. J. C* 38 (2004), pp. 1–28. DOI: [10.1140/epjc/s2004-02011-4](https://doi.org/10.1140/epjc/s2004-02011-4). arXiv: [hep-ex/0410017](https://arxiv.org/abs/hep-ex/0410017).
- [983] Mikolaj Misiak and Matthias Steinhauser. “Weak radiative decays of the B meson and bounds on  $M_{H^\pm}$  in the Two-Higgs-Doublet Model”. In: *Eur. Phys. J. C* 77.3 (2017), p. 201. DOI: [10.1140/epjc/s10052-017-4776-y](https://doi.org/10.1140/epjc/s10052-017-4776-y). arXiv: [1702.04571](https://arxiv.org/abs/1702.04571) [[hep-ph](#)].
- [984] Eung Jin Chun and Tanmoy Mondal. “Searching for a Light Higgs Boson via the Yukawa Process at Lepton Colliders”. In: *Phys. Lett. B* 802 (2020), p. 135190. DOI: [10.1016/j.physletb.2019.135190](https://doi.org/10.1016/j.physletb.2019.135190). arXiv: [1909.09515](https://arxiv.org/abs/1909.09515) [[hep-ph](#)].
- [985] Nivedita Ghosh and Jayita Lahiri. “Revisiting a generalized two-Higgs-doublet model in light of the muon anomaly and lepton flavor violating decays at the HL-LHC”. In: *Phys. Rev. D* 103.5 (2021), p. 055009. DOI: [10.1103/PhysRevD.103.055009](https://doi.org/10.1103/PhysRevD.103.055009). arXiv: [2010.03590](https://arxiv.org/abs/2010.03590) [[hep-ph](#)].
- [986] R. Aaij et al. “Analysis of Neutral B-Meson Decays into Two Muons”. In: *Phys. Rev. Lett.* 128.4 (2022), p. 041801. DOI: [10.1103/PhysRevLett.128.041801](https://doi.org/10.1103/PhysRevLett.128.041801). arXiv: [2108.09284](https://arxiv.org/abs/2108.09284) [[hep-ex](#)].
- [987] Armen Tumasyan et al. “Measurement of the  $B_s^0 \rightarrow \mu^+ \mu^-$  decay properties and search for the  $B^0 \rightarrow \mu^+ \mu^-$  decay in proton-proton collisions at  $\sqrt{s} = 13$  TeV”. In: *Phys. Lett. B* 842 (2023), p. 137955. DOI: [10.1016/j.physletb.2023.137955](https://doi.org/10.1016/j.physletb.2023.137955). arXiv: [2212.10311](https://arxiv.org/abs/2212.10311) [[hep-ex](#)].
- [988] Vardan Khachatryan et al. “Observation of the rare  $B_s^0 \rightarrow \mu^+ \mu^-$  decay from the combined analysis of CMS and LHCb data”. In: *Nature* 522 (2015), pp. 68–72. DOI: [10.1038/nature14474](https://doi.org/10.1038/nature14474). arXiv: [1411.4413](https://arxiv.org/abs/1411.4413) [[hep-ex](#)].
- [989] Christoph Bobeth, Martin Gorbahn, Thomas Hermann, Mikolaj Misiak, Emmanuel Stamou, and Matthias Steinhauser. “ $B_{s,d} \rightarrow l^+ l^-$  in the Standard Model with Reduced Theoretical Uncertainty”. In: *Phys. Rev. Lett.* 112 (2014), p. 101801. DOI: [10.1103/PhysRevLett.112.101801](https://doi.org/10.1103/PhysRevLett.112.101801). arXiv: [1311.0903](https://arxiv.org/abs/1311.0903) [[hep-ph](#)].
- [990] Andrzej J. Buras and Elena Venturini. “The exclusive vision of rare K and B decays and of the quark mixing in the standard model”. In: *Eur. Phys. J. C* 82.7 (2022), p. 615. DOI: [10.1140/epjc/s10052-022-10583-8](https://doi.org/10.1140/epjc/s10052-022-10583-8). arXiv: [2203.11960](https://arxiv.org/abs/2203.11960) [[hep-ph](#)].
- [991] Morad Aaboud et al. “Search for the direct production of charginos and neutralinos in final states with tau leptons in  $\sqrt{s} = 13$  TeV  $pp$  collisions with the ATLAS detector”. In: *Eur. Phys. J. C* 78.2 (2018), p. 154. DOI: [10.1140/epjc/s10052-018-5583-9](https://doi.org/10.1140/epjc/s10052-018-5583-9). arXiv: [1708.07875](https://arxiv.org/abs/1708.07875) [[hep-ex](#)].
- [992] Georges Aad et al. “Search for direct stau production in events with two hadronic  $\tau$ -leptons in  $\sqrt{s} = 13$  TeV  $pp$  collisions with the ATLAS detector”. In: *Phys. Rev. D* 101.3 (2020), p. 032009. DOI: [10.1103/PhysRevD.101.032009](https://doi.org/10.1103/PhysRevD.101.032009). arXiv: [1911.06660](https://arxiv.org/abs/1911.06660) [[hep-ex](#)].

- [993] “Search for the direct production of charginos and neutralinos in final states with tau leptons in  $\sqrt{s} = 13$  TeV  $pp$  collisions with the ATLAS detector”. In: (2022).
- [994] Georges Aad et al. “Search for a light CP-odd Higgs boson decaying into a pair of  $\tau$ -leptons in proton-proton collisions at  $\sqrt{s} = 13$  TeV with the ATLAS detector”. In: *JHEP* 12 (2024), p. 126. DOI: [10.1007/JHEP12\(2024\)126](https://doi.org/10.1007/JHEP12(2024)126). arXiv: [2409.20381](https://arxiv.org/abs/2409.20381) [[hep-ex](#)].
- [995] Lei Wang, Jin Min Yang, and Yang Zhang. “Two-Higgs-doublet models in light of current experiments: a brief review”. In: *Commun. Theor. Phys.* 74.9 (2022), p. 097202. DOI: [10.1088/1572-9494/ac7fe9](https://doi.org/10.1088/1572-9494/ac7fe9). arXiv: [2203.07244](https://arxiv.org/abs/2203.07244) [[hep-ph](#)].
- [996] Francisco J. Botella, Fernando Cornet-Gomez, and Miguel Nebot. “Electron and muon  $g - 2$  anomalies in general flavour conserving two Higgs doublets models”. In: *Phys. Rev. D* 102.3 (2020), p. 035023. DOI: [10.1103/PhysRevD.102.035023](https://doi.org/10.1103/PhysRevD.102.035023). arXiv: [2006.01934](https://arxiv.org/abs/2006.01934) [[hep-ph](#)].
- [997] Francisco J. Botella, Fernando Cornet-Gomez, Carlos Miró, and Miguel Nebot. “Muon and electron  $g - 2$  anomalies in a flavor conserving 2HDM with an oblique view on the CDF  $M_W$  value”. In: *Eur. Phys. J. C* 82 (2022), p. 915. DOI: [10.1140/epjc/s10052-022-10893-x](https://doi.org/10.1140/epjc/s10052-022-10893-x). arXiv: [2205.01115](https://arxiv.org/abs/2205.01115) [[hep-ph](#)].
- [998] Xiao-Fang Han, Tianjun Li, Lei Wang, and Yang Zhang. “Simple interpretations of lepton anomalies in the lepton-specific inert two-Higgs-doublet model”. In: *Phys. Rev. D* 99.9 (2019), p. 095034. DOI: [10.1103/PhysRevD.99.095034](https://doi.org/10.1103/PhysRevD.99.095034). arXiv: [1812.02449](https://arxiv.org/abs/1812.02449) [[hep-ph](#)].
- [999] Shao-Ping Li, Xin-Qiang Li, Yuan-Yuan Li, Ya-Dong Yang, and Xin Zhang. “Power-aligned 2HDM: a correlative perspective on  $(g - 2)_{e,\mu}$ ”. In: *JHEP* 01 (2021), p. 034. DOI: [10.1007/JHEP01\(2021\)034](https://doi.org/10.1007/JHEP01(2021)034). arXiv: [2010.02799](https://arxiv.org/abs/2010.02799) [[hep-ph](#)].
- [1000] Sudip Jana, Vishnu P. K., and Shaikh Saad. “Resolving electron and muon  $g - 2$  within the 2HDM”. In: *Phys. Rev. D* 101.11 (2020), p. 115037. DOI: [10.1103/PhysRevD.101.115037](https://doi.org/10.1103/PhysRevD.101.115037). arXiv: [2003.03386](https://arxiv.org/abs/2003.03386) [[hep-ph](#)].
- [1001] Tomohiro Abe, Ryosuke Sato, and Kei Yagyu. “Muon specific two-Higgs-doublet model”. In: *JHEP* 07 (2017), p. 012. DOI: [10.1007/JHEP07\(2017\)012](https://doi.org/10.1007/JHEP07(2017)012). arXiv: [1705.01469](https://arxiv.org/abs/1705.01469) [[hep-ph](#)].
- [1002] E. O. Iltan and H. Sundu. “Anomalous magnetic moment of muon in the general two Higgs doublet model”. In: *Acta Phys. Slov.* 53.1 (2003), p. 17. arXiv: [hep-ph/0103105](https://arxiv.org/abs/hep-ph/0103105).
- [1003] Lei Wang, Shuo Yang, and Xiao-Fang Han. “ $h \rightarrow \mu\tau$  and muon  $g-2$  in the alignment limit of two-Higgs-doublet model”. In: *Nucl. Phys. B* 919 (2017), pp. 123–141. DOI: [10.1016/j.nuclphysb.2017.03.013](https://doi.org/10.1016/j.nuclphysb.2017.03.013). arXiv: [1606.04408](https://arxiv.org/abs/1606.04408) [[hep-ph](#)].
- [1004] Lei Wang and Yang Zhang. “ $\mu$ - $\tau$ -philic Higgs doublet model confronted with the muon  $g-2$ ,  $\tau$  decays, and LHC data”. In: *Phys. Rev. D* 100.9 (2019), p. 095005. DOI: [10.1103/PhysRevD.100.095005](https://doi.org/10.1103/PhysRevD.100.095005). arXiv: [1908.03755](https://arxiv.org/abs/1908.03755) [[hep-ph](#)].
- [1005] Wei-Shu Hou, Rishabh Jain, Chung Kao, Girish Kumar, and Tanmoy Modak. “Collider Prospects for Muon  $g - 2$  in General Two Higgs Doublet Model”. In: *Phys. Rev. D* 104.7 (2021), p. 075036. DOI: [10.1103/PhysRevD.104.075036](https://doi.org/10.1103/PhysRevD.104.075036). arXiv: [2105.11315](https://arxiv.org/abs/2105.11315) [[hep-ph](#)].
- [1006] Wei-Shu Hou and Girish Kumar. “Charged lepton flavor violation in light of muon  $g - 2$ ”. In: *Eur. Phys. J. C* 81.12 (2021), p. 1132. DOI: [10.1140/epjc/s10052-021-09939-3](https://doi.org/10.1140/epjc/s10052-021-09939-3). arXiv: [2107.14114](https://arxiv.org/abs/2107.14114) [[hep-ph](#)].

- [1007] Kento Asai, Coh Miyao, Shohei Okawa, and Koji Tsumura. “Scalar dark matter with a  $\mu\tau$  flavored mediator”. In: *Phys. Rev. D* 106.3 (2022), p. 035017. DOI: [10.1103/PhysRevD.106.035017](https://doi.org/10.1103/PhysRevD.106.035017). arXiv: [2205.08998](https://arxiv.org/abs/2205.08998) [hep-ph].
- [1008] Monika Blanke and Syuhei Iguro. “Collider probe of heavy additional Higgs bosons solving the muon  $g-2$  and dark matter problems”. In: *Phys. Rev. D* 107.9 (2023), p. 095024. DOI: [10.1103/PhysRevD.107.095024](https://doi.org/10.1103/PhysRevD.107.095024). arXiv: [2210.13508](https://arxiv.org/abs/2210.13508) [hep-ph].
- [1009] Rachid Benbrik, Mohammed Boukidi, and Bouzid Manaut. “Interpreting the  $W$ -mass and muon  $(g\mu - 2)$  anomalies within a 2-Higgs doublet model”. In: *Nucl. Phys. B* 1005 (2024), p. 116593. DOI: [10.1016/j.nuclphysb.2024.116593](https://doi.org/10.1016/j.nuclphysb.2024.116593). arXiv: [2204.11755](https://arxiv.org/abs/2204.11755) [hep-ph].
- [1010] K. S. Babu, Sudip Jana, and Vishnu P. K. “Correlating  $W$ -Boson Mass Shift with Muon  $g-2$  in the Two Higgs Doublet Model”. In: *Phys. Rev. Lett.* 129.12 (2022), p. 121803. DOI: [10.1103/PhysRevLett.129.121803](https://doi.org/10.1103/PhysRevLett.129.121803). arXiv: [2204.05303](https://arxiv.org/abs/2204.05303) [hep-ph].
- [1011] Peter Athron, Andreas Crivellin, Tomás E. Gonzalo, Syuhei Iguro, and Cristian Sierra. “Global fit to the 2HDM with generic sources of flavour violation using GAMBIT”. In: *JHEP* 11 (2024), p. 133. DOI: [10.1007/JHEP11\(2024\)133](https://doi.org/10.1007/JHEP11(2024)133). arXiv: [2410.10493](https://arxiv.org/abs/2410.10493) [hep-ph].
- [1012] Peter Athron, Csaba Balazs, Tomás E. Gonzalo, Douglas Jacob, Farvah Mahmoudi, and Cristian Sierra. “Likelihood analysis of the flavour anomalies and  $g - 2$  in the general two Higgs doublet model”. In: *JHEP* 01 (2022), p. 037. DOI: [10.1007/JHEP01\(2022\)037](https://doi.org/10.1007/JHEP01(2022)037). arXiv: [2111.10464](https://arxiv.org/abs/2111.10464) [hep-ph].
- [1013] Giorgio Arcadi, Abdelhak Djouadi, and Farinaldo da Silva Queiroz. “Models with two Higgs doublets and a light pseudoscalar: A portal to dark matter and the possible  $(g-2)\mu$  excess”. In: *Phys. Lett. B* 834 (2022), p. 137436. DOI: [10.1016/j.physletb.2022.137436](https://doi.org/10.1016/j.physletb.2022.137436). arXiv: [2112.11902](https://arxiv.org/abs/2112.11902) [hep-ph].
- [1014] Giorgio Arcadi, Álvaro S. de Jesus, Téo B. de Melo, Farinaldo S. Queiroz, and Yoxara S. Villamizar. “A 2HDM for the  $g-2$  and dark matter”. In: *Nucl. Phys. B* 982 (2022), p. 115882. DOI: [10.1016/j.nuclphysb.2022.115882](https://doi.org/10.1016/j.nuclphysb.2022.115882). arXiv: [2104.04456](https://arxiv.org/abs/2104.04456) [hep-ph].
- [1015] Giorgio Arcadi and Abdelhak Djouadi. “2HD plus light pseudoscalar model for a combined explanation of the possible excesses in the CDF  $M_W$  measurement and  $(g-2)\mu$  with dark matter”. In: *Phys. Rev. D* 106.9 (2022), p. 095008. DOI: [10.1103/PhysRevD.106.095008](https://doi.org/10.1103/PhysRevD.106.095008). arXiv: [2204.08406](https://arxiv.org/abs/2204.08406) [hep-ph].
- [1016] Giorgio Arcadi, Nico Benincasa, Abdelhak Djouadi, and Kristjan Kannike. “Two-Higgs-doublet-plus-pseudoscalar model: Collider, dark matter, and gravitational wave signals”. In: *Phys. Rev. D* 108.5 (2023), p. 055010. DOI: [10.1103/PhysRevD.108.055010](https://doi.org/10.1103/PhysRevD.108.055010). arXiv: [2212.14788](https://arxiv.org/abs/2212.14788) [hep-ph].
- [1017] Giorgio Arcadi and Sarif Khan. “Axion dark matter and additional BSM aspects in an extended 2HDM setup”. In: *Phys. Rev. D* 110.1 (2024), p. 015011. DOI: [10.1103/PhysRevD.110.015011](https://doi.org/10.1103/PhysRevD.110.015011). arXiv: [2312.17099](https://arxiv.org/abs/2312.17099) [hep-ph].
- [1018] Eung Jin Chun and Tanmoy Mondal. “Leptophilic bosons and muon  $g-2$  at lepton colliders”. In: *JHEP* 07 (2021), p. 044. DOI: [10.1007/JHEP07\(2021\)044](https://doi.org/10.1007/JHEP07(2021)044). arXiv: [2104.03701](https://arxiv.org/abs/2104.03701) [hep-ph].
- [1019] Hrishabh Bharadwaj, Mamta Dahiya, Sukanta Dutta, and Ashok Goyal. “ $W$  mass and muon  $g-2$  in an inert 2HDM extended by a singlet complex scalar”. In: *Phys. Rev. D* 110.11 (2024), p. 115040. DOI: [10.1103/PhysRevD.110.115040](https://doi.org/10.1103/PhysRevD.110.115040). arXiv: [2407.00181](https://arxiv.org/abs/2407.00181) [hep-ph].

- [1020] Nabarun Chakrabarty. “Muon  $g-2$  in a type-X 2HDM assisted by inert scalars: A test at the LHC”. In: *Phys. Rev. D* 107.7 (2023), p. 075012. DOI: [10.1103/PhysRevD.107.075012](https://doi.org/10.1103/PhysRevD.107.075012). arXiv: [2112.13126](https://arxiv.org/abs/2112.13126) [[hep-ph](#)].
- [1021] Nabarun Chakrabarty and Indrani Chakraborty. “Muon  $g-2$  in a type-X 2HDM assisted by inert scalars: A test at the ILC”. In: *Phys. Rev. D* 107.7 (2023), p. 075013. DOI: [10.1103/PhysRevD.107.075013](https://doi.org/10.1103/PhysRevD.107.075013). arXiv: [2211.09863](https://arxiv.org/abs/2211.09863) [[hep-ph](#)].
- [1022] Chuan-Hung Chen, Cheng-Wei Chiang, and Takaaki Nomura. “Muon  $g-2$  in a two-Higgs-doublet model with a type-II seesaw mechanism”. In: *Phys. Rev. D* 104.5 (2021), p. 055011. DOI: [10.1103/PhysRevD.104.055011](https://doi.org/10.1103/PhysRevD.104.055011). arXiv: [2104.03275](https://arxiv.org/abs/2104.03275) [[hep-ph](#)].
- [1023] Mariana Frank and Ipsita Saha. “Muon anomalous magnetic moment in two-Higgs-doublet models with vectorlike leptons”. In: *Phys. Rev. D* 102.11 (2020), p. 115034. DOI: [10.1103/PhysRevD.102.115034](https://doi.org/10.1103/PhysRevD.102.115034). arXiv: [2008.11909](https://arxiv.org/abs/2008.11909) [[hep-ph](#)].
- [1024] Eung Jin Chun and Tanmoy Mondal. “Explaining  $g - 2$  anomalies in two Higgs doublet model with vector-like leptons”. In: *JHEP* 11 (2020), p. 077. DOI: [10.1007/JHEP11\(2020\)077](https://doi.org/10.1007/JHEP11(2020)077). arXiv: [2009.08314](https://arxiv.org/abs/2009.08314) [[hep-ph](#)].
- [1025] Radovan Dermisek, Keith Hermanek, Navin McGinnis, and Sangsik Yoon. “Predictions for muon electric and magnetic dipole moments from  $h \rightarrow \mu + \mu^-$  in two-Higgs-doublet models with new leptons”. In: *Phys. Rev. D* 108.5 (2023), p. 055019. DOI: [10.1103/PhysRevD.108.055019](https://doi.org/10.1103/PhysRevD.108.055019). arXiv: [2306.13212](https://arxiv.org/abs/2306.13212) [[hep-ph](#)].
- [1026] P. M. Ferreira, B. L. Gonçalves, F. R. Joaquim, and Marc Sher. “ $(g-2)_\mu$  in the 2HDM and slightly beyond: An updated view”. In: *Phys. Rev. D* 104.5 (2021), p. 053008. DOI: [10.1103/PhysRevD.104.053008](https://doi.org/10.1103/PhysRevD.104.053008). arXiv: [2104.03367](https://arxiv.org/abs/2104.03367) [[hep-ph](#)].
- [1027] Hrishabh Bharadwaj, Sukanta Dutta, and Ashok Goyal. “Leptonic  $g - 2$  anomaly in an extended Higgs sector with vector-like leptons”. In: *JHEP* 11 (2021), p. 056. DOI: [10.1007/JHEP11\(2021\)056](https://doi.org/10.1007/JHEP11(2021)056). arXiv: [2109.02586](https://arxiv.org/abs/2109.02586) [[hep-ph](#)].
- [1028] Radovan Dermisek, Keith Hermanek, Navin McGinnis, and Navin McGinnis. “Highly Enhanced Contributions of Heavy Higgs Bosons and New Leptons to Muon  $g-2$  and Prospects at Future Colliders”. In: *Phys. Rev. Lett.* 126.19 (2021), p. 191801. DOI: [10.1103/PhysRevLett.126.191801](https://doi.org/10.1103/PhysRevLett.126.191801). arXiv: [2011.11812](https://arxiv.org/abs/2011.11812) [[hep-ph](#)].
- [1029] Radovan Dermisek, Keith Hermanek, and Navin McGinnis. “Muon  $g-2$  in two-Higgs-doublet models with vectorlike leptons”. In: *Phys. Rev. D* 104.5 (2021), p. 055033. DOI: [10.1103/PhysRevD.104.055033](https://doi.org/10.1103/PhysRevD.104.055033). arXiv: [2103.05645](https://arxiv.org/abs/2103.05645) [[hep-ph](#)].
- [1030] Md. Raju, Abhi Mukherjee, and Jyoti Prasad Saha. “Investigation of  $(g - 2)_\mu$  anomaly in the  $\mu$ -specific 2HDM with vector like leptons and the phenomenological implications”. In: *Eur. Phys. J. C* 83.5 (2023), p. 429. DOI: [10.1140/epjc/s10052-023-11595-8](https://doi.org/10.1140/epjc/s10052-023-11595-8). arXiv: [2207.02825](https://arxiv.org/abs/2207.02825) [[hep-ph](#)].
- [1031] Md. Raju, Abhi Mukherjee, and Jyoti Prasad Saha. “Impact of Vector like quarks on  $(g - 2)_\mu$  with X-II-2HDM scenario and its phenomenological implications”. In: (June 2024). arXiv: [2406.00803](https://arxiv.org/abs/2406.00803) [[hep-ph](#)].
- [1032] H. Lee and A. E. Cárcamo Hernández. “Can the muon anomalous magnetic moment and the  $B$  anomalies be simultaneously explained in a minimally extended  $Z'$  model?” In: (July 2022). arXiv: [2207.01710](https://arxiv.org/abs/2207.01710) [[hep-ph](#)].

- [1033] Tanmoy Mondal and Hiroshi Okada. “Inverse seesaw and  $(g - 2)$  anomalies in B – L extended two Higgs doublet model”. In: *Nucl. Phys. B* 976 (2022), p. 115716. DOI: [10.1016/j.nuclphysb.2022.115716](https://doi.org/10.1016/j.nuclphysb.2022.115716). arXiv: [2103.13149](https://arxiv.org/abs/2103.13149) [hep-ph].
- [1034] Sayan Ghosh, Amit Dutta Banik, Eung Jin Chun, and Debasish Majumdar. “Leptophilic-portal dark matter in the light of AMS-02 positron excess”. In: *Phys. Rev. D* 104.7 (2021), p. 075016. DOI: [10.1103/PhysRevD.104.075016](https://doi.org/10.1103/PhysRevD.104.075016). arXiv: [2003.07675](https://arxiv.org/abs/2003.07675) [hep-ph].
- [1035] Takaaki Nomura and Prasenjit Sanyal. “Explaining Atomki anomaly and muon  $g - 2$  in  $U(1)_X$  extended flavour violating two Higgs doublet model”. In: *JHEP* 05 (2021), p. 232. DOI: [10.1007/JHEP05\(2021\)232](https://doi.org/10.1007/JHEP05(2021)232). arXiv: [2010.04266](https://arxiv.org/abs/2010.04266) [hep-ph].
- [1036] Takaaki Nomura, Hiroshi Okada, and Prasenjit Sanyal. “A radiatively induced inverse seesaw model with hidden  $U(1)$  gauge symmetry”. In: *Eur. Phys. J. C* 82.8 (2022), p. 697. DOI: [10.1140/epjc/s10052-022-10662-w](https://doi.org/10.1140/epjc/s10052-022-10662-w). arXiv: [2103.09494](https://arxiv.org/abs/2103.09494) [hep-ph].
- [1037] L. T. Hue, A. E. Cárcamo Hernández, H. N. Long, and T. T. Hong. “Heavy singly charged Higgs bosons and inverse seesaw neutrinos as origins of large  $(g-2)_{e,\mu}$  in two Higgs doublet models”. In: *Nucl. Phys. B* 984 (2022), p. 115962. DOI: [10.1016/j.nuclphysb.2022.115962](https://doi.org/10.1016/j.nuclphysb.2022.115962). arXiv: [2110.01356](https://arxiv.org/abs/2110.01356) [hep-ph].
- [1038] A. E. Cárcamo Hernández, D. T. Huong, and Ivan Schmidt. “Universal inverse seesaw mechanism as a source of the SM fermion mass hierarchy”. In: *Eur. Phys. J. C* 82.1 (2022), p. 63. DOI: [10.1140/epjc/s10052-022-10011-x](https://doi.org/10.1140/epjc/s10052-022-10011-x). arXiv: [2109.12118](https://arxiv.org/abs/2109.12118) [hep-ph].
- [1039] A. E. Cárcamo Hernández, S. F. King, and H. Lee. “Fermion mass hierarchies from vectorlike families with an extended 2HDM and a possible explanation for the electron and muon anomalous magnetic moments”. In: *Phys. Rev. D* 103.11 (2021), p. 115024. DOI: [10.1103/PhysRevD.103.115024](https://doi.org/10.1103/PhysRevD.103.115024). arXiv: [2101.05819](https://arxiv.org/abs/2101.05819) [hep-ph].
- [1040] A. E. Cárcamo Hernández, Catalina Espinoza, Juan Carlos Gómez-Izquierdo, and Myriam Mondragón. “Fermion masses and mixings, dark matter, leptogenesis and  $g - 2$  muon anomaly in an extended 2HDM with inverse seesaw”. In: *Eur. Phys. J. Plus* 137.11 (2022), p. 1224. DOI: [10.1140/epjp/s13360-022-03432-w](https://doi.org/10.1140/epjp/s13360-022-03432-w). arXiv: [2104.02730](https://arxiv.org/abs/2104.02730) [hep-ph].
- [1041] Hyun Min Lee, Jiseon Song, and Kimiko Yamashita. “Seesaw lepton masses and muon  $g - 2$  from heavy vector-like leptons”. In: *J. Korean Phys. Soc.* 79.12 (2021), pp. 1121–1134. DOI: [10.1007/s40042-021-00339-0](https://doi.org/10.1007/s40042-021-00339-0). arXiv: [2110.09942](https://arxiv.org/abs/2110.09942) [hep-ph].
- [1042] Jia Liu, Navin McGinnis, Carlos E. M. Wagner, and Xiao-Ping Wang. “ $\nu$  scalar in the early Universe and  $(g-2)_\mu$ ”. In: *Phys. Rev. D* 105.5 (2022), p. L051702. DOI: [10.1103/PhysRevD.105.L051702](https://doi.org/10.1103/PhysRevD.105.L051702). arXiv: [2110.14665](https://arxiv.org/abs/2110.14665) [hep-ph].
- [1043] Van Que Tran and Tzu-Chiang Yuan. “Charged lepton flavor violating radiative decays  $l_i \rightarrow l_j \gamma$  in G2HDM”. In: *JHEP* 02 (2023), p. 117. DOI: [10.1007/JHEP02\(2023\)117](https://doi.org/10.1007/JHEP02(2023)117). arXiv: [2212.02333](https://arxiv.org/abs/2212.02333) [hep-ph].
- [1044] Waleed Abdallah, Raj Gandhi, and Samiran Roy. “LSND and MiniBooNE as guideposts to understanding the muon  $g - 2$  results and the CDF II  $W$  mass measurement”. In: *Phys. Lett. B* 840 (2023), p. 137841. DOI: [10.1016/j.physletb.2023.137841](https://doi.org/10.1016/j.physletb.2023.137841). arXiv: [2208.02264](https://arxiv.org/abs/2208.02264) [hep-ph].
- [1045] N. T. Duy, D. T. Huong, and A. E. Carcamo Hernandez. “Flavor phenomenology of an extended 2HDM with inverse seesaw mechanism”. In: (Apr. 2024). arXiv: [2404.15935](https://arxiv.org/abs/2404.15935) [hep-ph].

- [1046] A. E. Cárcamo Hernández, Sergey Kovalenko, M. Maniatis, and Ivan Schmidt. “Fermion mass hierarchy and  $g - 2$  anomalies in an extended 3HDM Model”. In: *JHEP* 10 (2021), p. 036. DOI: [10.1007/JHEP10\(2021\)036](https://doi.org/10.1007/JHEP10(2021)036). arXiv: [2104.07047](https://arxiv.org/abs/2104.07047) [hep-ph].
- [1047] W. Buchmuller, R. Ruckl, and D. Wyler. “Leptoquarks in Lepton - Quark Collisions”. In: *Phys. Lett. B* 191 (1987). [Erratum: Phys.Lett.B 448, 320–320 (1999)], pp. 442–448. DOI: [10.1016/0370-2693\(87\)90637-X](https://doi.org/10.1016/0370-2693(87)90637-X).
- [1048] I. Doršner, S. Fajfer, A. Greljo, J. F. Kamenik, and N. Košnik. “Physics of leptoquarks in precision experiments and at particle colliders”. In: *Phys. Rept.* 641 (2016), pp. 1–68. DOI: [10.1016/j.physrep.2016.06.001](https://doi.org/10.1016/j.physrep.2016.06.001). arXiv: [1603.04993](https://arxiv.org/abs/1603.04993) [hep-ph].
- [1049] Andreas Crivellin and Martin Hoferichter. “Hints of lepton flavor universality violations”. In: *Science* 374.6571 (2021), p. 1051. DOI: [10.1126/science.abk2450](https://doi.org/10.1126/science.abk2450). arXiv: [2111.12739](https://arxiv.org/abs/2111.12739) [hep-ph].
- [1050] Martin Bauer and Matthias Neubert. “Minimal Leptoquark Explanation for the  $R_{D^{(*)}}$ ,  $R_K$ , and  $(g - 2)_\mu$  Anomalies”. In: *Phys. Rev. Lett.* 116.14 (2016), p. 141802. DOI: [10.1103/PhysRevLett.116.141802](https://doi.org/10.1103/PhysRevLett.116.141802). arXiv: [1511.01900](https://arxiv.org/abs/1511.01900) [hep-ph].
- [1051] Diganta Das, Chandan Hati, Girish Kumar, and Namit Mahajan. “Towards a unified explanation of  $R_{D^{(*)}}$ ,  $R_K$  and  $(g - 2)_\mu$  anomalies in a left-right model with leptoquarks”. In: *Phys. Rev. D* 94 (2016), p. 055034. DOI: [10.1103/PhysRevD.94.055034](https://doi.org/10.1103/PhysRevD.94.055034). arXiv: [1605.06313](https://arxiv.org/abs/1605.06313) [hep-ph].
- [1052] Oleg Popov and Graham A White. “One Leptoquark to unify them? Neutrino masses and unification in the light of  $(g - 2)_\mu$ ,  $R_{D^{(*)}}$  and  $R_K$  anomalies”. In: *Nucl. Phys. B* 923 (2017), pp. 324–338. DOI: [10.1016/j.nuclphysb.2017.08.007](https://doi.org/10.1016/j.nuclphysb.2017.08.007). arXiv: [1611.04566](https://arxiv.org/abs/1611.04566) [hep-ph].
- [1053] Yi Cai, John Gargalionis, Michael A. Schmidt, and Raymond R. Volkas. “Reconsidering the One Leptoquark solution: flavor anomalies and neutrino mass”. In: *JHEP* 10 (2017), p. 047. DOI: [10.1007/JHEP10\(2017\)047](https://doi.org/10.1007/JHEP10(2017)047). arXiv: [1704.05849](https://arxiv.org/abs/1704.05849) [hep-ph].
- [1054] Dario Buttazzo, Admir Greljo, Gino Isidori, and David Marzocca. “B-physics anomalies: a guide to combined explanations”. In: *JHEP* 11 (2017), p. 044. DOI: [10.1007/JHEP11\(2017\)044](https://doi.org/10.1007/JHEP11(2017)044). arXiv: [1706.07808](https://arxiv.org/abs/1706.07808) [hep-ph].
- [1055] Andreas Crivellin, Dario Müller, and Toshihiko Ota. “Simultaneous explanation of  $R(D^{(*)})$  and  $b \rightarrow s \mu^+ \mu^-$ : the last scalar leptoquarks standing”. In: *JHEP* 09 (2017), p. 040. DOI: [10.1007/JHEP09\(2017\)040](https://doi.org/10.1007/JHEP09(2017)040). arXiv: [1703.09226](https://arxiv.org/abs/1703.09226) [hep-ph].
- [1056] A. Angelescu, Damir Bečirević, D. A. Faroughy, and O. Sumensari. “Closing the window on single leptoquark solutions to the  $B$ -physics anomalies”. In: *JHEP* 10 (2018), p. 183. DOI: [10.1007/JHEP10\(2018\)183](https://doi.org/10.1007/JHEP10(2018)183). arXiv: [1808.08179](https://arxiv.org/abs/1808.08179) [hep-ph].
- [1057] Ilja Doršner, Svjetlana Fajfer, and Olcyr Sumensari. “Muon  $g - 2$  and scalar leptoquark mixing”. In: *JHEP* 06 (2020), p. 089. DOI: [10.1007/JHEP06\(2020\)089](https://doi.org/10.1007/JHEP06(2020)089). arXiv: [1910.03877](https://arxiv.org/abs/1910.03877) [hep-ph].
- [1058] Francesco D’Eramo, Nejc Košnik, Federico Pobbe, Aleks Smolkovič, and Olcyr Sumensari. “Leptoquarks and real singlets: A richer scalar sector behind the origin of dark matter”. In: *Phys. Rev. D* 104.1 (2021), p. 015035. DOI: [10.1103/PhysRevD.104.015035](https://doi.org/10.1103/PhysRevD.104.015035). arXiv: [2012.05743](https://arxiv.org/abs/2012.05743) [hep-ph].
- [1059] K. S. Babu, P. S. Bhupal Dev, Sudip Jana, and Anil Thapa. “Unified framework for  $B$ -anomalies, muon  $g - 2$  and neutrino masses”. In: *JHEP* 03 (2021), p. 179. DOI: [10.1007/JHEP03\(2021\)179](https://doi.org/10.1007/JHEP03(2021)179). arXiv: [2009.01771](https://arxiv.org/abs/2009.01771) [hep-ph].

- [1060] Valerio Gherardi, David Marzocca, and Elena Venturini. “Low-energy phenomenology of scalar leptoquarks at one-loop accuracy”. In: *JHEP* 01 (2021), p. 138. DOI: [10.1007/JHEP01\(2021\)138](https://doi.org/10.1007/JHEP01(2021)138). arXiv: [2008.09548](https://arxiv.org/abs/2008.09548) [[hep-ph](#)].
- [1061] Hyun Min Lee. “Leptoquark option for B-meson anomalies and leptonic signatures”. In: *Phys. Rev. D* 104.1 (2021), p. 015007. DOI: [10.1103/PhysRevD.104.015007](https://doi.org/10.1103/PhysRevD.104.015007). arXiv: [2104.02982](https://arxiv.org/abs/2104.02982) [[hep-ph](#)].
- [1062] Takaaki Nomura and Hiroshi Okada. “Explanations for anomalies of muon anomalous magnetic dipole moment,  $b \rightarrow s\mu\mu^-$ , and radiative neutrino masses in a leptoquark model”. In: *Phys. Rev. D* 104.3 (2021), p. 035042. DOI: [10.1103/PhysRevD.104.035042](https://doi.org/10.1103/PhysRevD.104.035042). arXiv: [2104.03248](https://arxiv.org/abs/2104.03248) [[hep-ph](#)].
- [1063] David Marzocca and Sokratis Trifinopoulos. “Minimal Explanation of Flavor Anomalies: B-Meson Decays, Muon Magnetic Moment, and the Cabibbo Angle”. In: *Phys. Rev. Lett.* 127.6 (2021), p. 061803. DOI: [10.1103/PhysRevLett.127.061803](https://doi.org/10.1103/PhysRevLett.127.061803). arXiv: [2104.05730](https://arxiv.org/abs/2104.05730) [[hep-ph](#)].
- [1064] Di Zhang. “Radiative neutrino masses, lepton flavor mixing and muon  $g - 2$  in a leptoquark model”. In: *JHEP* 07 (2021), p. 069. DOI: [10.1007/JHEP07\(2021\)069](https://doi.org/10.1007/JHEP07(2021)069). arXiv: [2105.08670](https://arxiv.org/abs/2105.08670) [[hep-ph](#)].
- [1065] Xin Wang. “Muon  $(g - 2)$  and flavor puzzles in the  $U(1)_X$ -gauged leptoquark model”. In: *JHEP* 08 (2022), p. 243. DOI: [10.1007/JHEP08\(2022\)243](https://doi.org/10.1007/JHEP08(2022)243). arXiv: [2108.01279](https://arxiv.org/abs/2108.01279) [[hep-ph](#)].
- [1066] Pavel Fileviez Perez, Clara Murgui, and Alexis D. Plascencia. “Leptoquarks and matter unification: Flavor anomalies and the muon  $g-2$ ”. In: *Phys. Rev. D* 104.3 (2021), p. 035041. DOI: [10.1103/PhysRevD.104.035041](https://doi.org/10.1103/PhysRevD.104.035041). arXiv: [2104.11229](https://arxiv.org/abs/2104.11229) [[hep-ph](#)].
- [1067] Admir Greljo, Peter Stangl, and Anders Eller Thomsen. “A model of muon anomalies”. In: *Phys. Lett. B* 820 (2021), p. 136554. DOI: [10.1016/j.physletb.2021.136554](https://doi.org/10.1016/j.physletb.2021.136554). arXiv: [2103.13991](https://arxiv.org/abs/2103.13991) [[hep-ph](#)].
- [1068] Shao-Long Chen, Wen-wen Jiang, and Ze-Kun Liu. “Combined explanations of B-physics anomalies,  $(g-2)_{e,\mu}$  and neutrino masses by scalar leptoquarks”. In: *Eur. Phys. J. C* 82.10 (2022), p. 959. DOI: [10.1140/epjc/s10052-022-10920-x](https://doi.org/10.1140/epjc/s10052-022-10920-x). arXiv: [2205.15794](https://arxiv.org/abs/2205.15794) [[hep-ph](#)].
- [1069] Andreas Crivellin, Benjamin Fuks, and Luc Schnell. “Explaining the hints for lepton flavour universality violation with three  $S_2$  leptoquark generations”. In: *JHEP* 06 (2022), p. 169. DOI: [10.1007/JHEP06\(2022\)169](https://doi.org/10.1007/JHEP06(2022)169). arXiv: [2203.10111](https://arxiv.org/abs/2203.10111) [[hep-ph](#)].
- [1070] Felipe F. Freitas, João Gonçalves, António P. Morais, Roman Pasechnik, and Werner Porod. “Interplay between flavor anomalies and neutrino properties”. In: *Phys. Rev. D* 108.11 (2023), p. 115002. DOI: [10.1103/PhysRevD.108.115002](https://doi.org/10.1103/PhysRevD.108.115002). arXiv: [2206.01674](https://arxiv.org/abs/2206.01674) [[hep-ph](#)].
- [1071] J. Julio, Shaikh Saad, and Anil Thapa. “A flavor-inspired radiative neutrino mass model”. In: *JHEP* 08 (2022), p. 270. DOI: [10.1007/JHEP08\(2022\)270](https://doi.org/10.1007/JHEP08(2022)270). arXiv: [2202.10479](https://arxiv.org/abs/2202.10479) [[hep-ph](#)].
- [1072] J. Julio, Shaikh Saad, and Anil Thapa. “Marriage between neutrino mass and flavor anomalies”. In: *Phys. Rev. D* 106.5 (2022), p. 055003. DOI: [10.1103/PhysRevD.106.055003](https://doi.org/10.1103/PhysRevD.106.055003). arXiv: [2203.15499](https://arxiv.org/abs/2203.15499) [[hep-ph](#)].
- [1073] Kingman Cheung, Wai-Yee Keung, and Po-Yan Tseng. “Isodoublet vector leptoquark solution to the muon  $g-2$ ,  $RK, K^*$ ,  $RD, D^*$ , and  $W$ -mass anomalies”. In: *Phys. Rev. D* 106.1 (2022), p. 015029. DOI: [10.1103/PhysRevD.106.015029](https://doi.org/10.1103/PhysRevD.106.015029). arXiv: [2204.05942](https://arxiv.org/abs/2204.05942) [[hep-ph](#)].

- [1074] P. S. Bhupal Dev, Srubabati Goswami, Chayan Majumdar, and Debashis Pachhar. “Neutrinoless double beta decay from scalar leptoquarks: interplay with neutrino mass and flavor physics”. In: *JHEP* 01 (2025), p. 004. DOI: [10.1007/JHEP01\(2025\)004](https://doi.org/10.1007/JHEP01(2025)004). arXiv: [2407.04670](https://arxiv.org/abs/2407.04670) [hep-ph].
- [1075] Arvind Bhaskar, Anirudhan A. Madathil, Tanumoy Mandal, and Subhadip Mitra. “Combined explanation of W-mass, muon  $g-2$ ,  $RK^{(*)}$  and  $RD^{(*)}$  anomalies in a singlet-triplet scalar leptoquark model”. In: *Phys. Rev. D* 106.11 (2022), p. 115009. DOI: [10.1103/PhysRevD.106.115009](https://doi.org/10.1103/PhysRevD.106.115009). arXiv: [2204.09031](https://arxiv.org/abs/2204.09031) [hep-ph].
- [1076] Talal Ahmed Chowdhury and Shaikh Saad. “Leptoquark-vectorlike quark model for the CDF  $m_W$ ,  $(g-2)_\mu$ ,  $RK^{(*)}$  anomalies, and neutrino masses”. In: *Phys. Rev. D* 106.5 (2022), p. 055017. DOI: [10.1103/PhysRevD.106.055017](https://doi.org/10.1103/PhysRevD.106.055017). arXiv: [2205.03917](https://arxiv.org/abs/2205.03917) [hep-ph].
- [1077] Shi-Ping He. “Leptoquark and vector-like quark extended model for simultaneous explanation of W boson mass and muon  $g-2$  anomalies\*”. In: *Chin. Phys. C* 47.4 (2023), p. 043102. DOI: [10.1088/1674-1137/ac9e4c](https://doi.org/10.1088/1674-1137/ac9e4c). arXiv: [2205.02088](https://arxiv.org/abs/2205.02088) [hep-ph].
- [1078] R. Aaij et al. “Test of lepton universality in  $b \rightarrow s\ell^+\ell^-$  decays”. In: *Phys. Rev. Lett.* 131.5 (2023), p. 051803. DOI: [10.1103/PhysRevLett.131.051803](https://doi.org/10.1103/PhysRevLett.131.051803). arXiv: [2212.09152](https://arxiv.org/abs/2212.09152) [hep-ex].
- [1079] Bernat Capdevila, Andreas Crivellin, and Joaquim Matias. “Review of semileptonic B anomalies”. In: *Eur. Phys. J. ST* 1 (2023), p. 20. DOI: [10.1140/epjs/s11734-023-01012-2](https://doi.org/10.1140/epjs/s11734-023-01012-2). arXiv: [2309.01311](https://arxiv.org/abs/2309.01311) [hep-ph].
- [1080] Debrupa Chakraverty, Debajyoti Choudhury, and Anindya Datta. “A Nonsupersymmetric resolution of the anomalous muon magnetic moment”. In: *Phys. Lett. B* 506 (2001), pp. 103–108. DOI: [10.1016/S0370-2693\(01\)00419-1](https://doi.org/10.1016/S0370-2693(01)00419-1). arXiv: [hep-ph/0102180](https://arxiv.org/abs/hep-ph/0102180).
- [1081] Uma Mahanta. “Implications of BNL measurement of delta  $a(\mu)$  on a class of scalar leptoquark interactions”. In: *Eur. Phys. J. C* 21 (2001), pp. 171–173. DOI: [10.1007/s100520100705](https://doi.org/10.1007/s100520100705). arXiv: [hep-ph/0102176](https://arxiv.org/abs/hep-ph/0102176).
- [1082] King-man Cheung. “Muon anomalous magnetic moment and leptoquark solutions”. In: *Phys. Rev. D* 64 (2001), p. 033001. DOI: [10.1103/PhysRevD.64.033001](https://doi.org/10.1103/PhysRevD.64.033001). arXiv: [hep-ph/0102238](https://arxiv.org/abs/hep-ph/0102238).
- [1083] Arvind Bhaskar, Diganta Das, Soumyadip Kundu, Anirudhan A. Madathil, Tanumoy Mandal, and Subhadip Mitra. “Vector leptoquark contributions to lepton dipole moments”. In: *Phys. Rev. D* 111.1 (2025), p. 015045. DOI: [10.1103/PhysRevD.111.015045](https://doi.org/10.1103/PhysRevD.111.015045). arXiv: [2408.11798](https://arxiv.org/abs/2408.11798) [hep-ph].
- [1084] Jonathan M. Arnold, Bartosz Fornal, and Mark B. Wise. “Phenomenology of scalar leptoquarks”. In: *Phys. Rev. D* 88 (2013), p. 035009. DOI: [10.1103/PhysRevD.88.035009](https://doi.org/10.1103/PhysRevD.88.035009). arXiv: [1304.6119](https://arxiv.org/abs/1304.6119) [hep-ph].
- [1085] Farinaldo S. Queiroz, Kuver Sinha, and Alessandro Strumia. “Leptoquarks, Dark Matter, and Anomalous LHC Events”. In: *Phys. Rev. D* 91.3 (2015), p. 035006. DOI: [10.1103/PhysRevD.91.035006](https://doi.org/10.1103/PhysRevD.91.035006). arXiv: [1409.6301](https://arxiv.org/abs/1409.6301) [hep-ph].
- [1086] Uladzimir Khasianevich, Dominik Stöckinger, Hyejung Stöckinger-Kim, and Johannes Wünsche. “Constraint on scalar leptoquark from low-energy leptonic observables”. In: *Phys. Rev. D* 108.9 (2023), p. 095027. DOI: [10.1103/PhysRevD.108.095027](https://doi.org/10.1103/PhysRevD.108.095027). arXiv: [2305.05016](https://arxiv.org/abs/2305.05016) [hep-ph].
- [1087] Estefania Coluccio Leskow, Giancarlo D’Ambrosio, Andreas Crivellin, and Dario Müller. “ $(g-2)_\mu$ , lepton flavor violation, and Z decays with leptoquarks: Correlations and future prospects”. In: *Phys. Rev. D* 95.5 (2017), p. 055018. DOI: [10.1103/PhysRevD.95.055018](https://doi.org/10.1103/PhysRevD.95.055018). arXiv: [1612.06858](https://arxiv.org/abs/1612.06858) [hep-ph].

- [1088] Kamila Kowalska, Enrico Maria Sessolo, and Yasuhiro Yamamoto. “Constraints on charmphilic solutions to the muon  $g-2$  with leptoquarks”. In: *Phys. Rev. D* 99.5 (2019), p. 055007. DOI: [10.1103/PhysRevD.99.055007](https://doi.org/10.1103/PhysRevD.99.055007). arXiv: [1812.06851 \[hep-ph\]](https://arxiv.org/abs/1812.06851).
- [1089] Wei-Chi Chiu, Chao-Qiang Geng, and Da Huang. “Correlation Between Muon  $g-2$  and  $\mu \rightarrow e\gamma$ ”. In: *Phys. Rev. D* 91.1 (2015), p. 013006. DOI: [10.1103/PhysRevD.91.013006](https://doi.org/10.1103/PhysRevD.91.013006). arXiv: [1409.4198 \[hep-ph\]](https://arxiv.org/abs/1409.4198).
- [1090] Innes Bigaran and Raymond R. Volkas. “Getting chirality right: Single scalar leptoquark solutions to the  $(g-2)_{e,\mu}$  puzzle”. In: *Phys. Rev. D* 102.7 (2020), p. 075037. DOI: [10.1103/PhysRevD.102.075037](https://doi.org/10.1103/PhysRevD.102.075037). arXiv: [2002.12544 \[hep-ph\]](https://arxiv.org/abs/2002.12544).
- [1091] Ilja Doršner, Svjetlana Fajfer, and Shaikh Saad. “ $\mu \rightarrow e\gamma$  selecting scalar leptoquark solutions for the  $(g-2)_{e,\mu}$  puzzles”. In: *Phys. Rev. D* 102.7 (2020), p. 075007. DOI: [10.1103/PhysRevD.102.075007](https://doi.org/10.1103/PhysRevD.102.075007). arXiv: [2006.11624 \[hep-ph\]](https://arxiv.org/abs/2006.11624).
- [1092] P. Arnan, D. Becirevic, F. Mescia, and O. Sumensari. “Probing low energy scalar leptoquarks by the leptonic  $W$  and  $Z$  couplings”. In: *JHEP* 02 (2019), p. 109. DOI: [10.1007/JHEP02\(2019\)109](https://doi.org/10.1007/JHEP02(2019)109). arXiv: [1901.06315 \[hep-ph\]](https://arxiv.org/abs/1901.06315).
- [1093] Andreas Crivellin, Dario Müller, and Francesco Saturnino. “Leptoquarks in oblique corrections and Higgs signal strength: status and prospects”. In: *JHEP* 11 (2020), p. 094. DOI: [10.1007/JHEP11\(2020\)094](https://doi.org/10.1007/JHEP11(2020)094). arXiv: [2006.10758 \[hep-ph\]](https://arxiv.org/abs/2006.10758).
- [1094] Stefan de Boer and Gudrun Hiller. “Flavor and new physics opportunities with rare charm decays into leptons”. In: *Phys. Rev. D* 93.7 (2016), p. 074001. DOI: [10.1103/PhysRevD.93.074001](https://doi.org/10.1103/PhysRevD.93.074001). arXiv: [1510.00311 \[hep-ph\]](https://arxiv.org/abs/1510.00311).
- [1095] Rusa Mandal and Antonio Pich. “Constraints on scalar leptoquarks from lepton and kaon physics”. In: *JHEP* 12 (2019), p. 089. DOI: [10.1007/JHEP12\(2019\)089](https://doi.org/10.1007/JHEP12(2019)089). arXiv: [1908.11155 \[hep-ph\]](https://arxiv.org/abs/1908.11155).
- [1096] Andrei Angelescu, Damir Bečirević, Darius A. Faroughy, Florentin Jaffredo, and Olcyr Sumensari. “Single leptoquark solutions to the B-physics anomalies”. In: *Phys. Rev. D* 104.5 (2021), p. 055017. DOI: [10.1103/PhysRevD.104.055017](https://doi.org/10.1103/PhysRevD.104.055017). arXiv: [2103.12504 \[hep-ph\]](https://arxiv.org/abs/2103.12504).
- [1097] W. Dekens, J. de Vries, M. Jung, and K. K. Vos. “The phenomenology of electric dipole moments in models of scalar leptoquarks”. In: *JHEP* 01 (2019), p. 069. DOI: [10.1007/JHEP01\(2019\)069](https://doi.org/10.1007/JHEP01(2019)069). arXiv: [1809.09114 \[hep-ph\]](https://arxiv.org/abs/1809.09114).
- [1098] Rachid Benbrik and Chun-Khiang Chua. “Lepton Flavor Violating  $l \rightarrow l'\gamma$  and  $Z \rightarrow \bar{l}l'$  Decays Induced by Scalar Leptoquarks”. In: *Phys. Rev. D* 78 (2008), p. 075025. DOI: [10.1103/PhysRevD.78.075025](https://doi.org/10.1103/PhysRevD.78.075025). arXiv: [0807.4240 \[hep-ph\]](https://arxiv.org/abs/0807.4240).
- [1099] Rachid Benbrik, Mohamed Chabab, and Gaber Faisal. “Lepton Flavour Violating  $\tau$  and  $\mu$  decays induced by scalar leptoquark”. In: (Sept. 2010). arXiv: [1009.3886 \[hep-ph\]](https://arxiv.org/abs/1009.3886).
- [1100] Innes Bigaran and Raymond R. Volkas. “Reflecting on chirality: CP-violating extensions of the single scalar-leptoquark solutions for the  $(g-2)_{e,\mu}$  puzzles and their implications for lepton EDMs”. In: *Phys. Rev. D* 105.1 (2022), p. 015002. DOI: [10.1103/PhysRevD.105.015002](https://doi.org/10.1103/PhysRevD.105.015002). arXiv: [2110.03707 \[hep-ph\]](https://arxiv.org/abs/2110.03707).
- [1101] Snehashis Parashar, Anirban Karan, Avnish, Priyotosh Bandyopadhyay, and Kirtiman Ghosh. “Phenomenology of scalar leptoquarks at the LHC in explaining the radiative neutrino masses, muon  $g-2$ , and lepton flavor violating observables”. In: *Phys. Rev. D* 106.9 (2022), p. 095040. DOI: [10.1103/PhysRevD.106.095040](https://doi.org/10.1103/PhysRevD.106.095040). arXiv: [2209.05890 \[hep-ph\]](https://arxiv.org/abs/2209.05890).

- [1102] Marco Fedele, Felix Wuest, and Ulrich Nierste. “Renormalisation group analysis of scalar Leptoquark couplings addressing flavour anomalies: emergence of lepton-flavour universality”. In: *JHEP* 11 (2023), p. 131. DOI: [10.1007/JHEP11\(2023\)131](https://doi.org/10.1007/JHEP11(2023)131). arXiv: [2307.15117](https://arxiv.org/abs/2307.15117) [[hep-ph](#)].
- [1103] Swagato Banerjee et al. “Averages of  $b$ -hadron,  $c$ -hadron, and  $\tau$ -lepton properties as of 2023”. In: (Nov. 2024). arXiv: [2411.18639](https://arxiv.org/abs/2411.18639) [[hep-ex](#)].
- [1104] Julian Heeck and Anil Thapa. “Explaining lepton-flavor non-universality and self-interacting dark matter with  $L_\mu - L_\tau$ ”. In: *Eur. Phys. J. C* 82.5 (2022), p. 480. DOI: [10.1140/epjc/s10052-022-10437-3](https://doi.org/10.1140/epjc/s10052-022-10437-3). arXiv: [2202.08854](https://arxiv.org/abs/2202.08854) [[hep-ph](#)].
- [1105] C. D. Froggatt and Holger Bech Nielsen. “Hierarchy of Quark Masses, Cabibbo Angles and CP Violation”. In: *Nucl. Phys. B* 147 (1979), pp. 277–298. DOI: [10.1016/0550-3213\(79\)90316-X](https://doi.org/10.1016/0550-3213(79)90316-X).
- [1106] Gudrun Hiller, Dennis Loose, and Kay Schönwald. “Leptoquark Flavor Patterns & B Decay Anomalies”. In: *JHEP* 12 (2016), p. 027. DOI: [10.1007/JHEP12\(2016\)027](https://doi.org/10.1007/JHEP12(2016)027). arXiv: [1609.08895](https://arxiv.org/abs/1609.08895) [[hep-ph](#)].
- [1107] Marzia Bordone, Oscar Catà, Thorsten Feldmann, and Rusa Mandal. “Constraining flavour patterns of scalar leptoquarks in the effective field theory”. In: *JHEP* 03 (2021), p. 122. DOI: [10.1007/JHEP03\(2021\)122](https://doi.org/10.1007/JHEP03(2021)122). arXiv: [2010.03297](https://arxiv.org/abs/2010.03297) [[hep-ph](#)].
- [1108] Sacha Davidson and Sebastien Descotes-Genon. “Minimal Flavour Violation for Leptoquarks”. In: *JHEP* 11 (2010), p. 073. DOI: [10.1007/JHEP11\(2010\)073](https://doi.org/10.1007/JHEP11(2010)073). arXiv: [1009.1998](https://arxiv.org/abs/1009.1998) [[hep-ph](#)].
- [1109] Otto Eberhardt, Geoffrey Herbert, Heiko Lacker, Alexander Lenz, Andreas Menzel, Ulrich Nierste, and Martin Wiebusch. “Impact of a Higgs boson at a mass of 126 GeV on the standard model with three and four fermion generations”. In: *Phys. Rev. Lett.* 109 (2012), p. 241802. DOI: [10.1103/PhysRevLett.109.241802](https://doi.org/10.1103/PhysRevLett.109.241802). arXiv: [1209.1101](https://arxiv.org/abs/1209.1101) [[hep-ph](#)].
- [1110] Abdelhak Djouadi and Alexander Lenz. “Sealing the fate of a fourth generation of fermions”. In: *Phys. Lett. B* 715 (2012), pp. 310–314. DOI: [10.1016/j.physletb.2012.07.060](https://doi.org/10.1016/j.physletb.2012.07.060). arXiv: [1204.1252](https://arxiv.org/abs/1204.1252) [[hep-ph](#)].
- [1111] Th. Kaluza. “Zum Unitätsproblem der Physik”. In: *Sitzungsber. Preuss. Akad. Wiss. Berlin (Math. Phys. )* 1921 (1921), pp. 966–972. DOI: [10.1142/S0218271818700017](https://doi.org/10.1142/S0218271818700017). arXiv: [1803.08616](https://arxiv.org/abs/1803.08616) [[physics.hist-ph](#)].
- [1112] Oskar Klein. “Quantum Theory and Five-Dimensional Theory of Relativity. (In German and English)”. In: *Z. Phys.* 37 (1926). Ed. by J. C. Taylor, pp. 895–906. DOI: [10.1007/BF01397481](https://doi.org/10.1007/BF01397481).
- [1113] Lisa Randall and Raman Sundrum. “A Large mass hierarchy from a small extra dimension”. In: *Phys. Rev. Lett.* 83 (1999), pp. 3370–3373. DOI: [10.1103/PhysRevLett.83.3370](https://doi.org/10.1103/PhysRevLett.83.3370). arXiv: [hep-ph/9905221](https://arxiv.org/abs/hep-ph/9905221).
- [1114] Nima Arkani-Hamed, Savas Dimopoulos, and G. R. Dvali. “The Hierarchy problem and new dimensions at a millimeter”. In: *Phys. Lett. B* 429 (1998), pp. 263–272. DOI: [10.1016/S0370-2693\(98\)00466-3](https://doi.org/10.1016/S0370-2693(98)00466-3). arXiv: [hep-ph/9803315](https://arxiv.org/abs/hep-ph/9803315).
- [1115] Nima Arkani-Hamed and Keisuke Harigaya. “Naturalness and the muon magnetic moment”. In: *JHEP* 09 (2021), p. 025. DOI: [10.1007/JHEP09\(2021\)025](https://doi.org/10.1007/JHEP09(2021)025). arXiv: [2106.01373](https://arxiv.org/abs/2106.01373) [[hep-ph](#)].
- [1116] Savas Dimopoulos, Nikolaos Tetradis, Rahim Esmailzadeh, and Lawrence J. Hall. “TeV Dark Matter”. In: *Nucl. Phys. B* 349 (1991). [Erratum: *Nucl.Phys.B* 357, 308–308 (1991)], pp. 714–726. DOI: [10.1016/0550-3213\(91\)90394-D](https://doi.org/10.1016/0550-3213(91)90394-D).

- [1117] Hsin-Chia Cheng, Jonathan L. Feng, and Konstantin T. Matchev. “Kaluza-Klein dark matter”. In: *Phys. Rev. Lett.* 89 (2002), p. 211301. DOI: [10.1103/PhysRevLett.89.211301](https://doi.org/10.1103/PhysRevLett.89.211301). arXiv: [hep-ph/0207125](https://arxiv.org/abs/hep-ph/0207125).
- [1118] Scott D. Thomas and James D. Wells. “Phenomenology of Massive Vectorlike Doublet Leptons”. In: *Phys. Rev. Lett.* 81 (1998), pp. 34–37. DOI: [10.1103/PhysRevLett.81.34](https://doi.org/10.1103/PhysRevLett.81.34). arXiv: [hep-ph/9804359](https://arxiv.org/abs/hep-ph/9804359).
- [1119] Marc Sher. “Charged leptons with nanosecond lifetimes”. In: *Phys. Rev. D* 52 (1995), pp. 3136–3138. DOI: [10.1103/PhysRevD.52.3136](https://doi.org/10.1103/PhysRevD.52.3136). arXiv: [hep-ph/9504257](https://arxiv.org/abs/hep-ph/9504257).
- [1120] A. Djouadi. “New fermions at  $e^+e^-$  colliders. 1. Production and decay”. In: *Z. Phys. C* 63 (1994), pp. 317–326. DOI: [10.1007/BF01411024](https://doi.org/10.1007/BF01411024). arXiv: [hep-ph/9308339](https://arxiv.org/abs/hep-ph/9308339).
- [1121] Kazuo Fujikawa. “A Vector - like extension of the standard model”. In: *Prog. Theor. Phys.* 92 (1994), pp. 1149–1160. DOI: [10.1143/PTP.92.1149](https://doi.org/10.1143/PTP.92.1149). arXiv: [hep-ph/9411258](https://arxiv.org/abs/hep-ph/9411258).
- [1122] Adam Falkowski, David M. Straub, and Avelino Vicente. “Vector-like leptons: Higgs decays and collider phenomenology”. In: *JHEP* 05 (2014), p. 092. DOI: [10.1007/JHEP05\(2014\)092](https://doi.org/10.1007/JHEP05(2014)092). arXiv: [1312.5329](https://arxiv.org/abs/1312.5329) [[hep-ph](#)].
- [1123] G. Cynolter and E. Lendvai. “Electroweak Precision Constraints on Vector-like Fermions”. In: *Eur. Phys. J. C* 58 (2008), pp. 463–469. DOI: [10.1140/epjc/s10052-008-0771-7](https://doi.org/10.1140/epjc/s10052-008-0771-7). arXiv: [0804.4080](https://arxiv.org/abs/0804.4080) [[hep-ph](#)].
- [1124] F. del Aguila, J. de Blas, and M. Perez-Victoria. “Effects of new leptons in Electroweak Precision Data”. In: *Phys. Rev. D* 78 (2008), p. 013010. DOI: [10.1103/PhysRevD.78.013010](https://doi.org/10.1103/PhysRevD.78.013010). arXiv: [0803.4008](https://arxiv.org/abs/0803.4008) [[hep-ph](#)].
- [1125] Gabriel Lourenço, André Milagre, Rui Santos, and João P. Silva. “Precision muon-related observables as a tool to constrain new physics models”. In: *Nucl. Phys. B* 1004 (2024), p. 116540. DOI: [10.1016/j.nuclphysb.2024.116540](https://doi.org/10.1016/j.nuclphysb.2024.116540). arXiv: [2310.06642](https://arxiv.org/abs/2310.06642) [[hep-ph](#)].
- [1126] Motoi Endo and Satoshi Mishima. “Muon  $g - 2$  and CKM unitarity in extra lepton models”. In: *JHEP* 08.08 (2020), p. 004. DOI: [10.1007/JHEP08\(2020\)004](https://doi.org/10.1007/JHEP08(2020)004). arXiv: [2005.03933](https://arxiv.org/abs/2005.03933) [[hep-ph](#)].
- [1127] A. L. Cherchiglia, G. De Conto, and C. C. Nishi. “Leptonic CP violation from a vector-like lepton”. In: *JHEP* 03 (2022), p. 010. DOI: [10.1007/JHEP03\(2022\)010](https://doi.org/10.1007/JHEP03(2022)010). arXiv: [2112.03943](https://arxiv.org/abs/2112.03943) [[hep-ph](#)].
- [1128] Koichi Hamaguchi, Natsumi Nagata, Genta Osaki, and Shih-Yen Tseng. “Probing new physics in the vector-like lepton model by lepton electric dipole moments”. In: *JHEP* 01 (2023), p. 100. DOI: [10.1007/JHEP01\(2023\)100](https://doi.org/10.1007/JHEP01(2023)100). arXiv: [2211.16800](https://arxiv.org/abs/2211.16800) [[hep-ph](#)].
- [1129] Kilian Möhling, Dominik Stöckinger, and Hyejung Stöckinger-Kim. “On-shell renormalization with vector-like leptons, one-loop muon–Higgs coupling and muon  $g - 2$ ”. In: *JHEP* 10 (2024), p. 170. DOI: [10.1007/JHEP10\(2024\)170](https://doi.org/10.1007/JHEP10(2024)170). arXiv: [2407.09421](https://arxiv.org/abs/2407.09421) [[hep-ph](#)].
- [1130] John Kearney, Aaron Pierce, and Neal Weiner. “Vectorlike Fermions and Higgs Couplings”. In: *Phys. Rev. D* 86 (2012), p. 113005. DOI: [10.1103/PhysRevD.86.113005](https://doi.org/10.1103/PhysRevD.86.113005). arXiv: [1207.7062](https://arxiv.org/abs/1207.7062) [[hep-ph](#)].
- [1131] Radovan Dermisek, Jonathan P. Hall, Enrico Lunghi, and Seodong Shin. “Limits on Vectorlike Leptons from Searches for Anomalous Production of Multi-Lepton Events”. In: *JHEP* 12 (2014), p. 013. DOI: [10.1007/JHEP12\(2014\)013](https://doi.org/10.1007/JHEP12(2014)013). arXiv: [1408.3123](https://arxiv.org/abs/1408.3123) [[hep-ph](#)].
- [1132] Nilanjana Kumar and Stephen P. Martin. “Vectorlike Leptons at the Large Hadron Collider”. In: *Phys. Rev. D* 92.11 (2015), p. 115018. DOI: [10.1103/PhysRevD.92.115018](https://doi.org/10.1103/PhysRevD.92.115018). arXiv: [1510.03456](https://arxiv.org/abs/1510.03456) [[hep-ph](#)].

- [1133] Guilherme Guedes and José Santiago. “New leptons with exotic decays: collider limits and dark matter complementarity”. In: *JHEP* 01 (2022), p. 111. DOI: [10.1007/JHEP01\(2022\)111](https://doi.org/10.1007/JHEP01(2022)111). arXiv: [2107.03429](https://arxiv.org/abs/2107.03429) [[hep-ph](#)].
- [1134] Junichiro Kawamura and Seodong Shin. “Current status on pair-produced muon-philic vectorlike leptons in multilepton channels at the LHC”. In: *JHEP* 11 (2023), p. 025. DOI: [10.1007/JHEP11\(2023\)025](https://doi.org/10.1007/JHEP11(2023)025). arXiv: [2308.07814](https://arxiv.org/abs/2308.07814) [[hep-ph](#)].
- [1135] Parham Dehghani, Mariana Frank, and Benjamin Fuks. “Collider imprint of vector-like leptons in light of anomalous magnetic moment and neutrino data”. In: (Mar. 2024). arXiv: [2403.11862](https://arxiv.org/abs/2403.11862) [[hep-ph](#)].
- [1136] Mikael Chala, Paweł Kozów, Maria Ramos, and Arsenii Titov. “Effective field theory for vector-like leptons and its collider signals”. In: *Phys. Lett. B* 809 (2020), p. 135752. DOI: [10.1016/j.physletb.2020.135752](https://doi.org/10.1016/j.physletb.2020.135752). arXiv: [2005.09655](https://arxiv.org/abs/2005.09655) [[hep-ph](#)].
- [1137] Georges Aad et al. “Search for type-III seesaw heavy leptons in leptonic final states in pp collisions at  $\sqrt{s} = 13$  TeV with the ATLAS detector”. In: *Eur. Phys. J. C* 82.11 (2022), p. 988. DOI: [10.1140/epjc/s10052-022-10785-0](https://doi.org/10.1140/epjc/s10052-022-10785-0). arXiv: [2202.02039](https://arxiv.org/abs/2202.02039) [[hep-ex](#)].
- [1138] Shrihari Gopalakrishna and Arunprasath Velusamy. “Higgs vacuum stability with vectorlike fermions”. In: *Phys. Rev. D* 99.11 (2019), p. 115020. DOI: [10.1103/PhysRevD.99.115020](https://doi.org/10.1103/PhysRevD.99.115020). arXiv: [1812.11303](https://arxiv.org/abs/1812.11303) [[hep-ph](#)].
- [1139] Amit Adhikary, Marek Olechowski, Janusz Rosiek, and Michal Ryzkowski. “Theoretical constraints on models with vectorlike fermions”. In: *Phys. Rev. D* 110.7 (2024), p. 075029. DOI: [10.1103/PhysRevD.110.075029](https://doi.org/10.1103/PhysRevD.110.075029). arXiv: [2406.16050](https://arxiv.org/abs/2406.16050) [[hep-ph](#)].
- [1140] Kivanc Y. Cingiloglu and Mariana Frank. “Stability of the Standard Model Vacuum with Vector-Like Leptons: A Critical Examination”. In: (Aug. 2024). arXiv: [2408.10898](https://arxiv.org/abs/2408.10898) [[hep-ph](#)].
- [1141] Ming-Lei Xiao and Jiang-Hao Yu. “Stabilizing electroweak vacuum in a vectorlike fermion model”. In: *Phys. Rev. D* 90.1 (2014). [Addendum: *Phys.Rev.D* 90, 019901 (2014)], p. 014007. DOI: [10.1103/PhysRevD.90.014007](https://doi.org/10.1103/PhysRevD.90.014007). arXiv: [1404.0681](https://arxiv.org/abs/1404.0681) [[hep-ph](#)].
- [1142] Koji Ishiwata and Mark B. Wise. “Phenomenology of heavy vectorlike leptons”. In: *Phys. Rev. D* 88.5 (2013), p. 055009. DOI: [10.1103/PhysRevD.88.055009](https://doi.org/10.1103/PhysRevD.88.055009). arXiv: [1307.1112](https://arxiv.org/abs/1307.1112) [[hep-ph](#)].
- [1143] Zijie Poh and Stuart Raby. “Vectorlike leptons: Muon g-2 anomaly, lepton flavor violation, Higgs boson decays, and lepton nonuniversality”. In: *Phys. Rev. D* 96.1 (2017), p. 015032. DOI: [10.1103/PhysRevD.96.015032](https://doi.org/10.1103/PhysRevD.96.015032). arXiv: [1705.07007](https://arxiv.org/abs/1705.07007) [[hep-ph](#)].
- [1144] Stuart Raby and Andreas Trautner. “Vectorlike chiral fourth family to explain muon anomalies”. In: *Phys. Rev. D* 97.9 (2018), p. 095006. DOI: [10.1103/PhysRevD.97.095006](https://doi.org/10.1103/PhysRevD.97.095006). arXiv: [1712.09360](https://arxiv.org/abs/1712.09360) [[hep-ph](#)].
- [1145] Andreas Crivellin, Fiona Kirk, Claudio Andrea Manzari, and Marc Montull. “Global Electroweak Fit and Vector-Like Leptons in Light of the Cabibbo Angle Anomaly”. In: *JHEP* 12 (2020), p. 166. DOI: [10.1007/JHEP12\(2020\)166](https://doi.org/10.1007/JHEP12(2020)166). arXiv: [2008.01113](https://arxiv.org/abs/2008.01113) [[hep-ph](#)].
- [1146] Ash Arsenault, Kivanc Y. Cingiloglu, and Mariana Frank. “Vacuum stability in the Standard Model with vectorlike fermions”. In: *Phys. Rev. D* 107.3 (2023), p. 036018. DOI: [10.1103/PhysRevD.107.036018](https://doi.org/10.1103/PhysRevD.107.036018). arXiv: [2207.10332](https://arxiv.org/abs/2207.10332) [[hep-ph](#)].

- [1147] Kivanc Y. Cingiloglu and Mariana Frank. “Vacuum stability and electroweak precision in the two-Higgs-doublet model with vectorlike quarks”. In: *Phys. Rev. D* 109.3 (2024), p. 036016. DOI: [10.1103/PhysRevD.109.036016](https://doi.org/10.1103/PhysRevD.109.036016). arXiv: [2309.03700](https://arxiv.org/abs/2309.03700) [hep-ph].
- [1148] Estefania Coluccio Leskow, Travis A. W. Martin, and Alejandro de la Puente. “Vector-like quarks with a scalar triplet”. In: *Phys. Lett. B* 743 (2015), pp. 366–376. DOI: [10.1016/j.physletb.2015.02.071](https://doi.org/10.1016/j.physletb.2015.02.071). arXiv: [1409.3579](https://arxiv.org/abs/1409.3579) [hep-ph].
- [1149] Da Huang, António P. Morais, and Rui Santos. “Anomalies in  $B$ -meson decays and the muon  $g - 2$  from dark loops”. In: *Phys. Rev. D* 102.7 (2020), p. 075009. DOI: [10.1103/PhysRevD.102.075009](https://doi.org/10.1103/PhysRevD.102.075009). arXiv: [2007.05082](https://arxiv.org/abs/2007.05082) [hep-ph].
- [1150] Sudip Jana, P. K. Vishnu, Werner Rodejohann, and Shaikh Saad. “Dark matter assisted lepton anomalous magnetic moments and neutrino masses”. In: *Phys. Rev. D* 102.7 (2020), p. 075003. DOI: [10.1103/PhysRevD.102.075003](https://doi.org/10.1103/PhysRevD.102.075003). arXiv: [2008.02377](https://arxiv.org/abs/2008.02377) [hep-ph].
- [1151] Bastián Díaz Sáez and Karim Ghorbani. “Singlet scalars as dark matter and the muon ( $g - 2$ ) anomaly”. In: *Phys. Lett. B* 823 (2021), p. 136750. DOI: [10.1016/j.physletb.2021.136750](https://doi.org/10.1016/j.physletb.2021.136750). arXiv: [2107.08945](https://arxiv.org/abs/2107.08945) [hep-ph].
- [1152] Junichiro Kawamura, Shohei Okawa, and Yuji Omura. “W boson mass and muon  $g-2$  in a lepton portal dark matter model”. In: *Phys. Rev. D* 106.1 (2022), p. 015005. DOI: [10.1103/PhysRevD.106.015005](https://doi.org/10.1103/PhysRevD.106.015005). arXiv: [2204.07022](https://arxiv.org/abs/2204.07022) [hep-ph].
- [1153] P. Ko, Takaaki Nomura, and Hiroshi Okada. “Muon  $g - 2$ ,  $B \rightarrow K^{(*)} \mu^+ \mu^-$  anomalies, and leptophilic dark matter in  $U(1)_{\mu-\tau}$  gauge symmetry”. In: *JHEP* 05 (2022), p. 098. DOI: [10.1007/JHEP05\(2022\)098](https://doi.org/10.1007/JHEP05(2022)098). arXiv: [2110.10513](https://arxiv.org/abs/2110.10513) [hep-ph].
- [1154] Lei Wang and Xiao-Fang Han. “The recent Higgs boson data and Higgs triplet model with vector-like quark”. In: *Phys. Rev. D* 86 (2012), p. 095007. DOI: [10.1103/PhysRevD.86.095007](https://doi.org/10.1103/PhysRevD.86.095007). arXiv: [1206.1673](https://arxiv.org/abs/1206.1673) [hep-ph].
- [1155] Sahar Bahrami and Mariana Frank. “Vector Quarks in the Higgs Triplet Model”. In: *Phys. Rev. D* 90.3 (2014), p. 035017. DOI: [10.1103/PhysRevD.90.035017](https://doi.org/10.1103/PhysRevD.90.035017). arXiv: [1405.4245](https://arxiv.org/abs/1405.4245) [hep-ph].
- [1156] A. S. De Jesus, S. Kovalenko, F. S. Queiroz, C. Siqueira, and K. Sinha. “Vectorlike leptons and inert scalar triplet: Lepton flavor violation,  $g - 2$ , and collider searches”. In: *Phys. Rev. D* 102.3 (2020), p. 035004. DOI: [10.1103/PhysRevD.102.035004](https://doi.org/10.1103/PhysRevD.102.035004). arXiv: [2004.01200](https://arxiv.org/abs/2004.01200) [hep-ph].
- [1157] Nabarun Chakrabarty. “Doubly charged scalars and vector-like leptons confronting the muon  $g-2$  anomaly and Higgs vacuum stability”. In: *Eur. Phys. J. Plus* 136.11 (2021), p. 1183. DOI: [10.1140/epjp/s13360-021-02168-3](https://doi.org/10.1140/epjp/s13360-021-02168-3). arXiv: [2010.05215](https://arxiv.org/abs/2010.05215) [hep-ph].
- [1158] Cesar Bonilla, A. E. Cárcamo Hernández, João Gonçalves, Felipe F. Freitas, António P. Morais, and R. Pasechnik. “Collider signatures of vector-like fermions from a flavor symmetric model”. In: *JHEP* 01 (2022), p. 154. DOI: [10.1007/JHEP01\(2022\)154](https://doi.org/10.1007/JHEP01(2022)154). arXiv: [2107.14165](https://arxiv.org/abs/2107.14165) [hep-ph].
- [1159] A. E. Cárcamo Hernández, Kamila Kowalska, Huchan Lee, and Daniele Rizzo. “Global analysis and LHC study of a vectorlike extension of the standard model with extra scalars”. In: *Phys. Rev. D* 109.3 (2024), p. 035010. DOI: [10.1103/PhysRevD.109.035010](https://doi.org/10.1103/PhysRevD.109.035010). arXiv: [2309.13968](https://arxiv.org/abs/2309.13968) [hep-ph].

- [1160] Sumit K. Garg and C. S. Kim. “Vector like leptons with extended Higgs sector”. In: (May 2013). arXiv: [1305.4712](#) [[hep-ph](#)].
- [1161] Pere Arnan, Andreas Crivellin, Marco Fedele, and Federico Mescia. “Generic Loop Effects of New Scalars and Fermions in  $b \rightarrow s\ell^+\ell^-$ ,  $(g-2)_\mu$  and a Vector-like 4<sup>th</sup> Generation”. In: *JHEP* 06 (2019), p. 118. DOI: [10.1007/JHEP06\(2019\)118](#). arXiv: [1904.05890](#) [[hep-ph](#)].
- [1162] Keiko I. Nagao, Takaaki Nomura, and Hiroshi Okada. “A model explaining the new CDF II W boson mass linking to muon  $g-2$  and dark matter”. In: *Eur. Phys. J. Plus* 138.4 (2023), p. 365. DOI: [10.1140/epjp/s13360-023-03992-5](#). arXiv: [2204.07411](#) [[hep-ph](#)].
- [1163] Tim Brune, Thomas W. Kephart, and Heinrich Päs. “Muon  $g-2$  anomaly from vector-like leptons in a 2-Higgs-doublet + scalar singlet model”. In: *Eur. Phys. J. C* 84.12 (2024), p. 1254. DOI: [10.1140/epjc/s10052-024-13617-5](#). arXiv: [2205.05566](#) [[hep-ph](#)].
- [1164] Takeo Moroi and Yasuhiro Okada. “Radiative corrections to Higgs masses in the supersymmetric model with an extra family and antifamily”. In: *Mod. Phys. Lett. A* 7 (1992), pp. 187–200. DOI: [10.1142/S0217732392000124](#).
- [1165] Stephen P. Martin. “Extra vector-like matter and the lightest Higgs scalar boson mass in low-energy supersymmetry”. In: *Phys. Rev. D* 81 (2010), p. 035004. DOI: [10.1103/PhysRevD.81.035004](#). arXiv: [0910.2732](#) [[hep-ph](#)].
- [1166] Peter W. Graham, Ahmed Ismail, Surjeet Rajendran, and Prashant Saraswat. “A Little Solution to the Little Hierarchy Problem: A Vector-like Generation”. In: *Phys. Rev. D* 81 (2010), p. 055016. DOI: [10.1103/PhysRevD.81.055016](#). arXiv: [0910.3020](#) [[hep-ph](#)].
- [1167] Yi Cai, Juan Herrero-García, Michael A. Schmidt, Avelino Vicente, and Raymond R. Volkas. “From the trees to the forest: a review of radiative neutrino mass models”. In: *Front. in Phys.* 5 (2017), p. 63. DOI: [10.3389/fphy.2017.00063](#). arXiv: [1706.08524](#) [[hep-ph](#)].
- [1168] K. S. Babu, P. S. Bhupal Dev, Sudip Jana, and Anil Thapa. “Non-Standard Interactions in Radiative Neutrino Mass Models”. In: *JHEP* 03 (2020), p. 006. DOI: [10.1007/JHEP03\(2020\)006](#). arXiv: [1907.09498](#) [[hep-ph](#)].
- [1169] Patrick Adolf, Martin Hirsch, and Heinrich Päs. “Radiative neutrino masses and the Cohen-Kaplan-Nelson bound”. In: *JHEP* 11 (2023), p. 078. DOI: [10.1007/JHEP11\(2023\)078](#). arXiv: [2306.15313](#) [[hep-ph](#)].
- [1170] Pablo Escribano, Mario Reig, and Avelino Vicente. “Generalizing the Scotogenic model”. In: *JHEP* 07 (2020), p. 097. DOI: [10.1007/JHEP07\(2020\)097](#). arXiv: [2004.05172](#) [[hep-ph](#)].
- [1171] Ritu Dcruz and Anil Thapa. “W boson mass shift, dark matter, and  $(g-2)_\ell$  in a scotogenic-Zee model”. In: *Phys. Rev. D* 107.1 (2023), p. 015002. DOI: [10.1103/PhysRevD.107.015002](#). arXiv: [2205.02217](#) [[hep-ph](#)].
- [1172] Dong Woo Kang, Jongkuk Kim, and Hiroshi Okada. “Muon  $g-2$  in  $U(1)_{\mu-\tau}$  symmetric gauged radiative neutrino mass model”. In: *Phys. Lett. B* 822 (2021), p. 136666. DOI: [10.1016/j.physletb.2021.136666](#). arXiv: [2107.09960](#) [[hep-ph](#)].
- [1173] Chuan-Hung Chen and Takaaki Nomura. “Two-loop radiative seesaw, muon  $g-2$ , and  $\tau$ -lepton-flavor violation with DM constraints”. In: *JHEP* 09 (2021), p. 090. DOI: [10.1007/JHEP09\(2021\)090](#). arXiv: [2001.07515](#) [[hep-ph](#)].

- [1174] Asmaa Abada, Nicolás Bernal, Antonio E. Cárcamo Hernández, Sergey Kovalenko, Têssio B. de Melo, and Takashi Toma. “Phenomenological and cosmological implications of a scotogenic three-loop neutrino mass model”. In: *JHEP* 03 (2023), p. 035. DOI: [10.1007/JHEP03\(2023\)035](https://doi.org/10.1007/JHEP03(2023)035). arXiv: [2212.06852](https://arxiv.org/abs/2212.06852) [[hep-ph](#)].
- [1175] A. E. Cárcamo Hernández and Ivan Schmidt. “A renormalizable left-right symmetric model with low scale seesaw mechanisms”. In: *Nucl. Phys. B* 976 (2022), p. 115696. DOI: [10.1016/j.nuclphysb.2022.115696](https://doi.org/10.1016/j.nuclphysb.2022.115696). arXiv: [2101.02718](https://arxiv.org/abs/2101.02718) [[hep-ph](#)].
- [1176] Lawrence M. Krauss, Salah Nasri, and Mark Trodden. “A Model for neutrino masses and dark matter”. In: *Phys. Rev. D* 67 (2003), p. 085002. DOI: [10.1103/PhysRevD.67.085002](https://doi.org/10.1103/PhysRevD.67.085002). arXiv: [hep-ph/0210389](https://arxiv.org/abs/hep-ph/0210389).
- [1177] Mayumi Aoki, Shinya Kanemura, and Osamu Seto. “Neutrino mass, Dark Matter and Baryon Asymmetry via TeV-Scale Physics without Fine-Tuning”. In: *Phys. Rev. Lett.* 102 (2009), p. 051805. DOI: [10.1103/PhysRevLett.102.051805](https://doi.org/10.1103/PhysRevLett.102.051805). arXiv: [0807.0361](https://arxiv.org/abs/0807.0361) [[hep-ph](#)].
- [1178] Yuji Kajiyama, Hiroshi Okada, and Kei Yagyu. “ $T_7$  Flavor Model in Three Loop Seesaw and Higgs Phenomenology”. In: *JHEP* 10 (2013), p. 196. DOI: [10.1007/JHEP10\(2013\)196](https://doi.org/10.1007/JHEP10(2013)196). arXiv: [1307.0480](https://arxiv.org/abs/1307.0480) [[hep-ph](#)].
- [1179] Amine Ahriche, Chian-Shu Chen, Kristian L. McDonald, and Salah Nasri. “Three-loop model of neutrino mass with dark matter”. In: *Phys. Rev. D* 90 (2014), p. 015024. DOI: [10.1103/PhysRevD.90.015024](https://doi.org/10.1103/PhysRevD.90.015024). arXiv: [1404.2696](https://arxiv.org/abs/1404.2696) [[hep-ph](#)].
- [1180] Chian-Shu Chen, Kristian L. McDonald, and Salah Nasri. “A Class of Three-Loop Models with Neutrino Mass and Dark Matter”. In: *Phys. Lett. B* 734 (2014), pp. 388–393. DOI: [10.1016/j.physletb.2014.05.082](https://doi.org/10.1016/j.physletb.2014.05.082). arXiv: [1404.6033](https://arxiv.org/abs/1404.6033) [[hep-ph](#)].
- [1181] Li-Gang Jin, Rui Tang, and Fei Zhang. “A three-loop radiative neutrino mass model with dark matter”. In: *Phys. Lett. B* 741 (2015), pp. 163–167. DOI: [10.1016/j.physletb.2014.12.034](https://doi.org/10.1016/j.physletb.2014.12.034). arXiv: [1501.02020](https://arxiv.org/abs/1501.02020) [[hep-ph](#)].
- [1182] Ricardo Cepedello, Pablo Escrivano, and Avelino Vicente. “Neutrino masses, flavor anomalies, and muon g-2 from dark loops”. In: *Phys. Rev. D* 107.3 (2023), p. 035034. DOI: [10.1103/PhysRevD.107.035034](https://doi.org/10.1103/PhysRevD.107.035034). arXiv: [2209.02730](https://arxiv.org/abs/2209.02730) [[hep-ph](#)].
- [1183] A. L. Cherchiglia, G. De Conto, and C. C. Nishi. “Connecting  $(g - 2)_\mu$  to neutrino mass in the extended neutrinophilic 2HDM”. In: *JHEP* 08 (2023), p. 170. DOI: [10.1007/JHEP08\(2023\)170](https://doi.org/10.1007/JHEP08(2023)170). arXiv: [2304.00038](https://arxiv.org/abs/2304.00038) [[hep-ph](#)].
- [1184] Rahool Kumar Barman, Ritu Dcruz, and Anil Thapa. “Neutrino masses and magnetic moments of electron and muon in the Zee Model”. In: *JHEP* 03 (2022), p. 183. DOI: [10.1007/JHEP03\(2022\)183](https://doi.org/10.1007/JHEP03(2022)183). arXiv: [2112.04523](https://arxiv.org/abs/2112.04523) [[hep-ph](#)].
- [1185] John C. Collins and J. A. M. Vermaseren. “Axodraw Version 2”. In: (May 2016). arXiv: [1606.01177](https://arxiv.org/abs/1606.01177) [[cs.OH](#)].
- [1186] Hermès Bélusca-Maïto, Amon Ilakovac, Paul Kühler, Marija Mađor-Božinović, Dominik Stöckinger, and Matthias Weißwange. “Introduction to Renormalization Theory and Chiral Gauge Theories in Dimensional Regularization with Non-Anticommuting  $\gamma_5$ ”. In: *Symmetry* 15.3 (2023), p. 622. DOI: [10.3390/sym15030622](https://doi.org/10.3390/sym15030622). arXiv: [2303.09120](https://arxiv.org/abs/2303.09120) [[hep-ph](#)].

- [1187] Herbi K. Dreiner, Howard E. Haber, and Stephen P. Martin. “Two-component spinor techniques and Feynman rules for quantum field theory and supersymmetry”. In: *Phys. Rept.* 494 (2010), pp. 1–196. DOI: [10.1016/j.physrep.2010.05.002](https://doi.org/10.1016/j.physrep.2010.05.002). arXiv: [0812.1594](https://arxiv.org/abs/0812.1594) [hep-ph].
- [1188] Ansgar Denner and Stefan Dittmaier. “Electroweak Radiative Corrections for Collider Physics”. In: *Phys. Rept.* 864 (2020), pp. 1–163. DOI: [10.1016/j.physrep.2020.04.001](https://doi.org/10.1016/j.physrep.2020.04.001). arXiv: [1912.06823](https://arxiv.org/abs/1912.06823) [hep-ph].
- [1189] Jorge C. Romao and Joao P. Silva. “A resource for signs and Feynman diagrams of the Standard Model”. In: *Int. J. Mod. Phys. A* 27 (2012), p. 1230025. DOI: [10.1142/S0217751X12300256](https://doi.org/10.1142/S0217751X12300256). arXiv: [1209.6213](https://arxiv.org/abs/1209.6213) [hep-ph].